

Excavation, Taphonomy and Biostratigraphy of the Late Miocene Hominid Locality Hammerschmiede and the Ecology of its Beavers

Dissertation

der Mathematisch-Naturwissenschaftlichen Fakultät
der Eberhard Karls Universität Tübingen
zur Erlangung des Grades eines
Doktors der Naturwissenschaften
(Dr. rer. nat.)

vorgelegt von
Thomas Sebastian Lechner
aus Trostberg

Tübingen
2023

Gedruckt mit Genehmigung der Mathematisch-Naturwissenschaftlichen Fakultät der
Eberhard Karls Universität Tübingen.

Tag der mündlichen Qualifikation:

26.01.2024

Dekan:

Prof. Dr. Thilo Stehle

1. Berichterstatter/-in:

Prof. Dr. Madelaine Böhme

2. Berichterstatter/-in:

PD Dr. Andreas T. Matzke

Table of Contents

Acknowledgements

Summary (English)	1
Zusammenfassung (Deutsch)	2
List of Publications	3
Chapter 1: Introduction and Objectives	8
1.1. Geology.....	8
1.2. Research history of the Hammerschmiede.....	10
1.3. Taphonomy and Biostratinomy.....	15
1.4. Mortality analyses.....	19
1.5. Objectives.....	21
Chapter 2: Excavation, Taphonomy and Biostratinomy	23
Chapter 3: Strewnfield case study of the great ape <i>Danuvius guggenmosi</i> (Mammalia, Hominidae)	107
Chapter 4: Strewnfield case study of the darter <i>Anhinga pannonica</i> (Aves, Anhingidae)	129
Chapter 5: Strewnfield case studies of the goose <i>Allgoviachen tortonica</i> and the duck cf. <i>Mioquerquedula</i> sp. (Aves, Anatidae)	149
Chapter 6: Strewnfield case study of a juvenile <i>Deinotherium levius</i> (Mammalia, Deinotheriidae)	160
Chapter 7: Taxonomy and Ecology of the beaver <i>Steneofiber depereti</i> (Mammalia, Castoridae)	201
Chapter 8: Taxonomy and Ecology of the beaver <i>Euroxenomys minutus</i> (Mammalia, Castoridae)	222
Chapter 9: Conclusion and future perspectives	239
References	246

Acknowledgements

First, I would like to thank my supervisors, Prof. Dr. Madelaine Böhme and PD Dr. Andreas T. Matzke for the supervision of this thesis. I am extremely grateful to Prof Böhme for the opportunity to be part of this ever-growing Hammerschmiede project and her working group. Without her the site would certainly not be what it is today – A world-class discovery site. She gave me the chance to live out my full potential in this project and to openly contribute all my ideas in improving scientific documentation and excavation techniques. Finally, she provided me with the funding that accompanied this project. My supervisors taught me in scientific thinking and writing, they were always friendly and attentive and gave me lots of helpful advice, which helped me a lot in completing this thesis.

Second, I would like to thank the co-authors of the papers that are included in this thesis (in alphabetical order): David R. Begun, Madelaine Böhme, Andrew S. Deane, Jochen Fuss, Panagiotis Kampouridis, Uwe Kirscher, George E. Konidaris, Gerald Mayr, Jerome Prieto, Nikolai Spassov and Adrian Tröscher. This collaboration was a special experience for me and helped me to advance my scientific way of thinking and working.

Third, I want to thank my colleagues and friends here at the University of Tübingen for fruitful discussions, and providing a pleasant working atmosphere. People I would like to absolutely highlight here are (in alphabetical order): Pascal Abel, Felix Augustin, Anna Ayvazyan, Christian Dietzel, Aaron Ebner, Martin Ebner, Haytham El Atfy, Agnes Fatz, Gabriel Ferreira, Lorenz Fischer, Jochen Fuss, Josephina Hartung, Panagiotis Kampouridis, Uwe Kirscher, Sabine Kötter, Christina Kyriakouli, Tobias Massonne, Tatiana Miranda, Henrik Stöhr, Adrian Tröscher and Ingmar Werneburg.

Finally, I would like to thank my friends and family for their invaluable support during all these years. My family always encouraged me to follow my interests and supported me wherever possible along the way. My father Wolfgang Lechner in particular, with his interest in the natural sciences, encouraged me to explore this subject in greater depth. Finally, and with the greatest respect, I would like to thank my girlfriend Ilona Gold. She has always been there for me over the years, giving me all the support and encouragement I needed, building me up again at low points and helping me to tackle projects with a new structure. She was always up for lengthy discussions about fossils and has at least the same fascination for fossilised creatures as I do.

Thank you very much!

Summary

Miocene sediments cover a large area of Eurasia and southern Germany. However, apart from sedimentological studies, a comprehensive insight into fossil ecosystems from this period is rarely possible. Many sites are known from single finds or were only accessible for a short period of time. The Hammerschmiede site (Allgäu region) enables the large-scale documentation of two fluvial fossil-enriched ecosystems of the early Late Miocene. In addition to a continuously growing taxonomic diversity, this site offers the opportunity to gain insights into taphonomy and, in particular, biostratinomy. Numerous field observations are described by different case studies. Sedimentological observations are evaluated and the discoveries are examined in three-dimensional analyses in relation to each other. Various elements can be attributed to autochthonous or allochthonous origin and testify to greater or lesser transportation and processing distances. Multiple proxies testify to the direction of flow of the water and its change of direction and provide evidence of meandering rivers and streams. Based on this information, isolated found bones and partially anatomically arranged skeletal elements can finally be reconstructed into single individuals that were scattered in strewnfields by the channel flow. A large number of destructive agents can be identified from traces on bones, demonstrating an extensive interplay of aquatic and terrestrial floral and faunal elements involved in the utilization of the carcasses. Finally, abiotic factors that have contributed to the preservation or destruction of fossils are documented and bear witness to compressions by large diagenetic loads. Nevertheless, possible destruction by mining equipment and activity, as well as the excavations themselves, cannot be ruled out. Furthermore, mineral neoformations of iron sulfides and uranium incorporation within bones reveal geochemical post-depositional processes. In addition to numerous case studies to field observations, mortality analyses are used to gain further ecological insights into the habitats along the fossil local stratigraphic levels HAM 5 (rivulet) and HAM 4 (river) using the selected example of two occurring beaver species, based on their assumed autochthony. The resulting age-frequency distributions allow conclusions on inter- and intraspecific relationships of the beavers within the habitat. The Hammerschmiede site proves that extensive excavations and comprehensive documentation can open up many other sources of information in addition to the usual findings on taxonomy. The result is a unique insight into the Miocene of southern Germany with an increasingly improved understanding of ecological parameters within those habitats and subsequent taphonomic and biostratinomic processes.

Zusammenfassung

Miozänen Sedimente bedecken weite Bereiche Eurasiens und auch Süddeutschlands. Dennoch ist ein umfassender Einblick in fossile Ökosysteme aus dieser Zeit, abgesehen von sedimentologischen Untersuchungen, nur selten möglich. Viele Fundstellen sind nur über Einzelfunde bekannt oder waren nur für kurze Zeit zugänglich. Die Fundstelle Hammerschmiede (Allgäu) ermöglicht die großflächige Dokumentation zweier fluvialer, fossilreicher Ökosysteme des frühen Obermiozäns. Neben einer stetig wachsenden taxonomischen Vielfalt bietet dieser Fundort die Möglichkeit, Einblicke in die Taphonomie und insbesondere in die Biostratinomie der Fundstelle zu gewinnen. Zahlreiche Feldbeobachtungen werden in Fallstudien beschrieben. Sedimentologische Beobachtungen werden ausgewertet und die Funde in 3-D Analysen in eine räumliche Beziehung gesetzt. Verschiedene Fossilien sind autochthoner oder allochthoner Herkunft und belegen mehr oder weniger weite Transport- und Aufarbeitungsdistanzen. Über verschiedene Beobachtungen werden die fossile Fließrichtung und Richtungsveränderungen konstruiert. Anhand dieser Informationen können fluvial verteilte Funde in Streufeldanalysen wieder zu einzelnen Individuen rekonstruiert werden. Anhand von Spuren auf den Knochen lassen sich eine Vielzahl von Verwertern identifizieren, die ein umfangreiches Zusammenspiel von aquatischen und terrestrischen Floren- und Faunenelementen bei der Nutzung von Fließgewässern belegen. Schließlich werden Faktoren, die zur Erhaltung oder Zerstörung von Fossilien beigetragen haben dokumentiert. Darüber hinaus lassen mineralische Neubildungen von Eisensulfiden und Uraneinlagerungen in Knochen auf geochemische Prozesse in den Ablagerungen schließen. Neben zahlreichen Fallstudien werden anhand von Mortalitätsanalysen weitere ökologische Erkenntnisse zu den Lebensräumen entlang des fossilen Bachlaufs HAM 5 und dem Flusslauf der HAM 4 am ausgewählten Beispiel zweier Biberarten gewonnen, welche als autochthone Elemente angesehen werden. Die resultierenden Mortalitätsprofile lassen Rückschlüsse auf inter- und intraspezifische Beziehungen der Biber innerhalb des Lebensraumes zu. Die Fundstelle Hammerschmiede belegt, dass umfangreiche Ausgrabungen und Dokumentationen neben den üblichen Erkenntnissen zur Taxonomie viele weitere Informationsquellen erschließen können. Das Ergebnis ist ein einzigartiger Einblick in das Miozän Süddeutschlands mit zunehmend besserem Verständnis über ökologische Parameter sowie taphonomische und biostratinomische Prozesse innerhalb dieser Lebensräume.

List of Publications

Publications and manuscripts included in this thesis. A manuscript that has not yet been submitted is included in Chapter 2. Published articles are found in the formatting type of the publication in the respective chapters below (Chapter 3-8). The publication list is sorted by ascending dates of publication.

a) Accepted publications

- 1.) Böhme, M., Spassov, N., Fuss, J., Tröscher, A., Deane, A.S., Prieto, J., Kirscher, U., Lechner, T., Begun, D.R., 2019. A new Miocene ape and locomotion in the ancestor of great apes and humans. *Nature* 575, 489–493.
<https://doi.org/10.1038/s41586-019-1731-0>
- 2.) Mayr, G., Lechner, T., Böhme, M., 2020. The large-sized darter *Anhinga pannonica* (Aves, Anhingidae) from the late Miocene hominid Hammerschmiede locality in Southern Germany. *PlosOne* 15, 1–19.
<https://doi.org/10.1371/journal.pone.0232179>
- 3.) Mayr, G., Lechner, T., Böhme, M., 2022. Nearly complete leg of an unusual, shelduck-sized anseriform bird from the earliest late Miocene hominid locality Hammerschmiede (Germany). *Historical Biology* 1–10.
<https://doi.org/10.1080/08912963.2022.2045285>
- 4.) Lechner, T., Böhme, M., 2022. The beaver *Steneofiber depereti* from the lower Upper Miocene hominid locality Hammerschmiede and remarks on its ecology. *Acta Palaeontologica Polonica* 67 (4), 807-826.
<https://doi.org/10.4202/app.00997.2022>
- 5.) Lechner, T., Böhme, M., 2023. The largest record of the minute beaver *Euroxenomys minutus* (Mammalia, Castoridae) from the early Late Miocene hominid locality Hammerschmiede (Bavaria, Southern Germany) and palaeoecological considerations. *Historical Biology*, 1–16.
<https://doi.org/10.1080/08912963.2023.2215236>

- 6.) Konidakis, G.E., Lechner, T., Kampouridis, P., Böhme, M., 2023. *Deinotherium levius* and *Tetralophodon longirostris* (Proboscidea, Mammalia) from the Late Miocene hominid locality Hammerschmiede (Bavaria, Germany), and their biostratigraphic significance for the terrestrial faunas of the European Miocene. *Journal of Mammalian Evolution*.
<https://doi.org/10.1007/s10914-023-09683-3>

b) Manuscripts not yet submitted

- 7.) Lechner, T., In Preparation. Excavation, Taphonomy and Biostratinomy of the early Late Miocene Hominid Locality Hammerschmiede.

This manuscript is in preparation for the submission to *Senckenberg Monographs*.



**Erklärung nach § 5 Abs. 2 Nr. 8 der Promotionsordnung der Math.-Nat.
Fakultät**

**-Anteil an gemeinschaftlichen Veröffentlichungen-
Nur bei kumulativer Dissertation erforderlich!**

**Declaration according to § 5 Abs. 2 No. 8 of the PhD regulations of the
Faculty of Science**

**-Collaborative Publications-
For Cumulative Theses Only!**

Last Name, First Name: Lechner, Thomas Sebastian

List of Publications

1. Böhme, M., Spassov, N., Fuss, J., Tröschler, A., Deane, A.S., Prieto, J., Kirscher, U., Lechner, T., Begun, D.R., 2019. A new Miocene ape and locomotion in the ancestor of great apes and humans. *Nature* 575, 489–493.
2. Mayr, G., Lechner, T., Böhme, M., 2020. The large-sized darter *Anhinga pannonica* (Aves, Anhingidae) from the late Miocene hominid Hammerschmiede locality in Southern Germany. *PlosOne* 15, 1–19.
3. Mayr, G., Lechner, T., Böhme, M., 2022. Nearly complete leg of an unusual, shelduck-sized anseriform bird from the earliest late Miocene hominid locality Hammerschmiede (Germany). *Historical Biology* 1–10.
4. Lechner, T., Böhme, M., 2022. The beaver *Steneofiber depereti* from the lower Upper Miocene hominid locality Hammerschmiede and remarks on its ecology. *Acta Palaeontologica Polonica* 67 (4), 807-826.
5. Lechner, T., Böhme, M., 2023. The largest record of the minute beaver *Euroxenomys minutus* (Mammalia, Castoridae) from the early Late Miocene hominid locality Hammerschmiede (Bavaria, Southern Germany) and palaeoecological considerations. *Historical Biology*, 1–16.
6. Konidaris, G.E., Lechner, T., Kampouridis, P., Böhme, M., 2023. *Deinotherium levius* and *Tetralophodon longirostris* (Proboscidea, Mammalia) from the Late Miocene hominid



locality Hammerschmiede (Bavaria, Germany), and their biostratigraphic significance for the terrestrial faunas of the European Miocene. *Journal of Mammalian Evolution*.

7. Lechner, T., In Preparation. Excavation, Taphonomy and Biostratinomy of the early Late Miocene Hominid Locality Hammerschmiede. This manuscript is in preparation for the submission to *Senckenberg Monographs*.

Nr.	Accepted publication yes/no	List of authors	Position of candidate in list of authors	Scientific ideas by the candidate (%)	Data generation by the candidate (%)	Analysis and Interpretation by the candidate (%)	Paper writing done by the candidate (%)
1	yes	9	8	10	10	10	10
2	yes	3	2	10	10	10	10
3	yes	3	2	10	10	10	10
4	yes	2	1	90	100	90	90
5	yes	2	1	90	100	90	90
6	yes	4	2	10	10	10	10
7	no	1	1	100	100	100	100

c) Publications not included in this thesis that were written during the PhD

The following publications have been fully published by the respective journals and are sorted according to their date of publication.

- 8.) Hartung, J., Lechner, T., Böhme, M., 2020. New cranial material of *Miotragocerus monacensis* (Mammalia: Bovidae) from the late Miocene hominid locality Hammerschmiede (Germany). *Neues Jahrbuch für Geologie und Paläontologie - Abhandlungen* 298, 269–284. <https://doi.org/10.1127/njgpa/2020/0948>
- 9.) Lechner, T., Böhme, M., 2020. Eine Fundgrube für Paläontologen. *Bayerische Archäologie* 26–31.
- 10.) Lechner, T.S., Böhme, M., 2020. Castor-like postcranial adaptation in an uppermost Miocene beaver from the Staniantsi Basin (NW Bulgaria). *Fossil Imprint* 76, 128–164. <https://doi.org/DOI 10.37520/fi.2020.009>
- 11.) Mayr, G., Lechner, T., Böhme, M., 2020. A skull of a very large crane from the late Miocene of Southern Germany, with notes on the phylogenetic interrelationships of extant Gruinae. *Journal of Ornithology* 161, 923–933. <https://doi.org/10.1007/s10336-020-01799-0>
- 12.) Kargopoulos, N., Kampouridis, P., Lechner, T., Böhme, M., 2021a. A review of *Semigenetta* (Viverridae, Carnivora) from the Miocene of Eurasia based on material from the hominid locality of Hammerschmiede (Germany). *Geobios* 69, 25–36. <https://doi.org/10.1016/j.geobios.2021.07.001>
- 13.) Kargopoulos, N., Kampouridis, P., Lechner, T., Böhme, M., 2021b. Hyaenidae (Carnivora) from the Late Miocene hominid locality of Hammerschmiede (Bavaria, Germany). *Historical Biology* 1–10. <https://doi.org/10.1080/08912963.2021.2010193>
- 14.) Kargopoulos, N., Valenciano, A., Kampouridis, P., Lechner, T., Böhme, M., 2021c. New early late Miocene species of *Vishnuonyx* (Carnivora, Lutrinae) from the hominid locality of Hammerschmiede, Bavaria, Germany. *Journal of Vertebrate Paleontology* 41, e1948858. <https://doi.org/10.1080/02724634.2021.1948858>
- 15.) Kargopoulos, N., Valenciano, A., Abella, J., Kampouridis, P., Lechner, T., Böhme, M., 2022. The exceptionally high diversity of small carnivorans from the Late Miocene hominid locality of Hammerschmiede (Bavaria, Germany). *PLOS ONE* 64.

Introduction and Objectives

1.1 Geology

During the Late Mesozoic (mid Cretaceous), a convergent movement of the African-Adriatic (Apulian) and the European Plates initiated the extensive tectonic processes which led to the formation of the Alpine mountain ranges – the Alpine (Alpide) orogeny (Schwerd et al. 1996). During the Cenozoic, the progressive and intensifying continental collision led to the extensive accumulation of mostly continental rocks in an orogenic wedge, which increasingly penetrated northwards into the European Plate. The crustal thickening (accumulation of mass) due to the orogeny caused the evolving mountain range to “sink” into the Earth's lithosphere and lithospheric mantle by density compensation and also flexed the peripheral lithosphere to the north of it. Based on the flexural rigidity of the lithosphere, the width and depth of the formed peripheral foreland basin is characterised (Schwerd et al. 1996). In the case of the North Alpine Foreland Basin (Molasse Basin after the German term: “Molassebecken” which is based on the French term “molasse” = very soft (see Doppler et al. 2005)) discussed here, the basin covers an east-west extension of over 1000 km (France, Switzerland, Germany, Austria) across the entire length of the Alpine front (Schwerd et al. 1996). The width of the basin reaches up to 130 km. The primary phase of subsidence dates from the Late Eocene to the Late Miocene (Schwerd et al. 1996; Doppler et al. 2005).

The basin structure acts as a sediment trap and is continuously filled with sediment during its progression. The sediments consist mainly of erosional products and debris from the rising Alps in the South but also from the Bohemian Massif to the North. This sediment accumulation (accumulation of mass) further drove the subsidence of the basin. Due to large differences in basin depth, sediment sources or water supply, the sedimented sequences differ, in some cases massively, across the entire depositional area. The basin is deepest directly at the orogenic front and rises low-angled to the North, so that sediment thicknesses of up to 5000 metres can be reached in the South (Schwerd et al. 1996). A borehole near Opfenbach (Bavaria, Allgäu region) documented a thickness of 3650 metres of Molasse basin sediments (Lemcke 1988).

The sedimentary record of the North Alpine Foreland Basin can be divided into four major sedimentary phases, that are typical for Southern Germany and the Allgäu region in particular (Steininger et al. 1989; Schwerd et al. 1996; Scholz 2016). Depending on the degree of basin subsidence and global sea level fluctuations, marine transgressions of the Paratethys ocean flooded the foreland basin (Schwerd et al. 1996; Scholz 2016). The oldest sediments of the

Molasse basin date to the Oligocene and comprise of a marine formation, the Lower Marine Molasse (German: Untere Meeresmolasse, UMM; Early Oligocene) (Schwerd et al. 1996, Doppler et al. 2005; Scholz 2016) (compare Fig. 1.1). They are followed by terrestrial fluvial sand, silt, clay and marl deposits of the second major formation, the Lower Freshwater Molasse (German: Untere Süßwassermolasse, USM; Late Oligocene – Early Miocene). This is again followed by a marine transgression phase with the deposits of the Upper Marine Molasse (German: Obere Meeresmolasse, OMM; Early Miocene). Terrestrial, mainly fluvial deposits occur again as the last major section, the Upper Freshwater Molasse (German: Obere Süßwassermolasse, OSM; late Early Miocene – Late Miocene). The continuing Alpine tectonic movement from the south (Austroalpine nappes, German: Alpine Decken, Fig. 1.1) overthrust some of the bottommost Molasse sediments (German: Überfahrene Molasse) and the southernmost region of the Molasse deposits was partly folded and straightened up (‘Folded Molasse’, German: Faltenmolasse, Fig. 1.1; ‘Straightened up Molasse’, German: Aufgerichtete Molasse) inclining to the South (Lemcke 1988; Schwerd et al. 1996). As a result of the continuing Alpine pressure from the south, the southern margin of the foreland Molasse (German: Vorlandmolasse, Fig. 1.1) was also raised and slightly inclined towards the north (Lemcke 1988) (Fig. 1.1).

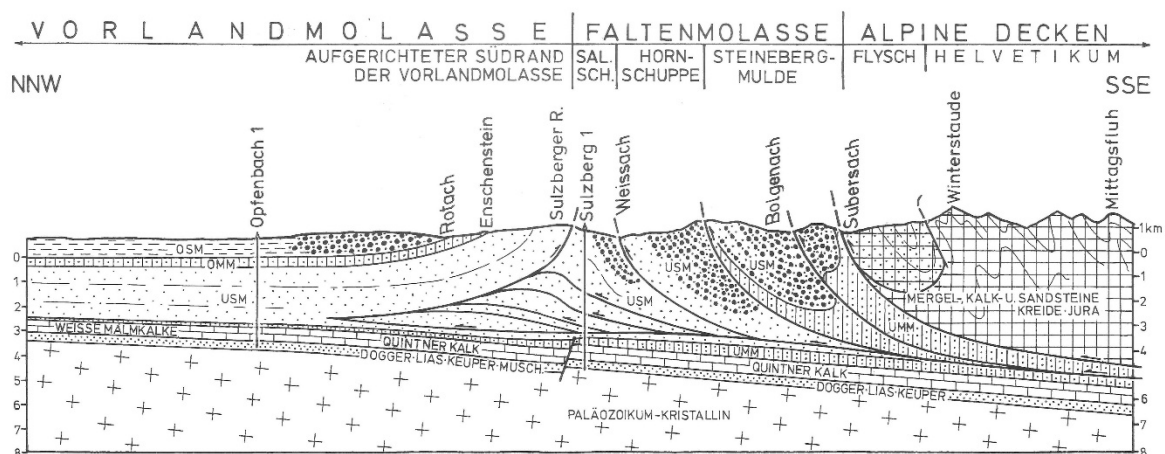


Figure 1.1. Geological section through the subsurface of the western Allgäu (southern Germany) and neighbouring areas (NNW-SSE). On the North, the undisturbed sediments of the Molasse basin, followed by the uplifted southern margin, the uplifted Molasse, the folded Molasse and the adjacent Alpine nappes of the Alpine orogen in the South. Reprinted from Scholz (2016).

During the Late Miocene, foreland basin subsidence stopped and the area slowly began to uplift again, probably due to isostatic rebound caused by increasing sediment erosion of the orogen (Schwerd et al. 1996). Finally, the increased uplift led to an increased denudation and erosion of the superimposed molasse sediments during the Pliocene and Pleistocene (Glaciers).

According to Doppler (1989) and Doppler et al. (2005) the Upper Freshwater Molasse of western Bavaria is divided into four units. It starts with the oldest “Limnische Untere Serie” (Limnic Lower Series), “Fluviatile Untere Serie” (Fluvial Lower Series) and “Geröllsandserie” (Gravel-Sand-Series) and ends with the youngest section of the “Obere Serie” (Upper Series). This last phase is characterised by fine grained fluvial deposits, which sometimes contain a considerable amount of carbonate. In addition to this, thin lignite seams also occur there. In regional geological terms, these argillaceous-marly to fine sandy deposits of the uppermost upper Freshwater Molasse are also known as “Flinz” because of the reflections caused by micas (Klein 1937, 1938, 1939; Kordiuk 1938).

Due to the strong erosion since the Pliocene, the youngest sections of the Upper Series are not preserved everywhere. A hill ridge at the western margin of the Wertach valley, in the area of the Hammerschmiede clay pit near Pforzen (Allgäu region) possibly comprises the youngest preserved areas of these deposits (Kirscher et al. 2016).

1.2 Research history of the Hammerschmiede locality

The Hammerschmiede fossil site is an active clay mine near the small village of Pforzen (Bavaria, Southern Germany). The clay pit comprises fluvio-alluvial flood plain deposits (clay, silt, fine-sand, lignite) of the Northern Alpine Foreland Basin (Fig. 1.2.1). The area around the municipality of Pforzen and Irsee has long been known for the occurrence of lignite (“coal”), which was even mined underground during the 19th and 20th century, and reported since at least 1836 (Wiedenmann 2011). Carl Wilhelm von Gümbel (1861, p. 791) is the first to list fossil finds (plant and mollusc remains) from the vicinity of ‘Irrsee’ (today Irsee), unfortunately without a detailed description of the site. While coal mining repeatedly fell into decline due to a lack of economic viability, clay began to be mined in 1947 (Wiedenmann 2011). In the description of a stratigraphic column of a 31 metre deep shaft at the Hammerschmiede from February 1948, the first fossils are localised and mentioned alongside the coal in the form of invertebrate fossils – gastropods – as components found in some clay layers within the profile (Observation by Dr. Heim 17.02.1948 to head miner Karl Zill, in Wiedenmann 2011). This historical profile reached an altitude of 657 metres above sea level and was thus situated below the current Hammerschmiede outcrop. A scientific report on paleobotanical (coal, leaves and palynology) finds and invertebrate fossils (helixid snails) is provided by Meyer (1956). As early as 1965, the amateur archaeologist and private collector Sigulf Guggenmos (Dösingen) possibly made the first vertebrate discovery (turtle carapace fragment). The first occurrence of

vertebrates (microvertebrates) and a more detailed description of fossil bearing strata was reported by Mayr and Fahlbusch (1975) and Fahlbusch and Mayr (1975) after S. Guggenmos informed those authors of further vertebrate fossil discoveries around 1972. This was followed by extensive sampling for microfossils by H. Mayr in May 1973 (HAM 1; pers. comm. to M. Böhme 2023).

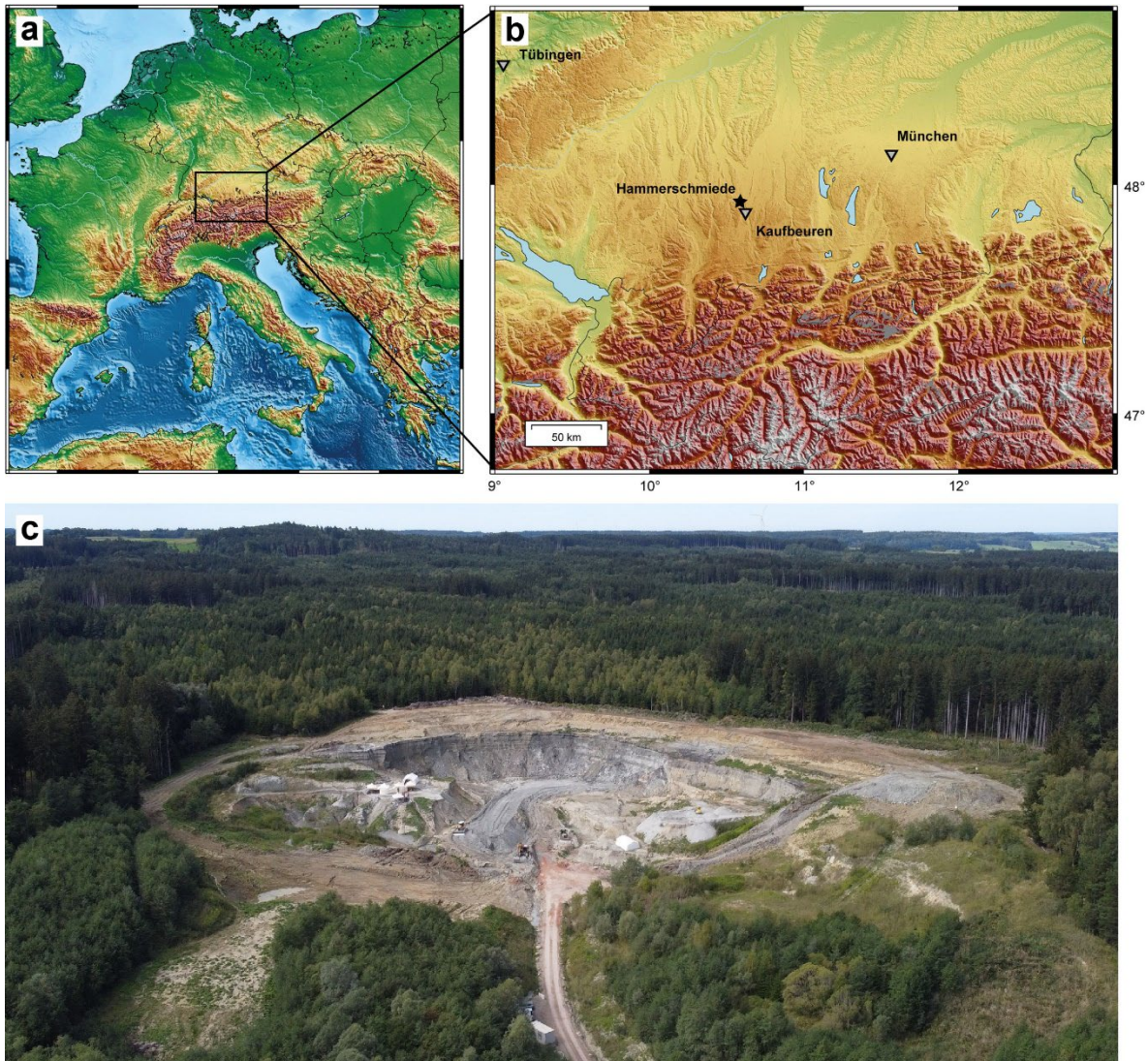


Figure 1.2.1. a) Topographical map of Europe. b) Magnification of the western part of the North Alpine Foreland Basin (south German Molasse Basin). The Hammerschmiede locality is highlighted with a black star. Modified from Böhme et al. (2019). c) Drone image of the Hammerschmiede clay pit looking west.

The private collectors Sigulf Guggenmos (Döisingen) and Manfred Schmid (Marktoberdorf) continued in documenting fossils from the Hammerschmiede during the late 1970s and early 1980s and discovered a fossil bearing level (now HAM 6) right below the topmost lignite seam, which yielded the partial skeleton of a large adult male proboscidean – *Tetralophodon longirostris* – in addition to several isolated finds of medium and small vertebrates (Konidaris

et al. 2023). Probably encouraged by this discovery, H. Mayr investigated two further levels containing small mammals in the 1980s (HAM 2 and HAM 3, one of which could correspond to HAM 6) (pers. comm. M. Böhme). The correlation of these "historical" fossil layers (HAM 1-3, HAM 6) to present-day fossil levels is restricted. Since that time, the material housed at the BSPG (Bayerische Staatssammlung für Geologie und Paläontologie) in Munich has been the subject of various publications. Jung and Mayr (1980) compared micromammals and palaeobotanical elements of several southern German localities and assigned the Hammerschmiede to the Mammal Neogene Unit MN 9. Gregor (1982) summarises the palaeobotanical findings of the Hammerschmiede and also deals with the discovery of a new leaf bearing level at the base of the pit by the private collector M. Schmid in 1979. He further provides an update on the vertebrate finds. Schleich (1984) provides the turtle finds of the Hammerschmiede. As part of her PhD thesis, Seitner (1987) analysed the microflora of the Hammerschmiede. Several authors support the placement of the Hammerschmiede in the Mammal Neogene Unit MN 9, as early Vallesian: Mein 1989; de Bruijn et al. 1992), or in the pre-Vallesian MN7/8 (Böhme et al. 2006, 2008; Prieto et al. 2011). In numerous publications especially the vertebrate fauna of the layers HAM 1-3 (mammals, amphibians, reptiles and fishes) is mentioned (Bollinger 1999; Daams 1999; Fejfar 1999; Huguency 1999; Ziegler 1999; Böhme 2002; Böhme et al. 2006, 2008, 2010, 2011, 2012; Prieto 2007; Prieto and Rummel 2009a; Prieto and Rummel 2009b; Klembara et al. 2010; van Dam 2010; Prieto 2011, 2012; Prieto and van Dam 2012).

From the early 2000s, M. Böhme (then Munich, today Tübingen) together with Jérôme Prieto (Munich) began to collect geological data in the Hammerschmiede clay pit (pers. comm. M. Böhme). It was precisely in the search for the youngest Molasse Basin deposits, that the outcrop of the actively mined Hammerschmiede clay pit on the western side of the Wertach river near Pforzen, a few kilometres northwest of the city of Kaufbeuren at the Allgäu region (Bavaria, Southern Germany), once again became the focus of scientific research. After a long break of research activity at this locality, the DFG funded a research project (grant BO1550/16 of the Deutsche Forschungsgemeinschaft, DFG, 2010-2013) including a borehole, that was put down on a hill just a few kilometres to the southwest of the Hammerschmiede, near the monastery Irsee (Kirscher et al. 2016). The drill core (150.5 m) recorded 28 metres of unconformably superimposed gravel, a Pleistocene fluvial terrace (meltwater gravel of the Günz glaciation) and 122 metres of Miocene sediments of the youngest part of the "Obere Serie" (Upper Series). In contrast to the drill core, the Pleistocene cover at the Hammerschmiede clay pit is only a few

metres thick and is composed of a glacial till of Middle Pleistocene age (Riss glaciation) (Kirscher et al. 2016) (Fig. 1.2.2). The Miocene sediments of the drill core and the Hammerschmiede are mainly composed of fluvial sediments (fine sand, silt, clay) and lignite seams and mainly represent river and floodplain deposits. With the help of various marker horizons and magnetostratigraphic investigations as well as the comparison of the topographic elevation with the Irsee drill core, a precise chronostratigraphic correlation of the sediments exposed at the Hammerschmiede clay pit was performed by Kirscher et al. (2016) and the 26 metres Hammerschmiede section was dated between 11.66 Ma and 11.42 Ma. Consequently, the sediments precisely cover the Middle- to Late Miocene transition (Late Serravallian and basal Tortonian) (Kirscher et al. 2016). In 2011 an apparently autochthonous mollusc fauna within a fluvial channel (HAM 4, discovered around 2009) was described by Schneider and Prieto (2011). In the same year, excavations began led by M. Böhme (Eberhard Karls University of Tübingen) in a smaller fossil-bearing channel, discovered by her in 2010 in the central pit profile (HAM 5), which were continued and more and more intensified over the following years. After initial small-scale sampling, extensive excavations have also been taking place in the local stratigraphic level HAM 4 since 2017. I myself have been actively involved in the excavations since field season 2015 and have been in charge of excavation management tasks since 2016.

The excavation work has not yet been completed and more than 30,000 finds from more than 1000 square metres of excavated area have been documented so far. In a new generation of publications, the new finds from the fossil layers HAM 5 and HAM 4 were supplemented by finds from HAM 1-3 and HAM 6. Fuss et al. (2015) and Hartung et al. (2020) studied the boselaphin bovids (*Miotragocerus monacensis*, Bovidae, Artiodactyla) of the locality. Hartung and Böhme (2022) published the first evidence of cranial sexual dimorphism in tragulids (*Dorcatherium nauti*, Tragulidae, Artiodactyla). Lechner and Böhme (2022, 2023) published two beaver species (*Steneofiber depereti* and *Euroxenomys minutus*, Castoridae, Rodentia) from the Hammerschmiede and presented palaeoecological observations. Several publications reported on the first avian finds of the Hammerschmiede with material of a darter (*Anhinga pannonica*, Anhingidae, Suliformes), the skull of a crane (Gruidae, Gruiformes),

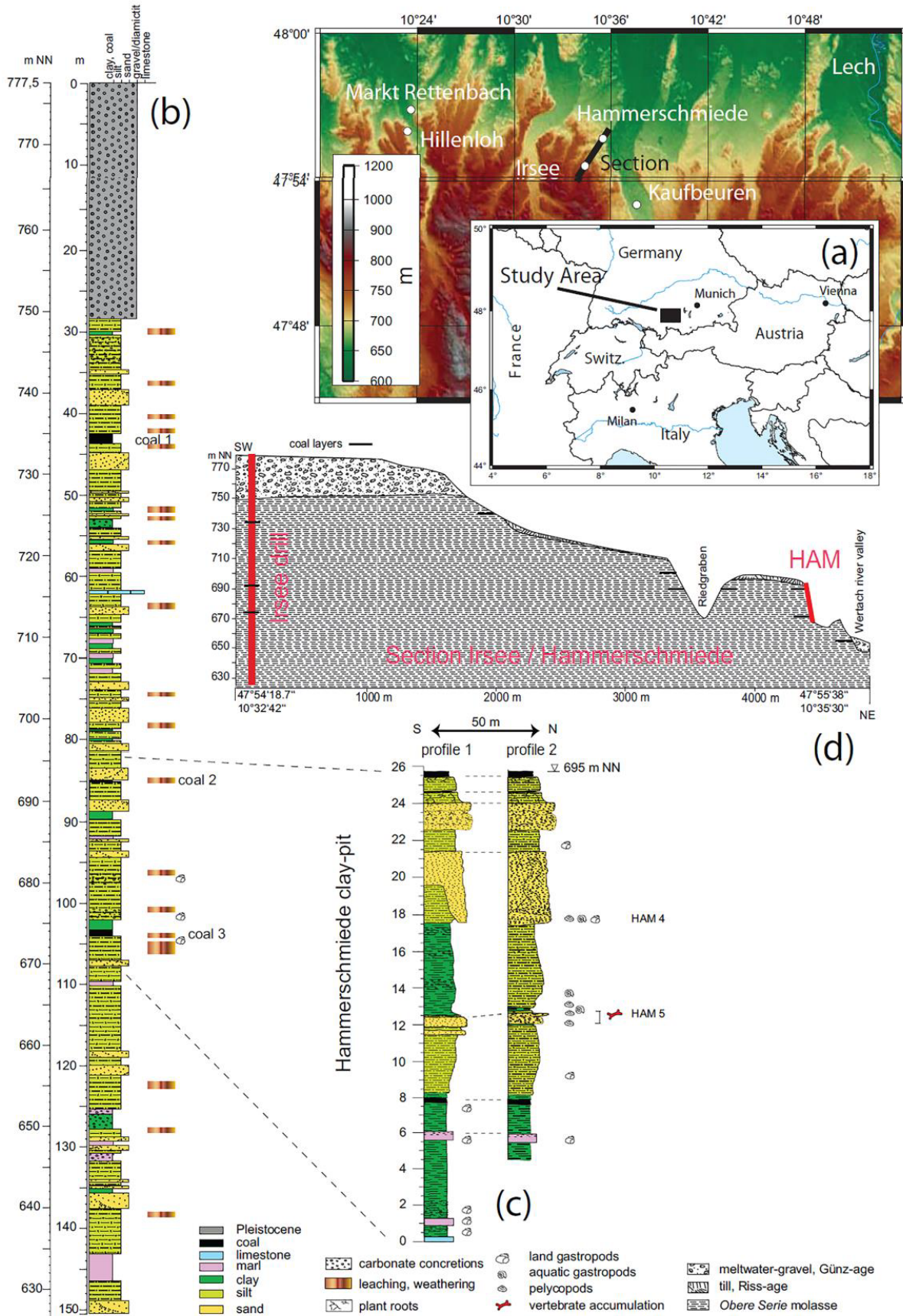


Figure 1.2.2. Stratigraphic profile of the Irsee drill core and the correlated Hammerschmiede sections including the local stratigraphic layers HAM 5 and HAM 4. Reprinted from Kirscher et al. (2016).

a leg of a new anseriform (*Allgoviachen tortonica*, Anatidae, Anseriformes) and material possibly belonging to a dabbling duck (cf. *Mioquerquedula*, Anatidae, Anseriformes) (Mayr et al. 2020a, 2020b, 2022). This was supplemented by a comprehensive description of the carnivore fauna of the Hammerschmiede (Kargopoulos et al. 2021a, 2021b, 2021c, 2022) and a study of the proboscidean finds (Konidaris et al. 2023). Nevertheless, the new great ape species of *Danuvius guggenmosi* Böhme et al. (2019), an arboreal biped hominid, still remains the most famous discovery of the Hammerschmiede and continues to attract public and scientific attention (Böhme et al. 2019, 2020; Kivell 2019; Williams et al. 2020).

1.3 Taphonomy and Biostratinomy

When analysing fossils and fossil localities, one not only has to deal with the fossils found, but also with the processes that played an important role in their preservation. In general, a fossil is an exception, since the majority of all ever-lived organisms were not transferred to the fossil record, but were returned to the regular cycles in decomposition processes. The palaeontological segment that deals with this topic is called taphonomy. The term taphonomy was first introduced by the palaeontologist Iwan Antonowitsch Efremov (other transcriptions read Yefremov) (1940). He understood this term to mean the totality of all processes that accompany the transition of an organism from the biosphere to the lithosphere (Efremov 1940; Müller 1963) (Fig. 1.3.1). The expression taphonomy is derived from the Greek *táphos* (τάφος), “burial” and *nomos* (νόμος), “law” and means something like the laws of burial or embedding. In addition to taxonomy, taphonomy plays a particularly important role in palaeontology, but is also widely used in an archaeological or zooarchaeological contexts. Particularly with regard to the latter areas of application, Behrensmeyer and Kidwell (1985) further refined the term to „*the study of processes of preservation and how they affect information in the fossil record*“. Taphonomy is divided into three major sub-disciplines (Fig. 1.3.2) (Behrensmeyer and Kidwell 1985). (1) Necrology, which is primarily concerned with how organisms die, or which body parts are shed and are thus available for taphonomic processes in the first place, and how soft parts (organic) decay. (2) Biostratinomy, which is dedicated to the sedimentary processes interacting with the preserved animal remains and includes all processes acting on a dying body, a carcass or components of this including the final burial and embedding (Behrensmeyer and Kidwell 1985, Laatsch 1931, Müller 1951, 1963). The third discipline is the (3) diagenesis, which deals with fossilisation and lithification and thus especially concerns processes of chemical alteration.

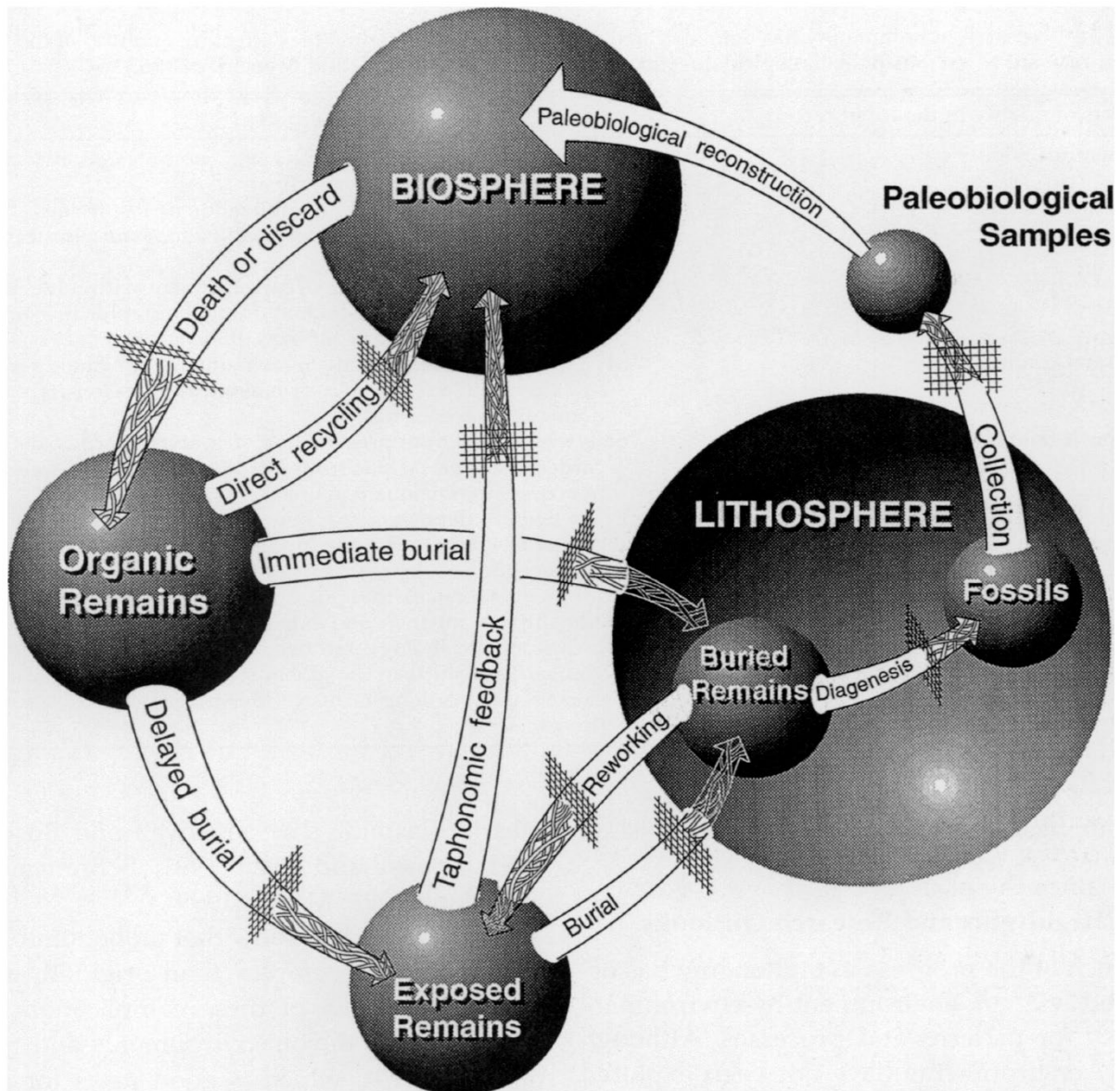


Figure 1.3.1. The main pathways for organic matter from death to preservation or total destruction. Every path is affected by taphonomic processes that affect preservation. Reprinted from Behrensmeier et al. (2000) that modified after Behrensmeier and Kidwell (1985).

Finally, the excavator, the palaeontologist or archaeologist also contributes to the taphonomic processes by exhuming the finds and influencing the fossils, and the storage conditions in the collection itself are not the end of the story (compare Figs. 1.3.1, 1.3.2). According to Müller (1963), the origins of systematic biostratigraphic observations go back to Johannes Walther (late 19th century). The term biostratigraphy was first introduced by Johannes Weigelt (1919) and was primarily limited to the science of fossil placement and alignment in sedimentary rocks (Weigelt 1919, 1928; Müller 1963). Today, the concept is much more comprehensive and includes mainly the differentiation between an autochthonous or an allochthonous embedding, i.e. whether an organism is embedded in situ (at the place of life or death) or after a more or

less long transport distance (Müller 1963). In both cases, external or internal forces (acting inside the carcass) can cause changes in the position of the carcass or parts of it. These include for instance the effects of scavengers, currents, gravity, upwelling due to decomposition or the accessibility for decomposers below the surface (e.g. plant roots) (e.g. Müller 1963). Etter (1994) divides biostratinomy into the phases of (1) death and decomposition, (2) transport and sorting phenomena, (3) disarticulation, (4) fragmentation, (5) corrosion and abrasion and (5) accumulation processes.

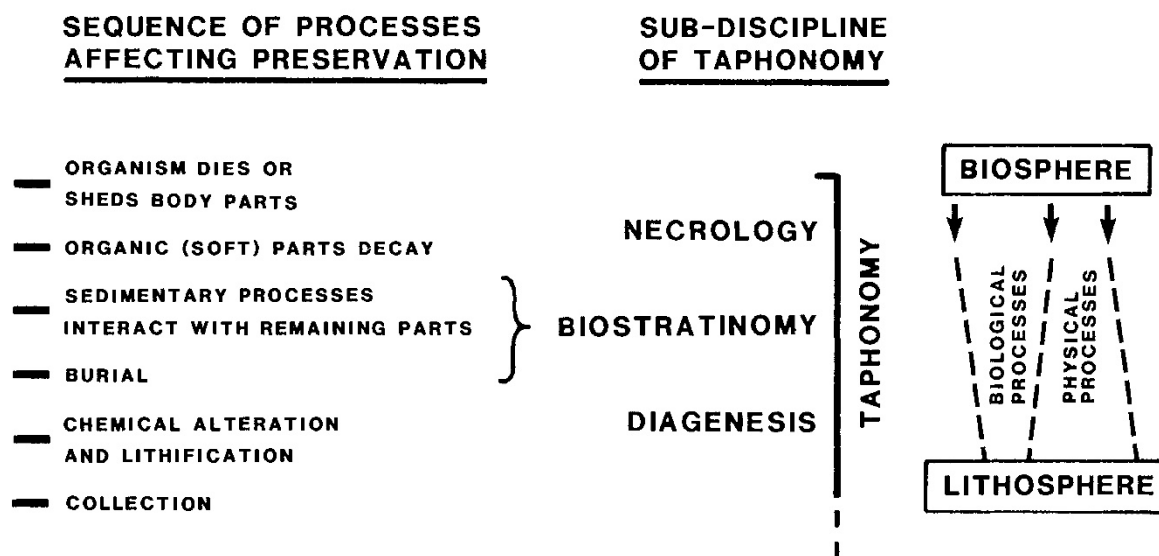


Figure 1.3.2. The subdisciplines of taphonomy according to Behrensmeyer and Kidwell (1985) divided into three major phases of post mortem processes: necrology, biostratinomy and diagenesis. Reprinted from Behrensmeyer and Kidwell (1985).

Especially in fluvial deposits, such as the Hammerschmiede site considered in this dissertation, taphonomic investigations are an important key to the evaluation of fossils and circumstances of discoveries in order to draw conclusions and reconstruct the fossil ecosystems. A multitude of small details must be investigated as clues to determine how deposits are formed. Which components are of autochthonous or of possible allochthonous origin. Which animals lived synchronous or were relocated from older deposits to younger ones. In addition to the actual age of a site, it is also important to get an indication of the duration of time within a layer. It is equally important to gain insight into the agents that have acted for either enrichment or depletion of certain components found. Finally, it must always be considered that that only preserved components or structures can be studied, but not in every deposit all available components are transferred to the fossil record to the same extent.

Especially in fluvial deposits, fossils can be deposited or transported with regard to their different size, density or surface properties (Voorhies 1969, Behrensmeyer 1975, 1988). Accordingly, fossils can be found accumulated or depleted as a result of currents and river dynamics (Voorhies 1969; Behrensmeyer 1975, 1988). Maturity (superficial abrasion) of bone surfaces can indicate longer transport distances of bones. Similarly, bones become abraded and fragmented over distance with increasing time and transportation range in the process. A skeleton that enters the channel system as a connected carcass can be transported as such or in pieces, depending on its size and its degree of decomposition (late ligament decomposition) or can be transported as a loose bone collection individually for each bone (Weigelt 1928, Müller 1963). In the same way, a transported carcass can be completely decomposed at an intermediate storage facility and then transported onwards in individual elements. Finally, deposits can be redistributed by changing flow conditions (e.g. meandering river that erodes old sediments) (Voorhies 1969; Behrensmeyer 1975, 1988). Overall, fluvial deposits are often turbulent and highly variable on a small scale. Only a comprehensive analysis, preferably of several depositional areas, can approximate reality.

In addition to the transport processes, sediments primarily consider the deposited, or sedimented, state, in other words the moment at which the component could no longer be transported further and was finally sedimented. The retention on the river bottom is a process that is influenced by bottom friction, adhesion and the weight, density and surface properties (contact surfaces) of the components (Voorhies 1969, Behrensmeyer 1975). Finally, the energy of the flow must not exceed the prevailing forces that keep the component on the ground. During the intermediate phase between transport and sedimentation, it is subsequently possible to orient objects, for example to align them in the direction of the flow by creating a kind of anchor effect with an asymmetrical (heavier or differently shaped) end, or by rolling them perpendicular to the flow (Lyman 1994). The evaluation of the statistical orientation of elongated objects within a certain deposit can thus provide decisive information about the flow direction or flow velocity of the depositing flow (Müller 1963; Lyman 1994). One possible method of analysis is the illustration of the orientation and length of longitudinal components such as bones or woods in so-called rose diagrams or line-direction histograms (e.g. Kreuzer 1988; Lyman 1994). Following Frison and Todd (1986), such diagrams can be used to distinguish between random and non-random long axes orientations. An asymmetry in the diagram is interpreted as a non-random positioning of components (Frison and Todd 1986; Lyman 1994).

1.4 Mortality analyses

According to most definitions (see previous section), taphonomy begins with the death of an organism. However, this is only true to a limited extent, as the organism itself naturally also has an influence on the mortality and thus on the taphonomy of its remains through its behaviour, ecological habits and life history (Lyman 1994). For example, the frequency of fossils belonging to certain age groups within a deposit depends massively on which interspecific and intraspecific parameters as well as behavioural and also abiotic factors influence the mortality of this species (Lyman 1994). Thus, a mortality analysis on the excavated material can help to shed light on the genesis of the fossil deposit. In principle, it is possible to clarify whether a composition of findings corresponds to a "normal" (attritional) and thus selective mortality or was caused, for example, by a "catastrophic", non-selective event (Lyman 1994). As a typical method of analysis, age-frequency distributions for a species at a site are examined in so-called mortality profiles (Hulbert 1982; Kurtén 1983; Voorhies 1969; Klein 1982; Lyman 1994). Here, individuals are clustered according to the minimum number of individuals per age class. Age groups are determined, for example, by dental wear stages and finally the minimum number of individuals is counted by the maximum number of specimens per used tooth position, wear stage and body side. This data are finally analysed in a histogram as an age-frequency distribution (compare Fig. 1.4.1; Lyman 1994).

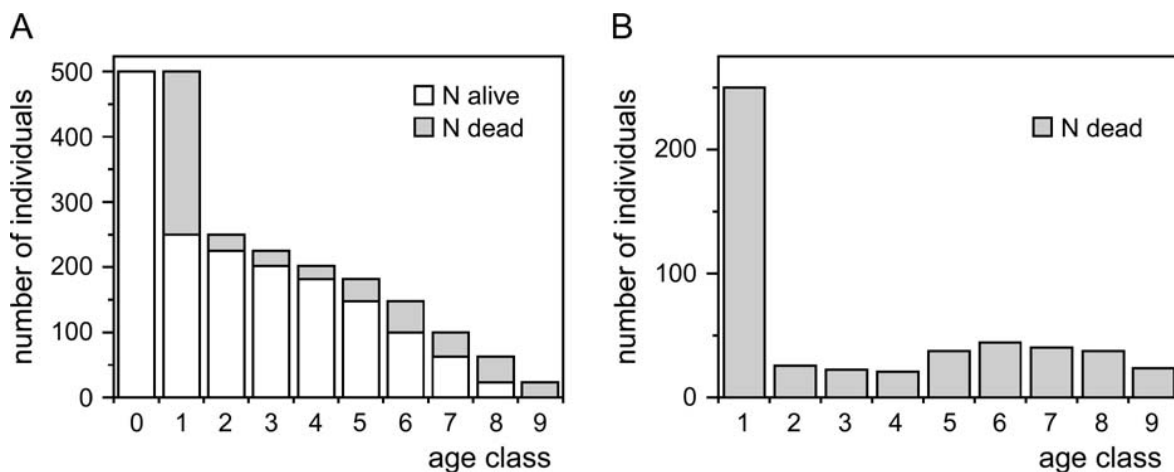


Figure 1.4.1. Basal type of "normal" or "attritional" mortality in age-frequency distributions (age mortality profiles). Blank bars indicate number of alive individuals. Grey bars indicate number of individuals that die each year. A) Age histogram shows an exemplary population breakdown into age groups and the annual deaths therein. B) Typical "attritional", "normal" or "U-shaped" age histogram as a consequence of the "normal" mortality from A). The "catastrophic", "mass" or "L-shaped" mortality pattern would result from the death of the entire population from A). Reprint from Lyman (1994).

A population is subject to a corresponding mortality probability per age group within normal conditions. This attritional mortality is typically reflected in "U-shaped" histograms,

comprising high infant mortality rates, low best-ager mortalities and increasing old-age mortalities (Fig. 1.4.1) (Klein 1982; Lyman 1994). This obviously selective mortality is mainly based on natural ecological parameters, where juveniles or young animals as well as senile individuals are more prone to die (caught by predators, more susceptible to diseases) than best agers (Lyman 1994). "Catastrophic", "mass" or "L-shaped" mortality typically shows a direct image of the population present at the time of a catastrophic event. Typically, the age classes contain fewer and fewer individuals with increasing age (Klein 1982; Lyman 1994).

Another method of visualisation and analysing mortality was introduced by Stiner (1994). She reduced the age groups to just three clusters (young, prime and old) and plotted the result in ternary diagrams. The advantage here is to visualise many mortality patterns for direct comparison in a single diagram (Stiner 1994; Kahlke and Gaudzinski 2005; Discamps and Costamagno 2015) (Fig. 1.4.2).

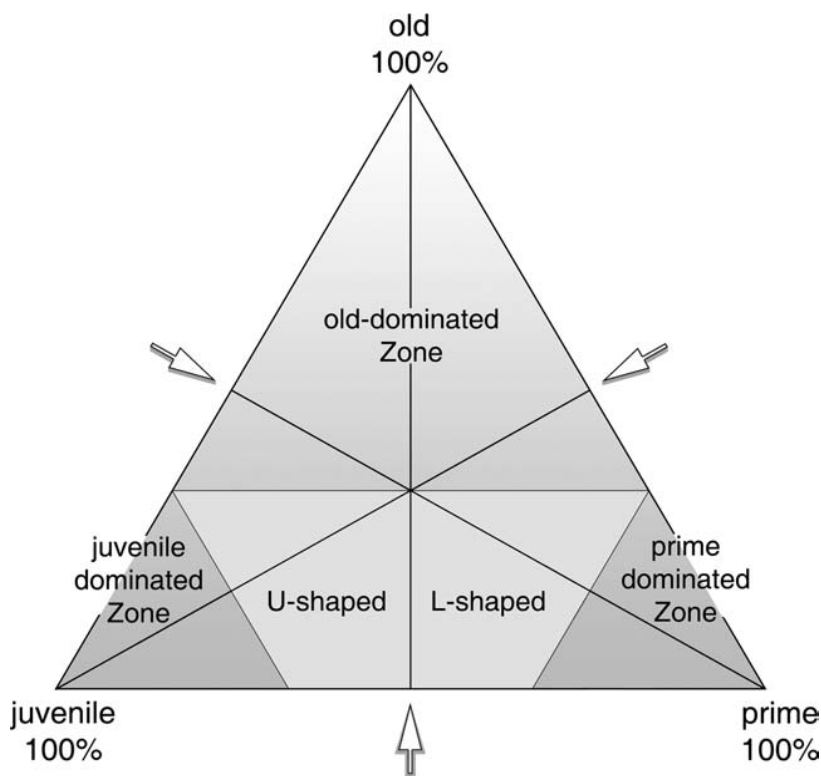


Figure 1.4.2. Ternary diagram for the analysis of mortality data as a possible tool for comparing different populations. Reprint from Kahlke and Gaudzinski (2005) after Stiner (1994).

In addition to the typical distinctions that mortality histograms allow (U- and L-shaped mortality), this diagram can be used to make significantly more differentiated distinctions between juvenile-dominated, prime-dominated, and old-dominated mortalities. By presenting the data in this way, it is easier to recognize and compare e.g. selective predator influences (Fig. 1.4.2).

The fluvial deposits at the Hammerschmiede site provide a large number of animal species for mortality investigations. In principle, sites with a high enrichment of a large number of individuals are best suited to deliver proper results. In addition to a population-dynamic evaluation of the animal species itself, an ecological indication of the deposition conditions is particularly important during a comprehensive taphonomic examination. It is therefore particularly important to select animals for this purpose which, in the best case, have inhabited the immediate study area according to their presumed habitat requirements. In addition, the statement is all the clearer when a large amount of material is available and a rather common animal is examined. This is the reason why beavers were selected for initial studies in mortality analyses in the Hammerschmiede (see chapters 7-8). In addition, the site contains two beaver species, one large and a small one, which thus provide the opportunity for direct comparison and because of their assumed semi-aquatic lifestyle fit perfectly into the presumed fluvial habitats on the assumption of an autochthonous origin.

1.5 Objectives:

Previous work has focused predominantly on taxonomic questions and improved the dating techniques of the sediments using biostratigraphic and geophysical methods. Little attention was paid to taphonomic and in particular, to biostratigraphic documentation and evaluation of the Hammerschmiede fossil site. In recent decades, new technologies have been developed for the documentation of finds on site and for the analysis of the collected data, which enable significantly larger data sets and speeds in fieldwork and evaluation. The Hammerschmiede site has changed to an equally important extent since its first examinations. An essential change in mining techniques, introducing a second mining floor and a legal protection of the main fossiliferous strata have freed up time and space to document and systematically excavate the site in large-scale excavations. This extensive documentation of finds and storage conditions provides an important basis to resolve numerous taphonomic and also more general palaeoecological questions. This dissertation is dedicated to precisely these new possibilities and aims to find answers to previously unsatisfactory or unanswered questions.

This dissertation investigates several aspects. The first is from a geological and sedimentological point of view, to generally resolve the depositional history of the local stratigraphic fossiliferous levels HAM 5 and HAM 4. This includes whether these deposits are of single- or multiphase origin and whether a distinction between different depositional facies

can be drawn and how fossils are distributed within the deposits. Besides clarifying which components are preserved in fossil form and how these finds relate to each other a possible detection of autochthonous and allochthonous components should also be carried out. In order to rule out potential connections, biostratigraphic analyses are necessary. These include the determination of the flow direction and its changes of the fossil watercourses and exposing potential transport phenomena as well as sorting processes. The aim is to clarify whether finds must be considered individually and in isolation or the existence of connections and the possibility of reconstructing disarticulated and scattered skeletons as a strewnfield of one and the same individual. For this purpose, hydrodynamic parameters must be taken into account in addition to taxonomic and age-specific questions about the individual organism. Furthermore, a comprehensive three-dimensional observation of the channel sediments is required. At the same time, it must be clarified which agents could cause disarticulation or be responsible for fragmentation, corrosion or abrasion on fossils. To explore ecological parameters for the fossil sites, presumed inhabitants of the habitats are analysed in mortality analyses to infer an ecological role supplemented by possible inter- and intraspecific relationships. For this purpose, the ecology and taxonomy of two beaver species from the Hammerschmiede fossil site (large: *Steneofiber depereti*; small: *Euroxenomys minutus*) should be examined for their possible autochthony and subjected to mortality analyses to detect mechanisms of control based on ecological or inter- and intraspecific parameters. Finally, post-depositional parameters are investigated, regarding diagenetic impacts and their potential influence on the fossil record.

Chapter 2

Excavation, Taphonomy and Biostratinomy

Manuscript prepared for submission to

Senckenberg Monographs

This chapter is structured independently and differs from the general chapter numbering of this dissertation. There is a separate table of contents for Chapter 2 on the next page.

Table of contents – Chapter 2

1	Abstract	25
2	Introduction	25
3	Excavation and documentation methods	26
3.1	Excavation techniques and historical review	26
3.2	Wet sieving	27
3.3	Processing of the wet sieve residues	30
3.4	Documentation of finds	31
3.4.1	Spatial documentation	31
3.4.2	On site registration of specimens	31
3.5	Excavation crew	32
3.6	Sample deposition	33
3.7	Quantity of material	33
4	Geology of the clay pit Hammerschmiede	34
4.1	Fossiliferous horizons of the Hammerschmiede	34
4.2	Channel morphology	38
4.3	Channel sediments	39
4.3.1	The HAM 5 channel infill	40
4.3.2	The HAM 4 channel infill	41
5	Palaeontology – Faunal list of the Hammerschmiede	43
6	Taphonomy and Biostratinomy	47
6.1	Area of excavation and documentation	47
6.1.1	HAM 5	47
6.1.2	HAM 4	50
6.2	Preserved material types	57
6.3	Spatial distribution of finds (large scale)	61
6.4	Spatial distribution of finds (small scale)	62
6.5	Reconstruction of flow direction	64
6.6	Postgenetic processes	71
6.6.1	Mineral neoformation and Uranium incorporation	71
6.6.2	Compaction	72
6.7	Case studies in strewnfield reconstructions	75
6.7.1	Case study I: HAM 5 – <i>Danuvius guggenmosi</i>	76
6.7.2	Case study II: HAM 5 – Lateral overbank extension	77
6.7.3	Case study III: HAM 4 – <i>Parachleuastochoerus steinheimensis</i>	81
6.7.4	Case study IV: HAM 4 – <i>Dorcatherium naui</i>	84
6.7.5	Case study V: HAM 4 – <i>Miotragocerus monacensis</i>	88
6.7.6	Case study VI: HAM 4 – Reassembled fossil broken and scattered bones	92
6.8	Biogenic bone modifications and possible producers	94

1 Abstract

Palaeontological sites often provide limited insights into the fossil environment of their time. In most cases there are only short-term outcrops, which can then often only be analysed with regard to their fauna. The present study investigates the early Late Miocene Hammerschmiede locality (MN 7/8) in the Northern Alpine Foreland Basin in Southern Germany (Bavaria, Allgäu region). The site has been known to science for several decades and is still accessible to science due to active clay mining activities. For almost a decade now, it has also been possible to carry out extensive and spatially documented area excavations and thus present taphonomic and biostratigraphic results in addition to investigations of flora and fauna. The extensive excavations and applied documentation techniques in the local fossiliferous layers HAM 5 and HAM 4 are described and taphonomic observations are presented. Field observations and the analysis of the spatial datasets of the excavated finds provide insights into the deposition and rearrangement processes of these two watercourses. Accumulation layers of coarse-grained sediments, as well as the orientation of elongated objects in relation to the documented erosive channel base structure show complex multi-phase depositional processes with flow-related accumulation, transportation and redepositional processes and give an indication of the flow direction and its change along the course of the channels. Several carcasses of vertebrates that were introduced into the processes of transport and sedimentation at various stages of the channel fill, some of which were scattered, are presented in case studies and reassigned to single individuals by means of these preliminary investigations. This improves our understanding of the biostratigraphic processes at the site of discovery and also expands our osteological and morphological knowledge of individual species. Finally, diagenetic and biogenic modifications to bones are described and possible producers are concerned.

2 Introduction

The Hammerschmiede clay pit has been known as a fossil site to science since the 1950s. First observations by Meyer (1956), Mayr and Fahlbusch (1975) and Fahlbusch and Mayr (1975) however, concentrated more on palaeobotanical or microvertebrate remains. For a long time, the Hammerschmiede was more of a sideshow in the species lists of various publications, which paid little attention to the site itself. In the late 1970s and early 1980s, the potential of the site for large mammal fossils was recognised for the first time by the two private collectors Sigulf Guggenmos (Dösingen) and Manfred Schmid (Marktobersdorf) who discovered the remains of an adult male *Tetralophodon* among numerous other vertebrate finds (Konidaris et al. 2023). Ultimately it was the search for the youngest preserved Miocene sediments of the North Alpine

Foreland Basin that brought the Hammerschmiede back into scientific focus (Kirscher et al. 2016). Triggered by this project and the discoveries of private collectors, first small and then increasingly extensive excavation campaigns were launched (2011-ongoing), which brought to light ever more substantial finds and features. By far the greatest scientific success around the Hammerschmiede site was probably achieved through the description of a new great ape species, *Danuvius guggenmosi*, which is considered to show partial bipedalism due to postcranial evidence (Böhme et al. 2019). The most recent publications deal more and more thoroughly with particular species or groups of mostly vertebrates, and in addition to taxonomic observations, ecological parameters of various faunal elements are becoming better known. Previously little recognized, research is increasingly including taphonomic observations and ecological conclusions that are unfolding the overall picture of the early Late Miocene Hammerschmiede ecosystems (e.g. Böhme et al. 2019; Mayr et al. 2020a, 2020b, 2022; Lechner and Böhme 2022, 2023; Konidaris et al. 2023). However, the circumstances of the fossil site itself were only dealt with superficially. There is little information on the constantly changing and optimising field methods and documentation techniques, which so far have generated an extremely extensive pool of metadata that can be used to obtain further information on the fossil habitats and shed light on the genesis of the fossil site itself. The present work is intended to present and discuss first results of taphonomic and especially biostratigraphic observations in addition to a methodological overview. Insights into documentation techniques, the spatial distribution and potential contexts of finds and sites, sedimentological findings, as well as observations in biostratigraphy, are presented. Due to the extensive data available, many topics are highlighted using case studies as examples. Many case studies provide an exemplary overview of the extensive data set, which can be expected to yield even much more information in the future.

3 Excavation and documentation methods

3.1 Excavation techniques and historical review

While excavations in the early days (2011-2015) were carried out over short periods of a few days or weeks with only a small number of participants, constant methodological and technical optimisation has led to a steady increase in the number and quality of finds. Digging is mostly done with shovels, spades, hand shovels, boning knives or spatula tools and for delicate work scalpels and dissecting needles are used. The rough work is thankfully done by workers of the clay mining company with their large construction machines that remove the several metres

thick overlaying sediments, whereas the final opening of the fossil layer is done by a small excavator on our own.

Stable finds are removed directly in the field and washed. Brittle or fragile objects are stabilised on the site with superglues of different viscosities. Usually, the moist matrix sediments prevent the adhesive from binding the matrix too strongly with the bone. More complex finds are recovered in a plaster jacket and prepared in the laboratory. Since 2021, more challenging finds are examined by micro-CT scanner before preparation in order to facilitate the subsequent procedure.

3.2 Wet sieving

In 2016, clay mining in the pit reached the areas of HAM 5 that had been exposed for the first time over a large area at that time. In a large-scale securing operation, about 23 tonnes of the fossil layer were extracted with an excavator and stored in a nearby small shed in front of the pit. At the time, there was no other way to protect the fossil bearing strata in situ, especially to prevent the potential loss of *Danuvius* specimens (Böhme et al. 2019). This pile of material (called "Schlammhaufen" in the German documentation) (Fig. 3.2.1 a) was processed by screen washing since 2016 in parallel to excavations in the clay pit itself until it was completed in the 2019 excavation year and finally yielded 6 specimens of *Danuvius* which could thus be saved from destruction.

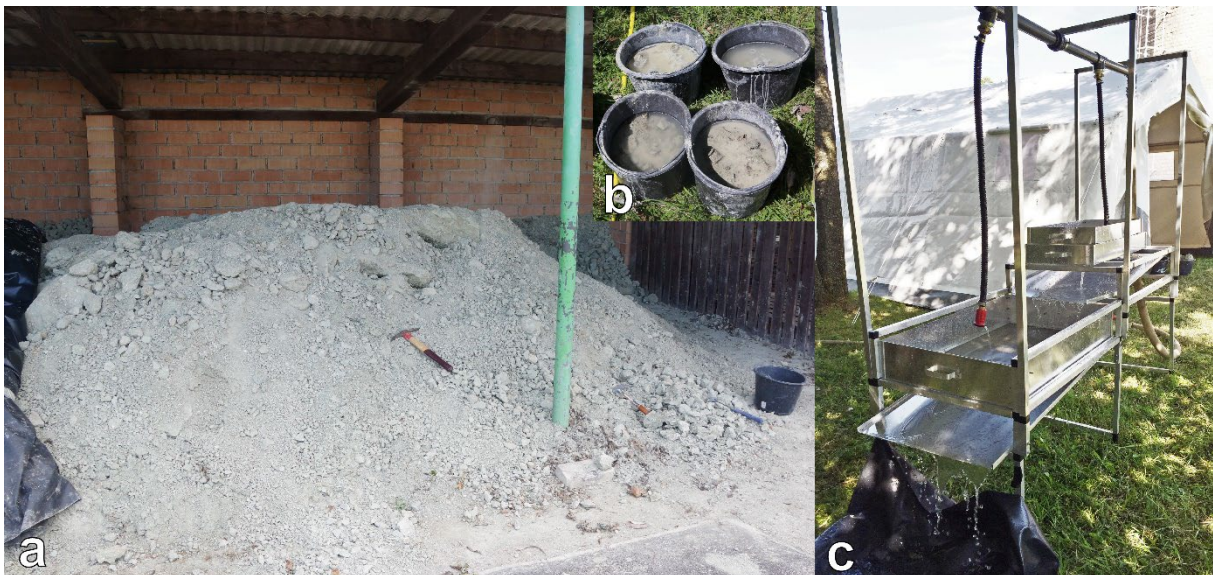


Figure 3.2.1. Overview of the first screen washing installation for the processing of the fossil sediments from the early Late Miocene Hammerschmiede site and the local stratigraphic level HAM 5. (a) Pile of secured and stored sediments from the fossil bearing layer HAM 5 in 2016, approximately 23 tonnes. (b) The sediments were looked through for fossils, carefully coarsely crushed and soaked with water in buckets for about 30 minutes. (c) The soaked material was screen washed and sieved by three grain sizes (>5mm, >1mm, >0,6mm) using a stacked sieve screen wash construction and water from the nearby hydrant.

The first construction used for screen washing is typical for palaeontological excavations, the material was wet sieved into three grain sizes (>5 mm, >1 mm, $>0,6$ mm) by stacked sieves with a direct water connection to the nearby hydrant. This work was done a few hundred metres in front of the clay pit near a small stream into which the sewage could be discharged. At this time, only excavations were taking place in HAM 5. The dried clayey material from HAM 5 was carefully coarsely crushed and soaked with water in buckets for about 30 minutes. At this point, about 60 buckets of clayey mud of 10 kg each could be processed at one day (Fig. 3.2.1 b-c). The coarsest fraction was already searched for finds in the field. The medium grain size was transported completely and the smallest grain size in a representative sample in bags to Tübingen for further processing and picking in the laboratory (see section processing of sieved material).

The extreme effort to cope with the large amounts of material and finally the possibility to examine all excavation tailings for small fossils has led to the self-design and construction of a more optimised screening device by the author (TL) in 2019. Based on existing designs used in industrial gold mining in North America, for example, the type selection fell on a portable Sieve trommel washing system or rotational sieving system, short “Rosie” (Fig. 3.2.2). Rosie includes a horizontally rotating screen drum with an adjustable angle, into which wet material is fed from a prewashing section. The trommel is powered by a chain drive from a windshield wiper motor via a car battery (12 V) and solar panels and rotates at a few revolutions per minute. The material is continuously washed by a spray bar from top and coarser material moves continuously to the drum outlet due to the slight inclination. Various sieve mesh sizes are assembled along the drum sections, so that grainsizes are sorted and specific removal is possible from fine to coarse. Because the particles are not thrown around as some might assume, but are slowly transported in the water film of the rotating system, hardly any damage is caused to the fossils by the washing process. In this way, more than 450 buckets per day could be processed in the clay material of the HAM 5 and considerably larger quantities in the sand material of HAM 4 which does not need to be pre-soaked. Rosie sorts the residuals into a grain size of 1-5 mm and >5 mm. The latter is now sorted out on site in the old screen wash plant, while the former grain size is packed in bags and transported to Tübingen for further processing in the laboratory. With the completion of the large material depots from HAM 5 outside the claypit, Rosie was directly installed and used at the excavation areas for the first time in 2020 (Fig. 3.2.2 a). The water required for this is fed to the system via around 750 metres of type B fire hose. The wastewater leaves the pit via a settling basin and the pit's own drainage channels to

the nearest stream. Since 2020, all tailings are screened for small fossils and with the certainty of discovering all the little things, the excavation speed was increased to a higher efficiency.



Figure 3.2.2. Fossil screening zone at the early Late Miocene Hammerschmiede locality and the HAM 4 excavation area in 2023. (a1) Water supply by type B and C fire hoses over 700 m from the next hydrant, (a2) piled up sediments, to be washed with (a3) the self constructed rotational sieving system "Rosie", that is powered by a solar panel (a4) with a car battery as buffer storage. The old sieve rack (a5) is used for picking of the washed material. The base of the area is slightly inclined and covered with pond foil and drainage pipes (a6) to effectively drain the waste water. (b) Inside view of "Rosie". A spray bar continuously cleans materials slowly transported to the outlet due to slow rotation and slight inclination of the system. (c) Technical overview of "Rosie": feed funnel with prewash and dosing of the material (c1); wiper motor and a motorcycle chain as drive (c2); the sieve trommel contains two mesh sizes (>1 mm and >5 mm) (c3); water supply (c4); Discharge section of the cleaned and sieved grain size 1-5 mm (c5) and >5 mm (c6).

3.3 Processing of the wet sieve residues

In HAM 4, about 10% of the wet sieved volume of tailings remains as residue. 20% of this corresponds to the coarse fraction (>5 mm) and 80% to the size range 1-5 mm. The latter fraction contains about 1% phosphatic (bones), siliciclastic, carbonate (shell fragments) and organic particles. The other part consists of approximately equal proportions of moist clay pebbles (resistant to first wet sieving) and pedogenic carbonate concretions. After drying and subsequent soaking in water the clay portion disintegrates and can be washed out, and the remaining residue can be directly picked for microfossils to document carbonate fossils (Fig. 3.3.1 a). The larger portion of the residue is further concentrated with the addition of acid.

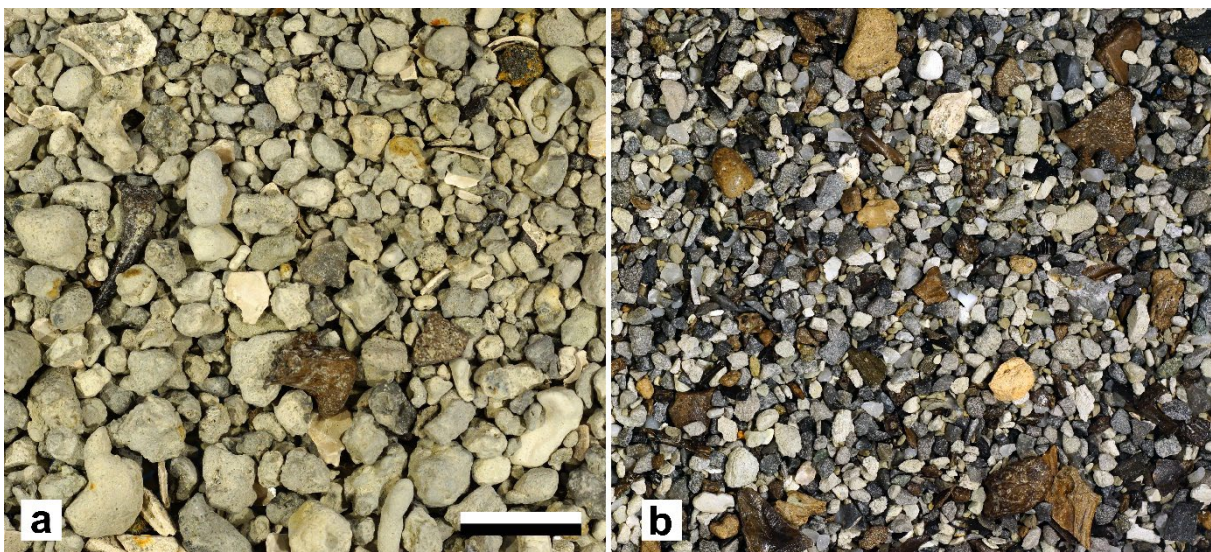


Figure 3.3.1. Overview of the particle grain sizes portion 1-5mm from the early Late Miocene Hammerschmiede site and the local stratigraphic level HAM 4. (a) Before and (b) after processing with 10% acetic acid solution. Scale bar equals 10mm.

The use of diluted acetic acid 5-10% has proven to be particularly gentle on bones and enamel, so that all carbonate components (shells and pedogenic carbonates) are dissolved and only phosphatic siliciclastic and organic components resist (Fig. 3.3.1 b). This procedure provides a minimal volume with maximum accumulation of osteological material for the microscopic search for microfossils, as only 1% of the material collected in the field and even only 0.1% of the total excavated sediment remains as residue here. Bones and teeth are not damaged by this process. The remaining material consists of siliceous, organic and phosphatic (bone) grains and is subsequently picked for microfossils under the binocular microscope. The processing of sieve residues has only just started and large quantities of material are still waiting for further treatment and will provide many more discoveries in the future.

3.4 Documentation of finds

3.4.1 Spatial documentation

Since the 2017 excavation, osteological specimens from a size of about 2 cm but also particularly interesting smaller finds are documented on site regarding their spatial location and distribution. For this purpose, total stations of the type Leica TCR 407 power (excavation period 2017-2018) and geo-FENNEL FTS 102 (as of 2019) are used. The stationing of the total stations is done using fix points in the pit area and in the excavation areas. Long objects are documented with at least 2 measuring points to obtain information on length and orientation. More complex find situations such as partly articulated or arranged finds were documented photographically and/or by find sketches.

3.4.2 On site registration of specimens

Since the excavation year 2015, An excavation register is kept, which provides a preliminary object identification and a chronological sequence of finds. Specimens from a size of approx. 2 cm and, in the case of more important finds, also below this size are registered with an identification number at the site. For surveying and documentation purposes, the item is removed and its position in the field is marked with a number tag and steel nail until a spatial measurement has taken place (Fig. 3.4.2.1).

Due to the weather problems, laminated number tags are used to mark the findspots, which correspond to a certain number range due to their colour at the respective point in time (Fig. 3.4.2.1). The advantage of this method is that the flags can be reprocessed, sorted and reused quite quickly. Longer objects are marked with a second number tag (handwritten A- and B-number) to generate two measurements for directional analysis (Fig. 3.4.2.1 b). Find complexes not recovered individually in the field, were stabilised with a plaster jacket on site. A small, handwritten label with the number is left next to every visible registered bone and plastered with it, so that an assignment to the inventory number remains until the final preparation in the laboratory (Fig. 3.4.2.1 c).

Since 2017, all finds marked with find numbers can be reconstructed with a spatial survey (X, Y, Z coordinate) with an accuracy of up to 1 mm. For finds from the wet-sieved tailings, a spatial reconstruction of the origin has been dispensed with so far. However, the tailings can be documented to the day and at least assigned to the corresponding excavated sectors. In this way, overlooked fragments can be more easily assigned and refitted to surveyed specimens and potential find connections (strewnfields) can be verified or rejected.

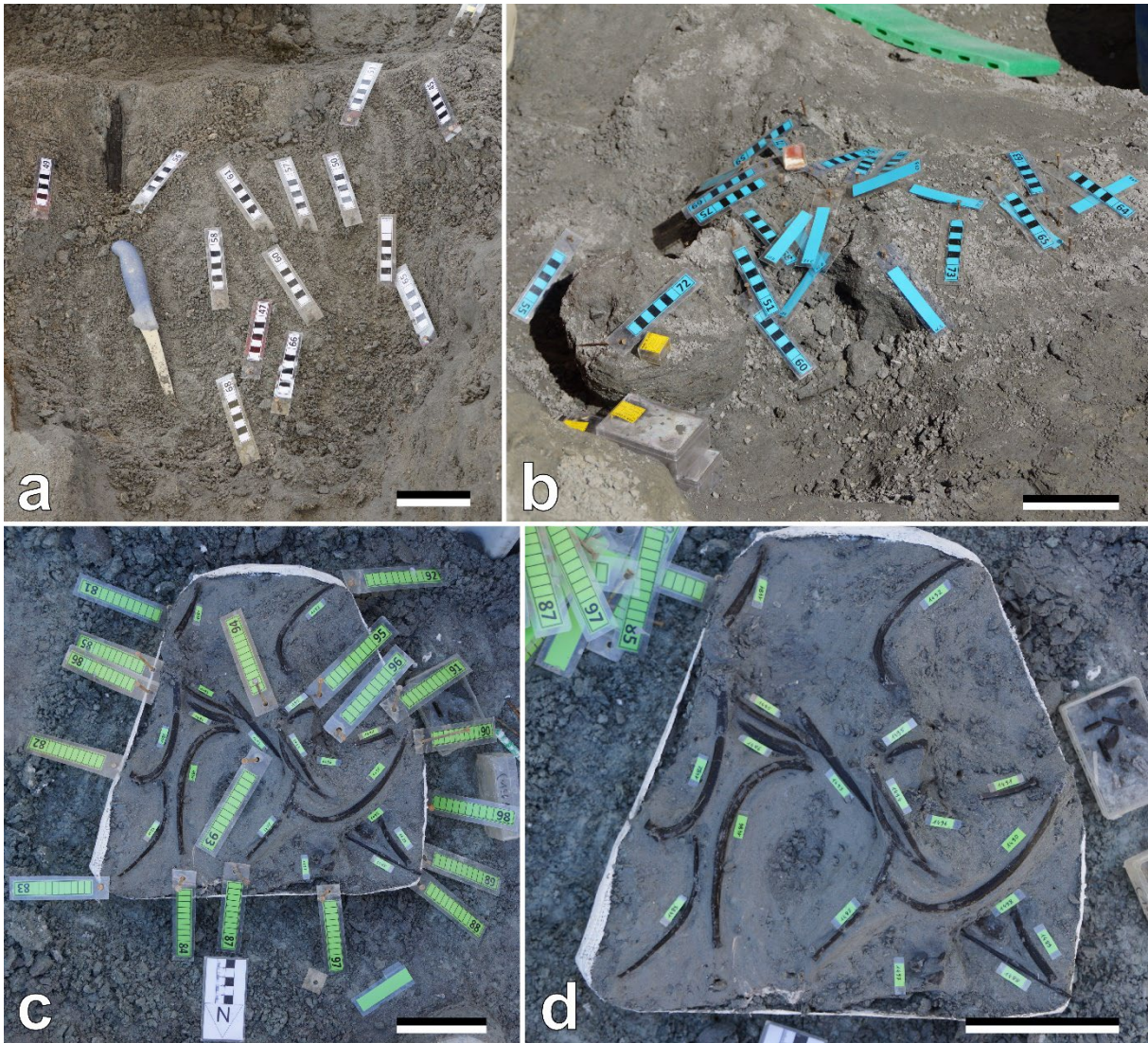


Figure 3.4.2.1. On-site views of the documentation of isolated finds (a) and find complexes (b-d) at the early Late Miocene Hammerschmiede site and the local stratigraphic level HAM 4. (a) Particularly specimen-rich spot with finds deposited in an incoherent manner next to each other. (b) Number tags mark multiple juvenile tragulid (*Dorcaterium nauti*) bones, which presumably resemble a single individual. (c-d) Complex finding arrangement of ribs and vertebrae of an adult tragulid (*Dorcaterium nauti*) stabilised by a plaster jacket. Number tag colour correspond to: green 14XX; white 37XX; blue 89XX. Scale bars equal 10 cm.

3.5 Excavation crew

In the early years 2011-2016 the excavation participants consisted mainly of staff and students of the University Tübingen working group. In the following years, the participation of volunteers from the surrounding area of the fossil site, as well as from Germany and abroad, was increased. In the meantime, more than 250 people are registered on our participant lists and in the last season (2022), 100 volunteer participants were able to take part in our citizen science excavation project “Bürgergrabung Hammerschmiede”, while in the same year the employed crew for the organization consisted of only 10 people.

3.6 Sample deposition

The samples and finds from the local stratigraphic levels HAM 1, HAM 2 and HAM 3 from earlier field work at the Hammerschmiede clay pit made by Helmut Mayr are stored in the Bavarian State Collection of Palaeontology and Geology in Munich, Germany and labelled as Hammerschmiede 1 (HAM 1): SNSB-BSPG 1973 XIX, Hammerschmiede 2 (HAM 2): SNSB-BSPG 1980 XXVII and Hammerschmiede 3 (HAM 3): SNSB-BSPG 1980 XXVIII. The material from HAM 4 and HAM 5 has been collected during excavations conducted by the University of Tübingen, Germany, since 2011. All material collected since then is currently stored in the Palaeontological Collection of the University of Tübingen, Germany (GPIT) and is labelled with numbers of both GPIT – for excavations from 2011 until 2019 – and SNSB-BSPG, for the excavations in the period 2020 to 2023 where the latter are indicated as Hammerschmiede 4 (HAM 4): SNSB-BSPG 2020 XCIV and Hammerschmiede 5 (HAM 5): SNSB-BSPG 2020 XCV. The private collection of Sigulf Guggenmos (Dösingen) from the find layer Hammerschmiede 6 (HAM 6) was donated to the Palaeontological Collection of the University of Tübingen (GPIT), Germany in 2018. A few finds from the Hammerschmiede are stored in the collection of the Kempten-Museum im Zumsteinhaus, Kempten, Germany and in the private collection of Manfred Schmid (Marktoberdorf) with casts of more relevant objects stored in Tübingen (GPIT).

3.7 Quantity of material (Tab. 1)

The constantly optimised techniques and methods allow for ever more effective excavations, which are constantly reflected in the growing number of specimens per field season. The find numbers are subdivided into measured objects, those that were already discovered in situ and spatially documented on site, and reading finds (“Lesefunde”, Rosie-specimens), those that were only registered in the wet sieving or from the collection boxes of the individual excavators afterwards. The numbers of the corresponding excavation years can be taken from Tab. 1. Note that geospatial measurements of finds have only taken place from the 2017 field season onwards. All numbers from previous years correspond to the numbers registered in the field book. It should also be noted that an extremely large number of microfossils are only archived in collection boxes or are still waiting for further processing, so that the actual number of finds is significantly higher.

Table 1. Quantity of material excavated at the Hammerschmiede fossil site and the corresponding data for local stratigraphic levels HAM 5 and HAM 4 respectively. Note, that geospatial measurement of objects started in the 2017 field season. The specimens recorded until (marked with an asterisk) then resemble the field book inventory. It should also be noted that an extremely large number of microfossils are only archived in collection boxes or are still waiting for further processing, so that the actual number of finds is significantly higher. The reading finds of HAM 4 for 2023 are still being processed, but a quantity of about 3500 objects can be expected.

HAM 4	2017	2018	2019	2020	2021	2022 south	2022 north	2023 north	TOTAL
Area [m ²]	56	70	197	60	70	140	50	85	728
Measured Nr.	534	528	3164	1089	1343	1323	160	669	8810
Reading Finds	539	224	719	2345	2729	3811	0	~3500	~13867
Total	1073	752	3883	3434	4072	5134	160	~4169	~22677

HAM 5	2014	2015	2016	2017	2018	2019	2020	2021	2022	2023	TOTAL
Area [m ²]	2	10	25	40	100	0	50	100	2	0	329
Measured Nr.	139*	368*	711*	342	833	0	260	215	23	0	2891
Reading Finds	158	81	104	136	50	0	80	1	0	0	610
Total	297	449	815	478	883	0	340	216	23	0	3501

4 Geology of the clay pit Hammerschmiede

4.1 Fossiliferous horizons of the Hammerschmiede

The actively mined Hammerschmiede clay pit exposes about 25 m of Miocene fluvio-alluvial sediments supplemented by two lignite seams on top and at mid position of the profile. Alluvial deposits include clays, silty clays, sands, marls and sandstone beds. In situ formed pedogenic carbonate concretions (Fig. 4.1.1) are observed in many regions within the profile of matrix-supported clays.



Figure 4.1.1. Pedogenic carbonates from the early Late Miocene Hammerschmiede site and the local stratigraphic levels HAM 5 and HAM 4. Less frequent particularly large (a) and very common small (b) pedogenic carbonate concretions. Scale bar equals 10 mm.

Within the fluvial deposits of the local stratigraphic and fossiliferous layers HAM 5 and HAM 4 there are grain-supported layers where these concretions enriched due to reworked sediment accumulation and contain various component sizes (Fig. 4.1.1). Consequently, a correlation of HAM 1 with HAM 5 is probably not given on the basis of the available topographical information.

Fossils are mainly found in certain fluvial channel deposits, with two main sites being the focus of the latest Hammerschmiede research since 2011 – HAM 5 and HAM 4 (Fig. 4.1.2).

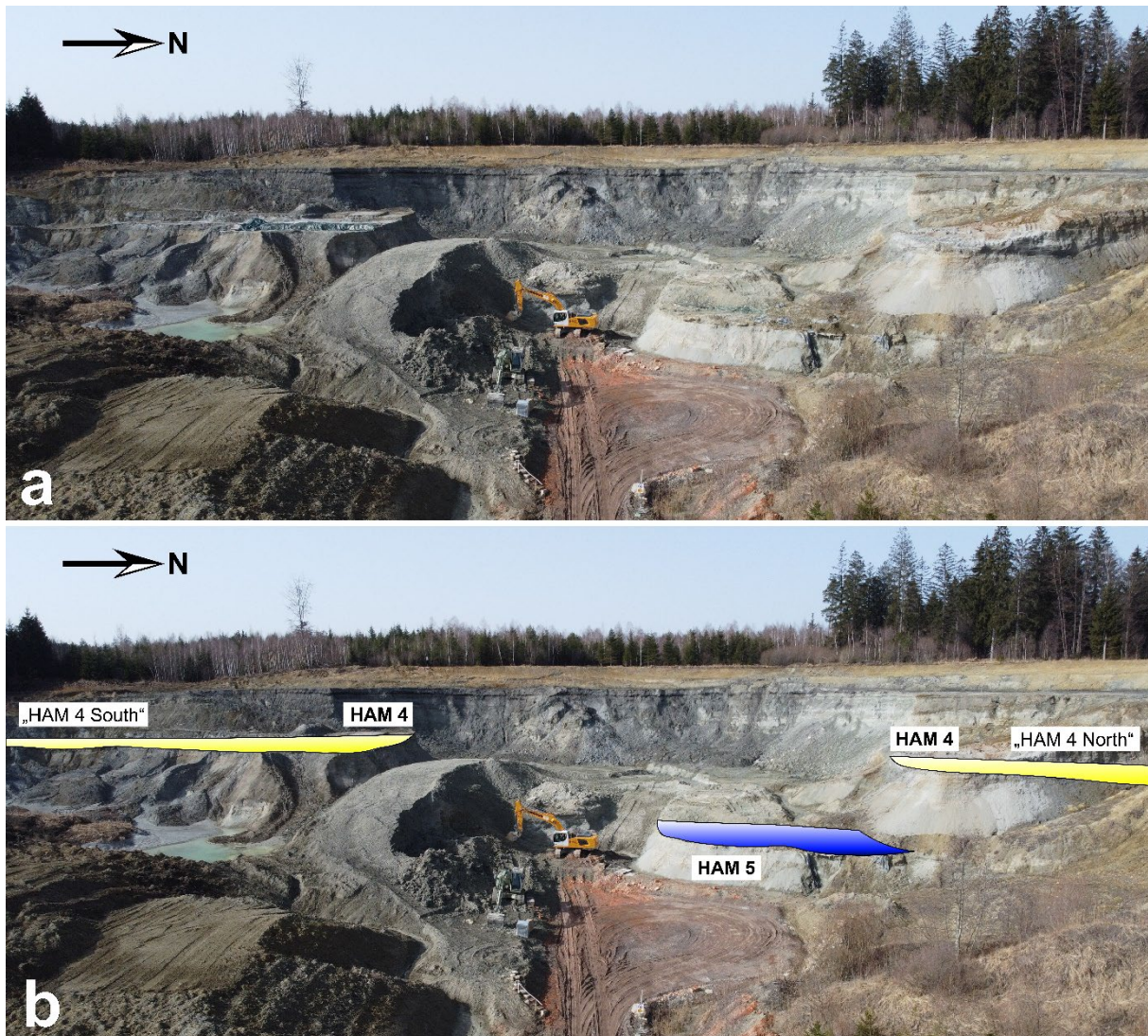


Figure 4.1.2. Overview of the Hammerschmiede clay pit and the approximate position of the local stratigraphic levels HAM 5 and HAM 4. (a) Drone image from the East, in the direction of active clay mining. (b) Indicated areas of the local stratigraphic levels HAM 5 (blue) and HAM 4 (yellow). “HAM 4 South” and “HAM 4 North” correspond to the same layer HAM 4, which artificially was interrupted in the central pit area due to mining activities. Image width approximately 150 metres.

A magnetostratigraphic examination by Kirscher et al. (2016) dates these layers to 11.62 Ma (HAM 5) and 11.44 Ma (HAM 4). The numbering of the local fossiliferous layers corresponds

to their order of discovery, not their stratigraphy (Fig. 4.1.3 and Fig. 4.1.4). The local stratigraphic levels HAM 1, HAM 2 and HAM 3 are known from previous collections of

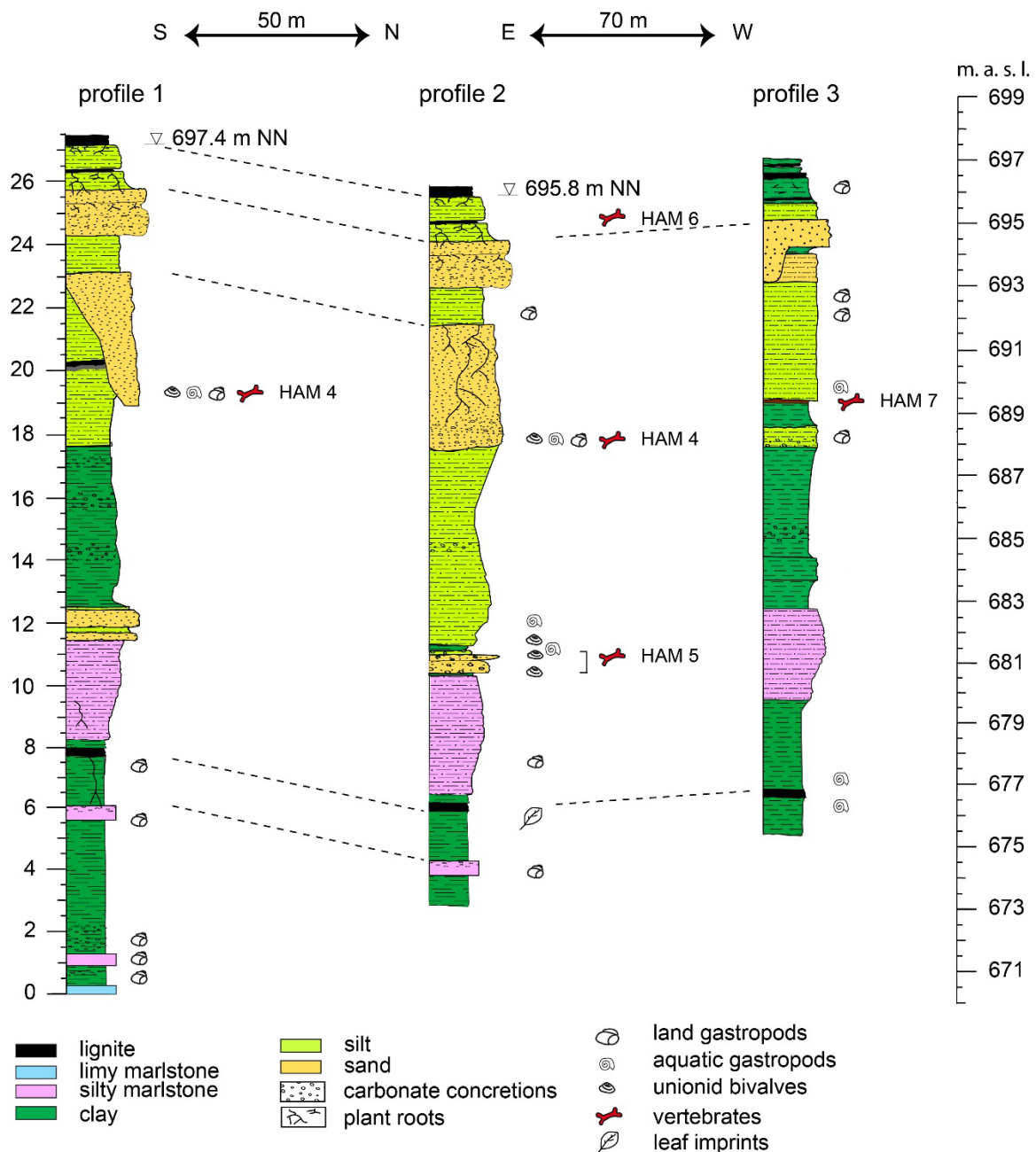


Figure 4.1.3. Stratigraphic profiles of three sections from the early Late Miocene Hammerschmiede (HAM) locality with lithological determinations. Profile 1 marks the southernmost section of the clay pit. Profile 2 is located approximately 50 metres to the north of profile 1. Profile 3 lies 70 metres to the west of the second profile. The profiles were created over the entire current exploration period of the Hammerschmiede and include sections in the east and in the central clay pit that have already been lost by mining activity. Fossil-bearing layers HAM 4, HAM 5 and HAM 7 are marked in the profiles, and the supposed location of the historical find layer HAM 6 from the end of the 1970s is noted. The historically introduced local stratigraphic levels HAM 1-3 cannot be correlated or assigned with certainty in the current profile. Figure updated and supplemented based on Kirscher et al. (2016) fig. 1c.

the Hammerschmiede (Mayr and Fahlbusch 1975, Prieto and Rummel 2009, Prieto 2012). Based on taxonomic overlaps, HAM 1 could possibly correlate with HAM 5 (Kargopoulos et

al. 2022). HAM 1 was found at the top of the Hammerschmiede section in 1973 (Mayr and Fahlbusch 1975), but since that time, the mining area of the clay pit extended to the west with a continuously increasing sediment thickness. Today, this historical "top" is no longer at the very top of the outcrop, but should still have been higher than today's HAM 5.

A freshwater mollusc community described by Schneider and Prieto (2011) stems from the fossil layer HAM 3 (Prieto and van Dam 2012). According to sedimentology, spatial position and fossil content, this layer possibly correlates with today's HAM 4 channel. However, the description of the layer as a fluvial channel at the top of the Hammerschmiede section with high contents of lignite pebbles (see Prieto and Rummel 2009) contrasts with today's observation. Such enrichments in lignite pebbles cannot be confirmed today.

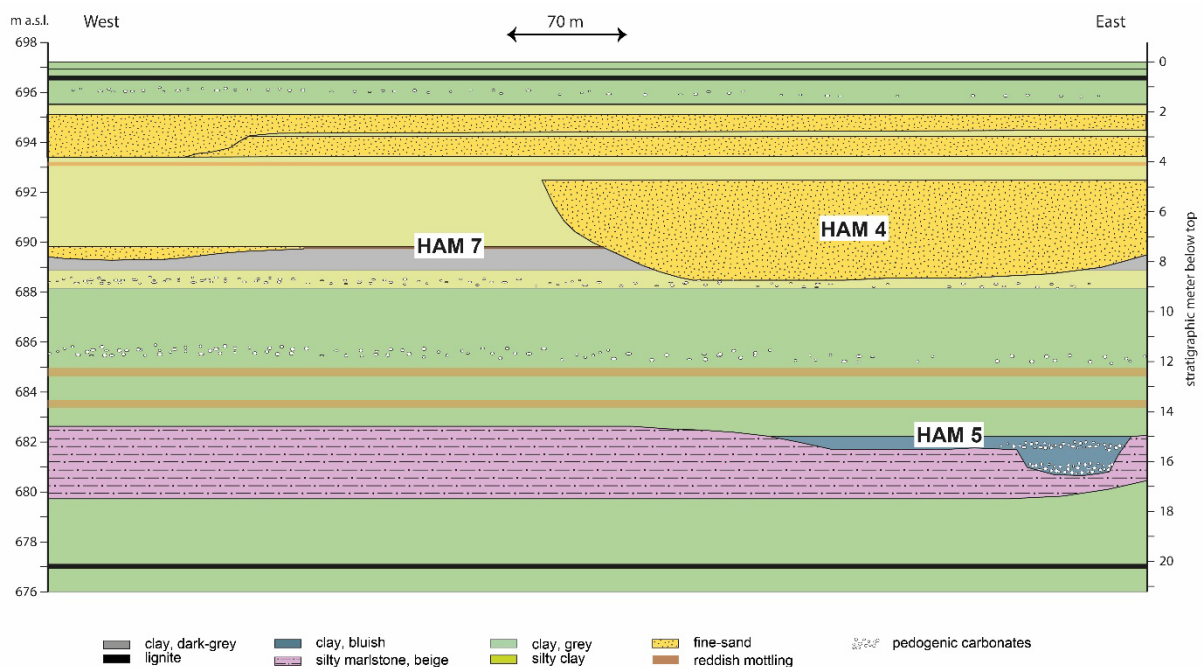


Figure 4.1.4. Detailed stratigraphic West-East section of the early Late Miocene Hammerschmiede (HAM) locality with lithological determinations. The fossil fluvial channel deposits of HAM 5 and HAM 4 are marked within the section, and the recently discovered HAM 7 is highlighted. Picture width corresponds to 70 metres in the central pit area with a view to the North.

This could probably mean that Prieto and Rummel observed different sedimentary facies within the HAM 4 that is no longer visible today or they observed a completely different channel structure no longer outcropping today. HAM 2 represents a fossil horizon that is possibly no longer available today and was probably stratigraphically placed between HAM 1(=5?) and HAM 3(=4?). HAM 2 could possibly be related to a recently discovered stratigraphic level (see HAM 7 below).

During the late 1970s and early 1980s the private collectors Sigulf Guggenmos (Dörsingen, Germany) and Manfred Schmid (Marktoberdorf, Germany) discovered another spatially

delimited fossil horizon (Gregor 1982, Kargopoulos et al. 2021b, Konidaris et al. 2023). This stratum was years later firstly classified as HAM 6 and the finds, which have only been secured through the efforts of those private collectors, are still being studied. From HAM 6 originate the recently studied remains of a male individual of the proboscidean *Tetralophodon longirostris* (see Konidaris et al. 2023), dental material of a the hyaenid *Thalassictis montadai* (see Kargopoulos et al. 2021b) as well as undescribed finds of amphibians, reptiles (turtles, snakes) and mammals (artiodactyles, carnivores and rodents). Based on photographs, notes and memories made by the private collectors, it was possible to place the find layer, which is no longer available today, stratigraphically at the top of the profile at the time of discovery and thus below the today present upper coal seam and above HAM 4 (Gregor 1982, S. Guggenmos pers. com. 2017 and 2018, M. Schmid pers. com. 2022). Inferring from the age model of Kirscher et al. (2016) an approximate age of about 11.42 Ma results for the site HAM 6 (Kargopoulos et al. 2022, Konidaris et al. 2023).

Recently, another fossil layer – HAM 7 – was discovered, which was missing due to erosion of the HAM 4 river in its channel area and therefore remained hidden until the western edge of the HAM 4 was reached and the channel bottom raised its topographic level. HAM 7 is represented by an approximately 10 cm thick chocolate brown organic-rich layer, representing clayey swamp to lacustrine facies, that appears to merge into a shallow channel fill of silty fine sands (50 cm thick in the current outcrop) in the western slope of the clay mining area. Besides the small beaver (*Euroxenomys minutus*), many remains of fish and aquatic turtles (*Chelydropsis* sp.) as well as charophyte gyrogonites and a multitude of gastropod opercula (*Bithynia*) have already been discovered there. A possible historical outcrop on the east side of the HAM 4 channel seems very likely and moreover a possible correlation to the local stratigraphic level HAM 2, in which also a mass occurrence of *Bithynia* opercula is known (Helmut Mayr pers. comm. to Madelaine Böhme 2000), cannot be ruled out. Further investigations for the classification and reliable correlation of the historical find layers to the current outcrop conditions are necessary.

4.2 Channel morphology

Due to the extensive work carried out in the past years, this study concentrates primarily on the local stratigraphic levels HAM 5 and HAM 4. The excavated areas during the period of 2011-2016 were documented in less detail and findings are mostly based on personal observations and reports. Since the 2017 field season, the excavation areas can be continued gapless and are documented coherently. Also, since that year, the shape of the channel base as well as the spatial

position of the finds within the channel structures is recorded using measuring technology (tachymeter).

The HAM 5 channel is north-south oriented and cuts into a consolidated sandy marl bank that is 2 metres thick in some areas (compare Fig. 4.1.4). In the deepest part of the HAM 5 channel, this bank seems fully eroded, and the channel base is possibly carved into underlying clays. The channel base is irregularly wavy and scattered with pool structures and rarely exhibits planar surfaces. There is a more deeply incised main channel of approximately 5-7 metres width, which is separated by a longitudinal mound from a shallower side channel (ca. 10 metres width) running to the west of it. The main channel is cut to a depth of about 1.2 metres, while the lowest passages of the side channel are eroded to only about half this depth (0.7 metres). The entire site is about 25 metres wide in transverse section. In the areas excavated before 2016, the HAM 5 layer was easier to distinguish with a single channel structure of about 5 metres width. The small-scale erosive structures indicate a small rivulet (approximately 5 metres in width) that changed its course several times and produced a heterogeneous channel base morphology. The HAM 4 channel is oriented SSW-NNE and is cut into green clays and silty clays (Fig. 4.2.1 and compare Fig. 4.1.4). Due to active clay mining in the western direction of the pit, HAM 4 is exposed in the south and north of the pit area and centrally intersected and lost. Due to the extensive outcrop conditions of HAM 4, a slightly S-shaped meander course can be assumed. HAM 4 shows a much larger depositional area of about 50 metres in width and an erosion depth of approximately 4-5 m. The base of the channel is mostly flat, and only rarely are there minor depressions or irregularities. Especially in the middle of the channel, an almost planar surface is visible. The fill of the channel is dominated by mobile fine sands and silts, which show countless small-scale erosion and redeposition events. However, the erosively uniform base of the channel indicates a significantly larger river than that of HAM 5, which probably also filled the entire channel width with water.

4.3 Channel sediments

Both local stratigraphic levels HAM 5 and HAM 4 are represented by alluvial channel fill deposits which were sedimented in a previously eroded channel structure. It is unclear and difficult to find out how much time is involved between the erosive and sedimentary phases until the final burial of both local stratigraphic levels. Fossil-rich sediments directly on the maximum erosional base (channel lag deposits) of the channels are typical for both Hammerschmiede layers. These accumulation zones of mainly bony remains are also characterised by an enormous cumulation of pedogenic carbonate concretions and clay rubbles which are most likely erosion products of surrounding sediments.

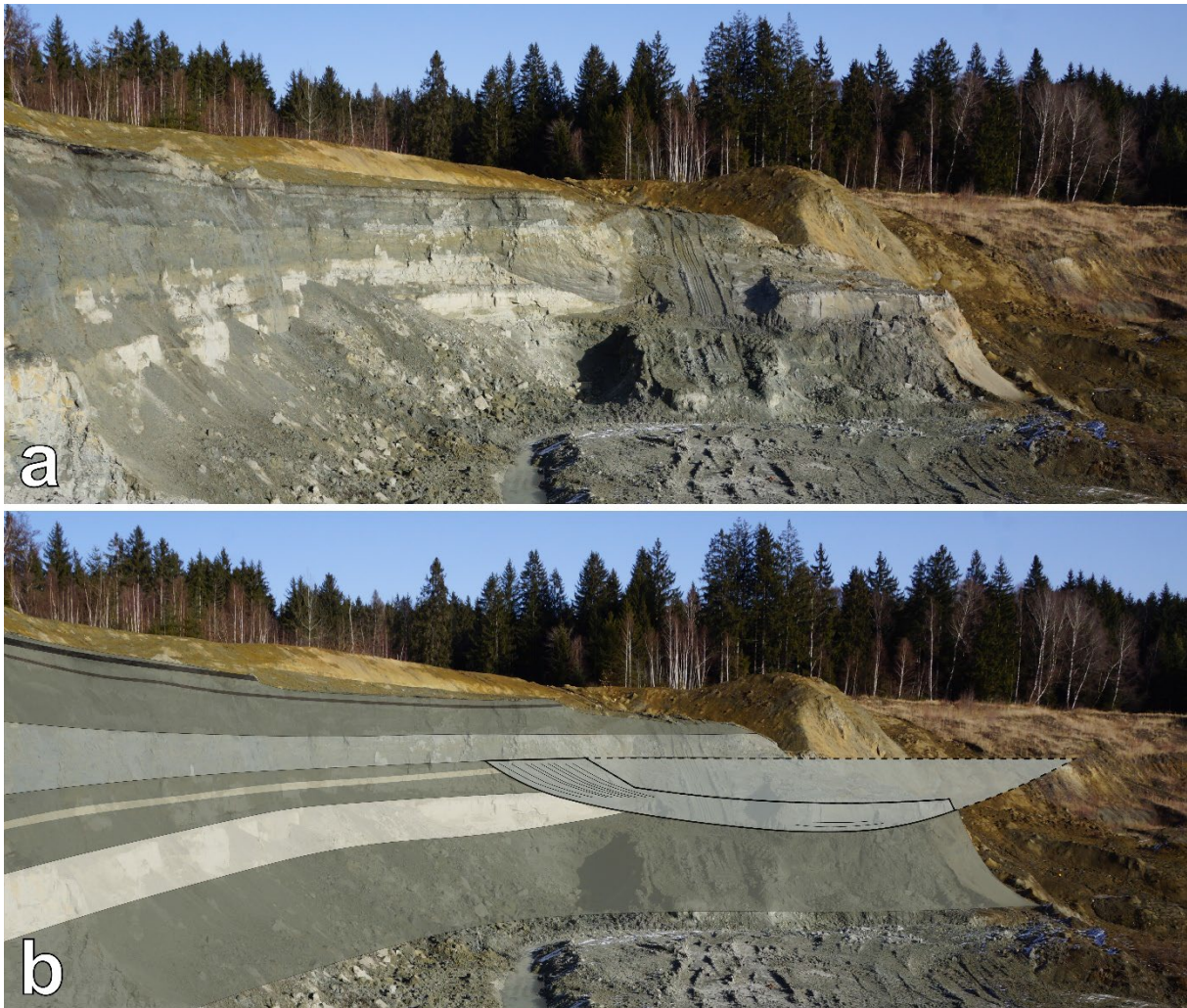


Figure 4.2.1. View of the northern pit wall of the Hammerschmiede clay pit in 2021 (a) and with a sketch overlay (b). The stratigraphic hiatus between the ochre-coloured glacial till deposits of Pleistocene age at the top of the profile and the underlying early late Miocene deposits is clearly visible. The Miocene sediments are characterised by clays, silty clays and sands (grey, green to bluish green), and one of the lignite seams (black) can be observed at the top of the pictured profile. Brighter colours indicate clay-rich strata, which dry out more quickly on the surface than the darker, sandier and partly water-bearing levels. The erosive channel base structure represents the level and excavation area HAM 4 North. HAM 5 is located at the lower right edge at the base of the pit wall. Reconstructed channel width (b) as an approximate scale corresponds to about 50 metres.

4.3.1 The HAM 5 channel infill

The sedimentation of the channel-fills is characterised by different phases. The HAM 5 channel shows at least three successive events, beginning with a basal channel lag deposit followed up by a fining upwards sequence of silty fine sand and clay (Fuss et al. 2015). The next overlying phase begins again with a channel lag deposit that accumulates coarse-grained material as an erosive enrichment phase and ends like the first sequence described. In the fine-grained top of those sequences, root traces indicate intermediate vegetation phases and consequently indicate a temporal separation. The first two phases largely fill the deeper main channel. The third and last phase fills, in addition to the top of the main channel, also a shallower lateral channel expansion with sediment. This last phase is also a fossil-bearing fining upwards sequence and

shows, especially in the area of the lateral side channel, a particular frequency of strewnfields of single individuals of many different vertebrate species. The channel base of HAM 5 is very irregular. There are repeatedly elevated and hollowed areas. The often basin- or pool-like hollows and undulations of the former rivulet bottom show in some cases accumulations of fossil material indicating the effect as fossil traps.

4.3.2 The HAM 4 channel infill

The river channel-fill of HAM 4 cannot be reconstructed as clearly as that of HAM 5. The erosive channel structure is broader and deeper in this case and reaches approximately 50 m in width and 4-5 m in depth (compare Fig. 4.2.1). The main fill, which consists primarily of fine sand and silt, is dominated by a much more dynamic and reworkable sediment than the clay-dominated HAM 5 channel-fill (Fig. 4.3.2.1).



Figure 4.3.2.1. Profile section in the local stratigraphic level HAM 4 (2018) at the early Late Miocene Hammerschmiede locality. The section is West-East oriented, looking to the North and roughly cuts transverse to the course of the HAM 4 channel. Yellow scale indicates the transition from the trough cross bedded fine sandy sediments to the erosive clay base. The sequence is characterized by coarse-grained layers with a high proportion of reworked pedogenic carbonate concretions, clay pebbles and dark (brown) coloured bones (area to the right of the white label). The bottom left shows an enrichment with freshwater pearl mussels. Reddish or brownish layers indicate heavy minerals (garnet). Scale bar equals 10 cm.

In the cross sections of HAM 4, an extremely large number of fine layering comprised by density and grain size sorting phases, oblique stratification sheets and unconformable beds, as well as smaller intersecting trough cross bedded channel structures are recognizable (Fig. 4.3.2.1). In particular, reddish layers show the accumulation of heavy minerals, especially garnet and demonstrate the strong rearrangement and sorting processes of the sediments (Fig. 4.3.2.1). These indicate many small erosive, enrichment and sedimentation phases.

Although bone finds can be expected in the entire area of the channel filling, several enrichment layers representing channel lag deposits are observed (Fig. 4.3.2.2). In general, one of these layers is found directly at the erosive base as a basal channel lag deposit. Furthermore, the channel fill shows minimum three further enrichment layers, which dip obliquely, possibly representing the point bar at the inner bank of the channel. Figure 4.3.2.2 demonstrates this overall observation at HAM 4 and shows an East-West section of the excavated areas of the years 2017/18 (right side) and 2019-2022 (left side). At the left-hand image area, a basal channel lag deposit and several obliquely East-dipping fossil enriched layers (minimum three) (Fig. 4.3.2.2). At the eastern ascending channel margin of HAM 4, it remains unclear whether there are two or only one large channel lag deposits. Possibly two layers meet each other asymptotically and form a shared channel lag, which does not exceed the lowermost 0.5 m of the channel fill at the easternmost channel margin (Fig. 4.3.2.2).

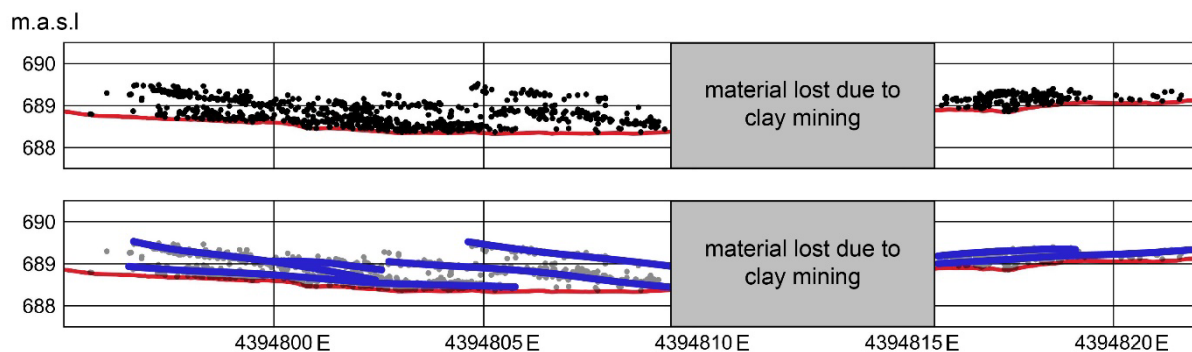


Figure 4.3.2.2. Accumulated profile section in the excavation area of the local stratigraphic level HAM 4 at the early Late Miocene Hammerschmiede locality. The section is West-East oriented, looking to the North and comprises data accumulated from a two metres wide transect between 5310824 N and 5310826 N (HAM 4 2017-2018 and 2020-2022). Excavated specimens (black dots) are plotted according to their elevation above the HAM 4 channel base (red line). The grey area has been lost due to clay mining. Blue lines indicate the location of potential channel lags found. Easting coordinates correspond to Gauss-Krüger Zone 4 grid in metres and elevation in m.a.s.l.

The western channel border (not included in Fig. 4.3.2.2 as the area is empty of finds) is characterised by an intermediate smaller channel structure which is filled by silty clay sediments and erosively cutting through and “cleaning” the western part of the first channel fill phase. The sediments of the first phase taper towards the west in a wedge shape below this fossil free second phase of a channel and document an unconformity by erosion. Subsequently,

the HAM 4 channel at the cut bank was possibly shifted to the east, leaving behind the successive channel lag deposits at the point bar of the inner bank in phases. In contrast to the HAM 5, the river bottom of the HAM 4 level is very evenly. The channel incises several metres in elevation from the east towards the centre of the channel structure, showing only minor differences surface texture of the river bottom. In the marginal area it is somewhat wavy and sometimes shows small depressions, while the central channel bottom of the HAM 4 area has a fairly flat surface.

5 Palaeontology – Faunal list of the Hammerschmiede

A first comprehensive faunal summary was provided by Kirscher et al. (2016) which was subsequently updated by Böhme et al. (2019). Every year and excavation, the Hammerschmiede site yields further new specimens and species which makes it necessary to update the already published lists and to make additions and corrections. Some animal species are completely new to science. Others are already known from other sites. Many records have probably not yet been worked on extensively, but it is clear that the fauna is characterised by a particular richness. To date, a total of 164 taxa can be recorded in the faunal list of the Hammerschmiede (HAM 1-6) (see Tab. 2). An overview of the major taxonomic groups comprises 14 molluscs (3 Bivalvia and 11 Gastropoda), 12 fishes, 13 amphibians, 25 reptiles (1 Choristodera, 9 Chelonia, 15 Squamata), 15 birds, 85 mammals (15 Eulipotyphla, 1 Chiroptera, 2 Primates, 28 Carnivora, 2 Proboscidea, 5 Perissodactyla, 6 Artiodactyla, 2 Lagomorpha and 24 Rodentia).

Table 2: Faunal list of the Hammerschmiede locality and the local stratigraphic levels HAM 5, HAM 4, HAM 6 and HAM 1-3 (combined). Updated and supplemented with new expertise based on Kirscher et al. (2016), Table 1 and Böhme et al. (2019), Supplementary Table 1.

Order	Family	Taxon	HAM 5	HAM 4	HAM 6	HAM 1-3
Unionida	Margaritiferidae	<i>Margaritifera (Pseudunio) flabellata</i>	X	X		X
Sphaeriida	Sphaeriidae	<i>Sphaerium (Amesoda) rivicola</i>	X			X
		<i>Pisidium (Pisidium) amnicum</i>	X	X		X
Architaenioglossa	Bithyniidae	<i>Bithynia</i> sp. 1	sp.	sp.		X
		<i>Bithynia</i> sp. 2				X
Heterobranchia	Valvatidae	<i>Borysthenia</i> sp.				X
Hygrophila	Planorbidae	<i>Segmentina</i> sp.				X
		<i>Gyraulus</i> sp.	?	?		X
Ellobiida	Carichiidae	<i>Carychium</i> sp.				X
Stylommatophora	Strobilopsidae	<i>Strobilops</i> sp.				X
	Filholidae	<i>Triptychia</i> sp.		X		X
	Helicidae	<i>Cepaea</i> sp.	X	X		
	Elonidae	<i>Tropidomphalus</i> sp.	X	X		
	Limacidae	<i>Limax</i> sp.	X	X		X
Esociformes	Esocidae	<i>Esox</i> cf. <i>lepidotus</i>	X	X		X

Order	Family	Taxon	HAM 5	HAM 4	HAM 6	HAM 1-3
Siluriformes	Siluridae	<i>Silurus cf. joergi</i>	X	X	X	X
Cypriniformes	Cyprinidae	<i>Tinca</i> sp.	X	X		X
		<i>Palaeoleuciscus</i> sp.	X			X
		<i>Leuciscus</i> sp.	X	X		X
		<i>Barbus</i> sp.	X	X		
	Cobitidae	<i>Cobitis</i> sp.		X		X
Perciformes	Gobiidae	<i>Gobius</i> sp.	X	X		X
	Percidae	<i>Perca</i> sp. 1		X		indet.
		<i>Perca</i> sp. 2			X	
Salmoniformes	Salmonidae	<i>Hucho hucho</i>	X	X		
Anguilliformes	indet.	indet.		X		
Urodela	Proteidae	<i>Mioproteus</i> sp.	X	X	X	X
	Cryptobranchidae	<i>Andrias scheuchzeri</i>	X	X		X
	Scapherpetontidae	Scapherpetontidae indet.	X	X		X
	Batrachosauroidae	Batrachosauroidae indet.	X	X		X
	Salamandridae	<i>Chelotriton</i> sp.	X	X	X	X
		<i>Triturus roehrsi</i>	sp.			X
		<i>Triturus</i> aff. <i>montadoni</i>				X
Anura	Palaeobatrachidae	<i>Palaeobatrachus</i> sp.		X		X
	Discoglossidae	<i>Latonia gigantea</i>	X	X	X	X
	Bufo	<i>Bufo</i> cf. <i>viridis</i>	X	sp.	X	X
	Hylidae	<i>Hyla</i> sp.		X		X
	Ranidae	<i>Pelophylax</i> sp.	X	X		X
	Pelobatidae	<i>Eopelobates</i> sp.	X	X		X
Choristodera		<i>Lazarussuchus</i> sp.	X	X		X
Chelonia	Trionychidae	<i>Trionyx</i> sp.	X	X	X	X
	Chelydridae	<i>Chelydopsis</i> sp.	X	X	X	X
	Geoemydidae	<i>Clemmysopsis</i> sp.	X	X	X	X
		<i>Mauremys sarmatica</i>	X	X	X	
		<i>Melanochelys</i> sp.		X		
		<i>Ptychogaster (T.) batalleri</i>		X		
	Testudinidae	<i>Testudo</i> sp.	X	X		X
		<i>Chersine</i> nov. sp.		X		
	incertae sedis	Chelonia incertae sedis		X		
Gruiformes	Gruidae	indet.		X		
Anseriformes	Anatidae	<i>Algoviachen tortonica</i>		X		
		cf. <i>Mioquerquedula</i> sp.		X		
		indet. 1	X	X		
		indet. 2		X		
Accipitriformes	indet.	indet. 1	X	X		
		indet. 2		X		
Strigiformes	Strigidae	indet.	X	X		
Suliformes	Anhingidae	<i>Anhinga pannonica</i>	X	X		
	Phalacrocoracidae	cf. <i>Microcarbo</i> sp.		X		
Galliformes	Phasianidae	<i>Miophasianus altus</i>		X		
	indet.	indet.	X			
		indet.		X		
Coraciiformes	Alcedinae	indet.		X		

Order	Family	Taxon	HAM 5	HAM 4	HAM 6	HAM 1-3	
Passeriformes	Corvidae	cf. <i>Pica</i> sp.		X			
Squamata	Chamaeleonidae	<i>Chamaeleo</i> sp.		X			
	Lacertidae	<i>Lacerta</i> sp. 1	X	indet.		X	
		<i>Lacerta</i> sp. 2				X	
		<i>Miolacerta</i> sp.		X			
	Scincidae	<i>Chalcides</i> sp.		X		X	
		Scincomorpha indet.		X			
	Anguidae	<i>Pseudopus pannonicus</i>	X	X	X		
		<i>Ophisaurus</i> sp.	X	X			
		<i>Anguis</i> sp.		X			
	Boidae	Erycinae indet.	X				
	Amphisbaenidae	Amphisbaenidae indet.		X		X	
	Colubridae	Colubrinae sp. 1	X	X	X	X	
		Colubrinae sp. 2	X	X		X	
		Natricinae sp. 1	X	X		X	
Natricinae sp. 2		X			X		
Eulipotyphla	Erinaceidae	<i>Galerix exilis</i>	indet.	X		X	
		? <i>Schizogalerix</i> sp.		X			
	Plesiosoricidae	<i>Plesiosorex schaffneri</i>	X	X	X	X	
	Talpidae	<i>Gehardstorchia quinquecupidata</i>	X	div. sp.	indet.	X	
		<i>Desmanella</i> sp.	X				
		<i>Talpa</i> sp.	X				
		<i>Proscapanus</i> sp.	X				
	Dimylidae	<i>Plesiodimylus johanni</i>	X	X			
		<i>Metacordylodon schlosseri</i>	X	X			
	Soricidae	<i>Crusafontina exulta</i>	X	X		X	
		<i>Paenelimnoecus crouzeli</i>	X				
		<i>Dinosorex</i> sp. nov.	X	X	X		
		<i>Paenesorex</i> sp.				X	
		Soricidae indet. 1	X	X			
		Soricidae indet. 2	X				
	Chiroptera		Chiroptera div. sp.	X	X		
	Primates	Hominidae	<i>Damivius guggenmosi</i>	X	X		
nov. gen. et sp.			X				
Carnivora	Amphicyonidae	Amphicyonidae indet.	X	X	X		
	Ursidae	<i>Kretzoiarctos beatrix</i>	X	X			
	Simocyonidae	<i>Alopecocyon goeriachensis</i>	X	X			
		gen. et sp. indet.		X			
	Mustelidae	<i>Martes sansaniensis</i>	X	X			
		<i>Martes munki</i>	X	X			
		<i>Martes</i> sp.				X	
		<i>Circamustela hartmanni</i> nov. sp.	X	X		X	
		<i>Laphictis mustelinus</i>		X			
		<i>Paralutra jaegeri</i>	X	X			
		<i>Vishnuonyx neptuni</i>		X			
		<i>Lartetictis</i> cf. <i>dubia</i>		X			
<i>Eomellivora moralesi</i>		X					
	Guloninae indet.	X					

Order	Family	Taxon	HAM 5	HAM 4	HAM 6	HAM 1-3
		<i>Proputorius sansaniensis</i>				X
		<i>Proputorius pusillus</i>				X
		<i>Palaeomeles pachecoi</i>	X	X		
	Leptarctinae	<i>Trocharion albanense</i>	X	X		
	Hyaenidae	<i>Thalassictis montadai</i>	X		X	
		Hyaenidae indet.	X			
	Viverridae	<i>Semigenetta sansaniensis</i>	X	X		X
		<i>Semigenetta grandis</i>		X		
		<i>Viverrictis modica</i>		X		
	Felidae	<i>Pseudaelurus quadridentatus</i>	X			
		Metailurini indet.	X			
	Barbourofelidae	<i>Sansanosmilus</i> sp.	X	X		
	Semantoridae	<i>Potamotherium</i> sp.	X			
Phocidae	Phocidae indet.	X	X			
Proboscidea	Gomphotheriidae	<i>Tetralophodon longirostris</i>	X		X	
	Deinotheriidae	<i>Deinotherium levius</i>	X	X		
Perissodactyla	Rhinocerotidae	<i>Hoploaceratherium belvederense</i>	X	X		
		<i>Aceratherium</i> sp.	X	X		
	Chalicotheriidae	Schizotheriinae indet.		X		
	Chalicotheriidae	<i>Chalicotheriinae, Anisodon</i> sp.	X			
	Equidae	<i>Sinhippus</i> sp.	X	X		
Artiodactyla	Suidae	<i>Listriodon splendens</i>	X	X	X	
		<i>Parachleuastochoerus steinheimensis</i>	X	X		
	Tragulidae	<i>Dorcatherium nauai</i>	X	X	X	
	Moschidae	Moschidae indet.	X	X		
	Cervidae	<i>Euprox furcatus</i>	X	X	indet.	
	Bovidae	<i>Miotragocerus monacensis</i>	X	X	X	
Lagomorpha	Ochotonidae	<i>Prolagus oeningensis</i>	X	X		
		<i>Eurolagus fontannesii</i>	X	X		X
Rodentia	Sciuridae	<i>Spermophilinus bredai</i>	X	X		X
		<i>Albanensia grimmi</i>	X	X		X
		<i>Blackia miocaenica</i>	X	X		
		<i>Miopetaurista</i> sp.	X	?		
	Castoridae	<i>Euroxenomys minutus</i>	X	X		X
		<i>Steneofiber depereti</i>	X	X	X	X
	Gliridae	<i>Microdyromys complicatus</i>	X			
		<i>Muscardinus hispanicus</i>	X	X		X
		<i>Muscardinus</i> sp.	X	X		
		<i>Bransatoglis</i> sp.	X			
		<i>Glirulus conjunctus</i>	X	?		X
		<i>Eliomys reductus</i>	sp.			X
		<i>Eliomys assimilis</i>				X
		<i>Myoglis meini</i>	X	X		X
	Eomyidae	<i>Eomyops catalaunicus</i>	X			X
		<i>Keramidomys</i> sp.	X			
	Cricetidae	<i>Democricetodon</i> sp. nov.	X	X		X
		<i>Collimys hiri</i>	X	X		X
		<i>Megacricetodon minutus</i>	X	X		X

Order	Family	Taxon	HAM 5	HAM 4	HAM 6	HAM 1-3
		<i>Microtocricetus molassicus</i>	X	X		X
		<i>Eumyarion latior</i>	X	X		
		Cricetodontini		X		
	Platacanthomyidae	<i>Neocometes</i> sp.		X		
	Anomalomyidae	<i>Anomalomys gaudryi</i>	X	X	X	X

6 Taphonomy and Biostratinomy

6.1 Area of excavation and documentation

The excavations were always clearly structured and documented separately according to their respective stratigraphic position in the profile. The local stratigraphic levels HAM 5 and HAM 4 are to be regarded as separate sites covering a different period and are also dealt with here in succession.

6.1.1 HAM 5 (Fig. 6.1.1.1)

In the years 2011 to 2014, no extensive excavations could take place. The exposure conditions of HAM 5 were in the steep slope of the excavation level of the active clay mining and only smaller excavations could be carried out. In the excavation year 2015, a larger HAM 5 area was exposed for the first time due to mining, as the overlying sediment was now removed. Here, for the first time, it was possible to excavate over a period of three weeks and to work on an area of approximately 10 m². The finds from this period can only be estimated within the excavation area by the chronological sequence of finds. Even before the 2016 summer excavation season, a significant portion of HAM 5 would have been lost to clay mining, as mining of the deeper layers was now to take place. Here, about 20 m³ of the find layer was recovered with an excavator and stored for later processing. In the subsequent excavation, HAM 5 was explored in further section of about 23 tonnes with a corresponding gap on areas from previous years and also only rough localisation of finds. Only from 2017 onwards it was possible to begin a coherent excavation of HAM 5, which also links up with a gap to previous areas. Starting in 2017, finds and features were spatially surveyed and exact find positions can now be placed in relation to each other. This was followed by excavations in 2017 (40 m²), 2018 (100 m²), 2020 (50 m²), 2021 (100 m²), 2022 (2 m²). No excavations took place at HAM 5 in 2019 and 2023.

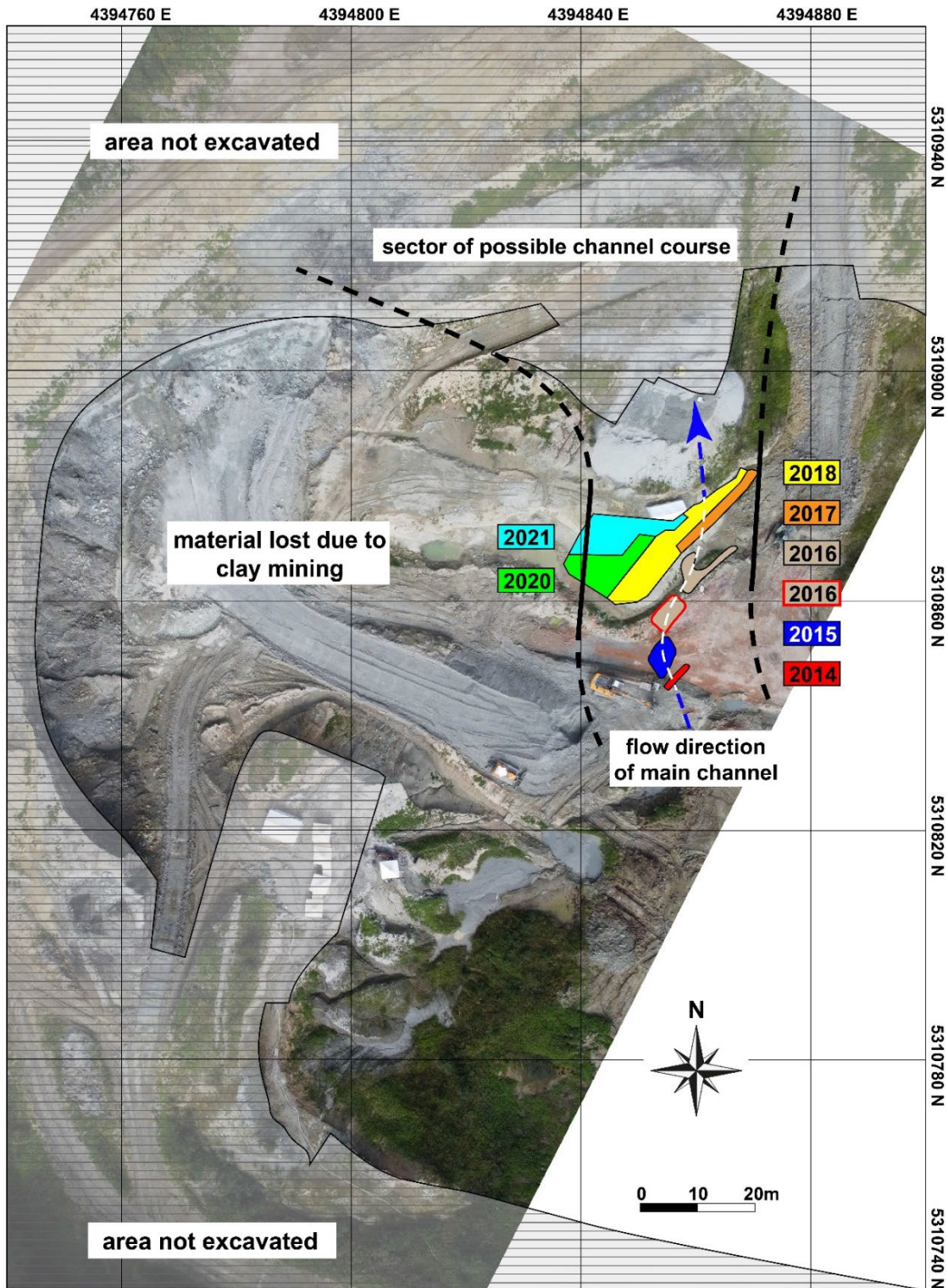


Figure 6.1.1.1. Top view of the Hammerschmiede clay pit (drone image) including the excavation areas within the local stratigraphic level HAM 5 at the early Late Miocene Hammerschmiede locality. The areas of 2017, 2018, 2020 and 2021 mark contiguously excavated and spatially documented areas. The areas of 2015 and 2016 correspond to approximate estimates. The red encircled 2016 polygon indicates an area that was under threat of destruction from mining activity. Sediments of this section have been removed, stored (approximately 23 tonnes) and separately processed over the following years. Thick black lines indicate the channel course based on outcrop observations. Dashed thick lines indicate the presumed course from the south and a possible area of the course to the north (secured by laterally delimiting outcrops). The thick blue and white dashed lines indicate the course of the deepest incised main channel of HAM 5. Not yet excavated areas are shaded and other areas at this elevation have been lost due to clay mining. Coordinates correspond to Gauss-Krüger Zone 4 grid in metres. Grid spacing equals 40 metres.

Currently, the overlying strata of HAM 4 are blocking further progress, so that the documentation of the overlying HAM 4 is necessary as preliminary work in order to continue HAM 5 excavations. For the excavated areas and years 2017-2018, 2020-2022 see Fig. 6.1.1.2. and for corresponding channel base morphology at the sections see Fig. 6.1.1.3.

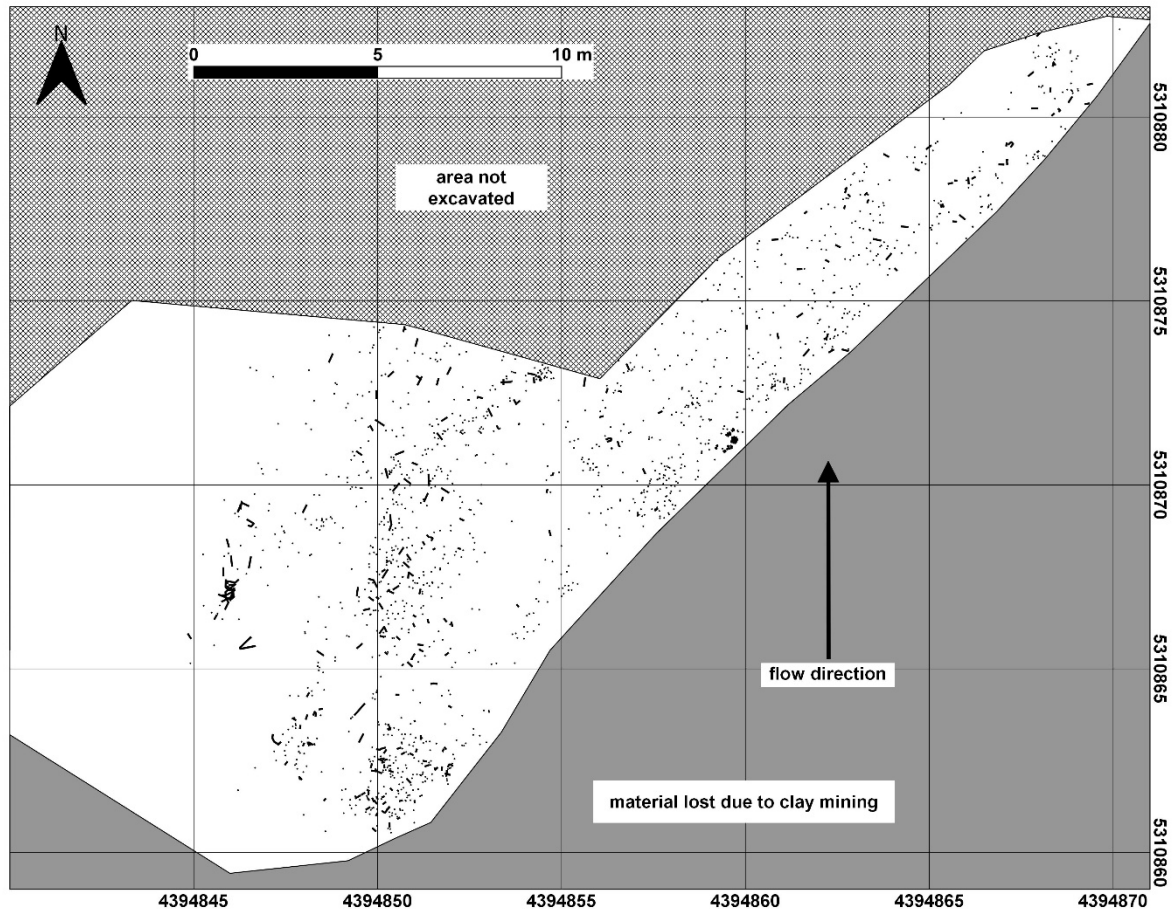


Figure 6.1.1.2. Detailed map of find distributions in the area of the local stratigraphic level HAM 5 at the early Late Miocene Hammerschmiede site. The white polygon frames fully excavated areas of the years 2017, 2018, 2020, 2021 and 2022 (no excavations took place in 2019 and 2023). Black dots mark excavated and measured isolated finds (mostly bones). Black lines represent elongated bones including length and orientation. The black arrow indicates the presumed flow direction of the watercourse. The grey area has been lost due to clay mining, and the shaded area includes unexcavated areas. Coordinates correspond to Gauss-Krüger Zone 4 grid in metres. Grid spacing equals 5 metres.

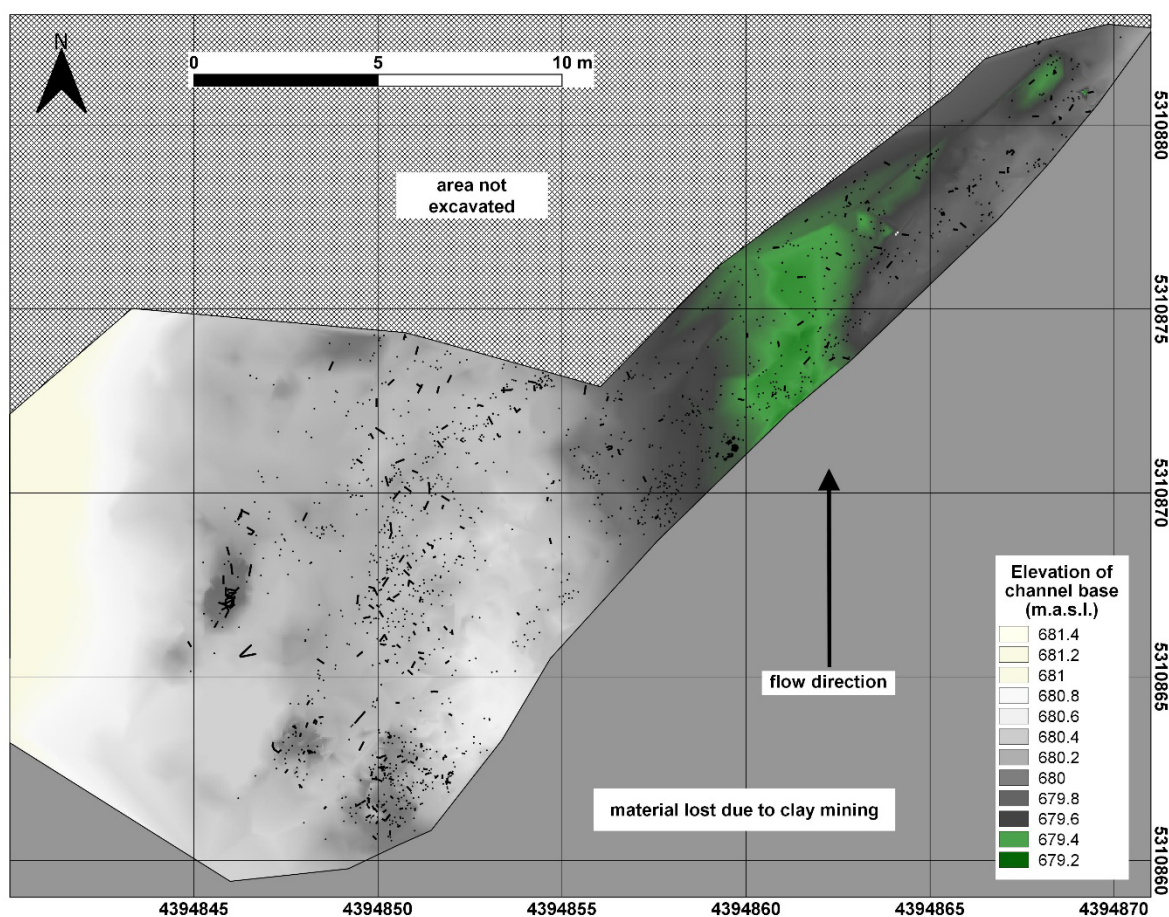


Figure 6.1.1.3. Relief map of the fossil HAM 5 channel base elevation at the early Late Miocene Hammerschmiede site. The polygon frames the excavation areas of the years 2017, 2018, 2020, 2021 and 2022. Black dots mark excavated and measured isolated finds (mostly bones). The map shows the maximum erosion depth of the HAM 5 channel based on measured points selected depending on the basement surface texture. The reconstructed flow direction (black arrow) is based on the course of the deepest channel base regions (darker colours) and the dip of the channel margin (brighter colours), supplemented by the orientation of elongated objects found (black lines). The grey area has been lost due to clay mining, and the shaded area includes unexcavated areas. Values for altitude in metres above sea level. Coordinates correspond to Gauss-Krüger Zone 4 grid in metres. Grid spacing equals 5 metres.

6.1.2 HAM 4 (Fig. 6.1.2.1)

The local stratigraphic level HAM 4 was already visible in the slope since the beginning of current research efforts. Due to its location in the middle of the mining slope, there was no possibility to realise larger excavations until 2017. Until then, only single finds could be recovered from the slope. Only a change in the mining strategy of the pit operator (the pit became too deep, as the sediment thickness increases in mining direction) with the creation of a mining floor in the stratigraphic level of HAM 4, made it possible there to excavate over a wide area.

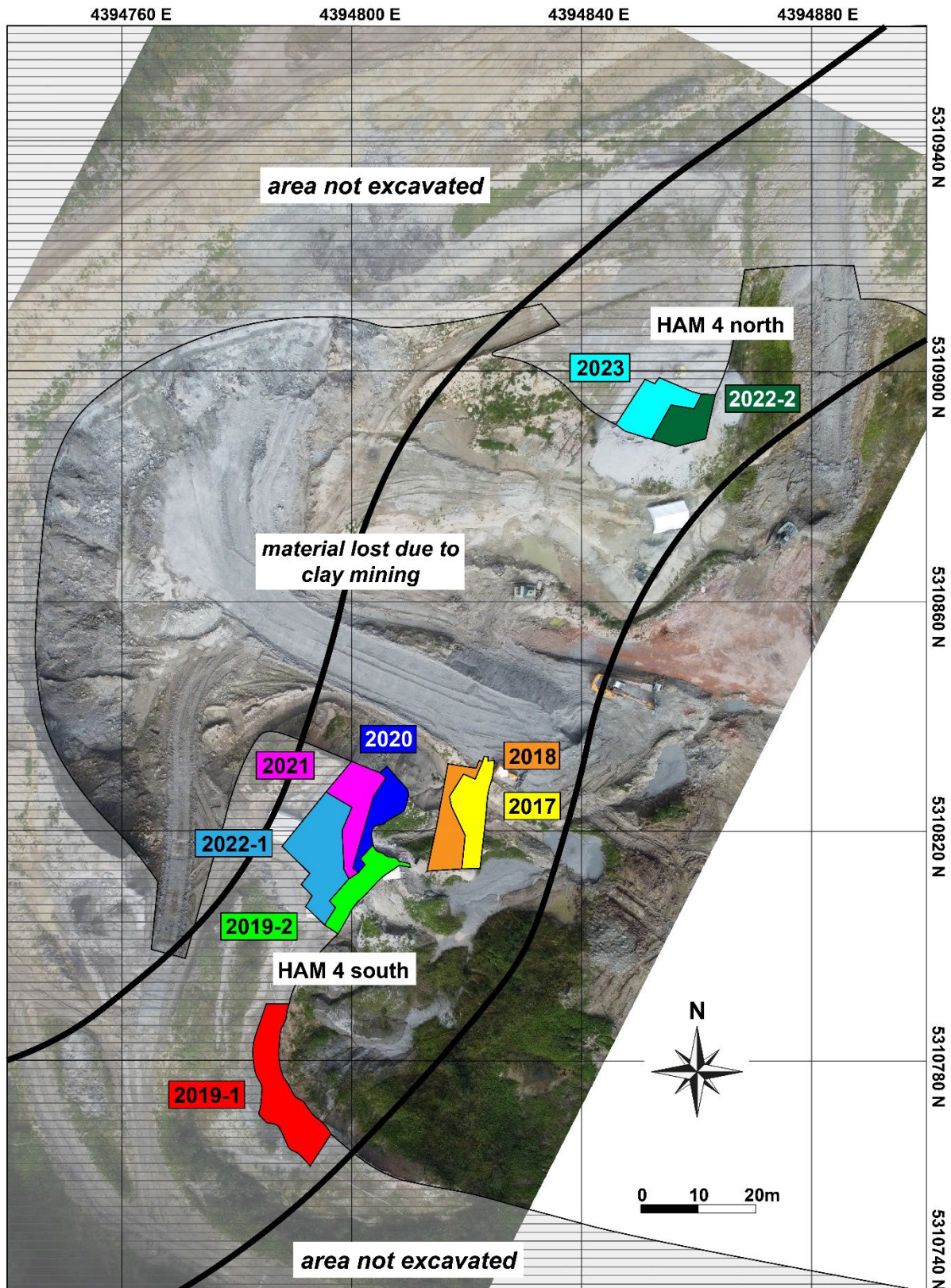


Figure 6.1.2.1. Top view of the Hammerschmiede clay pit (drone image) including the excavation areas within the local stratigraphic level HAM 4 at the early Late Miocene Hammerschmiede locality. The area between excavation sector “HAM 4 north” and “HAM 4 south” and to the east of those has been lost due to mining activities. The excavated and spatially documented areas of the years 2017 to 2023 are marked by coloured areas. Thick black lines indicate the potential slightly s-shaped meandering channel course based on field observations at the mining slopes. Shaded areas mark not excavated areas. Coordinates correspond to Gauss-Krüger Zone 4 grid in metres. Grid spacing equals 40 metres.

After the intended end of the excavations in 2017, the extreme density of finds in HAM 4, which was about to be mined, was recognised. The first finds were so promising that a new excavation campaign was carried out for a further 3 weeks in autumn of the same year and continued in the same area in spring 2018. Until the following excavation period, the clay mining was so extensive that only with a sufficiently large gap to the following areas in the south, middle and north out work could continue. Until the temporary protection since spring 2020 and the final protection declaration as a natural monument in 2021 by the district administration of Ostallgäu, large areas of the eastern rim of HAM 4 and the central pit area were lost due to clay mining. The 2017 and 2018 sites are thus contiguous sites separated by respective gaps from later excavations (2017: 56 m² and 2018: 70 m²; Fig. 6.1.2.2 and Fig. 6.1.2.3).

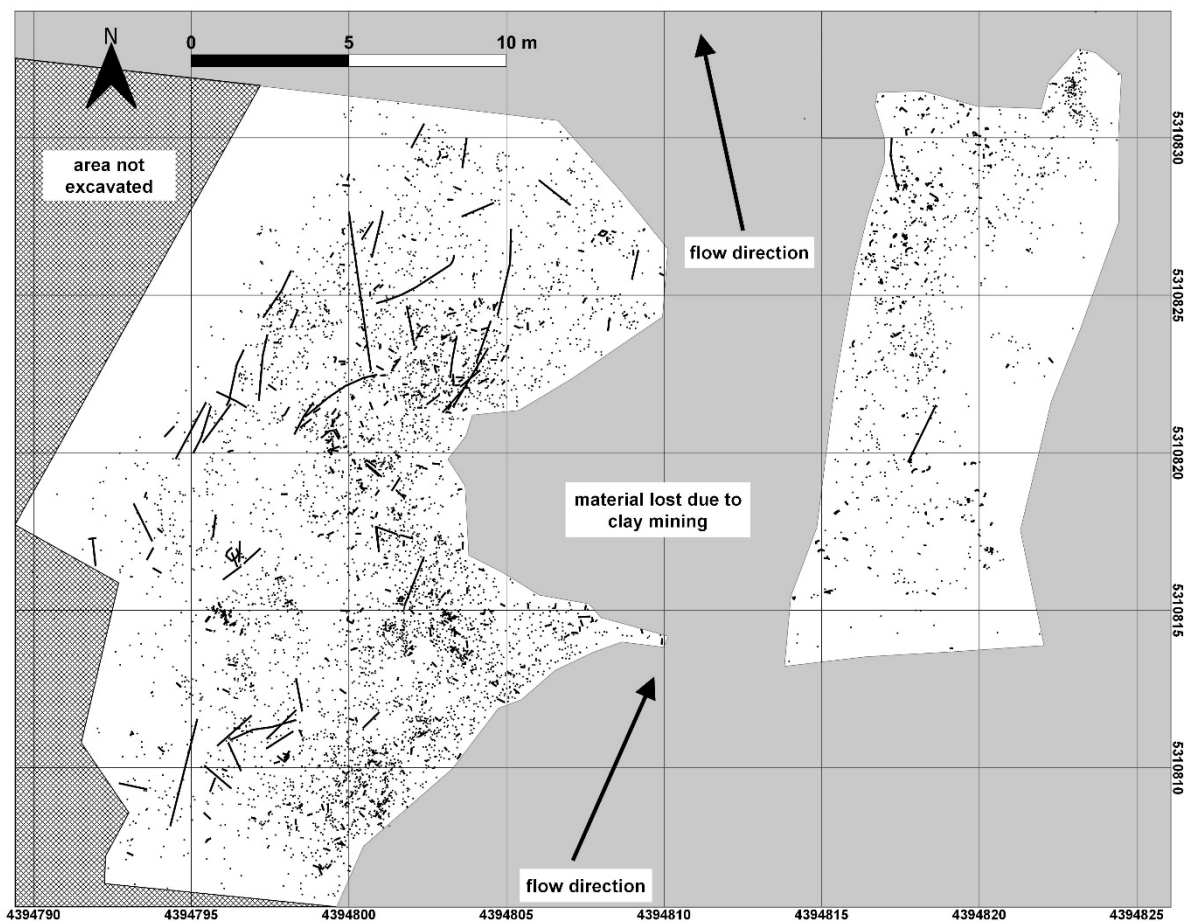


Figure 6.1.2.2. Detailed map of find distributions in the central excavation areas of the local stratigraphic level HAM 4 at the early Late Miocene Hammerschmiede site. The eastern polygon frames the contiguous excavation area 2017 to 2018. The western frame includes the excavation areas 2019-2, 2020, 2021 and 2022-2. Black dots mark excavated and measured isolated finds (mostly bones). Black lines represent elongated objects (the longest represent wood finds) including length and orientation. Black arrows indicate the presumed flow direction of the HAM 4 river and refer primarily to the orientation of the elongated objects found. The grey area has been lost due to clay mining, and the shaded area includes unexcavated areas. Coordinates correspond to Gauss-Krüger Zone 4 grid in metres. Grid spacing equals 5 metres.

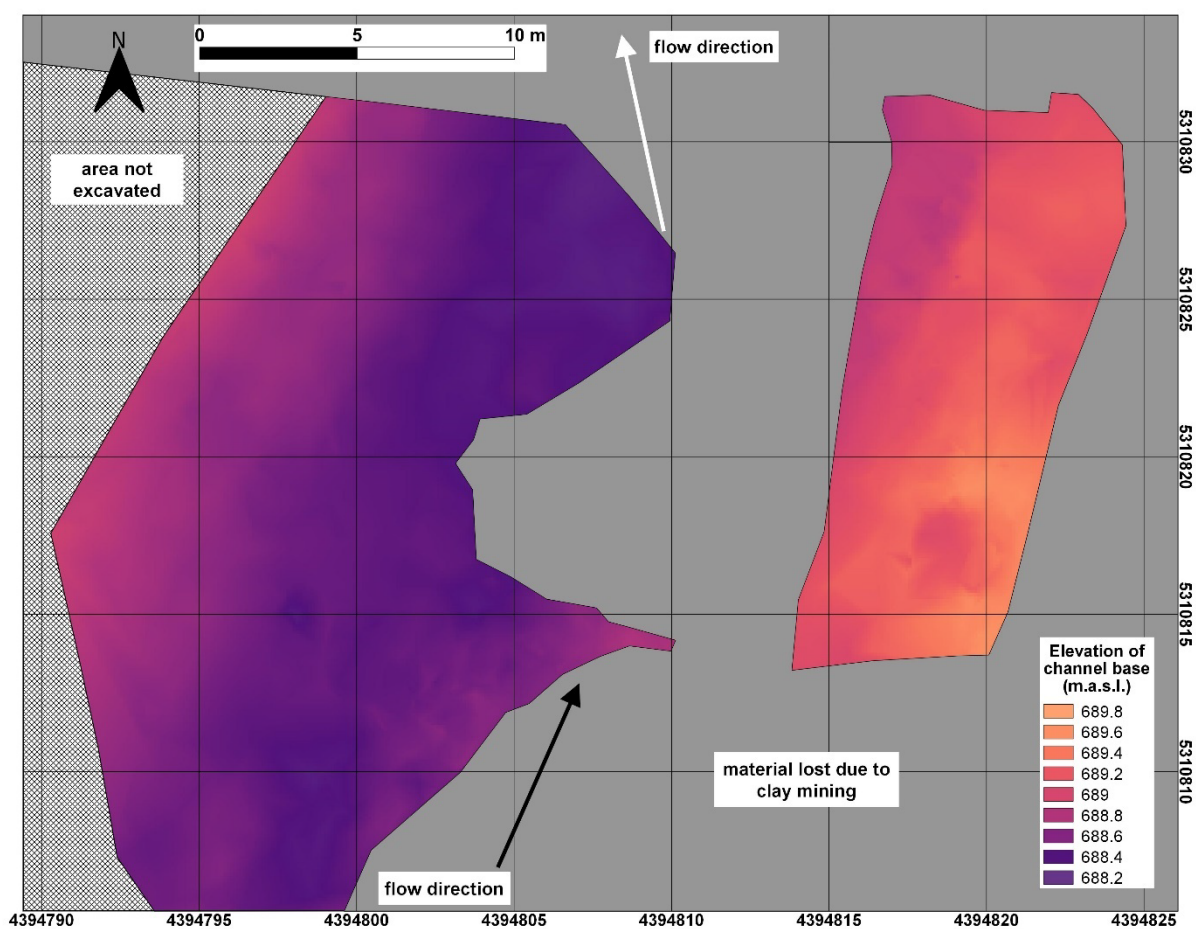


Figure 6.1.2.3. Relief map of the fossil river channel base elevation in the central excavation area of the local stratigraphic level HAM 4 at the early Late Miocene Hammerschmiede site. The eastern polygon frames the contiguous excavation area 2017 to 2018. The western frame includes the excavation areas 2019-2, 2020, 2021 and 2022-2. The map shows the maximum erosion depth of the HAM 4 channel based on measured points selected depending on the basement surface texture. The reconstructed flow direction (arrows) is based on the course of the deepest channel base regions (darker colours) and the dip of the channel margin (brighter colours), supplemented by the orientation of elongated objects found. The grey marked area has been lost due to clay mining, and the shaded area includes unexcavated areas. Values for altitude in metres above sea level. Coordinates correspond to Gauss-Krüger Zone 4 grid in metres. Grid spacing equals 5 metres.

This was followed by an excavation at the southern edge of pit 2019/1 (143 m²); Fig. 6.1.2.4 and Fig. 6.1.2.5). In the same year, in a second campaign, an excavation was carried out in the central pit area not far from the areas of the two previous years. Finally, it was possible to continue the previous year's excavations without any losses and to excavate the largest contiguous area of HAM 4 to date (2019/2: 54 m², 2020: 60 m², 2021: 70 m², 2022-1: south: 140 m²; Fig. 6.1.2.2 and Fig. 6.1.2.3). In the 2022 field season, excavation continued for the first time north of the large central gap of HAM 4, that was lost due to clay mining to regain access to HAM 5 below (2022-2: 50 m² and 2023: 85 m²; Fig. 6.1.2.6 and Fig. 6.1.2.7).

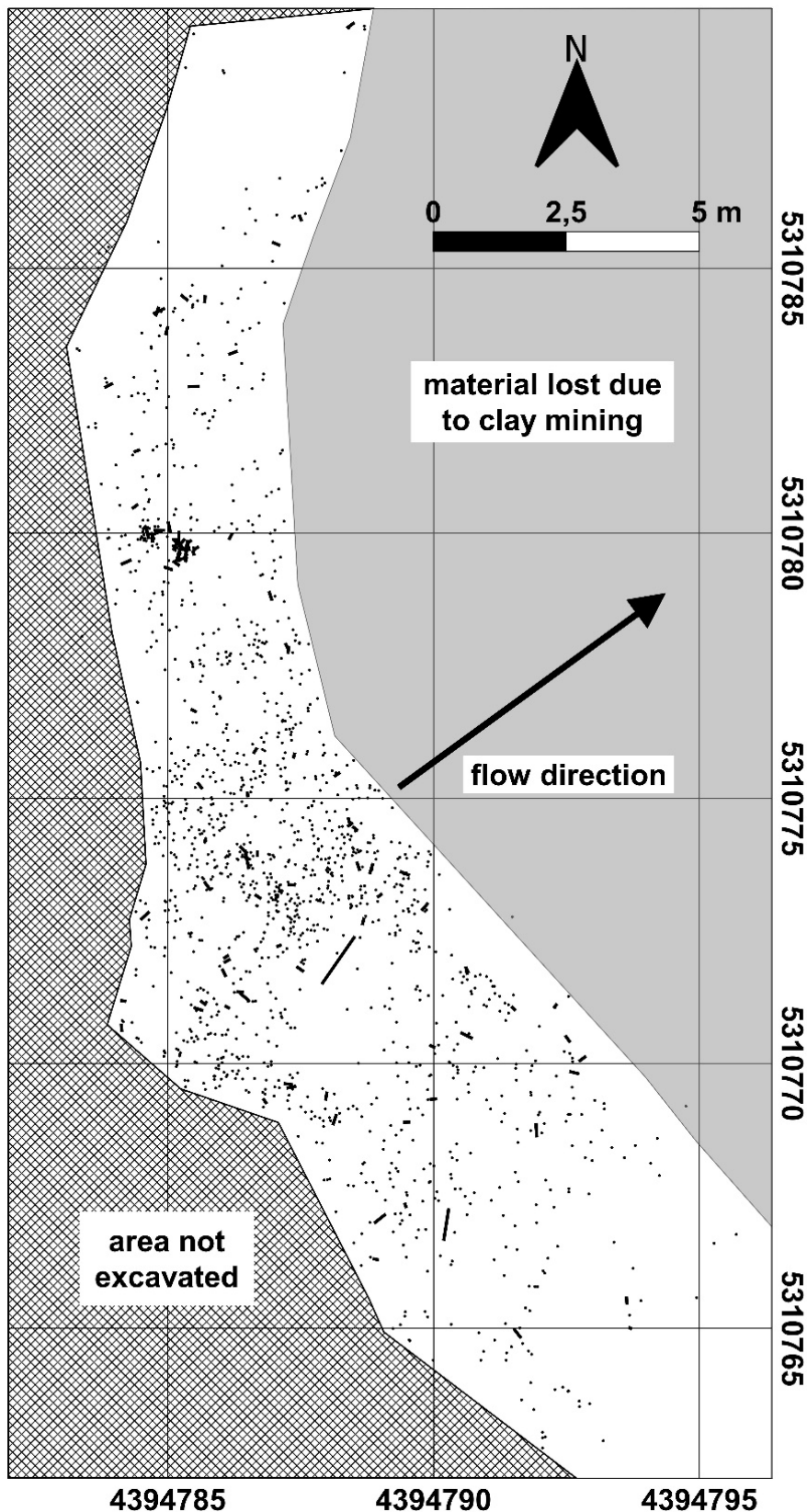


Figure 6.1.2.4. Detailed map of find distribution in the southernmost excavation area of the local stratigraphic level HAM 4 (2019-1) at the early Late Miocene Hammerschmiede site. Black dots mark excavated and measured isolated finds (mostly bones). Black lines represent elongated objects (the longest represent wood finds) including length and orientation. The black arrow indicates the presumed flow direction of the HAM 4 river and refers primarily to the orientation of the elongated objects found. The grey area has been lost due to clay mining, and the shaded area includes unexcavated areas. Coordinates correspond to Gauss-Krüger Zone 4 grid in metres. Grid spacing equals 5 metres.

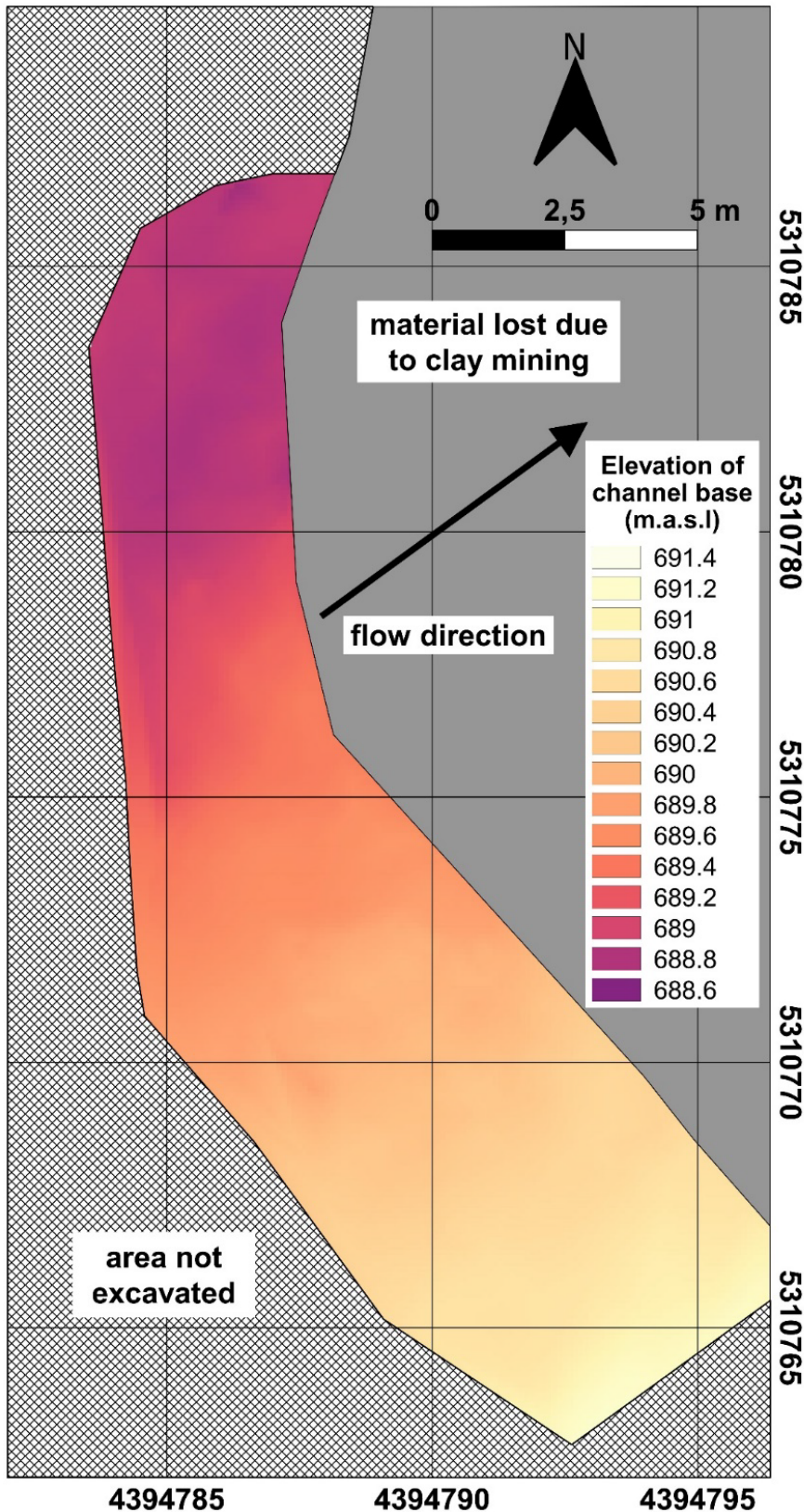


Figure 6.1.2.5. Relief map of the fossil river channel base elevation in the southernmost excavation area of the local stratigraphic level HAM 4 (2019-1) at the early Late Miocene Hammerschmiede site. The map shows the maximum erosion depth of the HAM 4 channel based on measured points selected depending on the basement surface texture. The reconstructed flow direction (arrow) is based on the course of the deepest channel base regions (darker colours) and the dip of the channel margin (brighter colours), supplemented by the orientation of elongated objects found. The grey marked area has been lost due to clay mining, and the shaded area includes unexcavated areas. Values for altitude in metres above sea level. Coordinates correspond to Gauss-Krüger Zone 4 grid in metres. Grid spacing equals 5 metres.

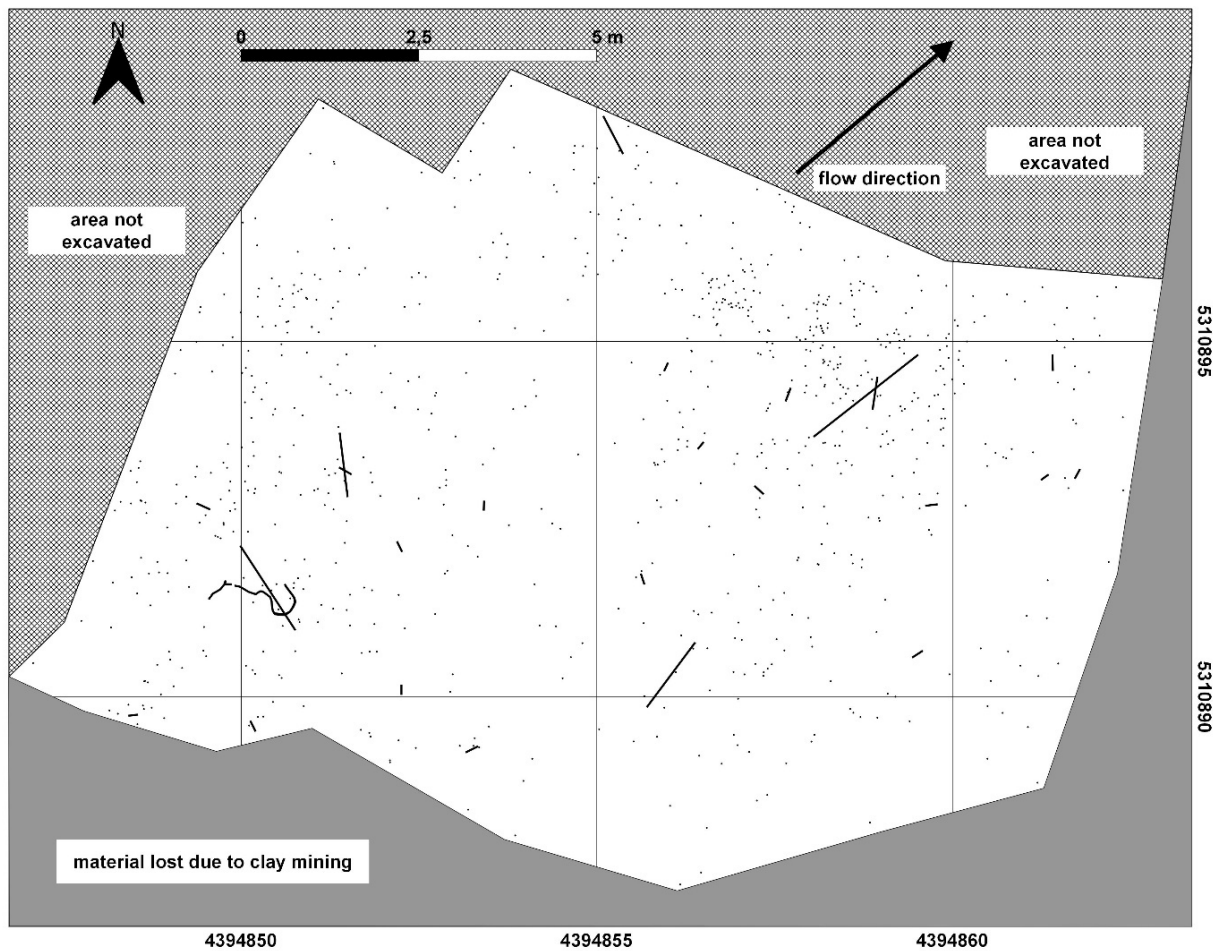


Figure 6.1.2.6. Detailed map of find distributions in the northernmost excavation area of the local stratigraphic level HAM 4 (2022-2 and 2023) at the early Late Miocene Hammerschmiede site. Black dots mark excavated and measured isolated finds (mostly bones). Black lines represent elongated objects (the longest represent wood finds) including length and orientation. The black arrow indicates the presumed flow direction of the HAM 4 river and refers primarily to the orientation of the elongated objects found. The grey area has been lost due to clay mining, and the shaded area includes unexcavated areas. Coordinates correspond to Gauss-Krüger Zone 4 grid in metres. Grid spacing equals 5 metres.

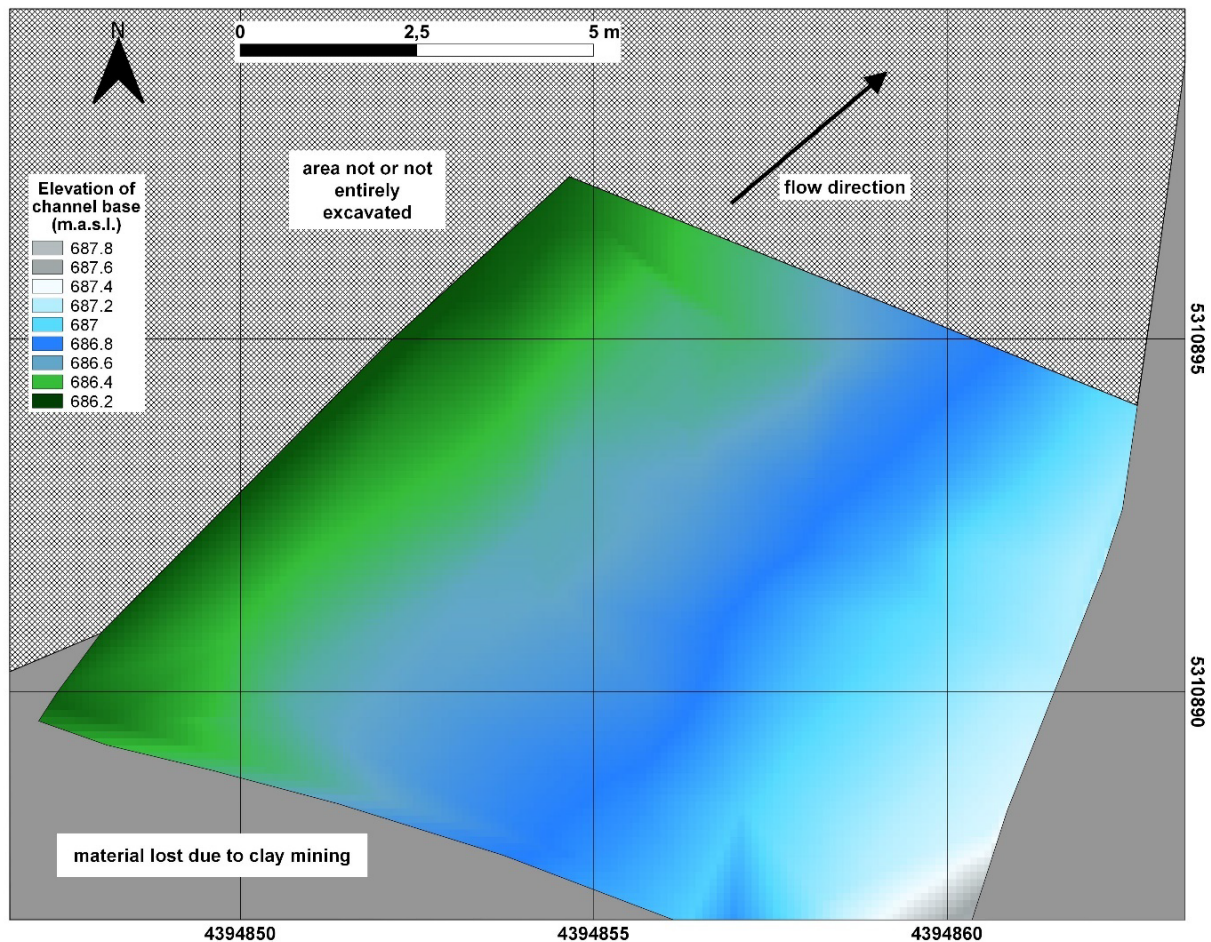


Figure 6.1.2.7. Relief map of the fossil river channel base elevation in the northernmost excavation area of the local stratigraphic level HAM 4 (2022-2 to 2023) at the early Late Miocene Hammerschmiede site. The map shows the maximum erosion depth of the HAM 4 channel based on measured points selected depending on the basement surface texture. The reconstructed flow direction (arrow) is based on the course of the deepest channel base regions (darker colours) and the dip of the channel margin (brighter colours), supplemented by the orientation of elongated objects found. The grey marked area has been lost due to clay mining, and the shaded area includes unexcavated areas. Values for altitude in metres above sea level. Coordinates correspond to Gauss-Krüger Zone 4 grid in metres. Grid spacing equals 5 metres.

6.2 Preserved material types

The preservation conditions in both layers of HAM 5 and HAM 4 are particularly favourable for the conservation of carbonate and phosphatic fossils. Especially bones and teeth of vertebrates show excellent preservation, whereas molluscs show different types of preservation. Freshwater pearl mussels (*Margaritifera flabellata*), for example, are preserved in HAM 5 as internal casts possibly preserving the periostracum without the original calcareous shell, whereas in HAM 4 bivalve and gastropod shells are preserved and some shells display a mother-of-pearl lustre. In the HAM 5 clays, in some gastropod specimens the shell is almost missing, whereby in some cases in the wet state the original shell colour pattern is still recognisable (see Fuss et al. 2015). There is also a clear distinction between the local stratigraphic levels

concerning the preservation of organics. Botanical remains are particularly poorly preserved in HAM 5 and are mostly indicated by a light purple coloured layer in the clay, whereby the actual organic matter is missing due to oxidisation and degradation processes. In HAM 4, on the other hand, pieces of wood are tree-dimensionally carbonized and pyritised, which makes preparation and conservation almost impossible (Fig. 6.2.1).



Figure 6.2.1. Wood finds from the early Late Miocene Hammerschmiede deposits and the local stratigraphic level HAM 4. (a) and (b) show typical finds of mostly elongated branchless wood that are used for flow direction analyses by measuring the longitudinal orientation within the fluvial channel. Reddish or brownish coatings (a) indicate a high content of iron sulphates that start to disintegrate after discovery. Scale bars equal 10 cm.

Leaf fossils are extremely rare in both layers and mostly only consist of badly preserved impressions. In the HAM 4 area reworked fragments of calcareous or pyritised root tubules (rhizocretions) can be found (Fig. 6.2.2), whereby Kirscher et al. (2016) also report on in situ root tubules. Particularly well preserved in both levels are charcoal pieces from micro charcoal to up to 65 mm in size, which are frequently found especially in HAM 4 (Fig. 6.2.3) and are evidence of vegetation fires in the catchment area or in the vicinity of the HAM 4 river. The freshwater pearl mussel is one of the most abundant finds within the HAM 4 channel fill. Most of the shells comprise both valves, slightly or completely opened and internally filled with surrounding fine-sand, suggesting a post-mortem embedding and allochthonous origin. A few

exceptions of found *Margaritifera flabellata* comprise a sedimentless internal filling and show a strong shell compression (Fig. 6.2.4 a-b). The enclosed core consists of a brownish, several millimetres thick organic filling (Fig. 6.2.4 b-d) which probably corresponds to remains of the original in vivo organics of the mussel and might represent a kind of soft-tissue preservation indicating an autochthonous origin. Since these specimens are mostly found in thicker silty fine-sand layers, a very fast embedding is indicated, most probably of the living shell which may have been killed by too great embedding depth.

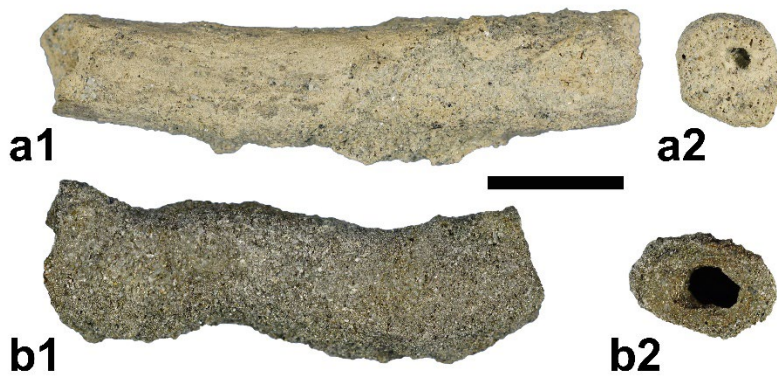


Figure 6.2.2. Allochthonous root tube fragments from the early Late Miocene Hammerschmiede deposits and the local stratigraphic level HAM 4. (a) Carbonated fragment of a root tube in lateral (a1) and cross-section (a2) view. (b) Pyritized fragment of a root tube in lateral (a1) and cross-section (a2) view. (a) GPIT/PL/21805; (b) GPIT/PL/21841. Scale bar equals 10 mm.

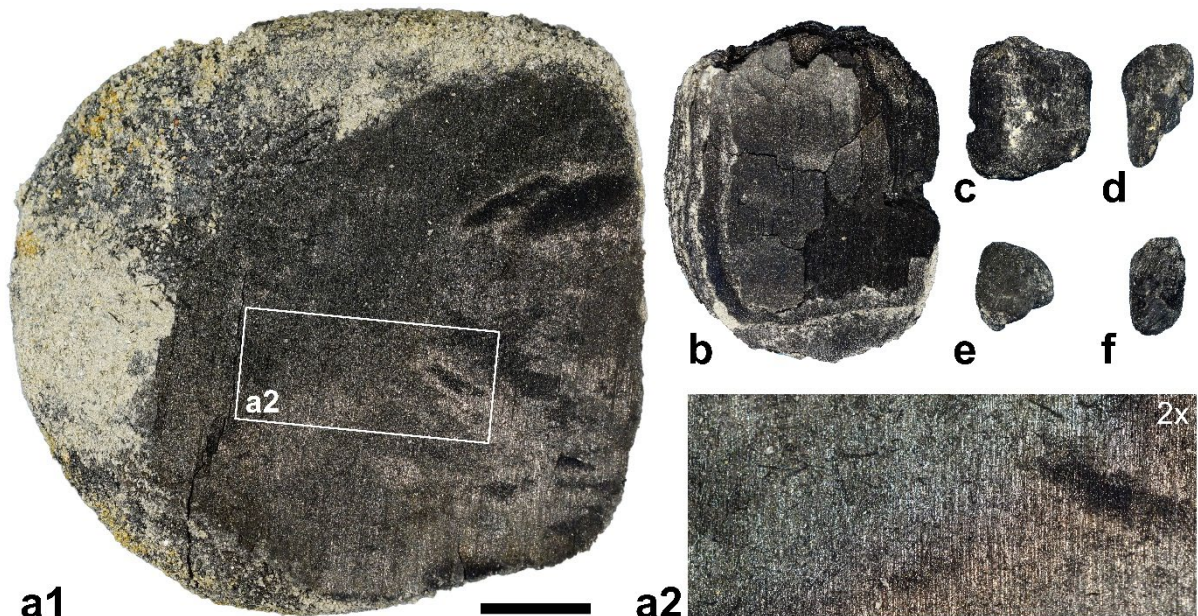


Figure 6.2.3. Charcoal specimens of different sizes from the early Late Miocene Hammerschmiede deposits and the local stratigraphic level HAM 4 (a-f). Most specimens are rolled and compressed but show a well preserved internal structure preservation (a2). Figure (a) represents the so far largest specimen of charcoal found at the HAM 4 layer. The majority of charcoal specimens shows smaller sizes (c-f). (a) GPIT/PL/21839, (b) GPIT/PL/21837; (c-f) SNSB-BSPG 2020 XCIV-7466. Scale bar equals 10 mm (a1, b-f) or 5 mm (a2).

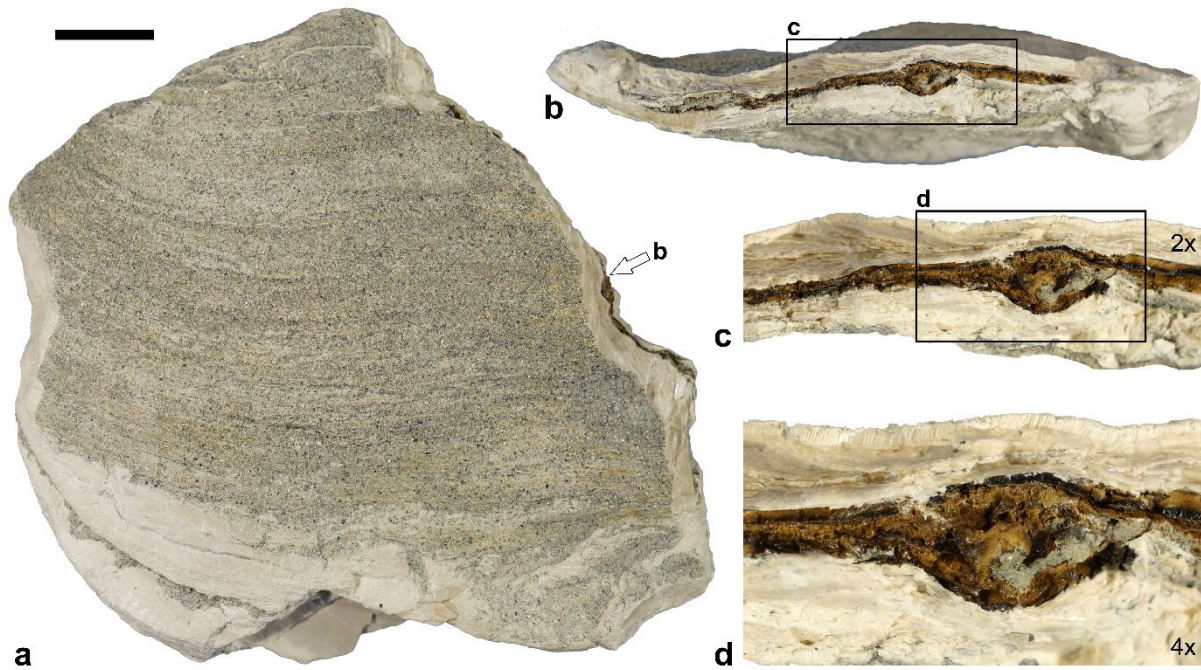


Figure 6.2.4. Preservation of organic matter within a freshwater pearl mussel (*Margaritifera flabellata*) from the early Late Miocene Hammerschmiede deposits and the local stratigraphic level HAM 4. The shell shows a sandless internal filling and strong compression (a-b). In the interior a brownish mass is found (b-d), which probably corresponds to remains of the original in vivo organics of the mussel and might represent soft-tissue preservation. (a-d) GPIT/BI/05904. Scale bar equals 10 mm (a-b), 5 mm (c) or 2.5 mm (d).

Component-supported coarse grained layers comprising of enriched pedogenic carbonate concretions, rolled greenish clay pebbles, and sometimes mass occurrence of terrestrial gastropods (*Helicoidea* / *Pseudochloris* sp.?) indicate strong rearrangement and sorting processes (Fig. 6.2.5 a-b). The terrestrial gastropods from HAM 4 mostly show a greenish clay filling, while the main HAM 4 components consist of greyish silts and fine sands (Fig. 6.2.5 c). This indicates an input of snails possibly washed in during rainfall from the surrounding terrestrial area of the Ham 4 river (paraautochthonous). As gastropods act as sediment traps, they catch green sediments of the river peripheral flood plain. Alternatively, the terrestrial gastropods could be redeposited secondarily, presumably from the green clays into which HAM 4 is cut. The same probably also applies to the pedogenic carbonate concretions and the green clay clasts from the reworking layers. Bone and tooth preservation are very good in both HAM 5 and HAM 4 layers. The preservation of osteological matter nevertheless is very heterogeneous. Different taphonomic processes and pathways seem to be responsible for this. In many cases bones are perfectly preserved, showing a medullary cavity preserved as a void, sometimes with pyrite crystallisations (HAM 4). Especially in HAM 4, these bones also remain three-dimensionally, as the surrounding sediment (silt and fine sand) is hardly compressible and stabilises the bone. In the clay layers of HAM 5, this stabilisation is missing, as the clay compresses and drains under load. A number of bones show significantly poorer preservation,

indicating different degrees of transport distance and strength. Some bones are also damaged by biogenic processes (see section 6.8). A number of finds show surface corrosion, which could be abiogenic chemical or biogenic (e.g. algae, bacteria; see section trace fossils) in nature. Root traces indicate post-depositional rooting, which would have taken place before further redepositional processes. The bones of ontogenetically older and individually more ossified animals are often better preserved than those of young animals, which were probably still quite porous when embedded. Some finds show polishing, rolling of broken edges, indicating greater transport distances for these. With few exceptions of partially articulated finds and narrower strewnfields of single individuals, the innumerable loose individual bone and tooth finds indicate transport and sorting processes in the river course.

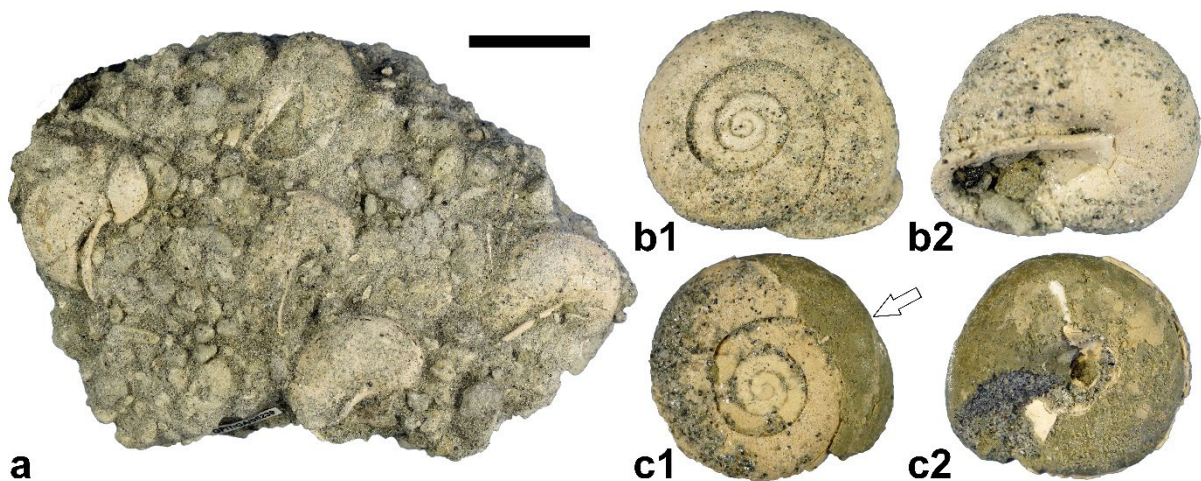


Figure 6.2.5. Terrestrial gastropods from the early Late Miocene Hammerschmiede deposits and the local stratigraphic level HAM 4. (a) In situ sample of a component-supported layer of reworked coarse sediments from the HAM 4 channel deposits consisting of pedogenic carbonate concretions, rolled clay pebbles and terrestrial gastropods (*Helicoidea* / *Pseudochloris* sp.?). (b) Completely preserved terrestrial gastropod (*Pseudochloris* sp.?) from HAM 4. (c) Terrestrial gastropod (*Pseudochloris* sp.?) from HAM 4 with partly broken and missing shell revealing a greenish fine-grained clay filling while coarser sediments adhere to the outer shell. (a) GPIT/GA/05239; (b) GPIT/GA/05228; (c) GPIT/GA/05227. Scale bar equals 20 mm (a) or 10 mm (b-c).

6.3 Spatial distribution of finds (large scale):

The distribution of finds within the documented excavation areas is based on a set of underlying geological and geomorphologic patterns. While for example finds of gastropods are possible over the whole pit area, bone finds are limited and enriched at carved channel courses. Within a fluvial eroded channel structure, it is not to be expected that objects are evenly distributed (Behrensmeyer 1988). The Hammerschmiede channels exhibit clear differences in the thickness of the fossil layers and in the density of finds between the channel margins and the centre of channels (see Figs. 6.1.1.2, 6.1.2.2, 6.1.2.4, 6.1.2.6). There are also sedimentary dependencies with regard to flow and sedimentation behaviour of fossils like the corresponding river bottom conditions and changes in the orientation of the flow direction due to meandering, sandbanks

or pool and riffle structures. As a result, different depositional zones within these channel structures are found. The spatial density of finds varies over the course of the channel, so that very rich zones (>50 objects per square metre) are located in close proximity to regions without finds. The orientation of elongated objects changes on a larger scale, as the channels do not run in a straight line. HAM 4 is particularly affected by this, as outcrops are compared over a larger distance throughout the entire claypit width. Basically, most objects are deposited at the channel base or in separate channel lag deposits within the channel fill (sensu Behrensmeyer 1988). Specimens at channel lags are mostly represented by disarticulated bones (reworked and enriched material). It is rather rare to find objects between those channel lag deposits, within the more quickly deposited channel fills. Due to the high degree of reprocessing within the channel lags, finds outside the enrichment layers, in the channel fill, are often of outstanding quality, even if they are extremely rare what exactly corresponds to observations described by Behrensmeyer (1988). With a corresponding distance to the channel base, the quantity of finds decreases significantly. Since the channel depth differs greatly between the central and the marginal area, the absolute thickness of the find layers in the marginal area is usually quite thin, while fossiliferous layers of more than a metre can be found in central regions. These days, there are no bones found outside the channel structures.

As a further indication of strong rearrangement processes, large- and small-scale sorting of objects can be detected. Only in the large-scale analysis it becomes visible that in the HAM 4 certain fossil-types are more frequent and accumulate on some areas while they are rare elsewhere. For example, areas with clustered mass accumulations of freshwater pearl mussels (*Margaritifera flabellata*) indicate sorting by density and object shape properties (see Fig. 6.5.2 later in the manuscript). Such processes can also be observed in HAM 5. Here in the excavation area of 2018 there was a pool-like depression in the western lateral channel base, which accumulated material of greater density (carbonate concretions and especially mammalian teeth). The depression in the base with slight edge undercuts rather indicates higher currents and possibly whirlpool-like circulating water, which only allowed particularly dense material to retain here. More than 50 teeth and tooth fragments were found within less than two square metres, while the surrounding area supplied not even close to such a high number of teeth.

6.4 Spatial distribution of finds (small scale):

The find layers HAM 5 and HAM 4 provide next to a majority of small and medium sized bones and fragments only a small quantity of larger bones. So far there is no find of a fully articulated

skeleton. This already indicates a strong mixing, reworking and transport of bones presumably also over larger distances. In addition, bones with excellent surface preservation can be found directly next to finds that have been crushed, corroded, rolled off, fragmented, and also covered with root marks. The largest quantity of finds are disarticulated bones or bone fragments from small and medium-sized vertebrates. Objects are very heterogeneously distributed and conclusions about related individuals are rarely possible. Especially the large mammal finds are in many cases limited to small fragments of teeth and bones broken down into small pieces of cm range. Depending on the localisation in the channel, there is one (channel margin) or several (channel centre) enrichment layers, which can be very thin at the margin or thicker at a more central position.

Anatomically connected units or anatomically slightly disarticulated but correctly arranged units are usually comprised by extremities (e.g. Fig. 6.4.1 a-b). Bones are often arranged in anatomical correct order, but joints are not in situ (Fig. 6.4.1 a-b). Findings of this kind indicate that only ligaments were present at the time of deposition which indicates a rearrangement after decomposition in a dry environment. There is only one case of true articulation in mammals comprised by a spinal column of most probably a female suid of the species *Parachleuastochoerus steinheimensis* from the local stratigraphic level HAM 5 (Fig. 6.4.1 c), in which the cranium and extremities are missing. Furthermore, there is the nearly complete and articulated bird leg of the new goose species *Allgoviachen tortonica* (Aves, Anatidae) from the HAM 4 (Mayr et al. 2022). Finally, there are three articulated turtle shell finds among the reptiles of HAM 4 (Reptilia, Chelonia: adult *Chelydropsis* sp.; adult *Testudo* sp.; juvenile *Clemmysopsis* sp.).

In some cases, partial skeletons can be assumed and reconstructed by matching parameters of spatial find density and proximity and strewnfield orientation according to the reconstructed flow direction, as well as taxonomic and age-specific characteristics, while there is no bone duplication and thus no intermixing with other individuals of similar characters. These so-called strewnfields are sometimes very small (radius less than 2 metres), or can sometimes be reconstructed over many tens of metres (Böhme et al. 2019, Mayr et al. 2020b, 2022). A separate treatment of selected case studies can be found in the taphonomy section (see section 6.8).

Particularly noteworthy is the frequency of anatomically arranged units, which are usually located within a heterogeneous mixture of isolated individual finds. In general, such finds are not very easy to identify, resulting in only a few known cases from HAM 4. Especially the

lateral overbank extension of HAM 5, however, consists of a number of already in the field well distinguishable and identified strewnfields, which in relation to other channel areas were not so strongly reworked and elongated and not so heavily mixed with material transported from far away. Here, lower flow velocities or shorter time and rearrangement factor seem to have acted, which at the same time only affected the last of the three sedimentation phases of HAM 5.

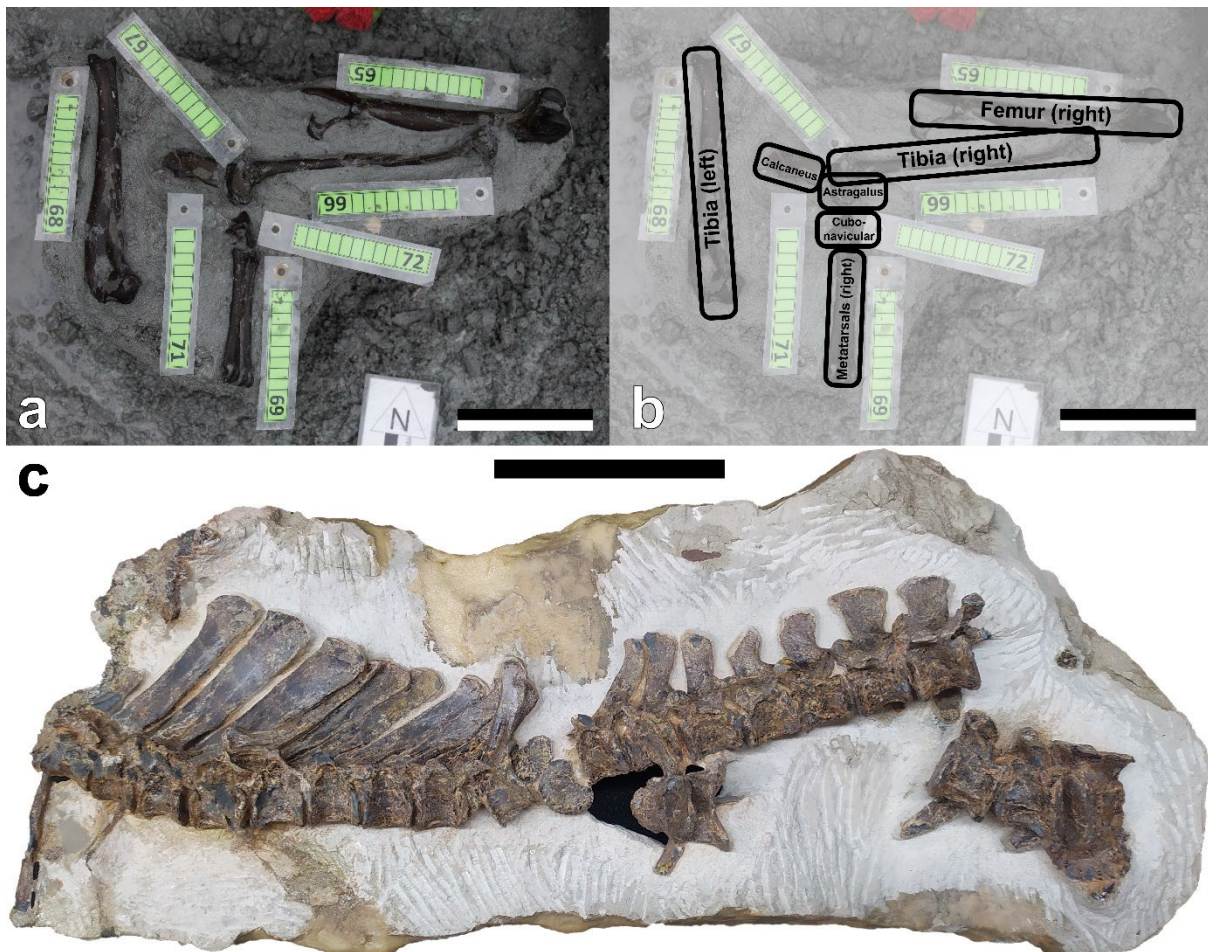


Figure 6.4.1. Examples of arranged or articulated mammalian skeletal finds from the early Late Miocene Hammerschmiede deposits and the local stratigraphic levels HAM 5 and HAM 4. (a-b) anatomically correctly arranged but not articulated hindlimb of the tragulid *Dorcatherium nauii* (GPIT/MA/18000) very probably belonging to a single individual, found at the southernmost excavated section HAM 4 2019-1. (a) Illustration of the find situation. (b) Superimposed labelling of the bone determination. Green number tag corresponds to the field inventory number range 14XX. (c) Spinal column probably of a female individual of the suid *Parachleuastochoerus steinheimensis* from HAM 5, the only mammal find from Hammerschmiede in which true articulation can be considered (GPIT/MA/10999). Scale bars equal 10 cm.

6.5 Reconstruction of flow direction

Several indicators can be used to determine the direction of flow of the palaeochannels. On the one hand, the erosional channels of both HAM 4 and HAM 5 deposits themselves and the distribution of finds within them give an indication of the direction and course of the flowing

waters. Furthermore, elongated objects and their orientation as well as the distribution patterns of originally connected skeletons of single individuals scattered by the water current (skeletal strewnfields) can be used to reconstruct orientation and flow direction of the actual fossil river.

The sediments of the HAM 4 channel are exposed at several places across the Hammerschmiede clay pit, what gives a good insight into the potential spatial channel course. The channel structure is exposed at the southern and northern edges of the pit (Fig. 6.1.1.1). In the central clay pit area and thus also the HAM 4 layer at this region, has been lost due to clay mining as well as larger sections of the eastern edge of the fossil river channel. The excavated and exposed areas of the HAM 4 channel base clearly show that the HAM 4 does not flow linearly at all, but can rather be described by a slightly meandering, S-shaped course, crossing the approximately 200 m width clay pit. This means, that flow direction reconstructions can only provide spatially focused, local results and do not have to apply to the entire HAM 4 area. Nevertheless, the main flow direction corresponds to a course from SSW to NNE due to the channel orientation and outcrop observations.

The erosive channel base was analysed as a further indication of a flow direction reconstruction. When digging for fossils, the channel fill is excavated and removed. Finally, the open channel base area (maximum erosion depth in the underlying clay) is measured with selected single points depending on the surface texture and a relief map is created (Figs. 6.1.2.3, 6.1.2.5, 6.1.2.7, 6.5.19). Based on the course of the deepest part of the channel and the dip of the channel margin, the course of the HAM 4 palaeochannel can be reconstructed (Fig. 6.5.1). It can be seen that in all excavated areas a section of a channel structure is visible, consisting of higher elevated margins and a deeper central area (Fig. 6.5.1). The difference in elevation and the eroded relief of the channel base was examined across the excavation areas of HAM 4 from the very south (HAM 4 South) to the northernmost area (HAM 4 North). The comparison of the points with the lowest elevation shows a difference of 2.1 metres (dipping to the North) between the southernmost and the northernmost excavation site (distance 135 metres; 1.55 % gradient). At first glance, this steep gradient within the HAM 4 channel over this length could indicate a flow direction to the north. A closer look at the Hammerschmiede profile, however, shows a slight tectonic dip of the profile by approximately 1.6% gradient (measured at the upper lignite seam) to the north, which roughly corresponds to the observation from the channel profile. This observation is therefore only of limited help in determining the actual direction of flow.

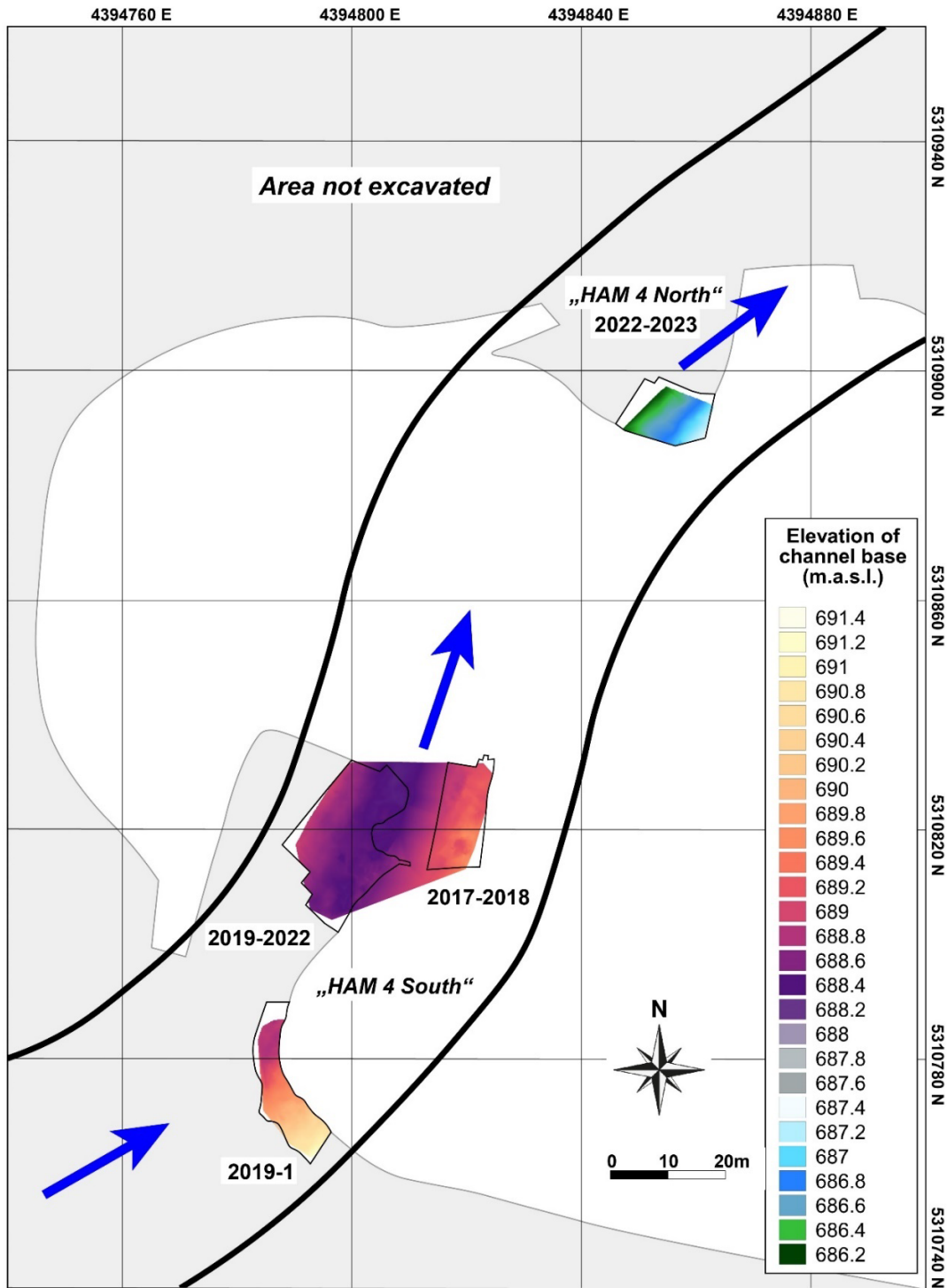


Figure 6.5.1. Relief map of the fossil river channel base elevation at the different excavation areas of the local stratigraphic level HAM 4 at the early Late Miocene Hammerschmiede fossil site. The map shows the maximum erosion depth of the HAM 4 channel based on measured points selected depending on the basement surface texture. Black polygons frame and combine neighbouring excavation areas HAM 4 2017 to 2023. The section between the areas HAM 4 2017-2018 and 2019-2022 has been lost due to clay mining and values for channel base elevation have been interpolated. Thick black lines indicate the assumed s-shaped meandering channel course based on outcrop observations of the channel structure. The reconstructed flow direction (blue arrows) is based on the course of the deepest channel base regions (darker colours) and the dip of the channel margin (brighter colours), supplemented by the orientation of elongated objects found. The channel base dips to the North (colour/scale change). The observed inclination matches the values observed in all Hammerschmiede sediments (approximately 1.6 % gradient to the North). Light grey colouring includes unexcavated areas and white areas have been lost due to clay mining. Coordinates correspond to Gauss-Krüger Zone 4 grid in metres. Grid spacing equals 40 metres.

At various locations in HAM 4, mass accumulations of freshwater pearl mussels of the species *Margaritifera flabellata* (Unionida, Margaritiferidae) were observed. Due to their elongated shape, an evaluation of the longitudinal axis orientation can be carried out to be used as a proxy for small-scale flow direction analyses. For this purpose, three mass accumulations of freshwater pearl mussels occurring in different areas of the HAM 4 were exposed and the individual shell orientations were documented (Fig. 6.5.2).

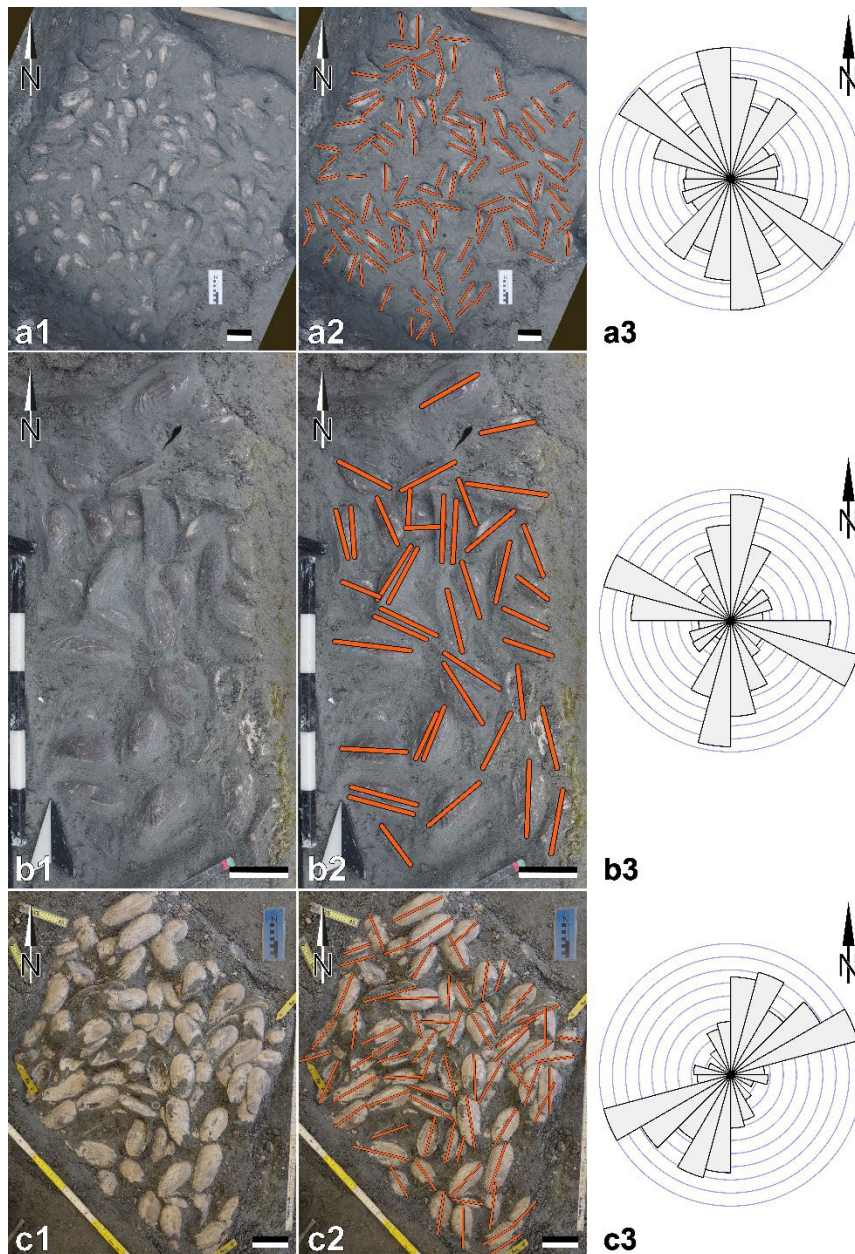


Figure 6.5.2. Mass accumulations of freshwater pearl mussels (*Margaritifera flabellata*) and longitudinal axis line direction histograms of the shells from the early Late Miocene Hammerschmiede deposits and the local stratigraphic level HAM 4. Freshwater pearl mussel beds were carefully uncovered at three different locations (a1, b2, c2) based on the orientation of the long axes of the individual shells (a2, b2, c2), line direction histograms were created (a3, b3, c3), indicating the prevailing flow direction during sedimentation. (a) Shell deposits from the central channel (HAM 4 2022-2; 119 orientations), (b) from the eastern channel margin at the central clay pit (HAM 4 2017; 41 orientations) and from the easternmost margin at the southernmost channel (HAM 4 2019-1; 70 orientations). All histograms show two main directions, which depending on the locality, merge somewhat diffusely (a3), show clear distinctions (b3) or converge strongly (c3). Scale bars equal 10 cm.

The long axis orientations were finally analysed in line direction histograms (Figs. 6.5.2 a3, b3, c3). It is particularly striking that the different survey areas yield different results, which is definitely an indication of different directional changes of the flow within HAM 4 channel and shows that such evaluations can always only apply to a specific small scale area. All three evaluations show two slightly different main directional distributions of the shell longitudinal axes. Following e.g. Voorhies (1969), Behrensmeyer (1990) or Lyman (1994) one direction possibly corresponds to the orientation of mussels that are turned longitudinally into the current and the other complies with bivalves "rolling" transverse to the current (Figs. 6.5.2 a3, b3, c3). It is noticeable that the angles vary between the prevailing directions which depending on the locality, merge somewhat diffusely (Fig. 6.5.2 a3), show clear distinctions (Fig. 6.5.2 b3) or converge strongly (Fig. 6.5.2 c3). One reason for this could possibly be the different river bottom positions, since two study areas are located in the still dipping margin area of the HAM 4 channel (Figs. 6.5.2 b3, c3) and one in the almost flat channel centre (Fig. 6.5.2 a3). The properties of the substrate and the different flow intensity due to the position certainly have an influence on the resulting shell orientation. Overall, the respective flow direction trends coincide with those suggested by channel-base morphology (compare Fig. 6.5.1).

Over slightly larger scales, several other long objects can be used in the HAM 4 for flow direction analyses (Fig. 6.5.3). A particularly good proxy for larger scale flow direction analyses are the often more than one metre long pieces of woods that are regularly found in HAM 4 sediments. Equally helpful are the numerous long bones, which are also recorded with their longitudinal orientation.

As longitudinal objects transported and deposited in fluvial environments changes in flow direction orientation must be assumed, and this analysis cannot simply be applied to the entire site, but must be subdivided into smaller study sections, so that changes in direction can be recognised. For this reason, in most of the excavation areas of HAM 4, a directional analysis of the long objects was carried out for a northern and a southern half of the areas (HAM 4 2017-2018, 2019-2, 2020-2023) or an east-west division was made (HAM 4 2019-1). As a result, the orientation trends indicated by line-direction histograms (Fig. 6.5.3) reproduce quite well the presumed S-shaped HAM 4 channel course from the geological observation (compare Fig. 6.1.2).

The proxies considered so far are more suitable for determining how the orientation of the flow could have proceeded. However, they are less suitable for determining the actual

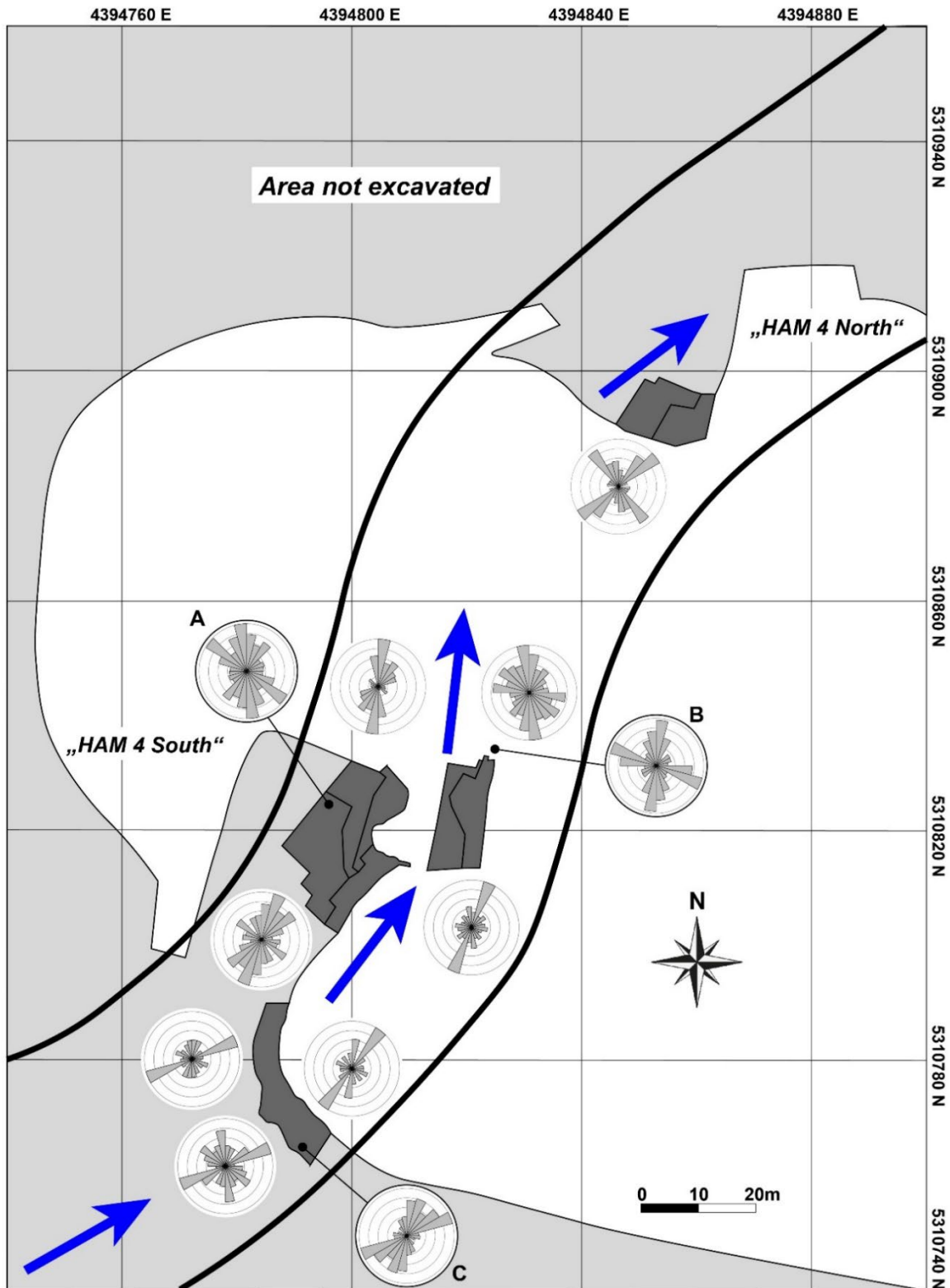


Figure 6.5.3. Line direction histograms from longitudinal objects (bones, wood and bivalves) at different locations of the excavation areas of the early Late Miocene Hammerschmiede deposits and the local stratigraphic level HAM 4. In order to be able to determine small scale changes in the flow direction of the HAM 4 channel, the excavation areas were analysed in several zones (approximate position of diagram near analysed area). The figure is supplemented by the line direction histograms of freshwater pearl mussels analysed in Fig. 6.5.2, localised within the HAM 4. Excavation areas in dark grey. Thick black lines indicate the assumed slightly S-shaped meandering channel course based on outcrop observations and blue arrows indicate the presumed and most likely direction (opposite direction also possible) of flow based on the orientation of long objects resulting from the line direction histograms. Light grey indicates unexcavated areas and white areas have been lost due to clay mining. Coordinates correspond to Gauss-Krüger Zone 4 grid in metres. Grid spacing equals 40 metres.

direction. From a theoretical point of view, a general flow direction from alpine direction in the south would be reasonable, but with such a flat and even landscape, it can be assumed that rivers and streams meander to a great extent and thus an apparent reversal of flow direction can also take place in river sections. To determine the actual direction of the water flow, bone strewnfields of distribution events of single vertebrate individuals can be used. The distribution of loose bones transported by currents follows specific patterns, which are determined by the bone properties of each bone type individually by parameters of surface area, weight and thus specific bone density. Furthermore, the bone shape itself can act like an anchor or promote rolling (Behrensmeyer 1975, 1988; Hanson 1980; Voorhies 1969). Particularly heavy and dense bones such as jaws and teeth, but also phalanges, should therefore lie more proximally, whereas vertebrae and ribs cover particularly distal strewnfield areas due to their less dense properties, which in some cases even extend to floating (Behrensmeyer 1975, 1988; Hanson 1980; Voorhies 1969). The longer a skeleton is exposed to currents, the exponentially longer the corresponding distribution area will be and the better the sorting (Behrensmeyer 1975, 1988; Hanson 1980; Voorhies 1969). In the present case, it appears that these arrangements found in the experimental tests (Behrensmeyer 1975, 1988; Voorhies 1969) can presumably be influenced by physical properties of the river bottom and the sediment contained therein and may differ from the known patterns.

In the case of two *Dorcatherium navi* (Artiodactyla, Tragulidae) skeletons, it is evident that, in addition to the cranial elements and some limb bones, large portions of the ribs have remained in place, while the vertebrae, with a few exceptions, are missing (details see section 6.8). If a carcass can decompose in the and all bones disarticulate, the flat ribs, which are characterised by a large bone surface, can adhere to the ground, while the vertebrae, for example, have a rather bulky three-dimensional shape, which is certainly easier to roll out of the arrangement and transport away with less contact with the ground. This gets possible due to the fact, that the Hammerschmiede rivers were very muddy (silt and clay) due to the lack of coarse grains (no boulders). Most actuopalaeontological taphonomy studies are tested on rivers with other bottom conditions (Behrensmeyer 1975; Voorhies 1969). In addition, a carcass settled on the bottom that is exposed to slowly increasing velocity of the flow is rarely considered. Thus, for example, certain areas may be exposed, excavated and transported downstream while others may be trapped by the sediments encountered.

6.6 Postgenetic processes

6.6.1 Mineral neoformation and Uranium incorporation

Postgenetic processes have affected the fossils of the Hammerschmiede for millions of years. The bone colours have changed due to permineralisation and mostly show brownish to black, in the weathered oxic area reddish and yellowish colours. In most cases, these colours are probably due to the deposition of manganese- or iron-oxides and iron-hydroxides or iron-sulphides like pyrite. Uncompressed bones (especially diaphyses of long bones or phalanges) from the HAM 4 level sometimes show pyrite mineralisation in the bone cavity if the bone breaks when it is found and provides an insight (Fig. 6.6.1 a-b). In the HAM 4 sands, iron sulphide (pyrite?) framboids of a few millimetres in diameter, can be observed, which most probably prove a postdepositional authigenic genesis, as they are found isolated in the sediment and envelop the surrounding sand (Fig. 6.6.1 c).

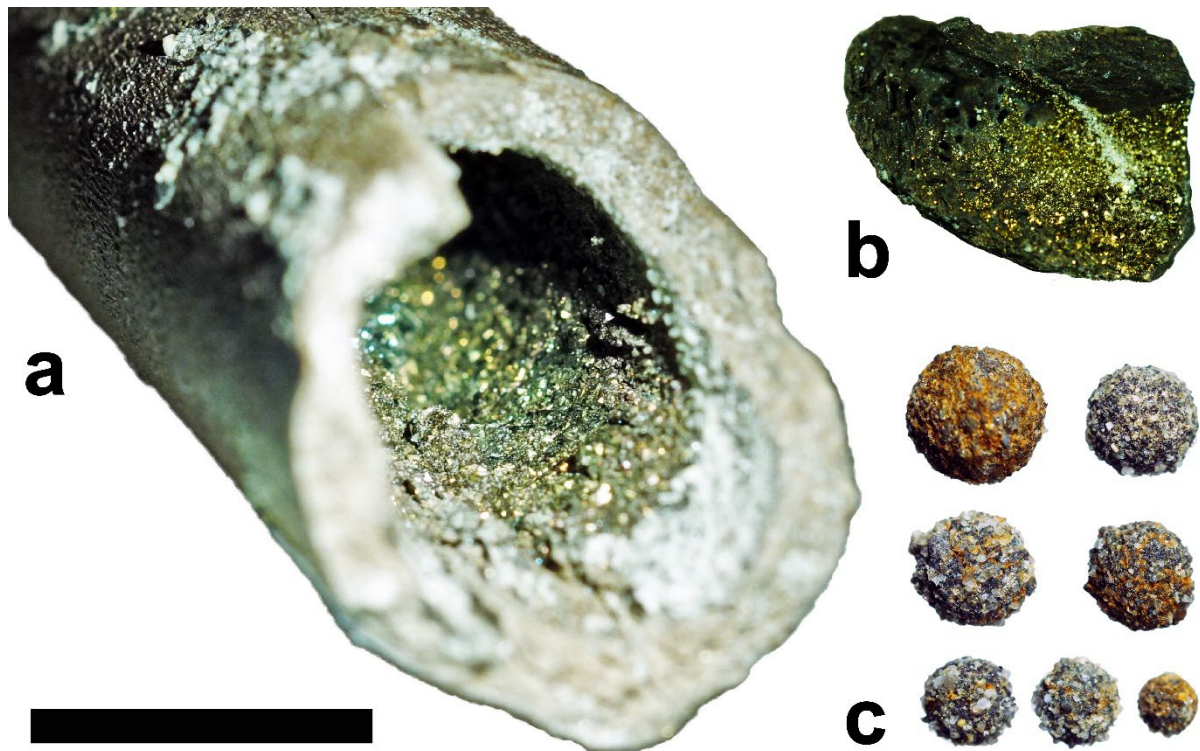


Figure 6.6.1. Mineralisations from the early Late Miocene Hammerschmiede fossil site and the local stratigraphic level HAM 4. (a-b) Authigenic mineral formation of iron sulphide (pyrite) within the cavities of vertebrate bones. (a) View into a femur diaphysis from the tragulid *Dorcatherium nawi* with idiomorphic pyrite mineralisations. (b) Bone fragment with a view of the cavity surface with pyrite coverage. (c) authigenic pyrite framboids from the silty fine-sand sediments of the HAM 4 channel fill. Scale bar equals 10 mm.

Furthermore, bones from the local stratigraphic Hammerschmiede levels HAM 5 and HAM 4 emit slight radioactive radiations produced by incorporations of mostly uranium isotopes into the bones (Albrecht pers. comm. 2017). Hitherto unpublished investigations have shown that the bones of HAM 5 exhibit a significantly higher enrichment of uranium isotopes than those

of HAM 4. It could be assumed that the uranium enrichment was introduced over a post-depositional diagenetic period, e.g. via the groundwaters, and is possibly due to the substitutional capability of uranyl (UO_2^{2+}) and calcium ions (Ca^{2+}) in the apatite of the bone. Uranium contents show a fluctuation of 0-3200 ppm (Albrecht pers. comm. 2017).

These partly high contents of iron sulphides and uranium in HAM 4 and HAM 5 indicate a strong redox potential within the sediments. As the fluvial channels HAM 5 and HAM 4 are regarded as well ventilated (rich in oxygen) by the observed faunal elements (e.g. fishes, freshwater pearl mussels, traces of ephemeropteran larvae), post-sedimentary processes remain causative for these anoxic mineral neoformations. Wang et al (2020) provide decisive indications in this regard, which point primarily to the sediment composition in terms of grain size as the cause of this. In coarse-grained river bed sediments, water is also transported through the already deposited sediments. In order to create anoxic redox conditions within the bottom sediments, this water exchange has to be limited (Wang et al. 2020). In particular, the high content of silt and clay ("siltation") reduces the permeability and thus the oxygen supply through and into the channel sediments and furthermore provides redox conditions for iron- or sulphate-reduction and thus also for the precipitation of uranium (Wang et al. 2020). The high silt and clay contents of HAM 5 and HAM 4 deposits are probably responsible for the reductive milieu in the sediments that presumably established shortly after deposition.

6.6.2 Compaction

Several postgenetic processes are responsible for preservability of the different types of material found at the Hammerschmiede site. One of the strongest postgenetic processes is the diagenetic compaction of the sediments mainly caused by the overburden loading (Fig. 6.6.2).

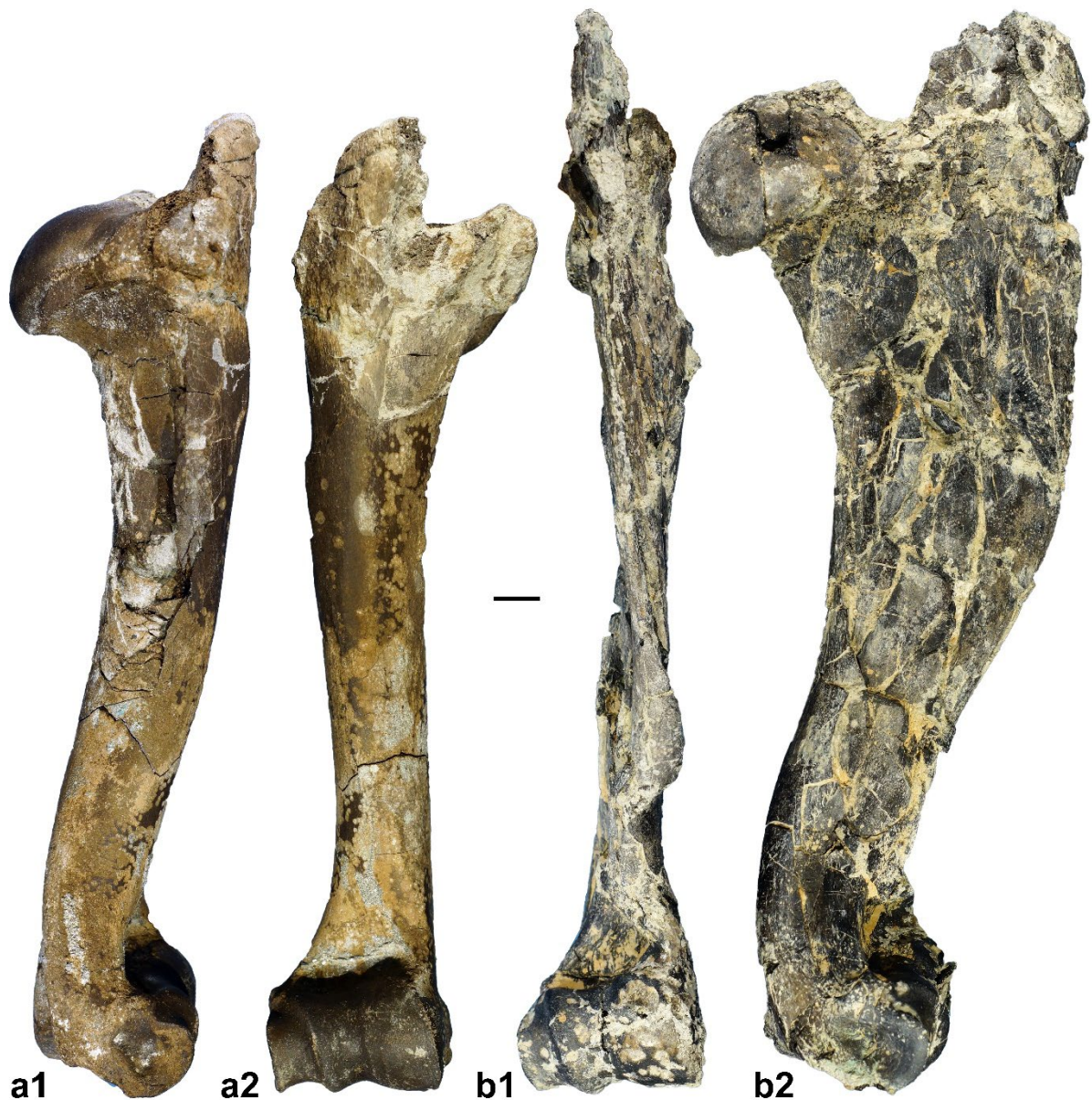


Figure 6.6.2. Different preservation conditions between the local stratigraphic levels HAM 5 and HAM 4 at the early Late Miocene Hammerschmiede site. (a-b) Two humeri of the antelope species *Miotragocerus monacensis* from the two different local stratigraphic levels HAM 4 (a) and HAM 5 (b) in lateral (a1, b2) and cranial (a2, b1) views. Note that the joints of the two bones shown indicate a humerus of nearly the same size. While the HAM 4 humerus (a) is preserved almost intact in 3D, the HAM 5 humerus diaphysis has undergone extreme medio-lateral compression resulting in significant lengthening (proximo-distal and cranio-caudal) while the distal joint itself is well preserved. (a) SNSB-BSPG 2020 XCIV-7776; (b) SNSB-BSPG 2020 XCV-480. Scale bar equals 10 mm.

This compaction is mainly based on the reduction of pore space through grain reorientation and water expulsion (e.g. Ulmer-Scholle et al. 2015), especially of the clayey sediments, and is thus partly responsible for bone compression found at the Hammerschmiede deposits (Fig. 6.6.2).

The sediments of the local stratigraphic level HAM 4 consist mainly of fine sands, which were already much more compacted when deposited and thus did not compress the bones much when further sediment load was deposited (Fig. 6.6.2 a). Consequently, the clay rich sediments of HAM 5 are particularly more affected by this type of compaction than the sandy HAM 4

sediments due to the higher compressibility. The deposits of the HAM 5 rivulet are clearly more heterogeneous and especially a layer in the western lateral channel shows a basal, very fine-grained and greasy clay layer, which obviously allowed a strong post-sedimentary compression, whereby some bones were literally rolled out and sometimes only the joints were preserved in their original three-dimensional shape (Fig. 6.6.2 b). Erosion (e.g. glaciers during the Pleistocene) removed a considerably high amount of overburden. At present, there is no estimate of the actual lack of sedimentary overlay at this locality, but approaches, especially concerning the rank of coalification (vitrinite-reflectance), could clarify this in the future. Since the observed rank of coalification is placed somewhere between lignite or bright coal rank, the assumed sediment cover was probably not insignificant. The Miocene Hammerschmiede section is overlain by several metres thick glacial till deposits of Middle Pleistocene age (Riss glaciation) (Kirscher et al. 2016). Consequently, loads by Pleistocene glaciers must be expected, which could also have contributed to the compaction. And last but not least, it is the large construction machines without which it would not be possible to reach the fossil layers. Particularly when exposing the strata, it cannot always be ruled out that the heavy weight of the excavators shears and compacts the underlying sediments, especially when there is no lateral sedimentary support due to the mining slopes. Especially the heavy compression and shearing of several bones found in a very greasy, only a few cm thick clay layer in the lateral overbank extension of the HAM 5 was most probably caused by the heavy machines (Fig. 6.6.2 b). In the same area of HAM 5, in 2018 a slipping tailing pile also sheared a not inconsiderable area of the discovery layer. Finally, there are the workers and palaeontologists themselves, who of course can cause damage to the finds in the form of mechanical fractures and displacements. The very sandy and silt-rich deposits of HAM 4 show significantly less susceptibility to these recent pressures. Bones were recovered only a few centimetres below the excavator trackway, which left the internal cavity of the shaft intact. In most cases, any compressive damage that occurs affects the bottom side of bones, which has collapsed. This possibly is caused by a historical ground failure of the surrounding sediments due to most probably very high lithostatic overburden pressures during diagenesis, as fragments are stabilised by mineralisation (Fig. 6.6.3).

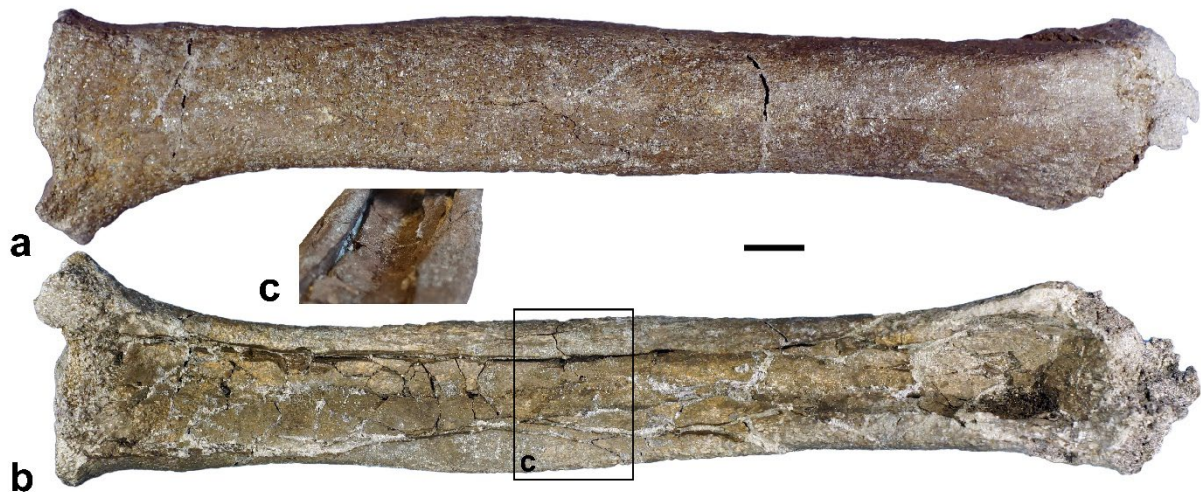


Figure 6.6.3. Compressive damage caused by diagenetic overburden pressures at the early Late Miocene Hammerschmiede fossil site and the local stratigraphic level HAM 4. (a-c) Radius of the bovid antelope *Miotragocerus monacensis* with for the HAM 4 typically impressed bottom side of the bone. (a) Anterior view of the radius, which pointed upwards at the discovery situation. (b) Posterior side of the radius, which in situ pointed downwards to the channel base. (c) Detailed view of the bottom side of the bone, which has been massively imprinted, while the top side remained intact. Scale bar equals 10 mm.

6.7 Case studies in strewnfield reconstructions

The deposits of the Hammerschmiede site include a large number of isolated finds, whose relationship to each other cannot be reconstructed at the moment. Among these objects, which were presumably repeatedly rearranged over long distances, there are nevertheless arrangements of bones that can be grouped together as one and the same individual on the basis of their taxonomic and age-specific identity as well as taphonomic parameters. The more excavation data are generated, the more case studies of partially articulated or disarticulated skeletal strewnfields become evident. In several studies, some of these examples were already described in more detail (Böhme et al. 2019; Konidaris et al. 2023; Mayr et al. 2020b, 2022). These include, as one of the most famous examples, the scattered remains of a male ape of the newly discovered ape species *Danuvius guggenmosi* at the site in addition to several remains of juveniles and females (strewnfield length 30 metres; Böhme et al. 2019). Due to its taxonomic particularity, this example is also discussed again in more detail here. Disarticulated avian bones of a darter — *Anhinga pannonica* (strewnfield length 10 metres; Mayr et al. 2020b), the articulated leg of a new tree goose — *Allgoviachen tortonica* (articulated leg; Mayr et al. 2022), bones of the right wing region of a very small dabbling duck — *Mioquerquedula* sp. (strewnfield length 10 metres; Mayr et al. 2022) have already been described in case studies and are not explained here again. The following will focus on a few cases that have not yet been published or that can be examined in more detail. The final evaluation of the countless single

finds is not yet complete and will certainly yield further surprises and evidence of correlations in future research.

6.7.1 Case study I: HAM 5 – *Danuvius guggenmosi* – The great apes from HAM 5

The new great ape species *Danuvius guggenmosi* is probably one of the most famous finds unearthed at the Hammerschmiede fossil site. The corresponding specimens were not found as an articulated skeleton, but represent reconstructed skeletal strewnfields over a distance of 30 metres length (Fig. 6.7.1).

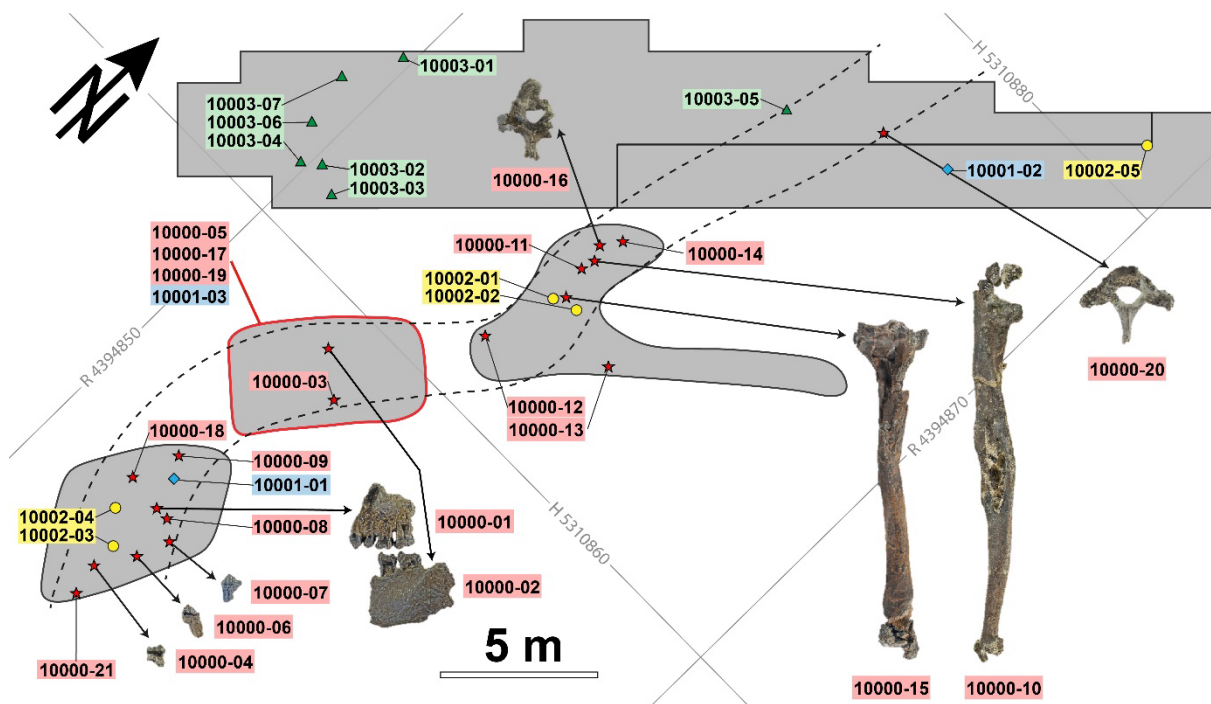


Figure 6.7.1. Excavation plan with localized *Danuvius guggenmosi* specimens at the early Late Miocene Hammerschmiede deposits. Excavated areas of the local stratigraphic level HAM 5 coloured in grey (excavation years 2015-2018). Intermediate regions represent material loss due to clay mining. Dashed lines indicate the supposed thalweg course of the palaeochannel. The Different colours and symbols indicate assumed different *Danuvius* individuals: Supposed adult male individual (Holotype; GPIT/MA/10000; red stars); Female 1 (Paratype; GPIT/MA/10001; blue diamonds); Juvenile individual (Paratype; GPIT/MA/10002; yellow circles); Female 2 (Paratype, GPIT/MA/10003, green triangles). The area outlined in red shows the sediments removed and stored separately, which were later processed and screen washed. To avoid mining-induced losses of specimens an imprecise localization of finds was accepted. Selected objects from the holotype and the most important strewnfield of the *Danuvius* finds were depicted according to their point of discovery. Coordinates correspond to Gauss-Krüger Zone 4 grid. Grid spacing equals 20 metres. Figure supplemented and revised based on Böhme et al. (2019): Extended Data Fig. 1.

For the taphonomic investigations of the Hammerschmiede sediments, a male *Danuvius* individual was one of the first and most important proofs that single specimens from the polyspecific bone accumulations of the fluvial Hammerschmiede deposits can be combined and reconstructed to individuals even over such large distances. The arguments for assigning some of these bones to a single individual are based on correspondences in age- and size-

specific characteristics but also on pathological consensus. Furthermore, the geospatial distribution of the bones and their arrangement within the suspected strewnfield of the reconstructed stream course of the HAM 5 rivulet plays a crucial role in this assignment. Due to individual density and surface properties of each skeletal object, the transportation and depositional characteristics differ decisively (Behrensmeyer 1975, 1988; Hanson 1980; Voorhies 1969). In the case of the male *Danuvius*, one of the crucial pieces of evidence that the bones belonged to one and the same individual is that the upper and lower jaws occlude perfectly. Since dental wear indicates a mature individual, the likelihood of this observation being a coincidence is reduced.

Furthermore, within the reconstructed strewnfield no duplicate skeletal elements were found. As with recent great apes, the hominid finds from the Hammerschmiede show a similar size difference, with the present case corresponding to a male, while other finds are attributed to juveniles and females. Finally, the arrangement of the bones within the rivulet deposits of HAM 5 correspond fairly closely to the classical sorting by different bone properties (Behrensmeyer 1975; Voorhies 1969), which begins with the most dens elements such as teeth and jaws, through long bones, and finally (if still present at all) vertebrae and ribs (there are no ribs present in the case at hand) (Fig. 6.7.1). The vertebrae specimens, which are particularly important for the functional morphological interpretation of this new great ape species, indicate that the origin of the carcass and the transport distance cannot be too large and probably lay in the area of the tooth finds, since vertebrae tend to be easily transported very far away due to their low density and voluminous appearance, which above certain flow velocities even allows flotation in the water body (Behrensmeyer 1975; Hanson 1980; Voorhies 1969).

6.7.2 Case study II: HAM 5 – Lateral overbank extension

The previously described bony strewnfield of a male *Danuvius guggenmosi* originates from the deeper main channel of the HAM 5. It was not until 2018, passing over a slight ridge of elevation in the channel base, which was originally thought to be the channel margin, that a connected side channel was discovered in parallel to the west of this main channel. This side channel more resembles a lateral overbank extension of the HAM 5 and reaches only about half the depth of the main channel itself and probably correlates only with the third and final sedimentation phase to the main channel. In this area, it was possible to excavate fully to the actual western slope and edge of the HAM 5 channel from 2018 to 2022 and to document and measure all finds. In contrast to the main channel, this secondary section shows much less

heterogeneity within the channel fill and fossil content. There were hardly any fin spines of catfish found and also turtle findings are much rarer, which characterize the classic enrichment layer of the HAM 5 main channel. This tends to suggest that this side area does not represent the permanently flooded channel, but rather a lateral overbank extension. Likewise, the vertebrate fill shows what appears to be a much less reworked fossil content that can be attributed to a few single individuals of different mammalian species, which will be discussed in more detail in the following. The channel bottom in the mentioned area is particularly heterogeneous and characterised by small depressions and minor elevated regions. Some of these depressions in the fossil river bottom seem to have acted as fossil traps and have accumulated particularly many bones.

In the present case study of the western HAM 5 channel area, several overlapping assumed skeletal strewnfields are to be evaluated in parallel. The selected cases are the best and most conspicuous bone accumulations, which are assigned to single individuals. Certainly, a more detailed evaluation will be able to reveal further skeletal strewnfields in this area. In the following the dispersed skeletons of a juvenile *Deinotherium*, an antelope, a large beaver, a large feliform and two tragulids will be examined in more detail and shall exemplify the enormous proximity and overlap of skeletal individuals in this area.

One of the most conspicuous skeletal strewnfields consists of 24 elements, all belonging to a juvenile (deciduous dentition) *Deinotherium levius*, which were found over a length of eight metres in the western part of the western overbank extension of the HAM 5 channel (Fig. 6.7.2). Konidaris et al. (2023) described and mapped this find taxonomically and discussed the corresponding taphonomy in more detail. The find contains the mandible, several deciduous teeth, skull fragments, two long bones, the pubis, and 14 ribs. A large number of ribs in particular was excavated in the basal area of a deeper longitudinal erosional channel base depression, which could represent a bone trap in which the fossils were deposited in the flow shadow (Konidaris et al. 2023). The rarity of proboscidean bones in the Hammerschmiede deposits at all, the integrity in taxonomy and life age, the taphonomic distribution of finds, and the absence of duplicate elements in this case support the assignment of these specimens to one and the same individual (Konidaris et al. 2023). The arrangement of the finds with the objects of higher density, teeth and mandibles in the southernmost direction and other bones further north, supports and confirms the flow direction from the south already assumed in other studies (e.g. Böhme et al. 2019).

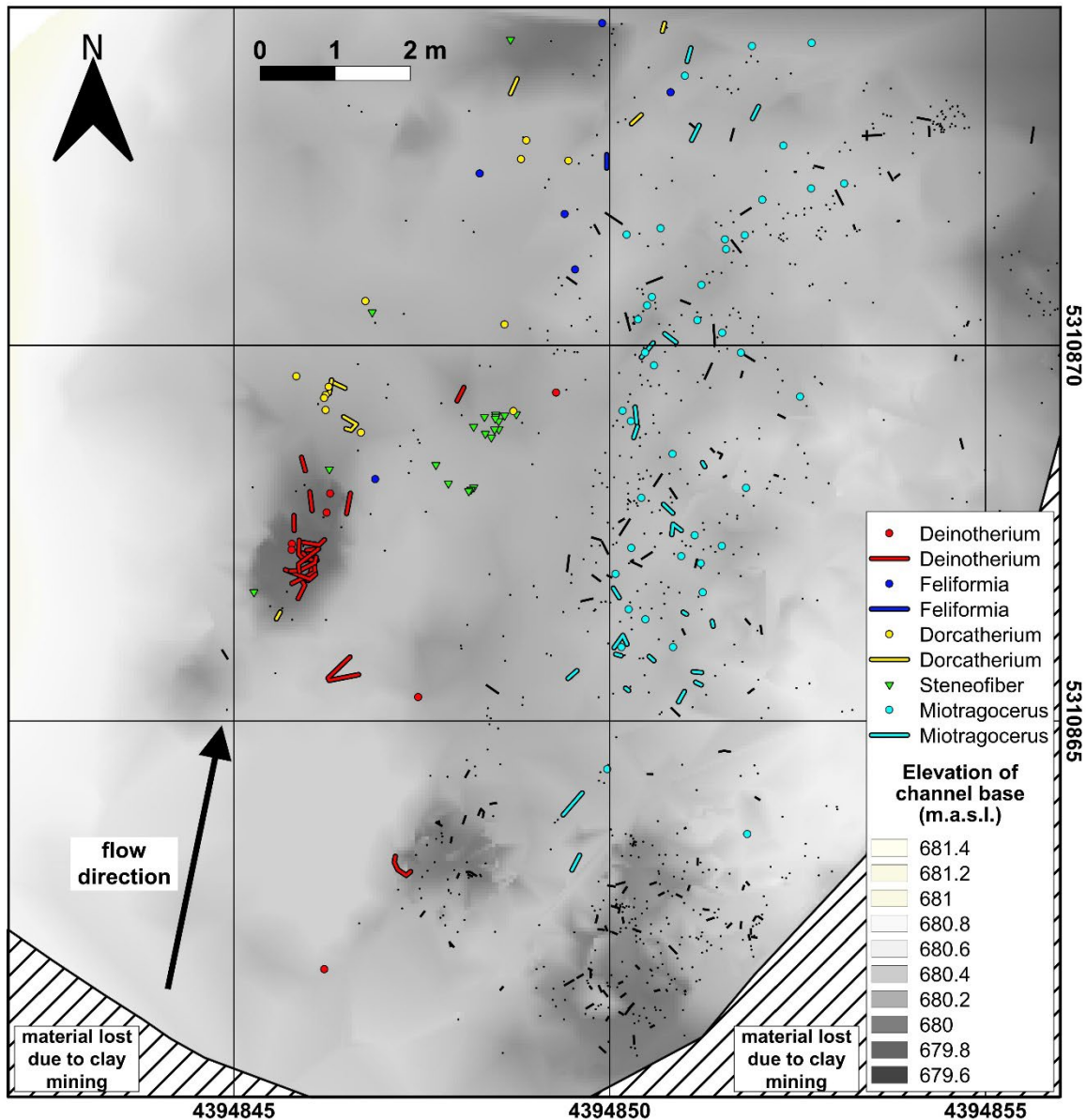


Figure 6.7.2. Distribution of finds in the western excavation plan section of the local stratigraphic level HAM 5 at the early Late Miocene Hammerschmiede fossil site. The shown section comprises the lateral overbank extension of the western HAM 5 channel excavated during the years 2018–2021. Black dots represent vertebrate fossil specimens, black lines denote elongated objects (long bones) and their orientation. Shaded areas have been lost to clay mining. The background colour indicates the differences in altitude of the excavated palaeochannel base. Dark colours represent lower and brighter ones higher elevations, with a total elevation difference of 1.5 m (finds only in the lowermost 70 cm). Note how the specimen density partly corresponds to the uneven channel base, which probably acted as bone traps in pool-like structures. Five skeletal strewnfields (including one double strewnfield) of potential single individuals are shown in coloured symbols: a juvenile *Deinotherium levius* (24 elements; red circles and lines); a larger feliform carnivore (seven elements; dark blue circles and lines); presumably two adult tragulids (*Dorcatherium navi*) (double strewnfield; 20 elements; yellow circles and lines); a large beaver (*Steneofiber depereti*) (29 elements; green triangles) and a boselaphin antelope (*Miotragocerus monacensis*) (64 elements; light blue circles and lines). Black arrow indicates the assumed flow direction of the palaeochannel and refers to long bone orientations, the channel morphology and the extension of the presumed skeletal strewnfields. Coordinates correspond to Gauss-Kruger Zone 4 grid in metres. Grid spacing equals 5 metres.

In the same westernmost HAM 5 area lies a somewhat more difficult to interpret distribution of bones. Over a length of (so far) 9.5 metres a strewnfield of bones extends, which belong to

two adult tragulids (some duplicate elements) of the species *Dorcatherium nauti* (Fig. 6.7.2). In the southern range, the high density of finds with a partially articulated hind leg and skull find most likely delineates a single individual. However, since at the northernmost excavated region another *Dorcatherium* skull find, representing nearly the same dental wear and life age, including both mandibles possibly indicates the beginning of a second strewnfield of a *Dorcatherium* individual. Especially the transitional area of the two skeleton distributions cannot be clearly delimited and an overlap of both strewnfields seems certain. At the moment, a more precise separation of the two strewnfields is not possible and the find complex remains unresolved as double-strewnfield. Beyond that, however, there is nothing to suggest that there is another adult *Dorcatherium* in this area. Even if a final separation is currently not possible, the distribution pattern of the *Dorcatherium* double-strewnfield fits very well with the general observations within the lateral overbank extension of HAM 5. The finds, like those of the other strewnfields from this area, are distributed in the assumed flow direction from southern direction. Bones of higher density such as long bones and cranial elements tend to remain in more southern spots, while lighter parts are transported to more northerly regions or distant regions (Behrensmeyer 1975, 1988; Hanson 1980; Voorhies 1969).

Likewise, in the western half of this lateral HAM 5 area there is a massive accumulation of bones, all of which can be taxonomically assigned to the large beaver species *Steneofiber depereti* (Fig. 6.7.2). There are 25 bones from the hind limbs and from the forelimbs, which, including a few vertebrae, suggest an original carcass position of one adult beaver on an area measuring only a little more than one square metre. At the westernmost edge of this lateral HAM 5 overbank extension four more beaver bones were found, which can also be assigned to this individual with high probability due to their assumed life age (adult), the absence of duplicate elements and the same bone size and proportions (e.g. left and right astragalus). The arrangement of all 29 specimens follows a similar longitudinal pattern (south-north), as already observed by the previously described strewnfields. A special feature of this find is that there is not a single rib find in the area and cranial elements that could be attributed to this individual are also missing. This and also the position of some bones further west could indicate that the initial carcass position was further south, outside the excavation area, as the cranial elements in particular should not be transported so easily due to their higher density (Behrensmeyer 1975, 1988; Hanson 1980; Voorhies 1969).

Seven isolated bones of a large adult carnivore were found dispersed very widely across the western half of the lateral overbank extension of HAM 5, which so far can taxonomically be

assigned to a feliform carnivore (Fig. 6.7.2). Due to the rarity of postcranial elements of large carnivores, the appropriate size and proportion, taxonomic classification and the lack of duplicate elements, it can be assumed that this is the strewnfield of only one individual. The seven elements were found isolated and widely scattered over a distance of 12 metres (north-southern extent) and mainly comprise limb elements. The isolated location of the specimens and the wide dispersion indicate a somewhat longer transportation route (Behrensmeyer 1975, 1988; Hanson 1980; Voorhies 1969). No direction of origin can be deduced from this find, but the strewnfield orientation in a south-north direction is consistent with the other strewnfields already observed at this area.

One of the probably most extensive bone distributions is located in the eastern part of the lateral overbank extension of HAM 5. 64 objects have already been found over a distance of 21 metres, which, are probably resemble a single individual of an adult antelope of the species *Miotragocerus monacensis* (Fig. 6.7.2). The corresponding skull find of this case study was already described by Hartung et al. (2020). The assignment of the specimens is performed on the basis of taxonomic classification, bone sizes and proportions and also no bone duplication (based on bone preservation and life age) is present. The bone preservation itself shows a tendency towards severe compression and flattening of many bones due to its location in a rather compressive thin and ductile clay layer (see Fig. 6.6.2 b). Particularly dense bones (long bones) and the cranial elements (skull fragments and lower jaws) are distributed within the southern third, while smaller bones like vertebrae or ribs are scattered over a greater distance to the north. According to this arrangement, which is typical for skeletal strewnfields, a transport direction to the north and an initial deposition of the carcasses at a southern position seems very certain (Behrensmeyer 1975, 1988; Hanson 1980; Voorhies 1969).

6.7.3 Case study III: HAM 4 – *Parachleuastochoerus steinheimensis*

In the HAM 4 excavation area of the years 2017 and 2018, the very well preserved skull of a juvenile (deciduous dentition) suid of the species *Parachleuastochoerus steinheimensis* was discovered. Within one metre of radius to the cranium, a mandible and various isolated teeth were found, which correspond to the missing tooth positions and fit into the alveoli. Based on concordant taxonomy, tooth wear, stage of tooth eruption and the absence of duplicate elements all of these objects are assigned to one and the same individual. The cranial finds were all located on an inclining layer of reworked sediments (pedogenic carbonate concretions) underlain by north-dipping, cross-bedded fine sands with the highest elevated finds about 40

cm above the channel base and the deepest on the base itself. Since these specimens indicate a connection over larger altitudinal differences, a special taphonomic significance persists. In the further southern excavation area additional postcranial objects were recovered, which probably also belong to the same individual complex. Just a few centimetres south of the skull discovery, an arrangement of four successive rib positions of the left body side were found in anatomically correct arrangement. Over the remaining excavation area, another 14 scattered ribs were found, all of which fit the juvenile suid in size, age and preservation.

Morphologically, all ribs of anterior and medial thoracic regions share a small additional process below the capitulum, which possibly occurs exclusively in suids or even in the species of *Parachleuastochoerus steinheimensis*. At least there is no other mammal from the Hammerschmiede deposits identified with this feature. In some distance to the south, the articulated left ulna and radius (GPIT/MA/16642) as well as a right ulna (GPIT/MA/16641) (Fig. 6.7.3). All findings correspond to a small, juvenile suid, suitable for a young female (small size, lack of epiphyses or unfused epiphyseal joints). More than 13 metres to the south of the cranial finds, a scapula (GPIT/MA/16625) and two articulated ribs (GPIT/MA/16635) mark the most distant find positions. Unfortunately, the continuing area was lost due to clay mining until excavations could continue, whereby it remains unclear whether there would have been further finds farther to the south. The described finds resemble the first recognised skeletal strewnfield of the eastern edge of the HAM 4 channel. The suid strewnfield shows, that the HAM 4 channel fill is very heterogenous and a fine stratigraphic differentiation of finds and the level at which they were found cannot exclude the possibility of a connection. The explicit altitude of a find is neither a proof nor a criterion for exclusion of a relationship of finds. In this case, it is assumed that the rather long strewnfield includes finds made about one metre above base with finds made on the base itself. Although the scatter of objects shows a quite high lateral dispersion, a single individual is assumed. Over the whole area no taxonomic object duplications exist with similar parameters of preservation, animal life age and even within 18 rib finds no duplication can be recognised. The excellent bone quality of all specimens assigned to this juvenile suid individual indicates a late entry of the carcass into the sediments, shortly before a final burial took place. The present case study is one of the most extensive strewnfields of the HAM 4 level (length of 15 metres).

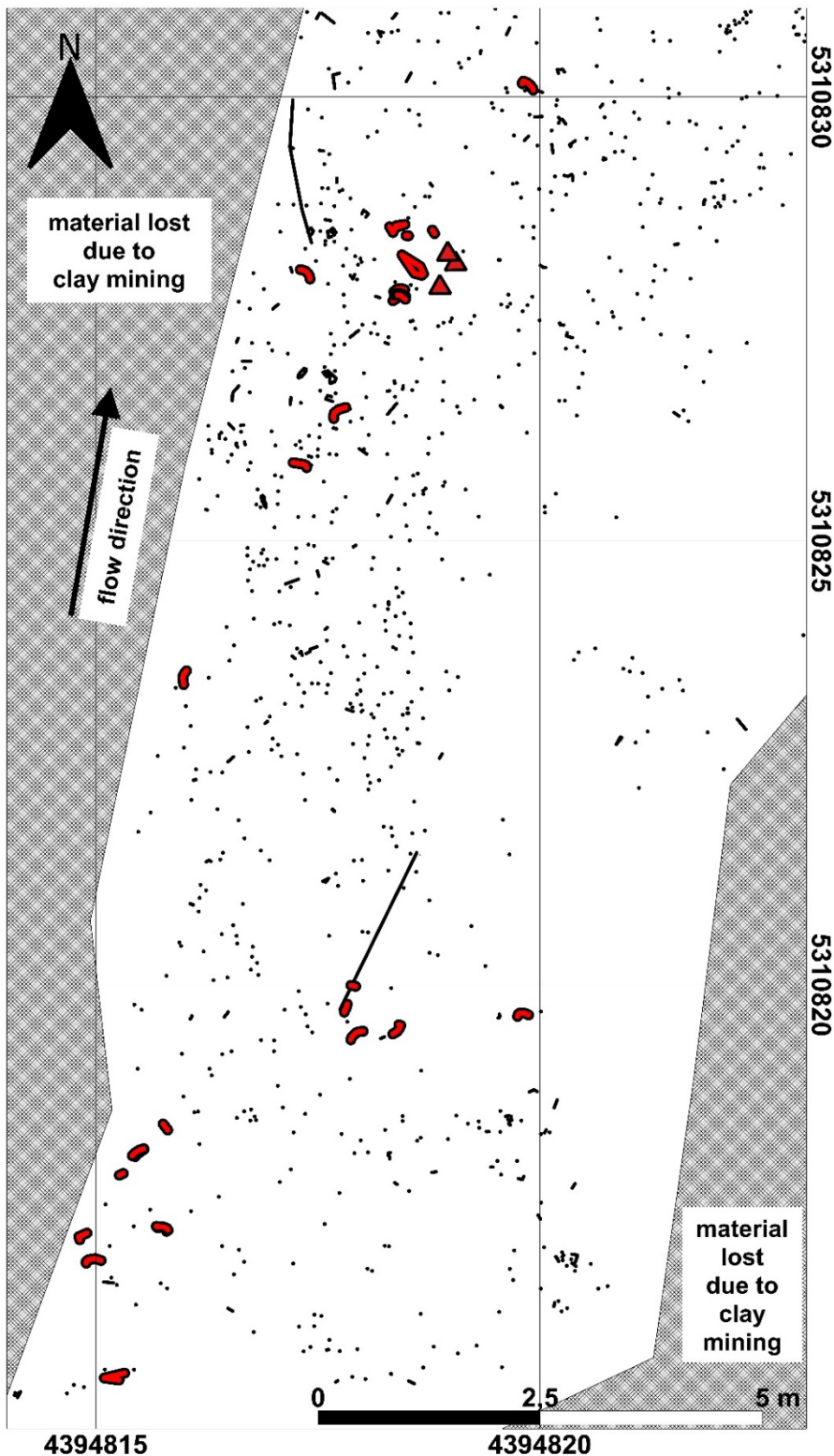


Figure 6.7.3. Section of the excavation plan of the local stratigraphic level HAM 4 at the early Late Miocene Hammerschmiede fossil site. The shown area comprises the lateral eastern margin of the HAM 4 channel excavated during the years 2017-2018. Black dots represent vertebrate fossil specimens, black lines denote elongated objects (the longest of these represent wood finds) and their orientation. Shaded areas have been lost due to clay mining. Excavated suid remains (30 specimens), most probably belonging to the same juvenile, female *Parachleuastochoerus steinheimensis* individual, are highlighted with red triangles, lines and outlines (skull). Associated bones (limb bones and mostly ribs) are arranged over a distance of 16 metres parallel to the reconstructed flow direction (black arrow). An enrichment of cranial elements (skull with mandible and associated isolated teeth) as well as partially articulated/arranged ribs is found in the northern strewnfield area. Coordinates correspond to Gauss-Kruger Zone 4 grid in metres. Grid spacing equals 5 metres.

The strewnfield is located on the eastern outer edge of an assumed left bend of the HAM 4 river course. Based on the order of arrangement and referring to taphonomic experiments and observations by Voorhies (1969), Behrensmeyer (1975, 1988) and Hanson (1980), the close proximity of cranial and thus particularly dense and heavy components and the dispersion of the less dense Bones (e.g. ribs) on the first view indicates a direction of dispersion and transport from north to south. Nevertheless, the flow direction for HAM 4 is assumed to be from the south via many other parameters and observations. However, the fact that the southern finds are located higher in elevation than the northern ones and above all that the skull itself was found on a foreset inclined to the north contradict a flow direction from the north. Many analyses indicate that a general flow direction of the HAM 4 river from the south must be assumed. Finally, there is a plausible explanation for the observed distribution. As later case studies will highlight, especially ribs in the case of the Hammerschmiede deposits do not behave as the classical experiments of Behrensmeyer (1975) and Voorhies (1969) show. The fine sediments probably tend to keep these flat and light bones sucked to the bottom and especially voluminous objects are better transported because these provide greater leverage and attack surfaces to be pulled out of the soft ground. Something like this could have occurred in the case of the suid individual. However, it is important to note that the cranial elements of the animal may have been held together by possibly desiccated soft tissue, which probably means a partial draining of the flow channel with a low water level of the HAM 4 river so that the semi-decomposed carcass could desiccate and the final decomposition took place at the further and final location of deposition. This would also explain why only dislocated teeth were found in the direct surrounding of the skull. Finally, the strewnfield of the juvenile female suid *Parachleuastochoerus steinheimensis* is a particularly interesting case study which contributes to a better understanding of HAM 4 taphonomy.

6.7.4 Case study IV: HAM 4 – *Dorcatherium nauti*

The tragulid *Dorcatherium nauti* represents one of the most abundant mammal finds of the Hammerschmiede deposits. Since finds of *Dorcatherium* are scattered almost everywhere, it is particularly difficult to reconstruct single individuals by strewnfields. In the southernmost excavation area (2019) within the very small proximity of a little more than one square metre at least 53 bones have been unearthed that are all anatomically assigned to the tragulid species *Dorcatherium nauti* (Fig. 6.7.4.1).

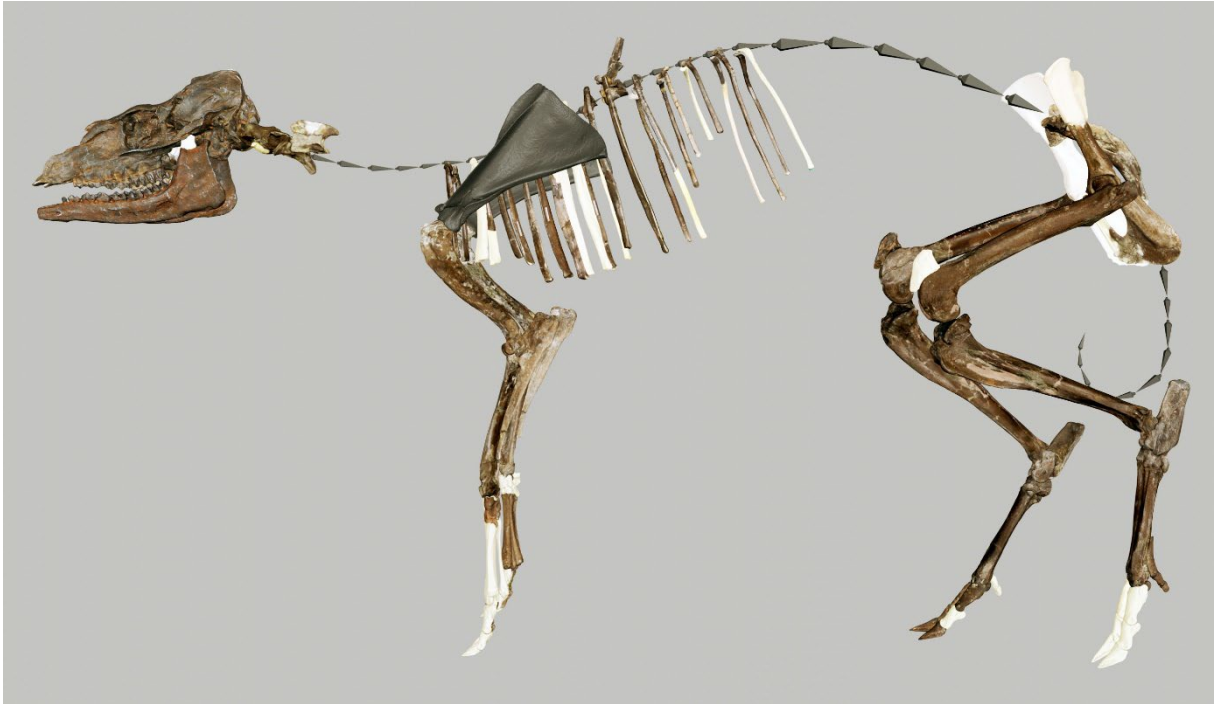


Figure 6.7.4.1 Reconstruction of the skeleton of *Dorcatherium naui* (Artiodactyla, Tragulidae) from the early Late Miocene Hammerschmiede fossil site and the local stratigraphic level HAM 4. The skeleton was digitally assembled from 53 bones, which presumably belong to one individual. Bones belonging to the skeleton find, which are only present on one body side, were mirrored. Supplemented elements in white. Scapula, for *Dorcatherium* from Hammerschmiede unknown, is reconstructed from living artiodactyles (black). The front legs do not belong to this individual, but were added from finds from the Hammerschmiede. Reconstruction created by C. Kyriakouli.

The western section consists of various bones of the left and right hind limbs (without pelvic bones) and the eastern section yields 20 ribs (eleven right, nine left) on an extremely small spot (Fig. 6.7.4.2). In the entire area one thoracic vertebra and four cervical vertebrae (including axis but no atlas) were found. Between the closely adjacent finding areas of the hind limbs and the ribs an excellent preserved skull of an adult female *Dorcatherium naui* was recovered (Hartung and Böhme 2022). Furthermore, a hemimandible was excavated in very close proximity to the main accumulations, which matches the dental tooth wear and state of the cranium and occludes perfectly the maxillary tooth row.

The monospecific accumulation of bones of *Dorcatherium naui* and the low density of finds in the vicinity of this enrichment spot, the anatomically correct arrangement (no perfect articulation) of many bones and skeletal regions, the perfect fit of pedal joints and the absence of duplicate skeletal elements leads to the conclusion that all of these bones belong to a single individual.

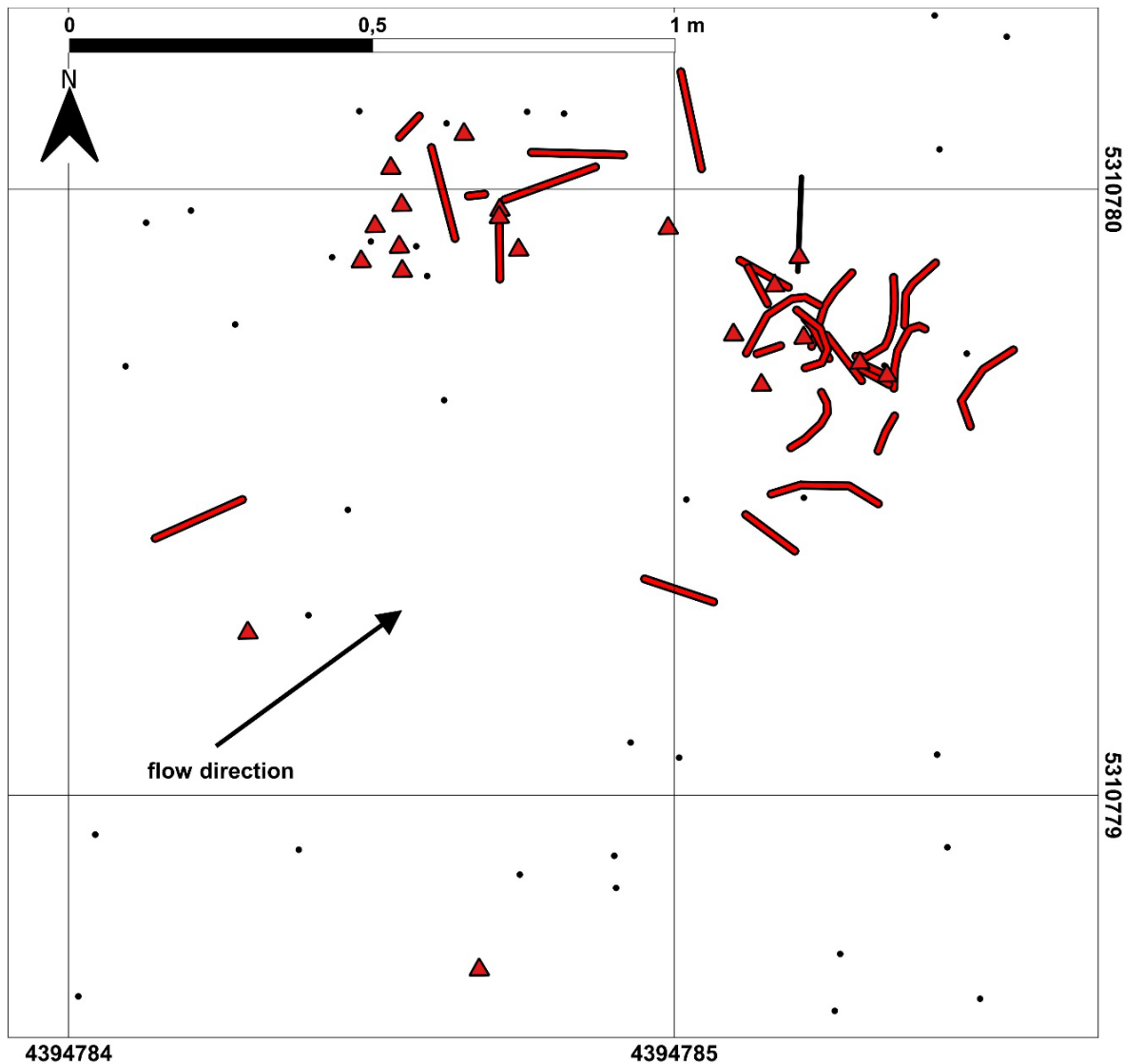


Figure 6.7.4.2 Section of the excavation plan of the local stratigraphic level HAM 4 at the early Late Miocene Hammerschmiede fossil site. The shown area comprises the part of the southernmost excavation area near to the deepest central channel area of the HAM 4 channel excavated in 2019. Black dots represent vertebrate fossil specimens, black line denotes an elongated bone and orientation. Excavated tragulid remains (53 specimens), most probably belonging to the same adult, female *Dorcatherium navi* individual, are highlighted with red triangles and lines. Associated bones (limb bones and mostly ribs) are arranged over a very small area (approximately one square metre) and long bone orientations correspond to the reconstructed flow direction (black arrow) for this area. Coordinates correspond to Gauss-Kruger Zone 4 grid in metres. Grid spacing equals one metre.

The present case is the first observation of a special taphonomic phenomenon observed at the Hammerschmiede deposits. The classical theory assumes that sedimentation or transport of bones is controlled by their physical properties, and especially by the density and shape of the bones (Behrensmeyer 1975, 1988; Hanson 1980; Voorhies 1969). According to this model, ribs and vertebrae are the "lightest" elements, which are transported the fastest and farthest away from the initial point a carcass enters the fluvial system. In this case study, ribs, of all things, were apparently not transported further and remained at the initial point along with the skull and some limb bones. An explanation must now be provided as to how it can be that the ribs

(of both sides of the body) remain on an extremely small spot, while nearly no vertebrae and especially virtually no thoracic vertebrae (which articulate anatomically in between the ribs) are present. A decisive different parameter to the classical observation models is that the Hammerschmiede deposits comprise of fine-grained and more soft sediments (clay, silt and fine sand). These muddy sediments could simply have adhesively attached the bones to the ground. The anatomical arrangement of the bones indicates that some decomposition must have taken place, separating the bones from each other, but perhaps also partially holding them in tendon union. It is remarkable that the finds where a reconstruction to a strewnfield is possible do not show any signs of feeding marks, so it can be assumed that the place where the carcasses decayed was not accessible to predators such as hyaenas. Furthermore, the carcass decomposed without great rearrangement processes acting. The carcass disintegrates and all the bones lie on the base when in a subsequent event (e.g. environmental events such as heavy rains) the flow velocity increases and the river level rises. The basal-most currents are almost non-existent due to friction. Bones that are somewhat more voluminous and protrude further into the flowing current (e.g. eddies) have considerably more surface area to be attacked by the current and to be detached from the muddy bottom. Ribs in particular are very flat and tend to remain adhesively attached to the soft bottom sediments, remain in place and eventually become quickly sedimented and thus even more stabilised.

As a result of this observation, adhesion is supposedly one of the primary physical parameters that influences the retention or detachment of bones from a river bottom consisting of fine-grained and thus muddy sediments as it is the case of the matrix dominated Hammerschmiede deposits. Accordingly, the fluid dynamic behaviour of a bone is superimposed by the bone-substrate interaction and whether this enables detachment or whether the bone remains in place and becomes sedimented. In this context, the shape and density of the surface to be attacked by the acting forces and their relationship to the adhesive suction of a bone surface to the underlain channel sediments also play a decisive role.

In this case study, the Hammerschmiede site contributes significantly to the understanding of transport and retention of bones in rivers with fine and rather muddy sediments. Understanding these special channel bottom properties seems to be essential to understand the dispersion and distribution of the skeletal strewnfields at the Hammerschmiede fossil sites and beyond that.

6.7.5 Case study V: HAM 4 – *Miotragocerus monacensis* (Fig. 6.7.5.1)

The boselaphin bovid *Miotragocerus monacensis* is beside the tragulids an equally common large mammal find of the HAM 4 river deposits. In general, randomly interspersed bone finds of this taxon are found throughout the entire channel fillings. Due to the presumably high number of multiple intermixed individuals, a particular assignment of bones to single carcasses is usually not possible. One conspicuous find distribution stands out exceptionally among these typically isolated finds and is examined in more detail below.

The directly adjacent excavation areas of the years 2021 and 2022 in the central HAM 4 channel yielded two restricted zones of particularly high enrichment of mainly limb bones of the bovid species *Miotragocerus monacensis*. This discovery includes at least 43 bones which were excavated at two locations (a northern and a southern spot), which lie approximately 12 metres apart from each other (Fig. 6.7.5.1).

The northern location comprises an area of two by three metres, with a north-south elongation, in which several non articulated but partly anatomically arranged bones of an anterior right limb and two (left and right) hind limbs were found along with the pelvis, sacrum, some tail and lumbar vertebrae (Fig. 6.7.5.2). All of these bones are anatomically assigned to the antelope *Miotragocerus monacensis*. The finds are distributed within the basal sediments of the HAM 4 channel fill and are located at about 10-20 cm above the channel base. Although they are not articulated, the partly correct anatomical arrangement indicates that these bones possibly correspond to a single individual. This is also supported by the fact that this conspicuously high number of larger long bones is untypical for the find layers of the Hammerschmiede.

The second and southern location consists of a small area of less than half a square metre on which the also not articulated but anatomically correctly arranged left forearm of a *Miotragocerus monacensis* was excavated (Fig. 6.7.5.3). The find elevation is similar to the northern locality at approximately 10 cm above channel base within the lower HAM 4 enrichment and reworking layer. Within both, the northern and the southern zone, the enrichment, the taxonomic integrity, the partially distinct anatomical arrangement, the similarity in age (young adult with some epiphyseal fissures already closed and some still open), the same level and the lack of duplicate bones indicate a relationship to a single individual. In addition, the bones of both sites show significantly better bone preservation compared to surrounding bones, suggesting late entry into the sediments with subsequent rapid embedding.

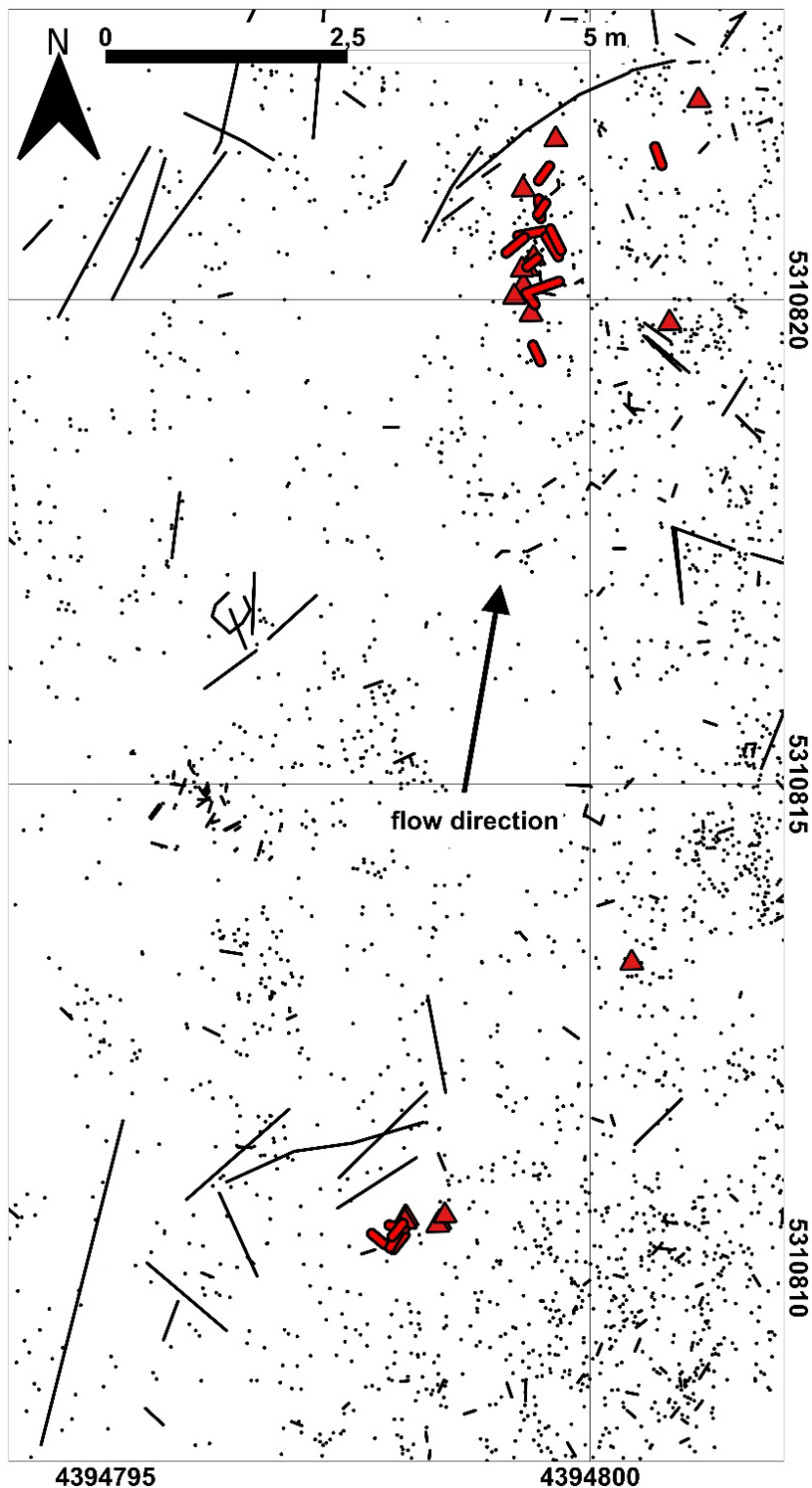


Figure 6.7.5.1. Section of the excavation plan of the local stratigraphic level HAM 4 at the early Late Miocene Hammerschmiede fossil site. The shown area comprises a part of central excavation area near to the deepest channel area of the HAM 4 excavated in 2021 and 2022. Black dots represent vertebrate fossil specimens, black lines denote elongated objects (the longest of these represent wood finds) and their orientation. Excavated bovid remains (43 specimens), most probably belonging to the same *Miotragocerus monacensis* individual, are highlighted with red triangles and lines. Associated bones (mostly limb bones) are arranged over a distance of approximately 12 metres corresponding to the reconstructed flow direction (black arrow) at this area. In addition to a few individual bones scattered in the wider area, there are two accumulation comprising of a very high bone density consisting of several elements belonging two both hind limbs and the right forelimb in the north and the partially articulated and arranged left forelimb in the south. Coordinates correspond to Gauss-Kruger Zone 4 grid in metres. Grid spacing equals 5 metres.

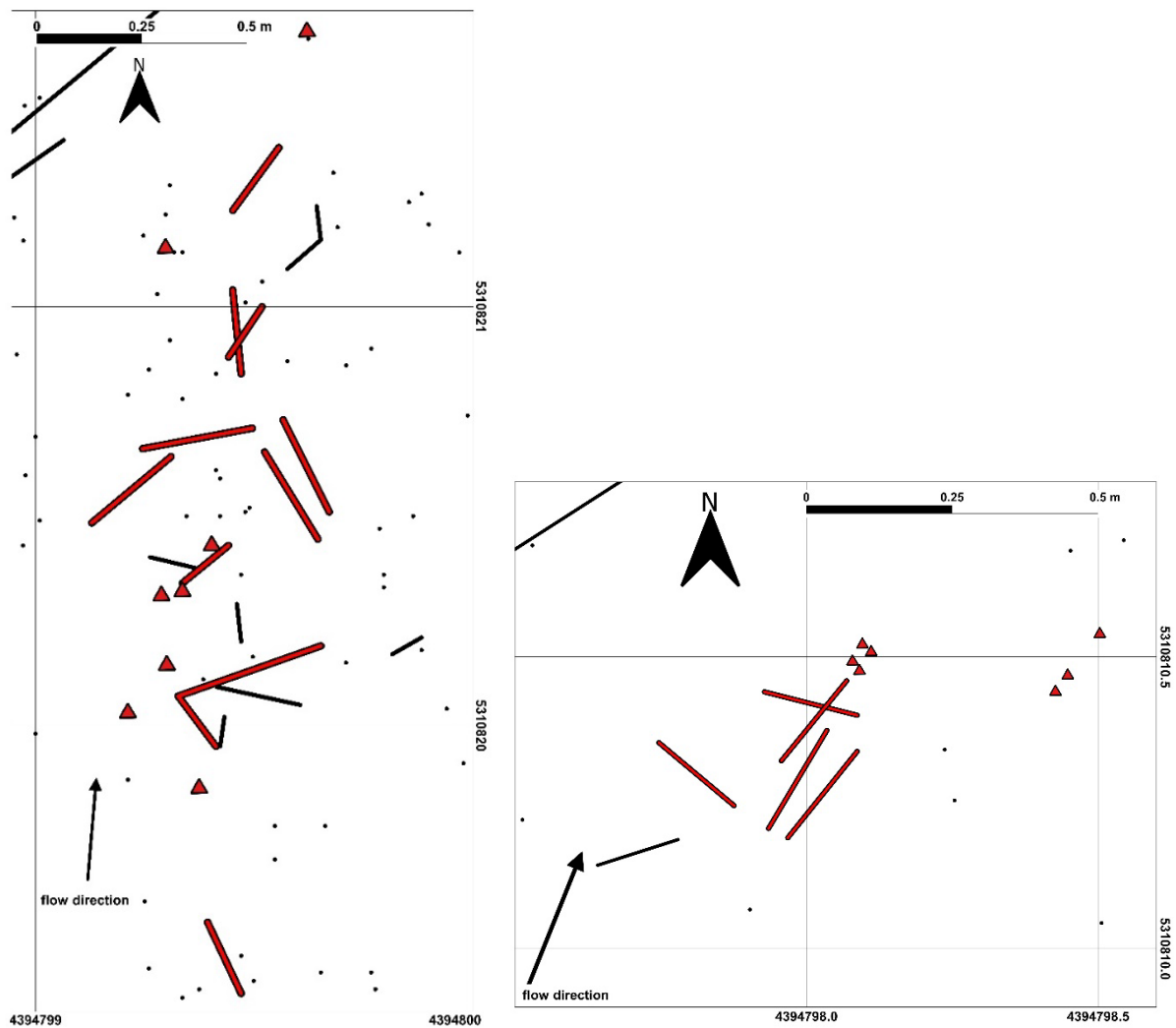


Figure 6.7.5.2. (left) Detailed view of the bovid strewnfield section of the excavation plan of the local stratigraphic level HAM 4 at the early Late Miocene Hammerschmiede fossil site. The shown area comprises a part of central excavation area near to the deepest channel area of the HAM 4 channel excavated in 2021 and 2022. Black dots represent vertebrate fossil specimens, black lines denote elongated objects and their orientation. Excavated bovid remains of the northern strewnfield section most probably belonging to the same *Miotragocerus monacensis* individual, are highlighted with red triangles and lines. Associated bones (mostly limb bones) are arranged and oriented in correspondence to the reconstructed flow direction (black arrow) at this area. The shown accumulation consists of several elements belonging to both hind limbs in addition to the pelvic region and lumbar vertebrae and the right forelimb. Coordinates correspond to Gauss-Kruger Zone 4 grid in metres. Grid spacing equals one metre.

Figure 6.7.5.3. (right) Detailed view of the bovid strewnfield section of the excavation plan of the local stratigraphic level HAM 4 at the early Late Miocene Hammerschmiede fossil site. The shown area comprises a part of central excavation area near to the deepest channel area of the HAM 4 channel excavated in 2021 and 2022. Black dots represent vertebrate fossil specimens, black lines denote elongated objects and their orientation. Excavated bovid remains of the southern strewnfield section most probably belonging to the same *Miotragocerus monacensis* individual, are highlighted with red triangles and lines. Associated bones belong to the left forelimb and are arranged and oriented in correspondence to the reconstructed flow direction (black arrow) at this area. Coordinates correspond to Gauss-Kruger Zone 4 grid in metres. Grid spacing equals 0.5 metres.

Although the two find zones with their northernmost and southernmost extents are about 12 metres apart, there are so many similarities between the two sites that it seems quite plausible that a larger dispersal field of the same individual is present here. Particularly noteworthy is the fact that the flow direction reconstructed on the basis of longitudinal objects (mainly wood) and their orientation corresponds quite precisely with the orientation of the two zones to each other. Likewise, the long bones within the certain specimen locations indicate this direction, whereby the flow direction of the river bottom-near deposits can be confirmed likewise. In the area between the two find complexes there is an area with a very low density of finds, which suggests that the flow in this area rather transported objects a bit further. Overall, a connection is also obvious with this find, since the bones of the right forelimb are virtually identical in size, anatomical proportion, and age characteristics. Also, the finds from both zones show an identical quality of bone preservation. While other antelope finds in the area indicate clearly further transport distances by signs of disintegration by fragmentation, corrosion or polishing and many antelope finds exhibit tooth or feeding marks by predators (“fresh/green fractures” and tooth marks presumably by hyaenas), these finds are all of particularly well preservation and indicate a contemporaneous embedding after deposition. This means that these finds represent the last deposited objects that were not reworked and redeposited by the river again. The presence of arranged and not exactly articulated bones indicates that the carcass had decomposed to a ligamentous skeleton and tendons and ligaments were the only connecting leftover units that hold the bones together, with the joint areas already completely disarticulated. These many similarities between the two find areas strengthen the suspicion that both finds were relocated and embedded in the same event and are likely attributable to the same individual.

In contrast to some of the other skeletal strewnfields, this find complex shows not a single assigned rib and no reliably assignable cranial elements. The bone preservation would suggest a completely preserved cranium, as no traces of feeding are visible on the bones, but such a skull of *Miotragocerus* has not yet been found in Hammerschmiede at all. Since the reconstructed flow direction is assumed to flow from south to north and in many other strewnfields of the Hammerschmiede skulls and ribs were found at the presumed initial point of the strewnfield, it seems possible that this spot has not yet been found and potentially exists in further southern (not yet excavated) direction and in this case study a rather distal strewnfield area is provided.

6.7.6 Case study VI: HAM 4 — Reassembled fossil broken and scattered bones

One of the best ways to obtain information about flow direction and potential individual dispersal fields are fragments that prove affiliation over long distances by an exact break edge match. So far only a few of these cases are documented, but in most cases, there are only a few metres distance between the components. The problem of this method is the ever-increasing amount of material at a greater comparative distance to find the counterpart to a fragmented object. There is one case of a mammalian fibula diaphysis represented by two similarly sized pieces which were found about 1.5 metres apart from each other within the HAM 4 excavation area of 2019-2 (Fig. 6.7.6.1). The alignment of the two fragments indicates a transport direction in north-south orientation in the HAM 4 channel.



Figure 6.7.6.1. Scattered found and reassembled fragments of a mammalian fibula diaphysis from the early Late Miocene Hammerschmiede deposits and the local stratigraphic level HAM 4. Both pieces were found about 1.5 metres apart and fit together perfectly at the fracture seam (a-b). (a-b) represent different view angles of the refit of the objects GPIT/MA/17170 and GPIT/MA/17180. Scale bar equals 10 mm.

A second case and one of the most comprehensive examples of reassembled bone fragments found over larger distance is a Proboscidean rib refit of three larger isolated pieces found within the southernmost excavation area of the HAM 4 channel (HAM 4 2019-1). In this case, due to the rarity of this animal group, the comparative material is manageable and led by chance to the result. This case proves via direct fracture fit the affiliation of three approx. 15 cm long rib fragments of a large proboscidean (Fig. 6.7.6.2).



Figure 6.7.6.2. Scattered found and reassembled large fragments of a Proboscidean rib from the early Late Miocene Hammerschmiede deposits and the local stratigraphic level HAM 4. The three specimens were found approximately 2 metres apart from each other but show perfect but slightly rolled and polished fracture seams (a-c). (a) GPIT/MA/16784; (b) GPIT/MA/16806; (c) GPIT/MA/16749. Scale bar equals 5 cm.

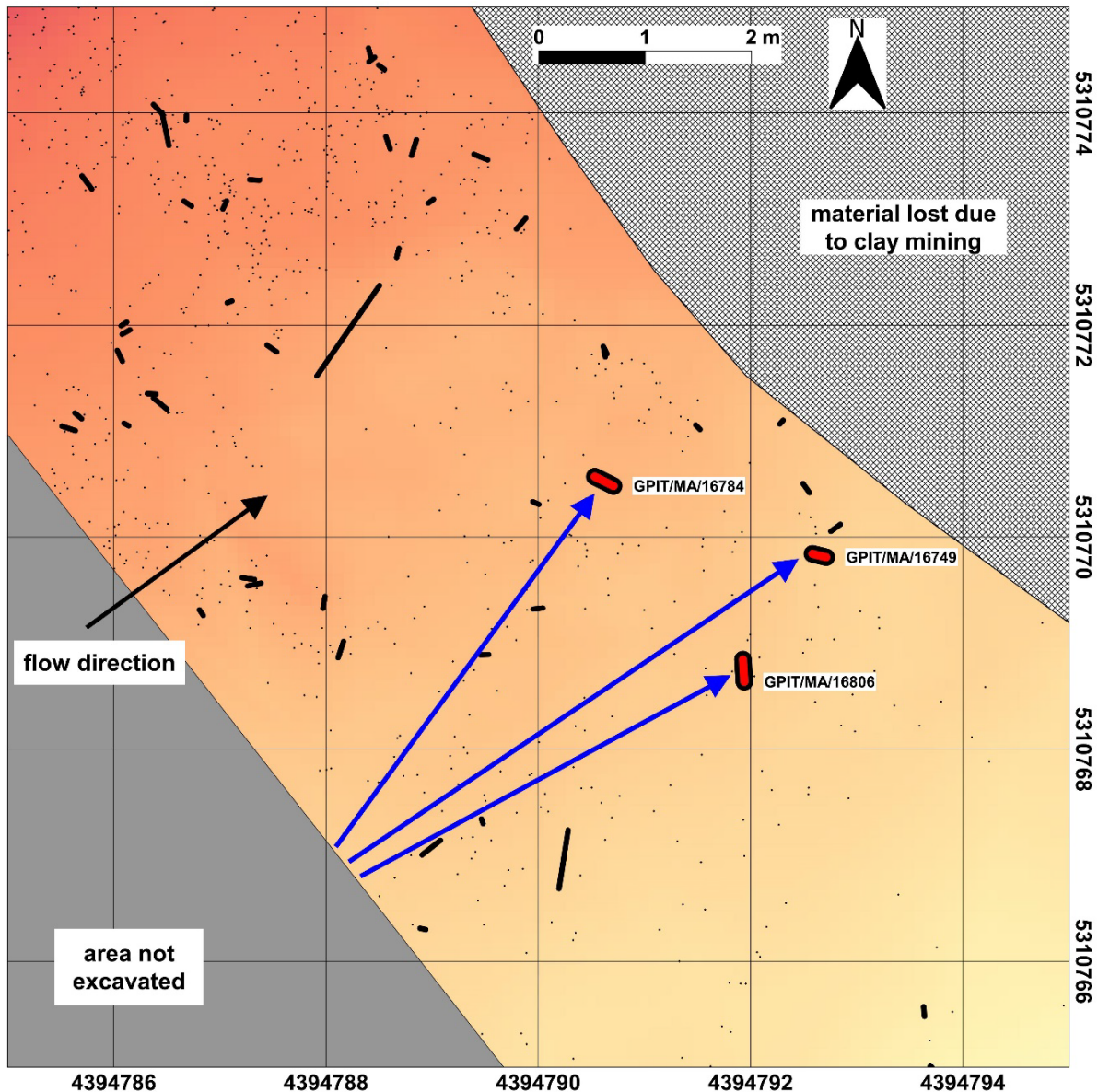


Figure 6.7.6.3. Detailed view of three scattered found and reassembled large fragments of a Proboscidean rib at the southernmost section of the excavation plan of the local stratigraphic level HAM 4 at the early Late Miocene Hammerschmiede fossil site. The three specimens (GPIT/MA/16784, 16806 and 16749) were found approximately 2 metres apart from each other in lateral disposition and one metre north-south offset and show perfectly fitting but slightly rolled and polished fracture seams. A transport origin and a lateral dispersion is indicated from a most probably further southern initial point of fragmentation (blue arrows). Black dots represent other vertebrate fossil specimens, black lines denote elongated objects and their orientation (the longest of them are wood finds). Coordinates correspond to Gauss-Kruger Zone 4 grid in metres. Grid spacing equals 2 metres.

The individual parts were found over an area of several metres and are not arranged linearly. The rather triangular relation of the individual bones gives rise to the assumption that the fragmentation and the original starting point of the rib was further upstream and all three elements were distributed slightly independently of each other, so that there is a laterally displaced position of each individual object (Fig. 6.7.6.3). Furthermore, the reassembled rib fragment is also freshly broken at both ends. This means that there may have been other pieces in the nearer and further surroundings and that they may still be found in future excavations if

they are located to the south. This example shows that objects starting from an origin are dispersed not only longitudinally (flow direction) but also laterally in the river with a larger transport distance. Certainly, effects at the edge of the flow channel (sweep water) and the observation that water tends to flow in a helical motion must also be considered. Nevertheless, the basic assumption is that the lateral width of dispersing elements increases with the transport distance.

6.8 Biogenic bone modifications and possible producers

A large number of the recovered bone finds from Hammerschmiede show possible traces of biogenic (animal or plant/algae/bacterial) modification. The following is an overview of the traces found in the Hammerschmiede material and an assignment to a possible producer. Traces are mainly found on disarticulated, isolated specimens and have not yet been recognised on bones, belonging to skeletal strewnfields of single vertebrate individuals. Related or associated finds possibly have not been available to the modifiers (temporally, spatially), what could possibly imply that the better-preserved skeletal find complexes arrived at the site rather late, shortly before the final sediment cover.

Splinter bones: A significant amount of bone finds show mechanical breakage and fracturing or is splintered into smaller parts and fragments (Fig. 6.8.1). Many of these splinters and bone shaft pieces show carnivorous tooth marks (puncture marks) in addition to fracture patterns possibly resulting from chewing (Fernández-Jalvo and Andrews 2016). The way the bones are fragmented indicates that they were manipulated mechanically in a "fresh" state (e.g. Fernández-Jalvo and Andrews 2016). Many bone shaft splinters collected as reading finds can be assigned in terms of size to the long bones of bovids, tragulids, cervids and suids. The majority of these bone shaft fragments show typical splinter fractures and tooth marks possibly produced by larger carnivores. Since the larger felids and barbourioides are not likely to be used for such fracture structures due to their already rather filigree canines, the marks were most likely produced rather by hyaenas, amphicyonids or large mustelids like *Eomellivora* who scavenged the bones for nutritious marrow. Overall the angled fragmentation patterns with curved cleavage is quite similar to regurgitated and chewed bones from recent hyena as it is shown by Fernández-Jalvo and Andrews (2016).

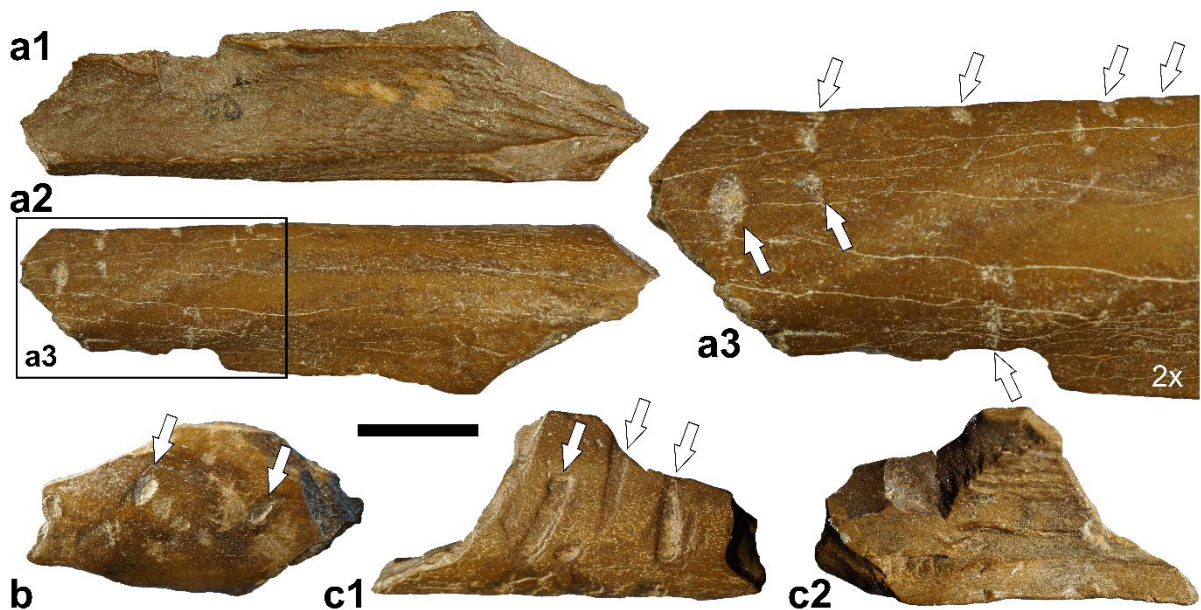


Figure 6.8.1. Bone splinters with tooth marks from the early Late Miocene Hammerschmiede deposits and the local stratigraphic levels HAM 5 and HAM 4. (a-c) Bone fragments most probably resembling diaphysis fragments of the antelope *Miotragocerus monacensis* showing surface pits (a2-3, b) and linear striations (b, c1) possibly produced by carnivore chewing. White arrows mark particularly conspicuous pits or linear striations. (a) GPIT/MA/19653; (b) GPIT/MA/19654; (c) GPIT/MA/16452. Scale bar equals 10 mm (a1-2, b, c) or 5 mm (a3).

Gnaw marks (vertebrates): Very few bones show gnaw marks on their margin possibly produced by the gnawing rodents or other small mammals like eulipotyphlans (Fig. 6.8.2). The found structures resemble quite well the typical parallel striations produced by rodents (compare to e.g. Fernández-Jalvo and Andrews 2016).

Arthropod bioerosion (small scale): In addition to previously described bone modifications by vertebrates, also possible invertebrate trace fossils are present. Rare, but probably quite inconspicuous and difficult to find, are very fine surface traces of very delicate parallel and intersecting furrows, a few mm long, which occur, or are best found mainly on smooth surfaces (e.g. interior turtle shell bone surfaces) (Fig. 6.8.3 a-b). These fine structures usually appear next to each other as small patches with similar patterns. It appears as if two adjacent columns made of more or less parallel furrows are arranged slightly crossed against each other. This could indicate a mechanical movement in opposing direction, as is the case with mouthparts of several arthropods (e.g. termites) where mandibles are able to cross over each other. The search for the producer of these traces is quite difficult. However, they possibly represent traces produced by arthropods like insects such as termites or ants. Accidental, non-biogenic scratching of the surface can be ruled out, as the traces appear at different bone sites with a similar pattern in a different orientation.

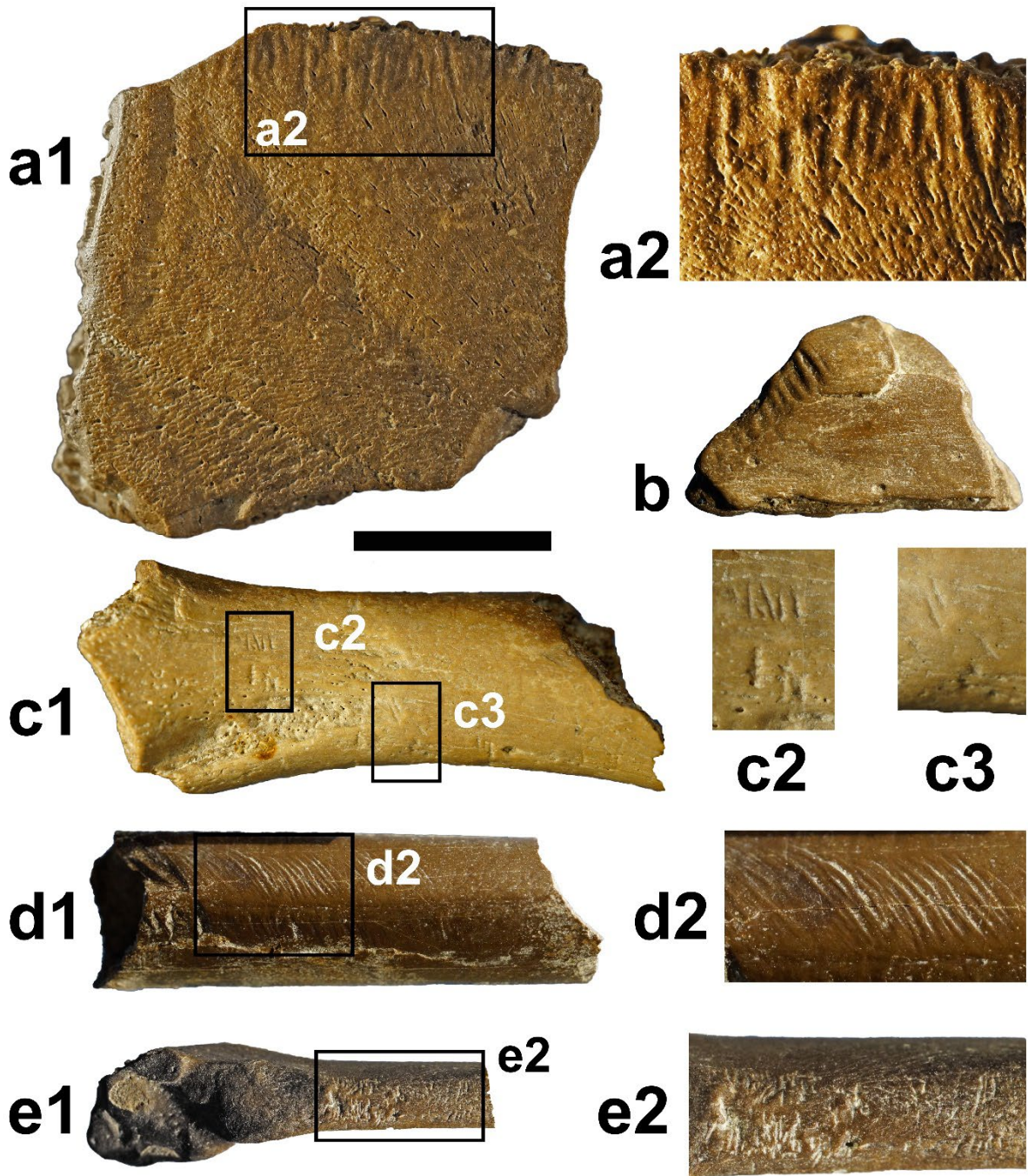


Figure 6.8.2. Gnaw marks on bones from the early Late Miocene Hammerschmiede deposits and the local stratigraphic levels HAM 5 and HAM 4. (a) Plastron fragment of a Testudinidae Turtle with linear marks possibly produced by rodent gnawing restricted to one side of the bone in the overview (a1) and detail view (a2). (b) Mammalian diaphysis fragment with linear marks at one fracture edge. (c) Diaphysis fragment (Humerus or Femur) of the snapping turtle *Chelydropsis* sp. with very few linear marks with bite and counterbite possibly produced by gnawing of small rodents or other small mammals like Eulipotyphla in the overview (c1) and detailed views (c2-3). d Avian diaphysis showing multiple linear striations possibly produced by gnawing of rodents or other small mammals in the overview (d1) and detail view (d2). (e) Right proximal metatarsal II of the beaver *Steneofiber depereti* with very tiny linear marks with bite and counterbite striations possibly produced by gnawing of a very small rodent or other very small mammal in overview (e1) and detail view (e2). (a) GPIT/RE/13656; (b) SNSB-BSPG 2020 XCIV-3102; (c) GPIT/RE/15229; (d) SNSB-BSPG 2020 XCIV-1015, (e) GPIT/MA/16621. Scale bar equals 10 mm (a1, b, c1, d1, e1) or 5 mm (a2, c2-3, d2, e2).

Arthropod bioerosion (large scale): Another rare pattern of most probable bioerosive origin, occurs mainly on flat bone areas and is characterised by a mainly star-shaped, centralised and deeper imprint made of intersecting linear furrows that are only slightly larger than one cm at the maximum (Fig. 6.8.3 c-d). These markings show great similarity to trace fossils described of other vertebrate sites and could possibly be attributed to termites (compare e.g. Watson and Abbey 1986; Parkinson et al. 2010; Backwell et al. 2012; Fernández-Jalvo and Andrews 2016; Augustin et al. 2019).

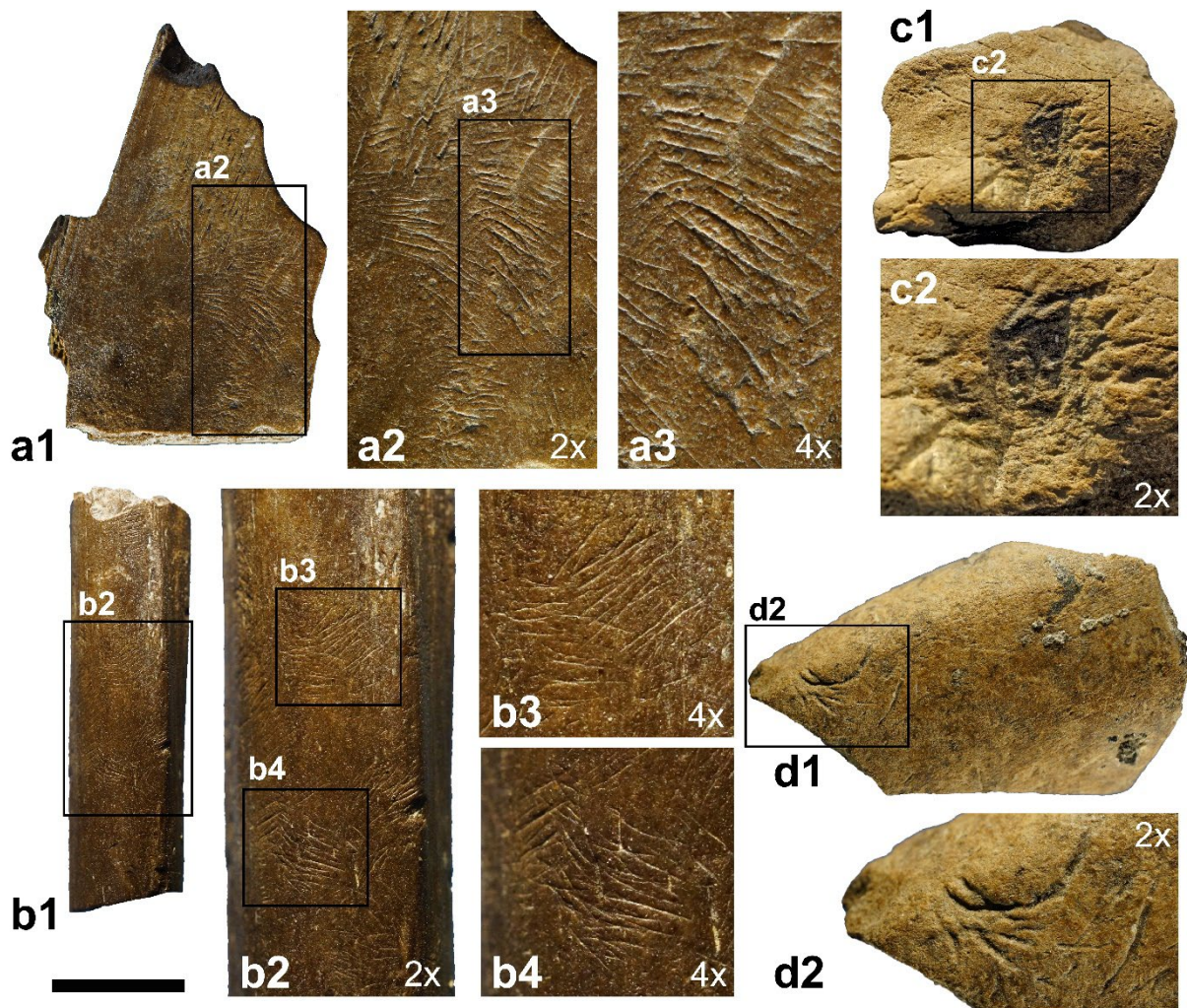


Figure 6.8.3. Insect marks on different bones from the early Late Miocene Hammerschmiede deposits and the local stratigraphic levels HAM 5 and HAM 4. (a-d) different bone types showing partly crisscrossing or intersecting linear or slightly curved marks possibly produced by insects or other Arthropods with their mandibles. (a) Plastron fragment of a trionychid turtle showing linear marks on the flat interior surface of the bone carapace possibly produced by insects in the overview (a1) and detailed views (a2-3). (b) Fragment of a snapping turtle (*Chelydropsis* sp.) scapula with linear marks on the surface possibly produced by arthropods such as insects in the overview (b1) and detailed views (b2-4). (c) Vertebra zygapophysis fragment of a large mammal with intersecting and carving curved marks possibly produced by larger arthropods like termites in overview (c1) and detail view (c2). d Mammalian diaphysis fragment with curved and intersecting marks possibly produced by larger arthropods like termites in overview (d1) and detail view (d2). (a) GPIT/RE/15230; (b) GPIT/RE/13198; (c) SNSB-BSPG 2020 XCIV-4696; (d) GPIT/MA/19655. Scale bar equals 10 mm (a1, b1, c1, d1), 5 mm (a2, b2, c2, d2) or 2.5 mm (a3, b3-4).

Dermestid bioerosion: Undercut small hollow forms and surface modifications occur, especially on bones of large mammals of poor preservation quality (Fig. 6.8.4). These hollows and furrowed surface areas could possibly be assigned to dermestid beetles and their feeding and carving activity of building pupation chambers (compare e.g. Kitching 1980; Fernández-Jalvo and Andrews 2016; Augustin et al. 2021).

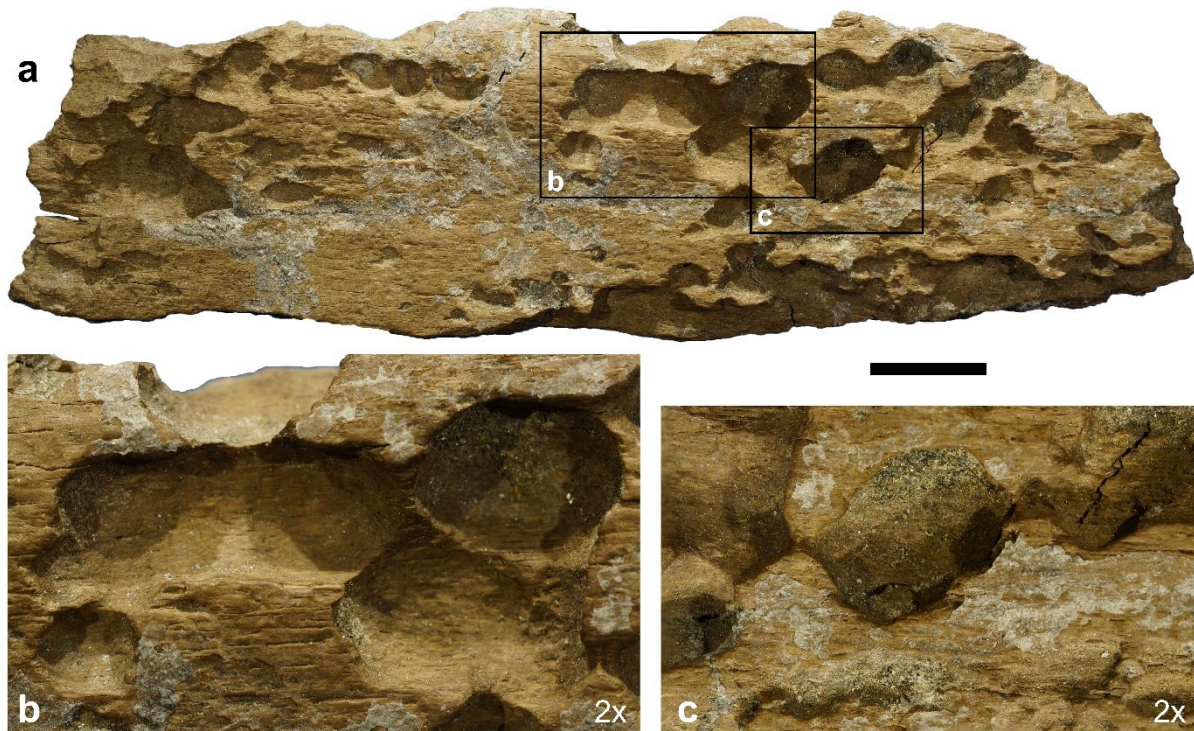


Figure 6.8.4. Insect marks on a large mammal bone from the early Late Miocene Hammerschmiede deposits and the local stratigraphic levels HAM 5 and HAM 4. (a-c) Large fragment of a large mammal diaphysis (possibly of a *Perissodactyla*) showing circular and ovoid shaped shows circular and ovoid depressions and furrows with partly undercut edges (overhanging) on the compacta surface of the bone in the overview (a) and detailed views (b, c). These structures possibly represent insect marks and could probably resemble pupation cavities produced by dermestid beetles. (a-c) SNSB-BSPG 2020 XCIV-3416. Scale bar equals 10 mm (a) or 5 mm (b, c).

Plant marks: A common feature on many isolated bones and bone fragments are linear, bifurcated and anastomosing furrow marks caused by roots (Fig. 6.8.5). Especially root traces are marks that require longer duration time. Root marks indicate the embedding of bones into the rooted zone of soils for a certain period of time, where plants leach out the bones as phosphate fertiliser with their roots. Since at the Hammerschmiede deposits affected bones and perfectly preserved bones are found next to each other, these traces indicate a secondary relocation of the affected specimens by the fluvial processes.



Figure 6.8.5. Root marks on different vertebrate bone and tooth fragments from the early Late Miocene Hammerschmiede deposits and the local stratigraphic levels HAM 5 and HAM 4. (a) Diaphysis fragment possibly belonging to the antelope *Miotragocerus monacensis* with intense linear marks most produced by plant root corrosion in internal (a1), breaking edge (a2) and compacta surface (a3) views and a detail view of the internal surface (a4). Note that root marks are found on both the internal and the external surface of the bone but not at the breaking edge (a2). This indicates that the bone did not break until after root penetration during a new redepositional process. (b) Peripheral bone fragment of a Geoemydidae swamp turtle (possibly *Mauremys* sp.) carapace with linear marks on the internal (b1) and external (b2) surface of the bone most probably produced by roots. (c) lower incisor of the small beaver *Euroxenomys minutus* with linear marks forming a dichotomous network structure produced by roots in lateral (c1), anterior (c2) and detail anterior views (c3). Note, that the dentine part is densely corroded without showing any detailed root structures while the enamel clearly exhibits root mark typical network patterns by differences in colouring. (a) GPIT/MA/19656; (b) GPIT/RE/15231; (c) GPIT/MA/17322. Scale bar equals 10 mm (a1-3, b1-2, c1-2) or 5 mm (a4, c3).

Corrosion by aquatic vegetation: The bone preservation in the sites of the Hammerschmiede are extremely heterogeneous. In addition to bones of excellent surface quality, there are also many pieces with severe bone surface damage and structures reminiscent of corrosion, such as corrugated, furrowed, and irregularly roughened surfaces and surface areas of bones (Fig. 6.8.6) that could possibly represent corrosion effects of “aquatic vegetation” (sensu e.g. Pesquero et al. 2010; Fernández-Jalvo and Andrews 2016). Some of these structures may be due to mechanical rolling, plant or animal traces. However, there are bone surfaces that are more suggestive of chemical dissolution processes. Since chemical bone corrosion would require pH values in the highly acidic or alkaline range, which would completely contradict the observations made in the deposits of a high water quality (freshwater pearl mussels and aquatic gastropods), another source must be responsible for these modifications. In the case of a suid

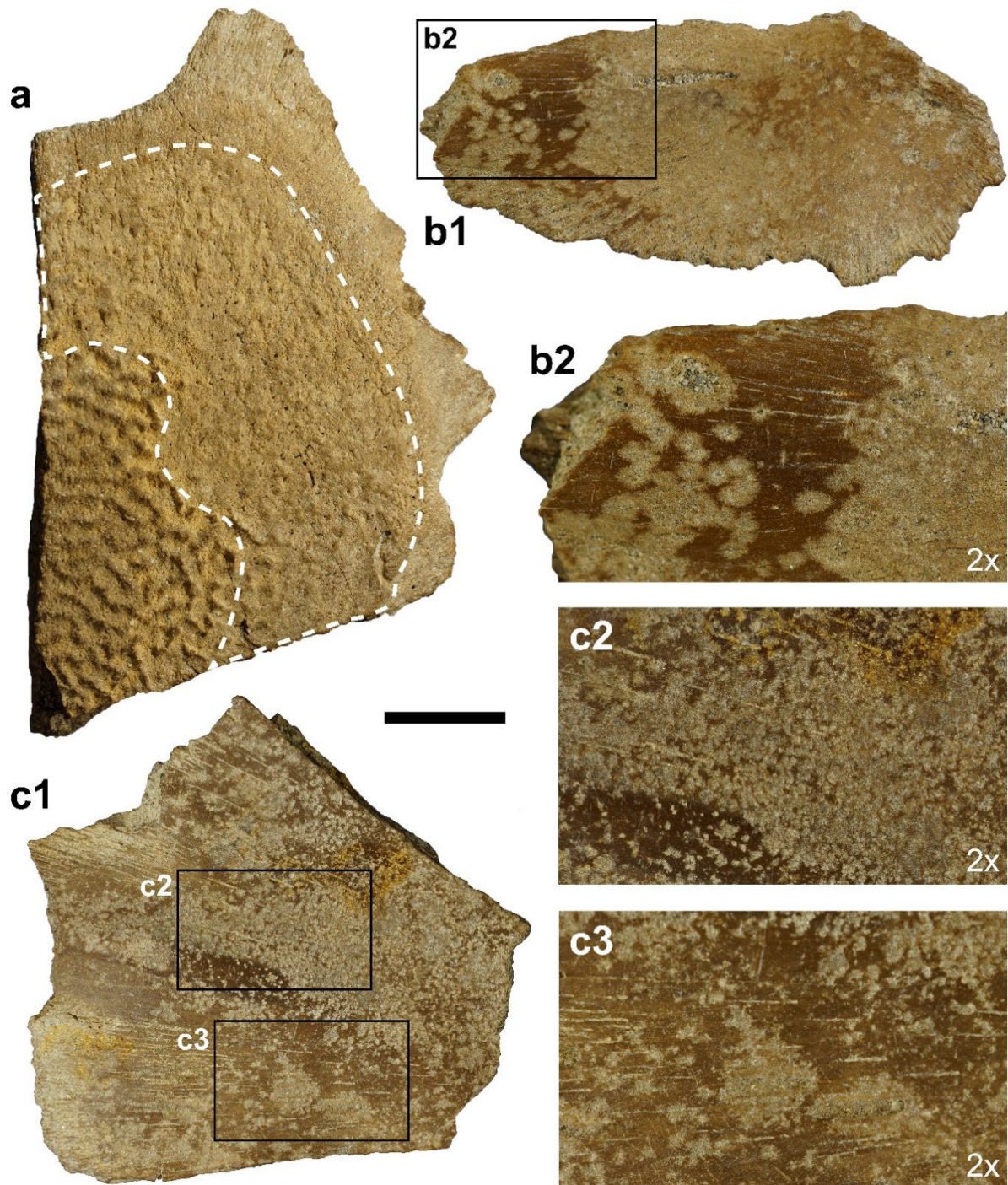


Figure 6.8.6. Bone surface corrosion on turtle bones from the early Late Miocene Hammerschmiede deposits and the local stratigraphic levels HAM 5 and HAM 4. (a) Plastron fragment of the trionychid turtle *Trionyx* sp. with preserved typical sculpture (bottom left) where a large part of the actual sculpture is missing (white dashed area) possibly corroded by bacteria or algae. (b) Epiplastron of the snapping turtle *Chelydropsis* sp. possibly corroded, while small zones remain unaffected preserving a smooth surface in the overview (b1) and a detail view (b2). (b2) shows irregularly distributed circular corrosion germs, that connect to larger patches while directly adjacent areas remain unaffected possibly produced by corrosive algal or bacterial mats. (c) internal view of a plastron fragment of the trionychid turtle *Trionyx* sp. showing very tiny dots and smaller circular areas of bone surface corrosion probably produced by aquatic vegetation (algal or bacterial corrosion) in the overview (c1) and detailed views (c2-3). (a) GPIT/RE/15143; (b) GPIT/RE/15232; (c) GPIT/RE/15233. Scale bar equals 10 mm (a, b1, c1) or 5 mm (b2, c2-3).

mandible, it becomes clear that this form of surface modification was only effective under certain conditions. While the bone surface of the left hemimandible is of a higher quality of preservation, the other side of the jaw, as if separated by an imaginary line, shows a strong corrosive impact (Fig. 6.8.7).

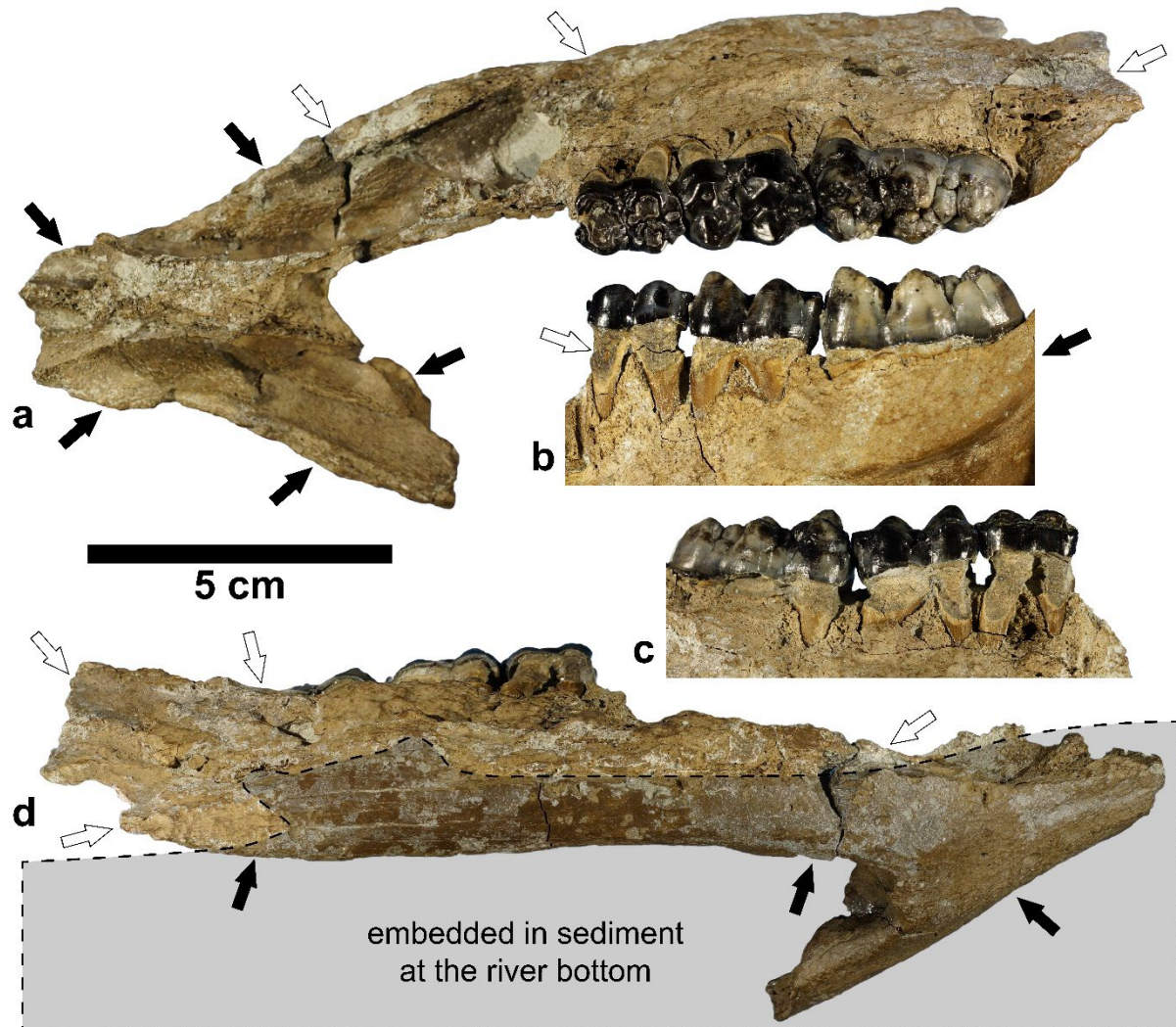


Figure 6.8.7. Bone surface corrosion on a suid mandible from the early Late Miocene Hammerschmiede deposits and the local stratigraphic level HAM 4. (a-d) Fragmentary mandible of the suid *Parachleuastochoerus steinheimensis* (SNSB-BSPG 2020 XCIV-9350) with right m1, m2 and m3 dentition in occlusal (a), lingual detail (b), buccal detail (c) and ventral (d) views. Black arrows indicate well preserved bone surface while white arrows point to the very corroded surface areas. An imaginary line divides the corroded and well preserved regions. This possibly demonstrates, that the specimen was half-embedded in the sediment at the river bottom. As a result, there was a division into a more protected half (embedded) and a counterpart which presumably was overgrown and corroded by aquatic vegetation (algae or bacterial mats) on the river bottom (d). Fractures and defects must have occurred before this embedding. Scale bar equals 5 cm.

A possible explanation for this is the assumption that some bones are placed over a longer period of time in one position (semi-buried in channel base sediments) and partly exposed at the river bottom. Larger bones are partially buried in the sediment and only reveal certain areas to the open water. In the light-flooded area of the flowing waters, algal or bacterial mats or water plants certainly settle on the bone surfaces, which use the bone as a phosphate fertilizer

source and hard ground in the surface area (compare e.g. Fernández-Jalvo and Andrews 2016; Pesquero et al. 2010). In addition to this, grazers such as snails might have fed on these biofilms together with the unstable bone surface and thus caused the massive irregular surface destruction as recurring combination. Similar modifications are described by e.g. Pesquero et al. (2010) or Fernández-Jalvo and Andrews (2016) as corrosion by aquatic vegetation (moss, algae or bacterial mats).

Rolling and polishing: In parallel with fragmentation, disarticulation and biogenic surface modifications, many bones and bone fragments show surface polishing and rolling defects such as rounded corners and edges. These traces are probably mainly due to fluvial transport processes and prove a correspondingly greater transport distance for these finds than for "fresh" and undamaged bones.

Digestive corrosion: Teeth and jaws of small mammals, especially of the small beaver *Euroxenomys minutus*, show a different form of corrosion. In addition to an observed high degree of fragmentation of the material, several dental fragments of this small beaver species show enamel lesions on the exposed tooth regions, while the dentin and jawbone themselves often is little or not affected by corrosion (Lechner and Böhme 2023, Figure 8). In incisor, the enamel is sometimes completely missing from the tip and in cheek teeth, lesions occur in the border area between the enamel and the jawbone, while other enamel areas still hardly show any dissolution. In this recent study it is concluded that such lesions, often involving only the enamel, can most probably be attributed to digestive corrosion by birds of prey or mammalian carnivores (Lechner and Böhme 2023). This probably indicates that the small beaver and many other small vertebrate finds from the Hammerschmiede represent a predatory bone assemblage.

Coprolites: In addition to bones with direct traces, there are also large numbers of phosphatic coprolites found. Besides many morphological differences, two main size categories can be distinguished. There are large coprolites in the size range of several cm, which probably originate from hyenas and also contain macroscopically recognisable bone fragments (Fig. 6.8.8.1; further compare e.g. Fernández-Jalvo and Andrews 2016; Gross et al. 2023).

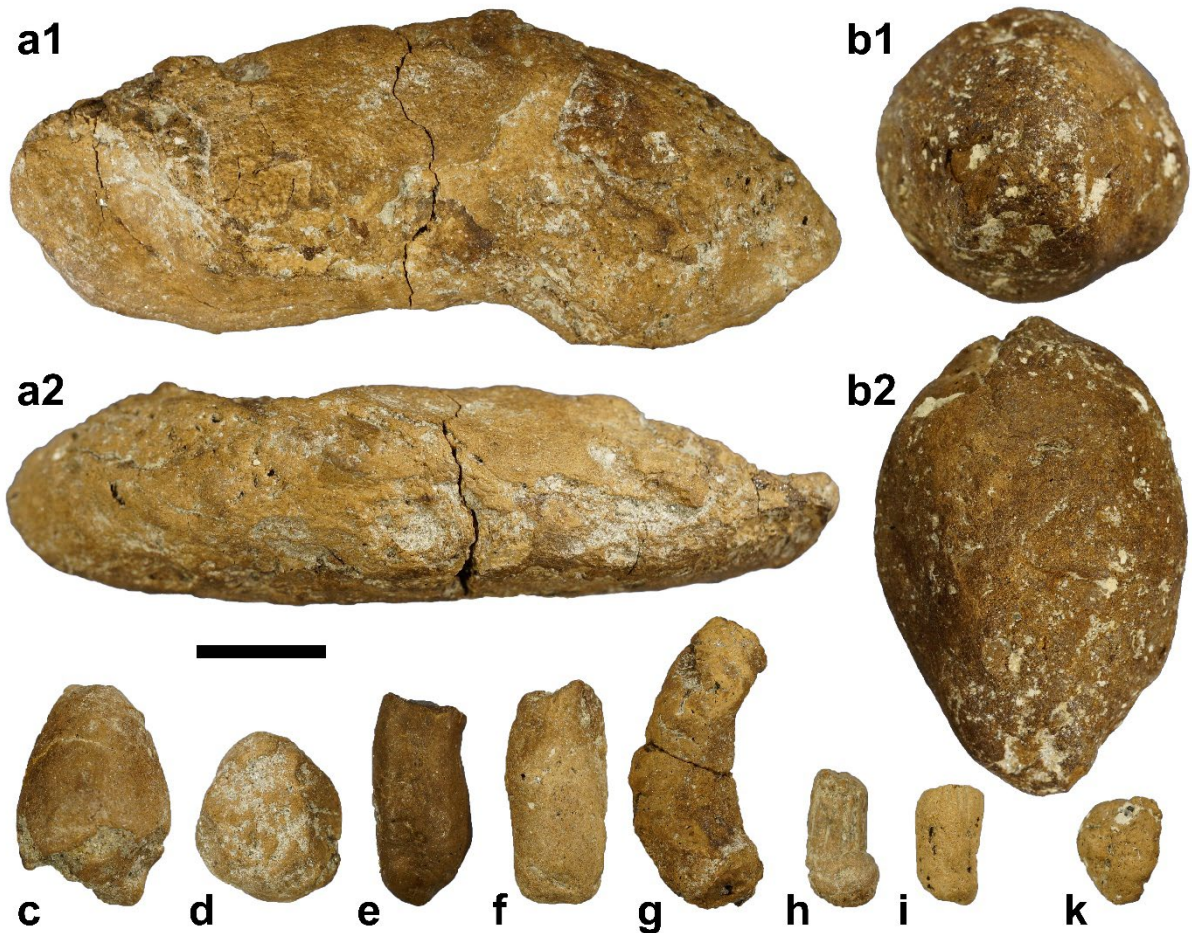


Figure 6.8.8.1. Coprolites from the early Late Miocene Hammerschmiede deposits and the local stratigraphic levels HAM 5 and HAM 4. (a-b) very large phosphatic coprolites of elongated (a) or more ovoid-shaped form (b) probably produced by larger mammalian carnivores such as hyaenids. c-k medium and small sized phosphatic coprolites of ovoid (c), knobby (d), oblong (e-g), striated oblong (h-i) or irregular flat (k) shapes. Due to the enormous diversity of shapes and sizes, various causative producers could certainly also be considered. (a) SNSB-BSPG 2020 XCIV-3603; (b) GPIT/MA/10968; (c-k) GPIT/MA/12554. Scale bar equals 10 mm.

Furthermore, a very large number of small and medium and also micro-coprolites are found, often containing prey bones of mainly aquatic (pharyngeal teeth of cyprinid fishes or fish vertebrae) or semi aquatic (vertebrae of proteid salamanders like *Mioproteus* sp.) vertebrates (Fig. 6.8.8.2, further compare e.g. Dentzien-Dias et al. 2021). Due to the numerical frequency, it is possible that these small coprolites originate from an aquatic or semiaquatic carnivorous predator. A great similarity exists with fish coprolites whereby catfish and pike could be considered as potential producers. Furthermore, the potential for production by otters, fish-hunting birds (cormorants) and also snapping turtles, large amphibians (*Andrias*) or even choristodere reptiles (*Lazarussuchus*) must be examined. Due to the enormous diversity of shapes and sizes, various causative agents could certainly also be considered.

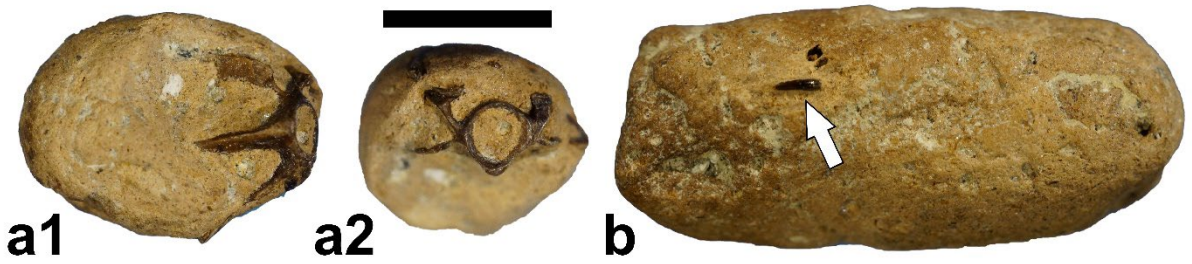


Figure 6.8.8.2. Coprolites with recognizable object inclusions from the early Late Miocene Hammerschmiede deposits and the local stratigraphic level HAM 4. (a) Small coprolite including an amphibian vertebra possibly belonging to the proteid salamander *Mioproteus* sp.. (b) Small coprolite containing a small tooth probably belonging to a fish. Both finds are only examples of several coprolites with recognizable object inclusions that possibly hint to an aquatic or semiaquatic carnivore as a producer of these coprolites. (a) SNSB-BSPG 2020 XCIV-3300; (b) GPIT/MA/12554. Scale bar equals 5 mm.

Aquatic insects (burrows): Not only the bones themselves, but also the surrounding sediments in some cases show trace fossils. In fine-grained intermediate layers in HAM 5 as well as in some channel base locations of HAM 4, fossil root traces are a clear indication of at least short-term vegetation (Fig. 6.2.2; Kirscher et al. 2016). Moreover, U-shaped structures (burrows) in different areas of the clay of the HAM 4 base indicate possibly colonisation by aquatic insects like Mayfly larvae (Ephemeroptera) (Fig. 6.8.9; Fürsich and Mayr 1981).

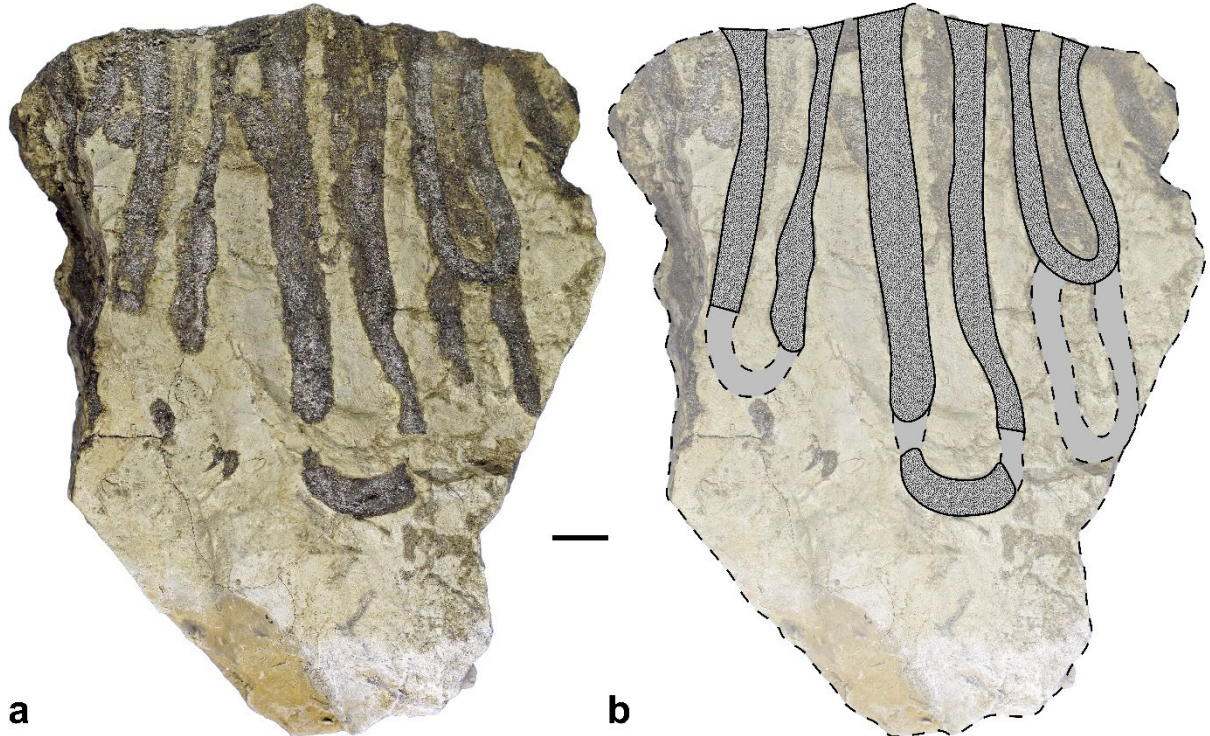


Figure 6.8.9. U-shaped ichno-fossils from the early Late Miocene Hammerschmiede deposits and the local stratigraphic level HAM 4. The clay-basement of the fine-sand filled HAM 4 channel shows at some areas U-shaped, fine-sand filled structures (a). These structures possibly represent burrows of aquatic insects or probably larvae of Mayflies (Ephemeroptera). (b) reconstruction and sketch of the burrows visible in figure (a). (a-b) SNSB-BSPG 2020 XCIV-8915. Scale bar equals 10 mm.

The found U-shaped tube-like structures in the clay, are filled with fine sand typical of HAM 4 sediments. Similar structures are produced by several fossil and extant mayfly species and represent burrows of larvae (e.g. Uchman et al. 2016). Larvae of Ephemeroptera represent filter-feeding aquatic organisms that are usually good indicators for unpolluted and clean rivers with a rich dissolved oxygen content (e.g. Iyagbaye et al. 2017 and citations therein). As a consequence, this would prove that there were also phases in the HAM 4 sedimentation in which the bare clay bottom of the channel was without sediment cover for a certain period of time.

As a last point in this chapter it should not remain unmentioned that there are also phenomena which at first glance could be placed in a taphonomic relationship, but which are probably of a more pathologic nature (Fig. 6.8.10).

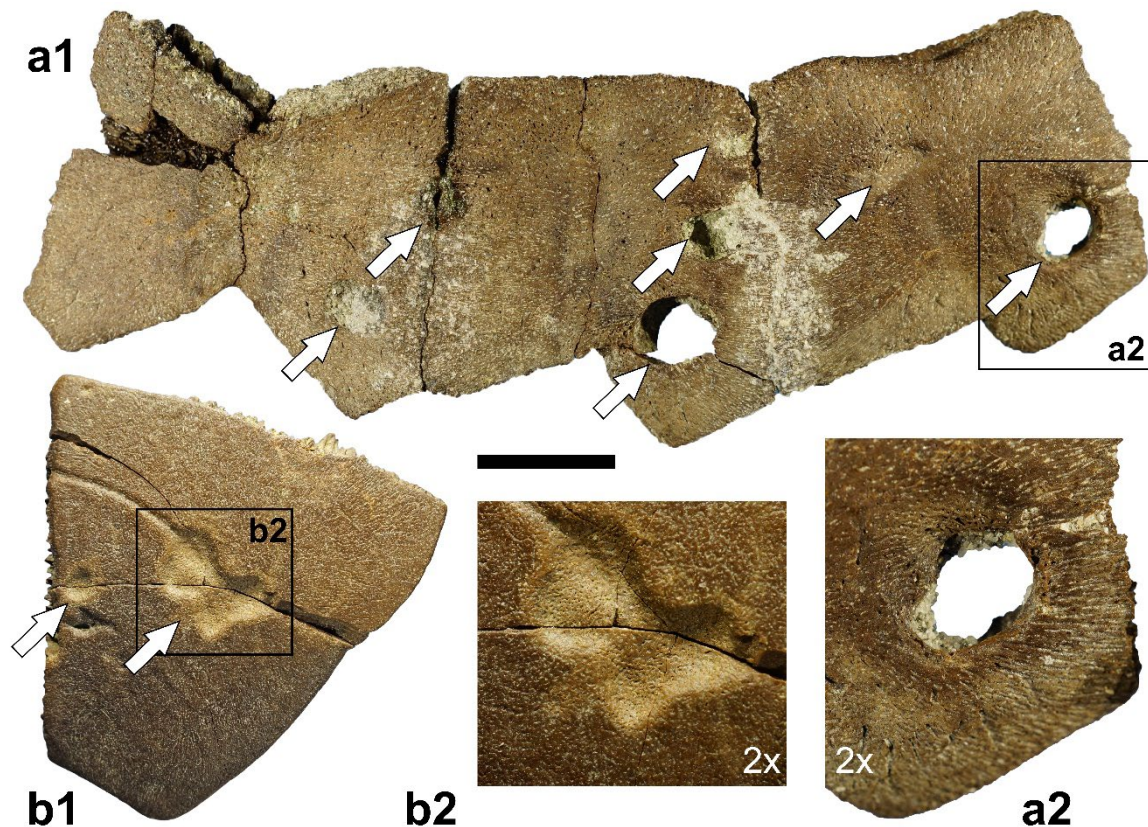


Figure 6.8.10. Pathologies on turtle bones from the early Late Miocene Hammerschmiede deposits and the local stratigraphic levels HAM 5 and HAM 4. (a) Pygal and two peripheral bones of the chelydrid snapping turtle *Chelydropsis* sp. showing bone lesions in form of dents and pits in overview (a1) and detail view (a2). The edges of the damaged areas show an active bone reaction, which suggests a healing process of an inflammation. (b) Xiphiplastron of a Geomydidae swamp turtle (possibly *Mauremys* sp.) showing bone lesions in form of irregular dents at the bone surface in the overview (b1) and detail view (b2). The cavity is not simply of mechanic origin, but the bone shows a reaction in the form of healing through bone remodeling and new formation. (a) GPIT/RE/13994; (b) GPIT/RE/13360. Scale bar equals 10 mm (a1, b1) or 5mm (a2, b2).

In several bone finds from the carapace of turtles, small lesions in form of dents or holes occur on the surface. These bone surface damages are especially exhibited in the areas of scale

margins and borders. In contrast to the afore mentioned taphonomic observations, in most of these bone lesions the bone shows a reaction to the damage in form of healing activity and remodelling of the bone what proves a process during lifetime (Fig. 6.8.10). These lesions most probably are of pathologic origin and most probably indicate disease, like a necrosis of the shell known from extant turtles presumably primarily caused by bacterial infections also in combination with fungi (e.g. Lovich et al. 1996).

Chapter 3

Strewnfield case study of the great ape *Danuvius guggenmosi* (Mammalia, Hominidae)

Published in

Böhme, M., Spassov, N., Fuss, J., Tröscher, A., Deane, A.S., Prieto, J., Kirscher, U., Lechner, T., Begun, D.R., 2019. A new Miocene ape and locomotion in the ancestor of great apes and humans. *Nature* 575, 489–493. <https://doi.org/10.1038/s41586-019-1731-0>

This chapter is a reprint of the published version and differs from the general chapter numbering of this dissertation.

A new Miocene ape and locomotion in the ancestor of great apes and humans

<https://doi.org/10.1038/s41586-019-1731-0>

Received: 10 July 2019

Accepted: 27 September 2019

Published online: 6 November 2019

Madelaine Böhme^{1,2*}, Nikolai Spassov³, Jochen Fuss^{1,2}, Adrian Tröscher², Andrew S. Deane⁴, Jérôme Prieto⁵, Uwe Kirscher^{1,6}, Thomas Lechner^{1,2} & David R. Begun⁷

Many ideas have been proposed to explain the origin of bipedalism in hominins and suspension in great apes (hominids); however, fossil evidence has been lacking. It has been suggested that bipedalism in hominins evolved from an ancestor that was a palmigrade quadruped (which would have moved similarly to living monkeys), or from a more suspensory quadruped (most similar to extant chimpanzees)¹. Here we describe the fossil ape *Danuvius guggenmosi* (from the Allgäu region of Bavaria) for which complete limb bones are preserved, which provides evidence of a newly identified form of positional behaviour—extended limb clambering. The 11.62-million-year-old *Danuvius* is a great ape that is dentally most similar to *Dryopithecus* and other European late Miocene apes. With a broad thorax, long lumbar spine and extended hips and knees, as in bipeds, and elongated and fully extended forelimbs, as in all apes (hominoids), *Danuvius* combines the adaptations of bipeds and suspensory apes, and provides a model for the common ancestor of great apes and humans.

Many studies since the nineteenth century have investigated the origin of human bipedalism. From Darwin and Huxley to the present, many researchers have added insights into this question but with little or no fossil evidence in support^{2–4}. Although many fossils have been discovered, none has shed light directly on this central question in palaeoanthropology.

Since the 1970s, many fossil apes from the middle to late Miocene epoch (13–5.3 million years ago (Ma)) from Europe have been discovered and described, along with smaller samples from the same time period in Africa^{5–7}. Apes and humans are thought to have diverged at this time⁸. Some of these discoveries include partial skeletons^{9,10}, but none shows preservation of completely intact long bones. Although opinions vary as to the relationship of these hominids to living hominids, nearly all researchers recognize European late Miocene apes as hominids as opposed to the stem hominoids of the early and middle Miocene epoch of Africa^{6,11,12}.

Postcranially, the most complete fossils from Europe include the well-preserved remains of the small bones of the hand, fragments of the long bones of the limbs, a partial pelvis and partially preserved vertebrae. These discoveries have provided insights into the anatomy of late Miocene apes. We know that these apes, including *Pierolapithecus*, *Dryopithecus*, *Hispanopithecus* and *Rudapithecus*, were suspensory and similar to modern great apes to varying degrees. However, without complete long bones of the limbs and well-preserved joint surfaces (especially of the lower limbs), interpretations of details of the positional behaviour of these apes remain limited.

Reconstructing the ancestral form of positional behaviour of great apes and humans is best accomplished through the analysis of fossils. On the basis of comparisons of *Ardipithecus*, extant catarrhines and Miocene apes, it has been argued that human bipedalism evolved from a

form of arboreal quadrupedalism in the last common ancestor of great apes and humans^{13,14}. Others have argued that bipedalism arose from a more suspensory ancestor, based largely on fossil evidence of late Miocene hominids^{6,11}. These scenarios are based on fragmentary fossil evidence. Here we present a different scenario based on our analysis of a well-preserved dryopithecine ape from Bavaria. The ulna, femur, tibia, vertebrae, hand and foot bones of this ape reveal unknown aspects of the anatomy of late Miocene apes and enable us to reconstruct what may be the ancestral morphology of the great apes and humans.

Extended limb clambering

The fossils (Fig. 1) include remains of at least four individuals, with a partial skeleton that is sufficiently complete to describe the morphology of the limbs and spine and proportions of the body in detail. The results reveal a combination of anatomical features that are indicative of a pattern of arboreal behaviour that we term extended limb clambering (ELC). It is characterized by generalized limb proportions superimposed on a unique combination of knee, ankle, elbow and wrist postures and strongly grasping extremities. ELC incorporates powerful hallux grasping, plantigrade feet, extended hip and knees, wide ranging elbow flexion–extension and pronation–supination, a mobile wrist, and hands with curved phalanges and a deep first metacarpal joint. It differs from previously identified forms of positional behaviour. Plantigrade and palmigrade quadrupeds (Old World monkeys and *Ekembo*) lack the suspensory attributes of the forelimb and the extension set of the knee. Knuckle-walkers (chimpanzees, bonobos and gorillas) lack the extended knee and have less powerfully developed hallux and pollical grasping. The hand phalanges of *Danuvius* also lack the robusticity typical of

¹Department of Geosciences, Eberhard-Karls-Universität Tübingen, Tübingen, Germany. ²Senckenberg Centre for Human Evolution and Palaeoenvironment, Tübingen, Germany.

³National Museum of Natural History, Bulgarian Academy of Sciences, Sofia, Bulgaria. ⁴Anatomy & Cell Biology, University of Indianapolis, Indianapolis, IN, USA. ⁵Paleontology & Geobiology, Ludwig-Maximilians-Universität, Munich, Germany. ⁶Earth Dynamics Research Group, School of Earth and Planetary Sciences, Curtin University, Perth, Western Australia, Australia.

⁷Department of Anthropology, University of Toronto, Toronto, Ontario, Canada. *e-mail: m.boehme@ifg.uni-tuebingen.de

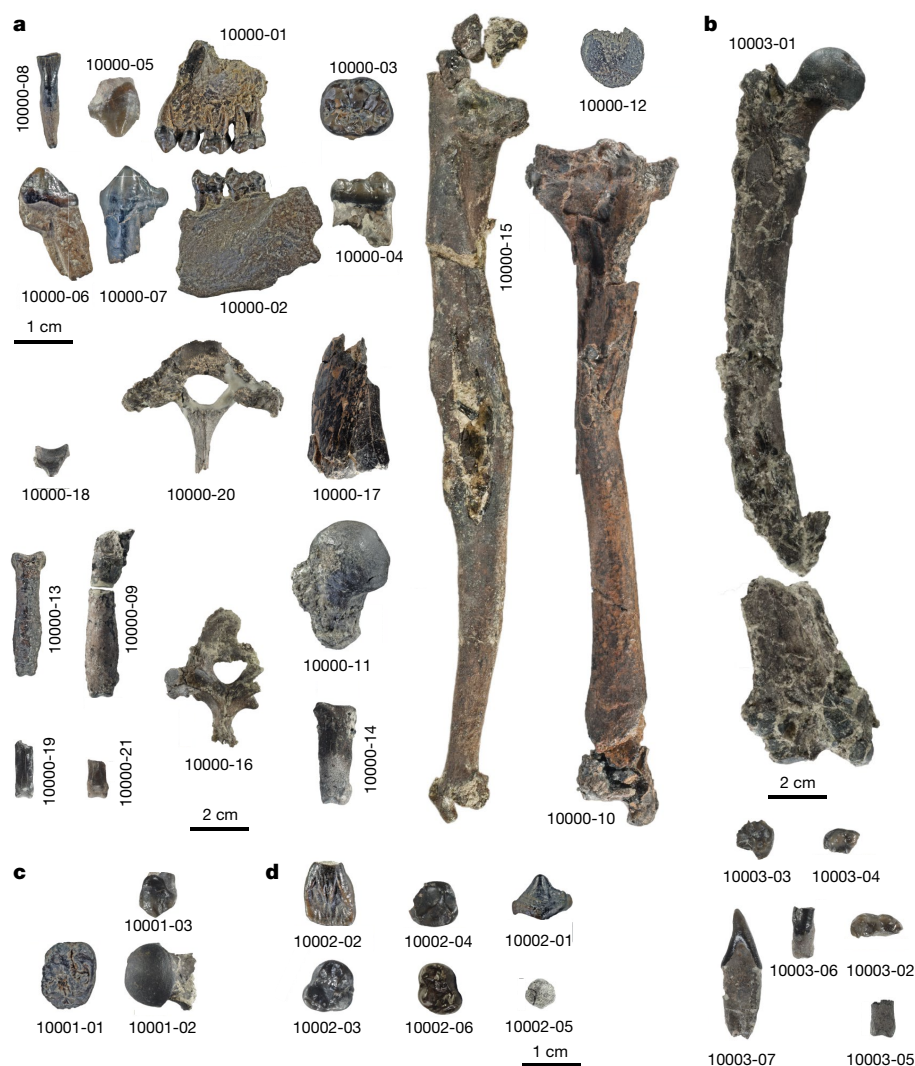


Fig. 1 | Fossil remains of four *D. guggenmosi* individuals from late Miocene sediments of Hammerschmiede. **a**, Holotype GPIT/MA/10000 male individual. **b–d**, Paratype individuals GPIT/MA/10003 (female), GPIT/MA/10001 (female) and GPIT/MA/10002 (juvenile). An excavation plan and a complete list of all elements can be found in Extended Data Fig. 1 and Supplementary Table 2. The scale bar is 20 mm for all bones and 10 mm for all isolated teeth.

knuckle-walkers. Arboreal clambering orangutans lack the weight-bearing adaptations present in the knee and ankle of *Danuvius* and have features that much more strongly emphasize forelimb postural and locomotor adaptations. *Danuvius* is distinguished from all known catarrhines in its vertebral morphology, with an elongated lumbar region combined with spinal invagination/lordosis, which shifts the body mass over the expanded proximal tibial joint surfaces. The uniqueness of ELC is that it does not favour the forelimb or the hindlimb, as in most primates, but utilizes both limbs in roughly equal proportions. ELC includes a combination of joint positions and loading patterns of both hominin bipedalism that emphasize hindlimb extension and spinal curvatures, and extant great ape suspension, which emphasizes powerful and mobile forelimbs. We propose ELC as a new model of the ancestral mode of positional behaviour of the last common ancestor of living great apes and humans. ELC is a precursor to obligate bipedalism, which shifts the emphasis of positional behaviour to the hindlimbs, and to suspension, in which the emphasis shifts to the forelimbs.

Systematic palaeontology

Order Primates Linnaeus, 1758
 Infraorder Catarrhini Geoffroy, 1812
 Family Hominidae Gray, 1825
Danuvius guggenmosi gen. et sp. nov.

Etymology. The genus name is derived from Celtic–Roman river god Danuvius. The trivial name honours the discoverer of the Hammerschmiede locality, Sigulf Guggenmos.

Holotype. Partial skeleton of male individual GPIT/MA/10000, comprising 21 elements (Fig. 1a): partial left mandible with M₁ and M₂, partial left maxilla with P³–M², isolated mandibular (left I₁, P₃; right P₃, M₂, M₃) and maxillary teeth (right P³), first and transitional thoracic vertebrae, left humeral shaft fragment, right ulna, left metacarpal I fragment, right proximal manual phalanges II and IV, two left intermediate manual phalanx fragments, right femoral head, right patella, left tibia, left proximal pedal phalanx I.

Paratypes. Two smaller adults (GPIT/MA/10001 (Fig. 1c), comprising left P³, M¹, left femur head; and GPIT/MA/10003 (Fig. 1b), comprising left I₁, I₂, fragments of M₁, M¹, M², left femur, proximal hallucal phalanx fragment) and one juvenile individual (GPIT/MA/10002 (Fig. 1d), comprising unerupted left P₃, left I₁, left and right DP₄, right DP⁴, epiphysis of the intermediate manual phalanx).

Locality and horizon. Hammerschmiede Clay pit near Pforzen (Allgäu region, Bavaria, Germany, Extended Data Fig. 1; 47.923° N, 10.588° E); level Hammerschmiede (HAM) 5 at stratigraphic metre 12 in the local section, which has been dated magnetostratigraphically to 11.62 million years ago¹⁵.

Diagnosis. Small hominid ranging in size from about 17 to 31 kg. The palate is narrow and deep with a thick palatine process; the maxilla is high, anteroposteriorly broad, with an anteriorly facing zygomatic root above the distal moiety of P⁴, maxillary sinus invaginating the zygomatic and alveolar processes, canine fossa deep and narrow, canine

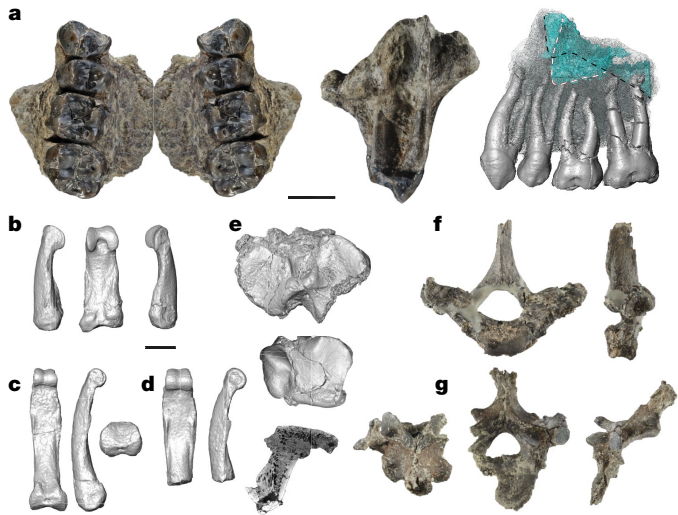


Fig. 2 | *D. guggenmosi* holotype. **a**, Palate (left; right side mirror-imaged) and left maxilla from superior (middle) and lateral (right) views, with a three-dimensional rendering of dental roots and maxillary sinus (blue). The sinus is invaginated by the posterobuccal and lingual roots of M^2 and is superior to the roots more anteriorly (dashed black line). Laterally the sinus extends into the zygomatic root (dashed white line); additional images are shown in Extended Data Fig. 10. **b**, Left proximal hallux phalanx in lateral (left), plantar (middle) and medial (right) views. **c**, Right proximal hand phalanx 2 in palmar (left), ulnar (middle) and proximal (right) views. **d**, Right proximal hand phalanx 4 in plantar (left) and ulnar (right) views. **e**, Tibial proximal (top) and distal (middle) articulations (anterior is up) and sagittal computed tomography cross-section through the middle of the lateral condyle (bottom; superior is up). **f**, First thoracic vertebra in superior (left) and left-lateral (right) views. **g**, Diaphragmatic vertebra in posterior (left), superior (middle) and right-lateral (right) views. Scale bars, 10 mm.

root alveolus vertically oriented; I^1 mesiodistally narrow, high-crowned with a strong lingual pillar and mesial marginal ridge; postcanine dentition with strongly developed crista, P^3 lacks the paraconule, molars are broad relative to the length with compressed trigons and thick enamel; mandibular corpus is low, robust with a prominent mandibular eminence and a broad extramolar sulcus; ulna has a straight shaft, moderately deep proximally, short olecranon, deep, strongly keeled, anteriorly oriented trochlear notch, large, laterally oriented radial notch, large head, short, non-articular styloid process; first metacarpal base strongly dorsopalmarly curved saddle-shaped joint; proximal hand phalanges are long, curved, with strongly developed flexor sheath ridges; femur head projects above the greater trochanter, extension of joint surface onto the superoposterior surface of femoral neck, neck compressed and strongly vertically oriented; tibia with broad proximal end, thickened metaphyses, mediolaterally concave condylar surfaces, lateral condyle anteroposteriorly flat, deeply incised and posteriorly oriented intercondylar notch, prominent intercondylar eminences, trochlear surface roughly square-shaped, strongly keeled, prominent malleolus deeply notched at its base with an anterolaterally expanded joint surface; patella with broad, flat joint surface; proximal hallux phalanx is large, robust at mid shaft, broad proximally, prominent flexor sheath ridges, strong lateral torsion of the distal end; first thoracic vertebra with short, divergent pedicles, strongly divergent zygapophyseal orientations, univertebral rib articulation; penultimate or antepenultimate diaphragmatic vertebra with a prominent metapophysis.

Differential diagnosis. The craniodental morphology of *Danuvis* is diagnostically dryopithecine ('Expanded differential diagnosis of *D. guggenmosi*' in the Methods). The anterior palate (Fig. 2a) is short in comparison with pongines, with a stepped subnasal fossa, as is typical

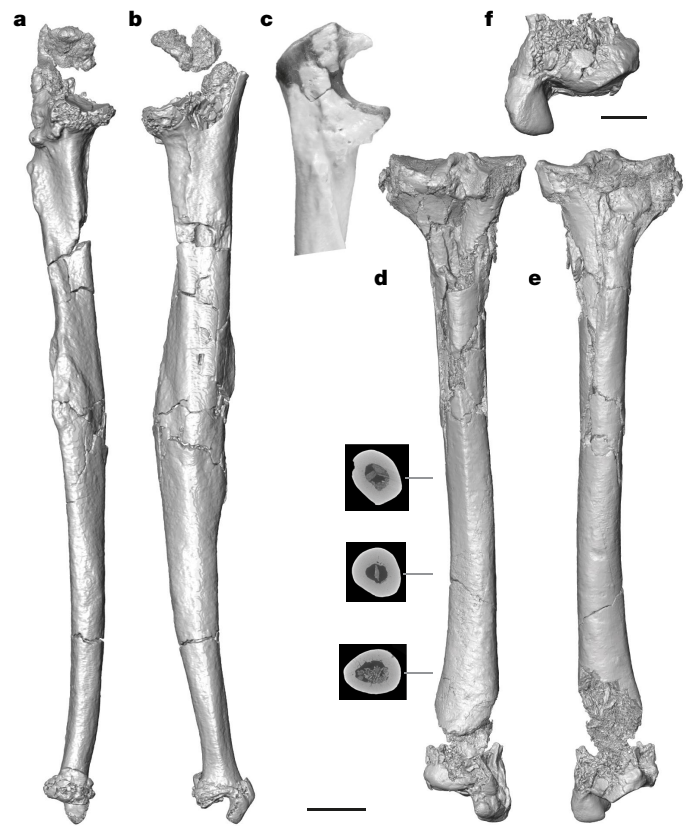


Fig. 3 | *D. guggenmosi*, right ulna (GPIT MA/10000-10) and left tibia (GPIT MA/10000-15). **a–c**, Anterolateral (a) and medial (b) views of the ulna and the reconstructed proximal end in lateral view (c). **d–f**, Posterior (d) and anterior (e) views of the tibia and the distal epiphysis in anterior view (f). Tibial shaft cross-sections are given at 20%, 35% and 50% of shaft length from the distal end. Additional images of the ulna and tibia are shown in Extended Data Fig. 4. Scale bars, 20 mm (a–e) and 10 mm (f).

of dryopithecines and extant hominines. *Danuvis* is distinguished from other dryopithecines in having a unique combination of facial attributes (compressed canine fossa, vertical canine implantation, anteriorly facing malar surface, robust mandible, prominent mandibular eminence, wide extramolar sulcus; Extended Data Fig. 2). The proximal ulna differs from *Hispanopithecus* and *Rudapithecus* in its anteriorly facing trochlear notch and expanded coronoid process (Fig. 3). The distal tibia differs from *Hispanopithecus* in its more squared outline and in details of articular morphology (see Supplementary Information for detailed descriptions and comparisons and Supplementary Tables 3–24 for measurements).

Limb proportions and posture

The postcrania of *Danuvis* reveals numerous previously unknown aspects of dryopithecine morphology. Compared with the length of the tibia, *Danuvis* has a relatively elongated ulna (Fig. 4a and Extended Data Fig. 3), comparable to *Pan paniscus*. In *Pongo*, the ulna is longer whereas in cercopithecoids and early hominins it is shorter. On the basis of reconstructed lengths, *Oreopithecus* and *Hispanopithecus* have tibia:ulna ratios that are comparable to that of *Danuvis*.

A mediolaterally broad thorax and orthograde is inferred from the dorsal orientation of the thoracic transverse processes, combined with a low costal facet angle on the first thoracic vertebra¹⁶ (Fig. 2f, g). Inferred from the difference in inclination of the spinous processes between the first vertebra and the lower thoracic vertebra, the upper spinal column was substantially curved (cervical lordosis/thoracic kyphosis)¹⁷.

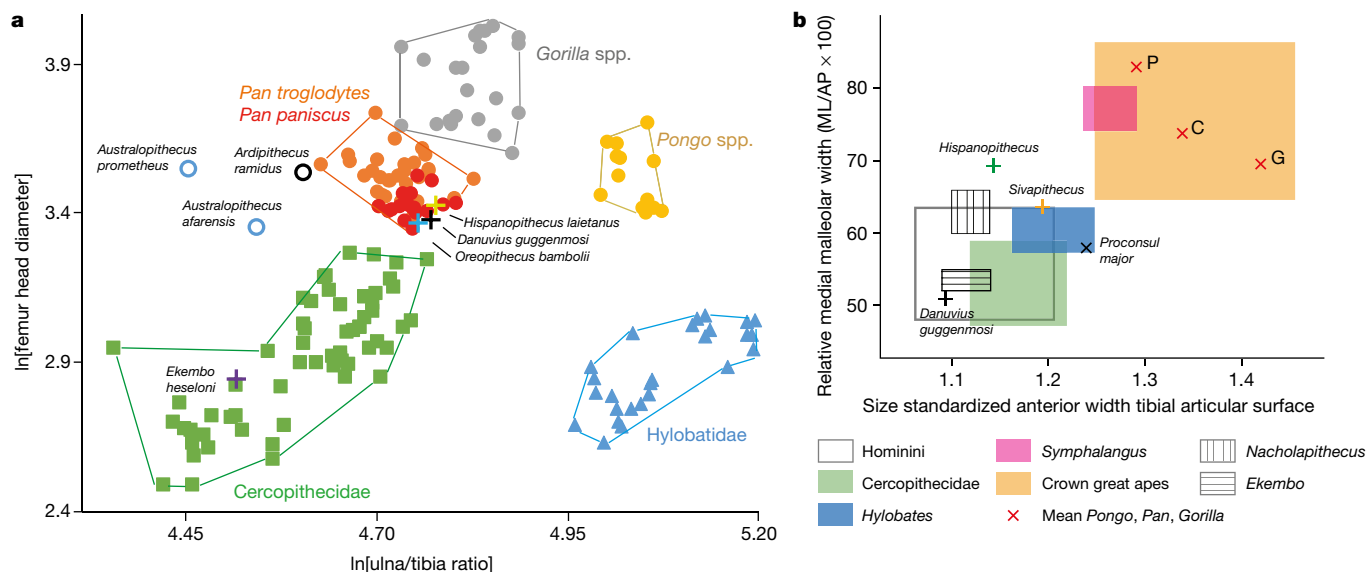


Fig. 4 | Body proportions and distal tibia articulation metrics. a, Ratio of ulna-to-tibia physiologic length (natural logarithm) in relation to body mass (natural logarithm of femur head diameter) of extant catarrhines ($n = 178$; for raw data see Supplementary Table 7) compared to fossil hominoids (*D. guggenmosi*, GPIT/MA10000; *Hispanopithecus laietanus*, IPS 18000; *Oreopithecus bamboli*, IGF 11778; *Ardipithecus ramidus*, ARA-VP-6/500; *Australopithecus prometheus*, StW 573; *Australopithecus afarensis*, A.L. 288-1; *Ekembo heseloni*, KNM-RU 2036; data are from previous studies^{9,13,37–40}). **b**, Plot of relative thickness of tibial

medial malleolus and size-standardized anterior width of tibial distal articular surface (measurements follow a previous study⁴¹) of extant catarrhines, compared to fossil hominoids (*D. guggenmosi*, GPIT/MA/10000; *H. laietanus*, IPS 18000; *Sivapithecus indicus*, YGSP 1656; *Nacholapithecus kerioi*, KNM-BG 35250; *E. heseloni*, KNM-RU 2036, 3589; *Proconsul major*, NAPI 58; comparative data were obtained from previous studies^{31,32,41}; for raw data see Supplementary Tables 19, 20). C, *Pan*; G, *Gorilla*; P, *Pongo*.

D. guggenmosi is, to our knowledge, the first Miocene hominid with evidence of diaphragmatic vertebra placement, which is important in interpreting thoracolumbar spine evolution in hominoids¹⁸. The well-developed costotransversal facet of GPIT/MA/10000-16 (Fig. 2g) indicates a non-ultimate thoracic position for the diaphragmatic vertebra and therefore a functionally longer lower back, as in early hominins, stem-hominoids and cercopithecids^{18–24}. On the basis of indirect evidence from the pelvis, a longer lower back has also been inferred for *Rudapithecus*²⁵. Extant hominoids including *Homo* show a diaphragmatic placement at the ultimate thoracic vertebra level²⁴. The contrasting vertebral configuration of *Danuivius* suggests that diaphragmatic cranial displacement is the symplesiomorphic hominoid condition, supporting the long-back model^{26,27}. The increased number of functional lumbar vertebrae allows sagittal flexibility to lordose the lumbar column, which contributes to effectively position the centre of mass over extended hips, knees and plantigrade feet (see below), implying at least some degree of habitual bipedal posture¹⁶.

Positional behaviour

Several skeletal elements of the upper limb bear unmistakable hallmarks of below-branch or suspensory positional behaviour (Fig. 3a–c and Extended Data Fig. 4). Despite the pathology evident on the ulna (Supplementary Information), these include a reduced olecranon process, broad, keeled trochlear notch with prominent medial and lateral surfaces for a trochlear humeral trochlea, large laterally oriented radial facet, robust proximal ulnar shaft and a reduced, non-articular ulnar styloid process. The proximal hand phalanges are curved with prominent flexor sheath ridges (Fig. 2c, d and Extended Data Figs. 5, 6), indicating that suspension played an important—but not dominant—part in its locomotory repertoire (for example, more similar to *Pan* than to *Pongo*). Powerful pollical grasping and increased thumb mobility are indicated by the strong dorsopalmar and radioulnar curvatures of the base of the first metacarpal (Fig. 1a).

The lower limb suggests postural extension at the hip and knee joints and a uniform force distribution in a stabilized ankle joint, combined with a powerful grasping hallux. On the femur (Fig. 1b and Extended

Data Fig. 7b–d), the low greater trochanter, the more vertically oriented neck and the posterosuperior expanded joint surface suggest that the femoral head articulated in habitual extension with an os coxae that was laterally rotated, which would have caused the iliac blade to be more tilted inferolaterally. This may have enhanced the function of the gluteal muscles as hip stabilizers (abductors) in bipedal posture, as in hominins. The flat patella (Fig. 1a and Extended Data Fig. 7a) and shallow rounded patellar surface suggest slow and deliberate movements (Supplementary Information). The absence of an anteroposterior convexity to the lateral tibial condyle (Fig. 2e and Extended Data Fig. 8), a character shared with hominins and hylobatids²⁸, suggests an extension set to the knee joint, as a flatter contour maximizes tibiofemoral contact area and joint stability during extended knee postures. A buttressing of the tibial metaphysis also reflects stereotypical extended knee postures under compressive load^{28,29}. The exceptional development of the intercondylar eminence is probably related to the presence of strongly developed cruciate ligaments. The subequal size of the tibial condyles indicate a more equally distributed weight transmission on the knee joint³⁰. Together, the morphology of the tibial plateau suggests an adaptation emphasizing an extended knee reinforced by strongly developed intra-articular ligaments. We interpret the distal tibia of *Danuivius*, with its mediolaterally short anterior trochlear margin and its mediolaterally narrow malleolus (Fig. 4b), to be an adaptation to a more uniform distribution of forces across the joint surface, with limited ankle loading in dorsiflexion and inversion compared to extant apes^{31,32}. The combination of the anteroposteriorly deep malleolus, medially expanded joint surface, prominent anterior margin with a strongly developed beak and strongly inclined medial and lateral trochlear surfaces produces a hinge-like morphology to the anterior talocrural joint, which would have been most stable with the foot roughly perpendicular to the long axis of the tibia. This is corroborated by the nearly perpendicularly orientated tibia relative to the horizontal plane of the ankle joint (Fig. 3d, e and Supplementary Information). Extant great apes, which load the ankle in inversion during climbing, have an obliquely oriented tibia relative to the plane of the ankle joint^{31,33}. The near perpendicular tibial angle is a shared

character between hominins and *Danuvius* and supports the inference of a habitual valgus knee position and bipedalism for the new genus.

A robust, elongated and strongly laterally torsioned hallux (Extended Data Figs. 5b, c, 9) with well-developed muscular attachments suggests an emphasis on powerful hallucal grasping with adducted ankle stabilized in a neutral position relative to the long axis of the tibia. In contrast to extant apes, the hallux was capable of interphalangeal hyperflexion, as indicated by the substantial plantar inter-condylar recess and depression (Fig. 2b), enabling *Danuvius* to securely grasp small-diameter arboreal supports.

Discussion

The uniqueness of *D. guggenmosi* is demonstrated by its small body size (between siamangs and bonobos; Supplementary Information and Supplementary Table 23) with limb proportions most similar to bonobos (Fig. 4a), a cranial shifted diaphragmatic vertebra (Fig. 2g), a strong grasping hallux (Fig. 2b) and a morphology of the tibia that is surprisingly similar to hominins (large-sized and flat lateral condyle with 'buttressed' plateau, tibial shaft perpendicular to talar facet, mediolaterally narrow malleolus and short anterior trochlear margin) (Fig. 3d–f, Extended Data Fig. 4 and Supplementary Information). The combination of morphological attributes of the limbs and vertebra of *Danuvius* point to a newly recognized form of positional behaviour. In contrast to suspensory behaviour, clambering and arm-assisted bipedalism in *Pongo*³⁴ or climbing and suspension in African apes, ELC involves equal contributions of the fore- and hindlimbs. The foot is flat and adducted on horizontal to mildly inclined branches with a hallux capable of powerful grasping, stabilizing the hindlimb. Torques resulting from body rotation above the knee are countered by powerfully developed cruciate ligaments. The knee is habitually extended and supported by a thickened plateau and large, flat-to-concave, proximally facing condyles. The elbow is capable of a full range of flexion–extension and pronation–supination as in extant hominoids. The hand was strong enough to generate the force to counter torques in a variety of positions ranging from suspensory to palmigrade, but without the hyperextension at the metacarpophalangeal joints that characterize Old World monkeys and *Pierolapithecus*. This newly defined locomotor category includes attributes of orthograde suspension and hominin bipedalism, making it a potential candidate for the positional behaviour of the last common ancestor of great apes and humans. *Danuvius* provides fossil evidence that hominin bipedalism and great ape suspension evolved from a form of arboreal locomotion that incorporates attributes of each^{35,36}, which has roots in the middle Miocene of Europe.

Online content

Any methods, additional references, Nature Research reporting summaries, source data, extended data, supplementary information, acknowledgements, peer review information; details of author contributions and competing interests; and statements of data and code availability are available at <https://doi.org/10.1038/s41586-019-1731-0>.

1. Begun, D. R. in *Biped to Strider: The Emergence of Modern Human Walking* (eds Meldrum, D. J. & Hilton, C. E.) 9–33 (Kluwer, 2004).
2. Begun, D. R. & Kivell, T. L. Knuckle-walking in *Sivapithecus*? The combined effects of homology and homoplasy with possible implications for pongine dispersals. *J. Hum. Evol.* **60**, 158–170 (2011).
3. Richmond, B. G., Begun, D. R. & Strait, D. S. Origin of human bipedalism: the knuckle-walking hypothesis revisited. *Am. J. Phys. Anthropol.* **116**, 70–105 (2001).
4. Crompton, R. H., Sellers, W. I. & Thorpe, S. K. Arboreality, terrestriality and bipedalism. *Phil. Trans. R. Soc. Lond. B* **365**, 3301–3314 (2010).
5. Begun, D. R. Dryopithecines, Darwin, de Bonis, and the European origin of the African apes and human clade. *Geodiversitas* **31**, 789–816 (2009).
6. Begun, D. R., Nargolwalla, M. C. & Kordos, L. European Miocene hominids and the origin of the African ape and human clade. *Evol. Anthropol.* **21**, 10–23 (2012).
7. Alba, D. M. Fossil apes from the vallès-penedès basin. *Evol. Anthropol.* **21**, 254–269 (2012).
8. Langergraber, K. E. et al. Generation times in wild chimpanzees and gorillas suggest earlier divergence times in great ape and human evolution. *Proc. Natl Acad. Sci. USA* **109**, 15716–15721 (2012).

9. Moyà-Solà, S. & Köhler, M. A *Dryopithecus* skeleton and the origins of great-ape locomotion. *Nature* **379**, 156–159 (1996).
10. Moyà-Solà, S., Köhler, M., Alba, D. M., Casanovas-Vilar, I. & Galindo, J. *Pierolapithecus catalaunicus*, a new Middle Miocene great ape from Spain. *Science* **306**, 1339–1344 (2004).
11. Alba, D. M., Almécija, S., Casanovas-Vilar, I., Méndez, J. M. & Moyà-Solà, S. A partial skeleton of the fossil great ape *Hispánopithecus laietanus* from Can Feu and the mosaic evolution of crown-hominoid positional behaviors. *PLoS ONE* **7**, e39617 (2012).
12. Begun, D. R. in *Handbook of Paleoanthropology* (eds Henke, W. & Tattersall, I.) 1261–1332 (Springer, 2015).
13. Lovejoy, C. O., Suwa, G., Simpson, S. W., Matternes, J. H. & White, T. D. The great divides: *Ardipithecus ramidus* reveals the postcrania of our last common ancestors with African apes. *Science* **326**, 73–106 (2009).
14. White, T. D., Lovejoy, C. O., Asfaw, B., Carlson, J. P. & Suwa, G. Neither chimpanzee nor human, *Ardipithecus* reveals the surprising ancestry of both. *Proc. Natl Acad. Sci. USA* **112**, 4877–4884 (2015).
15. Kirscher, U. et al. A biochronologic tie-point for the base of the Tortonian stage in European terrestrial settings: magnetostratigraphy of the topmost Upper Freshwater Molasse sediments of the North Alpine Foreland Basin in Bavaria (Germany). *Newsl. Stratigr.* **49**, 445–467 (2016).
16. Williams, S. A. & Russo, G. A. Evolution of the hominoid vertebral column: the long and the short of it. *Evol. Anthropol.* **24**, 15–32 (2015).
17. Latimer, B. & Ward, C. V. in *The Nariokotome Homo erectus Skeleton* (eds Walker, A. & Leakey, R.) 266–293 (Springer, 1993).
18. Williams, S. A., Middleton, E. R., Villamil, C. I. & Shattuck, M. R. Vertebral numbers and human evolution. *Am. J. Phys. Anthropol.* **159**, 19–36 (2016).
19. Haeusler, M., Regula, S. & Thomas, B. Modern or distinct axial bauplan in early hominins? A reply to Williams (2012). *J. Hum. Evol.* **63**, 557–559 (2012).
20. Nakatsukasa, M. & Kunimatsu, Y. *Nacholapithecus* and its importance for understanding hominoid evolution. *Evol. Anthropol.* **18**, 103–119 (2009).
21. Pilbeam, D. The anthropoid postcranial axial skeleton: comments on development, variation, and evolution. *J. Exp. Zool.* **302B**, 241–267 (2004).
22. Ward, C. V., Walker, A., Teaford, M. F. & Odhiambo, I. Partial skeleton of *Proconsul nyanzae* from Mfangano island, Kenya. *Am. J. Phys. Anthropol.* **90**, 77–111 (1993).
23. Ward, C. V., Nalley, T. K., Spoor, F., Tafforeau, P. & Alemseged, Z. Thoracic vertebral count and thoracolumbar transition in *Australopithecus afarensis*. *Proc. Natl Acad. Sci. USA* **114**, 6000–6004 (2017).
24. Williams, S. A. Placement of the diaphragmatic vertebra in catarrhines: implications for the evolution of dorsostability in hominoids and bipedalism in hominins. *Am. J. Phys. Anthropol.* **148**, 111–122 (2012).
25. Ward, C. V., Hammond, A. S., Plavcan, J. M. & Begone D. R. A late Miocene hominid partial pelvis from Hungary. *J. Hum. Evol.* <https://doi.org/10.1016/j.jhevol.2019.102645> (2019).
26. McCollum, M. A., Rosenman, B. A., Suwa, G., Meindl, R. S. & Lovejoy, C. O. The vertebral formula of the last common ancestor of African apes and humans. *J. Exp. Zool.* **314B**, 123–134 (2010).
27. Lovejoy, C. O. & McCollum, M. A. Spinopelvic pathways to bipedality: why no hominids ever relied on a bent-hip–bent-knee gait. *Phil. Trans. R. Soc. Lond. B* **365**, 3289–3299 (2010).
28. Landis, E. K. & Karnick, P. A three-dimensional analysis of the geometry and curvature of the proximal tibial articular surface of hominoids. In *Proc. SPIE 60560K Three-Dimensional Image Capture and Applications VII 60560K* (International Society for Optics and Photonics, 2006).
29. Frelat, M. A. et al. Evolution of the hominin knee and ankle. *J. Hum. Evol.* **108**, 147–160 (2017).
30. Tardieu, C. Ontogeny and phylogeny of femoro-tibial characters in humans and hominid fossils: functional influence and genetic determinism. *Am. J. Phys. Anthropol.* **110**, 365–377 (1999).
31. DeSilva, J. M. Functional morphology of the ankle and the likelihood of climbing in early hominins. *Proc. Natl Acad. Sci. USA* **106**, 6567–6572 (2009).
32. DeSilva, J. M., Morgan, M. E., Barry, J. C. & Pilbeam, D. A hominoid distal tibia from the Miocene of Pakistan. *J. Hum. Evol.* **58**, 147–154 (2010).
33. Latimer, B., Ohman, J. C. & Lovejoy, C. O. Talocrural joint in African hominoids: implications for *Australopithecus afarensis*. *Am. J. Phys. Anthropol.* **74**, 155–175 (1987).
34. Thorpe, S. K., Holder, R. L. & Crompton, R. H. Origin of human bipedalism as an adaptation for locomotion on flexible branches. *Science* **316**, 1328–1331 (2007).
35. Thorpe, S. K., McClymont, J. M. & Crompton, R. H. The arboreal origins of human bipedalism. *Antiquity* **88**, 906–914 (2014).
36. Wolpoff, M. *Australopithecus*: a new look at an old ancestor (part 2). *Gen. Anthropol.* **3**, 1–5 (1997).
37. Straus, W. in *Classification and Human Evolution* (ed. Washburn, S. L.) 146–177 (Aldine, 1963).
38. Asfaw, B. et al. *Australopithecus garhi*: a new species of early hominid from Ethiopia. *Science* **284**, 629–635 (1999).
39. Ruff, C. B. Long bone articular and diaphyseal structure in Old World monkeys and apes. II: estimation of body mass. *Am. J. Phys. Anthropol.* **120**, 16–37 (2003).
40. Haile-Selassie, Y. et al. An early *Australopithecus afarensis* postcranium from Woranso-Mille, Ethiopia. *Proc. Natl Acad. Sci. USA* **107**, 12121–12126 (2010).
41. DeSilva, J. M. *Vertical Climbing Adaptations in the Anthropoid Ankle and Midfoot: Implications for Locomotion in Miocene Catarrhines and Plio-Pleistocene Hominins*. PhD thesis, Univ. Michigan, (2008).

Publisher's note Springer Nature remains neutral with regard to jurisdictional claims in published maps and institutional affiliations.

© The Author(s), under exclusive licence to Springer Nature Limited 2019

Methods

Geology, age, fossils and taphonomy

The HAM 5 channel represents a riffle pool sequence of a small and shallow meandering rivulet with a talweg width of 4–5 m and a maximum pool depth of 1 m. The gravelly bed load is composed exclusively of reworked pedogenic carbonate concretions that are typically 4–8 mm in diameter. Similar concretions are abundant in Bk palaeosol horizons of the bedrock, indicating a local source of HAM 5 rivulet. Magnetostratigraphy of the local 26-m thick section, combined with a nearby 150 m deep drill core, revealed the date of the channel fill of 11.620 million years ago (± 5 thousand years), directly at the base of the Tortonian, late Miocene¹⁵. Excavation of about 200 m² between 2011 and 2018 revealed a high vertebrate diversity that comprised 100 species of fishes, amphibians, reptiles, birds and mammals (see Supplementary Table 1 for faunal list). Hominids are a common element in this thanatocoenosis, representing about 10% of all excavated large mammal individuals. Excavation demonstrates that fossil vertebrates are found exclusively along the channel, suggesting some sort of accumulation. Most finds are disarticulated skeletal elements, which tend to be complete in small- and medium-sized mammals (for example, carnivores, artiodactyls and primates) and broken and sometimes abraded in large-size taxa (for example, perissodactyls and proboscideans). Skeletal articulation occurs in rare cases. However, many medium-sized individuals are documented by associated specimens found within a few square metres, suggesting minor transport and sorting of bones. The 21 bones and teeth from the most complete hominid individual GPIT/MA/10000 represent about 15% of the skeleton. It is found within the talweg at a maximum distance of 20 m, except the first thoracic vertebra, which was found a further 10 m downstream. Moderate sorting of GPIT/MA/10000 is documented by proximal concentration of isolated teeth, followed by skull elements and more distally long bones and phalanges, whereas vertebrae are transported furthest down the channel (Extended Data Fig. 1). This arrangement follows experimentally observed patterns of bone taphocoenosis in rivers⁴².

Fossil repository

All Hammerschmiede fossils are stored in the palaeontological collection of the University of Tübingen (acronym GPIT), a research infrastructure of the Senckenberg Institute for Human Evolution and Palaeoenvironment (SHEP) Tübingen.

Bone preservation

The Hammerschmiede locality is an active clay-mining pit. Sediments from the fossiliferous rivulet channel HAM 5 are composed of fine-pebbly pedogenic carbonate nodules and marls with various degrees of silt and rare fine-sand admixture. Owing to mining activities, water-saturated clay-rich sediments on steep section walls tend to creep and heavy machinery add compressive load on the sediment surface. Therefore, postcranial long bones of smaller large mammals (for example, deer, tragulids, carnivores and primates) tend to be compressed at the shaft and occasionally laterally distorted. This strongly affected the complete femur of GPIT/MA/10003 (shaft compressed by machinery loading, folded along the shaft due to ground creeping), which was embedded in soft clay. The complete ulna of GPIT/MA/10000 is uncompressed, but at midshaft the cortical bone of the down-lying side is crushed and pushed into the shaft, probably by load compression. Computer tomographic images show that this preservation was facilitated by midshaft osteoporosis. By contrast, the complete tibia of GPIT/MA/10000, embedded in a less compressible silt-dominated matrix, is not crushed along the shaft, but laterally distorted at the tuberosity and slightly damaged at medial condyle and distal metaphysis, which are the result of excavation artefacts. Importantly, all cranial and small postcranial ape specimens (phalanges, metapodial, carpal bone and patella), as well as long-bone joint

articulations remained undisturbed, but occasionally show small excavation artefacts.

Length reconstruction

To measure the total and physiologic length of distorted long bones, we use three-dimensional prints of virtual reconstructions for the holotype tibia and ulna (GPIT/MA/10000-10 and -15, respectively). The total length of the crushed paratype femur (GPIT/MA/10003-01) is estimated with an accuracy of about ± 5 mm.

Expanded differential diagnosis of *D. guggenmosi*

The molars lack cingula and are elongated relative to length, with peripheralized cusps. These attributes and P₃ cusp morphology, P₄ length and M₁–M₂ proportions distinguish *Danuvius* from *Ekembo* and other early Miocene hominoids. The dentition is readily distinguished from thickly enamelled middle and late Miocene apes such as *Kenyapithecus*, *Nacholapithecus*, *Griphopithecus*, *Sivapithecus* and *Ouranopithecus*.

The maxilla of *D. guggenmosi* (Figs. 1a, 2a and Extended Data Figs. 2a, 3a) differs from *Anoiapithecus*, *Pierolapithecus* and *Dryopithecus* in its anteroposteriorly broad zygomatic root (zygomatico-alveolar crest) and convex and postero-inferiorly inclined temporal surface; deeply invaginated maxillary sinus floor; vertically implanted upper male canine (supero-inferiorly and mediolaterally); deep, anteroposteriorly narrow canine fossa and anteriorly facing zygoma. Differs from *Hispanopithecus* and *Rudapithecus* maxilla in its deep, anteroposteriorly narrow canine fossa and anteriorly facing zygoma, anteriorly positioned zygomaticoalveolar crest and deeper palate. Maxillary dentition differs from *Anoiapithecus*, *Pierolapithecus* and *Dryopithecus* by broader premolars; triangular P³; low mesial and distal P³ buccal shoulders; more mesiodistally centralized premolar cusps (shorter talon); broad, concave premolar trigon and talon basins; more strongly developed molar crista; more peripheralized cusps; mesiodistally compressed trigon. I¹ differs from *Pierolapithecus* and cf. *Dryopithecus* sp. (La Grive) in its more strongly developed mesial marginal ridge and convex lingual surface. The maxillary dentition differs from *Hispanopithecus* and *Rudapithecus* in its low P³ crown shoulders and broad upper premolars. The mandible (Fig. 1a and Extended Data Fig. 2b) differs from *Anoiapithecus* and *Dryopithecus* in its shallower, robust corpus (unknown in *Pierolapithecus*), prominent mandibular eminence and wide extramolar sulcus. Mandibular dentition differs from *Anoiapithecus* and *Dryopithecus* in its lower crowned, mesially more vertical P₃ with a prominent mesial beak; broader molar trigonid and talonid basins; shorter mesial fovea; absence of buccal cingula; elongated molars; short M₁ roots (not visible in *Anoiapithecus*). The mandible differs from *Hispanopithecus* and *Rudapithecus* mandibles in the same way as from *Anoiapithecus*, *Pierolapithecus* and *Dryopithecus* and from the lower teeth of *Hispanopithecus* and *Rudapithecus* in having restricted mesial and distal fovea. The mandibular dentition differs from *Ouranopithecus* as it is smaller with more thinly enamelled teeth and it differs in other attributes as in *Rudapithecus* and *Hispanopithecus*. It also differs from *Oreopithecus* in having lower postcanine cusps, less strongly developed crista/cristids, no centroconid, higher P₄ talonid, higher crowned I¹, no upper postcanine lingual cingula. The maxilla differs from early and middle Miocene hominoids in the high position of the zygomatic root. The dentition differs from early and middle Miocene hominoids in the absence of molar cingula, first and second molars of similar size, peripheralized molar cusps, more vertical mesiobuccal P³ surface and short P⁴ shoulders, and higher P₄ talonid.

The partial skeleton GPIT/MA/10000 includes dental and postcranial remains that are much larger than the other Hammerschmiede individuals. This along with the strongly flared mesiobuccal face of the P₃ (Fig. 1a and Extended Data Fig. 2g, j) and the large, elongated canine alveolus (Fig. 2a) strongly imply that GPIT/MA 10000 is a male.

Body mass calculations

For the calculation of the body mass of the individuals, we used metric traits (individual measurements) from hind limbs (femur and tibia) because they are most involved in weight carrying during locomotion in great apes³⁹. Our univariate body-mass predictions are based on regression equations from a previously published study³⁹ for sex/species means of hominoids. In addition, as we can show that body proportions of the male individual GPIT/MA/10000 fall within the range of bonobos and chimpanzees, we assume a comparable scaling pattern and apply regression equations established previously⁴³ for femur head size of the genus *Pan*. Both methods produce very similar results for the male individual within the 50% confidence interval (Supplementary Table 23). Femur size of the two female specimens GPIT/MA/10001 and GPIT/MA/10003 are significantly lower than of any extant great ape, and hence outside any hominid comparative sample. We therefore use the previously compiled regression equations³⁹ for the total primate sample (hominoids plus cercopithecoids) for the predictor femur head size and cercopithecoid equations for predictions based on femoral condyle breadth (as recommended in the previously published study³⁹).

Calculations of enamel thickness

We used the right M₂ of the holotype (GPIT/MA/10000-03) to calculate enamel thickness given its low occlusal wear (slightly higher on mesial half, wear stage 1–2 according to a previously published study⁴⁴). This tooth was scanned with a FF35 CT at the YXLON Application centre in Heilbronn (Germany) and captured at 170 kV and 55 μ A (500-ms exposure time), obtaining a voxel size of 15.8 μ m (Extended Data Fig. 3b). Following a previously published study⁴⁵, virtual buccolingual sections of the molar were performed using Avizo 9.0. Mesial and distal virtual sections were defined by the tips of the metaconid–protoconid and entoconid–hypoconid perpendicular to the cervical plane. The following variables were measured two-dimensionally in both planes: dentine area (*b*), enamel cap area (*c*), length of the enamel–dentine junction (*e*) and the bi-cervical diameter. The average enamel thickness was calculated as *c/e* and the relative enamel thickness (RET) was calculated as previously described⁴⁶ using $RET = 100 \times \left[\frac{(c/e)}{\sqrt{b}} \right]$. For GPIT/MA/10000-03, the RET = 19.36, based on data from the least worn distal section (Supplementary Table 6).

Ellipse estimates of lateral tibial condyle curvature

To estimate the shape of the lateral tibial condyle, we performed a cut through the sagittal mid-line of the condyle on the three-dimensional scans of tibiae from *D. guggenmosi* (Fig. 2e) and extant catarrhines (Extended Data Fig. 6) using an Artec Space Spider with Artec Studio 11 (three-dimensional scans) and Avizo 9 (cross-sections). Subsequently, the cross-sections were digitalized and a best-fit ellipse was obtained using a non-iterative MATLAB function ('EllipseDirectFit'; from

N. Chernov (code available from <https://www.mathworks.com/>)). To compare the individual ellipses, we further calculated the eccentricity $e = \sqrt{1 - (b/a)^2}$ in which *a* and *b* are the semi-major and semi-minor axes with $a \geq b$. The closer *e* is to 1, the more elongated the ellipse is, whereas $e = 0$ represents a circle.

Reporting summary

Further information on research design is available in the Nature Research Reporting Summary linked to this paper.

Data availability

All data generated or analysed during this study are included in this published Article (and its Supplementary Information). The computed tomography scans are available from the corresponding author on reasonable request. The new taxon has the following Life Science Identifier: <http://zoobank.org/References/E1573024-9543-4B1E-A79B-6E40896A4617>.

- Behrensmeyer, A. K. The taphonomy and paleoecology of Plio-Pleistocene vertebrate assemblages east of Lake Rudolf, Kenya. *Bull. Mus. Comp. Zool.* **146**, 473–578 (1975).
- Almécija, S. et al. The femur of *Orrorin tugenensis* exhibits morphometric affinities with both Miocene apes and later hominins. *Nat. Commun.* **4**, 2888 (2013).
- Smith, B. H. Patterns of molar wear in hunger-gatherers and agriculturalists. *Am. J. Phys. Anthropol.* **63**, 39–56 (1984).
- Smith, T. M., Olejniczak, A. J., Martin, L. B. & Reid, D. J. Variation in hominoid molar enamel thickness. *J. Hum. Evol.* **48**, 575–592 (2005).
- Martin, L. B. *The Relationships of the later Miocene Hominoidea*. PhD thesis, Univ. College London (1983).
- Wessel, P. et al. Generic mapping tools: improved version released. *EOS* **94**, 409–410 (2013).
- Amante, C. & Eakins, B. W. *ETOPO1 Arc-Minute Global Relief Model: Procedures, Data Sources and Analysis NOAA Technical Memorandum NESDIS NGDC-24* <https://www.ngdc.noaa.gov/mgg/global/relief/ETOPO1/docs/ETOPO1.pdf> (National Geophysical Data Center, NOAA, 2009).
- Reuter H. I., Nelson, A. & Jarvis, A. An evaluation of void-filling interpolation methods for SRTM data. *Int. J. Geogr. Inf. Sci.* **21**, 983–1008 (2007).
- Almécija, S., Alba, D. M. & Moyà-Solà, S. *Pierolapithecus* and the functional morphology of Miocene ape hand phalanges: paleobiological and evolutionary implications. *J. Hum. Evol.* **57**, 284–297 (2009).

Acknowledgements We are indebted to the following researchers and curators for granting access to collections under their care: S. Moyà-Solà and D. Alba, E. Gilissen, L. Costeur, A. van Heteren, S. Merker, E. Weber. We thank C. Schulbert and J.-F. Metayer for computed tomography scanning, and A. Fatz, H. Stöhr and W. Gerber for technical support.

Author contributions M.B. and D.R.B. designed the study; M.B., N.S., J.F., A.T., A.S.D., J.P., U.K., T.L. and D.R.B. collected the data and performed the analyses; M.B., D.R.B. and N.S. discussed the results and wrote the paper.

Competing interests The authors declare no competing interests.

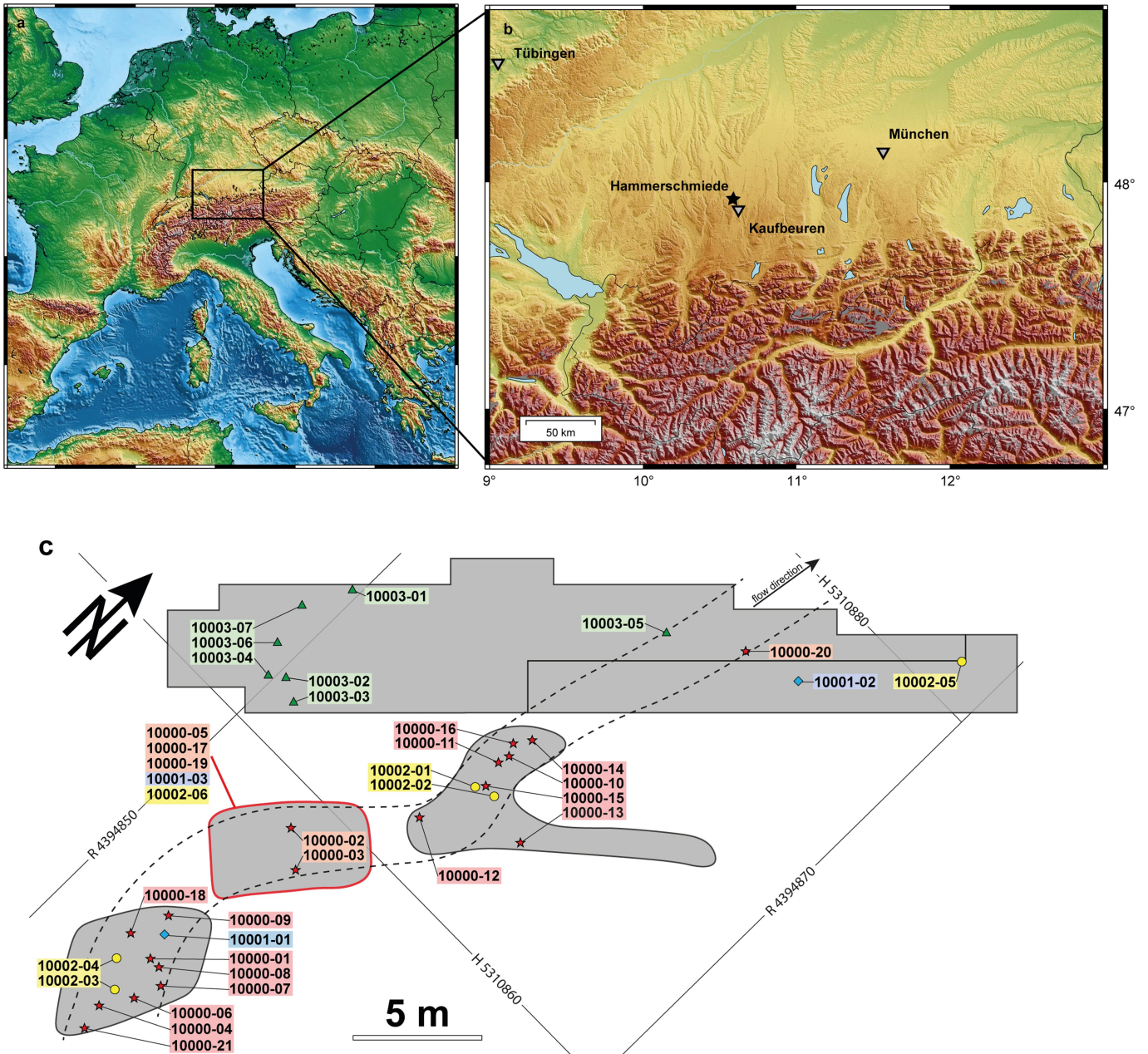
Additional information

Supplementary information is available for this paper at <https://doi.org/10.1038/s41586-019-1731-0>.

Correspondence and requests for materials should be addressed to M.B.

Peer review information Nature thanks Jeremy M. DeSilva, Tracy Kivell and Salvador Moyà-Solà for their contribution to the peer review of this work.

Reprints and permissions information is available at <http://www.nature.com/reprints>.



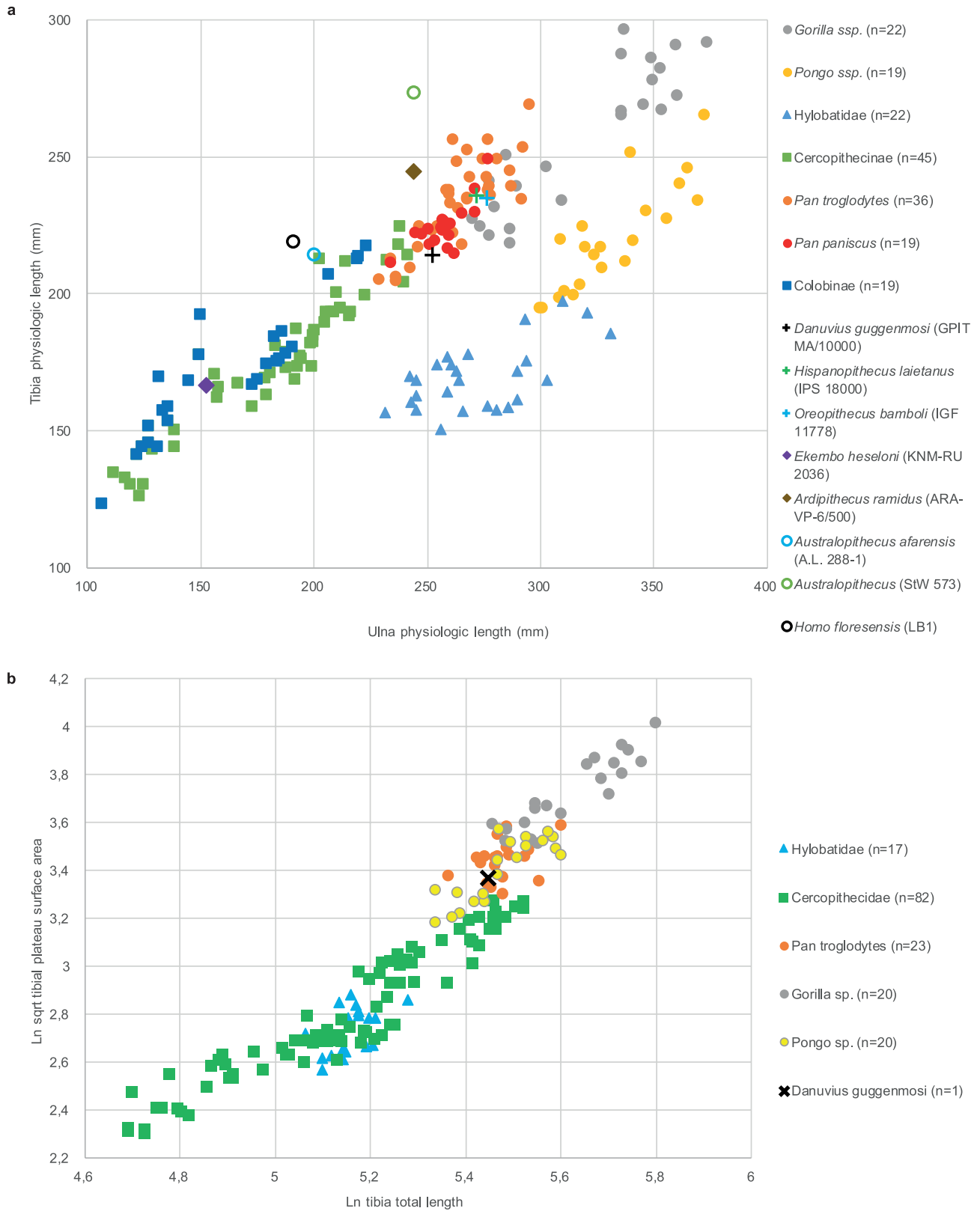
Extended Data Fig. 1 | Localization of Hammerschmiede locality and excavation plan with localized *D. guggenmosi* specimens. **a**, Topographical map of Europe. **b**, Magnification of the western part of the south German Molasse Basin (North Alpine Foreland Basin). The Hammerschmiede locality (47° 55' 37" N, 10° 35.5' E) is highlighted with a black star. Both maps were created using Generic Mapping Tools⁴⁷ and topographic datasets ETOPO1⁴⁸ and SRTM3⁴⁹. **c**, Excavation plan of the HAM 5 layer (the section has previously been published¹⁵) with excavated areas coloured in grey. Intermediate regions represent material lost due to clay mining. Dashed lines indicate the reconstructed thalweg course of the palaeochannel. Different colours and symbols indicate the individual context: holotype (GPIT/MA/10000) adult

male marked in red (stars), paratype (GPIT/MA/10001) female 1 in blue (diamonds), paratype (GPIT/MA/10002) juvenile individual in yellow (circles) and paratype (GPIT/MA/10003) female 2 in green (triangles). The red encircled sector indicates removed and stored sediments that were screen washed separately. This area was under threat of destruction from quarry activity. To avoid the complete loss of this sediment, approximately 25 tonnes were removed for remote processing. Two specimens were recovered in situ in this area. Five other specimens from this area were recovered during subsequent screen washing and cannot be more precisely localized. Coordinates correspond to Gauss-Krüger Zone 4 grid with easting (R) and northing (H) in metres.



Extended Data Fig. 2 | *D. guggenmosi*, dental and cranial specimens. **a**, Left maxilla with P³-M² (GPIT MA/10000-01) in lateral, anterior, medial (top), palatal, posterior, superior (bottom) views. **b**, Left mandible (GPIT MA/10000-02) in lateral, anterior, medial and occlusal views. **c**, Left upper central incisor (GPIT MA/10002-01) in labial, lingual and occlusal views. **d**, Right upper P³ fragment (GPIT MA/10000-05) in buccal, occlusal and mesial views. **e**, Left P³ (GPIT MA/10001-03) in buccal, occlusal and mesial views. **f**, Right upper M¹ (GPIT MA/10001-01) in occlusal, medial, distal and buccal views. **g**, Left lower P₃

(GPIT MA/10000-07) in medial, buccal, lingual and occlusal views. **h**, Left lower lateral incisor (GPIT MA/10003-5) in distal, mesial, lingual and labial views. **i**, Left lower central incisor (GPIT MA/10000-08) in distal, mesial and lingual views. **j**, Right lower P₃ (GPIT MA/10000-06) in mesial, distal, buccal and occlusal views. **k**, Right lower M₂ (GPIT MA/10000-03) in lingual, buccal (top), mesial, distal (bottom) and occlusal views. **l**, Right lower M₃ (GPIT MA/10000-04) in lingual, mesial (top), buccal, distal (bottom) and occlusal views. Scale bar, 10 mm.

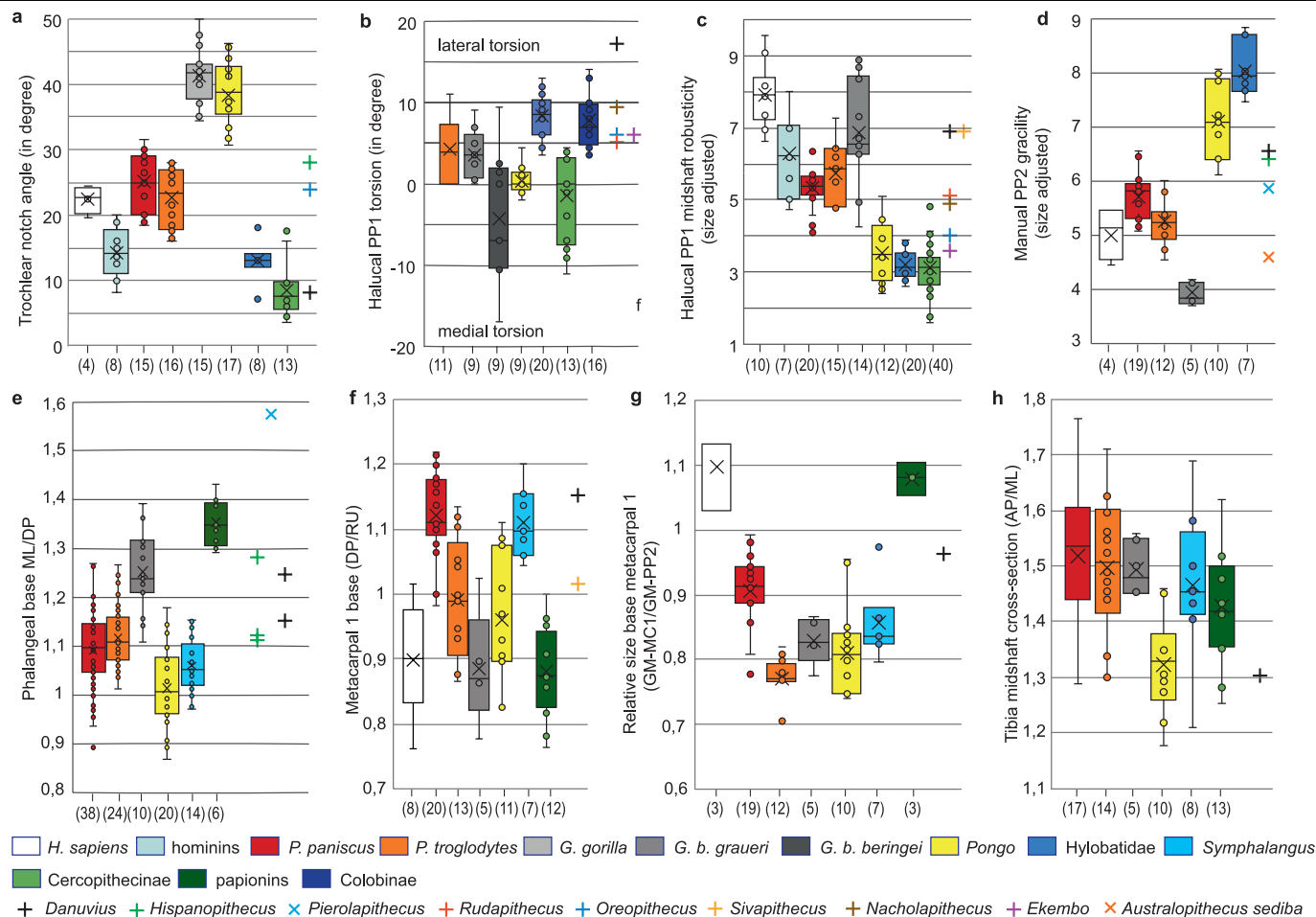


Extended Data Fig. 3 | Long-bone relationships and tibial plateau surface area. **a**, Relationships of physiologic lengths of tibia and ulna among extant and fossil catarrhines. **b**, Relationships of tibial plateau surface area (TPSA sensu³⁹, natural logarithm of square root) and tibial total length (natural logarithm) among extant hominids, hylobatids and cercopithecids (comparative data from a previous study³⁹). The tibial plateau surface area of GPIT MA/10000-10 is 1,457 mm².



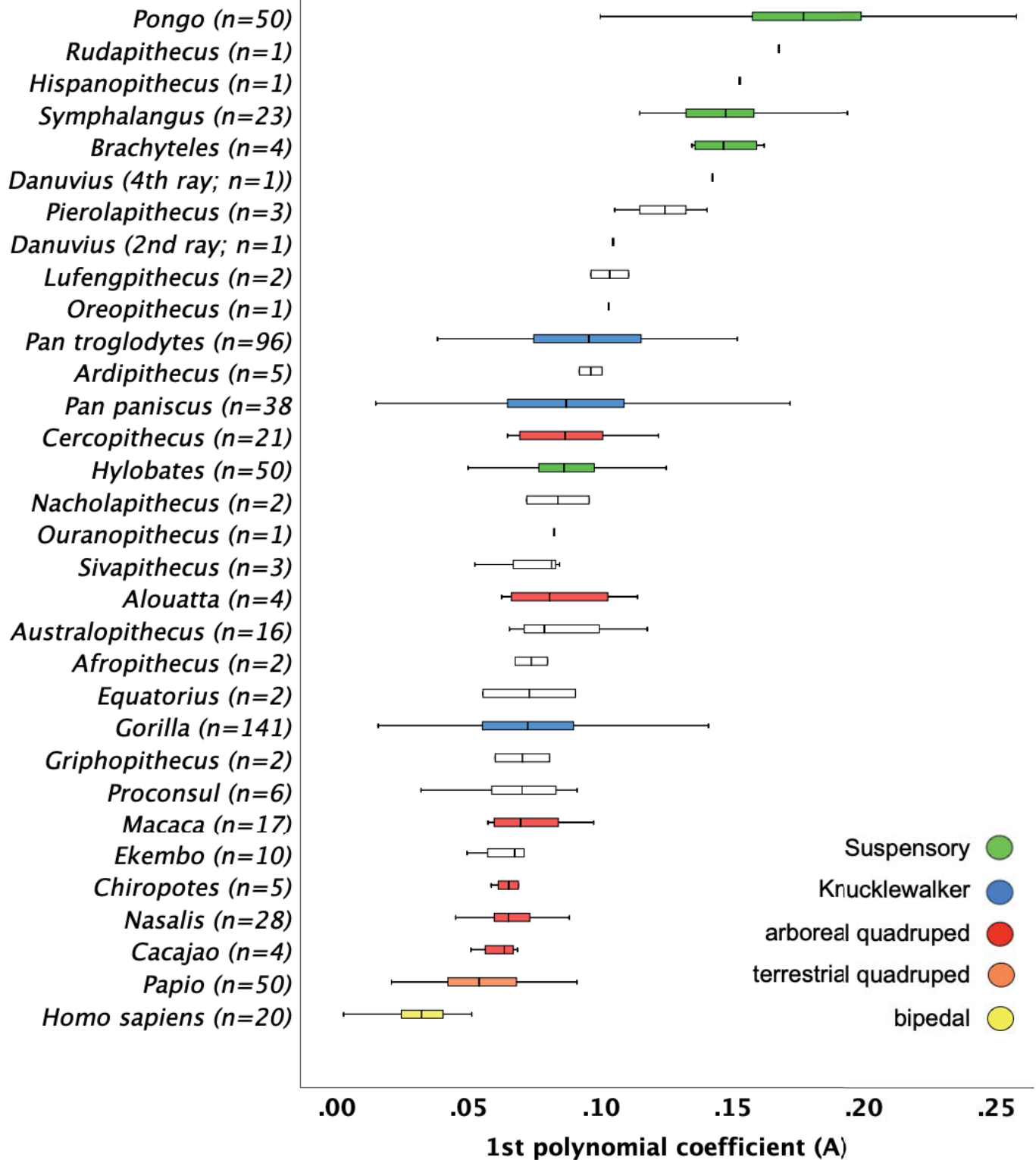
Extended Data Fig. 4 | *D. guggenmosi*, additional views of right ulna (GPIT MA/10000-10) and left tibia (GPIT MA/10000-15). a–d, Lateral (a), anteromedial (b) and posterior (c) views of the ulna and the reconstructed

olecranon in anterior view (d). e, f, Medial (e) and lateral (f) views of the tibia. Scale bar, 20 mm.



Extended Data Fig. 5 | Ulnar trochlear notch, phalangeal, metacarpal and tibial midshaft comparisons. **a**, Ulnar trochlear notch angle (for raw data, see Supplementary Table 9). **b**, Hallucal proximal phalanx (PP1) torsion (for measurement, see Methods; for raw data, see Supplementary Table 23). **c**, Size-adjusted hallucal proximal phalanx (PP1) midshaft robusticity (MLms \times DPms/GM in which MLms is the mediolateral width at midshaft, DPms is the dorsopalmar height at midshaft and GM is the geometric mean of the seven measurements: ML and DP at proximal, distal and midshaft, and total length; for raw data, see Supplementary Table 22). **d**, Size-adjusted second manual proximal phalanx (PP2) gracility (TL/GM in which TL is the total length and GM is the geometric mean of five measurements: ML and DP at distal and midshaft, and TL; five measurements are used to include *Pierolapithecus catalaunicus*, in which the proximal articulation is damaged⁵⁰; for raw data, see Supplementary

Table 11). **e**, Manual phalangeal base, ratio of mediolateral (ML) to dorsopalmar (DP) length (for raw data, see Supplementary Tables 11, 12). **f**, Manual metacarpal 1 base, ratio of dorsopalmar to radioulnar (RU) length (for raw data, see Supplementary Table 10). **g**, Relative size of manual metacarpal 1 base (geometric mean of dorsopalmar and radioulnar lengths) to proximal phalanx of ray 2 (geometric mean of seven measurements; for raw data, see Supplementary Tables 10, 11). **h**, Tibial cross-section at midshaft (ratio of anteroposterior and mediolateral width; for raw data see Supplementary Table 21). Sample sizes (*n*) of biologically independent animals are reported in parentheses below each box plot. All box plots show the centre line (median), box limits (upper and lower quartiles), crosses (arithmetic mean), whiskers (range) and individual values (circles).



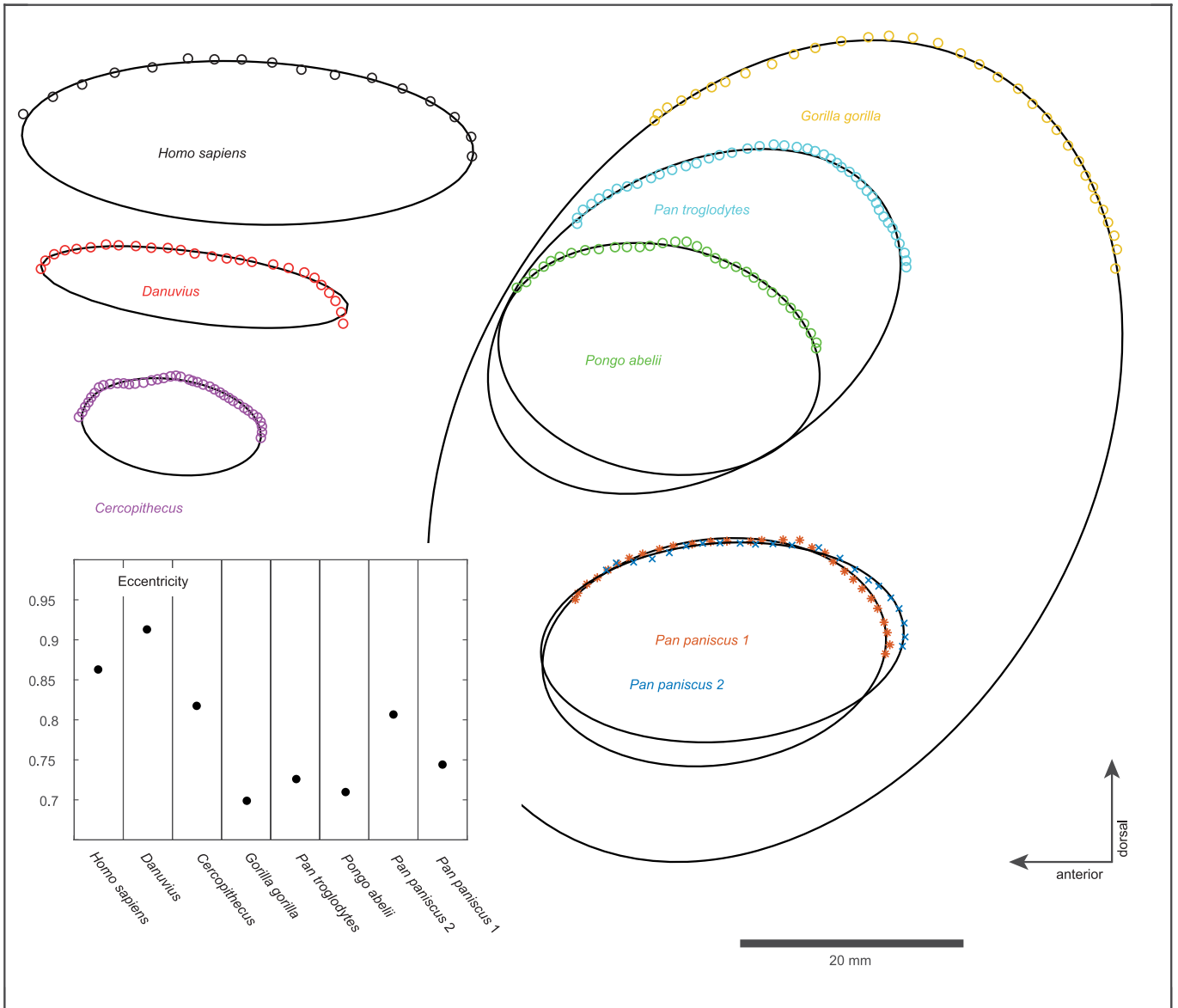
Extended Data Fig. 6 | Curvature manual proximal phalanges. Box plots of the first polynomial coefficient (A) of the second-order polynomial functional representing phalangeal shaft curvature. The box represents the interquartile range, which represents 50% of the sample values. The whiskers are lines that extend from the interquartile range box to the highest and lowest values,

excluding outliers. The line across the box indicates the median sample value for coefficient A. Extant primates are colour-coded according to locomotor adaptation. Taxa are arranged according to ascending median phalangeal shaft curvature. Sample sizes (*n*) of biologically independent animals are reported in parentheses after the species names.



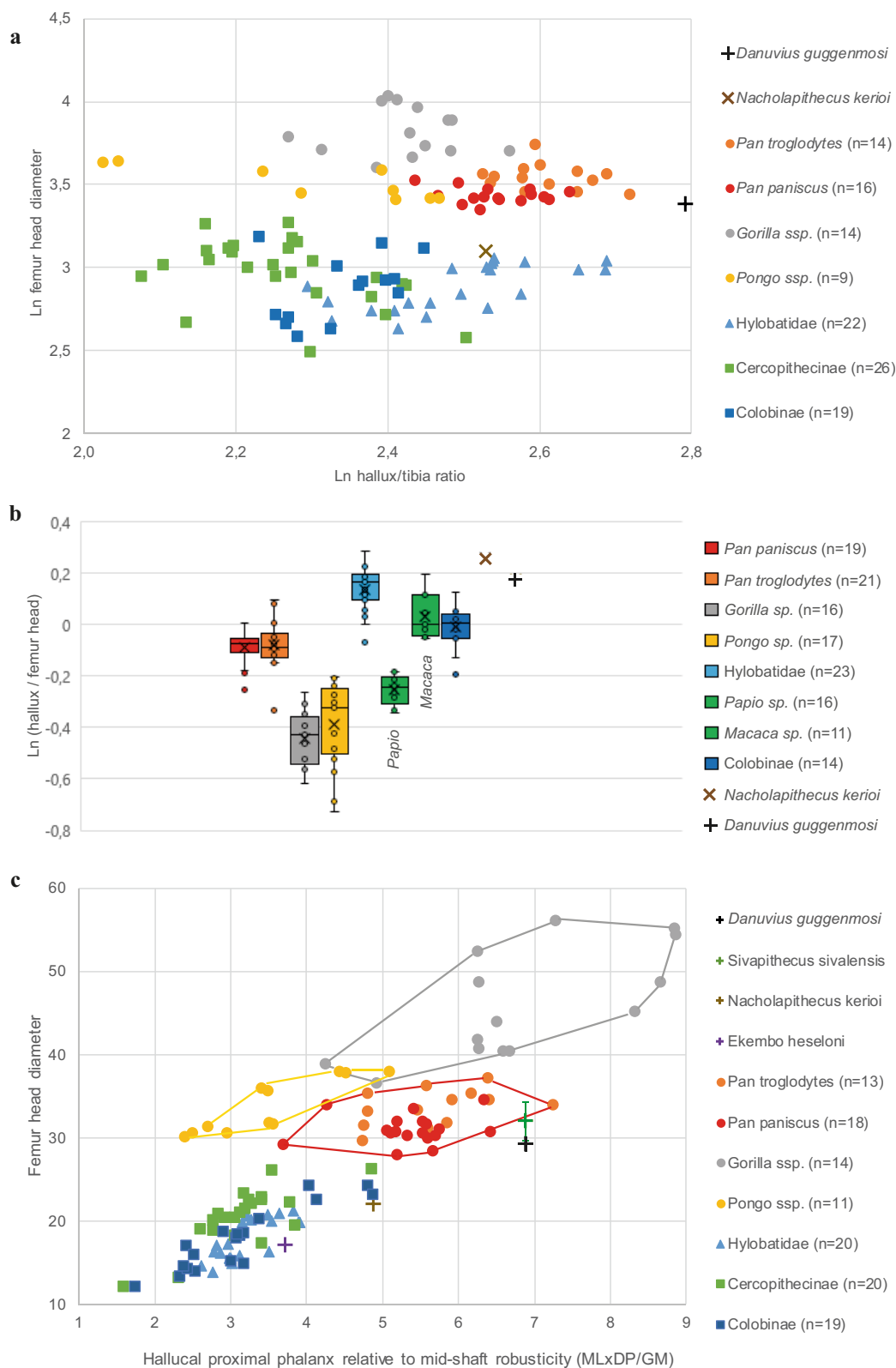
Extended Data Fig. 7 | *D. guggenmosi*, patella and femora. a, Right patella (GPIT MA/10000-12) in external and internal views. **b**, Right femur head (GPIT MA/10000-11) in medial, anterior, posterior (top), superior and lateral (bottom) views. **c**, Left femur head (GPIT MA/10001-02) in medial, posterior,

anterior (top), superior and lateral (bottom) views. **d**, Left femur, proximal half (GPIT MA/10003-01) in anterior (top) and posterior (bottom) views. Scale bar, 10 mm.



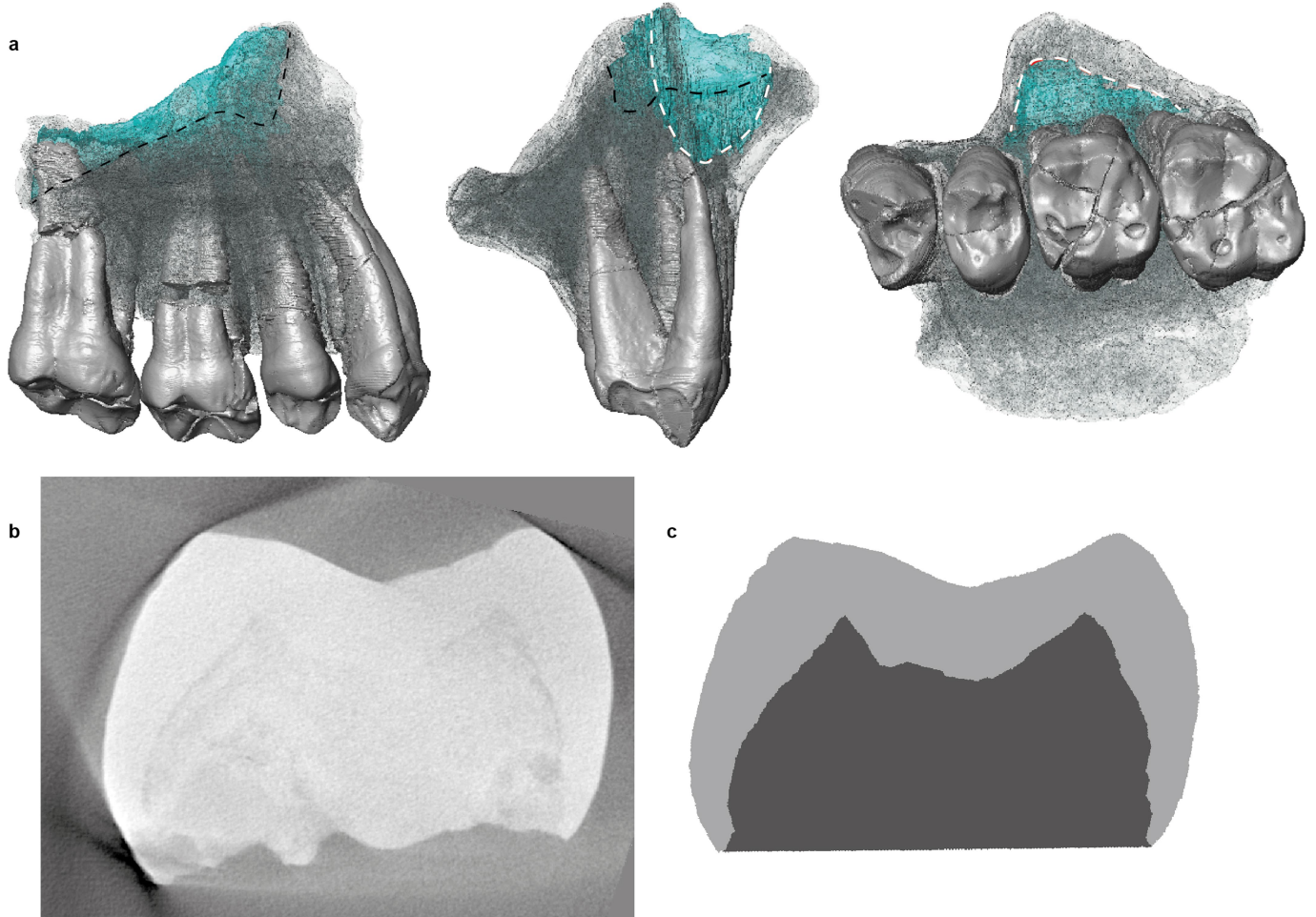
Extended Data Fig. 8 | Ellipse estimates of lateral tibial condyle. Best fit ellipses to digitalized portions of sagittal cross-sections through lateral tibial condyle of *D. guggenmosi* and extant catarrhines. Digitalized dots are shown in colour and best-fit ellipses in black. Orientation of ellipses follows the lateral condyle orientation (dorsal is up, anterior is left) at the same scale (scale bar,

20 mm). Inset shows calculated values of eccentricity for the obtained ellipses. Results indicate that both *Danuvius* and extant humans have a flat lateral tibial condyle (eccentricity >0.85), whereas great apes exhibit a convex lateral condyle (eccentricity <0.80) and *Cercopithecus* occupy an intermediate position.



Extended Data Fig. 9 | Hallux length and robusticity. a, Ratio (natural logarithm) of proximal hallucal phalanx total length to tibial physiologic length, relative to body mass (maximum femur head diameter). **b,** Box plots of hallux to femur head diameter ratios (natural logarithm). Box plots show the centre line (median), box limits (upper and lower quartiles), cross (arithmetic

mean), whiskers (range) and individual values (circles). **c,** Size-adjusted hallucal phalanx midshaft robusticity (for explanation, see Extended Data Fig. 8c), relative to femur head diameter. All sample sizes (*n*) of biologically independent animals are reported in parentheses after the species names. For raw data, see Supplementary Tables 7, 22.



Extended Data Fig. 10 | *D. guggenmosi*, maxillary sinus and enamel thickness. **a**, Left maxilla with three-dimensional rendering of molar roots and maxillary sinus (blue) in lingual (left), anterior (middle) and occlusal (right) views. Sinus runs deep between the posterobuccal and lingual roots of M^2 , rising anteriorly (dashed black line). Laterally the sinus extends deep into the

zygomatic root (dashed white line). **b, c**, Enamel thickness measured on right M_2 (GPIT/MA 10000-03). Computed tomography image of the cross-section at distal sectional plane (**b**) and graphical conversion (**c**; grey, enamel; dark grey; dentine).

Reporting Summary

Nature Research wishes to improve the reproducibility of the work that we publish. This form provides structure for consistency and transparency in reporting. For further information on Nature Research policies, see [Authors & Referees](#) and the [Editorial Policy Checklist](#).

Statistical parameters

When statistical analyses are reported, confirm that the following items are present in the relevant location (e.g. figure legend, table legend, main text, or Methods section).

n/a Confirmed

- The exact sample size (n) for each experimental group/condition, given as a discrete number and unit of measurement
- An indication of whether measurements were taken from distinct samples or whether the same sample was measured repeatedly
- The statistical test(s) used AND whether they are one- or two-sided
Only common tests should be described solely by name; describe more complex techniques in the Methods section.
- A description of all covariates tested
- A description of any assumptions or corrections, such as tests of normality and adjustment for multiple comparisons
- A full description of the statistics including central tendency (e.g. means) or other basic estimates (e.g. regression coefficient) AND variation (e.g. standard deviation) or associated estimates of uncertainty (e.g. confidence intervals)
- For null hypothesis testing, the test statistic (e.g. F , t , r) with confidence intervals, effect sizes, degrees of freedom and P value noted
Give P values as exact values whenever suitable.
- For Bayesian analysis, information on the choice of priors and Markov chain Monte Carlo settings
- For hierarchical and complex designs, identification of the appropriate level for tests and full reporting of outcomes
- Estimates of effect sizes (e.g. Cohen's d , Pearson's r), indicating how they were calculated
- Clearly defined error bars
State explicitly what error bars represent (e.g. SD, SE, CI)

Our web collection on [statistics for biologists](#) may be useful.

Software and code

Policy information about [availability of computer code](#)

Data collection

Data was collected on the original specimen using a phoenix v|tome|x s CT scanner at GeoZentrum Nordbayern (Friedrich-Alexander Universität Erlangen-Nürnberg, Germany) and a YXLON FF35 CT scanner at YXLON Inspection Service facility (Heidelberg / Germany). Comparative data of extant species were collected by using an Artec Space Spider surface scanner and Artec Studio software (versions 11-14).

Data analysis

For the micro CT-scan data analysis, we used Avizo 9.0 (ThermoFisher Scientific) and Geomagic Wrap 2017 (3D Systems Software) for the virtual reconstruction of longbones. 3D-prints were generated with Z-Suite 2.11 and printed on a Zortrax M200 FDM printer. Lateral tibia ellipse estimates we obtained using the Matlab function "EllipseDirectFit" of Nikolai Chernov available from mathworks.com

For manuscripts utilizing custom algorithms or software that are central to the research but not yet described in published literature, software must be made available to editors/reviewers upon request. We strongly encourage code deposition in a community repository (e.g. GitHub). See the Nature Research [guidelines for submitting code & software](#) for further information.

Data

Policy information about [availability of data](#)

All manuscripts must include a [data availability statement](#). This statement should provide the following information, where applicable:

- Accession codes, unique identifiers, or web links for publicly available datasets
- A list of figures that have associated raw data
- A description of any restrictions on data availability

All data generated or analysed during this study are included in the published article (and its supplementary information files). The CT-scans analysed during the current study are available from the corresponding author on reasonable request.

Field-specific reporting

Please select the best fit for your research. If you are not sure, read the appropriate sections before making your selection.

Life sciences Behavioural & social sciences Ecological, evolutionary & environmental sciences

For a reference copy of the document with all sections, see [nature.com/authors/policies/ReportingSummary-flat.pdf](https://www.nature.com/authors/policies/ReportingSummary-flat.pdf)

Ecological, evolutionary & environmental sciences study design

All studies must disclose on these points even when the disclosure is negative.

Study description	Morphologic description and functional interpretation of fossil hominid specimens.
Research sample	The research sample consists of 36 original fossil hominid bones/teeth from Hammerschmiede. The extant primates samples for skeletal comparison consists of about 350 adult and non-captive individuals of cercopithecids and hominids of both sexes.
Sampling strategy	No sample size calculation was performed. The sample size of fossils is limited by availability. The size of extant comparative samples (primates) varies between 10 and 60 individuals, which is a normal size in primatological anatomic comparisons.
Data collection	Data from the original fossil specimens were collected by M.B, D.R.B., N.S. and J.F. Micro-CT and surface scan data processing and collection was conducted by J.F. and A.T., in collaboration with A.S.D., U.K., T.L. and J.P.
Timing and spatial scale	Data collection started in spring 2018, followed by comparative data collection from summer 2018 to summer 2019.
Data exclusions	No data was excluded from the analysis.
Reproducibility	not applicable
Randomization	not applicable
Blinding	not applicable
Did the study involve field work?	<input type="checkbox"/> Yes <input type="checkbox"/> No

Field work, collection and transport

Field conditions	not applicable for palaeontological excavations
Location	Hammerschmiede, Allgäu, Bavaria, southern Germany;), coordinates N 47° 55' 38.5", E 10° 35.5'; fluvial channel of level HAM 5 at stratigraphic meter 12 in the local section, 685 m above sea level
Access and import/export	According to German (Bavarian) law no permissions needed for palaeontological excavations. Permission from the land owner have been obtained.
Disturbance	No disturbance (active mining pit)

Reporting for specific materials, systems and methods

Materials & experimental systems

n/a	Involvement	Included
<input checked="" type="checkbox"/>	<input type="checkbox"/>	Unique biological materials
<input checked="" type="checkbox"/>	<input type="checkbox"/>	Antibodies
<input checked="" type="checkbox"/>	<input type="checkbox"/>	Eukaryotic cell lines
<input type="checkbox"/>	<input checked="" type="checkbox"/>	Palaeontology
<input checked="" type="checkbox"/>	<input type="checkbox"/>	Animals and other organisms
<input checked="" type="checkbox"/>	<input type="checkbox"/>	Human research participants

Methods

n/a	Involvement	Included
<input checked="" type="checkbox"/>	<input type="checkbox"/>	ChIP-seq
<input checked="" type="checkbox"/>	<input type="checkbox"/>	Flow cytometry
<input checked="" type="checkbox"/>	<input type="checkbox"/>	MRI-based neuroimaging

Palaeontology

Specimen provenance	See above: According to German (Bavarian) law no permissions needed for palaeontological excavations. Non-formal permission from the land owner have been obtained.
Specimen deposition	All Hammerschmiede fossils are stored in the paleontological collection of the University of Tübingen (acronym GPIT), a research infrastructure of the Senckenberg Institute for Human Evolution and Palaeoenvironment (SHEP) Tübingen.
Dating methods	No new dates are provided.
<input checked="" type="checkbox"/> Tick this box to confirm that the raw and calibrated dates are available in the paper or in Supplementary Information.	

Terms and Conditions

Springer Nature journal content, brought to you courtesy of Springer Nature Customer Service Center GmbH (“Springer Nature”).

Springer Nature supports a reasonable amount of sharing of research papers by authors, subscribers and authorised users (“Users”), for small-scale personal, non-commercial use provided that all copyright, trade and service marks and other proprietary notices are maintained. By accessing, sharing, receiving or otherwise using the Springer Nature journal content you agree to these terms of use (“Terms”). For these purposes, Springer Nature considers academic use (by researchers and students) to be non-commercial.

These Terms are supplementary and will apply in addition to any applicable website terms and conditions, a relevant site licence or a personal subscription. These Terms will prevail over any conflict or ambiguity with regards to the relevant terms, a site licence or a personal subscription (to the extent of the conflict or ambiguity only). For Creative Commons-licensed articles, the terms of the Creative Commons license used will apply.

We collect and use personal data to provide access to the Springer Nature journal content. We may also use these personal data internally within ResearchGate and Springer Nature and as agreed share it, in an anonymised way, for purposes of tracking, analysis and reporting. We will not otherwise disclose your personal data outside the ResearchGate or the Springer Nature group of companies unless we have your permission as detailed in the Privacy Policy.

While Users may use the Springer Nature journal content for small scale, personal non-commercial use, it is important to note that Users may not:

1. use such content for the purpose of providing other users with access on a regular or large scale basis or as a means to circumvent access control;
2. use such content where to do so would be considered a criminal or statutory offence in any jurisdiction, or gives rise to civil liability, or is otherwise unlawful;
3. falsely or misleadingly imply or suggest endorsement, approval, sponsorship, or association unless explicitly agreed to by Springer Nature in writing;
4. use bots or other automated methods to access the content or redirect messages
5. override any security feature or exclusionary protocol; or
6. share the content in order to create substitute for Springer Nature products or services or a systematic database of Springer Nature journal content.

In line with the restriction against commercial use, Springer Nature does not permit the creation of a product or service that creates revenue, royalties, rent or income from our content or its inclusion as part of a paid for service or for other commercial gain. Springer Nature journal content cannot be used for inter-library loans and librarians may not upload Springer Nature journal content on a large scale into their, or any other, institutional repository.

These terms of use are reviewed regularly and may be amended at any time. Springer Nature is not obligated to publish any information or content on this website and may remove it or features or functionality at our sole discretion, at any time with or without notice. Springer Nature may revoke this licence to you at any time and remove access to any copies of the Springer Nature journal content which have been saved.

To the fullest extent permitted by law, Springer Nature makes no warranties, representations or guarantees to Users, either express or implied with respect to the Springer nature journal content and all parties disclaim and waive any implied warranties or warranties imposed by law, including merchantability or fitness for any particular purpose.

Please note that these rights do not automatically extend to content, data or other material published by Springer Nature that may be licensed from third parties.

If you would like to use or distribute our Springer Nature journal content to a wider audience or on a regular basis or in any other manner not expressly permitted by these Terms, please contact Springer Nature at

onlineservice@springernature.com

Chapter 4

Strewnfield case study of the darter *Anhinga pannonica* (Aves, Anhingidae)

Published in

Mayr, G., Lechner, T., Böhme, M., 2020. The large-sized darter *Anhinga pannonica* (Aves, Anhingidae) from the late Miocene hominid Hammerschmiede locality in Southern Germany. PlosOne 15, 1–19. <https://doi.org/10.1371/journal.pone.0232179>

This chapter is a reprint of the published version and differs from the general chapter numbering of this dissertation.

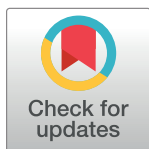
RESEARCH ARTICLE

The large-sized darter *Anhinga pannonica* (Aves, Anhingidae) from the late Miocene hominid Hammerschmiede locality in Southern Germany

Gerald Mayr^{1*}, Thomas Lechner², Madelaine Böhme²

1 Senckenberg Research Institute and Natural History Museum Frankfurt, Ornithological Section, Frankfurt am Main, Germany, **2** Senckenberg Center for Human Evolution and Paleoecology (HEP), Eberhard-Karls University Tübingen, Institute for Geoscience, Tübingen, Germany

* Gerald.Mayr@senckenberg.de



Abstract

We report fossils of the darter *Anhinga pannonica* Lambrecht, 1916 from two late Miocene (Tortonian, 11.62 and 11.44 Ma) avifaunas in Southern Germany. The material from the hominid locality Hammerschmiede near Pforzen represents the most comprehensive record of this species and includes most major postcranial elements except for the tarsometatarsus. We furthermore show that the putative cormorant *Phalacrocorax brunhuberi* (von Ammon, 1918) from the middle Miocene of Regensburg-Dechbetten is another, previously misclassified, record of *A. pannonica*, and this may also be true for early Miocene fossils described as *P. intermedius* Milne-Edwards, 1867. *A. pannonica* was distinctly larger than extant darters and reached the size of *A. grandis* from the late Miocene of North America. We detail that only fossils from the Miocene of Europe and Africa can be referred to *A. pannonica*, whereas putative records from Asia fall within the size range of extant darters. *A. pannonica* appears to have been a long-living species (16 to 6 Ma) with an extensive distribution from the equator to the northern mid-latitudes. The extinction of large-sized darters in Europe is likely to have been due to climatic cooling in the late Neogene, but the reasons for their disappearance in Africa and South America remain elusive.

OPEN ACCESS

Citation: Mayr G, Lechner T, Böhme M (2020) The large-sized darter *Anhinga pannonica* (Aves, Anhingidae) from the late Miocene hominid Hammerschmiede locality in Southern Germany. PLoS ONE 15(5): e0232179. <https://doi.org/10.1371/journal.pone.0232179>

Editor: Jun Liu, Chinese Academy of Sciences, CHINA

Received: March 3, 2020

Accepted: April 8, 2020

Published: May 6, 2020

Copyright: © 2020 Mayr et al. This is an open access article distributed under the terms of the [Creative Commons Attribution License](https://creativecommons.org/licenses/by/4.0/), which permits unrestricted use, distribution, and reproduction in any medium, provided the original author and source are credited.

Data Availability Statement: All relevant data are within the paper.

Funding: The authors received no specific funding for this work.

Competing interests: The authors have declared that no competing interests exist.

Introduction

Darters or snakebirds (Anhingidae) are the sister taxon of cormorants (Phalacrocoracidae) and include four extant species of highly aquatic birds, which occur in tropical and subtropical freshwater habitats of the Americas (*Anhinga anhinga*), Africa (*A. rufa*), Asia (*A. melanogaster*), and the Australian region (*A. novaehollandiae*) [1, 2]. Darters are leg-propelled divers, which forage by skewering larger prey items, mainly fishes and aquatic amphibians, with their long and pointed beak.

The fossil record shows that darters were much more diverse in the past and this is particularly true for South America, where species of the taxa *Macranhinga*, *Meganhinga*, and

Gigahinga reached a very large size and coexisted with smaller darters (*Anhinga minuta* and *A. hesterna*) during the Miocene and Pliocene [3–14]. Truly giant darters, some of which were probably flightless [5, 8], were restricted to South America. However a species that was distinctly larger than all extant darters, *Anhinga grandis*, was reported from the late Miocene of Nebraska and Florida [15, 16]; tentative records of *A. grandis* were also described from the late Miocene/early Miocene of Brazil [6] and the middle Miocene of Colombia [17]. *A. subvolans* from the early Miocene (ca. 18 Ma) of Florida, which is the oldest New World record of the Anhingidae, was somewhat larger than the largest extant Anhingidae but did not reach the size of *A. grandis* [18].

The Old World fossil record of darters includes the oldest unambiguously identified fossil species assigned to the clade, *Anhinga waltherbolesi* from the late Oligocene or early Miocene (24–26 Ma) of Australia, of which, however, only the tarsometatarsus is known [19] (the exact age and phylogenetic placement of *Protoplotus beauforti* from the early Paleogene of Sumatra is controversial [14, 20]). From Australia, several Neogene species of darters were described [21], and darters were also found in the Neogene of Africa and Asia [22–24].

Darters do not occur in Europe today, but the continent yielded one of the first fossil darters to have been described scientifically. This species, *Anhinga pannonica* (Lambrecht, 1916), was established on the basis of a 6th cervical vertebra from the late Miocene (MN 9; ~10 Ma) of Brusturi in Romania (the locality was then part of the Austro-Hungarian Empire and was termed Tataros); a carpometacarpus from the same site was also assigned to *A. pannonica* [25, 26]. Various fossils from the Miocene and Pliocene of Africa and Asia have subsequently at least tentatively been referred to *A. pannonica*. These include a cervical vertebra and a proximal humerus from the late Miocene Beglia Formation (MN 9; ca. 10–11 Ma) of Tunisia [27], a partial tarsometatarsus and a humerus fragment from the late Miocene of Pakistan [28], fragmentary leg bones from the early Miocene (MN 4; ca 16 Ma) of Thailand [29], a proximal humerus from the middle Miocene (12–13 Ma) Ngorora Formation of Kenya [30], as well as partial humeri from the late Miocene (7 Ma) of Toros-Menalla in Chad [23]. Bones of a large, unidentified darter were also reported from the latest Miocene Sahabi Formation of Libya [31, 32].

The European record of *A. pannonica* is much sparser and, in addition to the two bones described by Lambrecht [25], consists of two partial humeri from the late Miocene (MN 9; 9.8 Ma) of Götzendorf in Austria [33] and a proximal humerus from the early middle Miocene (MN 5; 16.0–15.2 Ma) of the Hambach opencast coal mine in Germany [34, 35]. A putative record of a darter from the middle Miocene (MN 6–8; ca. 13.5–11 Ma) of Hungary is only represented by an ungual pedal phalanx [36].

Here we report multiple remains of *Anhinga pannonica*, which significantly add to our knowledge of this species. The fossils stem from the Hammerschmiede clay pit near Pforzen (Allgäu region, Bavaria, Germany). The fossiliferous sediments of this locality were deposited in a subtropical, fluvial environment during the earliest late Miocene (Tortonian; MN 8). Bird fossils come from the stratigraphic levels Hammerschmiede 4 and 5 (HAM 4 and HAM 5). Both Hammerschmiede levels represent floodplain channels of meandering fluvial systems of different age and dimension [37]. The level HAM 5 (dated to 11.62 Ma) represents a small-sized channel with a width of four to five meters and a channel fill thickness of 0.8–1 meter, corresponding to a rivulet of local origin [38]. The channel dimensions of the stratigraphically younger level HAM 4 (11.44 Ma) indicate a medium-sized river (width ~50 m, thickness 4–5 m). Both channels are asymmetric in cross section with a more deeply incised outer bank and a shallower slip-off slope. Based on the depth of fluvial incision into the bedrock, the mean water depths can be estimated as ≤ 0.8 m for HAM 5 and ≤ 4 m for HAM 4. Based on the grain sizes of the channel fills (HAM 4: clay to fine sandy, HAM 5: clay to very fine sandy), estimated flow velocities were low to very low. Drift wood, sometimes as long as two meters, is

commonly observed in the deposits of HAM 4. Even the narrow and shallow rivulet HAM 5 is in agreement with the ecology of extant darters, which are as specialist shallow-water divers with observed dive depths < 0.5 m [39].

The Hammerschmiede locality has long been known for rich vertebrate assemblages [40, 41], and excavations of the past years have significantly augmented the diversity of the known fauna, which is so far represented by more than 120 vertebrate taxa. Most notable among the recent finds are fossils of the arboreal bipedal hominid *Danuvius guggenmosi* [38], but the vertebrate fossil record of the Hammerschmiede locality includes numerous other—from an extant European perspective—unusual vertebrate groups ([37]: Table 1), such as the giant urodele *Andrias scheuchzeri*, the latest records of the archosauromorph taxon Choristodera, and the bear *Kretzoiarctos*, which is a stem group representative of the Giant Panda [42]. Both Hammerschmiede channel fills contain abundant and diverse fish fossils, especially from small to medium-sized species (standard length 10–20 cm), such as true catfish (*Silurus*), cypriniforms (loach, minnows, barbs, and others) and perciforms (perch, goby), indicating that these fluvial systems provided ample food resources for piscivorous darters.

The Hammerschmiede clay pit has yielded more than 150 catalogued bird bones. Most of these belong to birds that lived in or near water, and in addition to the darter remains we identified at least five species of Anseriformes (waterfowl), a small species of Phalacrocoracidae (cormorants), and a fragmentary skull of a very large species of Gruidae (cranes). Remains of terrestrial or arboreal birds, by contrast, are very rare and include two species of Galliformes (landfowl), one or two species of Accipitridae (diurnal birds of prey), a passerine (Passeriformes) the size of the Eurasian Magpie (*Pica pica*; Corvidae), and a kingfisher (Alcedinidae) of about the size of the Collared Kingfisher (*Todiramphus chloris*), which is the first fossil record of an alcediniform bird from Europe. All of these fossils remain to be studied in detail, and in the present study we focus on the darter specimens.

Material and methods

The studied specimens are deposited in the palaeontological collection of the University of Tübingen, Germany (GPIT), in the ornithological collection of Senckenberg Research Institute

Table 1. Dimensions (in millimeters) of selected bones of *Anhinga pannonica* from the Hammerschmiede clay pit in comparison to fossil and extant Anhingidae (of *Giganhinga kikuyensis* and *Meganhinga chilensis* no comparable measurements were published, but these species are much larger than *A. pannonica*).

	Humerus, length	Humerus, midshaft width	Tibiotarsus, distal width	Carpometacarpus, length	Femur, length
† <i>Anhinga pannonica</i>	157.5	7.8	12.0	~77	~65
<i>A. rufa</i>	128.7–132.0 [23]	6.2–7.9 [18]	10.4–11.0 [22]	63.0; 69.3–71.0 [22]	55.3–59.2 [22]
<i>A. melanogaster</i>	133.1–140.9 [23]	6.4 [18]	N/A	N/A	56.5
<i>A. novaehollandiae</i>	137.0 [63]	7.0 [18]	12.2 [6]	72.6 [63]	58.0 [6]
<i>A. anhinga</i>	113.2–137.6 [16]	5.7–7.1 [18]	9.6–10.9 [16]	59.8–68.4 [16]	55.0–59.2 [6, 22]
† <i>A. minuta</i>	99.0 [6]	5.4 [6]	8.5 [6]	—	—
† <i>A. subvolans</i>	—	7.6 [18]	—	—	—
† <i>A. grandis</i>	~150 (est.) [16]	7.8–9.6 [16]	11.4 [16]	74.8 [16]	—
† <i>Macranhinga paranensis</i>	176.0–180 [4, 63]	10.2 [4]	20.0 [4]	81.2–84.4 [4]	87.0 [4]
† <i>M. ranzii</i>	—	—	—	—	95.2–~100 [6]
† <i>M.</i> (“ <i>Anhinga</i> ”) cf. <i>fraileyi</i>	~135.0 (est.) [6]	8.0 [6]	—	—	—

Extinct species are indicated by a dagger; unlabeled measurements are based on skeletons in the collection of Senckenberg Research Institute Frankfurt; references for values from the literature are given in brackets. N/A denotes that bone measurements of an extant species were not available, whereas a dash indicates that the corresponding bone is unknown for a fossil taxon.

<https://doi.org/10.1371/journal.pone.0232179.t001>

Frankfurt, Germany (SMF), and in the Bayerische Staatssammlung für Paläontologie und Geologie, Munich, Germany (BSPG). Of extant Anhingidae, skeletal material of *Anhinga anhinga*, *A. rufa*, and *A. melanogaster* (only trunk skeleton) was examined in the collection of Senckenberg Research Institute Frankfurt. Nomenclature of the extant species follows the IOC World Bird List at <https://www.worldbirdnames.org>.

All necessary permits were obtained for the described study, which complied with all relevant regulations (according to Bavarian law, no permits are required for palaeontological excavations; permission from the land owner has been obtained).

Systematic palaeontology

Aves Linnaeus, 1758

Suliformes Sharpe, 1891

Anhingidae Reichenbach, 1849

Anhinga pannonica (Lambrecht, 1916)

Referred specimens

GPIT/AV/00138: cervical (5th or 6th praesacral) vertebra (HAM 5); GPIT/AV/00215: thoracic (20th praesacral) vertebra (HAM 4); GPIT/AV/00223: partial right coracoid (HAM 4); GPIT/AV/00145: extremitas omalis of left coracoid (HAM 4); GPIT/AV/00217: right humerus (HAM 4); GPIT/AV/00127: distal and proximal ends of right ulna (HAM 5); GPIT/AV/00216: partial right carpometacarpus (HAM 4); GPIT/AV/00264: left femur lacking distal end (HAM 4); GPIT/AV/00220: proximal portion of right femur (HAM 4); GPIT/AV/00198: distal end of right tibiotarsus (HAM 4).

Locality and horizons

Hammerschmiede clay pit near Pforzen, Allgäu region, Bavaria, Germany (47.923° N, 10.588° E); early late Miocene, Tortonian, MN 8, regional stratigraphic levels HAM 5 (11.62 Ma) and HAM 4 (11.44 Ma) [37].

Measurements (in mm)

Cervical vertebra (GPIT/AV/00138), length: 31.7. Humerus (GPIT/AV/00217), length, 157.5; proximal width (from tuberculum ventrale to tuberculum dorsale), 21.0; distal width, 18.1. Carpometacarpus (GPIT/AV/00216), length as preserved, 72.7; estimated total length, ~77. Femur (GPIT/AV/00264), length as preserved, 62.3; estimated total length, ~65. Tibiotarsus (GPIT/AV/00198), distal width, 12.0.

Taphonomic remarks

In addition to numerous widely scattered finds of single bones and fragments, several partial mammal and turtle skeletons have been excavated in the Hammerschmiede locality. These include a male individual of the hominid *Danuvius guggenmosi* [38], as well as unpublished records of a boselaphine antelope (Bovidae: *Miotragocerus monacensis*), a chevrotain (Tragulidae: *Dorcatherium nauii*), and a snapping turtle (Chelydridae: *Chelydropsis* sp.). Here, we also assume that six bones of *Anhinga pannonica* from HAM 4 belong to the same individual. These specimens—GPIT/AV/00215 (thoracic vertebra), GPIT/AV/00216 (partial right carpometacarpus), GPIT/AV/00217 (right humerus), GPIT/AV/00220 and GPIT/AV/00264 (right and left femur), as well as GPIT/AV/00223 (right coracoid)—were excavated over a distance of nine meters parallel to the reconstructed flow direction (SSW-NNE) of the HAM 4 river (Fig 1). The bones appear to have been sorted according to density and bone volume [43, 44], with

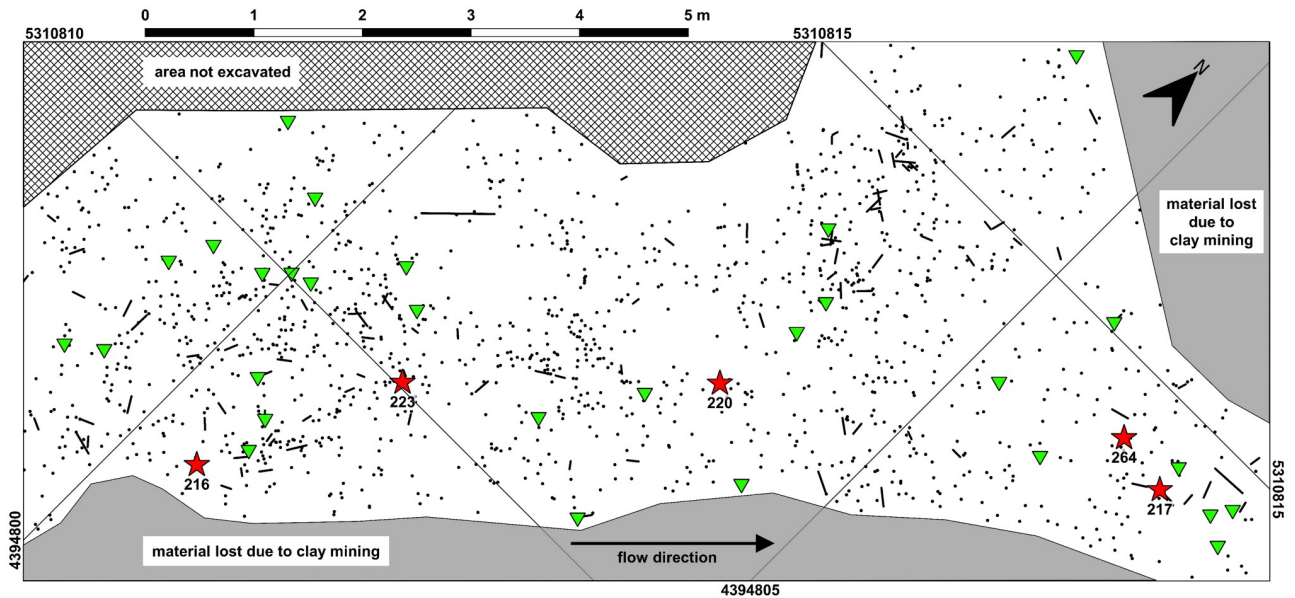


Fig 1. Section of the excavation plan Hammerschmiede level HAM 4 (excavation year 2019). Black dots represent vertebrate fossil specimens (black stripes denote the orientation of elongated objects). Excavated bird bones are shown with green triangles, and *Anhinga pannonica* bones, most probably belonging to the same individual, are highlighted with red stars (specimen GPIT/AV/00215 is a surface find from this area without coordinates). Associated bones of *A. pannonica* are arranged over a distance of nine meters parallel to the reconstructed flow direction (SSW-NNE) of the river.

<https://doi.org/10.1371/journal.pone.0232179.g001>

the femora and the long humerus having been transported a longer distance than the smaller carpometacarpus and coracoid. No duplicate skeletal elements are present and all of the surrounding avian finds belong to other taxa, so that we hypothesize that dispersal of the darter remains goes back to one taphonomic event, which involved a single individual. Four further individuals of *A. pannonica* are represented by two bones each from HAM 4 (GPIT/AV/00145, GPIT/AV/00198 –found 15 m downstream and 45 meters upstream, respectively, of the above-mentioned associated remains) and HAM 5 (GPIT/AV/00127, GPIT/AV/00138).

Description and comparisons

The cervical vertebra GPIT/AV/00138 exhibits a characteristic derived morphology that is only found in the cranial cervical vertebrae of the Anhingidae (Fig 2). Apart from being greatly elongated and narrow, GPIT/AV/00138 corresponds with the cranial cervical vertebrae of extant Anhingidae in that the processus costales are co-ossified with the corpus vertebrae and form ridge-like shelves along the ventrolateral margin of the corpus, which delimit a pair of lateral foramina (Fig 2F). The combination of these features is a diagnostic apomorphy of the Anhingidae. It is, however, less straightforward to identify the exact position of the fossil specimen within this series of cervical vertebrae, because it shows some differences to the cervical vertebrae of extant Anhingidae. The zygapophyses caudales project well beyond the facies articularis caudalis, and this derived morphology characterizes the 3rd to 6th (*A. anhinga*, *A. rufa*) or 3rd to 7th (*A. melanogaster*) cervical vertebrae of extant Anhingidae. The 3rd vertebra of extant darters differs from the fossil in the presence of a shallow, ridge-like processus ventralis, which runs along the midline of the cranial portion of the vertebral corpus. In its proportions, GPIT/AV/00138 corresponds to the very elongate and narrow 4th and 5th vertebrae of extant darters, whereas the 6th vertebra is proportionally shorter and stouter in extant darters (Fig 2). However, the fossil vertebra is only slightly longer (*A. anhinga*), as long as (*A. anhinga*,



Fig 2. 5th or 6th cervical vertebra of *Anhingia pannonica* from the late Miocene (MN 8) of the Hammerschmiede clay pit near Pforzen, Germany (A, C, D, F) in comparison to the holotype of *Anhingia pannonica* (B, E, G; from [25], original labeling removed) and the 4th (H–M) and 6th (N–S) cervical vertebrae of extant *A. anhingia* (SMF 9967) and *A. rufa* (SMF 9106). A, B, J, K, P, Q: dorsal view; C, right lateral view; D, E, H, I, N, O: left lateral view; F, G, L, M, R, S: ventral view. Abbreviations: car, sulcus caroticus; cir, circular expansion of vertebral corpus; fac, facies articularis; fcd, facies articularis caudalis; fcr, facies articularis cranialis; for, foramen delimited by the ridge-like shelf along the ventrolateral margin of the vertebral corpus; pcs, processus costalis; rdg, ridge bordering sulcus caroticus; slt, slit separating zygapophyses caudales; zcd, zygapophysis caudalis. The scale bar equals 10 mm (the size of the *A. pannonica* holotype is based on the measurements in [25]).

<https://doi.org/10.1371/journal.pone.0232179.g002>

A. rufa) or shorter (*A. melanogaster*) than the 4th and 5th vertebrae of extant darters, which conflicts with the fact that the limb bones of the fossil are distinctly longer than those of extant Anhingidae (Table 1). Therefore, and because the zygapophyses caudales appear to have been separated by a narrow slit (they are fused along their midlines in the 4th vertebra), we consider it most likely that GPIT/AV/00138 represents the 5th or 6th cervical vertebra. In size and morphology, GPIT/AV/00138 agrees well with the holotype of *A. pannonica* (identified as the 6th cervical vertebra [25]) and a tentatively referred vertebra from the late Miocene of Tunisia (identified as the 7th cervical vertebra [27]). With a length of 31.7 mm, GPIT/AV/00138 is slightly shorter than the holotype vertebra of *A. pannonica*, which has a length of 33 mm [25], whereas the vertebra from the late Miocene of Tunisia measures only 27.5 mm [27]. In lateral view, GPIT/AV/00138 is narrower than the holotype of *A. pannonica* and more closely resembles the vertebra from Tunisia [27]. However, as in the *A. pannonica* holotype and unlike in the Tunisian fossil, the zygapophyses caudales (the left one of which is broken in the fossil) are not fused along their midlines and appear to have been separated by a narrow slit. In ventral view, the corpus vertebrae has a keyhole-like shape and terminates in a circular expansion, which is situated caudal of a constriction of the vertebral corpus. The sulcus caroticus along the ventral surface of the corpus vertebrae is wider than in extant Anhingidae and is restricted to the cranial half of the vertebra, whereas it is laterally bordered by distinct ridges along the entire length of the vertebra in extant Anhingidae (Fig 2R). Cranially, the sulcus caroticus opens into a deep fossa. The facies articulares craniales correspond well with extant Anhingidae in their shape and orientation and are medially bordered by deep but narrow fossae.

The thoracic vertebra GPIT/AV/00215 exhibits a saddle-shaped cranial articulation facet and a deeply concave caudal articulation facet with an oblong-oval shape (Fig 3A–3C). This unique combination of very differently-shaped cranial and caudal articulation surfaces identifies it as the 20th vertebra of a darter (in the more cranial vertebrae of darters both articulation facets are saddle shaped, in the more caudal ones the cranial articulation facet is convex). As in extant Anhingidae, there is a small foramen on the lateral side of the corpus, just caudal of the processus transversus (Fig 3B). The processus ventrolaterales, which form distinct wings in extant Anhingidae, are broken and missing in the fossil specimen.

The coracoid (Figs 3D–3H, 4A–4F) differs from that of extant Anhingidae (Fig 4C) in that the processus acrocoracoideus is dorsoventrally narrower and the facies articularis clavicularis longer in sterno-omal direction. The facies articularis scapularis is slightly concave, whereas it is essentially flat in extant Anhingidae. As in *Meganhinga chilensis* [5], the processus procoracoideus is proportionally longer than in crown group Anhingidae and its tip is more pointed than the more “knob-like” processus procoracoideus of extant darters. The medial margin of the extremitas omalis forms a sharp ridge. On the ventral surface of the extremitas omalis, just omal of the facies articularis clavicularis, there is a distinct fossa, which is also present in extant Anhingidae, but which is absent in the Phalacrocoracidae. The extremitas sternalis resembles that of extant Anhingidae.

Several partial humeri were—tentatively, at least—referred to *A. pannonica* [23, 27, 30, 33, 34], but GPIT/AV/00217 (Fig 4M and 4N) is the first nearly complete humerus assigned to the species (on the proximal end of the bone, the tuberculum ventrale is broken and the margins of the crista deltopectoralis and crista bicipitalis exhibit some damage). In size, the humerus from the Hammerschmiede clay pit corresponds well with the proximal humeri assigned to *A. pannonica* by previous authors [27, 30, 34]. Mlíkovský [33] did not publish measurements for the partial humeri from Götzendorf in Austria and the plate lacks a scale. However, the more complete specimen has a length of 125 mm (U. Göhlich, pers. comm.) and was thus depicted in original size. Because the fossil lacks about one fifth of its proximal end, the original length of the bone was about 155 mm and compares well with the length of the humerus from the

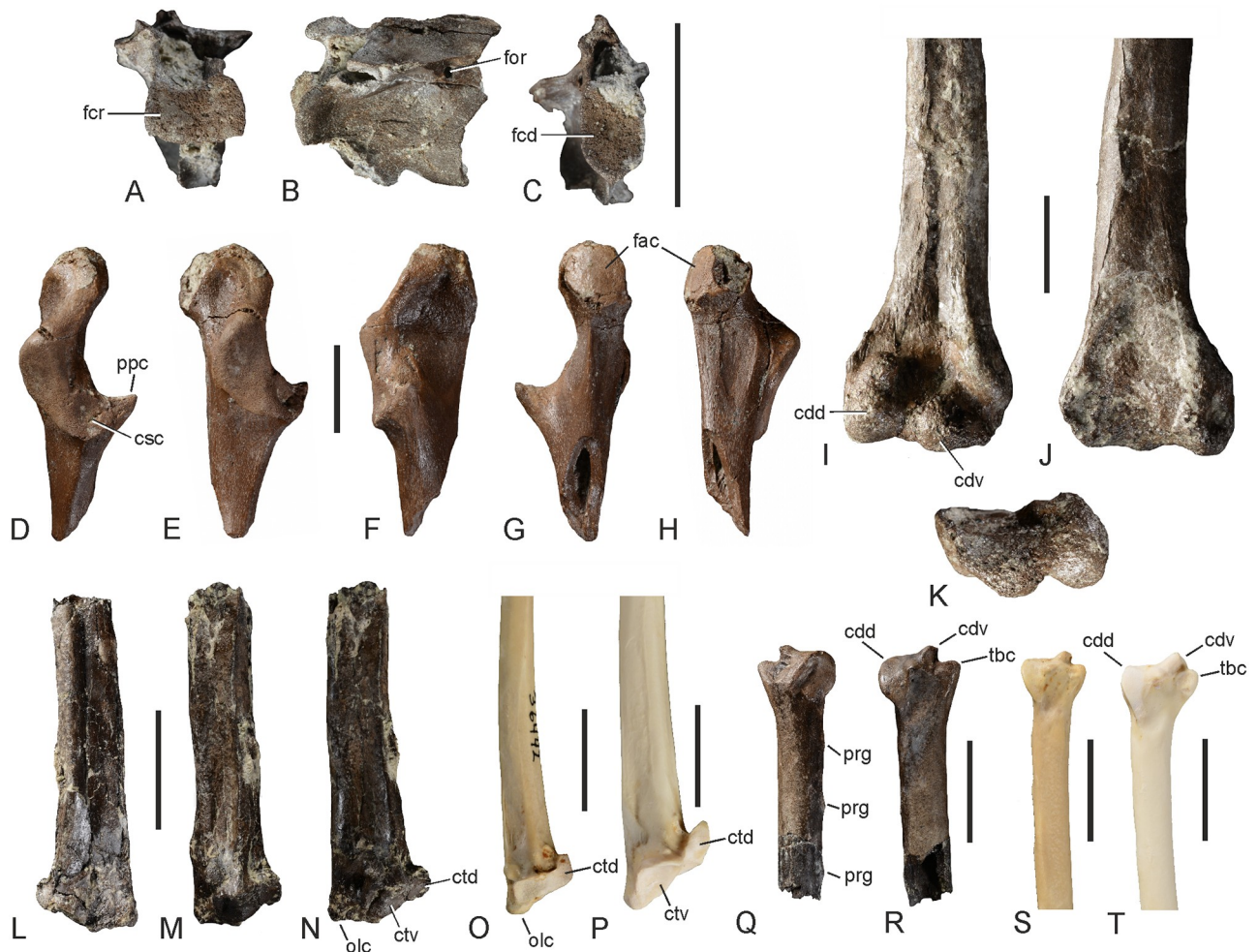


Fig 3. Various postcranial bones of *Anhinga pannonica* from the late Miocene (MN 8) of the Hammerschmiede clay pit near Pforzen, Germany. A–C, thoracic vertebra (GPIT/AV/00215) in cranial (A), left lateral (B), and caudal (C) view. D–H, extremitas omalis of left coracoid (GPIT/AV/00145) in dorsal (D), lateral (E), medial (F), ventromedial (G), and ventral (H) view. I–K, distal end of right humerus (GPIT/AV/00217) in cranial (I), caudal (J), and distal (K) view. L–N, proximal end of right ulna (GPIT/AV/00127) in caudodorsal (L), cranial (M), and cranioventral (N) view. O, *Anhinga anhinga* (SMF 9967), proximal end of right ulna in cranioventral view. P, *Phalacrocorax carbo* (Phalacrocoracidae; SMF 2939), proximal end of right ulna in cranioventral view. Q, R, distal end of right ulna (GPIT/AV/00127) in dorsal (Q) and ventral (R) view. S, A. *anhinga* (SMF 9967), distal end of right ulna in ventral view. T, P. *carbo* (SMF 2939), distal end of right ulna in ventral view. Abbreviations: cdd, condylus dorsalis; cdv, condylus ventralis; csc, cotyla scapularis; ctd, cotyla dorsalis; ctv, cotyla ventralis; fac, facies articularis clavicularis; fcd, facies articularis caudalis; fcr, facies articularis cranialis; for, foramen in vertebral corpus; olc, olecranon; ppc, processus procoracoideus; prg, papilla remigalis; tbc, tuberculum carpalae. The scale bars equal 10 mm.

<https://doi.org/10.1371/journal.pone.0232179.g003>

Hammerschmiede clay pit. The new fossil has similar overall proportions to the humerus of extant Anhingidae and is distinguished from the humerus of the Phalacrocoracidae in, e.g., the proportionally longer crista deltopectoralis (which reaches much farther distally than the crista bicipitalis), the poorly developed crus dorsale fossae, which does not overhang the fossa pneumotricipitalis, as well as the more expanded distal end. Furthermore as in extant Anhingidae, the crista bicipitalis is sheet-like with a flat cranial surface (convex in the Phalacrocoracidae) and the sulcus transversus is shallower than in the Phalacrocoracidae. The long shaft of the bone is slightly sigmoidally curved. On the distal end, the processus flexorius does not form a marked, distally projecting rim, which is present in *Anhinga grandis* and also found in extant Anhingidae (Fig 4O and 4P). However, the corresponding portion of the bone exhibits some



Fig 4. Major limb and pectoral girdle elements of *Anhingia pannonica* from the late Miocene (MN 8) of the Hammerschmiede clay pit near Pforzen, Germany. A, B, partial right coracoid (GPIT/AV/00223) in dorsal (A) and ventral (B) view. C, right coracoid of *Anhingia anhingia* (SMF 9967) in dorsal view. D–F, extremitas omalis of right coracoid GPIT/AV/00223 in dorsomedial (D), lateral (E) and ventromedial (F) view. G–I, partial right carpometacarpus (GPIT/AV/00216) in dorsal (G), ventral (H), and distal (I) view. J, right carpometacarpus of *A. rufa* (SMF 9106) in ventral view. K, L, right carpometacarpus of *A. anhingia* (SMF 9967) in ventral (K) and distal (L) view. M, N, right humerus (GPIT/AV/00217) in cranial (M) and caudal (N) view. O, right humerus of *A. rufa* (SMF 9106) in caudal view. P, right humerus of *A. anhingia* (SMF 9967) in caudal view. Q, R, proximal portion of right femur (GPIT/AV/00220) in cranial (Q) and caudal (R) view. S, T, left femur lacking distal end (GPIT/AV/00264) in caudal (S) and cranial (T) view. U, left femur (cranial view) of *A. melanogaster* (SMF 19890). V, left femur (cranial view) of *A. anhingia* (SMF 9967). W, left femur (cranial view) of *Phalacrocorax carbo* (Phalacrocoracidae; SMF 2939). X–Z, distal end of right tibiotarsus (GPIT/AV/00198) in caudal (X), cranial (Y), and distal (Z) view. AA, distal end of right tibiotarsus of *A. rufa* (SMF 9106) in cranial view. BB, distal end of right tibiotarsus of *P. carbo* (SMF 2939) in cranial view. Abbreviations: cbp, crista bicipitalis; cdf, crus dorsale fossae; cdl, condylus lateralis; cdm, condylus medialis; cdp, crista deltopectoralis; ext, sulcus extensorius; fib, fibula; flg, ridge-like flange on distal end of os metacarpale majus; flx, processus flexorius. The scale bars equal 10 mm; same scale bar for all images except I, L, and Z.

<https://doi.org/10.1371/journal.pone.0232179.g004>

damage and we hypothesize that this rim is broken in GPIT/AV/00217. Otherwise, the distal end of the specimen closely resembles the distal humerus of extant Anhingidae, but owing to the fact that the bone surface is eroded, many osteological details, such as the shape of the fossa musculi brachialis, cannot be discerned.

Of the ulna (GPIT/AV/00127), the proximal and distal ends are preserved (Fig 3L–3N, 3Q and 3R). Whereas the distal end is undistorted, the proximal end is dorsoventrally compressed, so that its original shape is deformed. However, it can still be observed that the tuberculum ligamenti collateralis ventralis is similar to that of extant darters in size and position, whereas it is shallower and more distally situated in the Phalacrocoracidae. The cotyla dorsalis is likewise similar to that of extant darters in its proportions; unlike in the Phalacrocoracidae it does not have a hook-like shape. The preserved distal portion of the shaft allows recognition of three papillae remigales. As in extant darters, the distal tip of the condylus ventralis, on the distal end of the bone, is strongly projected and is separated from the tuberculum carpale by a marked notch; unlike in the Phalacrocoracidae it is not cranially expanded and confluent with the tuberculum carpale. The condylus dorsalis has a somewhat more convex profile than in extant Anhingidae, whereas the cranial margin of the tuberculum carpale is straighter than in extant Anhingidae. In size, the distal end of the bone resembles a distal ulna that was tentatively assigned to *Anhinga grandis* [17], but the tuberculum carpale is narrower and more pointed than in the latter fossil and extant Anhingidae. On the dorsal surface, just proximal of the condylus ventralis, the bone has a rugose surface and exhibits several small pneumatic foramina.

The carpometacarpus GPIT/AV/00216 lacks the os metacarpale minus, the processus extensorius and the proximal portion of the trochlea carpalis (Fig 4G–4I). As far as comparisons are possible, the remaining sections of the bone closely correspond with a carpometacarpus referred to *A. pannonica* [25]. With an estimated length of ca. 77 mm, the carpometacarpus from the Hammerschmiede clay pit is, however, slightly longer than the latter specimen, for which a length of 73 mm was given [25]. In size and morphology, GPIT/AV/00216 resembles the carpometacarpus of *Phalacrocorax carbo* (Phalacrocoracidae), whereas the corresponding bone of extant Anhingidae has a more ridge-like flange on the distal end of the os metacarpale majus (Fig 4I and 4L). The bone is, however, too large to belong to the undescribed cormorant in the avian material from the Hammerschmiede clay pit and is here referred to *A. pannonica* based on its resemblance to the holotype of this species.

The femur (Fig 4Q–4T) closely corresponds with that of extant Anhingidae and is much more elongated than the stout femur of the Phalacrocoracidae. As in extant Anhingidae and unlike in the Phalacrocoracidae, the caput femoris is somewhat proximally directed and projects beyond the facies articularis antitrochanterica. The muscle insertion scars on the lateral surface of the proximal end, for musculus obturatorius lateralis and medialis, m. caudofemoralis, and m. ischiofemoralis ([45]: Fig 4O), closely match those of extant Anhingidae. On the lateral surface of the broken distal end of the more complete femur GPIT/AV/00264, a raised bulge presumably for musculus flexor perforans digiti II ([45]: Fig 4O) and a pit for the insertion of musculus flexor perforans et perforatus digiti II are preserved. The femur of *A. pannonica* is more elongated than the stout femora of the larger *Macranhinga paranensis* [4] and *M. ranzii* [6].

The tibiotarsus (Fig 4X–4Z) is likewise very similar to that of extant Anhingidae. As in other darters, the sulcus extensorius is centrally situated, whereas it is positioned more laterally in the Phalacrocoracidae. As in other Anhingidae but unlike in the Phalacrocoracidae, the distal end of the fibula seems not to have been fused to the tibiotarsus and the condylus medialis is less strongly protruding in distal direction (Fig 4BB).

Discussion

The fossil record of *Anhinga pannonica*

The specimens from the Hammerschmiede clay pit are assigned to *Anhinga pannonica*, which is the only previously described species of the Anhingidae from Europe. The cervical vertebra described in the present study agrees well with the holotype of *A. pannonica* in size and morphology (Fig 2), and the age of the fossils from the Hammerschmiede clay pit (11.62–11.44 Ma) is close to that of the holotype of *A. pannonica*, from Brusturi/Tataros (~10 Ma; Pannonian E, [46]).

Some bones of the Anhingidae, such as the cervical vertebrae, exhibit a unique derived morphology that makes an unambiguous identification straightforward. However, most limb and pectoral girdle elements of darters closely resemble those of cormorants (Phalacrocoracidae). Even though consistent differences exist, which allow a clear distinction of most major bones of darters and cormorants [15, 18], some Neogene darter fossils were initially assigned to the Phalacrocoracidae. This is true for *Anhinga* (“*Phalacrocorax*”) *subvolans* from the early Miocene of North America [18], and here we show that putative cormorants from the Miocene of Europe likewise represent a misidentified record of *A. pannonica*.

The specimens in question (Fig 5) stem from the early middle Miocene (MN 5) locality of Regensburg-Dechbetten (Germany) and were described by von Ammon [47] as a new cormorant species, *Phalacrocorax praecarbo* von Ammon, 1918 (omal extremity of a coracoid), and two new species of herons: *Ardea brunhuberi* von Ammon, 1918 (proximal carpometacarpus) and *Botaurites avitus* von Ammon, 1918 (cervical vertebra). The type material of these species is in the collection of Bayerische Staatssammlung für Paläontologie und Geologie in Munich and not in Senckenberg Research Institute Frankfurt, as erroneously indicated by Mlíkovský ([48]: 71), who also mistakenly considered the locality to be from the Mammalian Neogene Zones MN 7–8.

Brodkorb [49] hypothesized that the carpometacarpus described as “*Ardea brunhuberi*” is from a cormorant and synonymized *Phalacrocorax praecarbo* with *Phalacrocorax* (“*Ardea*”) *brunhuberi*, which is unfortunate, because the holotype of *A. brunhuberi* was badly damaged after von Ammon’s [47] description (Fig 5G and 5H) [50]. Olson ([51]: 167) subsequently noted that the vertebra, which constitutes the holotype of *Botaurites avitus* von Ammon, 1918 and was not considered by Brodkorb [49], is “almost certainly from a cormorant of the same size, so that this name likewise is best synonymized with *Phalacrocorax brunhuberi*.” This vertebra was also broken after von Ammon’s [47] publication, and the cranial and caudal portions of the bone are incorrectly glued and twisted at 90 degrees (Fig 5J–5P). However, it can still be discerned that the processus carotici are ankylosed along their midline and form a canalis caroticus, which is a derived characteristic of the Ardeidae (hence, von Ammon’s [47] identification), Anhingidae, and a few other taxa of the waterbird clade (Aequornithes), but which is absent in the Phalacrocoracidae. In other features, the holotypical vertebra of *B. avitus* also closely resembles the 9th or 10th praesacral vertebra of a darter. The coracoid that constitutes the holotype of *P. praecarbo* (Fig 5A–5E) is very similar to the coracoids of *A. pannonica* from the Hammerschmiede clay pit and differs from the coracoid of the Phalacrocoracidae in the shorter and more rounded processus acroracoides and the slightly concave cotyla scapularis. Accordingly, we transfer the vertebra, coracoid and carpometacarpus described by von Ammon [47] to the Anhingidae and synonymize *Ardea brunhuberi* von Ammon, 1918, *Phalacrocorax praecarbo* von Ammon, 1918, and *Botaurites avitus* von Ammon, 1918 with *Anhinga pannonica* Lambrecht, 1916.

Mlíkovský [48] synonymized *Phalacrocorax brunhuberi* (von Ammon, 1918) with *Phalacrocorax intermedius* Milne-Edwards, 1867, which is based on an incomplete proximal humerus

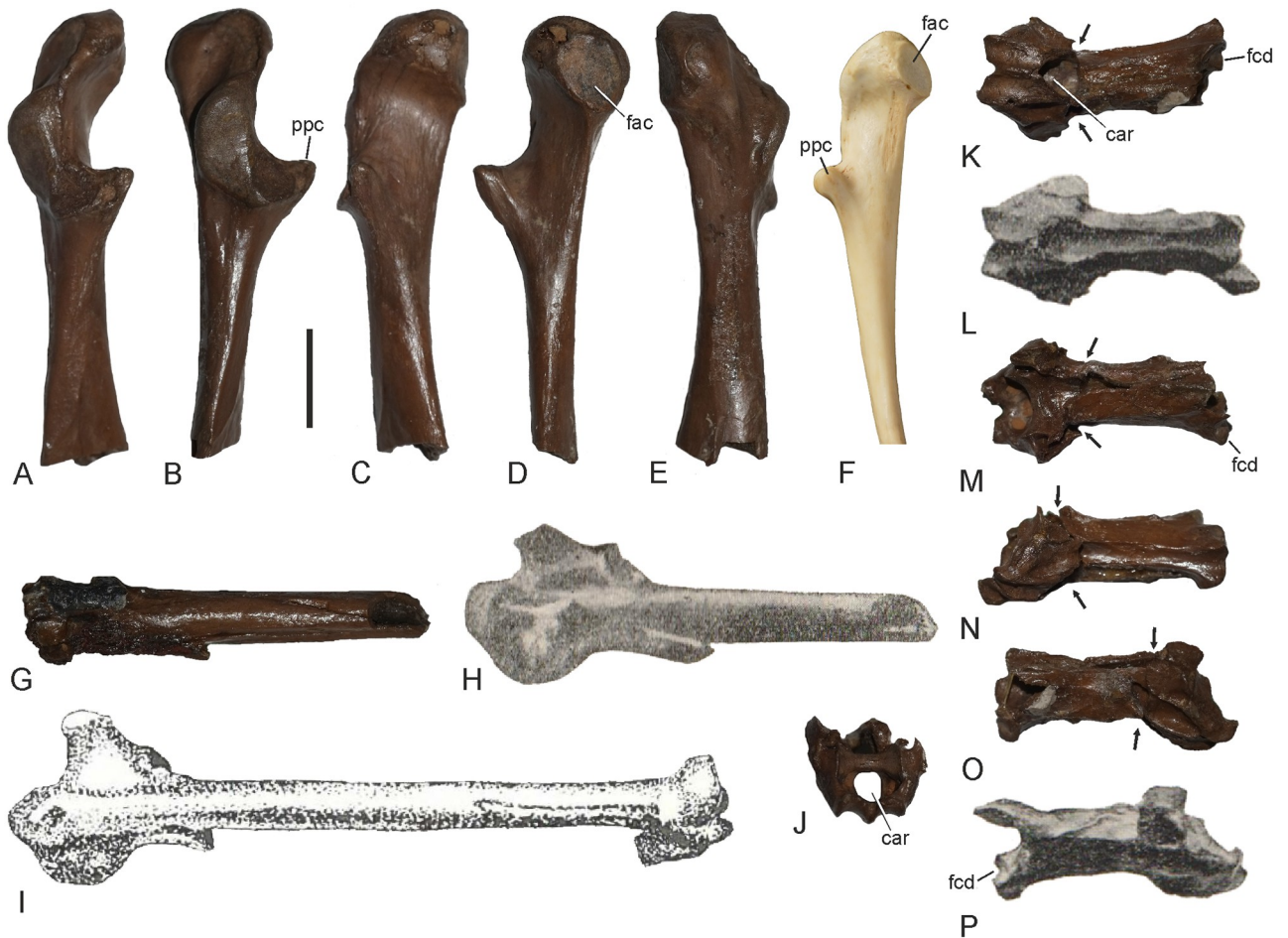


Fig 5. Fossils of *Anhinga pannonica* from the middle Miocene (MN 5) of Regensburg-Dechbetten near Regensburg, Germany. A–E, Left coracoid (BSPG 2008 LI 671; holotype of *Phalacrocorax praecarbo* von Ammon, 1918) in dorsal (A), dorsolateral (B), medial (C), ventromedial (D), and ventral (E) view. F, Left coracoid of the extant *Anhinga anhinga* (SMF 9967) in medial view. G, Partial left carpometacarpus (BSPG 2008 LI 607; holotype of *Ardea brunhuberi* von Ammon, 1918) in cranioventral view; H, the former specimen as it was figured by von Ammon [47]. I, referred left carpometacarpus of *A. pannonica* from the late Miocene of Brusturi in Romania (mirrored to ease comparisons and original labeling removed; from [25]). J–P, cervical vertebra (BSPG 2008 LI 676; holotype of *Botaurites avitus* von Ammon, 1918) in different views (J: cranial; K: ventral [cranial portion]/right lateral [caudal portion]; M: dorsal [cranial portion]/left lateral [caudal portion]; N: left lateral [cranial portion]/ventral [caudal portion]; O: right lateral [cranial portion]/dorsal [caudal portion]); L and P are from [47] and show the original condition of the bone in ventral (L) and right lateral (P) view; the arrows in K and M–O indicate the line of breakage separating the incorrectly reassembled cranial and distal portions of the vertebra. Abbreviations: car, canalis caroticus; fac, facies articularis clavicularis; fcd, facies articularis caudalis; ppc, processus procoracoideus. The scale bar equals 10 mm (the size of H, I, L, and P is based on measurements in [25] and [47]).

<https://doi.org/10.1371/journal.pone.0232179.g005>

from the early Miocene (MN 4) of France. This fossil, which was figured by Milne-Edwards ([52]: pl. 43, Figs 8–11), is of similar size to the humerus of *A. pannonica* and differs from the humerus of extant Phalacrocoracidae in the proportionally longer crista deltopectoralis, which reaches distally well beyond the distal end of the crista bicipitalis and in the less developed crus dorsale fossae (Fig 6). We consider it likely that *P. intermedius* is another misidentified darter, in which case *P. intermedius* Milne-Edwards, 1867 may be a senior synonym of *Anhinga pannonica* Lambrecht, 1916. However, a definitive taxonomic assessment of the species is only possible once the holotype has been directly examined. If anhingid affinities of *P. intermedius* can be shown, these need also to be considered for a pelvis with associated thoracic vertebrae from the early Miocene (MN 3) of the Czech Republic and a carpometacarpus from the middle Miocene (MN 5) of Austria, which were assigned to this species [53, 54].

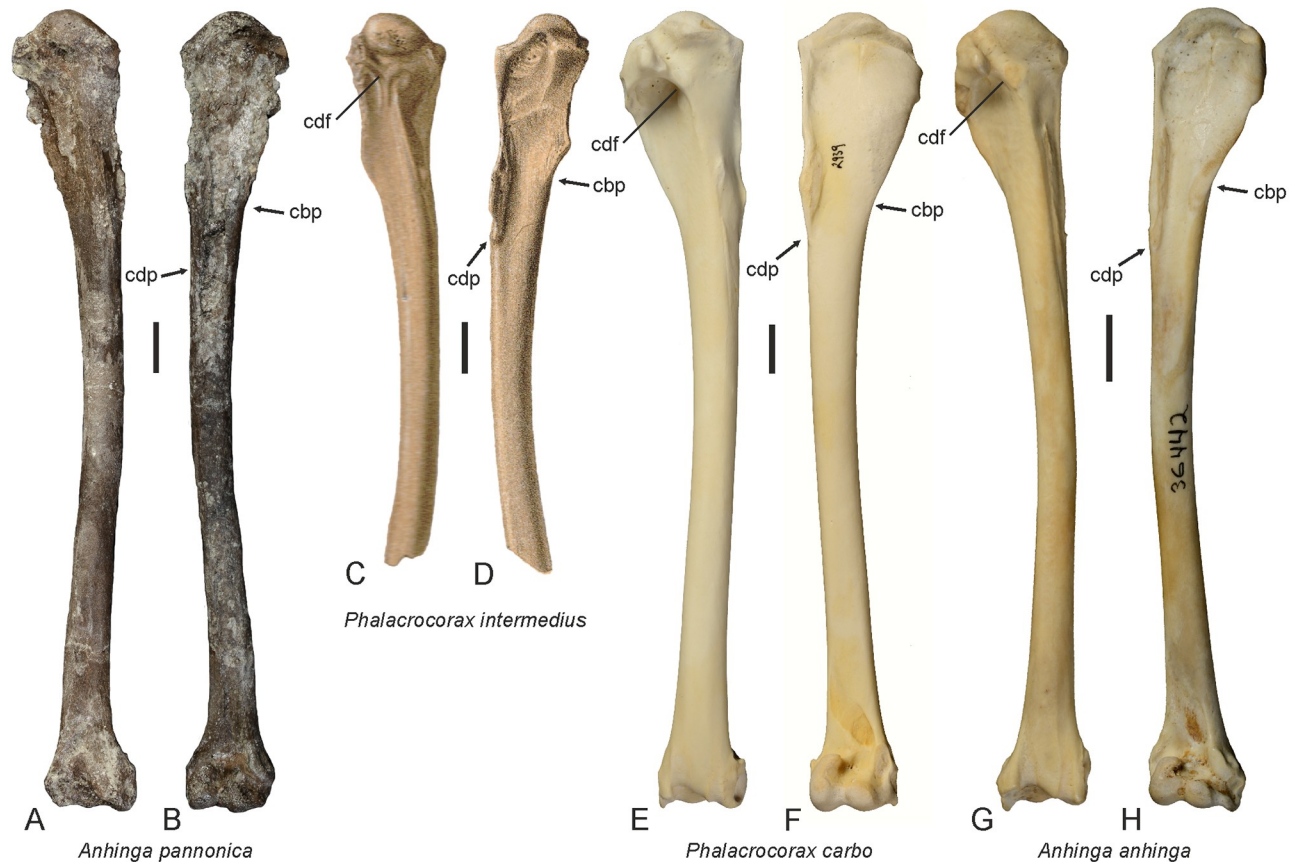


Fig 6. Humeri of extant and fossil Anhingidae and Phalacrocoracidae. A, B, *Anhinga pannonica* from the Hammerschmiede clay pit (GPIT/AV/00217), C, D, *Phalacrocorax intermedius* from the early Miocene of France; from ([52]: pl. 43), E, F, extant *Phalacrocorax carbo* (SMF 2939), and G, H, extant *Anhinga anhinga* (SMF 9967); the bones are shown in caudal (A, C, E, G) and cranial (B, D, F, H) view. The arrows indicate the distal ends of the crista bicipitalis and crista deltopectoralis. Note the long crista deltopectoralis and poorly developed crus dorsale fossae of *Phalacrocorax intermedius*. Abbreviations: cbp, crista bicipitalis; cdf, crus dorsale fossae; cdp, crista deltopectoralis. The scale bars equal 10 mm; the size of *P. intermedius* was inferred from ([52]: pl. 43), which depicts the fossil in natural size.

<https://doi.org/10.1371/journal.pone.0232179.g006>

As detailed above, the size of the humerus from the Hammerschmiede clay pit corresponds well with humeri of *A. pannonica* from Hambach in Germany [34] and Götzendorf in Austria [33]. With an estimated length of ca. 155 mm, the humerus of an unidentified darter from the latest Miocene of Libya [31] likewise has almost the same length as the fossil from the Hammerschmiede clay pit. A humerus from the late Miocene of Chad, which lacks only a part of the proximal shaft section, was tentatively assigned to *A. pannonica* and its total length was estimated at 167 mm [23]; although this bone is larger than other humeri assigned to *A. pannonica*, the size difference is not greater than that observed in extant Anhingidae (Table 1).

The Asian fossils of *Anhinga* cf. *pannonica* from Pakistan [28] and Thailand [29], by contrast, fall within the size range of extant darters, which suggests that they do not belong to *A. pannonica*. The distal width of the tibiotarsus of the species from Thailand measures 10.7 mm [29], which is less than in *A. pannonica* (12.0 mm; this study), and it was assumed that “the size of the elements [. . .] is somewhat intermediate between the size of the recent *A. anhinga* and the size of *Anhinga* of the *melanogaster* group” ([29]: 121). The putative *A. pannonica* bones from the late Miocene of Pakistan were considered to be “slightly larger than those of *A. anhinga*” ([28]: 56) and the specimens are of similar size to darter remains from the late

Pliocene of India [24]. We therefore conclude that only the records of *A. pannonica* from Europe (Romania, Austria, and Germany) and Africa (Kenya, Tunisia, Libya, and Chad) can be referred to the species (Fig 7) and that the taxonomic identity of the Asian material needs to be revised.

With nine occurrences from middle and late Miocene sediments of Europa and Africa (Fig 7), *Anhinga pannonica* exhibits a long stratigraphic occurrence over 10 million years as well as a large geographic distribution, stretching from the equator (Ngorora Formation) to 50° northern latitudes (Lower Rhine Basin). Its oldest records at the beginning of the middle Miocene from Regensburg-Dechbetten (~16 Ma) and Hambach 6 (~15 Ma) represent the northernmost localities. During the early late Miocene (11.6–9.8 Ma, Vallesian and early Tortonian), a period of considerably increased hydrologic cycle and spread of freshwater habitats in Europe and North Africa known as the first washhouse climate period [55], this species shows a wide circum-Mediterranean distribution (Fig 7). Its latest occurrences are documented from the early Messinian (6–7 Ma) of North Africa. The significant Northern Hemispheric meridional distribution is in accordance with the strongly reduced hemispheric temperature gradient during

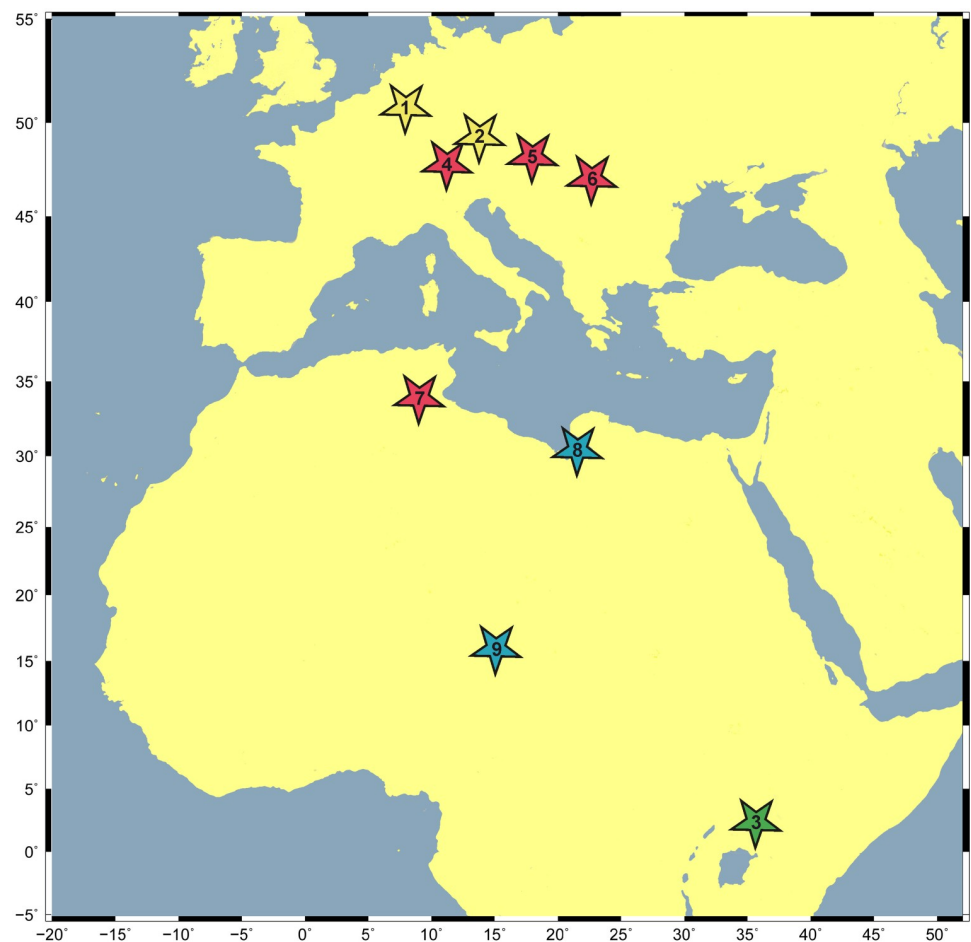


Fig 7. Geographic and stratigraphic distribution of *Anhinga pannonica* in Europe and Africa. Early middle Miocene (yellow stars): 1 –Hambach (Germany), 2 –Regensburg-Dechbetten (Germany). Late middle Miocene (green star): 3 –Ngorora Formation (Kenya). Early late Miocene (red stars): 4 –Hammerschmiede (Germany), 5 –Götzendorf (Austria), 6 –Brusturi/Tataros (Romania), 7 –Beglia Formation (Tunisia). Late late Miocene (blue stars): 8 –Sahabi Formation (Libya), 9 –Toros-Menalla (Chad).

<https://doi.org/10.1371/journal.pone.0232179.g007>

most of the Miocene, where topical temperatures prevail in mid-latitude southern Europe from the Langhian to the end of Tortonian (16–7.5 Ma) [56].

The size of *Anhinga pannonica* and the evolution of large-sized darters

Lambrecht [25] noted that *A. pannonica* was larger than *A. anhinga*, but owing to the limited material available to him, he did not further specify the size difference. Other authors considered the species to be “the size of a large *Anhinga anhinga*” ([27]: 48), “somewhat larger” than *A. rufa* ([34]: 115), or to fall “into the upper part of the range of extant *A. melanogaster*” ([31]: 114). The new fossils show that the size of *A. pannonica* has been underestimated by earlier authors and, with a length of 157.5 mm, the humerus is significantly longer than that of all extant Anhingidae and of similar length to the humerus of *A. grandis* from the late Miocene of North America (Table 1). Compared with extant darters, the humerus and all other sufficiently complete limb bones of *A. pannonica* are about 15% larger than those of extant Anhingidae and approach the size of the corresponding bones of the Great Cormorant, *Phalacrocorax carbo* (Figs 4 and 6).

The least circumference of the femur shaft (C_F) allows an assessment of the body mass (M) of a bird, with $\log_{10} M$ being proportional to $\log_{10} C_F$ [57]. For foot-propelled diving birds, mean $\log_{10} M = 2.938$ and mean $\log_{10} C_F = 1.209$ [57, 58]. With a least femur shaft circumference of 22.4 mm (GPIT/AV/00264), $\log_{10} C_F$ is 1.350 for *Anhinga pannonica*, which results in a mass estimate of about 3.3 kg. This value distinctly exceeds the body mass of extant darters, which is 1–1.8 kg [1], but it is less than the weight estimates of 5.4 to 25 kg for some of the extinct giant South American darters [8, 58].

Mlíkovský ([33]: 98) commented on the large size of *A. pannonica* and compared the species with *A. grandis*, noting that it “is worth mentioning that while *Anhinga pannonica* belonged to the Old World aningas, *Anhinga grandis* was a representative of the New World aningas, so that both these phyletic lines of aningas parallelly developed large-sized forms during the late Miocene”. Actually, however, the phylogenetic affinities of both *A. pannonica* and *A. grandis* are poorly constrained, and we note that *A. pannonica* can hardly be differentiated from the similar-sized (Table 1) *A. grandis* based on the published descriptions and photographs of the latter species. There even remains a possibility that *A. grandis* is a junior synonym of *A. pannonica*, but definitive taxonomic conclusions have to await a direct examination of the *A. grandis* material.

The sole published phylogeny of fossil Anhingidae [59] includes a single crown group representative, the New World *A. anhinga*, and is mainly based on features of the tarsometatarsus and pelvis. The tarsometatarsi of extant darters differ in the morphology of the hypotarsus, which exhibits a closed canal for the tendon of musculus flexor perforans et perforatus digiti 2 in the New World anhinga, *A. anhinga*, whereas this tendon is guided by an open sulcus in the three Old World species [60, 61]. It was hypothesized that the presence of a canal in *A. grandis* suggests close affinities between this fossil species and *A. anhinga* [16]. The canal for musculus flexor perforans et perforatus digiti 2 is absent in the oldest known darter, *Anhinga waltherbolesi* from the late Oligocene/early Miocene of Australia [19], which may indicate that its absence is indeed a plesiomorphic trait of crown group Anhingidae. Unfortunately, the tarsometatarsus is unknown for *A. pannonica* (as noted above, partial tarsometatarsi from the Miocene of Thailand and Pakistan probably do not belong to the species), and we can neither exclude the possibility that *A. pannonica* and *A. grandis* are closely related nor the alternative hypothesis that a large size evolved convergently in New World and Old World darters. Irrespective of their exact interrelationships, however, large-sized Anhingidae appear to have been widespread in the Miocene and Pliocene of Europe, Africa, and the Americas. At least in Africa and South

America, they coexisted with smaller forms, whose size was within the range of extant darters [22, 23, 62] or even fell below that of the smallest extant species (*Anhinga minuta* [6]).

The earliest definitive records of *A. pannonica* are the specimens from Regensburg-Dechbetten and Hambach in Germany (MN 5; ca. 15.2–16 Ma), but depending on the affinities of “*Phalacrocorax intermedius*” (see above), the species possibly already occurred in the early Miocene (MN 4 or even MN 3) of France and the Czech Republic, about 16–20 Ma. In Europe, *A. pannonica* therefore existed for at least 5 million years before it disappeared towards the early late Miocene (MN 10; 9–10 Ma). There is no Paleogene record of darters in Europe and the occurrence of *A. pannonica* in Europe is likely to be the result of an early or middle Miocene dispersal. Mayr ([14]: 183) hypothesized that it “may go back to a Miocene dispersal from Africa, which probably also led to range extensions of other African bird groups”. Removal of the Asian fossils from the record of *A. pannonica* seems to support this hypothesis, but the existence of similar-sized darters in North America places a caveat on premature biogeographic hypotheses.

With an age of about 8.5 Ma (early Hemphillian [16]), the North American fossils of *A. grandis* are roughly coeval to or only slightly younger than the latest European records of *A. pannonica*, but a tentatively referred ulna from the middle Miocene of Colombia was dated at 14.6–16.1 Ma [17] and therefore corresponds in age to the *A. pannonica* fossils from MN 5. A future revision of the early Miocene material assigned to *Phalacrocorax intermedius* and phylogenetic analyses including *A. grandis* and *A. pannonica* may eventually confirm an Old World origin of very large Anhingidae and their dispersal into the New World, but at present no well-founded biogeographic scenarios can be established.

Calibrated molecular data suggest that Old World and New World Anhingidae diverged 19–22 Ma [2]. This divergence estimate postdates the occurrence of the oldest known darter, *A. waltherbolesi* from Australia, which stems from strata that are 24–26 million years old and which is distinguished from crown group Anhingidae in a plesiomorphic hypotarsus morphology [19]. *A. waltherbolesi* was slightly larger than the largest extant Anhingidae, which possibly suggests that darters underwent a size decrease in their evolution. The smallest extant darter is the New World *A. anhinga*, but an even smaller species, *A. minuta*, occurred in the late Miocene/early Pliocene of Brazil [6]. The known records of *A. pannonica* and other very large darters are younger than the presumed divergence of Old World and New World darters. Even though a size decrease may have occurred in New World species after darters dispersed into the Americas, any considerations on trends in the evolution of the Anhingidae have to remain speculative in the absence of a robust phylogenetic framework.

To reduce buoyancy when diving, darters have a highly wettable plumage, which makes them prone to temperature loss during and after dives. Accordingly, these birds spend much time sunning on exposed perches, where they adopt a characteristic posture with widely spread wings [1]. These physiological constraints confine the extant distribution of darters to subtropical and tropical zones, and because a larger size results in a more favorable (with regard to heat loss) surface to volume ratio in endothermic animals, it may have been positively selected for in Neogene darters. This is in agreement with the reconstructed palaeoclimate of the Hammerschmiede locality, which was warm-subtropical with mean annual temperatures probably over 20°C. The extinction of darters in Europe is likely to have been due to climatic cooling in the late Neogene, but the reasons for the disappearance of large-sized Anhingidae in the Pliocene of Africa and in the Plio-Pleistocene of South America remain elusive.

Acknowledgments

We thank Sven Tränkner (Senckenberg Research Institute Frankfurt) for taking the photographs, Getrud Rößner (Bayerische Staatssammlung für Paläontologie und Geologie, Munich)

for providing access to the type material of von Ammon, and Ursula Göhlich (Naturhistorisches Museum Wien) for photographs of the *Anhinga pannonica* humerus from Götzendorf. Uwe Kirscher is acknowledged for assistance in the preparation of the map for Fig 7. Finally, we thank Federico Degrange and an anonymous reviewer for comments, which improved the manuscript.

Author Contributions

Conceptualization: Gerald Mayr.

Data curation: Madelaine Böhme.

Formal analysis: Gerald Mayr.

Investigation: Gerald Mayr, Thomas Lechner, Madelaine Böhme.

Methodology: Thomas Lechner, Madelaine Böhme.

Validation: Gerald Mayr.

Visualization: Gerald Mayr, Madelaine Böhme.

Writing – original draft: Gerald Mayr, Thomas Lechner, Madelaine Böhme.

References

1. Orta J. Family Anhingidae (darters). In: del Hoyo J, Elliott A, Sargatal J, editors. Handbook of the birds of the world, vol. 1. Barcelona: Lynx Edicions; 1992, pp. 354–361.
2. Kennedy M, Seneviratne SS, Mendis UK, Spencer HG. Sorting out the snakebirds: The species status, phylogeny, and biogeography of the darters (Aves: Anhingidae). *J Zool Syst Evol Res.* 2019; 57:892–899.
3. Noriega JI. Un nuevo género de Anhingidae (Aves: Pelecaniformes) de la Formación Ituzaingó (Mioceno superior) de Argentina. *Not Mus de la Plata.* 1992; 109:217–223.
4. Noriega JI. Additional material of *Macranhinga paranensis* (Aves: Pelecaniformes: Anhingidae) from the Upper Miocene Ituzaingó Formation of Entre Rios Province, Argentina. In: Zhou Z, Zhang Z., editors. Proceedings of the 5th Symposium of the Society of Avian Paleontology and Evolution, Beijing, 1–4 June 2000. Beijing: Science Press; 2002, pp. 51–61.
5. Alvarenga HMF. A large and probably flightless anhinga from the Miocene of Chile. *Courier Forsch-Inst Senckenberg.* 1995; 181:149–161.
6. Alvarenga HMF, Guilherme E. The anhingas (Aves: Anhingidae) from the Upper Tertiary (Miocene-Pliocene) of southwestern Amazonia. *J Vertebr Paleont.* 2003; 23:614–621.
7. Campbell KE Jr. A new species of giant anhinga (Aves: Pelecaniformes: Anhingidae) from the Upper Miocene (Huayquerian) of Amazonian Peru. *Nat Hist Mus Los Angeles Cty, Contrib Sci.* 1996; 460:1–9.
8. Rinderknecht A, Noriega JI. Un nuevo género de Anhingidae (Aves: Pelecaniformes) de la Formación San José (Plioceno-Pleistoceno) del Uruguay. *Ameghiniana.* 2002; 39:183–192.
9. Areta JI, Noriega JI, Agnolín F. A giant darter (Pelecaniformes: Anhingidae) from the Upper Miocene of Argentina and weight calculation of fossil Anhingidae. *N Jb Geol Paläontol, Abh.* 2007; 243:343–350.
10. Cenizo MM, Agnolín FL. The southernmost records of Anhingidae and a new basal species of Anatidae (Aves) from the lower-middle Miocene of Patagonia, Argentina. *Alcheringa.* 2010; 34:493–514.
11. Diederle JM. Systematic status of the Miocene darter '*Liptornis hesternus* Ameghino, 1895 (Aves, Suliformes, Anhingidae) from Patagonia, Argentina. *Alcheringa.* 2015; 39:589–594.
12. Diederle JM. Taxonomic status of the Neogene snakebird *Anhinga fraileyi* (Aves, Anhingidae). *Ameghiniana.* 2017; 54:341–348.
13. Diederle JM, Agnolín F. New anhingid (Aves, Suliformes) from the middle Miocene of Río Negro province, Patagonia, Argentina. *Hist Biol.* 2017; 29:1056–1064.
14. Mayr G. *Avian Evolution: The Fossil Record of Birds and its Paleobiological Significance.* Chichester: Wiley-Blackwell; 2017.

15. Martin LD, Mengel RM. A new species of anhinga (Anhingidae) from the Upper Pliocene of Nebraska. *Auk*. 1975; 92:137–140.
16. Becker JJ. Additional material of *Anhinga grandis* Martin and Mengel (Aves: Anhingidae) from the late Miocene of Florida. *Proc Biol Soc Washington*. 1987; 100:358–363.
17. Rasmussen DT, Kay RF. A Miocene anhinga from Colombia, and comments on the zoogeographic relationships of South America's Tertiary avifauna. *Papers in Avian Paleontology honoring Pierce Brodkorb*. *Nat Hist Mus Los Angeles Cty, Sci Ser*. 1992; 36:225–230.
18. Becker JJ. Reidentification of "*Phalacrocorax*" *subvolans* Brodkorb as the earliest record of Anhingidae. *Auk*. 1986; 103:804–808.
19. Worthy TH. A new species of Oligo-Miocene darter (Aves: Anhingidae) from Australia. *Auk*. 2012; 129:96–104.
20. Mayr G. *Paleogene fossil birds*. Heidelberg: Springer; 2009.
21. Mackness B. *Anhinga malagurala*, a new pygmy darter from the Early Pliocene Bluff Downs local fauna, north-eastern Queensland. *Emu*. 1995; 95:265–271.
22. Brodkorb P, Mourer-Chauviré C. Fossil aningas (Aves: Anhingidae) from Early Man sites of Hadar and Omo (Ethiopia) and Olduvai Gorge (Tanzania). *Geobios*. 1982; 15:505–515.
23. Louchart A, Haile-Selassie Y, Vignaud P, Liskius A, Brunet M. Fossil birds from the late Miocene of Chad and Ethiopia and zoogeographical implications. *Oryctos*. 2008; 7:147–167.
24. Stidham T, Patnaik R, Krishan K, Singh B, Ghosh A, Singla A, et al. The first darter (Aves: Anhingidae) fossils from India (late Pliocene). *PLoS ONE*. 2017; 12(5):e0177129. <https://doi.org/10.1371/journal.pone.0177129> PMID: 28542291
25. Lambrecht K. Die Gattung *Plotus* im ungarischen Neogen. *Mitt Jb Königl Ungar Geol Reichsanst*. 1916; 24:1–24.
26. Lambrecht K. *Handbuch der Palaeornithologie*. Berlin: Gebrüder Borntraeger; 1933.
27. Rich PV. A fossil avifauna from the Upper Miocene Beglia Formation of Tunisia. *Notes Serv Géol, Tunis*. 1972; 35:29–66.
28. Harrison CJO, Walker CA. Fossil birds from the Upper Miocene of northern Pakistan. *Tert Res*. 1982; 4:53–69.
29. Cheneval J, Ginsburg L, Mourer-Chauviré C, Ratanasthien B. The Miocene avifauna of the Li Mae Long locality, Thailand: systematics and paleoecology. *J Southeast Asian Earth Sci*. 1991; 6:117–126.
30. Dyke GJ, Walker CA. New records of fossil 'waterbirds' from the Miocene of Kenya. *Am Mus Novit*. 2008; 3610:1–10.
31. Ballmann P. A fossil bird fauna from the Pliocene Sahabi formation of Libya. In: Boaz NT, El-Arnauti A, Gaziry AW, de Heinzelin J, Boaz DD, editors. *Neogene paleontology and geology of Sahabi*. New York: Alan R. Liss, Inc.; 1987, pp. 113–118.
32. Boaz NT, El-Arnauti A, Agustí J, Bernor RL, Pavlakis P, Rook L. Temporal, lithostratigraphic, and biochronologic setting of the Sahabi Formation, North-Central Libya. *Geol East Libya*. 2008; 3:959–972.
33. Mlíkovský J. Late Miocene birds of Götzendorf/Leitha, Austria. *Ann Naturhist Mus Wien, Ser A*. 1988; 92:97–100.
34. Dalsätt J, Mörs T, Ericson PGP. Fossil birds from the Miocene and Pliocene of Hambach (NW Germany). *Palaeontographica A, Paläozool, Stratigr*. 2006; 277:113–121.
35. Mörs T. The platacanthomyine rodent *Neocometes* Schaub & Zapfe, 1953 from the Miocene of Hambach (NW Germany). *Beitr Paläontol*. 2006; 30:329–337.
36. Gál E, Hír J, Kessler E, Kókay J, Mészáros L, Vencel M. Középső-miocén ősmaradványok, a Mátraszőlős, Rákóczi-kápolna alatti útbevágásból. I. A Mátraszőlős 1. lelőhely [Middle Miocene fossils from the sections at the Rákóczi chapel at Mátraszőlős. I. Locality Mátraszőlős 1.] *Folia Hist Nat Mus Matraensis*. 1999; 23:33–78. [In Hungarian].
37. Kirscher U, Prieto J, Bachtadse V, Aziz HA, Doppler G, Hagmaier M, et al. A biochronologic tie-point for the base of the Tortonian stage in European terrestrial settings: Magnetostratigraphy of the topmost Upper Freshwater Molasse sediments of the North Alpine Foreland Basin in Bavaria (Germany). *Newslett Stratigr*. 2016; 49:445–467.
38. Böhme M, Spassov N, Fuss J, Tröscher A, Deane AS, Prieto J, et al. A new Miocene ape and locomotion in the ancestor of great apes and humans. *Nature*. 2019; 575:489–493. <https://doi.org/10.1038/s41586-019-1731-0> PMID: 31695194
39. Ryan PG. Diving in shallow water: the foraging ecology of darters (Aves: Anhingidae). *J Avian Biol*. 2007; 38:507–514.

40. Fahlbusch V, Mayr H. Microtoide Cricetiden (Mammalia, Rodentia) aus der Oberen Süßwasser-Molasse Bayerns. *Paläontol Z.* 1975; 49:78–93.
41. Prieto J, van den Hoek Ostende LW, Böhme M, Braze M. Reappearance of *Galerix* (Erinaceomorpha, Mammalia) at the Middle to Late Miocene transition in South Germany: biostratigraphic and palaeoecologic implications. *Contrib Zool.* 2011; 80:179–189.
42. Abella J, Alba DM, Robles JM, Valenciano A, Rotgers C, Carmona R, et al. *Kretzoiarctos* gen. nov., the oldest member of the giant panda clade. *PLoS ONE.* 2012; 7(11):e48985. <https://doi.org/10.1371/journal.pone.0048985> PMID: 23155439
43. Behrensmeyer AK. The taphonomy and paleoecology of Plio-Pleistocene vertebrate assemblages east of Lake Rudolf, Kenya. *Bull Mus Comp Zool.* 1975; 146:473–578.
44. Voorhies MR. Taphonomy and population dynamics of an early Pliocene vertebrate fauna, Knox County, Nebraska. *Rocky Mountain Geol.* 1969; 8:1–69.
45. Owre OT. Adaptations for locomotion and feeding in the Anhinga and the Double-crested Cormorant. *Ornithol Monogr.* 1967; 6:1–138.
46. Kretzoi M. Wichtigere Streufunde aus der wirbeltierpaläontologischen Sammlung der Ungarischen Geologischen Anstalt. 7. Mitteilung: Funde der Hipparion-Faunen im Pannon des Karpathenbeckens. *Magy All Földt Int Évi Jel.* 1982; 1980:385–394.
47. von Ammon L. Tertiäre Vogelreste von Regensburg und die jungmiocäne Vogelwelt. *Abh naturwiss Ver Regensburg.* 1918; 12:1–69.
48. Mlíkovský J. *Cenozoic Birds of the World. Part 1: Europe.* Praha: Ninox Press; 2002.
49. Brodkorb P. A new fossil heron (Aves: Ardeidae) from the Omo Basin of Ethiopia, with remarks on the position of some other species assigned to the Ardeidae. In: Campbell KE, editor. *Papers in avian paleontology honoring Hildegard Howard.* Nat Hist Mus Los Angeles Cty, Contrib Sci. 1980; 330:87–92.
50. Göhlich UB. Catalogue of the fossil bird holdings of the Bavarian State Collection of Palaeontology and Geology in Munich. *Zitteliana.* 2017; 89:331–349.
51. Olson SL. The fossil record of birds. In: Farner DS, King JR, Parkes KC, editors. *Avian Biology*, vol. 8. New York: Academic Press; 1985, pp. 79–238.
52. Milne-Edwards A. *Recherches anatomiques et paléontologiques pour servir à l'histoire des oiseaux fossiles de la France*, vol. 1. Paris: Victor Masson et fils; 1867–1869.
53. Mlíkovský J. Early Miocene birds of Břešťany, Czech Republic. *Cas Nar Muz Praze Rad Prirodoved.* 1998; 167:103–109.
54. Göhlich UB. The avifauna of the Grund Beds (middle Miocene, early Badenian, northern Austria). *Ann Naturhist Mus Wien, Ser A.* 2003; 104:237–249.
55. Böhme M, Ilg A, Winklhofer M. Late Miocene “washhouse” climate in Europe. *Earth Planet Sci Lett.* 2008; 275:393–401.
56. Tzanova A, Herbert TD, Peterson L. Cooling Mediterranean Sea surface temperatures during the Late Miocene provide a climate context for evolutionary transitions in Africa and Eurasia. *Earth Planet Sci Lett.* 2015; 419:71–80.
57. Campbell KE Jr, Marcus L. The relationship of hindlimb bone dimensions to body weight in birds. *Papers in Avian Paleontology honoring Pierce Brodkorb.* Nat Hist Mus Los Angeles Cty, Sci Ser. 1992; 36:395–412.
58. Noriega JI. Body mass estimation and locomotion of the Miocene peleciform bird *Macranhinga*. *Acta Palaeontol Pol.* 2001; 46:247–260.
59. Noriega JI, Alvarenga HMF. Phylogeny of the Tertiary giant darters (Pelecaniformes: Anhingidae) from South America. In Zhou Z-H, Zhang F-Z, editors. *Proceedings of the 5th Symposium of the Society of Avian Paleontology and Evolution*, 1–4 June 2000. Beijing: Science Press; 2002, pp. 41–49.
60. Harrison CJO. Osteological differences in the leg bones of two forms of anhinga. *Emu.* 1978; 78:230–231.
61. Mayr G. Variations in the hypotarsus morphology of birds and their evolutionary significance. *Acta Zool.* 2016; 97:196–210.
62. Stewart JR, Beech M. The Miocene birds of Abu Dhabi (United Arab Emirates) with a discussion of the age of modern species and genera. *Hist Biol.* 2006; 18:103–113.
63. Noriega JI, Piña CI. Nuevo material de *Macranhinga paranensis* (Aves: Pelecaniformes: Anhingidae) del Mioceno Superior de la Formación Ituzaingó, provincia de Entre Ríos, Argentina. *Ameghiniana.* 2004; 41:115–118.

Chapter 5

Strewnfield case studies of the goose *Allgoviachen tortonica* and the duck cf. *Mioquerquedula* sp. (Aves, Anatidae)

Published in

Mayr, G., Lechner, T., Böhme, M., 2022. Nearly complete leg of an unusual, shelduck-sized anseriform bird from the earliest late Miocene hominid locality Hammerschmiede (Germany). *Historical Biology* 1–10. <https://doi.org/10.1080/08912963.2022.2045285>

This chapter is a reprint of the published version and differs from the general chapter numbering of this dissertation.

Nearly complete leg of an unusual, shelduck-sized anseriform bird from the earliest late Miocene hominid locality Hammerschmiede (Germany)

Gerald Mayr ^a, Thomas Lechner^b and Madelaine Böhme^b

^aOrnithological Section, Senckenberg Research Institute and Natural History Museum Frankfurt, Frankfurt Am Main, Germany; ^bSenckenberg Centre for Human Evolution and Palaeoenvironment (HEP), Eberhard Karls University Tübingen, Institute for Geoscience, Tübingen, Germany

ABSTRACT

We describe leg bones of a larger-sized representative of the Anatidae from the Tortonian of the Hammerschmiede clay pit in southwestern Germany. *Allgoviachen tortonica*, n. gen. et sp. differs from most other representatives of the Anatidae in tarsometatarsus characters. The holotype is among the most substantial records of an anatid from this stratigraphic period in Central Europe and shows unusual morphological features that impede a straightforward phylogenetic assignment. In overall proportions, the tarsometatarsus resembles that of the extant taxon *Sarkidiornis* and some Tadornini, whereas the hypotarsus morphology differs from all extant Anatidae. Because of its resemblance to the early Miocene taxa *Paranyroca* and *Cygnopterus*, the new species may be a stem group representative of the Anatidae, but more osteological data are required for a firm phylogenetic placement. We show that anseriform birds exhibit a previously unnoticed diversity of the ungual phalanges of the pedal digits, and the curved unguals of the fossil indicate a predominantly non-aquatic way of living. The Hammerschmiede avifauna also includes a very small anseriform, which may belong to the extinct taxon *Mioquerquedula*; equally small species of the Anatidae are today restricted to tropical and subtropical regions.

ARTICLE HISTORY

Received 1 November 2021
Accepted 18 February 2022

KEYWORDS

Allgoviachen tortonica, n. gen. et sp.; Anatidae; Aves; fossil birds; Hammerschmiede locality; Tortonian

Introduction



Extant Anseriformes include the South American Anhimidae (screamers) and the Australo-Papuan Anseranatidae (magpie-geese), which are successive sister taxa of the globally distributed Anatidae (ducks and allies). The latter are the most species-rich group of waterfowl and the only one that occurs in Europe today. The phylogenetic interrelationships and evolutionary history of anatids are not well understood. There exists a consensus that the Dendrocygninae (whistling ducks or tree ducks) are the sister taxon of a clade including the Anserinae (geese and swans) and the Anatinae (ducks and allies). Otherwise, however, molecular analyses yield conflicting tree topologies concerning the interrelationships of anatids (Donne-Goussé et al. 2002; Gonzalez et al. 2009; Sun et al. 2017; Buckner et al. 2018).

Taxonomically diverse assemblages of Miocene anseriforms are known from Europe (Mlíkovský 2002), Australia and New Zealand (Worthy et al. 2007; Worthy 2009) as well as Central Asia (Zelenkov 2011, 2012a, b, 2020; Zelenkov and Kurochkin 2012). In Europe, the earliest unambiguously identified anatids occur towards the late Eocene and earliest Oligocene, and these are also the oldest fossils of the Anatidae on a global scale (Mayr in press). Fossils of the anatid taxon *Mionetta* are fairly abundant in some early Miocene European sites (Cheneval 1987), whereas the middle and late Miocene record of the Anatidae is much scarcer (Mlíkovský 2002; Zelenkov 2020). The affinities of most fossil taxa are furthermore poorly constrained. Earlier authors assigned small duck-like anatids to the taxon *Anas*, whereas larger species were often classified into *Anser* (Mlíkovský 2002). In fact, however, these extant taxa appear to have diverged quite recently (Sun et al. 2017). Miocene anatids often represent distinctive morphologies and virtually all of the described taxa belong to extinct genus-level taxa (Worthy et al.

2007; Worthy 2009; Mayr and Pavia 2014; Zelenkov 2011, 2012a, b, 2020; Zelenkov and Kurochkin 2012, 2015; contra Mlíkovský 2002). Even the affinities of the well-represented *Mionetta* are controversially resolved, and the taxon has either been assigned to the Dendrocygninae (Cheneval 1983), resulted as a basal representative of the clade formed by Anserinae and Anatinae (Livezey and Martin 1988), or was found nested within the Anatinae (Worthy and Lee 2008). In the early Miocene, there still appear to have existed some stem group representatives of the Anatidae, such as the taxa *Paranyroca* and *Cygnopterus* (Cheneval 1984; Mayr and Smith 2017), whereas late Miocene Anseriformes were considered to be of essentially modern aspect (Zelenkov 2020).

A major obstacle impeding an understanding of the evolution of waterfowl from a fossil perspective is the fact that many extinct taxa are only known from fragmentary bones, and often there is no overlap of the holotype material of the various species described. This is particularly true for larger, shelduck- or goose-sized species, of which few fossils have been described so far, most of which are based on isolated fragmentary bones.

One of the best-represented species is *Anserobranta tarabukini* from the early late Miocene (MN 9) of Moldova. The holotype of this species is a partial carpometacarpus, but in the original description (Kurochkin and Ganea 1972) other wing bones and the distal end of a tarsometatarsus were also referred to *A. tarabukini*; a largely complete humerus was furthermore reported by Kessler (1984). Mainly based on a similar size and geological age, the distal end of a humerus from the middle Miocene (MN 6) of Sansan in France, described as *Anas robusta* by Milne-Edwards (1867–1869), was tentatively assigned to *Anserobranta* by Cheneval (2000). A record of ‘*Anas*’ cf. *robusta* from the early middle Miocene (MN 5) locality of Regensburg-Dechbetten (Germany) is likewise based on the distal

CONTACT Gerald Mayr  Gerald.Mayr@senckenberg.de  Senckenberg Research Institute and Natural History Museum Frankfurt, Ornithological Section, Senckenberganlage 25, D-60325 Frankfurt Am Main, Germany.

© 2022 The Author(s). Published by Informa UK Limited, trading as Taylor & Francis Group.

This is an Open Access article distributed under the terms of the Creative Commons Attribution-NonCommercial-NoDerivatives License (<http://creativecommons.org/licenses/by-nc-nd/4.0/>), which permits non-commercial re-use, distribution, and reproduction in any medium, provided the original work is properly cited, and is not altered, transformed, or built upon in any way.

Published online 07 Mar 2022

end of a humerus (von Ammon 1918). A similar-sized anatid, ‘*Anser oeningensis*’ from the middle Miocene (MN 7) of Öhningen in Germany (von Meyer 1865) is represented by crushed wing and pectoral girdle bones on a slab. Two larger species of the Anatidae, *Heteroanser vicinus* and *Bonibernicla ponderosa*, were furthermore described from the late Miocene (MN 13) of Hyargas Nuur 2 in Mongolia and are known from a proximal tarsometatarsus and a distal humerus, respectively (Zelenkov 2012a).

Here, we report a leg of a larger-sized anseriform bird, as well as the bones of a very small duck from the Hammerschmiede clay pit near Pforzen (Allgäu region, Bavaria, Germany). The fossiliferous sediments of this locality stem from the middle to late Miocene transition (MN 8) and the local stratigraphic level HAM 4, which yielded most of the described bones, is dated to the earliest Tortonian, at 11.44 Ma (Kirscher et al. 2016). The HAM 4 level represents a large-sized, fluvial, and meandering channel filled with cross-bedded fine sand. The somewhat older level HAM 5 is dated to 11.62 Ma and stems from a smaller-sized channel (Kirscher et al. 2016). The Hammerschmiede locality yielded a diversified vertebrate fauna, and as yet more than 120 non-avian species have been reported, most of which are represented by isolated bones or fragments thereof (Böhme et al. 2019). Previously described bird fossils from the Hammerschmiede site include bones of a large-sized darter (Mayr et al. 2020a) and a partial skull of a crane (Mayr et al. 2020b), but the site also yielded remains of various other undescribed avian taxa.

Material and methods

The examined fossil and extant material is stored in the Palaeontological Collection of the University of Tübingen, Germany (GPIT) and is labelled with both GPIT (for Hammerschmiede fossils excavated until 2019) and SNSB-BSPG (Staatliche Naturwissenschaftliche Sammlungen Bayerns – Bayerische Staatssammlung für Paläontologie und Geologie, Munich, Germany; for excavations of 2020). All measurements are in millimetres.

Skeletons of the following species of the Anatidae were examined in the collection of the Senckenberg Research Institute Frankfurt (SMF; the nomenclature follows the IOC World Bird List at <https://www.worldbirdnames.org>; the classification follows Carboneras 1992; Gonzalez et al. 2009): Dendrocygninae: *Dendrocygna arborea*, *D. autumnalis*, *D. bicolor*, *D. eytoni*, *D. guttata*, *D. viduata*, *Thalassornis leuconotus*. Anserinae: *Anser albifrons*, *A. anser*, *A. brachyrhynchus*, *A. canagicus*, *A. cygnoides*, *A. erythropus*, *A. fabalis*, *A. indicus*, *A. rossii*, *Branta bernicla*, *B. canadensis*, *B. leucopsis*, *B. ruficollis*, *B. sandvicensis*, *Coscoroba coscoroba*, *Cygnus atratus*, *C. cygnus*, *C. melanocoryphus*, *C. olor*. Cereopsini: *Cereopsis novaehollandiae*. Anatinae: Stictonettini: *Stictonetta naevosa*. Tadornini: *Alopochen aegyptiaca*, *Chloephaga melanoptera*, *Ch. picta*, *Ch. poliocephala*, *Ch. rubidiceps*, *Cyanochen cyanopterus*, *Neochen jubata*, *Radjah radjah*, *Tadorna cana*, *T. ferruginea*, *T. tadorna*, *T. tadornoides*, *T. variegata*. Tachyerini: *Tachyeres magellanicus*, *T. pteneres*. ‘Cairinini’: *Aix galericulata*, *A. sponsa*, *Amazonetta brasiliensis*, *Asarcornis scutulata*, *Cairina moschata*, *Callonetta leucophrys*, *Chenonetta jubata*, *Nettapus auritus*, *N. coromandelianus*, *N. pulchellus*, *Plectropterus gambensis*, *Pteronetta hartlaubi*. Merganettini: *Merganetta armata*. Anatini: *Anas acuta*, *A. bahamensis*, *A. bernieri*, *A. capensis*, *A. castanea*, *A. crecca*, *A. erythrorhyncha*, *A. flavirostris*, *A. formosa*, *A. gibberifrons*, *A. luzonica*, *A. melleri*, *A. platyrhynchus*, *A. sparsa*, *A. superciliosa*, *Hymenolaimus malacorhynchus*, *Malacorhynchus membranaceus*, *Mareca americana*, *M. strepera*, *M. falcata*, *M. penelope*, *M. sibilatrix*, *Marmaronetta angustirostris*, *Spatula clypeata*, *S. cyanoptera*, *S. discors*, *S. hottentota*, *S. platalea*, *S. puna*, *S. querquedula*, *S. versicolor*, *Specularnas specularis*. Aythyini: *Aythya ferina*, *A. fuligula*, *A. marila*,

A. nyroca, *Netta peposaca*, *N. rufina*. Mergini: *Bucephala albeola*, *B. clangula*, *B. islandica*, *Clangula hyemalis*, *Histrionicus histrionicus*, *Lophodytes cucullatus*, *Melanitta fusca*, *M. nigra*, *Mergellus albellus*, *Mergus merganser*, *M. serrator*, *M. squamatus*, *Polysticta stelleri*, *Somateria fischeri*, *S. mollissima*, *S. spectabilis*. Oxyurini: *Heteronetta atricapilla*, *Oxyura jamaicensis*, *O. leucocephala*, *O. vittata*.

Systematic palaeontology

Aves Linnaeus, 1758
Anseriformes Wagler, 1831
Anatidae Leach, 1820
Allgoviachen, n. gen.

Type species

Allgoviachen tortonica, n. sp.

Diagnosis

Characterised by tarsometatarsus (1) fairly long and slender, with (2) deep fossa infracotylaris dorsalis, (3) prominent and mediolaterally narrow eminentia intercotylaris; (4) proximal articular surface deep with fossa between cotyla medialis and cotyla lateralis; (5) dorsomedial side of shaft with marked furrow for musculus extensor hallucis longus; (6) hypotarsus without canal for tendon of musculus flexor digitorum longus and (7) with plantarly prominent and proximodistally long crista medialis; (8) trochlea metatarsi II short, reaching only to middle of trochlea metatarsi IV; (9) fossa metatarsi I absent; (10) ungual phalanges with well developed and proximally situated tuberculum flexorium.

Differential diagnosis

The new species differs from:

- all extant taxa of the Anatidae in the plantarly more prominent and proximodistally longer crista medialis, the narrower and more pointed eminentia intercotylaris, and the deeper fossa infracotylaris dorsalis.
- the Oligo-Miocene *Cygnopterus* Lambrecht, 1931 in: tarsometatarsus shaft somewhat stouter in its distal section; cotyla medialis more strongly medially protruding; eminentia intercotylaris more projected; crista medialis hypotarsi less laterally deflected; trochlea metatarsi II proportionally larger; plantar articular surface of trochlea metatarsi IV proportionally longer.
- the early Miocene *Paranyroca* Miller and Compton, 1939 in: fossa infracotylaris dorsalis deeper; hypotarsus with sulcus for tendon of musculus flexor perforatus digiti 2; crista medialis more prominent.
- the late Miocene *Anserobranta* (Kurochkin and Ganea 1972) in: tarsometatarsus shaft stouter and trochlea metatarsi II proportionally larger.
- the late Miocene *Heteroanser* (Zelenkov 2012a) in: eminentia intercotylaris narrower and more pointed; crista medialis hypotarsi proximodistally longer.

Taxonomic remarks

Owing to a lack of overlap in the known bones, the new taxon cannot be differentiated from *Bonibernicla* (Zelenkov 2012a).

Etymology

From allgovia (Lat.: Allgäu), in reference to the geographic provenance of the fossil, and chen (Gr.: goose).

Allgoviachen tortonica, n. gen. et sp.

Holotype

SNSB-BSPG 2020 XCIV 1058: left leg including the distal portion of the femur as well as the tibiotarsus, tarsometatarsus and most pedal phalanges (Figures 1,2).

Etymology

The species epithet refers to the stratigraphic age of the new species.

Diagnosis

As for genus.

Referred specimen

GPIT/AV/00143: fragmentary distal portion of left tarsometatarsus (HAM 5).

Type locality and horizon

Hammerschmiede clay pit near Pforzen (Allgäu region, Bavaria, Germany); stratigraphic horizon HAM 4, earliest late Miocene, Tortonian (MN 8, 11.44 Ma).

Measurements

Tibiotarsus, length, 125.8; distal width, 14.1. Tarsometatarsus, length, 74.1; proximal width, 14.7; width of trochlea metatarsi III, ~6.2. Pedal phalanges: I1, 14.1; I2, 6.1; II1, 33.3; II2, 26.5; II3, >11.0; III1, 33.5; III2, >23.4; IV1, 27.1; IV2, 18.7; IV3, >12.7; IV4, 16.7; IV5, >8.4.

Description and comparisons

Owing to the fragmentary condition of GPIT/AV/00143, the following description is based on the partial leg SNSB-BSPG 2020 XCIV 1058, which was found in articulation (Figure 1). The bones belong to a species about the size of the extant *Anser indicus* (Anserinae) and *Alopochen aegyptiaca* (Anatinae), which are medium-sized anatids with body masses of about two kilograms (Carboneras 1992). Of the femur, only the crushed distalmost portion is preserved, which is attached to the proximal end of the tibiotarsus (Figure 2(c-d)) and does not allow a meaningful description. Tibiotarsus, tarsometatarsus, and the pedal phalanges, however, are nearly complete.

The crista cnemialis cranialis of the tibiotarsus has a similar shape to that of, e.g., *Anser indicus*, whereas it is proximodistally shorter in, e.g., *Alopochen aegyptiaca*. The distal end of the bone is medially inflected, even though the curvature appears more pronounced than it actually was owing to the fact that the distalmost portion is broken and displaced. Condylus medialis and condylus lateralis are of similar size and separated by a wide incisura intercondylaris. The epicondylus medialis is only weakly protruding.

In its proportions, the tarsometatarsus corresponds to that of some Tadornini (Figure 3) and the taxon *Sarkidiornis* (which is more closely related to the Aythyini and Anatini; Gonzalez et al. 2009; Sun et al. 2017; Buckner et al. 2018). Compared with other fossil taxa, the bone most closely resembles the tarsometatarsus of the Oligo-Miocene *Cygnopterus* and *Paranyroca* (Figure 4; Mayr and Smith 2017). As in *Heteroanser* from the late Miocene of Mongolia (Zelenkov 2012a) but unlike most extant Anatidae, the fossa infracotylaris dorsalis is very deep. The eminentia intercotylaris is more pointed and mediolaterally narrower than in crown group Anatidae. The cotyla medialis is mediolaterally wide, as it is in extant Anserinae and some Anatinae (e.g., *Alopochen*), whereas this cotyla is proportionally narrower in other Anatinae and the Dendrocygninae (Figure 3(h), (i)). Unlike in crown group Anatidae, there is a fossa between the cotyla medialis and the cotyla lateralis, in the plantar portion of the proximal articular surface of



Figure 1. In-situ photo of the partial leg of *Allgoviachen tortonica*, n. gen. et sp. from the earliest late Miocene (Tortonian) of the Hammerschmiede clay pit (holotype, SNSB-BSPG 2020 XCIV 1058). Abbreviations: tbt, tibiotarsus; tmt, tarsometatarsus. The toes are numbered. Photo by Henrik Stöhr. [Colour online].



Figure 2. Partial leg of *Allgoviachen tortonica*, n. gen. et sp. from the earliest late Miocene (Tortonian) of the Hammerschmiede clay pit (holotype, SNSB-BSPG 2020 XCIV 1058). (a)–(d) Left tibiotarsus in (a) cranial, (b) medial, (c) caudal, and (d) lateral view, with details of the distal end in (e) cranial and (f) distal view. (g)–(j) Left tarsometatarsus in (g) dorsal, (h) medial, (i) plantar, and (j) lateral view. (k) Pedal phalanges. Abbreviations: brg, breakage; ccc, crista cnemialis cranialis; cdl, condylus lateralis; cdm, condylus medialis; crf, crista fibularis; fib, fibula; ito, intratendinous ossification; pst, pons supratendineus. Scale bars equal 10 mm. [Colour online].



Figure 3. (a–e) Left tarsometatarsus of *Allgoviachen tortonica*, n. gen. et sp. from the Hammerschmiede locality (holotype, SNSB-BSPG 2020 XCIV 1058) in (a) dorsal, (b) dorsomedial, (c) plantar, (d) medial, and (e) proximal view; the specimen was coated with ammonium chloride. (f) Proximal tarsometatarsus (proximal view) of *Anser indicus* (Anserinae; SMF 19855). (g) Proximal tarsometatarsus (proximal view) of *Anseranas semipalmata* (Anseranatidae; SMF 11276). (h), (j) Detail of the proximal tarsometatarsus of SNSB-BSPG 2020 XCIV 1058 in (h) dorsal and (j) plantar view. (i), (k) Proximal tarsometatarsus of *Dendrocygna arborea* (Dendrocygnae; SMF 6175) in (i) dorsal and (k) plantar view. Left tarsometatarsi (left: dorsal view, right: plantar view) of (l) *Anser indicus* (Anserinae; SMF 19855), (m) *Alopochen aegyptiaca* (Anatinae; SMF 1925), (n) *Dendrocygna arborea* (Dendrocygnae; SMF 6175), and (o) *Stictonetta naevosa* (Anatinae; SMF 17151). The small arrows in (j) and (k) indicate the distal extent of the crista medialis hypotarsi. Abbreviations: cmh, crista medialis hypotarsi; ehl, furrow for musculus extensor hallucis longus; eic, eminentia intercotylaris; fdl, hypotarsal sulcus/canal for tendon of musculus flexor digitorum longus; fhl, hypotarsal sulcus for tendon of musculus flexor hallucis longus; fid, fossa infracotylaris dorsalis; fos, fossa between cotyla medialis and cotyla lateralis; fp2, hypotarsal sulcus for tendon of musculus flexor perforatus digiti 2; fvd, foramen vasculare distale; fvp, foramen vasculare proximale; ire, impressio retinaculi extensorii; ito, intratendinous ossification; trt, tuberositas retinaculi muscoli tibialis. Scale bars equal 10 mm. [Colour online].

the bone (Figure 3(e)). As in crown group Anatidae, the tuberositas retinaculi muscoli tibialis is bipartite, with the longer, medially situated ridge being aligned with the lateral impressio retinaculi extensorii. Of the foramina vascularia proximalia, only the medial one is clearly visible and situated between the medial ridge of the tuberositas retinaculi muscoli tibialis and the lateral impressio retinaculi extensorii.

As in extant Anatidae, the hypotarsus appears to have formed three sulci for the tendons of musculus flexor digitorum longus, musculus flexor perforatus digiti 2, and musculus flexor hallucis longus, but the most lateral hypotarsal crest is broken, so that only

the two medial sulci (for m. flexor digitorum longus and m. flexor perforatus digiti 2) are well delimited (Figure 3(e), (j)). Otherwise, however, the hypotarsus has a distinctive morphology, which shows a resemblance to the hypotarsus of *Cygnopterus alphonsi* (Figure 4 (i)) but is different from that of all other Anatidae, of which the hypotarsus is known. In particular, the crista medialis hypotarsi is much more plantarly prominent than in extant Anatidae (Figure 3 (e), (f)) and the hypotarsal crest between the sulci for m. flexor digitorum longus and m. flexor perforatus digiti 2 is proximodistally shorter and mediolaterally less wide (Figure 3(j), (k)). Even though the tarsometatarsus is slightly crushed, the unusual

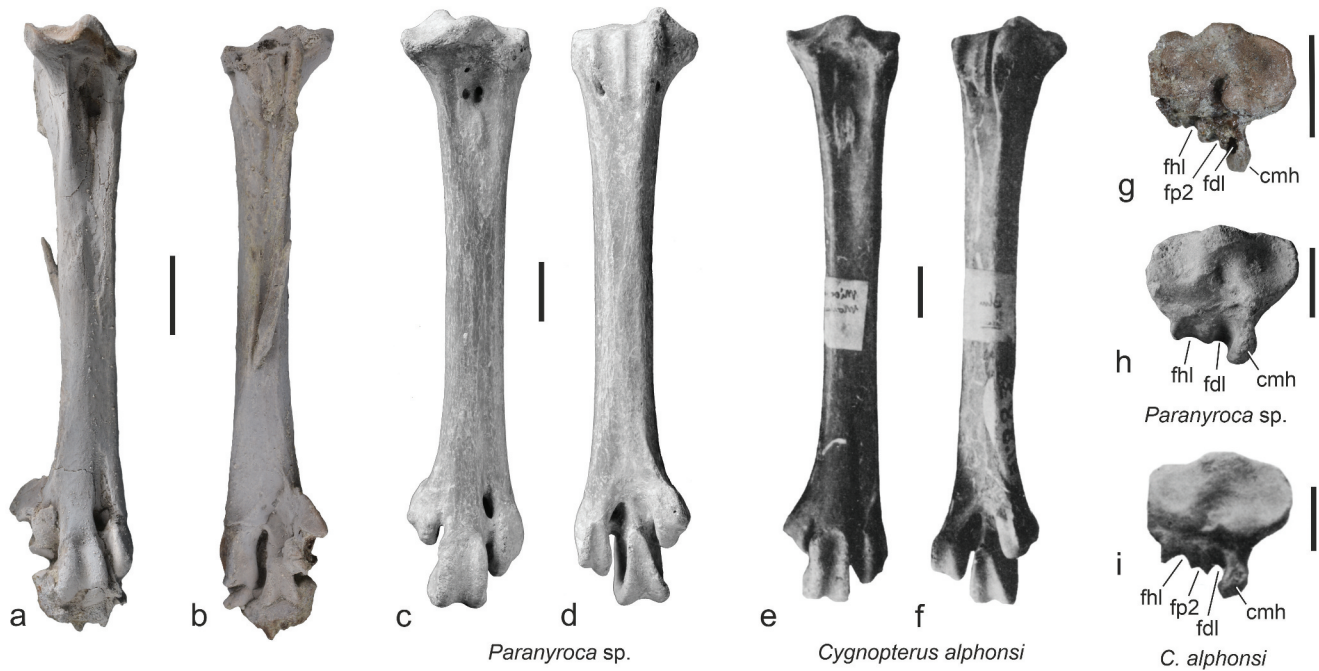


Figure 4. Tarsometatarsi of (a), (b), (g) *Allgoviachen tortonica*, n. gen. et sp. from the Hammerschmiede locality (holotype, SNSB-BSPG 2020 XCIV 1058), (c), (d), (h) *Paracygnopterus* sp. from the early Miocene of the Saint-Gérard-le-Puy area in France (University of Leuven, Department of Earth and Environmental Sciences, Leuven, Belgium; PLV 1988/17–1), and (e), (f), (i) *Cygnopterus alphonsi* from Saint-Gérard-le-Puy (from Cheneval 1983: pl. 9; mirrored to ease comparisons). Abbreviations: cmh, crista medialis hypotarsi; fdl, hypotarsal sulcus/canal for tendon of musculus flexor digitorum longus; fhl, hypotarsal sulcus for tendon of musculus flexor hallucis longus; fp2, hypotarsal sulcus for tendon of musculus flexor perforatus digiti 2. Scale bars equal 10 mm. [Colour online].

morphology of the hypotarsal crests does not seem to be an artefact of preservation, and the two medial crests are fully preserved, with their morphologies being unaltered by breakage or compression. With regard to the plantar prominence of the crista medialis, the hypotarsus of the Hammerschmiede anatid resembles that of extant Anseranatidae (Figure 3(g)). Unlike in the latter and crown group Anatidae, however, there appears to be no canal for the tendon of musculus flexor digitorum longus, even though an assessment of this feature is less ambiguous and the osseous bridge connecting the two medial hypotarsal crests may be broken in the fossil.

On the dorsomedial side of the shaft, there is a marked furrow for musculus extensor hallucis longus (Figure 3(b)), which is less developed in most crown group Anatidae. A splint on the plantar surface of the bone represents an intratendinous ossification (Figure 2(h)).

The distal end of the tarsometatarsus is not medially inflected, as it is in most extant Anatini. The dorsal opening of the foramen vasculare distale is situated at the end of a marked sulcus extensorius; as in extant Anatidae, the plantar opening is recessed. A fossa metatarsi I is absent. Adhering matrix and bone fragments obscure the shapes of the trochleae. The trochlea metatarsi II is short and reaches distally only to the middle of the trochlea metatarsi III. Its plantar surface bears a prominent lobe, similar to *Alopochen*. Unfortunately, the distomedial portion of the trochlea is damaged so that it is not possible to discern whether there was a groove on the trochlea metatarsi II (which is absent in the Anseranatidae and the dendrocygine taxon *Dendrocygna* but present in *Thalassornis*, the Anserinae, and the Anatinae). The plantar articular surface of the trochlea metatarsi III tapers proximally and has a subtriangular shape. The trochlea metatarsi IV is mediolaterally narrow and its lateral plantar rim reaches farther proximally than the medial one.

The processus articularis tarsometatarsalis of the os metatarsale I (Figure 5(a)) is of similar shape to that in *Alopochen aegyptiaca*, whereas it is wider in many other extant Anatidae. The fossil lacks the two distalmost phalanges of the third toe. The pedal digits are of similar proportions to those of extant Anatidae. The hallux is quite short and its first phalanx is shorter than the second phalanx of the fourth toe, whereas both phalanges are of equal length in many Anatinae (e.g., Figure 6(b–d)). As in most extant Dendrocygnae and Anatinae, but unlike some terrestrial Anserinae (e.g., *Anser indicus*, Figure 6(c)), the fourth toe is much longer than the second. The ungual phalanges of the Hammerschmiede anseriform correspond to those of extant Anseranatidae, the dendrocygine taxon *Dendrocygna* (Figure 5(e)), the anserine *Cereopsis* (Figure 5(d)), and some Tadornini and Cairinini in that the tuberculum flexorium is prominent and proximally located, as it is in most other neornithine birds. In highly aquatic anatids, by contrast, the unguals are straighter, and the tuberculum flexorium is proximodistally stretched and low (Figure 5(c), (f), (h)).

Discussion

Allgoviachen tortonica, n. gen. et sp. is identified as a representative of the Anatidae by the short trochlea metatarsi II (which reaches only to the middle of the trochlea metatarsi IV) and the absence of a fossa metatarsi I. Unfortunately, the fossil bones do not show unambiguous character evidence for a well-founded further phylogenetic placement. The proximal end of the tarsometatarsus differs from all extant Anatidae in the very deep fossa infracotyleris dorsalis, the mediolaterally narrower eminentia intercotylaris, the more plantarly protruding crista medialis of the hypotarsus, and – possibly (see above) – the absence of a hypotarsal canal for the tendon of musculus flexor digitorum longus. The latter character (absence of a hypotarsal canal for

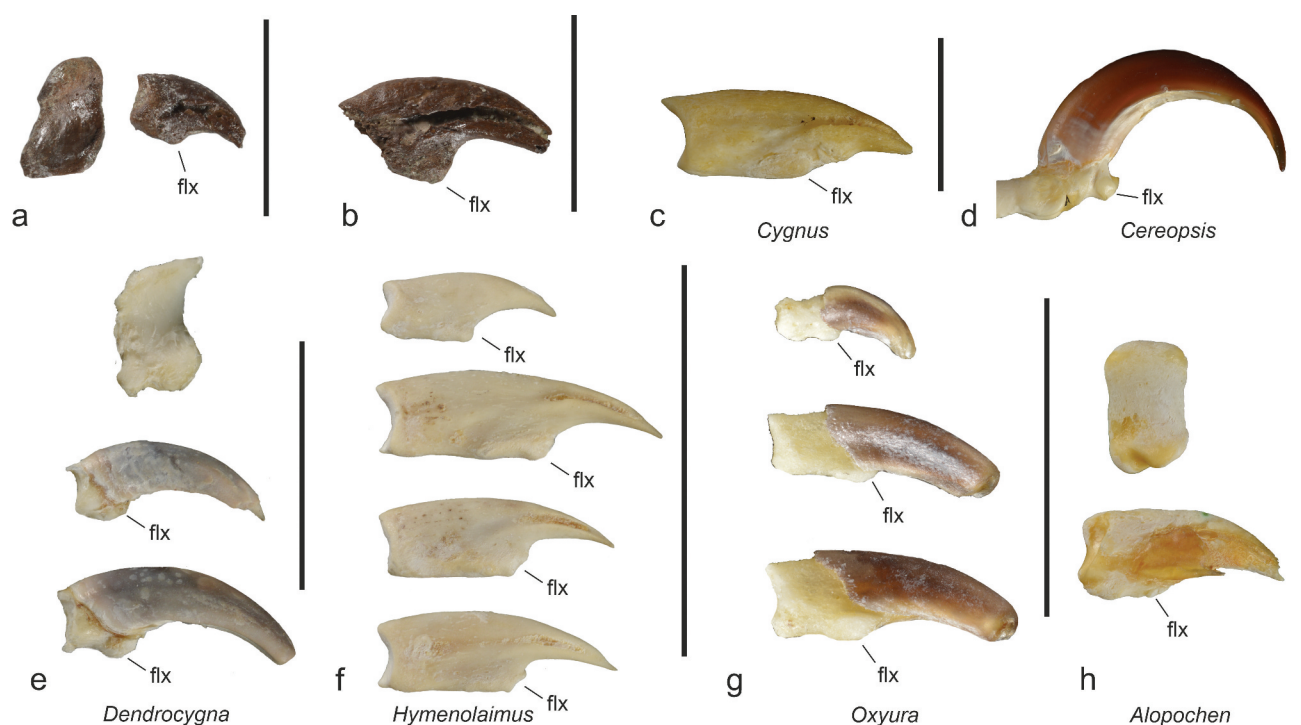


Figure 5. (a) Left os metatarsale I and unguis phalanx of the hallux of *Allgoviachen tortonica*, n. gen. et sp. from the Hammerschmiede locality (holotype, SNSB-BSPG 2020 XCIV 1058). (b) Unguis phalanx of the second toe of *A. tortonica* (holotype, SNSB-BSPG 2020 XCIV 1058). (c) Unguis phalanx of *Cygnus atratus* (Anserinae; SMF 3423). (d) Unguis phalanx of the second toe of *Cereopsis novaehollandiae* (Anserinae; SMF 19923). (e) Left os metatarsale I and unguis phalanges of the hallux and second toe (left side) of *Dendrocygna viduata* (Dendrocygnae; SMF 2271). (f) Four unguis phalanges of *Hymenolaimus malacorhynchus* (Anatinae; SMF 10257). (g) Unguis phalanx of the hallux (top) and two other unguis phalanges of *Oxyura jamaicensis* (Oxyurini; SMF 10472). (h) Left os metatarsale I and unguis phalanx of the second toe of *Alopochen aegyptiaca* (Anatinae; SMF 1925). Abbreviation: flx, tuberculum flexorium. Scale bars equal 10 mm. [Colour online].

musculus flexor digitorum longus) may be plesiomorphic for the Anatidae, but its occurrence in the new species needs to be verified by future specimens. The resemblance to the taxa *Paranyroca* and *Cygnopterus* potentially also indicates that *A. tortonica* is a stem group representative of the Anatidae (see Mayr and Smith 2017 for a discussion of the affinities of the latter two taxa). However, more data on the osteology of the new species are required for a robust phylogenetic placement, and the above-listed characteristics do not allow a well-supported assignment to any anatid subtaxon.

With regard to the shape of the unguis phalanges, *A. tortonica* resembles extant Dendrocygnae (*Dendrocygna* spp., but not *Thalassornis leuconotus*), the anserine *Cereopsis*, and some Tadornini (shelducks, e.g. *Tadorna*, *Alopochen*, and *Chloephaga*). Most other extant Anatidae have less curved unguis phalanges, in which the tuberculum flexorium is hardly protruding and more distally situated Figure 5(c), (f). To the best of our knowledge, no surveys of the different shapes of the unguis phalanges of extant Anatidae exist, and the marked variability appears to have been unnoticed before. Outgroup comparisons with the Anhimidae, Anseranatidae, and other neornithine birds suggest that a low and distally situated tuberculum flexorium represents a derived morphology, which evolved several times independently, in the Dendrocygnae (*Thalassornis*), Anserinae (Cygnetini and Anserini), and Anatinae (Anatini). This derived morphology is found in highly aquatic anatids, and the plesiomorphic shape of the unguis phalanges of *A. tortonica* indicates a predominantly non-aquatic and more terrestrial species, which – in analogy to the extant *Dendrocygna* – may have had perching capabilities.

Concerning the deep fossa infracotylaris dorsalis, *A. tortonica* agrees with *Heteroanser vicinus* from Mongolia (Zelenkov 2012a), but otherwise there are distinct differences (see differential diagnosis). Owing to a lack of overlap in the known bones, *A. tortonica* cannot be differentiated from ‘*Anser*’ *oeningensis*, ‘*Anas*’ *robusta*, and *Bonibernicla ponderosa*. These three species are from strata that are either slightly older (‘*A.*’ *oeningensis*, ‘*A.*’ *robusta*) or somewhat younger (*B. ponderosa*) than those yielding the specimens from the Hammerschmiede site. Well-founded morphological comparisons will, however, only be possible on the basis of the eventual future discovery of further fossils.

Irrespective of its exact phylogenetic affinities, the holotype of *A. tortonica* is of interest from a taphonomic point of view, because it constitutes the only skeletal remains of a bird from the Hammerschmiede clay pit that were found in articulation. Even though some bones of the large darter *Anhinga pannonica* from the Hammerschmiede locality may belong to a single individual (Mayr et al. 2020a), these were scattered over a larger area owing to transport of the disarticulated bones in the flow direction of the river channel in which they were deposited. The preservation of the anseriform leg indicates a rapid burial in the sediment without subsequent reworking, and the fact that the femur lacks the proximal portion suggests that the specimen represents the feeding remains of a scavenger or predator. Isolated legs or feet are commonly found in the Eocene fossil locality Messel, where they were interpreted as feeding remains of crocodylians (Mayr 2016). Crocodylians no longer existed in the late Miocene of Central Europe (Böhme 2003), but snapping turtles (Chelydridae) are commonly found in the Hammerschmiede locality (Kirscher et al. 2016) and may have scavenged bird carcasses.

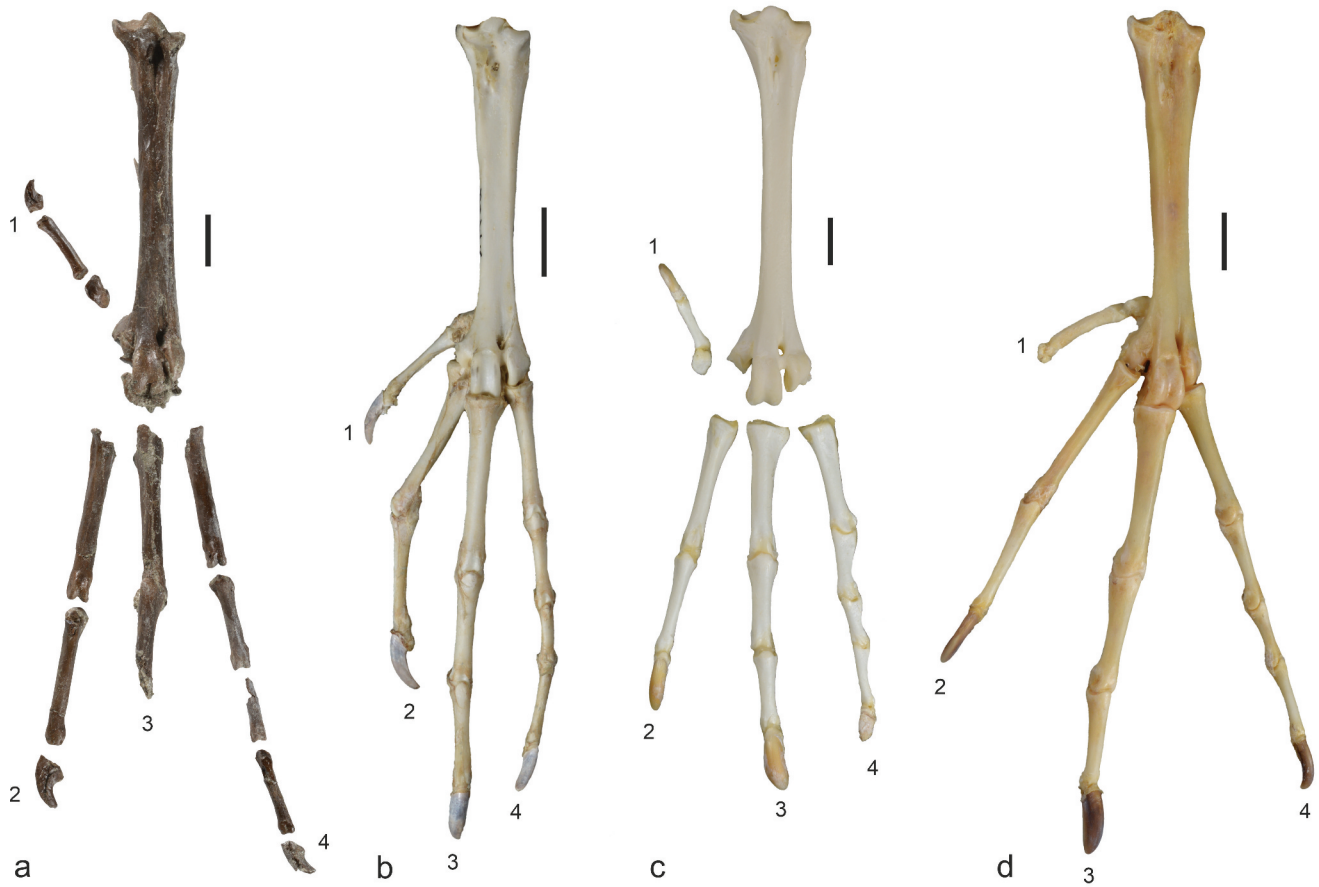


Figure 6. Left feet of (a) *Allgoviachen tortonica*, n. gen. et sp. from the earliest late Miocene (Tortonian) of the Hammerschmiede clay pit (holotype, SNSB-BSPG 2020 XCIV 1058), (b) *Dendrocygna viduata* (Dendrocygnae; right foot, mirrored; SMF 2271), (c) *Anser indicus* (Anserinae; SMF 19855), and (d) *Sarkidiornis melanotos* (Anatinae; ungual phalanx of hallux truncated; SMF 19912). The toes are numbered. Scale bars equal 10 mm. [Colour online].

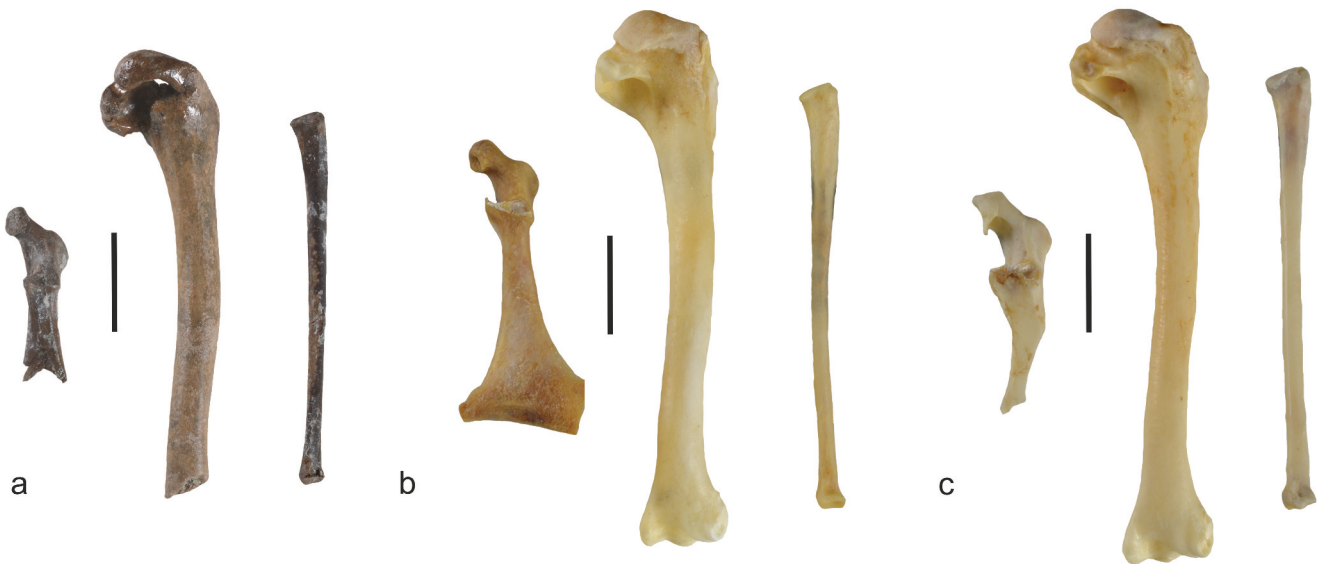


Figure 7. (a) Omal extremity of right coracoid (GPIT/AV/00236; dorsal view), right humerus lacking distal end (GPIT/AV/00232; caudal view), and right radius (GPIT/AV/00213; ventral view) of a very small anatid from the Hammerschmiede clay pit (cf. *Mioquerquedula*). (b) Right coracoid, humerus, and radius of the extant *Spatula hottentota* (SMF 5794). (c) Omal extremity of right coracoid as well as right humerus and right radius of the extant *Nettapus auritus* (SMF 255). Scale bars equal 10 mm. [Colour online].

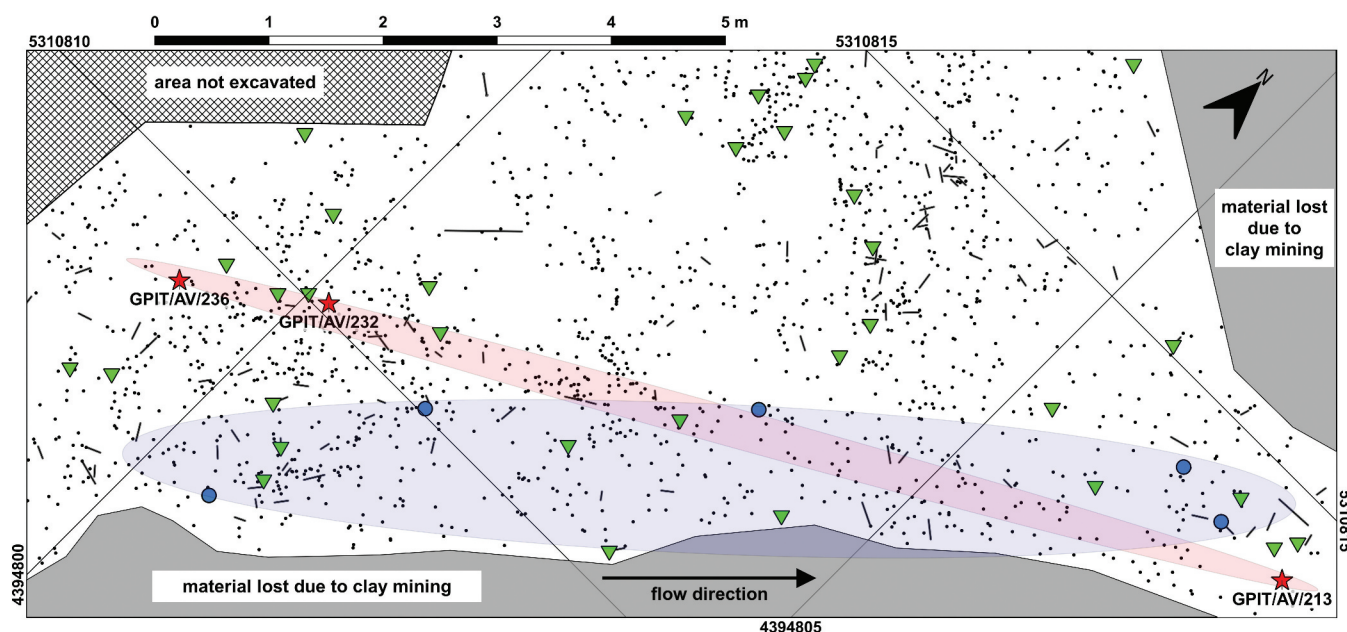


Figure 8. Section of the excavation plan Hammerschmiede level HAM 4 (excavation years 2019–2021). Black dots represent vertebrate fossils, black stripes denote the orientation of elongated objects. Bird bones are indicated by green triangles, cf. *Mioquerquedula* bones (likely belonging to the same individual) are highlighted with red stars, and bones that probably belong to a single individual of the large-sized darter *Anhinga pannonica* are shown with blue circles. The three wing and pectoral girdle bones that likely belong to a single individual of cf. *Mioquerquedula* are scattered over a distance of ten metres in an area (red field) of similar length to that containing putatively associated bones of *A. pannonica* (blue field). Coordinates correspond to a Gauss-Krüger Zone 4 grid with values in metres. Modified after Mayr et al. (2020a). [Colour online].

The Hammerschmiede clay pit also yielded remains of further anseriform taxa. Most notable among these are four bones of a very small species, which was even smaller than the smallest extant anatids, *Spatula hottentota* and *Nettapus auritus* (Figure 7). The material includes the omal extremities of two right coracoids (GPIT/AV/00236 and GPIT/AV/00245) as well as a right humerus lacking the distal end (GPIT/AV/00232) and a right radius (GPIT/AV/00213). These bones, all of which stem from the local stratigraphic level HAM 4, are likely to belong to the taxon *Mioquerquedula*. The type species of this taxon, *M. minutissima*, was described from the middle Miocene Sharga locality of Mongolia (Zelenkov and Kurochkin 2012). *Mioquerquedula* seems to have been quite common during the middle and early late Miocene in Eurasia, between approximately 14 and 10 Ma. Another species, *M. velox* occurs in the middle Miocene of France (Sansan locality, Zelenkov and Kurochkin 2012). A tentative record of *Mioquerquedula* was furthermore reported from the middle Miocene (Volhynian) of the northern Caucasus near Tsurevsky in the Krasnodar region of Russia (Zelenkov 2017a), and the taxon was also identified in the late Miocene (MN 9) of Rudabanya, Hungary (Zelenkov 2017b).

The specimens of this very small dabbling duck are also of interest from a taphonomic point of view. Due to the presence of duplicate coracoids from the same body side, a minimal number of two individuals is obvious. Judging from the presumed direction of transport and the spatial data of the finds, three specimens – a right coracoid (GPIT/AV/00236), a right proximal humerus (GPIT/AV/00232) and a right radius (GPIT/AV/00213) – are likely to belong to the same individual (the other coracoid, GPIT/AV/00245, was gathered without spatial data several metres NNW in the deeper parts of the HAM 4 channel). These three bones were discovered within a distance of ten metres and were scattered in accordance with the

reconstructed flow direction (SSW–NNE) (Figure 8). The specimens are anatomically sorted from proximal (SSW) to distal bones (NNE), and their spatial distribution within the 150 cm thick fossiliferous profile of the HAM 4 layer is within a range of 23 cm only. This observation is consistent with a similar taphonomic event regarding the scattered bones of a darter (*Anhinga pannonica*). The latter are also likely to stem from a single individual and were dispersed in a stray field with a similar direction and expansion to the closely adjacent one of the small dabbling duck (Mayr et al. 2020a). The small-scale transport and redeposition of the wing and pectoral girdle bones of the small duck (cf. *Mioquerquedula*) sharply contrasts with the preservation of the articulated leg of *A. tortonica*.

In conclusion, the anseriform assemblage of the Hammerschmiede clay pit, and that of the HAM 4 level in particular, is represented by four species: *Allgoviachen tortonica*, cf. *Mioquerquedula*, and two so far undetermined medium-sized anatids. This association shows notable differences to extant anseriform faunas from Central Europe. *A. tortonica* represents an unusual morphotype unknown from extant avifaunas, which places a caveat on attempts to shoehorn Miocene anseriforms into extant genus-level taxa (e.g., Mlíkovský 2002). Today, very small-sized Anatidae are only found in the tropical and subtropical regions and their occurrence at the Hammerschmiede site, and elsewhere in Eurasia, is likely to be due to a warmer paleoenvironment, which featured mean annual temperatures above 20°C in the Hammerschmiede locality (Mayr et al. 2020a). Climatic cooling after the late Miocene was also hypothesised to have accounted for the disappearance of other taxa found in the Hammerschmiede locality, that is, the large-sized darter *Anhinga pannonica* (Anhingidae) and a very large crane (Mayr et al. 2020a, b). Currently, early late Miocene avifaunas remain poorly studied, and it is to be hoped that future finds from the Hammerschmiede clay pit and coeval

sites will add to our understanding of the avifaunas of this time period.

Acknowledgments

We thank the members of the Hammerschmiede excavation team from 2020 for their invaluable assistance in the field. This excavation was supported by the Bavarian State Ministry of Research and the Arts, and by the Bavarian Natural History Collections (SNSB). We furthermore thank Sven Tränkner (Frankfurt) for taking the photographs and Henrik Stöhr (Tübingen) for the preparation of the fossil. Comments from an anonymous reviewer improved the manuscript.

Disclosure statement

No potential conflict of interest was reported by the authors.

ORCID

Gerald Mayr  <http://orcid.org/0000-0001-9808-748X>

References

- Böhme M. 2003. The Miocene Climatic Optimum: evidence from ectothermic vertebrates of Central Europe. *Palaeogeogr, Palaeoclimatol, Palaeoecol.* 195 (3–4):389–401. doi:10.1016/S0031-0182(03)00367-5.
- Böhme M, Spassov N, Fuss J, Tröscher A, Deane AS, Prieto J, Kirscher U, Lechner T, Begun DR. 2019. A new Miocene ape and locomotion in the ancestor of great apes and humans. *Nature.* 575:489–493.
- Buckner JC, Ellingson R, Gold DA, Jones TL, Jacobs DK. 2018. Mitogenomics supports an unexpected taxonomic relationship for the extinct diving duck *Chendytes lawi* and definitively places the extinct Labrador Duck. *Mol Phylogenet Evol.* 122:102–109.
- Carboneras C. 1992. Family Anatidae (ducks, geese, and swans). In: Del Hoyo J, Elliott A, Sargatal J, editors. *Handbook of the Birds of the World* (Vol. 1). Barcelona: Lynx Edicions; p. 536–628.
- Cheneval J. 1983. Les Anatidae (Aves, Anseriformes) du gisement Aquitainien de Saint-Gerand-le-Puy (Allier, France). In: Buffetaut E, Mazin JM, Salmon E, editors. *Actes du symposium paleontologique Georges Cuvier*. Montbéliard: la Ville; p. 85–98.
- Cheneval J. 1984. Les oiseaux aquatiques (Gaviiformes à Anseriformes) du gisement aquitainien de Saint-Gerand-le-Puy (Allier, France): révision systématique. *Palaeovertebr.* 14:33–115.
- Cheneval J. 1987. Les Anatidae (Aves, Anseriformes) du Miocène de France. Révision systématique et évolution. *Doc Lab Géol* (Lyon). 99:137–157.
- Cheneval J. 2000. L'avifaune de Sansan. In: Ginsburg L, editor. *La faune miocène de Sansan et son environnement*, Vol. 183. *Mém Mus natl Hist nat.*; p. 321–388.
- Donne-Goussé C, Laudet V, Hänni C. 2002. A molecular phylogeny of anseriformes based on mitochondrial DNA analysis. *Mol Phylogenet Evol.* 23:339–356.
- Gonzalez J, Düttmann H, Wink M. 2009. Phylogenetic relationships based on two mitochondrial genes and hybridization patterns in Anatidae. *J Zool.* 279 (3):310–318. doi:10.1111/j.1469-7998.2009.00622.x.
- Kessler E. 1984. Noi contribuții privind studiul avifaunei din Paratethys [New contributions to the study of the avifauna in the Paratethys]. *Crisia.* 14: 521–532. in Romanian.
- Kirscher U, Prieto J, Bachtadse V, Aziz HA, Doppler G, Hagmaier M, Böhme M. 2016. A biochronologic tie-point for the base of the Tortonian stage in European terrestrial settings: magnetostratigraphy of the topmost Upper Freshwater Molasse sediments of the North Alpine Foreland Basin in Bavaria (Germany). *Newslett Stratigr.* 49(3):445–467. doi:10.1127/nos/2016/0288.
- Kurochkin EN, Ganea IM. 1972. Birds of the Middle Sarmatian of Moldavia. In: David AI, editor. *Neogene and Pleistocene Vertebrates of Moldavia*. Kishniev: Akademiya Nauk Moldavskoy SSR. [in Russian]; p. 45–70.
- Livezey BC, Martin LD. 1988. The systematic position of the Miocene anatid *Anas* [?] *blanchardi* Milne-Edwards. *J Vertebr Paleontol.* 8:196–211.
- Mayr G. 2016. Avian feet, crocodylian food and the diversity of larger birds in the early Eocene of Messel. *Palaeobiodiv Palaeoenviron.* 96:601–609.
- Mayr G. *in press*. *Paleogene fossil birds*. 2nd edition ed. Heidelberg: Springer.
- Mayr G, Lechner T, Böhme M. 2020a. The large-sized darter *Anhinga pannonica* (Aves, Anhingidae) from the late Miocene hominid Hammerschmiede locality in Southern Germany. *PLoS ONE.* 15(5):e0232179. doi:10.1371/journal.pone.0232179.
- Mayr G, Lechner T, Böhme M. 2020b. A skull of a very large crane from the late Miocene of Southern Germany, with notes on the phylogenetic interrelationships of extant Gruinae. *J Ornithol.* 161:923–933.
- Mayr G, Pavia M. 2014. On the true affinities of *Chenornis graculoides* Portis, 1884 and *Anas lignitifila* Portis, 1884 – an albatross and an unusual duck from the Miocene of Italy. *J Vertebr Paleontol.* 34:914–923.
- Mayr G, Smith T. 2017. First Old World record of the poorly known, swan-sized anseriform bird *Paranyroca* from the late Oligocene/early Miocene of France. *N Jb Geol Paläontol, Abh.* 286:349–354.
- Milne-Edwards A. 1867–1869. *Recherches anatomiques et paléontologiques pour servir à l'histoire des oiseaux fossiles de la France*, vol. 1. Paris: Victor Masson et fils.
- Mlíkovský J. 2002. *Cenozoic Birds of the World*, Vol. Part 1. Europe: Ninox Press, Praha.
- Sun Z, Pan T, Hu C, Sun L, Ding H, Wang H, Zhang C, Jin H, Chang Q, Kan X, et al. 2017. Rapid and recent diversification patterns in Anseriformes birds: inferred from molecular phylogeny and diversification analyses. *PLoS ONE.* 12(9):e0184529. doi:10.1371/journal.pone.0184529.
- von Ammon L. 1918. Tertiäre Vogelreste von Regensburg und die jungmiocäne Vogelwelt. *Abh naturwiss Ver Regensburg.* 12:1–69.
- von Meyer H. 1865. Fossile Vögel von Radoboy und Oehningen. *Palaeontogr.* 14:125–131.
- Worthy TH. 2009. Descriptions and phylogenetic relationships of two new genera and four new species of Oligo-Miocene waterfowl (Aves: anatidae) from Australia. *Zool J Linn Soc.* 156(2):411–454. doi:10.1111/j.1096-3642.2008.00483.x.
- Worthy TH, Lee MS. 2008. Affinities of Miocene waterfowl (Anatidae: *manuherikia*, *Dunstanetta* and *Miotadorna*) from the St Bathans Fauna, New Zealand. *Palaeontol.* 51:677–708.
- Worthy TH, Tennyson AJ, Jones C, McNamara JA, Douglas BJ. 2007. Miocene waterfowl and other birds from Central Otago, New Zealand. *J Syst Palaeontol.* 5:1–39.
- Zelenkov NV. 2011. Diving ducks from the middle Miocene of western Mongolia. *Paleontol J.* 45:191–199.
- Zelenkov NV. 2012a. Neogene geese and ducks (Aves: anatidae) from localities of the Great Lakes Depression, western Mongolia. *Paleontol J.* 46:607–619.
- Zelenkov NV. 2012b. A new duck from the Middle Miocene of Mongolia, with comments on Miocene evolution of ducks. *Paleontol J.* 46:520–530.
- Zelenkov NV. 2017a. Finds of fragmentary bird skeletons in the Middle Miocene of the northern Caucasus. *Dokl Biol Sci.* 477:223–226.
- Zelenkov NV. 2017b. The revised avian fauna of Rudabanya (Hungary, Late Miocene). *Paleontología y evolución de las Aves. Contrib Museo Argentino Cienc Nat* 7:253–266.
- Zelenkov NV. 2020. Cenozoic evolution of Eurasian anatids (Aves: anatidae s.l.). *Biol Bull Rev.* 10(5):417–426. doi:10.1134/S2079086420050096.
- Zelenkov NV, Kurochkin EN. 2012. Dabbling ducks (Aves: anatidae) from the middle Miocene of Mongolia. *Paleontol J.* 46:421–429.
- Zelenkov NV, Kurochkin EN. 2015. Class Aves. In: Kurochkin EN, Lopatin AV, Zelenkov NV, editors. *Fossil vertebrates of Russia and adjacent countries, Fossil reptiles and birds, part 3*. Moscow: Geos; p. 86–290. in Russian.

Chapter 6

Strewnfield case study of a juvenile *Deinotherium levius* (Mammalia, Deinotheriidae)

Published in

Konidaris, G.E., Lechner, T., Kampouridis, P., Böhme, M., 2023. *Deinotherium levius* and *Tetralophodon longirostris* (Proboscidea, Mammalia) from the Late Miocene hominid locality Hammerschmiede (Bavaria, Germany), and their biostratigraphic significance for the terrestrial faunas of the European Miocene. *Journal of Mammalian Evolution*. <https://doi.org/10.1007/s10914-023-09683-3>

This chapter is a reprint of the published version and differs from the general chapter numbering of this dissertation.



Deinotherium levius and *Tetralophodon longirostris* (Proboscidea, Mammalia) from the Late Miocene hominid locality Hammerschmiede (Bavaria, Germany), and their biostratigraphic significance for the terrestrial faunas of the European Miocene

George E. Konidaris^{1,2} · Thomas Lechner^{2,3} · Panagiotis Kampouridis³ · Madelaine Böhme^{2,3}

Accepted: 8 August 2023
© The Author(s) 2023

Abstract

During the Miocene, proboscideans reached their greatest diversification, and due to their marked evolutionary changes in dental size and morphology, they comprise an important biostratigraphic/biochronological tool. In this article, we study the proboscideans from the Late Miocene hominid locality Hammerschmiede (Germany), whose fossiliferous layers HAM 6, HAM 4 and HAM 5 are dated to 11.42, 11.44 and 11.62 Ma, respectively. The studied material consists of mandibular, tusk and cheek tooth specimens, which are attributed to the deinothere *Deinotherium levius* and the tetralophodont gomphothere *Tetralophodon longirostris*. An almost complete juvenile mandible of *D. levius* was CT-scanned and revealed that the erupting lower tusks represent the permanent ones. The mandible is most possibly associated with a lower deciduous tusk, and therefore these specimens capture the rare, and short in duration, moment of transition between deciduous and permanent lower tusks in fossil proboscideans and represent the first such example in deinotheres. The chronologically well-constrained proboscidean fauna from Hammerschmiede and the examination of other assemblages from European localities indicate that the coexistence of *D. levius* and *T. longirostris* characterizes the late Astaracian–earliest Vallesian, while Hammerschmiede may showcase the transition from the Middle Miocene trilophodont (*Gomphotherium*)-dominated faunas of central Europe to the Late Miocene tetralophodont-dominated ones. Finally, in order to decipher the dietary preferences of the Hammerschmiede *Tetralophodon* we performed dental mesowear angle analysis, which revealed a mixed-feeding diet with an important browsing component, significantly different from the heavily browsing one of *Deinotherium* known from other localities. Such distinct feeding habits between the taxa indicate niche partitioning, which allowed their sympatry.

Keywords Biostratigraphy · Deinotheres · Dental mesowear · Gomphotheres · Tusk replacement

Introduction

The Miocene is the period of the Cenozoic that evidenced the greatest diversity of proboscideans and additionally documents their first wide distribution outside of Africa

(Shoshani and Tassy 1996). After their arrival in Europe during the Early Miocene, as part of the complex “Proboscidean Datum Event” (Tassy 1990), deinotheres, gomphotheres, and mammutids formed the proboscidean faunas of this epoch, and by their rapid diversification and expansion, combined with marked evolutionary changes in terms of dental size and morphology, they comprise an important biostratigraphic and biochronological tool for the whole Miocene. However, certain issues remain still partially explored, either due to the rarity of proboscidean discoveries or due to absence of secure (bio)chronological frameworks, that prohibit the recognition of bioevents (e.g., dispersals, extinctions). The latter is particularly obscured because many important specimens/assemblages that play a crucial role in evolutionary schemes and interpretations are part of historical collections lacking stratigraphic control.

✉ George E. Konidaris
georgios.konidaris@uni-tuebingen.de

¹ Palaeoanthropology, Institute for Archaeological Sciences, Department of Geosciences, Eberhard Karls University of Tübingen, Rümelinstr. 23, 72070 Tübingen, Germany

² Senckenberg Centre for Human Evolution and Palaeoenvironment, Tübingen, Germany

³ Terrestrial Palaeoclimatology, Department of Geosciences, Eberhard Karls University of Tübingen, Sigwartstraße 10, 72074 Tübingen, Germany

Here, we present the proboscidean assemblage (deinotheres and tetralophodont gomphotheres) from the faunal-rich and chronologically well-constrained hominid locality of Hammerschmiede (Germany) dated at the very base of the Late Miocene. The aim of the study is (1) to describe and compare the proboscidean dental and mandibular remains, (2) contribute to the taxonomy, evolution, biostratigraphy and palaeoecology of Miocene deinotheriids and gomphotheriids, and (3) add new data on the replacement of deciduous by permanent lower tusks in deinotheriids, a rarely captured moment of transition in fossil proboscideans, based on a mostly complete juvenile mandible.

Fossiliferous locality and geological setting

The active clay-pit of Hammerschmiede is situated in the North Alpine Foreland Basin (NAFB), 5 km north of the city of Kaufbeuren (Fig. 1). It uncovers 25 m of fine-grained fluvial and overbank deposits, including two lignite seams, belonging to the Upper Series lithostratigraphic unit of the Upper Freshwater Molasse (Doppler 1989). Magnetostratigraphic investigations date this succession to the Middle-to-Late Miocene transition (Kirscher et al. 2016). Fossil vertebrates are preserved mainly in fluvial channels (Fig. 2) and two of these channel structures, HAM 4 (dated to 11.44 Ma) and HAM 5 (dated to 11.62 Ma), have been intensively excavated since 2011. The HAM 4

channel represents a larger meandering stream of about 50 m width, whereas the structure HAM 5 is interpreted as a meandering rivulet of 4–5 m width (Kirscher et al. 2016; Lechner and Böhme 2022).

In addition to these main fossiliferous horizons, a third vertebrate-bearing level (HAM 6) has been discovered and sampled by private collectors (Sigulf Guggenmos, Dösingen and Manfred Schmid, Marktoberdorf) during the late 1970s and early 1980s (Fig. 3). This horizon, which contained a partial proboscidean skeleton, was found directly below the upper lignite seam at the uppermost limit of the Miocene succession exposed in the clay-pit (see below), which imply, according to the age-model (Kirscher et al. 2016), an age of about 11.42 Ma for the site HAM 6.

These three fossil-bearing horizons, but especially the actively excavated HAM 4 and HAM 5, are decidedly productive, resulting in a high diversity and disparity of vertebrates, including so far 146 species from 75 families. Most spectacular was the discovery of associated skeletons of the partially bipedal hominid *Danuvius guggenmosi* (Böhme et al. 2019, 2020) in HAM 5. So far, only a fraction of the enormous vertebrate fauna has been studied in detail, including carnivores (Kargopoulos et al. 2021a, b, c, 2022), ruminants (Fuss et al. 2015; Hartung et al. 2020; Hartung and Böhme 2022), beavers (Lechner and Böhme 2022, 2023), small mammals (Mayr and Fahlbusch 1975; Prieto and Rummel 2009; Prieto et al. 2011; Prieto 2012; Prieto and Dam 2012) and birds (Mayr et al. 2020a, b, 2022).

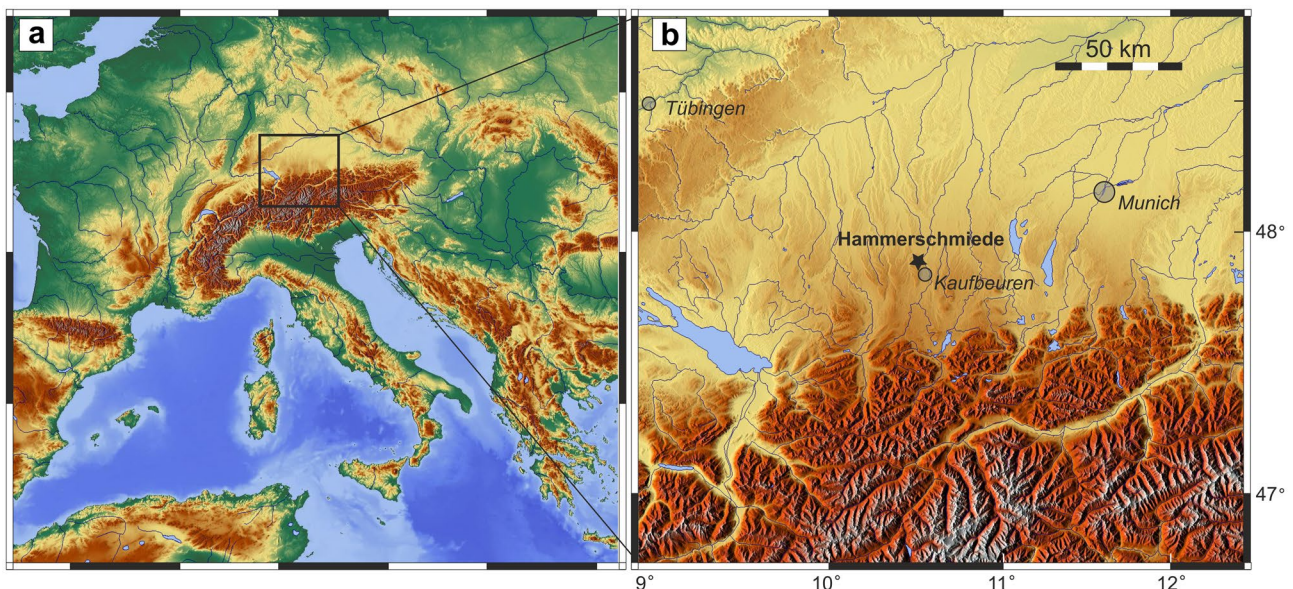


Fig. 1 Geographic position of the Hammerschmiede locality (Bavaria, Germany) in Europe (**a**) and in the North Alpine Foreland Basin (**b**)

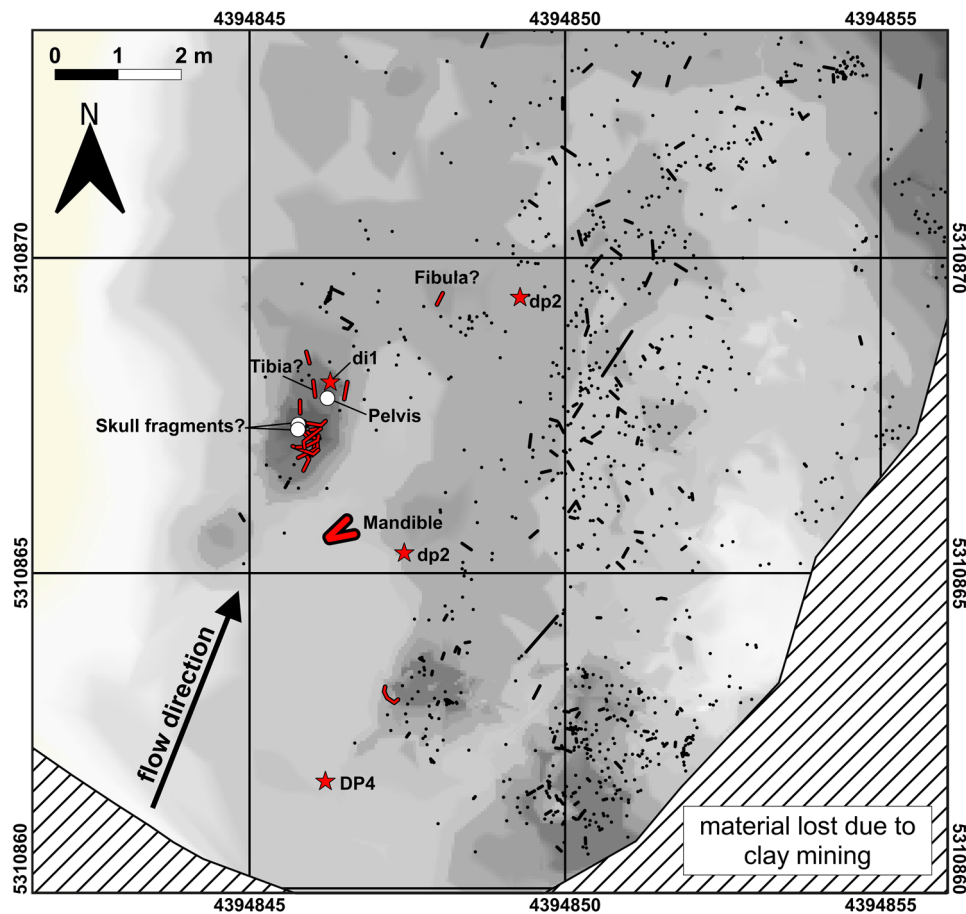


Fig. 2 Section of the excavation plan at Hammerschmiede HAM 5 (excavation years 2018–2021). Black dots represent vertebrate fossil specimens, black stripes denote elongated objects and their orientation. Excavated deinothere bones, most probably belonging to the same juvenile individual of *Deinotherium levius*, are highlighted with red stars (single teeth), a thick red angled line (mandible), white circles (pelvis and two skull fragments) and red lines (14 ribs, one tibia? and fibula?). Associated bones of the juvenile *Deinotherium* individual are arranged over a distance of eight meters parallel to the

reconstructed flow direction in a shallower side branch of the HAM 5 rivulet. The background color indicates the elevation differences of the excavated palaeo-channel base, dark areas represent lower and brighter ones for higher elevations of the riverbed with a total height difference of 1.5 m, with finds only in the lowermost 70 cm. Note the uneven channel base and accumulation of most of the finds in pit-like depressions, which probably acted as bone traps. Coordinates correspond to Gauss-Krüger Zone 4 grid in meters

Material and methods

The herein studied proboscidean material originates from the layers HAM 4, HAM 5 and HAM 6 of the Hammerschmiede clay pit. All specimens are stored at the Palaeontological Collection of the University of Tübingen, Germany (GPIT), and are labelled as either GPIT/MA (for excavation years 2011–2019) or SNSB-BSPG (for excavation years 2020–2021). SNSB-BSPG-2020-XCIV refers to specimens from HAM 4 and SNSB-BSPG-2020-XCV from HAM 5. Comparative material was studied at FSL, HGI, HLMD, HNHM, ML, MNHN, NHMW, SNSB-BSPG and SU. The deinothere dental terminology follows Pickford and Pourabrishami (2013), and the gomphothere one is according to Tassy (1996a). For the cheek teeth, the metric parameters

measured are the mesiodistal crown length (L), the maximum buccolingual crown width (W) in each loph(id), and the maximum height for unworn (or minimally worn) teeth. For the lower tusk of *Tetralophodon*, the compression index (Ci) was calculated as $\text{height} \times 100 / \text{width}$. The measurements were taken with a digital caliper or, in the case of some large mandibular measurements, with a measuring tape; those in parentheses indicate the greatest measurable value of a parameter in incomplete or inadequately preserved specimens. Mandibular measurements follow Tassy (1996b). All measurements are given in Tables 1 and 2. Comparative dental measurements were obtained from the literature or directly acquired from specimens at several museums and institutions (Tables 3 and 4). For each deciduous tooth measurement and deinothere species used in the analysis,

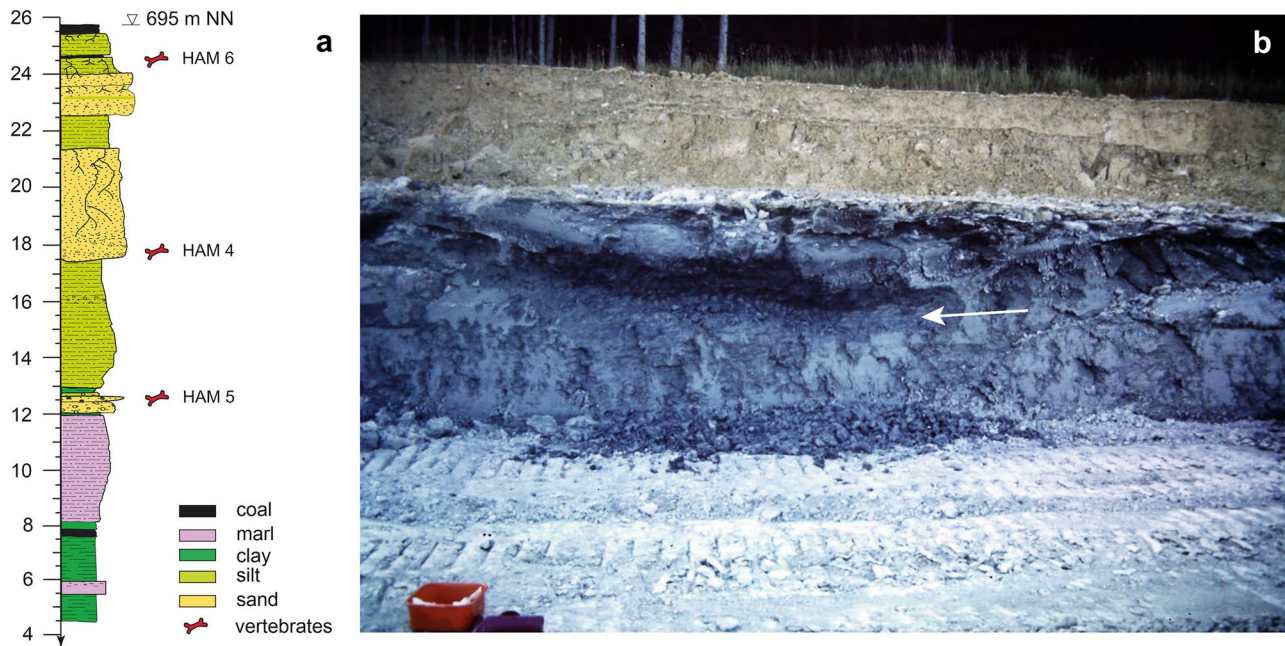


Fig. 3 **a.** Stratigraphic sequence (left) of the Hammerschmiede clay-pit (northern profile of Kirscher et al. 2016) indicating all three fossiliferous levels containing proboscideans. **b.** Finding position of the adult *Tetralophodon* skeleton (photo: M. Schmid, 1980). The Mio-

cene clay-rich sediments are greyish-bluish in color and overlaid by bright-yellowish meltwater deposits of the Günz glaciation (earliest Middle Pleistocene). The excavated layer (HAM 6) is marked by the white arrow

the z-score was computed as $z = (x - m) / SD$, where x is the dental measurement of the HAM specimens (mean value in case both right and left deciduous premolar are preserved), and m and SD the mean and standard deviation of the comparative sample, respectively (Table 5).

Table 1 Mandibular measurements (in mm) of the *Deinotherium levius* mandible from Hammerschmiede 5

	<i>Deinotherium levius</i>
Mandibular measurements	SNSB-BSPG-2020-XCV-0096
preserved length	435
symphyseal length	91
alveolar distance	220
maximal width	277
mandibular width at the root of the rami	239
width of corpus at the root of the ramus	(75)
width of corpus in front of the dp2 alveolus	47
posterior symphyseal width	125
anterior symphyseal width	95
maximal width of the rostral trough	51
minimal width of the rostral trough	28
internal width between the dp2 alveoli	43
maximal height of corpus	(57)
rostral height at the symphyseal border	52
maximal depth of the ramus	139

In order to estimate the age at death of the *Tetralophodon* individual(s) from HAM 6, we applied the dental-wear-based criteria proposed by Metz-Muller (2000) for the tetralophodont gomphothere *Anancus arvernensis* (note, however, that *A. arvernensis* did not possess premolars and is thus not precisely comparable). Wear was codified as f, p, d, D and C (Metz-Muller 2000: figs. 20 and 21) for each of the four or five loph(id)s, and when necessary, separated between pretrite/posttrite lophids. Age estimation was based on the extant African elephant *Loxodonta africana* (Haynes 1991; Metz-Muller 2000: fig. 22) and thus the results should be considered indicative.

The deinotherere mandible SNSB-BSPG-2020-XCV-0096 was scanned with an X-ray tube containing a multi-metal reflection target with a maximum acceleration voltage of 225 kV in the Nikon X TH 320 μ CT scanner of the 3D imaging lab of the University of Tübingen using a 0.1 mm copper filter with 3500 projections, 200 kV and 27 μ A, with a voxel size of 0.006741 mm. 3D models of the mandible, as well as from the associated to it right and left dp2 can be viewed in Online Resources 1–3. 3D renderings of the mandible are given in Online Resource 4, Figs. S1–S6.

In order to decipher the dietary habits of the Hammerschmiede proboscideans, we performed dental mesowear angle analysis (Saarinen et al. 2015). This method was originally applied in proboscideans with lamellar structure on their cheek teeth, and was later employed also in bunodont (e.g., *Gomphotherium*, *Tetralophodon*), zygodont

Table 2 Dental measurements (in mm) of *Deinotherium levius* and *Tetralophodon longirostris* from Hammerschmiede. Measurements in parentheses indicate the greatest measurable value of a parameter in incomplete or inadequately preserved specimens, or worn cusps in case of height values. Values noted with an asterisk were acquired from the CT-scan. Abbreviations: **L**, mesio-distal crown length; **H**, preserved crown height and cusp measured; **W**, maximum buccolingual crown breadth (at first, second, third and fourth loph/rid)

Species	Inventory number	Site	Tooth	Side	L	W	W1	W2	W3	W4	W5	H
<i>Deinotherium levius</i>	SNSB-BSPG-2020-XCV-0199	HAM-5	dp2	right	31.4		18.3	20.1				29.3 (protoconid)
	SNSB-BSPG-2020-XCV-0092	HAM-5		left	30.7		17.4	19.9				27.6 (protoconid)
	SNSB-BSPG-2020-XCV-0257	HAM-5	di1	right	28.1	18.4						12.4
	SNSB-BSPG-2020-XCV-0096	HAM-5	dp3	right	(46.8)			37.0				29.0 (protoconid)
	SNSB-BSPG-2020-XCV-0096	HAM-5		left	52.2		31.1	35.4				-
	SNSB-BSPG-2020-XCV-0096	HAM-5	dp4	right	70.4			41.4*				-
	SNSB-BSPG-2020-XCV-0096	HAM-5		left	70.0			41.5				30.0 (3 rd labial)
	SNSB-BSPG-2020-XCV-0096	HAM-5	i2	right	34.1*	27.8*						12.8*
	SNSB-BSPG-2020-XCV-0096	HAM-5	i2	left	37.5*	30.5*						-
	GPIT/MA/16490	HAM-4	DP2	right	36.9		28.8	32.1				28.3 (paracone)
<i>Tetralophodon longirostris</i>	GPIT/MA/09552	HAM-5	DP3	left	47.8		42.8	47.0				(24.8) (paracone)
	GPIT/MA/13794	HAM-5	DP4	right	70.2		52.7	53.9	50.3			32.4 (protocone)
	GPIT/MA/12313	HAM-5	dp4	right	78.6		36.6	38.9	42.4	35.4		-
	GPIT/MA/12196	HAM-5	DP3	left	51.1		32.5	41.8	39.7			(23.8) (metacone)
	GPIT/MA/09554	HAM-5	P3	right	(39.6)		41.1					
	GPIT/MA/10800-05	HAM-6	M1		(116)		(72)					
	GPIT/MA/10800-03	HAM-6	m2	right	143.3		64.0	71.5	80.1	65.8		(45.9) (3 rd posttrite)
	GPIT/MA/10800-04	HAM-6	M2	left	144.0		85.9	83.0	85.0	79.1		(51.9) (3 rd posttrite)
	GPIT/MA/10800-02	HAM-6	M3	right	191.2		97.3	96.3	94.1	92.4	77.3	49.6 (4 th pretrite)

Table 3 Comparative sample of deinotheriid deciduous teeth used in the analyses

Taxon	Locality	Country	Age/MN	Source
<i>Prodeinotherium cuvieri</i>	Langenau 1	Germany	MN 4	Sach and Heizmann (2001)
	Chevilly	France	MN 4	Ginsburg and Chevrier (2001)
	Montreal-du-Gers	France	MN 4	Ginsburg and Chevrier (2001)
	Zagyvapalfalva	Hungary	MN 4	Gasparik (2004)
<i>Prodeinotherium bavaricum</i>	Grund	Austria	MN 5	G.K. at NHMW
	Gračanica	Bosnia-Herzegovina	late MN 5 or early MN 6	Göhlich (2020)
	Channay-sur-Lathan	France	MN 5	Ginsburg and Chevrier (2001)
	Hommès	France	MN 5	Ginsburg and Chevrier (2001)
	Noyant	France	MN 5	Ginsburg and Chevrier (2001)
	Pont-Boutard	France	MN 5	Ginsburg and Chevrier (2001)
	Pontlevoy	France	MN 5	Stehlin (1925); Ginsburg and Chevrier (2001)
	Savigne-sur-Lathan	France	MN 5	Ginsburg and Chevrier (2001)
	Tavers	France	MN 5	Ginsburg and Chevrier (2001)
	<i>Deinotherium levius</i> or <i>D. ?levius</i>	Hollabrunn	Austria	?
Atzelsdorf		Austria	earliest MN 9	Göhlich and Huttunen (2009)
Mannersdorf bei Leithagebirge		Austria	?	Huttunen (2002b)
Vetren		Bulgaria	?	Vergiev and Markov (2012)
La Grive		France	MN 7/8	Ginsburg and Chevrier (2001); G.K. at ML
Emmering bei Fürstenfeldbruck		Germany	?	Stromer (1940)
Massenhausen		Germany	MN 7/8	G.K. at SNSB-BSPG
Sopron		Hungary	late MN 7/8	G.K. at HNHM
Charmoile		Switzerland	MN 9	Gagliardi et al. (2021)
<i>Deinotherium giganteum</i> or <i>D. ?giganteum</i>		Nessebar	Bulgaria	late Miocene
	Montredon	France	MN 10	G.K. at FSL and ML
	Rudabanya	Hungary	MN 9	Gasparik (2005)
<i>D. proavum</i>	Kayadibi	Turkey	late Miocene (?Vallesian)	Gaziry (1976)
	Wolfau	Austria	Pannonian	G.K. at NHMW
	Rogozen	Bulgaria	late Miocene	G.K. at SU
	Pikermi	Greece	MN 12	Wagner (1848, 1857); Konidaris et al. (2017)
	Samos	Greece	Turolian	Konidaris and Koufos (2019)
	Baltavar	Hungary	MN 12	Gasparik (2004); G.K. at HNHM
	Pestszentlőrinc	Hungary	Turolian	Gasparik (2004)
	Polgardi	Hungary	MN 13	G.K. at HNHM
	Cimislia	Moldova	MN 12	Simionescu and Barbu (1939)
	Taraklia	Moldova	MN 12	Khomenko (1914)
Kiro Kucuk	North Macedonia	Turolian	Garevski and Markov (2011)	
Sinap 49	Turkey	late MN 10	Sanders (2003)	

(e.g., *Mammuth*) and lophodont (deinotheres) proboscideans (Saarinen and Lister 2016; Xafis et al. 2020). Here we apply the method only in *Tetralophodon* molars, because the HAM deinotheres teeth are deciduous, they are almost unworn and do not have sufficiently worn facets. Angles were measured

from the bottom (deepest point) of the dentine valleys in moderately worn main cusps to the top of the cusp's enamel ridges. For this purpose, we used a contour gauge that we have precisely fit within the cusp where the angle was to be measured. The contour gauge was photographed

Table 4 Comparative sample of tetralophodont molars used in the analyses (“Dinotheriensande” sites are noted with D)

Taxon	Locality	Country	Age/MN	Source
<i>Tetralophodon longirostris</i>	Atzelsdorf	Austria	earliest MN 9	Göhlich and Huttunen (2009)
	Auersbach	Austria	Vallesian	Göhlich (1998)
	Belvedere	Austria	Vallesian	Göhlich (1998); G.K. at NHMW
	Breitenfeld	Austria	MN 9	Göhlich (1998)
	Eggersdorf	Austria	Vallesian	Göhlich (1998)
	Geiereck	Austria	?	Göhlich (1998)
	Gschmeier	Austria	Vallesian	Göhlich (1998)
	Kornberg	Austria	MN 9	Göhlich (1998)
	Laaerberg	Austria	MN 9	Göhlich (1998)
	Lasnitz	Austria	Vallesian	Schlesinger (1917)
	Laßnitzhöhle	Austria	?	Göhlich (1998)
	Mannersdorf	Austria	?	Göhlich (1998); G.K. at NHMW
	Meidling	Austria	Vallesian	Göhlich (1998)
	Obertiefenbach	Austria	Vallesian	Göhlich (1998)
	Stettenhof	Austria	Vallesian	Göhlich (1998)
	Wolfau	Austria	Vallesian	Göhlich (1998)
	Dinotheriensande (D)	Germany	middle-late Miocene	Göhlich (1998)
	Bermersheim (D)	Germany	middle-late Miocene	Göhlich (1998); G.K. at HLMD
	Eppelsheim (D)	Germany	middle-late Miocene	Klähn (1931); Göhlich (1998); Gaziry (1994); G.K. at HLMD and MNHN
	Esselborn (D)	Germany	middle-late Miocene	Bergounioux and Crouzel (1960); Göhlich (1998)
	Gegend Alzey (D)	Germany	middle-late Miocene	Göhlich (1998)
	Kahlig bei Bermersheim (D)	Germany	middle-late Miocene	Göhlich (1998)
	Westhofen (D)	Germany	middle-late Miocene	Gaziry (1994)
	Wissberg (D)	Germany	middle-late Miocene	Göhlich (1998)
	Rudabanya	Hungary	MN 9	Gasparik (2004, 2005); G.K. at HGI
	Azambujeira (middle level)	Portugal	Vallesian	Antunes and Mazo (1983)
	Kapellen	Slovenia	Vallesian	Göhlich (1998)
Polinya	Spain	MN 9	Alberdi (1971)	
Maritsa-Iztok	Bulgaria	Turolian	Kovachev (2004)	
Oryahovo	Bulgaria	late Miocene	G.K. at SU	
Pestszentlőrinc	Hungary	Turolian	G.K. at HNHM	
Yulafli	Turkey	MN 10	Geraads et al. (2005)	
Crevilente 2	Spain	MN 11	Mazo and Montoya (2003)	
Mannersdorf bei Angern	Austria	Pannonian F/H	G.K. at NHMW	
Küçükçekmece	Turkey	MN 10	Tassy (2016)	
<i>?Stegotetralobodon</i>				
tetralophodont indet.				

Table 5 Descriptive statistics and calculated z-scores for the dental measurements (in mm) of the HAM deinothereiid deciduous teeth compared to *Prodeinotherium cuvieri*, *Prodeinotherium bavaricum*, *Deinotherium levis*, *Deinotherium giganteum* and *Deinotherium proavum* from several localities (see Materials and methods, and Table 3). When $z > |1.96|$, the null hypothesis that the HAM specimens fit within the variation of the comparative sample can be rejected at $p < 0.05$; in such cases the z-score is typed in bold). Abbreviations: **CI**, confidence interval; **L**, mesiodistal crown length; **n**, number of specimens; **W**, maximum buccolingual crown breadth; **SD**, standard deviation

		n	mean	minimum	maximum	SD	95% CI (lower)	95% CI (upper)	z-score
LDP2	HAM	1	36.90	-	-	-	-	-	-
	<i>P. cuvieri</i>	1	28.30	-	-	-	-	-	-
	<i>P. bavaricum</i>	3	26.33	24.8	29.0	2.32	20.58	32.09	4.56
	<i>D. levis</i>	4	36.25	35.0	39.0	1.86	33.28	39.22	0.35
	<i>D. giganteum</i>	5	41.26	36.4	44.0	2.93	37.63	44.89	-1.49
	<i>D. proavum</i>	7	48.57	40.6	53.9	4.49	44.42	52.72	-2.60
	HAM	1	32.10	-	-	-	-	-	-
WDP2	<i>P. cuvieri</i>	1	24.30	-	-	-	-	-	-
	<i>P. bavaricum</i>	3	22.83	19.7	27.0	3.76	13.50	32.17	2.47
	<i>D. levis</i>	4	30.93	29.5	32.2	1.37	28.74	33.11	0.85
	<i>D. giganteum</i>	5	37.70	32.6	42.0	3.60	33.23	42.17	-1.56
	<i>D. proavum</i>	7	45.03	41.9	47.1	2.04	43.15	46.91	-6.34
	HAM	1	47.80	-	-	-	-	-	-
	<i>P. cuvieri</i>	3	33.47	32.1	34.4	1.21	30.46	36.47	11.84
LDP3	<i>P. bavaricum</i>	5	35.72	33.0	38.0	1.92	33.34	38.10	6.29
	<i>D. levis</i>	4	44.58	42.0	48.0	2.92	39.93	49.22	1.10
	<i>D. giganteum</i>	2	52.65	51.3	54.0	1.91	35.50	69.80	-2.54
	<i>D. proavum</i>	12	58.39	48.0	64.2	4.51	55.52	61.26	-2.35
	HAM	1	47.00	-	-	-	-	-	-
	<i>P. cuvieri</i>	3	27.83	24.0	31.0	3.55	19.02	36.65	5.40
	<i>P. bavaricum</i>	5	31.96	29.0	34.0	2.39	28.99	34.93	6.29
WDP3	<i>D. levis</i>	4	40.23	38.6	42.3	1.74	37.46	42.99	3.89
	<i>D. giganteum</i>	2	50.00	50.0	50.0	0	-	-	-
	<i>D. proavum</i>	12	57.47	52.4	64.7	3.24	55.41	59.53	-3.23
	HAM	1	70.20	-	-	-	-	-	-
	<i>P. cuvieri</i>	2	55.05	55.0	55.1	0.07	54.41	55.69	216.43
	<i>P. bavaricum</i>	9	53.84	49.0	60.8	3.97	50.80	56.89	4.12
	<i>D. levis</i>	4	67.23	64.2	71.8	3.26	62.04	72.41	0.91
LDP4	<i>D. giganteum</i>	3	75.47	70.4	78.0	4.39	64.57	86.37	-1.20
	<i>D. proavum</i>	5	86.82	82.9	91.2	3.58	82.37	91.27	-4.64
	HAM	1	53.90	-	-	-	-	-	-
	<i>P. cuvieri</i>	2	37.90	37.8	38.0	0.14	36.63	39.17	114.29
	<i>P. bavaricum</i>	9	38.33	34.0	40.8	2.53	36.39	40.28	6.15

Table 5 (continued)

	<i>n</i>	mean	minimum	maximum	SD	95% CI (lower)	95% CI (upper)	z-score
Ldp2	<i>D. levius</i>	50.75	48.5	54.7	2.86	46.20	55.30	1.10
	<i>D. giganteum</i>	56.33	52.0	59.0	3.79	46.93	65.74	-0.64
	<i>D. proavum</i>	67.42	63.0	69.0	2.50	64.32	70.52	-5.41
	HAM	31.05	30.7	31.4	0.49	-	-	-
	<i>P. cuvieri</i>	19.00	-	-	-	-	-	-
	<i>P. bavaricum</i>	20.93	17.5	23.3	3.04	13.37	28.49	3.33
	<i>D. levius</i>	27.70	26.4	28.9	1.24	25.73	29.67	2.70
	<i>D. giganteum</i>	31.50	29.9	33.5	1.66	29.44	33.56	-0.27
	<i>D. proavum</i>	34.37	33.8	35.4	0.90	32.14	36.59	-3.69
	HAM	20.00	19.9	20.1	0.14	-	-	-
Wdp2	<i>P. cuvieri</i>	11.50	-	-	-	-	-	-
	<i>P. bavaricum</i>	14.87	11.0	17.2	3.37	6.49	23.24	1.52
	<i>D. levius</i>	18.65	16.8	20.0	1.45	16.34	20.97	0.93
	<i>D. giganteum</i>	22.82	21.0	25.0	1.66	20.76	24.88	-1.70
	<i>D. proavum</i>	27.83	23.2	30.2	4.01	17.87	37.80	-1.95
	HAM	52.20	-	-	-	-	-	-
	<i>P. bavaricum</i>	36.23	34.0	38.5	1.60	34.89	37.56	9.98
	<i>D. levius</i>	45.90	45.7	46.2	0.26	45.24	46.56	24.23
	<i>D. giganteum</i>	54.20	51.1	56.0	1.76	52.37	56.06	-1.14
	<i>D. proavum</i>	60.60	54.6	64.1	3.75	56.63	64.50	-2.24
Ldp3	HAM	35.40	-	-	-	-	-	-
	<i>P. bavaricum</i>	25.01	20.0	29.9	3.31	22.25	27.78	3.14
	<i>D. levius</i>	31.37	30.8	31.7	0.49	30.14	32.59	8.22
	<i>D. giganteum</i>	37.40	34.5	40.1	1.86	35.45	39.35	-1.08
	<i>D. proavum</i>	42.55	37.3	44.8	2.77	39.65	45.46	-2.58
	HAM	70.20	70.0	70.4	0.28	-	-	-
	<i>P. bavaricum</i>	50.94	39.5	58.1	1.54	47.45	54.43	12.51
	<i>D. levius</i>	66.25	57.7	69.7	4.40	61.63	70.87	0.90
	<i>D. giganteum</i>	77.73	71.0	82.0	3.74	74.27	81.19	-2.01
	<i>D. proavum</i>	86.30	79.5	90.3	4.28	80.98	91.62	-3.76
Wdp4	HAM	41.45	-	-	-	-	-	-
	<i>P. bavaricum</i>	29.50	1.90	28.1	30.9	26.5	32.8	6.29
	<i>D. levius</i>	39.43	2.63	36.7	42.2	37	44.3	0.77
	<i>D. giganteum</i>	46.06	2.95	43.6	48.5	42.6	50	-1.56
	<i>D. proavum</i>	52.54	6.13	44.9	60.2	42.6	58	-1.81

Table 6 Dental mesowear angles of the *Tetralophodon longirostris* sample from Hammerschmiede 6 and summary statistics. Abbreviations as in Table 5

Tooth	Inventory number	Cusp measured	Mesowear angle (°)	Mean mesowear angle (°)
m2	GPIT/MA/10800-03	2 pretrite	117.6	117.1
		2 posttrite	116.5	
M2	GPIT/MA/10800-04	2 pretrite	116.7	116.7
M3	GPIT/MA/10800-02	3 posttrite	105.3	104.3
		3 pretrite	103.3	
Mean				112.7
Median				116.7
SD				7.28
95% CI (lower)				94.6
95% CI (upper)				130.8

horizontally from a vertical position and was subsequently processed in ImageJ (Abràmoff et al. 2004; <https://imagej.nih.gov/ij/index.html>), where the angle was measured from the relief formed at the upper (counter) side of the contour gauge (see Saarinen et al. 2015: fig. 1b). This process was applied in all measurable cusps of each tooth (pretrite and/or posttrite sides) and the mean value was calculated for each tooth (Table 6). The mesowear angles from HAM were compared with the dataset of Xafis et al. (2020), which includes mesowear angles for Miocene proboscideans of Eurasia.

Box-and-whisker plots and statistical computations were performed with PAST v. 4.12 (Hammer et al. 2001; <https://www.nhm.uio.no/english/research/resources/past/>).

Institutional abbreviations: **FSL**, Faculté des Sciences de Lyon (France); **HGI**, Hungarian Geological Institute (Budapest); **HLMD**, Hessisches Landesmuseum Darmstadt (Germany); **HNHM**, Hungarian National History Museum, Budapest (Hungary); **ML**, Musée des Confluences, Lyon (France); **MNHN**, Muséum National d'Histoire Naturelle (Paris, France); **NHMW**, Naturhistorisches Museum Wien (Austria); **SNSB-BSPG**, Staatliche Naturwissenschaftliche Sammlungen Bayerns—Bayerische Staatssammlung für Paläontologie und Geologie, München (Germany); **SU**, Palaeontology Museum of Sofia University (Bulgaria).

Dental abbreviations: **aprc1, 2, 3**, anterior pretrite central conule of the first, second or third loph(id); **di**, lower deciduous tusk; **dp/DP**, lower/upper deciduous premolar; **m/M**, lower/upper molar; **ppoc1, 2**, posterior posttrite central conule of the first or second loph (id); **pprc1, 2, 3**, posterior pretrite central conule of the first, second or third loph(id).

Taphonomic remarks on the partial skeletons from HAM 5 and HAM 6

Deinotherium at HAM 5: In total 24 bones and isolated teeth of a juvenile *Deinotherium* from the overbank extension of the HAM 5 rivulet belong to the same individual.

The proposed strewnfield consists of a mandible, right DP4, left and right dp2, di1, two cranial fragments of unknown position, possibly the tibia and the fibula, the pubis and 14 ribs. These specimens were excavated during the field seasons in 2018, 2020 and 2021 over a distance of eight meters parallel to the reconstructed flow direction (SSW–NNE) of the rivulet (Fig. 2). The arrangement of the bones corresponds approximately to the typical sorting by density and bone volume (Voorhies 1969; Behrensmeyer 1975), with the heavier and denser DP4 and mandible in the southernmost limit of the strewnfield and the lighter and less dense bones north of it. A special feature is the accumulation of a large proportion of the finds (especially ribs) in a pit-like erosion depression on the more lithified bedrock. This depression in the channel base probably acted as a bone trap through the resulting flow shadow. The proximate spatial accumulation of the deinotherium remains, the absence of duplicate skeletal elements, the consistency in ontogenetic age of both dental and postcranial remains, as well as in dental wear, combined with the fact that all of the surrounding finds belong to other taxa, indicate that the *Deinotherium* remains were deposited in a single taphonomic event and represent a single individual.

Tetralophodon at HAM 6: A partial adult skeleton has been independently excavated by the two private collectors Sigulf Guggenmoos (Dösingen) in the end of 1970ies and Manfred Schmid (Marktoberdorf) in early 1980ies. The finding position of the material was at the uppermost part of the Miocene sediments exposed at the time in the Hammerschmiede clay-pit, below the presently exposed upper lignite seam (Fig. 3). Both collections contain, besides upper and lower tusks and molars, hundreds of heavily fractured bone fragments. This fragmentation, which prohibits morphological and taphonomic investigations, is probably related to the heavy machinery removing the directly overlying till (Fig. 3) of Middle Pleistocene

age (Riss glaciation) or was caused by Pleistocene glacial processes. While the tooth collections show no duplicates, however, and although there is consistency in dental wear between the m2 and M2, the substantially more worn M3 than M2 (see below) is not compatible with the dental succession and normal wear pattern known in elephantiform proboscideans indicating the presence of either two individuals, or one with anomalous/pathologic condition.

Systematic palaeontology

Mammalia Linnaeus, 1758

Proboscidea Illiger, 1811

Deinotherioidea Osborn, 1921

Deinotheriidae Bonaparte, 1845

Deinotherium Kaup, 1829

Deinotherium levius Jourdan, 1861

Type material: ML-LGR-962 (lectotype), right upper tooththrow with P3–M3; figured in Depéret (1887: pl. 18, fig. 1).

Type locality: La Grive Saint-Alban, quarry Peyre et Beau, France, Middle Miocene (MN 8).

Material (HAM 4): right DP2, GPIT/MA/16490.

Material (HAM 5): partial juvenile skeleton (see Fig. 2), represented by 24 specimens including the mandible with erupting right and left lower tusks and right and left dp3–dp4, SNSB-BSPG-2020-XCV-0096; right di1, SNSB-BSPG-2020-XCV-0257; right dp2, SNSB-BSPG-2020-XCV-0199; left dp2, SNSB-BSPG-2020-XCV-0092; right DP4, GPIT/MA/13794, two cranial fragments of unknown position, SNSB-BSPG-2020-XCV-0253–11 and 0253–12, as well as the pubis SNSB-BSPG-2020-XCV-0256; ?fibula, SNSB-BSPG-2020-XCV-0358; ?tibia, SNSB-BSPG-2020-XCV-0433; and 14 ribs GPIT/MA/13773, SNSB-BSPG-2020-XCV-0252, 0253–01, 0253–02, 0253–03, 0253–04, 0253–05, 0253–06, 0253–07, 0253–08, 0253–09 and 0253–10. In addition to this partial skeleton, this horizon yields a left DP3, GPIT/MA/09552, and multiple worn and unworn molar fragments (GPIT/MA/09553, 09867, 10,338, 10,340).

Description

Mandible and lower dentition The mandible is almost complete, preserving the corpora with the symphysis and the rami with their coronoid processes; both hemimandibles lack the region of the mandibular angle and have partially damaged condyles (Fig. 4; Online Resources 1 and 4; Figs. S1–S6). The mandible bears the right and left dp3 and dp4,

while the alveoli of the dp2 are open (Fig. 4a); these alveoli most possibly fit the isolated right and left dp2s (described below), which were found in spatial proximity with the mandible and are compatible in terms of wear stage with the other deciduous dentition. Additionally, two emerging lower tusks are visible inside their alveoli within the symphysis; they are postdepositionally compressed dorsoventally. They are covered with enamel, but there is no distinct cervix, and the pulp cavity is open (Figs. 4d, f and 5); as such the tusks are identified as permanent (juvenile) lower tusks (i2). The enamel is thick at their tips and becomes thinner distally. The symphysis is ventrally deflected. Two foramina are present, one large at the level of the caudal symphyseal border, and one smaller at the level of the distal part of the dp2 alveolus. Both rostral and caudal margins of the ramus are caudally inclined relative to the corpus.

The lower deciduous tusk SNSB-BSPG-2020-XCV-0257 is complete (total length: 100 mm) and strongly curved (Fig. 6j–m). Its tip is covered by a short enamel cap, which is well separated by a distinct cervix from the root. The maximum diameters of the root (21.1×13.4 mm) are almost at its middle, while it narrows towards the proximal part. The pulp cavity is closed.

Both left and right dp2s (SNSB-BSPG-2020-XCV-0092 and 0199) are almost unworn apart from the worn ectolophid and hypoconid (Fig. 6n–s; Online Resources 2 and 3). They most probably both belong to the same individual as the mandible SNSB-BSPG 2020-XCV-0096. They have a triangular shape with narrow and high mesial part, and two fused roots. The paracristid consists of several weak conelets decreasing in height, but there is one strong one in front of the protoconid. The protoconid, which is set in a more mesiolabial position than the metaconid, is separated from the latter and there are two conelets in between them. The ectolophid connects the protoconid with the hypoconid. The hypoconid and entoconid are opposite to each other and are connected with a series of weak conelets positioned in line and decreasing in size from the former to the latter cusp; hypoconid is higher than entoconid. The distal cingulum is low and is comprised by several weak conelets in a row.

The right dp3 is slightly damaged, especially in its mesiolingual part, whereas the left one is well-preserved (Fig. 4; Online Resource 4). It is almost unworn, apart from the protoconid, which shows a worn facet at its tip, and the crests connecting the main cusps in each lophid. The tooth consists of two lophids, of which the mesial one is narrower. The strong and curved mesial cingulum, which is comprised by a series of cusplets, is connected through the preprotocristid (paracristid) with the protoconid. On the lingual side, the mesial cingulum extends until the pre-matacristid, which runs in front of the metaconid. One low

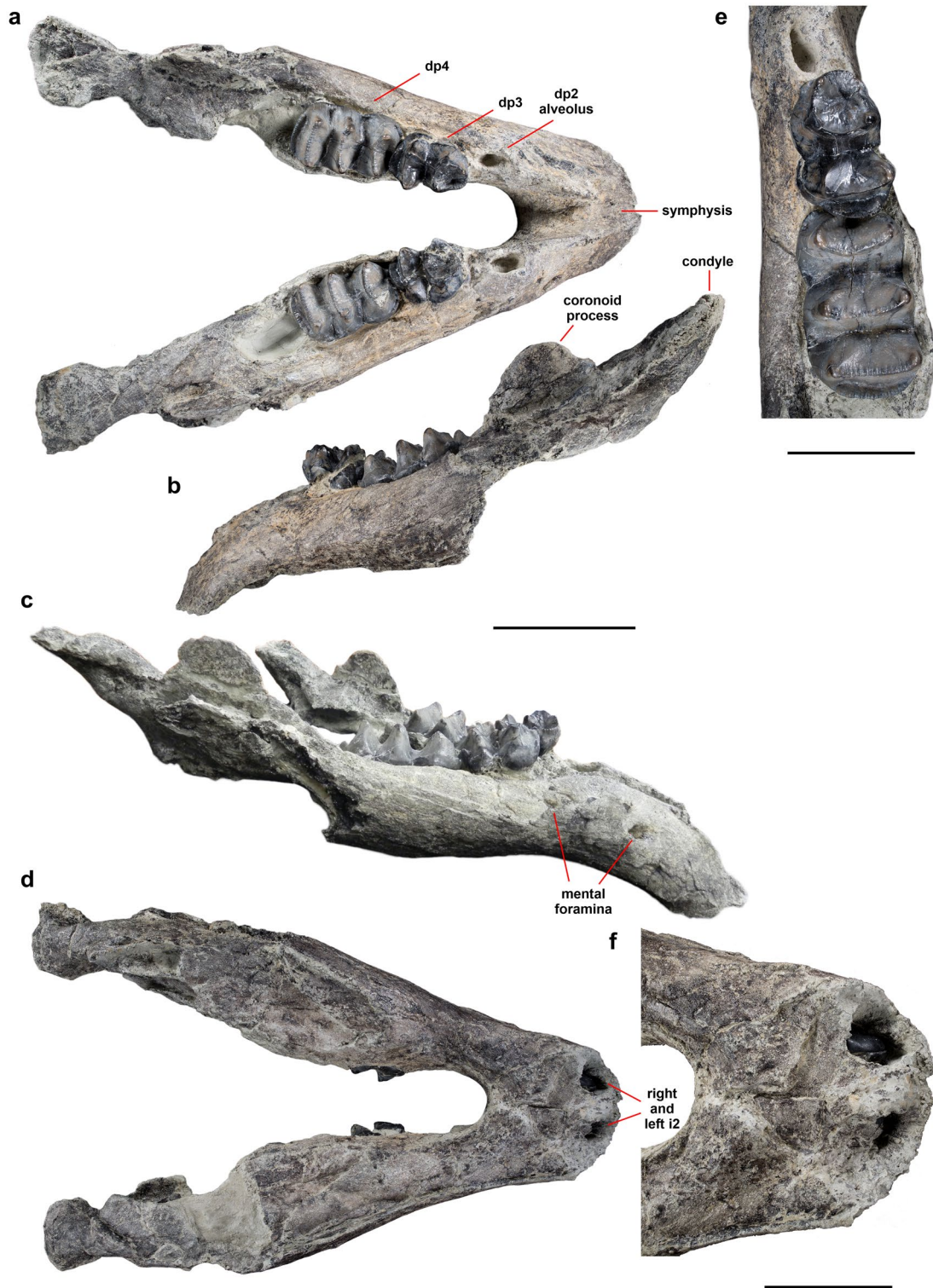
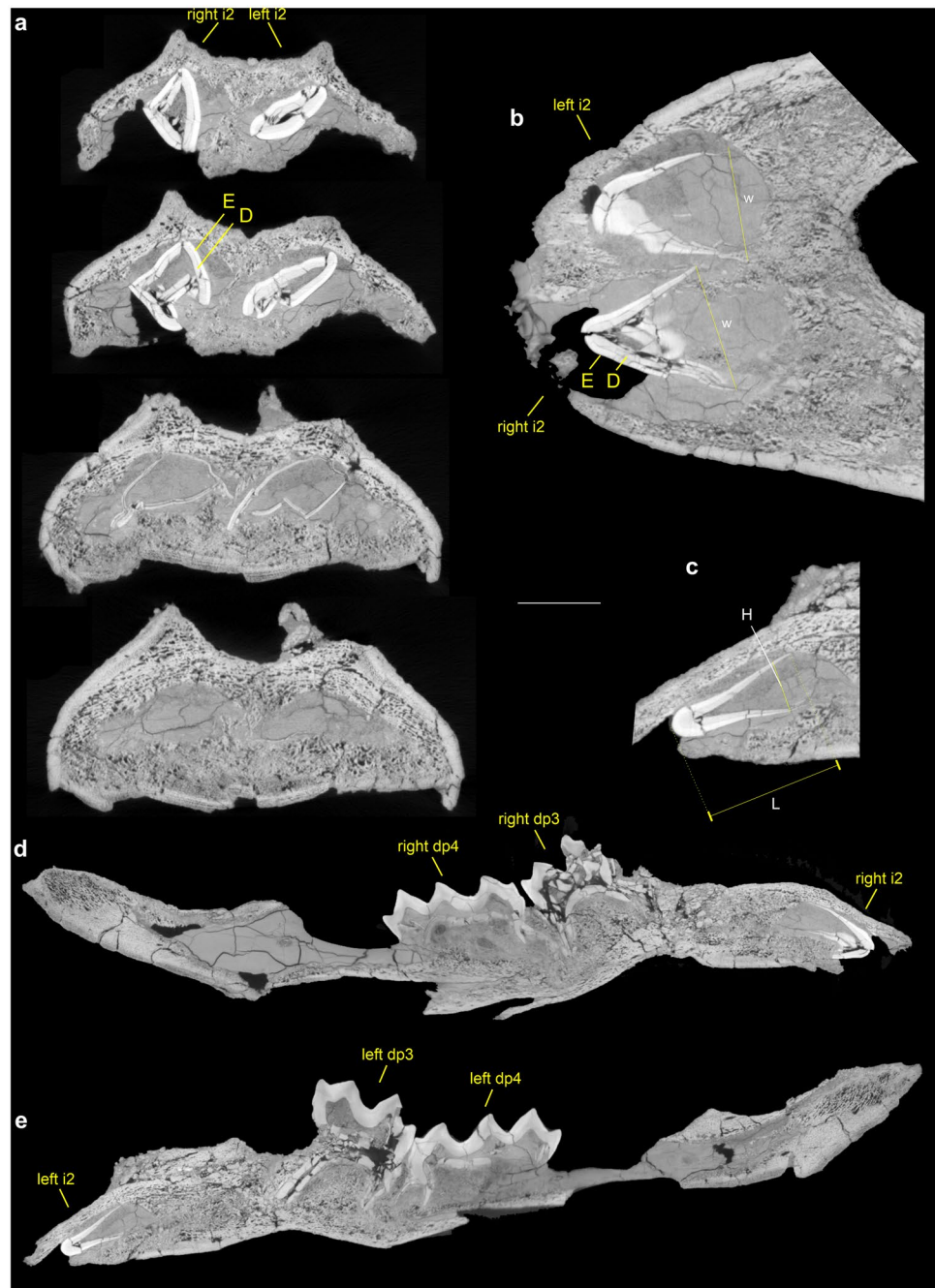


Fig. 4 Juvenile mandible (SNSB-BSPG-2020-XCV-0096) with erupting right and left i2, and right and left dp3–dp4 of *Deinotherium levius* from Hammerschmiede 5 in dorsal (a), left lateral (b), right lateral (c) and ventral (d) view; occlusal view of the left dp3 and dp4 (e); close-up view of the ventral side of the symphysis showing the emerging i2 (f). Scale bars equal 10 cm in a–d, and 5 cm in e–f

eral (c) and ventral (d) view; occlusal view of the left dp3 and dp4 (e); close-up view of the ventral side of the symphysis showing the emerging i2 (f). Scale bars equal 10 cm in a–d, and 5 cm in e–f

Fig. 5 CT-scan slices of the *Deinotherium levius* mandible (SNSB-BSPG-2020-XCV-0096) from Hammerschmiede 5. **a.** Coronal slices in the symphysis showing the right and left lower permanent tusks (i2) and their alveoli (from anterior to posterior from top to bottom). **b.** Transverse slice in the symphysis showing the right and left i2; noted are the enamel (E) and the dentine (D) of the tusks, and the measured width (W). **c.** Parasagittal slice in the symphysis showing the right lower tusk, and the measured length (L) and height (H). **d.** Parasagittal slice of the right hemimandible. **e.** Parasagittal slice of the left hemimandible. Scale bars equal 20 mm in **a–c** and 100 mm in **d–e**. Additional CT-scan slices are given in Online Resource 4, Fig. S7



cusplet (rudimentary cingulum?) is located at the mesiolabial side of the tooth. The slightly worn and distally curved protolophid connects proto- and metaconid. The transverse valley is open. The hypolophid is only slightly curved and connects the hypo- and entoconid. The pre-entocristid and prehypocristid are strong. The distal cingulum is separated from the hypolophid; it is strong but low and formed by a series of conelets.

The dp4 is trilophodont (Fig. 4; Online Resource 4). It is erupting from the mandible and is unworn. The mesial cingulum is weak and low. The crest connecting in the mesial

lophid the main cusps is curved; this crest in lophid 2 is less curved, whereas in distal one is straight. The mesial cristid of the main cusps are visible in all lophids; those in the labial side are stronger and even more the more mesial one. The transverse valleys are open, but there are remnants of cingulum in the labial side. The distal cingulum is low and consists of a series of conelets.

Two erupting tusks are partially visible within the symphysis of the mandible, but their morphology can be further observed in virtual cross-section of the μ CT-scan of the mandible (Fig. 5). They are recognized as permanent ones



Fig. 6 Dental remains of *Deinotherium levius* from Hammer-schmiede. **a–c.** Right DP2, HAM 4, GPIT/MA/16490 in occlusal (**a**), labial (**b**) and lingual (**c**) view. **d–f.** Left DP3, HAM 5, GPIT/MA/09552 in occlusal (**d**), labial (**e**) and lingual (**f**) view. **g–i.** Right DP4, HAM 5, GPIT/MA/13794 in occlusal (**g**), labial (**h**), lingual (**i**) view. **j–m.** Right di1, HAM 5, SNSB-BSPG-2020-XCV-0257 in

dorsal (**j**), ventral (**k**), lateral (**l**) and medial (**m**) view. **n–p.** Right dp2, HAM 5, SNSB-BSPG-2020-XCV-0199 in occlusal (**n**), lingual (**o**) and labial (**p**) view. **q–s.** Left dp2, HAM 5, SNSB-BSPG-2020-XCV-0092 in occlusal (**q**), lingual (**r**) and labial (**s**) view. Scale bar equals 5 cm

due to the absence of an enamel cap with distinct cervix and the clearly open pulp cavity. Like the rest of the mandible, the tusks are dorsoventrally compressed postdepositionally, and the enamel and the dentine are in several places offset. Despite this deformation, the cross-section can be generally regarded as subcircular. The tusks are covered by a continuous enamel layer, which becomes thinner towards the proximal part. Some small enamel buds are visible at the tip.

Upper dentition The isolated DP2 is bilophodont and practically unworn (Fig. 6a–c). It has a mesial cingulum, stronger and more pointed at the mesiolabial side, consisting of several conelets, while on its lingual side there are five to six low conelets. A slightly worn curved crest in loph 1 connects the protocone with the metacone. The ectoloph, connecting the paracone with the metacone, is continuous. On the lingual side, the proto- and hypocone are well separated by an open valley. The hypocone, which is damaged at its tip, is ornamented with several weak conelets at its labial side. The distal cingulum is low and consists of a series of very weak conelets, increasing in height labially and connect with the metacone.

The DP3 consists of two lophs, both of which are much worn, and as a result confluent dentine is exposed on proto- and metaloph (Fig. 6d–f). The mesial cingulum is developed, and the stronger parastyle is connected to the weaker protostyle by a worn ridge. A worn weak ridge connects the parastyle and the paracone. The lophs are clearly separated by marked ecto- and entoflexus; the transverse valley is open lingually, but blocked labially. The postparacrista and postmetacrista are well developed, the latter connected to the metastyle. The distal cingulum is partially damaged; it is low and weaker on the labial side.

The DP4 is trilophodont (Fig. 6g–i). The mesial cingulum is rather low, almost half the height of loph 1, but the parastyle is strong and is connected with the paracone by a weak ridge. Slightly mesially curved crests (more curved in loph 3) consisting of numerous conelets connect the main cusps of each loph. Both ectoflexus are pronounced, especially the first one. The postparacrista and postmetacrista are strong. There is “double” distal cingulum; the distalmost one is longer but lower, consisting of a series of weak conelets.

Remarks

Based on several dental, cranial and postcranial features, European deinotheres are represented by the Early–Middle Miocene *Prodeinotherium* and the Middle–Late Miocene *Deinotherium* (e.g., Huttunen 2002a; Aiglstorfer et al. 2014a; Konidaris et al. 2017). Five species are considered valid here: *Prodeinotherium cuvieri* (Kaup, 1832a)

from the early–middle Orleanian, *Prodeinotherium bavarium* (von Meyer, 1831) from the late Orleanian–early Astaracian, *Deinotherium levius* Jourdan, 1861 from the late Astaracian, *Deinotherium giganteum* Kaup, 1829 from the Vallesian and *Deinotherium proavum* (Eichwald, 1831) (= *Deinotherium gigantissimum* Stefanescu, 1892) from the latest Vallesian–Turolian. In the absence of clear-cut evidence of coexistence between chronologically successive species, it is generally regarded that European deinotheres did not have overlapping chronostratigraphic ranges. Distinctive features among the species include: a) dental dimensions, b) traits of the mandible (shape of the symphysis and the mandibular angle), and c) morphology of the p3 and the dp2/DP2. Further details on the taxonomy of European deinotheres are given in Aiglstorfer et al. (2014a), Konidaris et al. (2017), Alba et al. (2020) and Konidaris and Tsoukala (2022).

Comparison

Dental morphology remained relatively conservative throughout the evolutionary history of deinotheres, however, dental dimensions increased progressively throughout the Miocene in the European species, and besides their taxonomic value, they most importantly have biochronologic significance. The metric comparison (bivariate, and box-and-whisker plots) of the deciduous dentition reveals that although some overlap in the size ranges between chronologically successive species for certain tooth positions, their interquartile ranges are mostly non-overlapping, while the average dimensions are larger in each chronologically succeeding species. Such a distinction among the species, allows the metric comparison of the available teeth from HAM. For all tooth positions, the crown dimensions of the HAM deciduous teeth (Figs. 7 and 8) are clearly distinguished from both *Prodeinotherium* (*P. cuvieri* and *P. bavarium*) and *D. proavum*. Therefore, we focus the comparison on *D. levius* and *D. giganteum*. For all tooth positions, the HAM crown dimensions are greater than the L and W mean and median values of *D. levius*, and lower than the values of *D. giganteum* (Figs. 8 and 9). The LDP2 and WDP2 values from HAM are at the lowermost range or outside, respectively, of *D. giganteum*; LDP2 stands within the upper part of the interquartile range, and WDP2 at the upper quartile of *D. levius* (Fig. 8). The HAM DP2 is plotted close to the *D. levius* specimens from La Grive (France), Massenhausen (Germany), Atzelsdorf (Austria) and to the *D. levius*-sized DP2 from Emmering bei Fürstenfeldbruck (Germany), while it overlaps only with the DP2 of *D. ?giganteum* from Nessebar (Bulgaria) (Fig. 7). The LDP3 value from HAM is much below the lower range of *D. giganteum* and plots at the upper range of *D. levius* [the

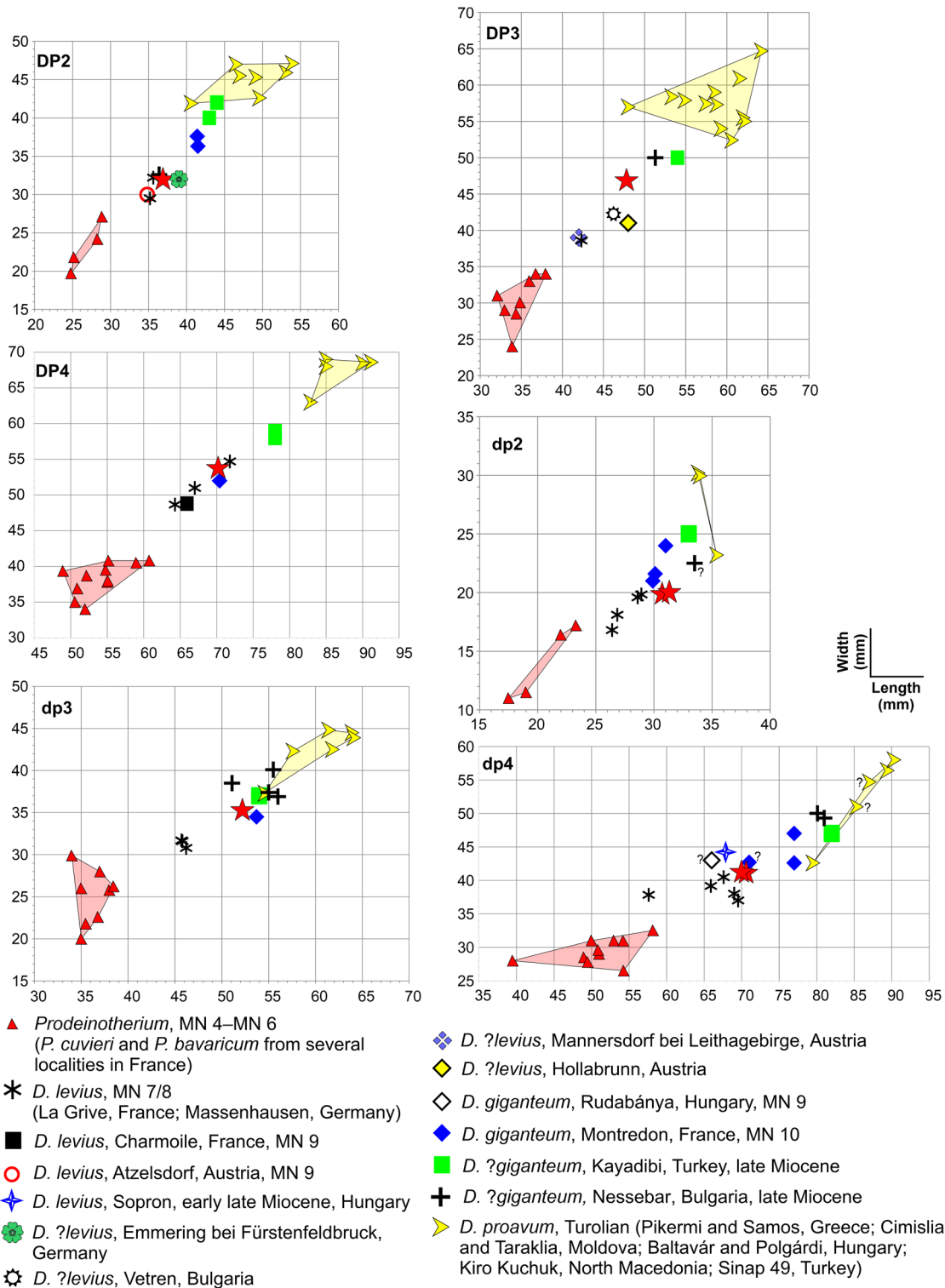


Fig. 7 Bivariate plots of length vs. maximum width (in mm) for deinothereiid lower and upper deciduous premolars from various localities. The symbol “?” indicates incomplete or inadequately preserved

specimens; the convex hulls for *Prodeinotherium* and *Deinotherium proavum* are also shown. For the comparative sample, see Table 3

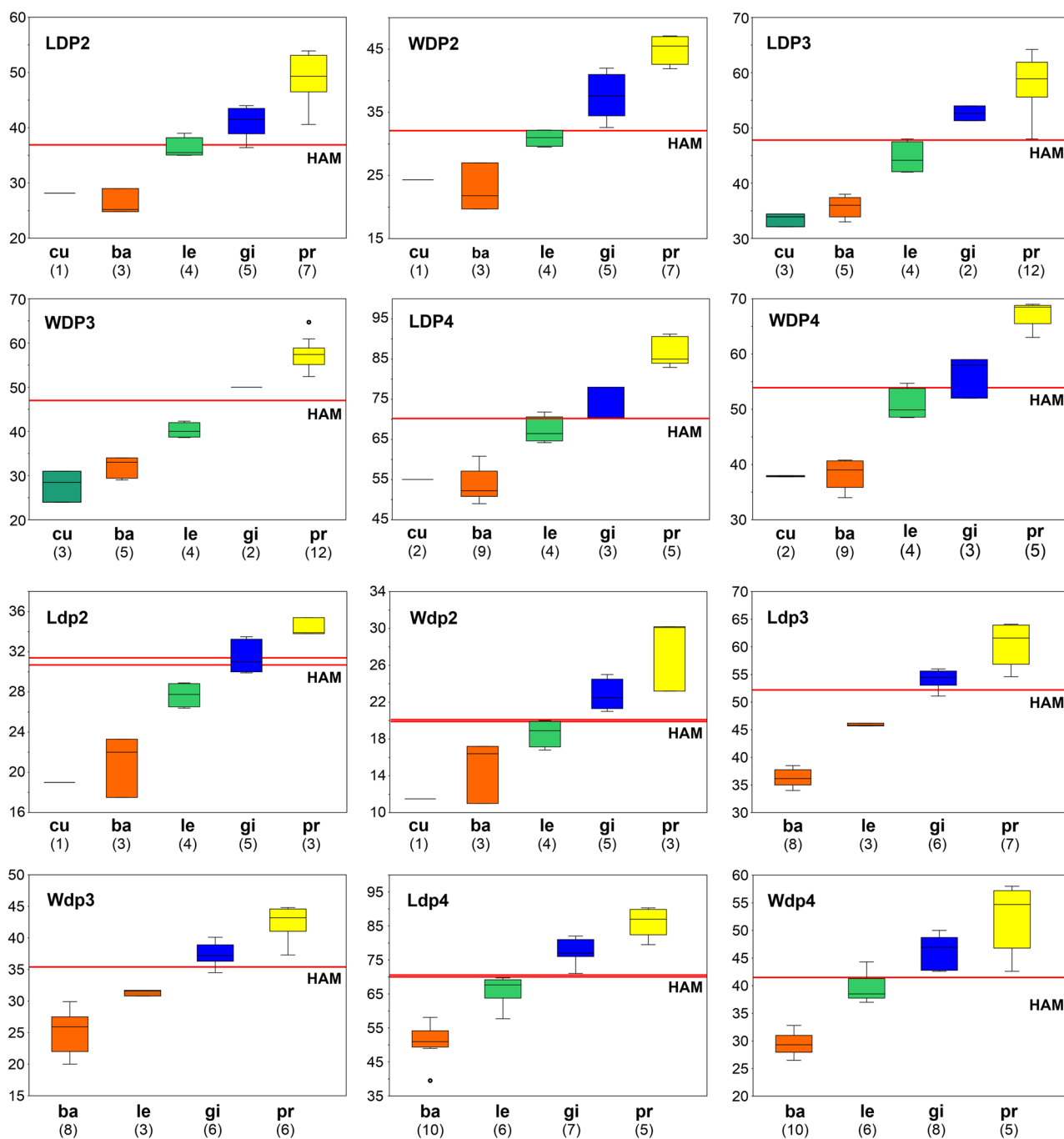


Fig. 8 Box-and-whisker plots of length (L) and width (W) (in mm) for the lower and upper deciduous premolars of European deinotheriid species compared to specimens from Hammerschmiede (red horizontal line). Black horizontal lines represent the median, boxes the 25 and 75 percentiles (interquartile range); whiskers the max-

imum-minimum values; circles the outliers; numbers in parentheses the number of specimens. Abbreviations: **cu**, *Prodeinotherium cuvieri*; **ba**, *Prodeinotherium bavaricum*; **le**, *Deinotherium levius*; **gi**, *Deinotherium giganteum*; **pr**, *Deinotherium proavum*. For the comparative sample see Table 3

specimens from Hollabrunn (Austria) and the similar-sized DP3 from Vetren (Bulgaria), both tentatively referred here to this species; see discussion below and Vergiev and Markov (2012)], while the WDP3 value stands between *D. levius* and *D. giganteum* (Figs. 7 and 8). The LDP4 value from HAM

is plotted within the uppermost part of the interquartile range of *D. levius* and at the lower quartile of *D. giganteum*, while the WDP4 stands at the upper quartile of *D. levius* and the lower part of the interquartile range of *D. giganteum* (Fig. 8). The HAM DP4 plots together with the *D. levius* specimens

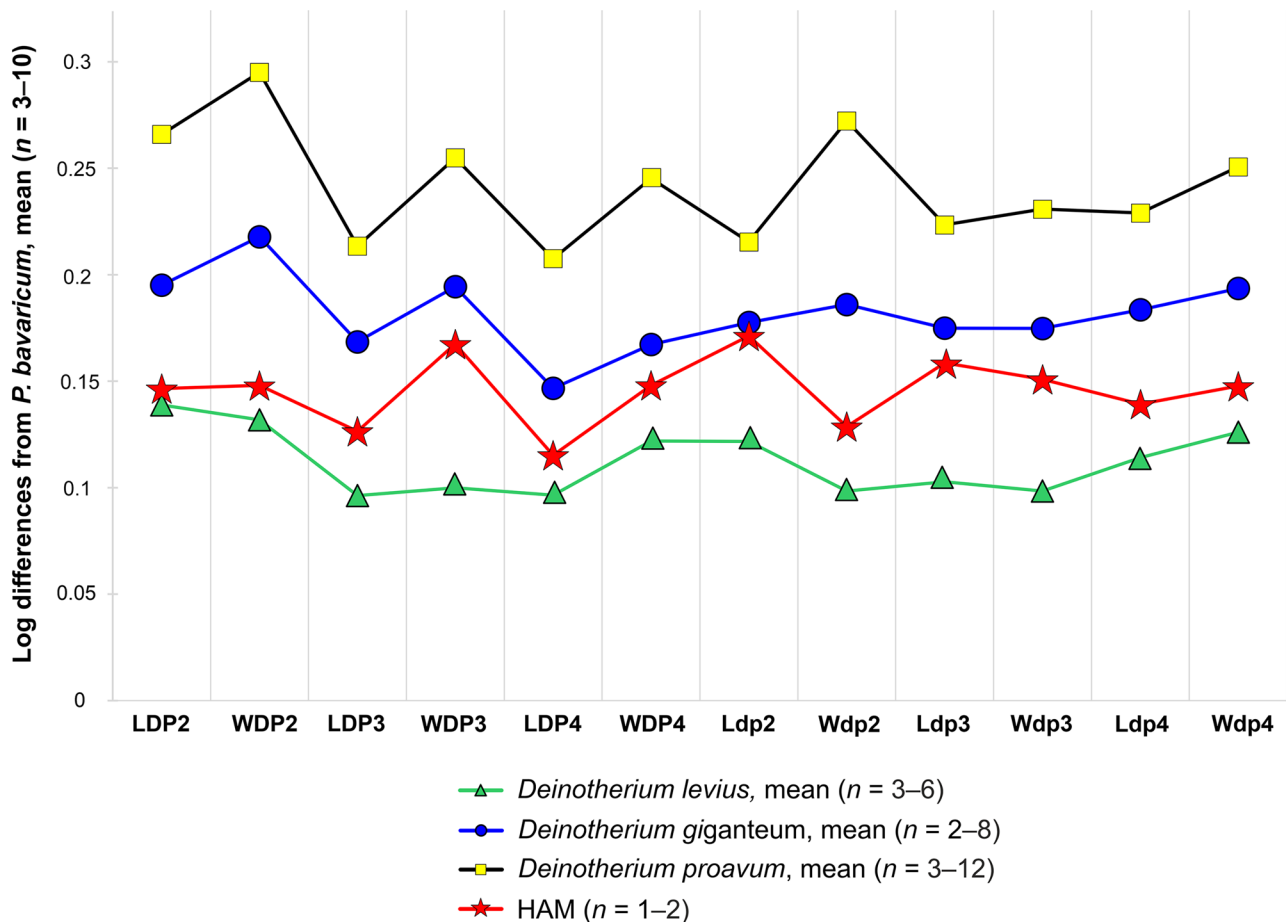


Fig. 9 Logarithmic ratio diagram comparing length (L) and width (W) of the lower and upper deciduous premolars from Hammer-schmiede with *Deinotherium levius*, *Deinotherium giganteum* and

Deinotherium proavum from various localities (see Table 3). Standard of comparison: mean values of *Prodeinotherium bavaricum*

from La Grive and Massenhausen, as well as with the single known DP4 from Montredon (France) (Figs. 7 and 8). The Ldp2 value from HAM is outside the range of *D. levius* and within *D. giganteum*, whereas the Wdp2 is outside the range of *D. giganteum* and at the upper quartile of *D. levius* (Fig. 8). The HAM dp2 is overall plotted close to the larger specimens from La Grive and the smaller ones from Montredon (Fig. 7). Both Ldp3 and Wdp3 values from HAM exceed the upper range of *D. levius* and are plotted at the lower range of *D. giganteum* (Fig. 8). The Ldp4 stands between *D. levius* and *D. giganteum*, while the Wdp4 values (CT-scan measurements) are at the upper quartile of *D. levius* (Fig. 8). The HAM dp4 is plotted close to the dp4 from Sopron [Hungary; the deinotherium material from Sopron is attributed to *D. levius* by Aiglstorfer et al. (2014a)], the larger specimens from La Grive and Massenhausen, and the smaller one from Montredon (Fig. 7).

Similar results are obtained by the statistical comparison using z-scores of the HAM specimens with the *Prodeinotherium* and *Deinotherium* species from Europe. We must note, however, that the comparative sample for

some species/tooth positions is insufficient, and therefore the results have to be considered indicative but treated with caution. The analysis detects significant differences of the HAM teeth for all tooth position and variables (except of Wdp2, and Wdp4 only for *D. proavum*) from *P. cuvieri*, *P. bavaricum* and *D. proavum* (Table 5). The HAM teeth are most similar with the Ldp4 and LDP3 (positive values) of *D. levius*, and the Ldp2, Ldp3 and Wdp3 (negative values) of *D. giganteum*, while they are within the variation of both these species for Wdp2, Wdp4, LDP2, WDP2, LDP4 and WDP4, for which variables however (except WDP4) the z-score is closer to zero for *D. levius*. Comparable results are acquired from the 95% confidence intervals for *D. levius* and *D. giganteum*, where the only differences compared to the z-scores is that in this case the HAM LDP2 is within *D. levius*, while the HAM LDP3 falls within both *D. levius* and *D. giganteum* (Table 5).

Morphological traits of the dp2 and DP2 provide further evidence for the taxonomic identification of the HAM specimens. Konidaris et al. (2017) and Konidaris and

Koufos (2019) noted that the morphology of the dp2, and in particular the position of the protoconid in regard to the metaconid, and the connection of the ectolophid with either of these cusps, differs among the European deinotheriid species. In this aspect the HAM dp2 (Fig. 6n, q) is different from both *P. cuvieri* from Montréal-du-Gers (France; Ginsburg and Chevrier 2001: fig. 2l, m) where the proto- and metaconid are clearly separated, as well as from *D. proavum* from Pikermi (Greece; AMPG-PA3950/91) and Samos (Greece; SMF-M 3604), where the proto- and metaconid are fused, and the ectolophid is connected with the metaconid (Konidaris and Koufos 2019: fig. 4). HAM dp2 is also different from the dp2s of *D. giganteum* from Montredon (ML-MR- 52, FSL-210393), where the protoconid and the metaconid are almost or totally fused (Konidaris and Koufos 2019: fig. 4d, e). In *D. levius* from La Grive (ML-LGR 893, LGR 900, LGR 959; Ginsburg and Chevrier 2001: fig. 7) these cusps are either connected (but clearly distinct) or almost/totally fused and the ectolophid is connected with the protoconid. The best match of the HAM dp2s is with ML-LGR 893 of *D. levius*, where proto- and metaconid are located in a slightly more distant position (a primitive trait, not observed so far in *D. giganteum*).

The DP2 presents also some morphological differences among the European deinotheriid taxa (Konidaris et al. 2017; Konidaris and Koufos 2019). Based on these, the HAM DP2 (Fig. 6a) differs from that of *P. bavaricum* from Tavers, Pontlevoy (France, both MN 5) and Esselborn (Germany; HLMD-Din 237) in that the latter have a triangular shape due to the narrower protoloph in regard to the metaloph, resulting in the closer position of the proto- and paracone; a strongly curved crest that connects proto- and paracone (Stehlin 1925: fig. 21b; Ginsburg and Chevrier 2001: fig. 4b; Konidaris and Koufos 2019: fig. 4); and a relatively weak mesial projection of the mesial cingulum. On the other side, the DP2 of *D. giganteum* and *D. proavum* have a more rectangular shape, with an L-shaped connection of the proto- and ectoloph (Gaziry 1976; Sanders 2003; Garevski and Markov 2011; Konidaris and Koufos 2019; Fig. 4). The HAM DP2 matches with *D. levius* from La Grive ML-LGR 970, Massenhäusen (SNSB-BSPG-1959 I 430) and Atzelsdorf (Göhlich and Huttenen 2009: pl. 1, fig. 1; Konidaris and Koufos 2019: fig. 4l, m), in which the crest connecting the protocone and paracone is curved (though less than *Prodeinotherium*), and these cusps stand in a more distant position to each other compared with *Prodeinotherium*, giving a trapezoid shape to the tooth due to the widening of the protoloph, while the mesial projection of the mesial cingulum is prominent.

Overall, the metric and morphological comparison reveals a clear distinction of the HAM deciduous teeth from *Prodeinotherium* spp. and *D. proavum*. Although the metric separation between *D. levius* and *D. giganteum* is not

clear-cut for some deciduous teeth, the HAM specimens are for most tooth positions within the range of dimensions of *D. levius*, while additionally the morphology of the dp2 and DP2 matches best with *D. levius*. Therefore, we attribute the deinotheriid specimens from HAM to this species.

The shape and inclination of the mandibular symphysis (Fig. 4b, c) is also an important trait to be noted as it is shown that the symphysis of adult deinotheriid mandibles became evolutionary more ventrally inclined and contributes to the separation of species (see e.g., Gräf 1957: fig. 12). The mandibles SU-190 of *D. giganteum* from Nessebar (Bakalov 1914: pl. 1, 2; Bakalov and Nikolov 1962: pl. 42) and SMF-M 3604 of *D. proavum* from Samos (Konidaris and Koufos 2019) are ontogenetically comparable to the HAM mandible and their symphyses are stronger (note, however, that the Nessebar symphysis is partially reconstructed) and more ventrally inclined. Although the ontogenetic development (growth pattern) of the symphysis is unknown in deinotheres, due to the rarity of juvenile preserving this part, it seems that in addition to interspecific differentiation, the ontogenetic age is also of importance. For example, the mandible MGL-S 1048 of *D. proavum* from Samos (dp4 erupting), which is ontogenetically slightly younger than SMF-M 3604 (dp4 erupted), bears a less inclined symphysis than the latter specimen. Accordingly, the mandible from Isle-en-Dodon (MN 7, France; Lartet 1859: pl. 13, fig. 4; Duranthon et al. 2007) belonging to an older individual (m1 erupted) than HAM possesses a fairly deflected symphysis. Indeed, proboscidean mandibles are characterized by an evident intraspecific variability in morphology and dimensions affected mainly by the ontogenetic age, and these ontogenetic changes continue during the adult stages, when also sexual dimorphism influences the variation (e.g., Huttunen and Göhlich 2002; Tassy 2013; Álvarez-Lao and Méndez 2011). Therefore, for any taxonomic conclusion it is important to compare only mandibles of similar or at least approximate ontogenetic age.

Replacement of deciduous by permanent lower tusks in Deinotheriidae

Another important aspect of the deinotheriid partial juvenile skeleton from HAM 5 is the presence of juvenile lower tusks, both deciduous and permanent ones (Figs. 4d, f and 6j–m). The presence of deciduous lower tusks is well known in elephantimorphs (e.g., Tassy 1987; Göhlich 2010), but in more basal proboscideans, such as the deinotheriids, their presence is only scarcely documented. Following the criteria of distinguishing deciduous and juvenile permanent tusks (e.g., enamel cap with distinct cervix, closed pulp cavity; Tassy 1987) and the proposed tooth positions (Delmer 2009), we consider the lower tusk SNSB-BSPG-2020-XCV-0257

(Fig. 6j–m) to be deciduous (di1). This tusk was found in close spatial association (Fig. 2) with the juvenile mandible SNSB-BSPG-2020-XCV-0096 (the deciduous tusks may have become loose in the sockets and removed from the mandible soon after the death of the individual, like it may happen with elephants' upper tusks at the initial post-mortem stages during the decay of the carcass; Haynes 1988) whose symphysis preserves the emerging permanent lower tusks (Figs. 4 and 5), and therefore the isolated di1 and the mandible belong most possibly to the same juvenile individual (as also do the isolated right and left dp2s SNSB-BSPG-2020-XCV-0199 and 0092). Therefore, the HAM deinotheriid material not only provides another example of the possession of both deciduous and permanent tusks in deinotheres (Stehlin 1925: fig. 27; Harris 1976, 1983), but most importantly it captures the rare moment of transition between deciduous and permanent lower tusks in fossil proboscideans, a succession which corresponds to a short period of time during the early life of an individual, and to our knowledge it represents the first such well-documented example in deinotheriids.

Two juvenile mandibles (SU-190 and 191) of *D. ?giganteum* from Nessebar are important in this aspect for comparison. SU-190 (Bakalow 1914: pl. 1, 2; Bakalov and Nikolov 1962: pl. 42) lacks the dp2, but preserves the slightly worn dp3s, and the erupting, still inside their crypts, dp4s. Two laterally curved lower tusks are protruding from the ventrally deflected symphysis and are identified as the deciduous ones. Of approximate ontogenetic age is the juvenile mandible consisting of the specimens MGL-S 1048 and S 380 from "Adriano" of Samos Island (Greece; Konidaris and Koufos 2019: figs. 2g, h and 3c), which preserves the dp2 alveolus, the unworn dp3, the erupting dp4, and a partially broken lower tusk that most possibly corresponds to a deciduous one. The second and ontogenetically older mandible from Nessebar, SU-191 (Bakalow 1914: pl. 3, 4, 5, fig. 1; Bakalov and Nikolov 1962: pl. 43, fig. 1, a), bears the much-worn dp2s and dp3s, the slightly worn dp4s, and the erupting but still inside the alveolus, m1s. The two lower tusks that are preserved in the symphysis correspond in this case most possibly to permanent ones. Based on the tooth eruption and wear, the mandible of *Deinotherium bozasi* Arambourg, 1934 KNM-ER 354 from East Turkana (Kenya; Harris 1976: pl. 2b, 1983: pl. 2.3b, 2.4) belongs to an individual of comparable ontogenetic age and preserves the permanent lower tusks. The HAM mandible with the minimally worn dp2 (associated to the mandible) and dp3, the unworn dp4 that is not completely erupted, and with not preserved and most likely not formed m1, belongs to an individual of intermediate ontogenetic age between SU-190, and SU-191 and KNM-ER 354, and is perhaps close to KNM-ER 518 (Harris 1976: pl. 2c, 1983: pl. 2.3c). Therefore, the replacement of deciduous lower tusks by their permanent

successors occurs around the time when the m1 is formed within the mandible, and the di1 is already shed when m1 is erupting.

Elephantimorpha Tassy and Shoshani in Shoshani et al., 1998
 Elephantida Tassy and Shoshani in Shoshani et al., 1998
 Gomphotheriidae Hay, 1922
 Tetralophodontinae van der Maarel, 1932
Tetralophodon Falconer, 1857
Tetralophodon longirostris (Kaup, 1832a, b).

Type material: HLMD-Din 111 (holotype), left mandibular fragment with m2–m3; originally figured in Kaup (1835: pl. 19, figs. 1 and 2) and later in Tobien (1978: pl. 10, fig. 1).

Type locality: Eppelsheim, Germany, Miocene.

Material (HAM 5): left i2, GPIT/MA/13792; right dp4, GPIT/MA/12313; left DP3, GPIT/MA/12196; right P3, GPIT/MA/09554.

Material (HAM 6): right i2 (cast, original belongs to the private collection of M. Schmid, Marktoberdorf), GPIT/MA/19246; right m2, GPIT/MA/10800–03; right I2, GPIT/MA/10800–01; right M1?, GPIT/MA/10800–05; left M2, GPIT/MA/10800–04; right M3, GPIT/MA/10800–02; left m3 fragment (cast, original belongs to the private collection of M. Schmid, Marktoberdorf), GPIT/MA/19247; as well as numerous fragments of long bones and vertebrae (partial skeleton).

Description

Lower dentition The small-sized lower tusk GPIT/MA/13792 (total length: 54.8 mm) from HAM 5 has a rather oval cross-sectional shape (width: 10.9 mm; height: 15.0 mm), but with a longitudinal dorsal concavity (Fig. 10a, b). There is neither an enamel cap nor any other traces of enamel, but there is a small wear facet at the dorsomedial side of the tip.

The lower tusk (Fig. 10c–e) from HAM 6 is almost straight and its maximum preserved length is 440 mm; however, in its proximal part the tusk is roughly transversally broken, indicating that the original tusk was longer. The proximal cross-Sect. (64.1 × 50.8 mm; circumference: 180 mm) is subcircular and bears a shallow dorsal concavity, while ventrally it is convex. The Schreger lines that are visible in the cross-section form slightly acute angles of ~87–88° (Fig. 10c). The dorsal concavity runs longitudinally until the wear facet (ca. 110 mm in length and 41.8 mm in width), which is present at the dorsolateral side of the tip.

The dp4 GPIT/MA/12313 from HAM 5 exhibits four lophids (Fig. 11d–f). The mesial cingulum is damaged in its lingual part; in its labial part it is worn and connects with pretrite lophid 1. All lophids are worn, and the dentine is confluent on the pretrite and posttrite half-lophids. In lophid 1, the half-lophids are transversely opposite to each other,

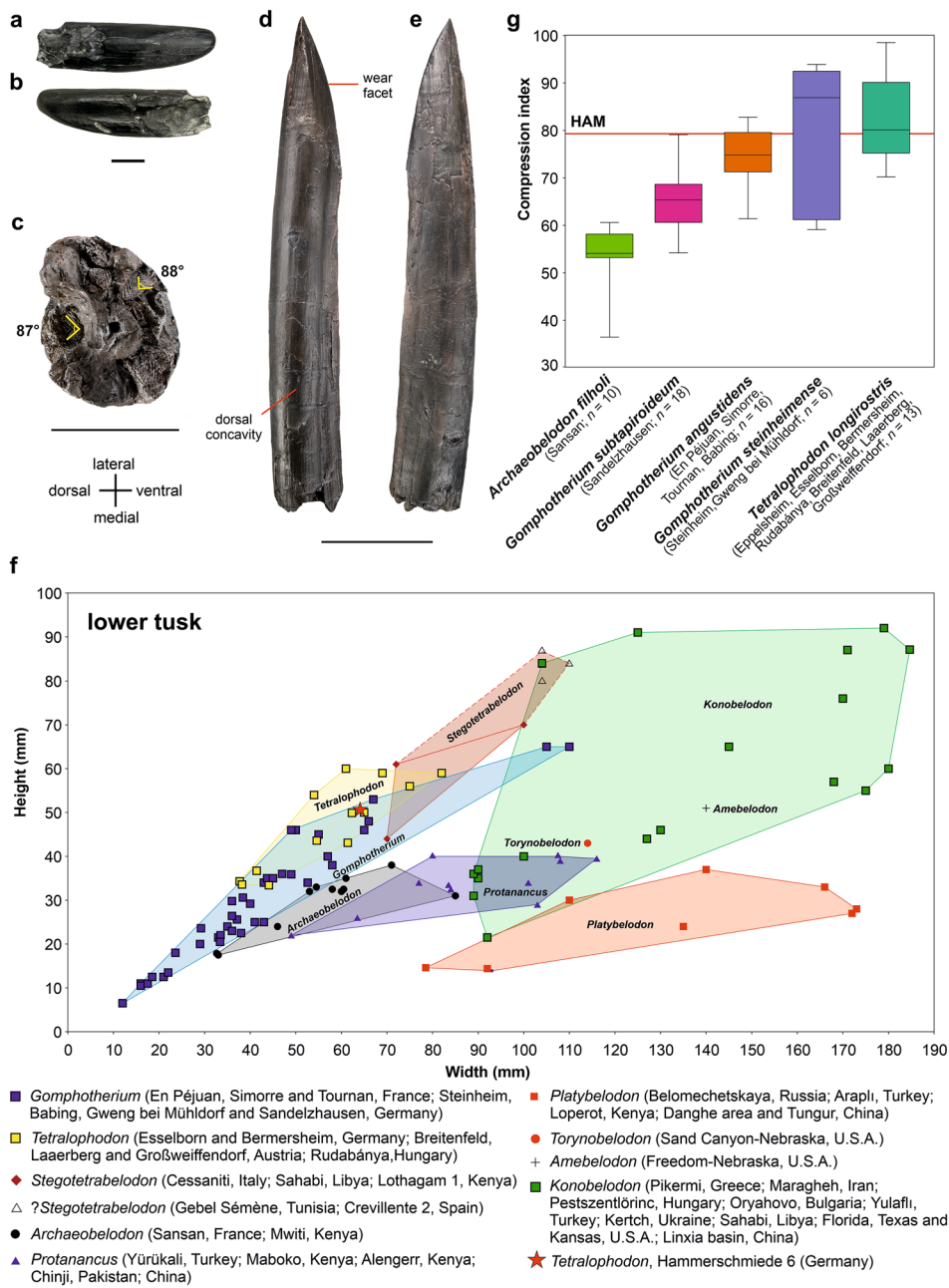


Fig. 10 Morphology and metric comparison of the lower tusks (i2) of *Tetralophodon longirostris* from Hammerschmiede. **a–b.** Left (juvenile permanent) i2, HAM 5, GPIT/MA/13792 in ventral (**a**) and dorsal (**b**) view. **c–e.** right (adult) i2 (cast), HAM 6, GPIT/MA/19246 in cross-sectional (**c**), dorsal (**d**) and ventral (**e**) view; in **c** the slightly acute Schreger lines are also shown. Scale bars equal 1 cm in **a–b**, 5 cm in **c**, and 10 cm in **d–e**. **f.** Bivariate plot (width vs. height) comparing the lower tusk of *T. longirostris* from Hammerschmiede 6 with lower tusks of various Miocene proboscideans. Note that the lower tusks belong to individuals of different ontogenetic ages and the location of the measurements differs among them (e.g., maximal preserved diameters if isolated or in front of the mandibular symphysis if embedded). The symbol ‘?’ indicates incomplete or inadequately

preserved specimens. Bivariate plot based on Konidaris and Tsoukala (2020: Fig. 5d, and references cited in the corresponding caption) plus Steininger (1965), Göhlich (1998, 2010) and Gasparik (2004); it is noted that the upper range for *Archaeobelodon* in the figure of Konidaris and Tsoukala (2020) was extended due to an oversight in the measurements. **g.** Box-and-whisker plot comparing the compression index of the lower tusks of *Archaeobelodon filholi*, *Gomphotherium* spp. and *Tetralophodon longirostris* from various localities with GPIT/MA/19246 from Hammerschmiede (red horizontal line); data from Klähn (1931), Steininger (1965), Mottl (1969), Tobien (1973), Göhlich (1998, 2010), Gasparik (2004), Tassy (2014), and own measurements at HLMD

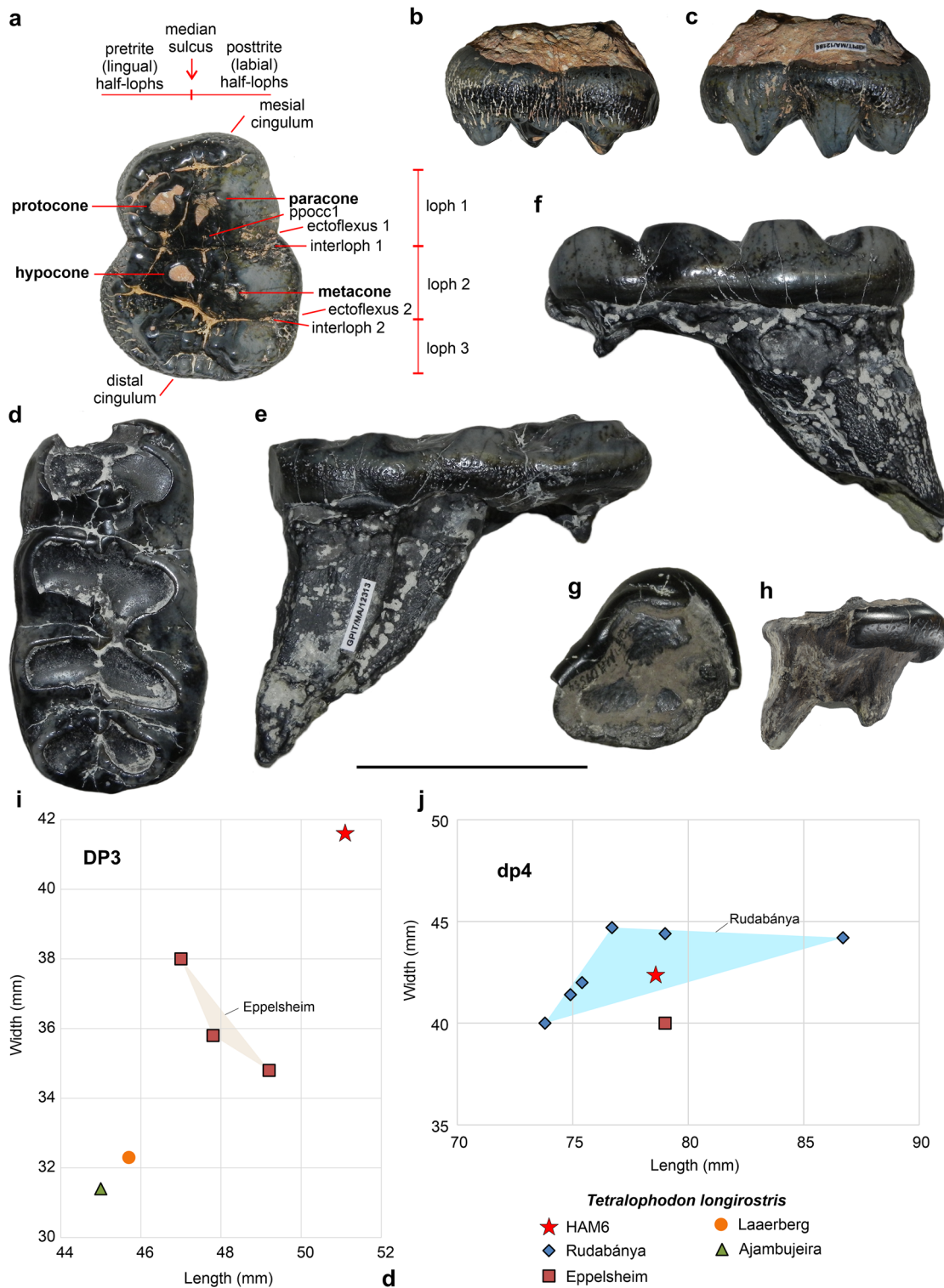


Fig. 11 Morphology and metric comparison of the third upper deciduous premolar (DP3), fourth lower deciduous premolar (dp4) and third upper premolar (P3) of *Tetralophodon longirostris* from Hammerschmiede. **a–c.** Left DP3, HAM 5, GPIT/MA/12196 in occlusal (**a**), (**b**) and (**c**) view. **d–f.** Right dp4, HAM 5, GPIT/MA/12313, in occlusal (**d**), labial (**e**) and lingual (**f**) view. **g–h.** right

P3, HAM 5, GPIT/MA/09554 in occlusal (**g**) and labial (**h**) view. Scale bar equals 5 cm. **i.** Bivariate plot of length vs. maximum width (in mm) for DP3 of *T. longirostris* from various localities. **j.** Bivariate plot of length vs. maximum width (in mm) for dp4 of *T. longirostris* from various localities (see Table 4)

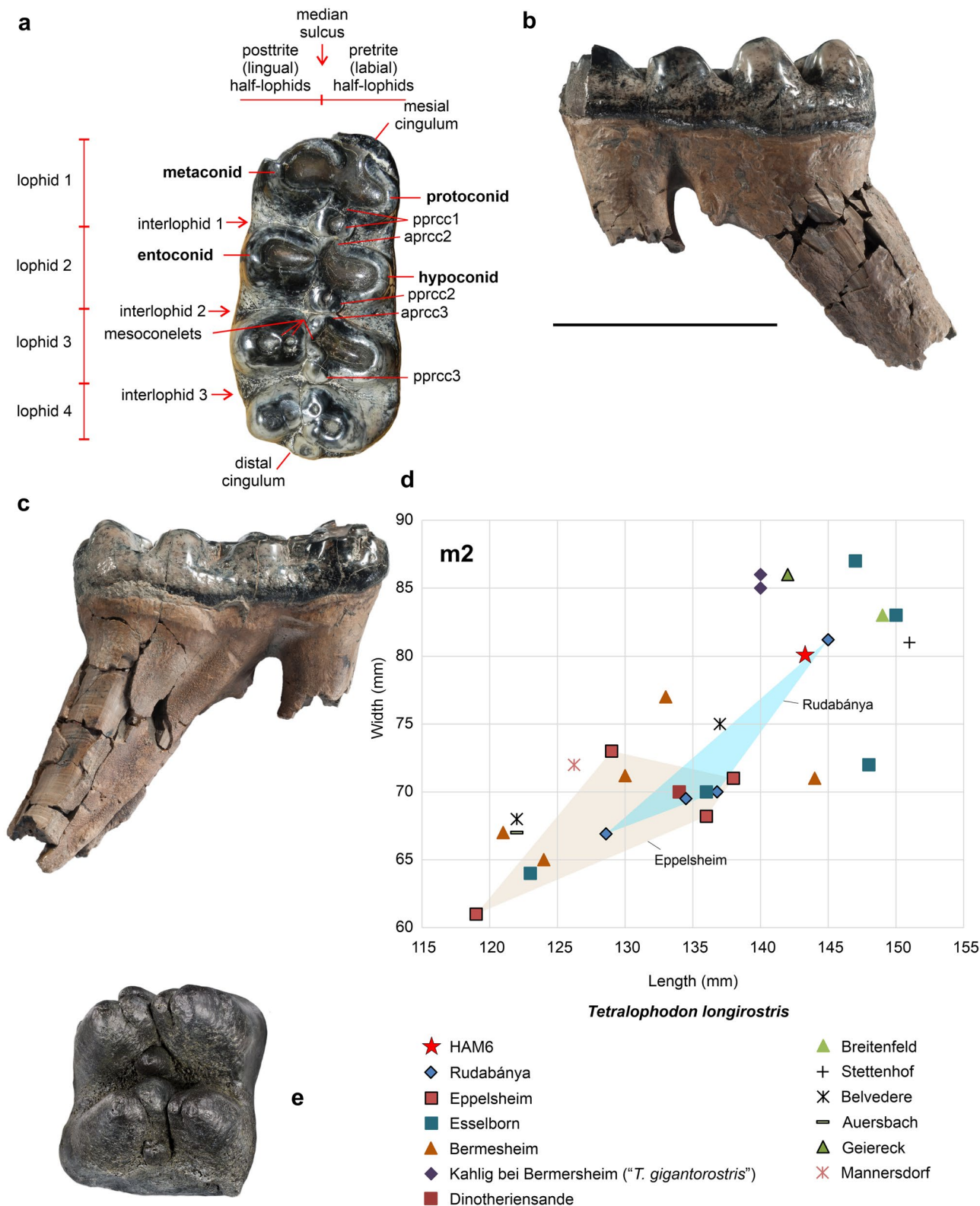
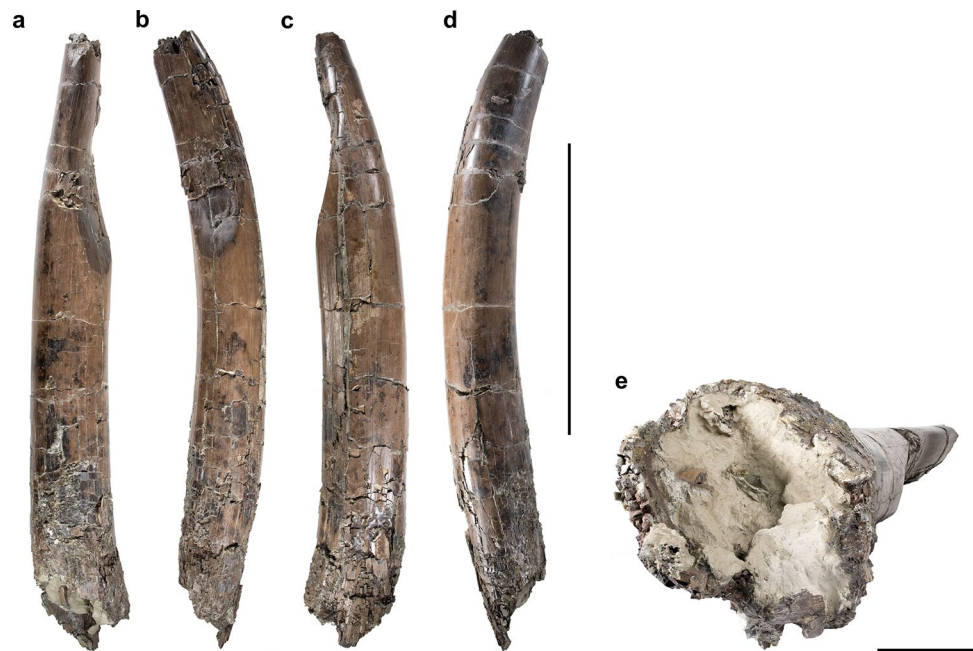


Fig. 12 Morphology and metric comparison of the lower molars of *Tetralophodon longirostris* from Hammerschmiede 6. **a–c.** Right m2, GPIT/MA/10800–03, in occlusal (**a**), lingual (**b**), and labial (**c**) view. **d.** Bivariate plot of length vs. maximum width (in mm) for m2 of *T.*

longirostris from various localities (see Table 4). **e.** Left m3 fragment (cast; GPIT/MA/19247) of *Tetralophodon longirostris* from Hammerschmiede 6. Scale bar equals 10 cm

Fig. 13 Right upper tusk (GPIT/MA/10800–01) of *Tetralophodon longirostris* from Hammerschmiede 6 in ventral (a), medial (b) dorsal (c), lateral (d) and cross-sectional (e) view. Scale bars equal 50 cm in a–d, and 5 cm in e



whereas in lophid 2 and more pronounced in lophid 3 the pretrite half-lophids are set in a more diagonal position relative to the posttrite ones; in lophid 4, the half-lophids form a mesially pointed chevron structure. In interlophids 1 and 2, the larger pprcc1 and 2 abut the smaller aprcc2 and 3, respectively, blocking the labial sides of the interlophids; lingually the interlophids are open. A similar structure is visible in interlophid 3, but the pprcc3 is smaller than the corresponding ones of lophids 1 and 2. The distal cingulum is formed by three cuspules, of which the most pretrite one is the stronger and higher. The enamel is slightly corrugated towards the distal, and less worn, part of the tooth. The mesial root is damaged, while the two distal ones are fused.

The tetralophodont m2 from HAM 6 is very worn and dentine is exposed on all lophids (Fig. 12a–c). The mesial cingulum is damaged at its lingual part; at the labial part it is low but strong and is connected through the confluent due to wear dentine with pretrite half-lophid 1. Lophid 1 is very worn. There are two ppcc1, of which the more distal one is robust, labially blocking the interlophid 1 and abutting the weak aprcc2. At the labial side of interlophid 1, there are remnants of cingulum. Lophid 2 is also very worn, but the two half-lophids are separated by the median sulcus. In interlophid 2, the strong (but slightly less than pprcc1) pprcc2 abuts the weaker aprecc3. In lophid 3, the pretrite half-lophid is set diagonal relative to the posttrite one. The latter bears two mesoconelets, of which the adaxial one is stronger. Interlophid 3 is blocked at its labial part by the pprcc3. In lophid 4, the two mesoconelets are set mesially relative to the main cusps. The distal cingulum consists of two cuspules, of which the labial one is higher and larger.

A middle fragment of a m3 (cast) from HAM 6 preserves two lophids (Fig. 12e). Each pretrite and posttrite half-lophid bears a mesoconelet, which on the pretrite side is in a slightly more mesial position in regard to the main cusp. This is more strongly expressed in the distal lophid. The preserved mesial lophid has one anterior and one posterior pretrite central conule, while the distal lophid only a weaker posterior one.

Upper dentition The upper tusk GPIT/MA/10800–01 (length arc: 1030; length chord: 920; circumference: 410; maximal diameters: 140 × 126 proximal; all in mm) from HAM 6 is ventrally curved, has an ovoid cross-section and lacks an enamel band (Fig. 13). In the proximal part, the pulp cavity is open (indicating that the tusk is almost completely preserved) and partially filled with sediment, while the distal part (tip) is missing. There is a long medial wear facet (maximal diameters wear facet: 370 × 104 mm).

The slightly worn DP3 GPIT/MA/12196 from HAM 5 is trilophodont with narrow loph 1, and wide lophs 2 and 3 (Fig. 11a–c). Mesially it shows a polished surface due to the contact with the DP2. The mesial cingulum is low, but strong, and consists of worn cusplets in a row. It continues and becomes high at the lingual side, and even stronger and higher at the level of loph 2. The cingulum ends at interloph 2. In loph 1, protocone and paracone are opposite to each other, but the latter is higher. The paracone bears a lower and worn mesoconelet set in a more distal position, as well as a low and worn posterior central conule. The protocone bears a similar in height mesoconelet, but it is directed mesially. Lophs 1 and 2 are separated by clearly marked ento- and ectoflexus. Interloph 1 is straight and open but closed

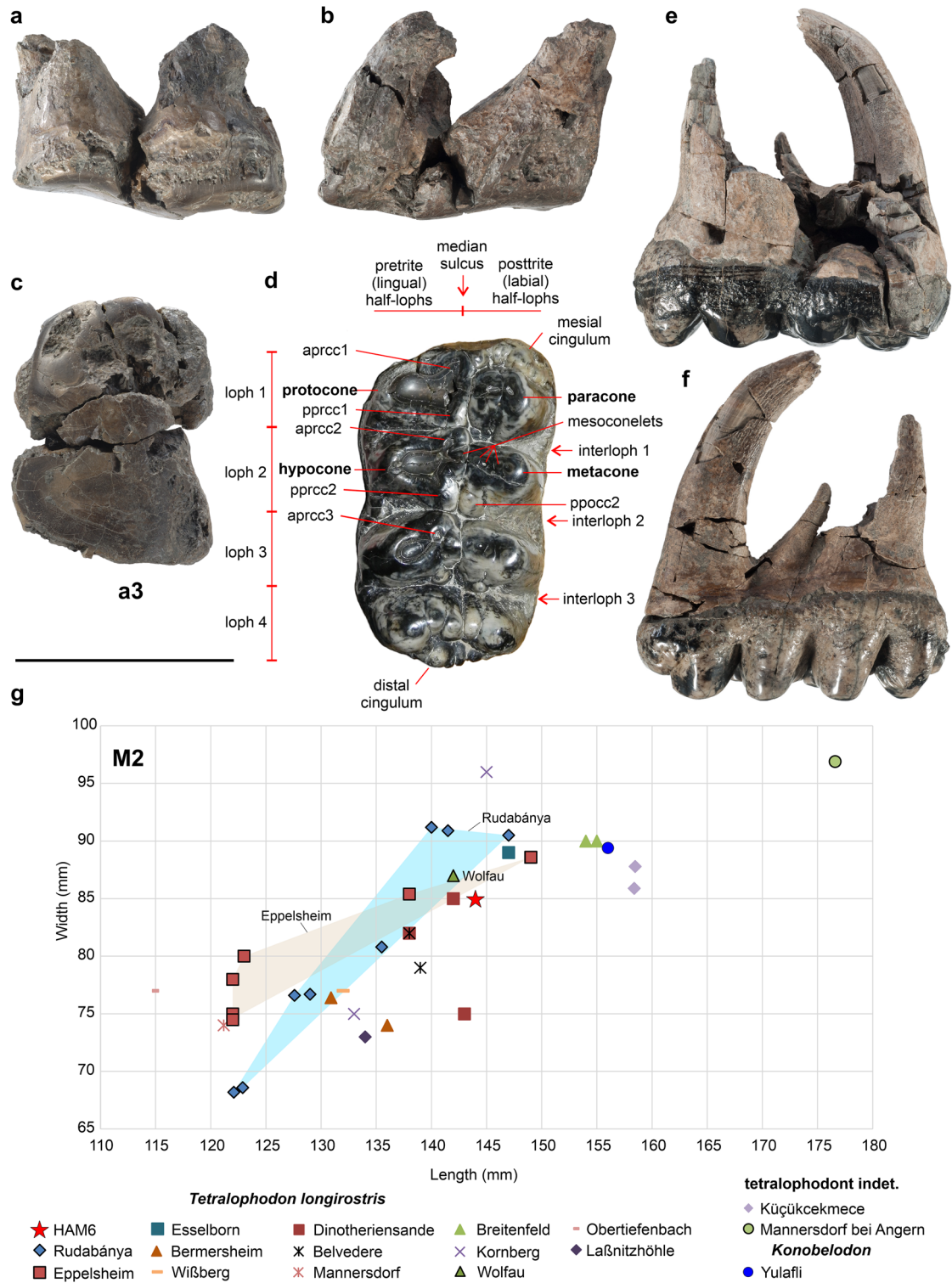


Fig. 14 Morphology and metric comparison of the first (M1) and second (M2) upper molars of *Tetralophodon longirostris* from Hamerschmiede 6. **a–c.** Right first upper molar? (M1?, GPIT/MA/10800–05) in lingual (**a**), labial (**b**) and occlusal (**c**) view. **d–f.** Left M2,

GPIT/MA/10800–04, in occlusal (**d**), labial (**e**) and lingual (**f**) view. Scale bar equals 10 cm. **g.** Bivariate plot of length vs. maximum width (in mm) for M2 of *T. longirostris*, *Konobelodon* and tetralophodont indet. from various localities (see Table 4)

lingually by the strong cingulum. Loph 2 is set diagonally. The metacone is higher than the hypocone and is fused with one mesoconelet; the hypocone and mesoconelet are worn and confluent. There is no second entoflexus and the second ectoflexus is very weak. The transverse valley is relatively sinuous and open, apart from the blocked by the cingulum lingual part. In loph 3, the posttrite main cusp is unworn and located in a more distal position relative to the slightly worn pretrite main cusp. The mesoconelets are lower than the main cusps. The distal cingulum is formed by four to five relatively low cusplets, which increase in height and strength towards the lingual side. The enamel is corrugated.

GPIT/MA/09554 from HAM 5 is a small-sized, deeply worn, tooth; it is of triangular shape with narrow mesial part and wider distal one (Fig. 11g, h). In its mesial part the enamel is thick, indicating that the specimen is not a deciduous premolar. The tooth is tentatively identified as a third upper premolar. There is a strong mesial cingulum which is connected to the pretrite side of the mesial loph. Enamel is missing from the distal side of the tooth.

GPIT/MA/10800–05 is a severely worn tooth (complete absence of enamel) from HAM 6, which is tentatively identified here as an upper M1 due to its length (116.2 mm), which is much smaller than the M2 GPIT/MA/10800–04 (144.0 mm) (Fig. 14a–c). The preservation of two single roots at the mesial part of the tooth indicate that no substantial loss of the original length could have happened although the advanced wear stage, excluding an identification as a M3. However, alternatively, it may be a smaller-sized M2.

The tetralophodont M2 from HAM 6 is relatively worn, and dentine is exposed in the first three lophs (Fig. 14d–f). There is a polished interproximal surface due to contact with the M1. The tooth is slightly damaged mesiolingually. On the mesiolabial side, the cingulum is low but strong. In loph 1, the paracone and one mesoconelet are fused. The pretrite half-loph is much worn and the dentine is confluent; however, the strong aprcc1 is connected to the mesial cingulum, while the pprcc1 and the aprcc2 are connected blocking interloph 1 lingually. On its lingual-most part there is a strong bulge, while on its labial side there is low and weak cingulum. In posttrite half-loph 2, there are three fused to each other mesoconelets in a slightly more mesial position than the metacone, and one ppoc2. Pretrite half-loph 2 is very worn, but at least one mesoconelet is visible. The pprcc2 abuts the aprcc3 in interloph 2; on its lingual-most part four rather strong cusps are located. In loph 3, the mesoconelets are set mesially relative to the main cusps; there are three mesoconelets in the posttrite half-loph and at least one in the worn pretrite one. Interloph 3 is open, but there are two weak cusps, one in the posttrite and one in the pretrite side. Loph 4 is almost straight; there are two pretrite mesoconelets and one posttrite. The distal cingulum

consists of five cusps, larger and higher towards the lingual side.

The two mesial lophs of the M3 from HAM 6 are completely worn and the dentine is confluent (Fig. 15a–c). However, the molar preserves the mesial roots indicating that there is no loss of additional mesial lophs, and therefore the M3 was comprised of five lophs. There are strong bulges in the labial side of interloph 1; weaker ones are located in interloph 2 and even weaker in interloph 3. In the lingual side, there are two low but strong cusps in interloph 2, two very large ones in interloph 3, and one strong in interloph 4. In loph 3, the pretrite half-loph is set diagonal to the posttrite one; it bears one strong aprcc3. In lophs 4 and 5, the mesoconelets (one for each half-loph) are positioned more mesially than the main cusps. Besides these mesoconelets, there is one very strong additional one located at the middle of the lophs, which is larger than the main cusps. The distal cingulum consists of three cusps, of which the most lingual one is the strongest, while at the distal-most part of the tooth there are three additional weak cusps.

Remarks

Tetralophodon encompasses tetralophodont gomphotheres with a long mandibular symphysis, pyriform to oval in cross-section lower tusks (in contrast to the brevirostrine and tuskless *Anancus*) that consist of concentric lamellar dentine (no dentinal rods like the amebelodontid *Konobelodon*), intermediate and third molars that show trefoil wear patterns (not plate like pattern such as the elephantid *Stegotetrabelodon*) and rounded upper tusks that lack enamel bands (Konidaris and Tsoukala 2022). In Europe, *Tetralophodon* is represented by its type species *T. longirostris*, the known biostratigraphic distribution of which ranges from the late Astaracian (MN 7/8; Middle Miocene) to the late Vallesian (MN 10; Late Miocene) (Tassy 1985). The type locality of *T. longirostris*, Eppelsheim, belongs to the Eppelsheim Formation (“Dinotheriensande”) of the Mainz Basin in Germany, from where most of the known specimens originate. Originally, the tetralophodont proboscidean remains from “Dinotheriensande” were allocated by Kaup (1832b) to the species *Tetracaulodon longirostre* (*Tetracaulodon* is now regarded as a junior synonym of *Mammuth*); slightly later (Kaup 1835) they were assigned to *Mastodon longirostris*, a species that was subsequently included within the subgenus *Mastodon* (*Tetralophodon*) by Falconer (1857). Besides *T. longirostris*, several other taxa have been proposed in the past based on material from “Dinotheriensande”, e.g., *Mastodon grandis* Kaup and Scholl, 1864, *Mastodon wahlheimensis* Klähn, 1922, *Mastodon esselbornensis* Klähn, 1922, *Mastodon gigantorostri* Klähn, 1922, *Tetralophodon curvirostris* Bergounioux and Crouzel, 1960, mainly

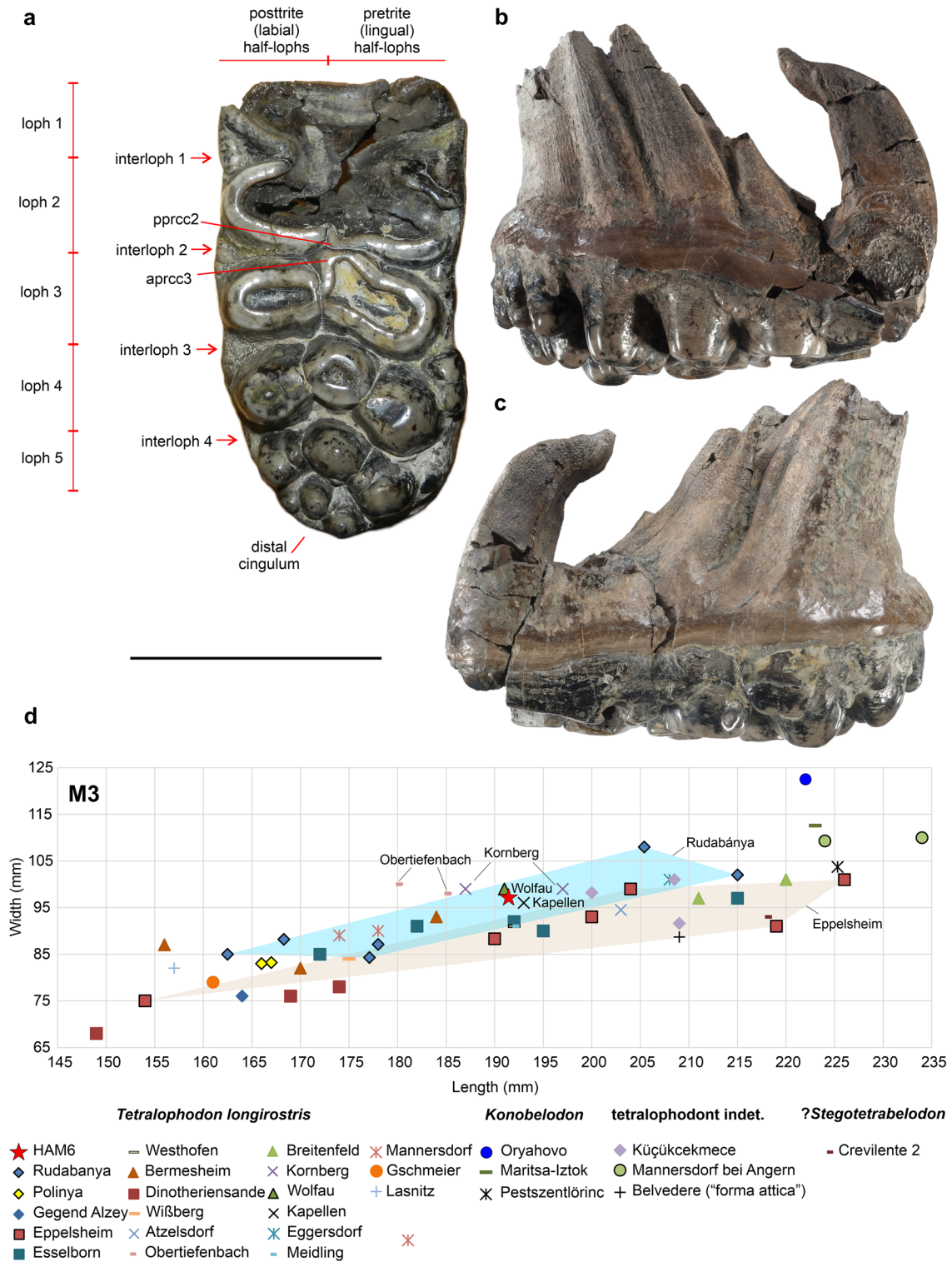


Fig. 15 Morphology and metric comparison of the third upper molar of *Tetralophodon longirostris* from Hammerschmiede 6. **a–c.** Right M3, GPIT/MA/10800–02, in occlusal (**a**), lingual (**b**) and labial (**c**) view. Scale bar equals 10 cm. **d.** Bivariate plot of length vs. maxi-

imum width (in mm) for M3 of *T. longirostris*, *Konobelodon*, tetralophodont indet. and ?*Stegotetabelodon* from various localities (see Table 4)

on the grounds of dental size, and mandibular and dental and morphology. However, these species are considered junior synonyms and within the intraspecific variation (polymorphism) of *T. longirostris* (Tobien 1980; Tassy 1985, 1999). “Dinotheriensande” were generally considered to be of Vallesian age; however, recent studies indicate the stratigraphic inhomogeneity due to reworking of the sediments and a chronological range of the fauna from the Middle to the Late Miocene (Böhme et al. 2012; Pickford and Pourabrishami 2013). Taking also into account that, as in several historical collections, the fossils lack precise stratigraphic information, the revision of all known material from Europe and the discovery of new specimens with certain stratigraphic context are necessary to clarify the taxonomy and evolution of *Tetralophodon* from Europe.

Comparison

The combination of several morphological and metric traits, exclude the allocation of all HAM specimens to the trilophodont elephantimorphs *Archaeobelodon*, *Protanancus*, *Platybelodon*, *Choerolophodon* and *Gomphotherium*, as well as to the mammutids *Zygalophodon* and *Mammut*. In particular:

- Trilophodont DP3, tetralophodont dp4, m2 and M2, and five loph with a distal cingulum in the M3, indicate that all HAM cheek teeth belong to a tetralophodont elephantimorph. Even the later and larger *Gomphotherium* (cf.) *steinheimense* (Klähn, 1922) (e.g., Steinheim, Massenhäuser, Gweng bei Mühlendorf; Germany) possesses M3 with four loph that may bear a developed cingulum or 4 ½ loph (Göhlich 1998; Göhlich and Huttunen 2009), but not five loph.
- The absence of an enamel band (a derived trait) in the upper tusk from HAM further corroborates the exclusion of a more basal bunodont elephantimorph (see e.g., Tassy 2014), while an attribution to *Choerolophodon*, which also lacks an enamel band is ruled out, because this genus is characterized by strongly curved and double-twisted upper tusks (e.g., Konidaris and Koufos 2016).
- The subcircular cross-section of the lower tusk from HAM 6 combined with the presence of only concentric lamellar dentine in the inner part clearly precludes an attribution to the amebelodontid *Platybelodon*, whose lower tusks bear tubular dentine and are dorsoventrally strongly compressed (Fig. 10f). The lower tusks of the other amebelodontids *Protanancus* and *Archaeobelodon* are also more dorsoventrally compressed than the HAM specimen (Fig. 10f, g). On the other hand, the morphological and metric distinction with *Gomphotherium* is more difficult as the lower tusks of *Gomphotherium* and *Tetralophodon* are morphologically close and partially overlap metrically (Fig. 10f, g). The HAM lower tusk is distinct

from *Gomphotherium suptapiroideum* (Schlesinger, 1917). In terms of the Ci, it stands at the upper quartile of *Gomphotherium angustidens* (Cuvier, 1817), and within the interquartile range of *Gomphotherium steinheimense* (Fig. 10g). However, the lower tusks of *G. angustidens* are mostly pyriform in cross-section (Tassy 2014: fig. 24), while those of *G. steinheimense* are circular in cross-section (Steinheim; Klähn 1931: pl. 2, fig. 1) or much larger (*G. cf. steinheimense*; Gweng bei Mühlendorf; Göhlich 1998). The lower tusks of the zygalophodonts *Zygalophodon* and *Mammut* differ also from the HAM specimen by their oval cross-section (Tobien 1996).

On the other hand, tetralophodont elephantimorphs of Europe include *Tetralophodon*, *Anancus*, *Konobelodon*, *Stegotetralophodon* and the “Crevillente 2 taxon” from Spain. Although the elephantid *Stegotetralophodon* (present in Europe so far only in the region of Calabria in Southern Italy, which at that time was a northern extension of the African continent; Ferretti et al. 2003) retains some gomphotherid traits, it differs from the HAM specimens in the straight and not ventrally curved upper tusks, the pentalophodont (or almost) m2/M2, and the equal development of the cusps which are aligned forming a plate-like pattern (Tassy 1999). These elephantid traits are also present in the molars of the derived tetralophodont taxon from the Turolian of Crevillente 2 (Spain), originally attributed to *Tetralophodon cf. longirostris* ‘grandincisivoform’, but with possible *Stegotetralophodon* affinities (Mazo and Montoya 2003; Mazo and Made 2012; Tassy 2016). Additionally, the not completely preserved M3 of this taxon (Mazo and Montoya 2003: pl. 7, figs. 1 and 2) shows six loph and is characterized by a multiplication of cusps, while its dimensions are larger than the HAM M3 (Fig. 15d). An attribution of the HAM cheek teeth to *Anancus* can also be excluded because this genus [including the earliest representative from the Late Miocene of Europe *Anancus lehmanni* (Gaziry, 1997)] is characterized by the dislocation of the pretrite and posttrite half-loph(id)s, which results in the alternate arrangement of the successive loph(id)s (anancoidy), a feature not present on the studied specimens, while this genus is equipped with almost straight upper tusks and does not bear lower tusks (Tassy 1986; Hautier et al. 2009; Konidaris and Roussiakis 2019). The other tetralophodont candidate is the tetralophodont amebelodontid *Konobelodon*, represented in Europe by *Konobelodon atticus* (Wagner, 1857). The latter is diagnosed among others by its enlarged loph 3 in the DP3 with well-marked second ento- and ectoflexus, and by large-sized, dorsoventrally flattened lower tusks bearing internally tubular dentine (Fig. 10f; Konidaris et al. 2014; Konidaris and Tsoukala 2020, 2022); on the contrary, in the HAM DP3 loph 3 is short, there is no entoflexus 2, the ectoflexus 2 is weak, while the lower tusk is subcircular, is formed only by

concentric dentine and is of smaller size (Figs. 10c, f and 11a). Additionally, the dimensions of the known M2, M3 of European *Konobelodon* (e.g., Pestszentlőrinc, Hungary; Oryahovo, Maritsa Iztok, Bulgaria; Yulafli Turkey; and perhaps Mannersdorf bei Angern, Austria), and the M2 and M3 from Küçükçekmece (Turkey), attributed to “tetralophodont form, gen. and sp. indet.” (Tassy 2016) are larger than the HAM specimen (Figs. 14g and 15d).

On the other hand, the HAM specimens match well with *Tetralophodon longirostris*. In particular (based on Tassy 1985: p. 723–724):

- Trilophodont DP3, tetralophodont intermediate molars, and M3 with five lophs (Figs. 11, 12, 14, 15).
- Tetrabelodont with rounded upper tusk lacking an enamel band, and subcircular/pyriform lower tusk with a dorsal concavity and without a ventral one (Figs. 10a–e, 13).
- Alternate contact (posttrite-pretrite) between the two mesial lophs (a derived trait) in the DP3 (Fig. 11a). The HAM specimen is morphologically similar to corresponding specimens of *T. longirostris* from Eppelsheim (HLMD-Din 1062 and casts MNHN-268, A.C. 1987; Kaup 1835: pl. 16, fig. 1a, pl. 17, fig. 12, pl. 20, fig. 2), Stierlingsandgrube am Geiereck (Laaerberg, Austria; Schlesinger 1917: pl. 12, fig. 1) and Azambujeira (Portugal; Antunes and Mazo 1983: pl. 1 fig. 6), in which loph 3 is not enlarged, ectoflexus 2 is weak (more marked in HLMD-Din 1062), and entoflexus 2 is absent or not very marked. Nonetheless, the HAM DP3 is larger than all other known *T. longirostris* specimens (Fig. 11i).
- Asymmetry in the pretrite trefoils with smaller posterior central conules compared to the anterior ones in the M3 (Fig. 15a).
- In the lophs distally of loph 3 in the M3, the mesoconulets are shifted mesially, and are as high as the main cusps of the loph (Fig. 15a).

However, within *T. longirostris* there are certain variable features in the last molars, the main of which relate to the complexity of the occlusal morphology, the crown dimensions, and the number of loph(id)s, as well as differences in the size, shape and Ci of upper/lower tusks.

Size, cross-sectional shape and compression index of upper/lower tusks The size, cross-sectional shape and Ci of the adult HAM 6 lower tusk match well with *T. longirostris* (Fig. 10c–g). However, the known *T. longirostris* lower tusks vary in size, cross-sectional shape and CI. The cross-section is roughly rounded (and accordingly the Ci is close to 100) in the Esselborn (HLMD-Din 1087; L tusk protruding from the symphysis = 320 mm) and Bermersheim

(L tusk protruding from the symphysis = 700 mm; Klähn 1931) lower tusks, whereas it is reported as pyriform in the Breitenfeld specimen (Mottl 1969). The Ci of the tusks from Rudabánya ranges from 70.2 (the lowest value for the species *T. longirostris* in general) to 91.0 highlighting the great variability within a sample. In terms of size and Ci, the HAM tusk fits best with Laaerberg and HGI-V.11953 from Rudabánya, while in terms of cross-sectional shape is close to the Grossweissendorf specimen (Austria; Steininger 1965) and HLMD-Din 999 from Eppelsheim. The general morphology is also similar with the specimen from Breitenfeld (Mottl 1969: pl. 1, fig. 2).

Only few upper tusks of *T. longirostris* are known. The upper tusk from HAM has a similar morphology but is larger than one from Rudabánya [Hungary; maximal diameters cross-section: 123 × 114 mm; Gasparik, 2004, 2005; originally attributed to “*Tetralophodon*” *gigantorostris* (Klähn, 1922), see below), as well as from one from Belvedere (Austria; maximal diameters cross-section: 122 × 100, circumference: 352 mm; Schlesinger, 1917: pl. 19, fig. 2; Göhlich, 1998). On the other side, the length and cross-sectional dimensions are very close to the specimen from Villavieja del Cerro (Spain; 920 mm and 142 × 127 mm, respectively; Mazo and Jordá Pardo 1997). In terms of length, the HAM tusk is similar to the Polinya (Spain; 950 mm) one, with which it shares a similar general morphology (Alberdi 1971: pl. 2, figs. 3 and 4). Two more upper tusks are known preserving the distal part, one comes from Eppelsheim (HLMD-Din 998) and is figured in Kaup (1835: pl. 3, fig. 2) and the other from Altmannsdorf (Austria) described in Schlesinger (1917: pl. 12, fig. 4).

Complexity of the occlusal morphology Tetralophodont molars vary greatly in the complexity of their occlusal morphology, e.g., pretrite central conules may be weak or strong, posttrite central conules may be present or not, alternating contacts may be present or absent, while in addition the degree of complexity may vary among the upper and lower molars of the same individual, within the toothrow (e.g., M2–M3) or even between the mesial and distal part of a single tooth (Tassy 1985: p. 735; Metz-Muller 1995; Göhlich 1998: p. 88; Hautier et al. 2009). This is also the case for *Tetralophodon longirostris*, e.g., within the samples from Rudabánya and Eppelsheim. Therefore, the complexity of the molars, at least in small samples where the degree cannot be statistically evaluated, cannot be of taxonomic significance and provide evolutionary conclusions.

The HAM 6 m2 is much worn but shows a relatively simple structure, with the complex traits pertaining to the presence of a ppoccl1 and pprcc3. The M2 shows a slightly more complex pattern, showing compressed posttrite

mesoconelets in loph 2 and 3, as well as two ppoc2 and two cusps (posttrite and pretrite) in interloph 3. The mesial loph in the HAM M3 are worn and thus the degree of complexity cannot be observed; in the rest of the tooth the complexity of the occlusal morphology can be regarded as relatively simple (e.g., absence of posttrite central conules), but with additional weak to strong cusplets present in the lingual and labial sides of the interlophs. The HAM molars differ from the complex ones such as the M2 from Gars (SNSB-BSPG-1974 I 342) and the M3 from Atzelsdorf that show heavy ornamentation with multiplication of the conelets and the central conules (however, particularly in the mesial loph that are not observable in the HAM molar). Another difference with the Atzelsdorf molar is that the latter bears in its distal half equal size main cusps and mesoconelets, whereas on loph 4 and 5 of the HAM M3 there are particularly strong conelets in the central parts of the lophs.

Size variation Proboscideans are characterized by variation in the size of their molars, especially of the m3/M3, evident when large samples from a single site are available. Particularly informative is the sample of *G. angustidens* from the Middle Miocene (Astaracian) of En Pélujan (France). The studies of Tassy (1996b, 2014) proved that the size variation in the m3/M3 from a single site should be attributed primarily to sexual dimorphism and not to the presence of two species, concluding that in most cases small-sized gomphotheriid molars from the Miocene correspond to female individuals and not to small-sized species. On the other hand, size variation between distant population of the same species might be a response to local environmental factors reflecting thus differences at population level (Tassy 1996b).

Another example might be *Mastodon giganteostris* of Klähn (1922) [or *Mastodon longirostris* forma *giganteostris* in Klähn (1931)] from Kahlig bei Bermersheim (Dinotheriensande, Germany), a taxon which was later included in *Tetralophodon* by Osborn (1936) and in *Stegotetabelodon* by Tobien (1978, 1980), followed also by Gaziry (1994). Besides some differences in the morphology of the holotypic mandible (mandibular angle, symphysis, and position of condyle in respect to the coronoid process), the main differences from *T. longirostris* are the more complicated structure, the presence of cement and the larger size of the molars (Klähn 1922, 1931; Tobien 1978, 1980; Gaziry 1994). According to Tassy (1985, 1999), however, this taxon is part of the polymorphism observed in European *T. longirostris*, while Göhlich (1999) notes that it is similar, if not identical, to *T. longirostris*. In this aspect, the rich tetralophodont material from Rudabánya plays an important role. The material consists primarily of isolated teeth, while unfortunately the preserved mandibles are fragmentary (and thus no comparison with the mandible of *Mastodon giganteostris* is possible). The tetralophodont assemblage was separated into two species based mainly on size, *T. longirostris* and “*T.*” *giganteostris*

(Gasparik 2005). Indeed, the size range of the six preserved M3 is wide, which in Fig. 15d results into two clusters (see also Fig. 16). Such size variation is observed also in the m3 (Konidaris et al. 2014: fig. 7). However, this might be part of the intraspecific size variation of *T. longirostris* reflecting sexual dimorphism. The material from Dinotheriensande localities (e.g., Eppelsheim, Esselborn), part of historical collections, lacks precise stratigraphic information and cannot be regarded as homogenous, however, it also shows evident size variability (Figs. 15d and 16).

The m2 from the HAM 6 individual is plotted at the upper range of *T. longirostris* (Fig. 12d) close to the m2s from Kahlig bei Bremersheim (Germany; holotype of *Mastodon giganteostris*), HGI-M.93.7 from Rudabánya (“*T.*” *giganteostris* in Gasparik 2005), Stierlingsandgrube am Geiereck (Laaerberg; *Stegotetabelodon grandicisivus* in Tobien 1978), Breitenfeld, Stettenhof (Austria), and to the larger specimens from Esselborn (HLMD-Din 856 and 1067) and Bremersheim (HLMD-Din 1072). For both Lm2 and Wm2 the HAM 6 m2 is plotted above the upper quartile of Rudabánya and Dinotheriensande (Fig. 16). Likewise, the M2 from HAM 6 is also plotted at the upper range of *T. longirostris* (Fig. 14g) close to the M2 from Wolfau (Austria), and to the larger specimens from Rudabánya (“*T.*” *giganteostris* in Gasparik 2005), Eppelsheim (HLMD-Din 770), Esselborn (HLMD-Din 755), “Dinotheriensande”, and Kornberg (Austria; LMJ 60.114; in terms of length). The HAM 6 LM2 stands above the upper quartile of Rudabánya and Dinotheriensande, while the WM2 at the upper part of the interquartile range of the former locality and at the upper quartile of the latter (Fig. 16). The M3 from the same HAM 6 individual is plotted roughly at the middle of the size variation of *T. longirostris* (note that the maximum length is likely affected by the advanced wear at the mesial part and thus it may be slightly an underestimate of the original, unworn, one), close to the M3s from Kornberg, Wolfau, Meidling (Austria), Kapellen (Slovenia; Bach 1910), Westhofen (Germany), and to HLMD-Din 751 from Esselborn (Fig. 15d). For both LM3 and WM3 the HAM 6 M3 is plotted at the upper part of the interquartile range of Rudabánya (separation into male and female individuals is possible) and Dinotheriensande, (Fig. 16). Overall, the HAM 6 *T. longirostris* belongs to a large-sized individual (probably male; see remarks below).

Number of loph(id)s The HAM 6 M3 is formed of five lophs, of which the last one is short and is accompanied by a rather reduced distal cingulum (Fig. 15a). This occlusal pattern differs from M3s of *T. longirostris* that consist of 4–4 ½ lophs, such as Obertiefenbach bei Fehring (Austria; Bach 1910: p. 66, pl. 7, fig. 14), Bermersheim (HLMD-Din 600) and Atzelsdorf (Göhlich and Huttunen 2009; *T. cf. longirostris*). It also differs from specimens having a wide loph

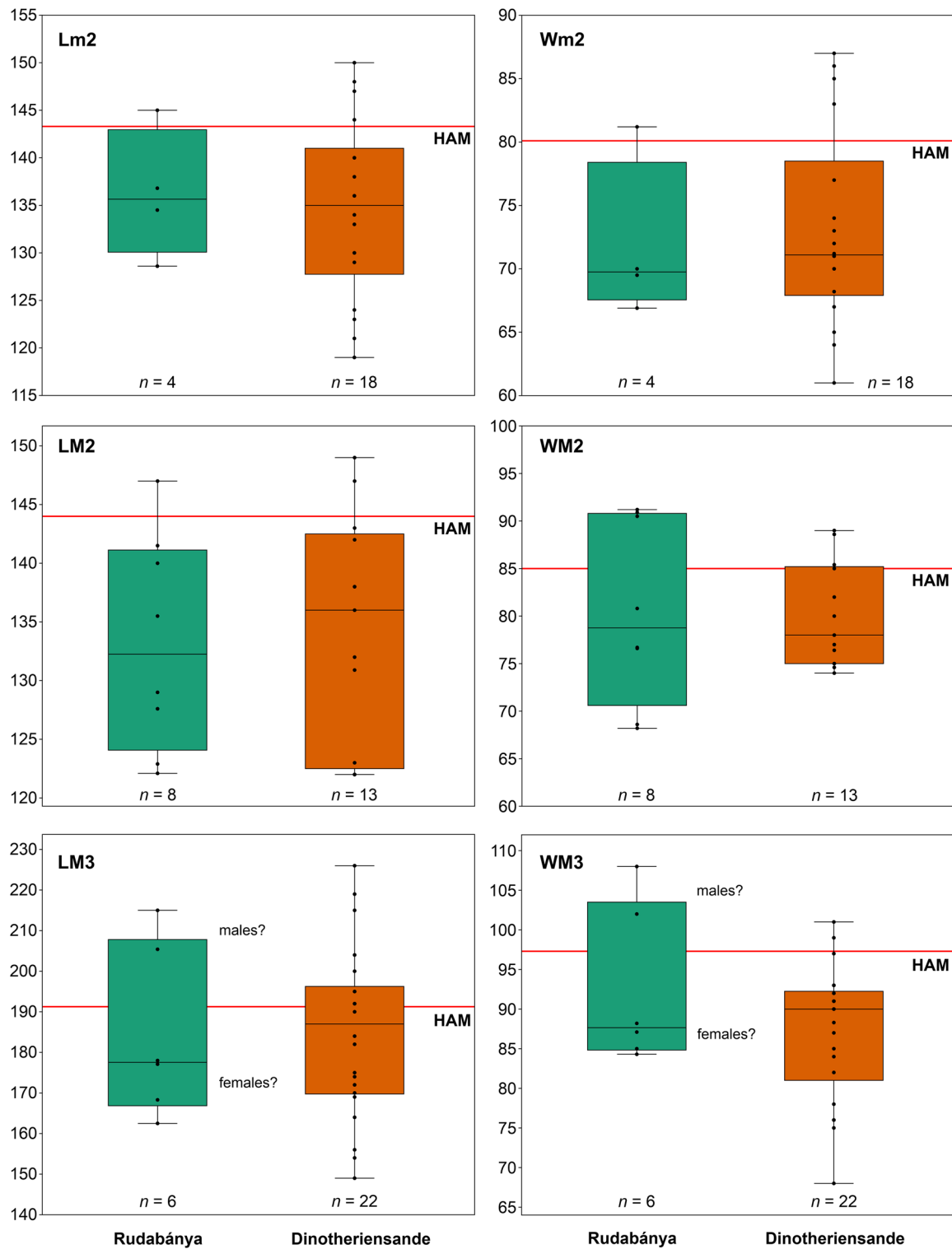


Fig. 16 Box-and-whisker plots of length (L) and width (W) (in mm) for the m2, M2 and M3 (specimens appear with black dots) of *Tetraodon longirostris* from Rudabánya (Hungary) and from Dinotheriensande (Germany) sites compared to the specimens from Hammer-schmiede (red horizontal line). For explanation see Fig. 8 and for the comparative sample Table 4

riensande (Germany) sites compared to the specimens from Hammer-schmiede (red horizontal line). For explanation see Fig. 8 and for the comparative sample Table 4

5, e.g., HLMD-Din 751 from Esselborn (Gaziry 1994: pl. 2, fig. 5) or even a sixth loph, e.g., HLMD-Din 651 from Eppelsheim (Gaziry 1994: pl. 3, fig. 3). The HAM M3 is comparable with HLMD-Din 757 from Wißberg (Germany; Gaziry 1994: pl. 2, fig. 6), HLMD-Din 759 from Westhofen (Gaziry 1994: pl. 2, fig. 4), and the molars from Kapellen (Bach 1910: pl. 10, fig. 2) and Eggersdorf (Austria; Bach 1910: pl. 10, fig. 5), and matches best with the M3 from Kornberg (Mottl 1969: pl. 12).

Overall, there exists evident metric and morphological variability within the *Tetralophodon* sample of Europe, while the uncertain stratigraphic position for some of them obscures whether this variability has taxonomic/biochronologic importance. Additionally, it should be noted that none of the above dental traits should be used on its own for any taxonomic/biochronologic conclusions (e.g., Obertiefenbach with 4–4 ½ lophs and Kornberg with five lophs have approximately similar age; Fig. 18) especially when studying limited/fragmentary samples. In this aspect, the secure chronological placement of the HAM 6 morphological traits allows their chronological control and can form a reliable comparative sample, contributing thus to the investigation of the evolution of European *Tetralophodon*.

Minimum number of individuals – age, sex, health, and hypotheses on the cause of death

Based on the degree of dental wear and the dental eruption sequence in deinotheres and elephantimorph proboscideans, we can calculate the Minimum Number of Individuals for each HAM layer. HAM 4 includes one juvenile *Deinotherium* individual; HAM 5 two juveniles (of which one partial skeleton is preserved) and one adult (based on tooth fragments) *Deinotherium* individuals, and two juveniles and one adolescent (based on the P3) *Tetralophodon* individuals; HAM 6 one (or perhaps two; see below) adult *Tetralophodon* individual (partial skeleton).

The *Deinotherium* mandible from HAM 5 belonged to an individual in its infancy (dp4 not fully erupted) in accordance with the developmental stage of the preserved postcranial bones. Although hypothetical, this very early age at death of the individual might be the result of predation. The damaged angles of the mandible might be attributed to carnivore gnawing, because this region (which includes the masseteric fossa where the masseter muscle is attached) is commonly attacked by carnivorans (Binford 1981: p. 63, fig. 3.27; Brain 1981: pp. 69–70, fig. 62). Interestingly, HAM 5 is the only layer of Hammerschmiede that documents both a machairodont felid (*Pseudaelurus*) and a large-sized hyaenid (Kargopoulos 2022; Kargopoulos et al. 2022), both formidable predators capable for foraging on juvenile

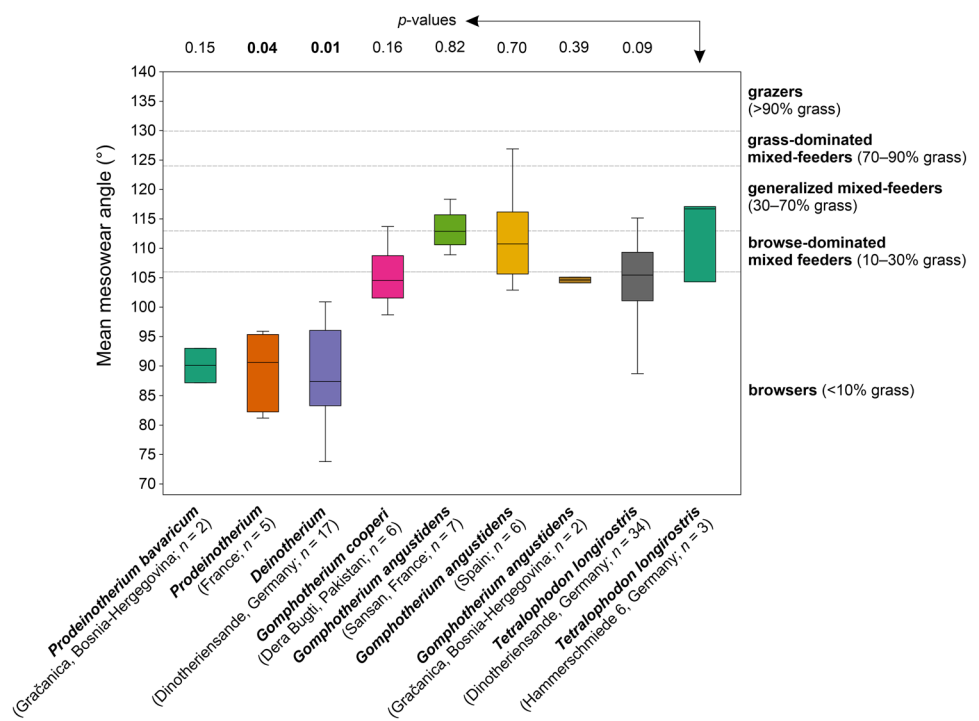
proboscideans, which might have been inattentive or were possible left unprotected by the herd.

Applying the dental age classes of Metz-Muller (2000) (see Material and methods) in the HAM 6 *Tetralophodon* molars, the m2 (C, D, D/d, d) and M2 (D/d, D/d, d/p, f) correspond to an age class of ~10 (compatible with the severely worn M1, and the practically unworn m3 fragment), and the M3 (C, C, D, d, f) to ~13. The m2/M2 provide an ontogenetic age estimation ~25–36, and the M3 ~37–48, in *Loxodonta africana* equivalent years (Metz-Muller 2000: fig. 22). As noted in the taphonomic section, the excavation of fossils at HAM 6 took place in the end of 1970ies and early 1980ies, and therefore there are not precise spatial data available. The wear of the right m2 is roughly compatible (but slightly in a more advanced stage indicating a stronger right-side component in the food consumption) with the left M2. Unfortunately, the right M2 is not available, however, the right M3 is significantly more worn than the left M2, as well as than the right m2. This is not compatible with the normal wear pattern and dental succession known in elephantimorph proboscideans, in which the preceding tooth is more worn than the succeeding one. This means either the presence of two individuals at HAM 6, or of a single one (of about 35–40 years old) with anomalous/pathologic dental condition. Another interesting aspect is the marked difference in the wear along the M3, whose mesial half is severely affected by wear, whereas the distal one is minimally worn.

For the HAM 6 *Tetralophodon* individual(s) a sex determination is possible. The large size of the m2/M2, in particular compared with the Rudabánya and Dinotheriensande ones (Fig. 16), indicates a male individual; the LM3 might be a slight underestimate of the original unworn condition, but it also fits better with a male determination. In further agreement, the cross-sectional dimensions of the upper tusk are close to those of the Villavieja del Cerro upper tusk (associated with a much-worn M3), which is attributed to a male individual (Mazo and Jordá Pardo 1997; Larramendi 2016). The live shoulder height (including flesh) of the latter individual is estimated at ~3.45 m and its body mass at ~10 tons (Larramendi 2016). Comparable shoulder height and body mass estimations could also be considered for the HAM 6 individual(s).

Male proboscideans (documented also by their abundance in the fossil record of open-air sites where partial skeletons are preserved) show a high mortality at their subadult/adult (but not senile) stage, which is possibly attributed to the fact that males on puberty are forced out of the family and acquire a more solitary and nomadic life associated with increased risks (Konidaris and Tourloukis 2021, and references cited therein). Whether one or two individuals at HAM 6, the dental wear evidence indicates an adulthood stage, certainly younger than the expected longevity, and therefore a comparable way of life can be hypothesized also for the HAM 6 *Tetralophodon*. Additionally,

Fig. 17 Box-and-whisker plots comparing the dental mesowear angles of *Tetralophodon longirostris* from Hammerschmiede with various Miocene proboscideans. Estimated dietary composition and categories are indicated with dashed lines based on Saarinen et al. (2015); comparative data from Xafis et al. (2020). The *p*-values above the graph were calculated by pairwise Mann–Whitney test comparing the mesowear angles of *Tetralophodon longirostris* from Hammerschmiede with the other proboscideans; significant differences at $p < 0.05$ are bolded



the HAM 6 molars exhibit some enamel hypoplasia (e.g., Fig. 15b–c), indicating episodes of stress (physiological, ecological, predatory, or competitive) during the life history (see e.g., Ameen et al. 2020), which may have rendered the individual(s) weakened, and potentially could have also contributed to a premature death (based on the available tooth positions and the degree of dental wear).

Dental mesowear analysis and palaeoecological remarks

The mean mesowear angles of the three *Tetralophodon longirostris* molars from HAM range from $\sim 104^\circ$ to $\sim 117^\circ$ (Table 6), thus showing moderately angled wear facets and modestly deep worn dentine valleys. This provides a mixed-feeding mesowear signal with an important browsing component (Fig. 17). The mean mesowear angles from HAM are significantly different from the heavily browse-dominated diet of *Prodeinotherium* (Gračanica and France) and *Deinotherium* (Dinotheriensande), supported also by the low *p*-values from the pairwise Mann–Whitney test (Fig. 17). On the other hand, the HAM signal fits within the variable range of *Gomphotherium* spp. and *Tetralophodon longirostris* (Dinotheriensande), which broadly show a browsing to mixed feeding diet. The mean value (112.7°) plots the HAM *Tetralophodon* within

the browse-dominated mixed feeding category and closer to the Middle Miocene *G. angustidens* populations from Sansan (France; mean value 113.5°) and Spain (mean value 111.7°), supported also by the *p*-values. However, the median value (116.7°) of the HAM 6 *T. longirostris* exceeds those of all comparative samples, while its upper range exceeds the upper quartile of both *G. angustidens* populations, implying perhaps a slightly higher incorporation of grasses in the diet. Interestingly, the HAM 6 *T. longirostris* shows a more expressed generalized mixed-feeding signal than the *T. longirostris* population from Dinotheriensande, which could perhaps reflect slightly different palaeoenvironmental conditions. We note, however, that the Dinotheriensande material lacks stratigraphic control and may be mixed, encompassing a long biostratigraphic range, that may cover both Astaracian and Vallesian. Additionally, the HAM sample is limited, and therefore the results should be considered indicative but not conclusive. Although mesowear angles were not acquired for the HAM deinotheres, several studies support the browsing character and the consumption of C_3 vegetation of *D. levius* / *D. giganteum* populations from the Middle–Late Miocene of central Europe (Calandra et al. 2008; Aiglstorfer et al. 2014b; Xafis et al. 2020). As such, the different feeding habits of *D. levius* and *T. longirostris* indicate niche partitioning between these two species, i.e., they did not compete for the same food resources, thus reducing the competitive pressure and permitting their viable coexistence at Hammerschmiede.

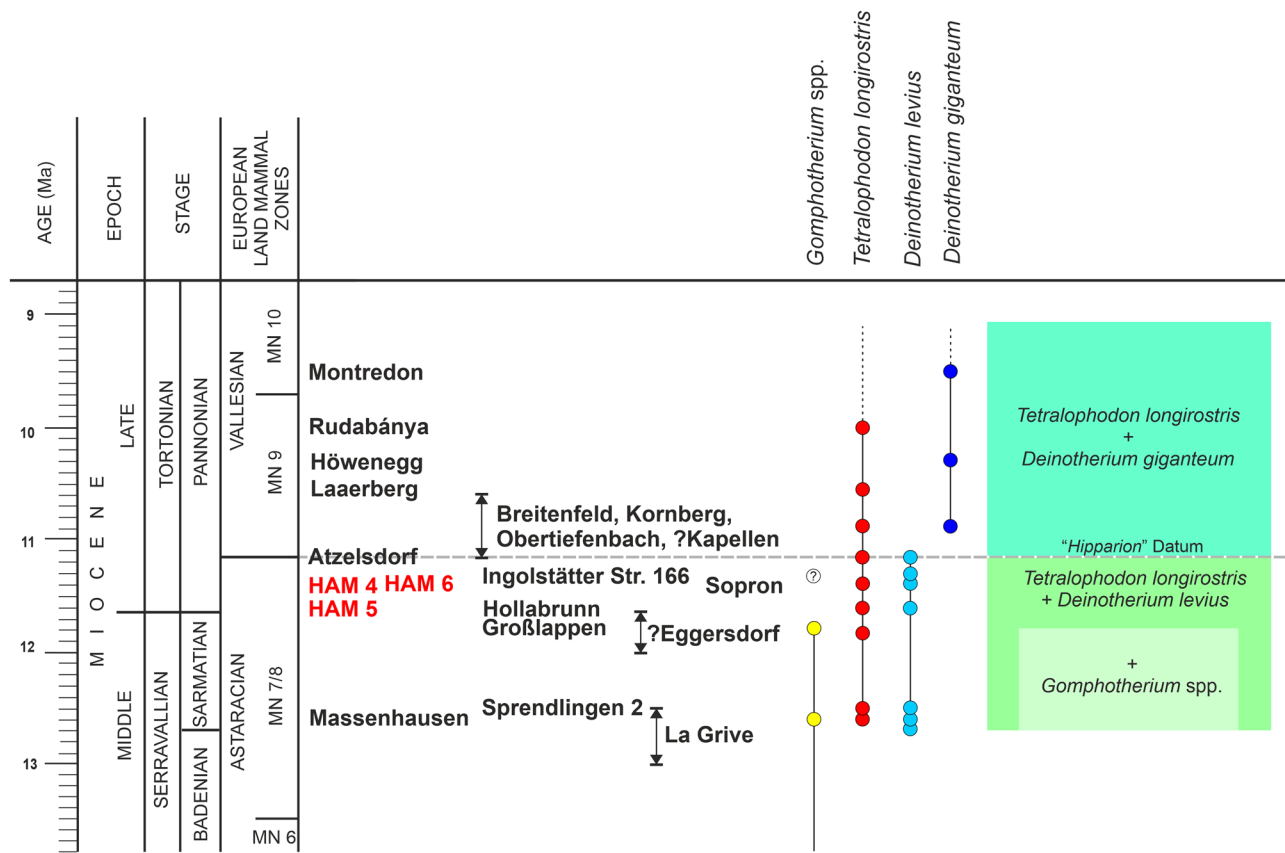


Fig. 18 Biochronological distribution of *Deinotherium levius*, *Deinotherium giganteum*, *Gomphotherium* spp. and *Tetralophodon longirostris* close to the Middle–Late Miocene transition, and chronology

of selected central European localities. Data from Göhlich (1998), Böhme et al. (2012) and Kirscher et al. (2016)

Biostratigraphic remarks – conclusions

The proboscidean sample from Hammerschmiede includes complete and important specimens of the deinotheriid *Deinotherium levius* and the gomphotheriid *Tetralophodon longirostris*. Besides its taxonomic value, the securely bio- and magnetostratigraphically constrained age of the HAM localities (Kirscher et al. 2016), renders the HAM proboscidean assemblage important for biostratigraphic conclusions within the wider central European context, close to the Middle/Late Miocene transition (Fig. 18).

Evidence of association of *D. levius* and *T. longirostris* is so far relatively meager and besides Hammerschmiede, these species coexisted at the late Middle Miocene (MN 7/8) localities Massenhausen (Gräf 1957; Göhlich 1998), Sprendlingen 2 (Germany; Böhme et al. 2012) and Montréjeau (France; Crouzel 1947; Crouzel and Debeaux 1957; Duranthon et al. 2007), and the early Late Miocene localities Atzelsdorf (earliest MN 9; Göhlich and Huttunen 2009, see also Konidaris and Koufos 2019) and Polinya (MN 9; Alberdi 1971; Casanovas-Vilar et al. 2016). Both species are recorded at Dinotheriensande (e.g., p3 of *D. levius* from Eppelsheim

HLMD-Din 311), but the absence of stratigraphic data and the reworking of the fossils (Böhme et al. 2012; Pickford and Pourabrishami 2013) makes their coexistence only hypothetical. Another locality with possible such coexistence is Hollabrunn (formerly Oberhollabrunn; Austria), from where Sickenberg (1928, 1929) mentions *Deinotherium* sp. and *Mastodon* sp. A deinother P3 from Hollabrunn is attributed to *D. aff. giganteum* by Thenius (1952: p. 133, table), who notes (p. 132) that such an attribution corresponds to a form between *D. levius* and *D. giganteum*. Indeed, the dimensions of the tooth plot at the lower values of *D. giganteum* from Montredon (MN 10, France; Tobien 1988; Ginsburg and Chevri er 2001), but also within *D. levius* from Massenhausen, Hinterauerbach (Germany; Gr af 1957) and Gusyatin (Ukraine; Svistun 1974). Additionally, a DP3 from Hollabrunn is attributed to *D. giganteum* by Huttunen (2002a, b; the author followed the two European deinother species concept of *Prodeinotherium bavaricum*–*Deinotherium giganteum*), but the tooth is smaller than the few known specimens of *D. giganteum*, and interestingly has close dimensions to the corresponding one from HAM, especially in terms of length (Fig. 7). The preserved cheek tooth of *Mastodon* sp. from

Hollabrunn (Sickenberg 1929) is much worn and does not provide any taxonomic information, however, a distal fragment of a M3 from “Schottergrube in Haslach am Reisberg bei Oberhollabrunn” is attributed by Schlesinger (1917: p. 101, pl. 17, fig. 1) to *Tetralophodon longirostris*. Importantly, the overall large mammal faunas from Hollabrunn and HAM have almost half of the taxa in common and are regarded roughly contemporaneous by Kirscher et al. (2016). The latter authors note faunal similarities also between HAM and Ingolstädter Straße 166 of Munich city (likewise in the central North Alpine Foreland Basin in Bavaria, Germany). From this site Stromer (1938) described a partial deinotherium skeleton and attributes it to *D. giganteum*, noting its small dental dimensions; later on, Gräf (1957: p. 144) places this find in the synonymy list of *D. levius*. Stromer (1938: p. 26, 1940: p. 60, pl. 3, fig. 13) described two m3 distal fragments of a gomphothere, ascribing them to cf. *Trilophodon angustidens* var. *subtapiroidea*, which later on Göhlich (1998: p. 67) attributes them to *G. cf. steinheimense*. Both authors note the difficulty in the identification of these fragments and the possibility that they could instead belong to *Tetralophodon*. Therefore, the presence of *Gomphotherium* at Ingolstädter Straße 166 is considered tentative.

Although the absence of a faunal element in a fossil assemblage (especially in the smaller ones and in particular concerning the rarer proboscideans) cannot be regarded as evidence of its nonexistence, the presence of *Gomphotherium* (together with *Tetralophodon*) at Massenhausen, and its absence to date at HAM (as well as at Atzelsdorf and other contemporaneous sites; *Gomphotherium* in the Eppelsheim Formation originates most probably from pre-Late Miocene deposits; see Göhlich 2020) may indicate a younger character for the HAM proboscidean fauna (Fig. 18). Hammerschmiede is either correlated after the extinction of *Gomphotherium* or at least to the period that captures its decline, which roughly coincides with the appearance of tetralophodont gomphotheres. Therefore, HAM (beginning of Tortonian; earliest Late Miocene) showcases the transition from the Middle Miocene trilophodont (*Gomphotherium*)-dominated faunas of central Europe (with Massenhausen and Großlappen, Germany, documenting some of the *Gomphotherium* last occurrences, and one of the first ones of *Tetralophodon* at the former) to the Late Miocene tetralophodont-dominated ones (*Tetralophodon*, and later on *Konobelodon* and *Anancus*). It seems thus possible that *Gomphotherium* did not manage to enter into the Late Miocene and possibly vanished close to the Seravallian/Tortonian boundary, when tetralophodonts seem to have been the major elephantimorph component. Therefore, the association *D. levius* and *T. longirostris* covers the Sarmatian and the base of Pannonian (Tortonian), while their association with *Gomphotherium* spp. correlates

to the Sarmatian, and thus can be regarded as a useful biochronologic tool for the central Europe terrestrial settings (Fig. 18). The demise and extinction of trilophodont gomphotheres could potentially be linked to the climatic changes that occurred during this epoch (see e.g., Böhme et al. 2008) as well as to the competition with the tetralophodont ones (see e.g., their broadly similar dental mesowear signal), or both. Whether tetralophodont gomphotheres contributed to the extinction of trilophodont gomphotheres through direct competition for resources or filled the gap left by the decline and extinction of the latter is difficult to prove, and beyond the scope of this study. However, it emphasizes the need for further and systematic research into this topic, and proboscidean material from localities correlated to this time interval such as HAM, as well as the discovery of new ones from controlled stratigraphic contexts, is crucial.

Supplementary information The online version contains supplementary material available at <https://doi.org/10.1007/s10914-023-09683-3>.

Acknowledgements The authors would like to express their special thanks to the two private collectors †S. Guggenmos (Dörsingen) and M. Schmid (Marktobersdorf) for the great cooperation and the transfer and making available of their finds and records. Further, we wish to thank C. Kyriakouli and A.-C. Grupp for the preparation of the partial skeleton of the juvenile deinotherium (both at that time at SNSB) and H. Stöhr (GPIT) for the preparation of the other specimens. We thank A. Fatz (Tübingen) for providing photographs of the fossil material, and G. Ferreira and C. Kyriakouli (both Tübingen) for realizing the μ CT scanning. We acknowledge all participants of the numerous excavations in the Hammerschmiede fossil site since 2011, who helped to detect and collect the studied material. Since 2020, the excavations and associated research were supported by the Bavarian State Ministry of Research and the Arts, and by the Bavarian Natural History Collections (SNSB). G.K. would like to thank for granting access to collections at their disposal: O. Sandrock (HLMD), G. Rössner (SNSB-BSPG), U. Göhlich (NHMW), P. Tassy (MNHN), M. Gasparik (HNHM), L. Kordos (HGI), D. Berthet (ML), A. Prieur (FSL), and I. Werneburg (GPIT). G.K. was supported by the European Union-funded Integrated Activities grant SYNTHESES (AT-TAF-3825 and HU-TAF-1683), and DFG-463225251 (“MEGALOPOLIS”). We thank the editor D. Croft, and the reviewers J. Saarinen and one anonymous, for their constructive comments and suggestions.

Authors' contributions Conceptualization: G.K., M.B. Formal analysis: G.K. Investigation: G.K., T.L., P.K., M.B. Methodology: G.K. Project administration: M.B. Validation: G.K., M.B. Visualization: G.K., T.L., M.B. Writing – original draft: G.K., T.L., M.B. Writing – review and editing: G.K., T.L., P.K., M.B.

Funding Open Access funding enabled and organized by Projekt DEAL.

Availability of data and materials All data are included in this published article and its supplementary information files.

Declarations

Competing interests The authors have no competing interests to declare that are relevant to the content of this article.

Open Access This article is licensed under a Creative Commons Attribution 4.0 International License, which permits use, sharing, adaptation, distribution and reproduction in any medium or format, as long as you give appropriate credit to the original author(s) and the source, provide a link to the Creative Commons licence, and indicate if changes were made. The images or other third party material in this article are included in the article's Creative Commons licence, unless indicated otherwise in a credit line to the material. If material is not included in the article's Creative Commons licence and your intended use is not permitted by statutory regulation or exceeds the permitted use, you will need to obtain permission directly from the copyright holder. To view a copy of this licence, visit <http://creativecommons.org/licenses/by/4.0/>.

References

- Abramoff MD, Magalhães, PJ, Ram SJ (2004) Image processing with ImageJ. *Biophotonics Int* 11:36–42.
- Alba DM, Gasamans N, Pons-Monjo G, Luján ÀH, Robles JM, Obradó P, Casanovas-Vilar I (2020) Oldest *Deinotherium proavum* from Europe. *J Vertebr Paleontol* 40:e1775624.
- Álvarez-Lao DJ, Méndez M (2011) Ontogenetic changes and sexual dimorphism in the mandible of adult woolly mammoths (*Mammuthus primigenius*). *Geobios* 44:335–343.
- Aiglstorfer M, Göhlich UB, Böhme M, Gross M (2014a) A partial skeleton of *Deinotherium* (Proboscidea, Mammalia) from the late Middle Miocene Gratkorn locality (Austria). *Palaeobiodivers Palaeoenvirons* 94:49–70.
- Aiglstorfer M, Bocherens H, Böhme M (2014b) Large mammal ecology in the late Middle Miocene Gratkorn locality (Austria). *Palaeobiodivers Palaeoenvirons* 94:189–213.
- Alberdi MT (1971) Primer ejemplar completo de un *Tetralophodon longirostris* Kaup, 1835, encontrado en España. *Estud Geol* 27:181–196.
- Ameen M, Khan A, Tahir Waseem M, Ahmad R, Iqbal A, Rafeh A, Imran M (2020) Were late gomphotheres (Plio-Pleistocene) of the Siwaliks at more stress as compared to early gomphotheres (middle to late Miocene)? *J Bioresour Manag* 7:117–130.
- Antunes MT, Mazo AV (1983) Quelques mastodontes Miocènes du Portugal. *Ciênc Terra* 7:115–128.
- Arambourg C (1934) Le *Deinotherium* des gisements de l'Omo. *C R Soc Géol Fr* 1934:86–87.
- Bach F (1910) Mastodonreste aus der Steiermark. *Beitr Paläont Geol Öster-Ung und des Orients* 23:63–123.
- Bakalov P, Nikolov I (1962) Les Fossiles de Bulgarie. X. Mammifères Tertiaires. *Académie des Sciences de Bulgarie, Sofia*.
- Bakalov P (1914) Beiträge zur Paläontologie Bulgariens. II. *Dinotheriumreste aus Bulgarien*. *Ann Univ Sofia* 8–9:1–29.
- Behrensmeyer AK (1975) The taphonomy and paleoecology of Plio-Pleistocene vertebrate assemblages east of Lake Rudolf, Kenya. *Bull Mus Comp Zool* 146:473–578.
- Bergounioux FM, Crouzel F (1960) *Tetralophodon curvirostris* n. sp. (Mamm., Proboscidea) aus dem Unterpliozän (Pontien) von Esselborn (Rheinessen). *Jahresber Mitt Oberrhein Geol Ver* 42:109–121.
- Binford LR (1981) *Bones: Ancient Men and Modern Myths*. Academic Press, New York.
- Böhme M, Ilg A, Winkhofer M (2008) Late Miocene “washhouse” climate in Europe. *Earth Planet Sci Lett* 275:393–401.
- Böhme M, Aiglstorfer M, Uhl D, Kullmer O (2012) The antiquity of the Rhine River: Stratigraphic coverage of the Dinotheriensande (Eppelsheim Formation) of the Mainz Basin (Germany). *PLoS One* 7:e36817.
- Böhme M, Spassov N, Fuss J, Tröscher A, Deane AS, Prieto J, Kirscher U, Lechner T, Begun DR (2019) A new Miocene ape and locomotion in the ancestor of great apes and humans. *Nature* 575:489–493.
- Böhme M, Spassov N, DeSilva JM, Begun DR (2020) Reply to: Reevaluating bipedalism in *Danuvius*. *Nature* 586: E4–E5.
- Bonaparte CL (1845) *Catalogo Metodico dei Mammiferi Europei*. Luigi di Giacomo Pirola, Milan.
- Brain CK (1981) *The Hunters or the Hunted? An Introduction to African Cave Taphonomy*. The University of Chicago Press, Chicago and London.
- Calandra I, Göhlich UB, Merceron G (2008) How could sympatric megaherbivores coexist? Example of niche partitioning within a proboscidean community from the Miocene of Europe. *Naturwissenschaften* 95:831–838.
- Casanovas-Vilar I, Madern A, Alba DM, Cabrera L, García-Paredes I, van den Hoek Ostende LW, DeMiguel D, Robles JM, Furió M, van Dam JA, Garcés M, Angelone C, Moyà-Solà S (2016) The Miocene mammal record of the Vallès-Penedès Basin (Catalonia). *C R Palevol* 15:791–812.
- Crouzel F (1947) Une variété de *Dinotherium levius* dans le Miocène de Montréjeau. *Bull Soc hist nat Toulouse* 82:105–109.
- Crouzel F, Debeaux M (1957) Découverte de *Tetralophodon longirostris* près de Montréjeau (Haute-Garonne). *Bull Soc hist nat Toulouse* 92:202–204.
- Cuvier G (1817) *Le Règne Animal*. Déterville, Paris.
- Delmer C (2009) Reassessment of the generic attribution of *Numidotherium savagei* and the homologies of lower incisors in proboscideans. *Acta Palaeontol Pol* 54:561–580.
- Depéret C (1887) Recherches sur la succession des faunes de vertébrés miocènes de la vallée du Rhône. *Arch Mus hist nat Lyon* 4:45–313.
- Doppler G (1989) Zur Stratigraphie der nördlichen Vorlandmolasse in Bayerisch-Schwaben. *Geol Bavar* 94:83–133.
- Duranthon F, Antoine PO, Laffont D, Bilotte M (2007) Contemporanéité de *Prodeinotherium* et *Deinotherium* (Mammalia, Proboscidea) à Castelnau-Magnoac (Hautes-Pyrénées, France). *Rev Paléobiol* 26:403–411.
- Eichwald E (1831) *Zoologia Specialis Quam Expositis Animalibus Tum Vivis, Tum Fossilibus Potissimum Rossiae in Universum, et Poloniae in Specie*. Josephi Zawadzki, Vilnae.
- Falconer H (1857) On the species of mastodon and elephant occurring in the fossil state in Great Britain. Part I. *Mastodon*. *Q J Geol Soc Lond* 13:307–360.
- Ferretti MP, Rook L, Torre D (2003) *Stegotetralodon* (Proboscidea, Elephantidae) from the Late Miocene of southern Italy. *J Vertebr Paleontol* 23:659–666.
- Fuss J, Prieto J, Böhme M (2015) Revision of the boselaphin bovid *Miotragocerus monacensis* Stromer, 1928 (Mammalia, Bovidae) at the Middle to Late Miocene transition in Central Europe. *N Jb Min Geol Paläont – Abh* 276:229–265.
- Gagliardi F, Maridet O, Becker D (2021) The record of Deinotheriidae from the Miocene of the Swiss Jura Mountains (Jura Canton, Switzerland). *bioRxiv* 244061, ver. 4 peer-reviewed by PCI Paleo, 2020.2008.2010.244061.
- Garevski R, Markov GN (2011) A *Deinotherium gigantissimum* (Mammalia, Proboscidea) palate with deciduous dentition from the area of Veles, Republic of Macedonia. *Paläont Z* 85:33–36.
- Gasparik M (2004) *Magyarországi Neogén és Also-Pleisztocén Proboscidea Maradványok*. Dissertation, Magyar Természettudományi Múzeum, Budapest.
- Gasparik M (2005) Proboscidean remains from the Pannonian of Rudabánya. *Palaeontogr Ital* 90:181–192.
- Gaziry AW (1976) Jungtertiäre Mastodonten aus Anatolien (Türkei). *Geol Jb* 22:3–143.
- Gaziry AW (1994) Über Mastodonten (Mammalia, Proboscidea) aus den Dinotheriensanden (M-Europa: Ober-Miozän): Materialien des Hessischen Landesmuseums Darmstadt. *Verh naturwiss Ver Hamburg* 34:95–112.

- Gaziry AW (1997) Die Mastodonten (Proboscidea, Mammalia) aus Dorn-Dürkheim I (Rheinhausen). Cour Forsch-Inst Senckenberg 197:73–115.
- Geraads D, Kaya T, Mayda S (2005) Late Miocene large mammals from Yulafli, Thrace region, Turkey, and their biogeographic implications. Acta Palaeontol Pol 50:523–544.
- Ginsburg L, Chevrier F (2001) Les Dinotheres du bassin de la Loire et l'évolution du genre *Deinotherium* en France. Symbioses 5:9–24.
- Göhlich UB (1998) Elephantoidea (Proboscidea, Mammalia) aus dem Mittel- und Obermiozän der Oberen Süßwassermolasse Süddeutschlands: Odontologie und Osteologie. Münchner Geowiss Abh A Geol Paläont 36:1–245.
- Göhlich UB (1999) Order Proboscidea. In: Rössner GE, Heissig K (eds) The Miocene Land Mammals of Europe. Dr. Friedrich Pfeil, Munich, pp 157–168.
- Göhlich UB (2010) The Proboscidea (Mammalia) from the Miocene of Sandelzhausen (southern Germany). Paläont Z 84:163–204.
- Göhlich UB (2020) The proboscidean fauna (Mammalia) from the middle Miocene lignites of Gračanica near Bugojno (Bosnia–Herzegovina). Palaeobiodivers Palaeoenviron 100:413–436.
- Göhlich UB, Huttunen K (2009) The early Vallesian vertebrates of Atzelsdorf (Late Miocene, Austria) 12. Proboscidea. Ann Naturhist Mus Wien 111A:635–646.
- Gräf IE (1957) Die Prinzipien der Artbestimmung bei *Dinotherium*. Palaeontographica 108:131–185.
- Hammer Ø, Harper DAT, Ryan PD (2001) PAST: paleontological statistics software package for education and data analysis. Palaeontol Electron 4:1–9.
- Harris JM (1976) Cranial and dental remains of *Deinotherium bozasi* (Mammalia: Proboscidea) from East Rudolf, Kenya. Zool J Linn Soc 178:57–75.
- Harris JM (1983) Deinotheriidae. In: Harris JM (ed) Koobi Fora Research Project, Volume 2: The Fossil Ungulates: Proboscidea, Perissodactyla, and Suidae. Clarendon Press, Oxford, pp 22–39.
- Hartung J, Böhme M (2022) Unexpected cranial sexual dimorphism in the tragulid *Dorcatherium naui* based on cranial material from the middle to late Miocene localities of Eppelsheim and Hammerschmiede (Germany). PLoS ONE 17: e0267951.
- Hartung J, Lechner T, Böhme M (2020) New cranial material of *Miotragocerus monacensis* (Mammalia: Bovidae) from the late Miocene hominid locality Hammerschmiede (Germany). Neues Jahrb Geol Paläontol - Abh 298:269–284.
- Hautier L, Mackaye HT, Lihoreau F, Tassy P, Vignaud P, Brunet M (2009) New material of *Anancus kenyensis* (Proboscidea, Mammalia) from Toros-Menalla (Late Miocene, Chad): Contribution to the systematics of African anancines. J African Earth Sci 53:171–176.
- Hay OP (1922) Further observations on some extinct elephants. Proc Biol Soc Wash 35:97–101.
- Haynes G (1988) Longitudinal studies of African elephant death and bone deposits. J Archaeol Sci 15:131–157.
- Haynes G. (1991) Mammoths, Mastodonts and Elephants: Biology, Behavior, and the Fossil Record. Cambridge University Press, Cambridge.
- Huttunen K (2002a) Systematics and taxonomy of the European Deinotheriidae (Proboscidea, Mammalia). Ann Naturhist Mus Wien 103A:237–250.
- Huttunen K (2002b) Deinotheriidae (Proboscidea, Mammalia) dental remains from the Miocene of Lower Austria and Burgenland. Ann Naturhist Mus Wien 103A:251–285.
- Huttunen K, Göhlich UB (2002) A partial skeleton of *Prodeinotherium bavarium* (Proboscidea, Mammalia) from the Middle Miocene of Untertzolling (Upper Freshwater Molasse, Germany). Geobios 35:489–514.
- Illiger C (1811) Prodromus Systematis Mammalium et Avium Additis Terminis Zoographicis Utriusque Classis. C. Salfeld, Berlin.
- Jourdan M (1861) Des terrains sidérolitiques. C R Hebd Séances Acad Sci 53:1009–1014.
- Kargopoulos N (2022) The carnivorans (Carnivora, Mammalia) from the hominid locality of Hammerschmiede (Bavaria, Germany). Dissertation, University of Tübingen, Tübingen.
- Kargopoulos N, Kampouridis P, Lechner T, Böhme M (2021a) A review of *Semigenetta* (Viverridae, Carnivora) from the Miocene of Eurasia based on material from the hominid locality of Hammerschmiede (Germany). Geobios 69:25–36.
- Kargopoulos N, Kampouridis P, Lechner T, Böhme M (2021b) Hyainidae (Carnivora) from the Late Miocene hominid locality of Hammerschmiede (Bavaria, Germany). Hist Biol 34:2249–2258.
- Kargopoulos N, Valenciano A, Abella J, Kampouridis P, Lechner T, Böhme M (2022) The exceptionally high diversity of small carnivorans from the Late Miocene hominid locality of Hammerschmiede (Bavaria, Germany). PLoS ONE 17: e0268968.
- Kargopoulos N, Valenciano A, Kampouridis P, Lechner T, Böhme M (2021c) New early late Miocene species of *Vishnuonyx* (Carnivora, Lutrinae) from the hominid locality of Hammerschmiede, Bavaria, Germany. J Vertebr Paleontol 41:e1948858.
- Kaup J (1829) *Deinotherium giganteum*. Eine Gattung der Vorwelt aus der Ordnung der Pachydermen. Isis 22:401–404.
- Kaup JJ (1832a) Description d'Ossements Fossiles de Mammifères Inconnus Jusqu'à Présent, qui se Trouvent au Muséum Grand-ducal de Darmstadt. J.G. Heyer, Darmstadt.
- Kaup J (1832b) Ueber zwei Fragmente eines Unterkiefers von *Mastodon angustidens* Cuv., nach welchen diese Art in die Gattung *Tetracaulodon* Godmann gehört. Isis 25:628–631.
- Kaup JJ (1835) Description d'Ossements Fossiles de Mammifères Inconnus Jusqu'à-Présent qui se Trouvent au Muséum Grand-ducal de Darmstadt. Diehl, J.P., Darmstadt, pp 65–89.
- Kaup JJ, Scholl JB (1864) Verzeichnis der Gypsabgüsse von den ausgezeichnetsten urweltlichen Thierresten des Großherzoglichen Museums zu Darmstadt, Darmstadt.
- Khomenko J (1914) La faune méotique du village Taraklia du district de Bendery. Trudy Bessarab Obsh Est liub est 5:1–55
- Kirscher U, Prieto J, Bachtadse V, Abdul Aziz H, Doppler G, Hagmaier M, Böhme M (2016) A biochronologic tie-point for the base of the Tortonian stage in European terrestrial settings: Magnetostratigraphy of the topmost Upper Freshwater Molasse sediments of the North Alpine Foreland Basin in Bavaria (Germany). Newsl Stratigr 49:445–467.
- Klähn H (1922) Die badischen Mastodonten und ihre süddeutschen Verwandten. Verlag von Gebrüder Borntraeger, Berlin.
- Klähn H (1931) Rheinhesisches Pliozän besonders Unterpliozän im Rahmen des Mitteleuropäischen Pliozäns. Geol Paläont Abh 18:279–340.
- Konidaris GE, Koufos GD (2016) Palaeontology of the upper Miocene vertebrate localities of Nikiti (Chalkidiki Peninsula, Macedonia, Greece). Proboscidea. Geobios 49:37–44.
- Konidaris GE, Koufos G (2019) Late Miocene proboscideans from Samos Island (Greece) revisited: new specimens from old collections. Paläont Z 93:115–134.
- Konidaris GE, Roussiakis SJ (2019) The first record of *Anancus* (Mammalia, Proboscidea) in the late Miocene of Greece and reappraisal of the primitive anancines from Europe. J Vertebr Paleontol 38:e1534118.
- Konidaris GE, Tsoukala E (2020) Proboscideans from the upper Miocene localities of Thermopigi, Neokaisareia and Platania (Northern Greece). Ann Paléontol 106:102380.
- Konidaris GE, Tsoukala E (2022) The fossil record of the Neogene Proboscidea (Mammalia) in Greece. In: Vlachos E (ed) The Fossil Vertebrates of Greece Vol. 1. Springer – Nature Publishing Group, Cham, pp 299–344.
- Konidaris GE, Tourloukis V (2021) Proboscidea-*Homo* interactions in open-air localities during the Early and Middle Pleistocene of

- western Eurasia: a palaeontological and archaeological perspective. In: Konidaris GE, Barkai R, Tourloukis V, Harvati K (eds) *Human-Elephant Interactions: From Past to Present*. Tübingen University Press, Tübingen, pp 67–104.
- Konidaris GE, Roussiakis SJ, Theodorou GE, Koufos GD (2014) The Eurasian occurrence of the shovel-tusker *Konobelodon* (Mammalia, Proboscidea) as illuminated by its presence in the late Miocene of Pikermi (Greece). *J Vertebr Paleontol* 34:1437–1453.
- Konidaris GE, Roussiakis SJ, Athanassiou A, Theodorou GE (2017) The huge-sized deinother *Deinotherium proavum* (Proboscidea, Mammalia) from the Late Miocene localities Pikermi and Halmypopotamos (Greece). *Quat Int* 430:5–21.
- Kovachev D (2004) Cranium of *Stegotrabelodon* (Proboscidea, Mammalia) from the Neogene in the East Maritsa basin. *Rev Bulg Geol Soc* 65:167–173.
- Larramendi A (2016) Shoulder height, body mass, and shape of proboscideans. *Acta Palaeontol Pol* 61:537–574.
- Lartet E (1859) Sur la dentition des proboscidiens fossiles (*Dinotherium*, mastodontes et éléphants) et sur la distribution géographique et stratigraphique de leurs débris en Europe. *Bull Soc Géol Fr* 16:469–515.
- Lechner T, Böhme M (2022) The beaver *Steneofiber depereti* from the lower Upper Miocene hominid locality Hammerschmiede and remarks on its ecology. *Acta Palaeontol Pol* 67: 807–826.
- Lechner T, Böhme M (2023) The largest record of the minute beaver *Euroxenomys minutus* (Mammalia, Castoridae) from the early Late Miocene hominid locality Hammerschmiede (Bavaria, Southern Germany) and palaeoecological considerations. *Hist Biol*. <https://doi.org/10.1080/08912963.2023.2215236>
- Linnaeus C (1758) *Systema Naturae per Regna Tria Naturae, Secundum Classes, Ordines, Genera, Species, cum Characteribus, Differentiis, Synonymis Locis*. Tomus 1. Laurentius Salvius, Stockholm.
- Mayr G, Lechner T, Böhme M (2020a) A skull of a very large crane from the late Miocene of Southern Germany, with notes on the phylogenetic interrelationships of extant Gruinae. *J Ornithol* 161:923–933.
- Mayr G, Lechner T, Böhme M (2020b) The large-sized darter *Anhinga pannonica* (Aves, Anhingidae) from the late Miocene hominid Hammerschmiede locality in Southern Germany. *PLoS ONE* 15:e0232179.
- Mayr G, Lechner T, Böhme M (2022) Nearly complete leg of an unusual, shelduck-sized anseriform bird from the earliest late Miocene hominid locality Hammerschmiede (Germany). *Hist Biol* 35:465–474.
- Mayr H, Fahlbusch (1975). Eine unterpliozäne Kleinsäugerfauna aus der Oberen Süßwasser-Molasse Bayerns. *Mitt Bayer Staatssamm Paläontol Hist Geol* 15:91–111.
- Mazo AV, Montoya P (2003) Proboscidea (Mammalia) from the Upper Miocene of Crevillente (Alicante, Spain). *Scr Geol* 126:79–109.
- Mazo AV, van der Made J (2012) Iberian mastodonts: Geographic and stratigraphic distribution. *Quat Int* 255:239–256.
- Mazo AV, Jordá Pardo JF (1997) Un *Tetralophodon longirostris* (Kaup, 1832) (Proboscidea, Mammalia) en el Mioceno medio de Villavieja del Cerro (sector central de la cuenca del Duero, Valladolid). *Rev Soc Geol Esp* 10:219–235.
- Metz-Muller F (1995) Mise en évidence d'une variation intraspécifique des caractères dentaires chez *Anancus arvernensis* (Proboscidea, Mammalia) du gisement de Dorkovo (Pliocène ancien de Bulgarie, biozone MN14). *Geobios* 28:737–743.
- Metz-Muller F (2000) La population d'*Anancus arvernensis* (Proboscidea, Mammalia) du Pliocène de Dorkovo (Bulgarie); étude des modalités évolutives d'*Anancus arvernensis* et phylogénie du genre *Anancus*. Dissertation, Muséum National d'Histoire Naturelle, Paris.
- Mottl M (1969) Bedeutende Proboscider-Neufunde aus dem Altpliozän (Pannonien) Südost-Österreichs. *Österreichische Akademie der Wissenschaften. Mathematisch-naturwissenschaftliche Klasse. Denkschriften* 115:1–50.
- Osborn HF (1921) The evolution, phylogeny, and classification of the Proboscidea. *Am Mus Novit* 1:1–15.
- Osborn HF (1936) Proboscidea. A Monograph of the Discovery, Evolution, Migration and Extinction of the Mastodonts and Elephants of the World, Volume I: Moeritherioidea, Deinotherioidea, Mastodontoidea. American Museum Press, New York.
- Pickford M, Pourabrishami Z (2013) Deciphering Dinotherien-sande deinotheriid diversity. *Palaeobiodivers Palaeoenviro* 93:121–150.
- Prieto J (2012) The genus *Eomyops* Engesser, 1979 (Rodentia, Eomyidae) from the youngest deposits of the German part of the North Alpine Foreland Basin. *Swiss J Palaeontol* 131:95–106.
- Prieto J, Rummel M (2009) Evolution of the genus *Collimys* Daxner-Höck, 1972 (Rodentia, Cricetidae) a key to Middle to Late Miocene biostratigraphy in Central Europe. *Neues Jahrb Geol Paläontol Abh* 252:237–247.
- Prieto J, van Dam JA (2012) Primitive Anourosoricini and Allosoricinae from the Miocene of Germany. *Geobios* 45:581–589.
- Prieto J, van den Hoek Ostende LW, Böhme M, Braze M (2011) Reappearance of *Galerix* (Erinaceomorpha, Mammalia) at the Middle to Late Miocene transition in South Germany: biostratigraphic and palaeoecologic implications. *Contrib Zool* 80:179–189.
- Saarinen J, Lister AM (2016) Dental mesowear reflects local vegetation and niche separation in Pleistocene proboscideans from Britain. *J Quat Sci* 31:799–808.
- Saarinen J, Karne A, Cerling TE, Uno K, Säilä L, Kasiki S, Ngene S, Obari T, Mbua E, Manthi FK, Fortelius M (2015) A new tooth wear-based dietary analysis method for Proboscidea (Mammalia). *J Vertebr Paleontol* 35:e918546.
- Sach VJ, Heizmann EPJ (2001) Stratigraphie und Säugetierfaunen der Brackwassermolasse in der Umgebung von Ulm (Südwestdeutschland). *Stuttgarter Beiträge zur Naturkunde, Serie B (Geologie und Paläontologie)* 310:1–95.
- Sanders WJ (2003) Proboscidea. In: Fortelius M, Kappelman J, Sen S, Bernor RL (eds) *Geology and Paleontology of the Miocene Sinap Formation, Turkey*. Columbia University Press, New York, pp 202–219.
- Schlesinger G (1917) Die Mastodonten des K. K. Naturhistorischen Hofmuseums. *Denkschr K K Nat Hofmus* 1:1–230.
- Shoshani J, Tassy P (1996) Summary, conclusions, and a glimpse into the future. In: Shoshani J, Tassy P (eds) *The Proboscidea: Evolution and Palaeoecology of Elephants and their Relatives*. Oxford University Press, New York, pp 335–348.
- Shoshani J, Golenberg EM, Yang H (1998) Elephantidae phylogeny: morphological versus molecular results. *Acta Theriol Suppl* 5:89–122.
- Sickenberg O (1928) Säugetierreste aus der Umgebung von Oberholbrunn. *Verhandl Geol Bundesanst Wien* 9–10:205–210.
- Sickenberg O (1929) Eine neue Antilope und andere Säugetierreste aus dem Obermiozän Niederösterreichs. *Paläobiologica* 2:62–88.
- Simionescu I, Barbu V (1939) Mamiferele pliocene dela Cimişlia (România). III. Proboscidieni. *Acad Rom Public Fondul V Adam* 9:1–20.
- Stefanescu G (1892) On the existence of the *Dinotherium* in Roumania. *Bull Geol Soc Am* 3:81–83.
- Stehlin HG (1925) Catalogue des ossements de mammifères Tertiaires de la collection Bourgeois à l'École de Pont-Levoy (Loiret-Cher). *Bull Soc hist nat Anthropol Loiret-Cher* 18:77–277.
- Steininger F (1965) Ein bemerkenswerter Fund von *Mastodon (Bunolophodon) longirostris* Kaup 1832 (Proboscidea, Mammalia) aus dem Unterpliozän (Pannon) des Hausruck-Kobernauberwald-Gebietes in Oberösterreich. *Jb Geol Bundesanst* 108:195–212.

- Stromer E (1938) Huftier-Reste aus dem unterstpliocänen Flinzsande Münchens. Abh Bayer Akad Wiss Math-Naturwiss Abt 44:1–39.
- Stromer E (1940) Die jungtertiäre Fauna des Flinzes und des Schweißsandens von München. Nachträge und Berichtigungen. Abh Bayer Akad Wiss Math-naturwiss Abt 48:1–106.
- Svistun VI (1974) Dinotheriums of Ukraine. Naukova Dumka, Kiev.
- Tassy P (1985) La place des mastodontes Miocènes de l’Ancien Monde dans la phylogénie des Proboscidea (Mammalia): Hypothèses et conjectures. Dissertation, Université Pierre et Marie Curie, Paris.
- Tassy P (1986) Nouveaux Elephantoidea (Mammalia) dans le Miocène du Kenya. CNRS, Paris.
- Tassy P (1987) A hypothesis on the homology of proboscidean tusks based on paleontological data. Am Mus Novit 2895:1–18.
- Tassy P (1990) The “Proboscidean Datum Event”: how many proboscideans and how many events? In: Lindsay EH, Mein P, Fahlbusch V (eds) European Neogene Mammal Chronology. Plenum Press, New York, pp 237–252.
- Tassy P. (1996a) Dental homologies and nomenclature in the Proboscidea. In: Shoshani J, Tassy P (eds) The Proboscidea: Evolution and Palaeoecology of Elephants and their Relatives. Oxford University Press, New York, pp 21–25.
- Tassy P (1996b) Growth and sexual dimorphism among Miocene elephantoids: the example of *Gomphotherium angustidens*. In: Shoshani J, Tassy P (eds) The Proboscidea: Evolution and Palaeoecology of Elephants and their Relatives. Oxford University Press, New York, pp 92–100.
- Tassy P. (1999) Miocene elephantids (Mammalia) from the emirate of Abu Dhabi, United Arab Emirates: Palaeobiogeographic implications. In: Whybrow PJ, Hill A (eds) Fossil Vertebrates of Arabia. Yale University Press, New Haven and London, pp 209–233.
- Tassy P (2013) L’anatomie cranio-mandibulaire de *Gomphotherium angustidens* (Cuvier, 1817) (Proboscidea, Mammalia): données issues du gisement d’En Pèjouan (Miocène moyen du Gers, France). Geodiversitas 35:377–445.
- Tassy P (2014) L’odontologie de *Gomphotherium angustidens* (Cuvier, 1817) (Proboscidea, Mammalia): données issues du gisement d’En Pèjouan (Miocène moyen du Gers, France). Geodiversitas 36:35–115.
- Tassy P (2016) Proboscidea. In: Sen S (ed) Late Miocene mammal locality of Küçükçekmece, European Turkey. Geodiversitas 38(2):261–271.
- Thenius E (1952) Die Säugetierreste aus dem Jungtertiär des Hausruck und Kobernauberwaldes (O.-Österr.) und die Alterstellung der Fundschichten. Jb Geol Bundesanst Wien 95:119–144.
- Tobien H (1973) On the evolution of mastodonts (Proboscidea, Mammalia). Part I: The bunodont trilophodont groups. Notizbl hess Landesamt Bodenforsch 101:202–276.
- Tobien H (1978) On the evolution of mastodonts (Proboscidea, Mammalia). Part 2: The bunodont tetralophodont groups. Geol Jb Hessen 106:159–208.
- Tobien H. (1980) A note on the mastodont taxa (Proboscidea, Mammalia) of the “Dinotheriensande” (Upper Miocene, Rheinhessen, Federal Republic of Germany). Mainzer geowiss Mitt 9:187–201.
- Tobien H (1988) Contributions a l’étude du gisement miocene supérieur de Montredon (Herauld). Les grands mammifères. 7 – les proboscidiens Deinotheriidae. Palaeovertebrata, Mém ext 1988:135–175.
- Tobien H (1996) Evolution of zygodons with emphasis on dentition. In: Shoshani J, Tassy P (eds) The Proboscidea: Evolution and Palaeoecology of Elephants and their Relatives. Oxford University Press, New York, pp 76–85.
- van der Maarel FH (1932) Contributions to the knowledge of the fossil mammalian fauna of Java. Wet Meded Dienst Mijnb Nederlandsch-Indië 15:1–208.
- Vergiev S, Markov GN (2012) Fossil proboscideans (Mammalia) from the collections of the Varna Regional Museum of History. Acta Zool Bulg 64:427–438.
- von Meyer H (1831) Mittheilung an geheimen Rath von Leonhard. Jb Min Geogn Geol Petrefaktenkunde 2:296–297.
- Voorhies MR (1969) Taphonomy and population dynamics of an early Pliocene vertebrate fauna, Knox County, Nebraska. Rocky Mt Geol 8:1–69.
- Wagner A (1848) Urvweltliche Säugthier-Ueberreste aus Griechenland. Abh Bayer Akad Wiss 5:335–378.
- Wagner A (1857) Neue Beiträge zur Kenntnis der fossilen Säugthier-Ueberreste von Pikermi. Abh Bayer Akad Wiss 8:109–158.
- Xafis A, Saarinen J, Bastl K, Nagel D, Grímsson F (2020) Palaeodietary traits of large mammals from the middle Miocene of Gračanica (Bugojno Basin, Bosnia-Herzegovina). Palaeobiodivers Palaeoenvir 100:457–477.

Terms and Conditions

Springer Nature journal content, brought to you courtesy of Springer Nature Customer Service Center GmbH (“Springer Nature”).

Springer Nature supports a reasonable amount of sharing of research papers by authors, subscribers and authorised users (“Users”), for small-scale personal, non-commercial use provided that all copyright, trade and service marks and other proprietary notices are maintained. By accessing, sharing, receiving or otherwise using the Springer Nature journal content you agree to these terms of use (“Terms”). For these purposes, Springer Nature considers academic use (by researchers and students) to be non-commercial.

These Terms are supplementary and will apply in addition to any applicable website terms and conditions, a relevant site licence or a personal subscription. These Terms will prevail over any conflict or ambiguity with regards to the relevant terms, a site licence or a personal subscription (to the extent of the conflict or ambiguity only). For Creative Commons-licensed articles, the terms of the Creative Commons license used will apply.

We collect and use personal data to provide access to the Springer Nature journal content. We may also use these personal data internally within ResearchGate and Springer Nature and as agreed share it, in an anonymised way, for purposes of tracking, analysis and reporting. We will not otherwise disclose your personal data outside the ResearchGate or the Springer Nature group of companies unless we have your permission as detailed in the Privacy Policy.

While Users may use the Springer Nature journal content for small scale, personal non-commercial use, it is important to note that Users may not:

1. use such content for the purpose of providing other users with access on a regular or large scale basis or as a means to circumvent access control;
2. use such content where to do so would be considered a criminal or statutory offence in any jurisdiction, or gives rise to civil liability, or is otherwise unlawful;
3. falsely or misleadingly imply or suggest endorsement, approval, sponsorship, or association unless explicitly agreed to by Springer Nature in writing;
4. use bots or other automated methods to access the content or redirect messages
5. override any security feature or exclusionary protocol; or
6. share the content in order to create substitute for Springer Nature products or services or a systematic database of Springer Nature journal content.

In line with the restriction against commercial use, Springer Nature does not permit the creation of a product or service that creates revenue, royalties, rent or income from our content or its inclusion as part of a paid for service or for other commercial gain. Springer Nature journal content cannot be used for inter-library loans and librarians may not upload Springer Nature journal content on a large scale into their, or any other, institutional repository.

These terms of use are reviewed regularly and may be amended at any time. Springer Nature is not obligated to publish any information or content on this website and may remove it or features or functionality at our sole discretion, at any time with or without notice. Springer Nature may revoke this licence to you at any time and remove access to any copies of the Springer Nature journal content which have been saved.

To the fullest extent permitted by law, Springer Nature makes no warranties, representations or guarantees to Users, either express or implied with respect to the Springer nature journal content and all parties disclaim and waive any implied warranties or warranties imposed by law, including merchantability or fitness for any particular purpose.

Please note that these rights do not automatically extend to content, data or other material published by Springer Nature that may be licensed from third parties.

If you would like to use or distribute our Springer Nature journal content to a wider audience or on a regular basis or in any other manner not expressly permitted by these Terms, please contact Springer Nature at

onlineservice@springernature.com

Chapter 7

Taxonomy and Ecology of the beaver *Steneofiber depereti* (Mammalia, Castoridae)

Published in

Lechner, T., Böhme, M., 2022. The beaver *Steneofiber depereti* from the lower Upper Miocene hominid locality Hammerschmiede and remarks on its ecology. *Acta Palaeontologica Polonica* 67 (4), 807-826.
<https://doi.org/10.4202/app.00997.2022>

This chapter is a reprint of the published version and differs from the general chapter numbering of this dissertation.

The beaver *Steneofiber depereti* from the lower Upper Miocene hominid locality Hammerschmiede and remarks on its ecology

THOMAS LECHNER and MADELAINE BÖHME



Lechner, T. and Böhme, M. 2022. The beaver *Steneofiber depereti* from the lower Upper Miocene hominid locality Hammerschmiede and remarks on its ecology. *Acta Palaeontologica Polonica* 67 (4): 807–826.

Dental remains of a medium sized beaver from the early Late Miocene Hammerschmiede locality (MN 7/8) in the Northern Alpine Foreland Basin (Southern Germany, Bavaria) are described and assigned to *Steneofiber depereti*. The numerous material (160 teeth) was collected in the two fossiliferous layers HAM 5 and HAM 4 and comprises beaver individuals of a large range of age classes, from juvenile to old. The dental remains metrically and morphologically overlap the stratigraphic older *Steneofiber* spp. and the younger *Chalicomys* spp. This supports the hypothesis of the European anagenetic evolutionary lineage *Steneofiber depereti*–*Chalicomys jaegeri*. The morphological characters to differentiate *Steneofiber depereti* and *Chalicomys jaegeri* are discussed and redefined. The performed age–frequency distribution (Mortality profile) indicates a natural ecological mortality and confirms that at least the fluvial channel of the HAM 4 deposits was the actual optimal beaver habitat and continuously populated by larger family groups of beavers. Furthermore, there are indications that the Hammerschmiede beaver had a similar parental investment as today's beavers, where young adults migrate to poorer habitats in the second year, in search of their own territory. The shallower channel of HAM 5 possibly represents such a “second choice” habitat.

Key words: Mammalia, Rodentia, Castoridae, *Steneofiber depereti*, ecology, mortality, Miocene, Germany, Bavaria.

Thomas Lechner [thomas.lechner@senckenberg.de] and Madelaine Böhme [m.boehme@ifg.uni-tuebingen.de], Senckenberg Centre for Human Evolution and Palaeoenvironment (HEP), Eberhard Karls University of Tübingen, Institute for Geoscience, Sigwartstraße 10, 72074 Tübingen, Germany.

Received 22 march 2022, accepted 16 June 2022, available online 23 November 2022.

Copyright © 2022 T. Lechner and M. Böhme. This is an open-access article distributed under the terms of the Creative Commons Attribution License (for details please see <http://creativecommons.org/licenses/by/4.0/>), which permits unrestricted use, distribution, and reproduction in any medium, provided the original author and source are credited.

Introduction

The early Late Miocene Hammerschmiede locality (Allgäu region, Bavaria) is long known for its rich vertebrate fauna (Fahlbusch and Mayr 1975; Mayr and Fahlbusch 1975). Since the early 2000s, excavations by the University of Tübingen yielded approximately 20 000 new specimens. Currently, the vertebrate fauna of the Hammerschmiede locality comprises more than 130 vertebrate taxa (Kirscher et al. 2016; Böhme et al. 2019). Since the description of the arboreal biped hominid *Danuvius guggenmosi* Böhme, Spassov, Fuss, Tröscher, Deane, Prieto, Kirscher, Lechner, and Begun, 2019, the Hammerschmiede locality became internationally renowned (Böhme et al. 2020; Williams et al. 2020). Apart from this exceptional finding, other groups of the vertebrate fauna of the Hammerschmiede have been published, including the antelope *Miotragocerus monacensis* Stromer von Reichenbach, 1928 (Fuss et al. 2015; Hartung et al. 2020), the mouse deer *Dorcatherium naui* Kaup, 1833 (Hartung

and Böhme 2022), birds including a large crane, the darter *Anhinga pannonica* Lambrecht, 1916, and anseriforms represented by the small cf. *Mioquerquedula* sp. and the new anatid *Allgoviachen tortonica* Mayr, Lechner, and Böhme, 2022 (Mayr et al. 2020a, b, 2022), carnivores (Kargopoulos et al. 2021a–c, 2022) and small mammals including soricids, erinaceids, eomyids and cricetids (Prieto and Rummel 2009; Prieto et al. 2011; Prieto 2012; Prieto and Dam 2012). Turtles, artiodactyles, carnivores, fishes, and rodents are the most common vertebrates in the Hammerschmiede fauna, indicating a diverse ecosystem consisting of arboreal, terrestrial, semiaquatic and aquatic habitats. One of the most common groups of semiaquatic vertebrates are the beavers (Castoridae) that are represented by numerous specimens.

Today, beavers are solely represented by the genus *Castor*, but during the European Miocene a much higher diversity of up to seven genera are known, *Anchitheriomys* Roger, 1898, *Chalicomys* Kaup, 1832, *Dipoides* Jaeger, 1835, *Eucastor?* (*Schreuderia*) Aldana Carrasco, 1992, *Euroxenomys* Samson

and Radulesco, 1973, *Steneofiber* Geoffroy-Saint-Hilare, 1833 and *Trogontherium* Fischer von Waldheim, 1809 (Hugueney 1999; Stefen 2009). All these beavers are usually interpreted to inhabit similar ecological niches. Therefore, it is not surprising that in most localities that contain fossil beavers, only a single beaver species is known (Rekovets et al. 2020). But there are several localities with two beaver taxa (Hugueney 1999; Rekovets et al. 2020) including: Hambach (MN 5; Stefen and Mörs 2008; Mörs and Stefen 2010) with the equal-sized *Steneofiber depereti* Mayet, 1908, and *Anchitheriomys suevicus* Schlosser, 1884, as well as other localities with beaver taxa that have a notable size difference including: Dorn-Dürkheim 1 (MN 11; Franzen and Storch 1975; Rekovets et al. 2009, 2020; Casanovas-Vilar and Alba 2011) and Grytsiv (MN 9; Rekovets et al. 2020) with *Chalicomys jaegeri* (= *C. plassi*) Kaup, 1832, and *Euroxenomys minutus* (Von Meyer, 1838), and Sansan (MN 6; Hugueney and Duranthon 2012) with *Steneofiber* aff. *eseri* (Von Meyer, 1846) and *Euroxenomys minutus*. Only few localities comprise more than two beaver taxa, including Staniantzi (MN 13; Lechner and Böhme 2020) with *Castor* sp. Linnaeus, 1758, *Dipoides problematicus* Schlosser, 1902 and *Euroxenomys minutus*. At the locality Hammerschmiede two different beavers, the medium sized *Steneofiber depereti* and the small *Euroxenomys minutus* are found, though previous publications assigned the incisor fragment of a medium sized beaver from Hammerschmiede to *Chalicomys jaegeri* (Mayr and Fahlbusch 1975; Hugueney 1999; Kirscher et al. 2016: table 1; Böhme et al. 2019: supplementary table S1).

In this study we report new dental material of the larger castorid from Hammerschmiede (consisting of 142 specimens including 160 teeth). Based on diagnostic features we assign this material to *Steneofiber depereti*. The exceptionally high number of specimens with different age stages, provides insights into the intraspecific and ontogenetic variability of the *Steneofiber* population. The presence of beavers in Hammerschmiede is indicative for a freshwater dominated river ecosystem. This interpretation is also supported by the sediments of the Hammerschmiede clay pit (Fuss et al. 2015; Kirscher et al. 2016).

Institutional abbreviations.—GPIT, University of Tübingen, Germany; SNSB-BSPG, Bavarian State Collection of Palaeontology and Geology, Munich, Germany.

Other abbreviations.—D/d, upper/lower deciduous teeth; HAM, Hammerschmiede layers (HAM 5 and HAM 4); I/i, upper/lower incisor; M/m, upper/lower molar; M1/2 or m1/2, upper or lower first or second molar, more precise differentiation of the tooth position not possible; P/p, upper/lower premolar; WS 1–6, dental wear stages.

Geological setting

The locality Hammerschmiede is situated close to the small town Pforzen, only a few kilometres northwest of

Kaufbeuren (Bavaria, Southern Germany) in the Northern Alpine Foreland Basin. The active clay pit (clay, silty-clay and fine-sand) comprises a 26-metre-thick sediment section mainly represented by floodplain and channel deposits from the early Late Miocene age (Tortonian, MN 7/8). Within this section there are two main fossiliferous layers, HAM 5 and HAM 4 with an approximate depositional age of 11.62 and 11.44 Ma, respectively (Kirscher et al. 2016). The younger HAM 4 horizon can be interpreted as a river channel of about 50 m width and 4–5 m depth (Mayr et al. 2020a) whereas the slightly older HAM 5 most likely represents a small rivulet of only four to five metres width (Mayr et al. 2020a). According to the classic stream order (Hack's stream order following Hack 1957) it is assumed, that HAM 4 represents a deeper 2nd order stream and HAM 5 a shallower 3rd order stream.

Material and methods

The material used in this study was excavated at the Hammerschmiede locality. In total 160 teeth (142 specimens) were examined, of which 42 (39 specimens) are from the HAM 5 layer and 118 (103 specimens) from the HAM 4 layer.

The entire material is stored in the palaeontological collection of the University of Tübingen, Germany (GPIT), and is labelled either with GPIT (for excavation years 2011 to 2019 inclusive) or SNSB-BSPG (Bavarian State Collection of Palaeontology and Geology in Munich, Germany; for excavation years 2020 to 2021). SNSB-BSPG 2020 XCIV identifies specimens from HAM 4 and SNSB-BSPG 2020 XCV from HAM 5.

The morphological nomenclature of dental material follows Stirton (1935) and Hugueney (1999) (Fig. 1). The nomenclature of skull and mandibular features follows Freye (1959). Dental measurements were taken with a digital caliper (rounded to the first decimal point) at the occlusal surface and at the position of maximum extent (basal tooth) when possible. Evaluation of dental wear stages (WS) is modified according to Stefen (1997, 2001, 2018), Stefen and Mörs (2008), and Heinrich and Maul (2020): WS 1, unworn: no wear can be observed, deciduous dentition in use; WS 2, slightly worn: first occlusal contact; WS 3, worn: para-/metaflexus/-id is closing or just closed; WS 4, medium worn: mesoflexus/-id is closing or just closed; WS 5, deeply worn: hypoflexus/-id is near to closing; WS 6, heavily worn: hypoflexus/-id is closed.

Systematic palaeontology

Class Mammalia Linnaeus, 1758

Order Rodentia Bowdich, 1821

Family Castoridae Hemprich, 1820

Subfamily Castorinae Hemprich, 1820

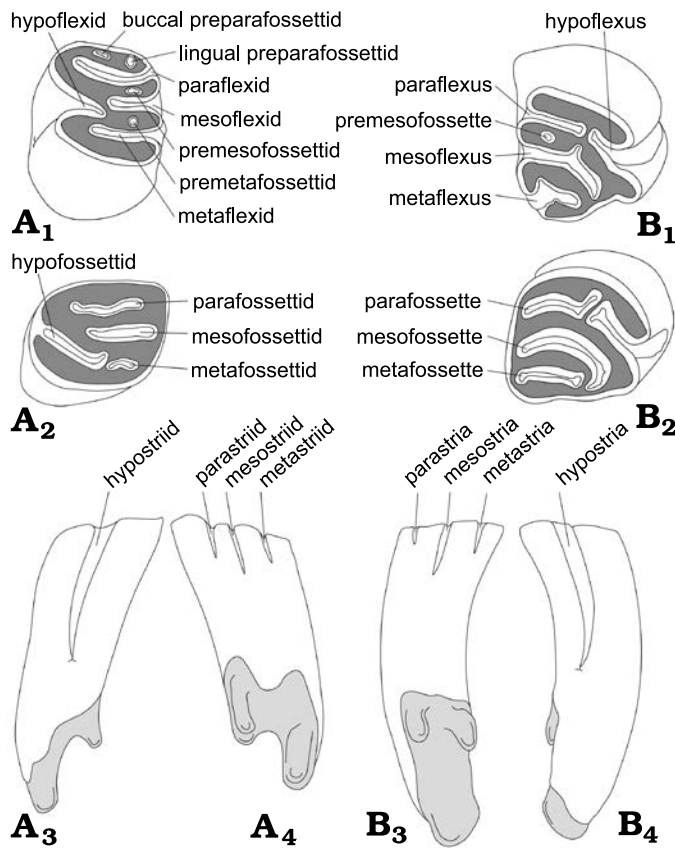


Fig. 1. General tooth scheme and morphological nomenclature used for the descriptions and comparisons of right lower (A) and upper (B) cheek teeth (premolars and molars) of the beaver *Steneofiber depereti* Mayet, 1908, from the early Late Miocene locality of Hammerschmiede (Bavaria, Germany). A₁, B₁, occlusal view of an early wear stage; A₂, B₂, occlusal view of a later wear stage; A₃, B₃, buccal view; A₄, B₄, lingual view. Enamel in white, dentine in dark grey, roots in light grey, cement not shown. Line drawings are not based on specific specimens and are not to scale. Nomenclature follows Stirton (1935) and Huguency (1999).

Genus *Steneofiber* Geoffroy-Saint-Hilaire, 1833

Type species: Steneofiber eseri (*Chalicomys eseri* Meyer, 1846 = *Steneofiber castorinus* Pomel, 1847). Following Huguency 1999, the genus *Steneofiber* “published before 1931 ... (as) uninominal genus group named without associated nominal species is accepted as consistent with the Principles of Binomial Nomenclature in the absence of evidence to the contrary” (ICZN, art 11 c, i). Saint-Gérant-le-Puy (France), Early Miocene (MN 2).

Steneofiber depereti Mayet, 1908

Figs. 2–6.

For synonymy see Huguency (1999).

Material.—Hammerschmiede locality, Germany, lower Upper Miocene, MN 7/8, base of Tortonian, for measurements see Tables 1 and 2). *HAM 5, upper dentition:* left I2: GPIT/MA/10749; right I2: GPIT/MA/10753; left DP4: GPIT/MA/10744, 10781; left P4: GPIT/MA/10746; left M1/2: GPIT/MA/10731, 13820; right M1/2: GPIT/MA/12604, 13825; left M3: GPIT/MA/10748, 12152. *HAM 5, lower dentition:* left i2: GPIT/MA/10743; right i2: GPIT/MA/10729; left dp4:

GPIT/MA/10782; right dp4: GPIT/MA/10785, 13826; left p4: GPIT/MA/09896, 10727, 13980, SNSB-BSPG 2020 XCV-0303; right p4: GPIT/MA/10745; left m1/2: GPIT/MA/09897, 09902, 09906, 10728, 10784, 12342, 13822, 13824; right m1/2: GPIT/MA/09903, 12032, 12260, 13821; right m3: GPIT/MA/09907, 10751, 13823; right mandible with angular process, part of the coronoid process, i2 and m1: GPIT/MA/13813; right mandible with angular process, p4, m1 and m3: GPIT/MA/09909; right mandible (frag.) with i2: GPIT/MA/10742. *HAM 4, upper dentition:* right I2: GPIT/MA/17456, 17807, SNSB-BSPG 2020 XCIV-0661; left DP4: GPIT/MA/12416, 12489; right DP4: GPIT/MA/17763, SNSB-BSPG 2020 XCIV-0879, 1731; left P4: GPIT/MA/17205, 10989, SNSB-BSPG 2020 XCIV-1725, 3891, 5375; right P4: GPIT/MA/17422, 17772, 16935, 17081, SNSB-BSPG 2020 XCIV-1510; left M1/2: GPIT/MA/16755, 12490, 16134, SNSB-BSPG 2020 XCIV-1724, 5366, 5371; right M1/2: GPIT/MA/17358, 16845, SNSB-BSPG 2020 XCIV-1391, 1726, 1727, 4059, 5367, 5368, 5369, 5370, 5372, 5374, 5376, 5377, 5378; left M3: GPIT/MA/12562, 16530, SNSB-BSPG 2020 XCIV-0415, 1320, 1728, 1729; right M3: GPIT/MA/10990, SNSB-BSPG 2020 XCIV-0446, 1730, 3388, 5373; maxillae and palatine (frag.) with left P4–M1 and right P4: GPIT/MA/17163; right P4–M2 (frag.): GPIT/MA/17367; left maxilla (frag.) with P4: GPIT/MA/16979.

Table 1. Dimensions (in mm) of upper and lower teeth of the beaver *Steneofiber depereti* Mayet, 1908, from the lower Upper Miocene locality of Hammerschmiede (Bavaria, Germany), with combined treatment of material from the local stratigraphic levels HAM 5 and HAM 4. L, mesio-distal length at occlusal surface and at basal position (where possible) for cheek teeth and length across anterior enamel band for incisors; W, bucco-lingual width at occlusal surface and at basal position (where possible) for cheek teeth; m, measurement; N, number of measurements.

Tooth position	m	N	Min	Max	Mean	Standard deviation	Variance
i	L	11	4.14	7.92	6.43	1.28	1.64
	W	11	4.15	7.47	6.01	1.28	1.64
I	L	4	5.77	7.06	6.54	0.56	0.32
	W	5	5.85	7.42	6.56	0.61	0.37
dp4	L	8	6.56	8.26	7.26	0.61	0.38
	W	8	4.52	5.66	5.13	0.39	0.15
p4	L	29	6.47	12.34	10.07	1.31	1.71
	W	29	5.98	8.23	7.34	0.53	0.28
m1/2	L	71	5.74	8.02	6.56	0.48	0.23
	W	71	4.55	8.37	6.89	0.89	0.80
m3	L	26	5.78	7.77	6.60	0.49	0.24
	W	26	5.17	7.05	6.31	0.39	0.15
DP4	L	10	5.00	6.80	5.94	0.63	0.40
	W	13	4.19	9.82	6.71	1.62	2.63
P4	L	34	7.59	9.56	8.21	0.53	0.28
	W	34	7.39	9.84	8.72	0.59	0.35
M1/2	L	52	4.98	7.40	5.89	0.46	0.21
	W	52	4.06	7.97	6.65	0.91	0.83
M3	L	24	5.16	6.41	5.82	0.33	0.11
	W	24	3.97	7.00	5.93	0.78	0.61

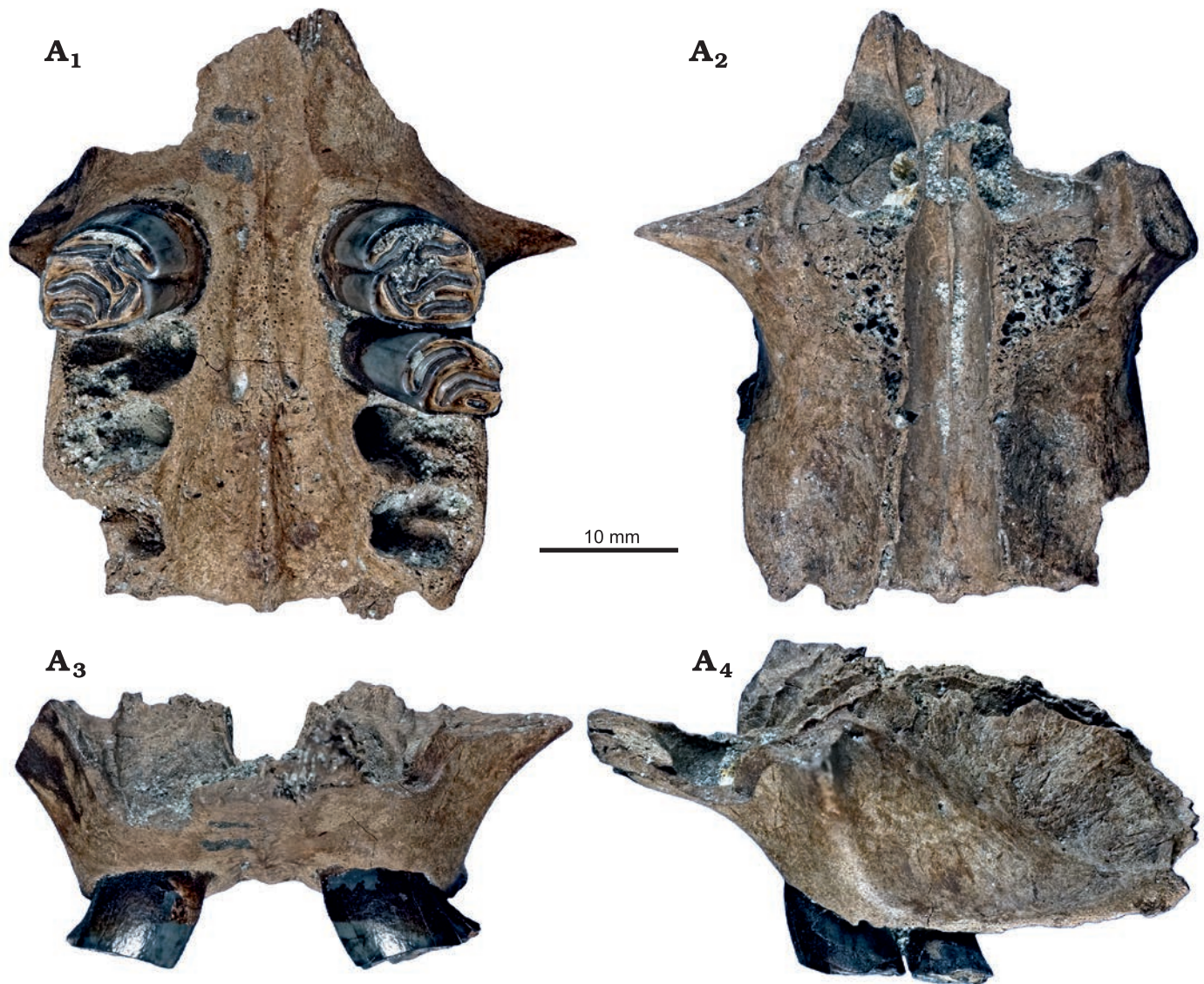


Fig. 2. Maxillae and fragmentary palatine of the beaver *Steneofiber depereti* Mayet, 1908 (GPIT/MA/17163), from the early Late Miocene locality Hammerschmiede (Bavaria, Germany), local stratigraphic level HAM 4. Maxillae and fragmentary palatine with left P4–M1 and right P4 in inocclusal (A₁), dorsal (A₂), mesial (A₃), and left buccal (A₄) views.

HAM 4, lower dentition: left i2: GPIT/MA/16985, SNSB-BSPG 2020 XCIV-1100; right i2: GPIT/MA/16512, 16928, 16436; left dp4: SNSB-BSPG 2020 XCIV-5365; left p4: GPIT/MA/17296, 17352, SNSB-BSPG 2020 XCIV-0179, 0487, 1246, 3726; right p4: GPIT/MA/18113, SNSB-BSPG 2020 XCIV-2276, 5362; left m1/2: GPIT/MA/16908, SNSB-BSPG 2020 XCIV-3572, 3745, 5359, 5363, 5364; right m1/2: GPIT/MA/10987, 16672, 16915, SNSB-BSPG 2020 XCIV-1185, 1468, 1723, 3903, 5357, 5358, 5360; left m3: GPIT/MA/17388, SNSB-BSPG 2020 XCIV-0416, 1114, 1719, 5361; right m3: GPIT/MA/17666, SNSB-BSPG 2020 XCIV-1720, 1721, 1722; left mandible with i2, dp4, m1, m2 (juvenile): GPIT/MA/17569; left mandible with dp4, m1, m2, m3 (juvenile): GPIT/MA/16950; left mandible with i2 (frag.), p4 (frag.), m1, m2: GPIT/MA/17068; left mandible with p4, m1, m2: SNSB-BSPG 2020 XCIV-1494; right mandible with p4 (frag.), m1, m2: GPIT/MA/16839; right mandible

(frag.) with m2, m3: GPIT/MA/17280; left mandible (frag.) with m1: GPIT/MA/18106; right mandible (frag.) with m2: SNSB-BSPG 2020 XCIV-2134; left angular process: GPIT/MA/16586; right angular process: GPIT/MA/17215.

Description.—In general, all cheek teeth are subhypsodont to hypsodont, developing complete and closed roots with age. Hypostriid and hypostria are always the longest striid/stria, but they never extend to the crown base although they can get quite close to it in the lower premolars. Mesostrid/-ia are usually longer than para- and metastrid/-stria, with the latter always terminating within the first quarter of tooth crown. The premolar is the largest tooth of the cheek teeth. Flexus/-ids, fossettes/-ids and striae/striids are gradually filled with cement with increasing wear stages and age.

Upper dentition: GPIT/MA/17163 is the most complete specimen with parts of the maxillae and palatine including

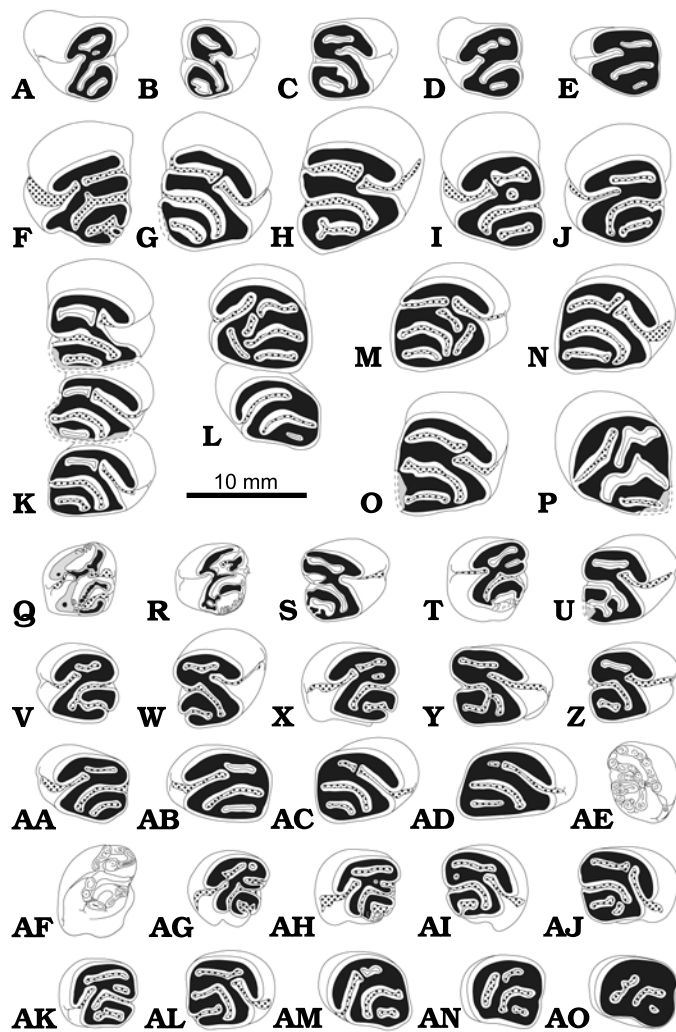


Fig. 3. Occlusal pattern of upper cheek teeth of the beaver *Stenofiber depereti* Mayet, 1908, from the early Late Miocene locality Hammerschmiede (Bavaria, Germany), local stratigraphic levels HAM 5 and HAM 4. Deciduous premolars (A–E), premolars (F–J, M–P), maxillary tooth rows (K, L), molars (Q–AQ). Left DP4: (A) GPIT/MA/12416, HAM 4; (D) GPIT/MA/10744, HAM 5; (E) GPIT/MA/10781, HAM 5. Right DP4: (B) SNSB-BSPG XCIV-0879, HAM 4; (C) GPIT/MA/17763, HAM 4. Left P4: (F) SNSB-BSPG XCIV-3891, HAM 4; (I) SNSB-BSPG XCIV-5375, HAM 4; (J) GPIT/MA/10989, HAM 4; (P) GPIT/MA/10746, HAM 5. Right P4: (G) GPIT/MA/17422, HAM 4; (H) GPIT/MA/17772, HAM 4; (M) GPIT/MA/17163, HAM 4; (N) GPIT/MA/16935, HAM 4; (O) GPIT/MA/17081, HAM 4. Right P4–M2: (K) GPIT/MA/17367, HAM 4. Left P4–M1: (L) GPIT/MA/17163, HAM 4. Left M1/2: (Q) SNSB-BSPG XCIV-5366, HAM 4; (R) GPIT/MA/13820, HAM 5; (T) SNSB-BSPG XCIV-5371, HAM 4; (S) SNSB-BSPG XCIV-5372, HAM 4; (V) GPIT/MA/16134, HAM 4; (X) SNSB-BSPG XCIV-1724, HAM 4; (AA) GPIT/MA/12490, HAM 4; (AB) GPIT/MA/16755, HAM 4. Right M1/2: (U) SNSB-BSPG XCIV-1391, HAM 4; (W) GPIT/MA/16845, HAM 4; (Y) SNSB-BSPG XCIV-5370, HAM 4; (Z) SNSB-BSPG XCIV-5368, HAM 4; (AC) GPIT/MA/17358, HAM 4; (AD) SNSB-BSPG XCIV-1726, HAM 4. Right M3: (AE) SNSB-BSPG XCIV-3388, HAM 4; (AI) GPIT/MA/10990, HAM 4; (AJ) SNSB-BSPG XCIV-5373, HAM 4; (AL) SNSB-BSPG XCIV-0446, HAM 4. Left M3: (AF) SNSB-BSPG XCIV-1320, HAM 4; (AG) SNSB-BSPG XCIV-0415, HAM 4; (AH) GPIT/MA/12562, HAM 4; (AK) GPIT/MA/10748, HAM 5; (AM) GPIT/MA/16530, HAM 4; (AN) SNSB-BSPG XCIV-1728, HAM 4; (AO) SNSB-BSPG XCIV-1729, HAM 4. Enamel in white, dentine in black, cement as dotted area, completions or hypothetical area of first wear in grey.

both P4, the left M1 and the alveoli of all other molars. Another maxilla fragment (GPIT/MA/16979) consists of a left P4 (Fig. 2). GPIT/MA/17367 comprises a right P4, M1 and M2; however, the remains of the maxilla were too weathered to be rescued. The rest of the material of the upper dentition is represented by isolated teeth; in total, five I2 fragments, seven DP4, 15 P4 (three in situ), 28 M1/2 (three in situ) and 13 M3.

I2: Five upper incisor fragments were excavated, all with their tips preserved. Their wear facets are all terraced and divided into two different parts. The labial tooth surface shows a smooth enamel band. A sharp and steep anterior tip consisting of mostly the labial enamel band and the angled lingual part of the dentine shows small and irregularly stepped wear marks parallel to the enamel band. The cross section of the upper incisor depicts an equilateral triangle with slightly convex sides (Reuleaux triangle). The lingual tip of this triangle is directed mesially.

DP4: All seven DP4 are worn and their para- and meta-fossettes are clearly visible (Figs. 3A–E, 4A, B), but only in four specimens an open mesoflexus is exposed (Figs. 3A–D, 4A, B). GPIT/MA/10781 is the most worn DP4 and its mesoflexus is closing (Fig. 3E). In all DP4 the hypoflexus/-stria are still open and do not reach the base of the crown (Figs. 3A–E, 4A, B₁). Two DP4 show an additional small fossette, one laterally to the para-fossette (GPIT/MA/10744; Figs. 3D, 4A) and one between para-fossette and mesoflexus (GPIT/MA/12416; Fig. 3A). Synclines of DP4 are never filled with cement. Only two DP4 have their entire base preserved (GPIT/MA/10744 and 17763) that consists of three roots with two small uniform buccal roots and one large dominant lingual root (Fig. 4B₁, B₂).

P4: In general, the occlusal surface of the P4 is nearly as wide as long (Figs. 3F–P, 4C–F). Mesiolingually the P4 is rounded, whereas the posterior and buccal margins are straight, forming an angular edge. The hypostria always closes well above the tooth base (Fig. 4D₂, E₂, F). Striae, flexus and fossettes of all P4 are at least slightly filled with cement in the least worn specimens (SNSB-BSPG 2020 XCIV-1510 and 3891; Figs. 3F, 4C) and cement filling increases with wear and age. The P4 is double-rooted with one minor root located at the distobuccal edge (Fig. 4D₃). The dominant root forms a wide arch that follows the mesiolingual tooth margin. The least worn P4 (SNSB-BSPG 2020 XCIV-1510) is the only unrooted P4 consisting of the tooth crown solely.

Only in the least worn SNSB-BSPG 2020 XCIV-3891 a metaflexid and a tiny enamel styloid at the buccal margin are expressed, but near to closure (Figs. 3G, 4C). All other available P4 are worn and the meta-fossette is exposed (Fig. 3G–P). Their para- and mesostria are very short or in higher wear stages they are already closed as fossettes (Figs. 3H–P, 4D–F).

On the buccal side, the least worn teeth (GPIT/MA/17422 and SNSB-BSPG 2020 XCIV-1510) show a longer parastris and shorter mesostria (Fig. 3G). In contrast, similarly worn GPIT/MA/10989, 17367, and 17772 show an already closed



parastria (parafossette) and an open and therefore longer mesostria (Figs. 3H, I, 4D₃).

In occlusal view, the length of the hypoflexus is slightly shorter than the paraflexus, but both are curved mesially and almost meet lingually to the centre of the tooth (Figs. 3F–P, 4C, D₁, E₁, F₁).

The hypoflexus and paraflexus/fossette are highly variable. In five specimens they meet facing in a straight line (GPIT/MA/17772, 17422, 17163, SNSB-BSPG 2020 XCIV-3891 and 5375) (Figs. 3F–I, 4C). In contrast, five other specimens show a different pattern. In three of those teeth the curved ending of the paraflexus/fossette is oriented mesially to the hypoflexus (GPIT/MA/16935, 17081, and 10989), whereas in the two other teeth they are situated distally to the hypoflexus (GPIT/MA/10746 and SNSB-BSPG 2020 XCIV-1725). In general, the mesoflexus/fossette of the P4 is curved and elongated far to the posterior occlusal tooth margin. The metafossette is encompassed by the mesoflexus/fossette and relatively short. In the deeply worn GPIT/MA/10746 para- and mesofossette are more irregular and wavier in shape (Fig. 3P).

Only in one specimen with both P4s (GPIT/MA/17163) in situ, two additional fossettes are exposed. The smaller fossette is situated in between the hypoflexus and the mesofossette and the larger one is located in the distolingual corner and perpendicular to the lingual ends of the para-, meso-, and metafossette as well as the hypoflexus (Figs. 2A₁, 3L, M).

M1/2: The occlusal outline of upper M1/2 is longer (mesio-distally) than wide (bucco-lingually) in early wear stages; with further wear this ratio changes to wider than long (compare Figs. 3Q–AD, 4G–M, N₁).

The hypostria ends well above the crown base and is the longest stria (Fig. 4K₃, N₃). Buccal striae are only present in early wear stages and thus very short, terminating within the first third of the tooth crown (Fig. 4K₂, N₂). The parastria and metastrria are very short and nearly non-existent in one very slightly worn M1/2 (GPIT/MA/13820; Figs. 3R, 4H). The similarly slightly worn M1/2 SNSB-BSPG 2020 XCIV-5366 exhibits no parastria (and thus a primary parafossette) but a well-expressed (4 mm long) metastrria (Figs. 3Q, 4G). The mesostria is the longest buccal stria, only present in

M1/2 of earlier wear stages (GPIT/MA/13820, 16134, 16845, SNSB-BSPG 2020 XCIV-1391, 1724, 5366, 5367, 5368, 5370, 5371, 5372 and 5377; Figs. 3Q–AA, 4G–M). In four of these (GPIT/MA/16134, 16845, SNSB-BSPG 2020 XCIV-1724 and 5366) an additional, but very short metastrria is also exposed (Figs. 3Q, V–X, 4G, K).

Form and orientation of flexus and fossettes on the occlusal surface are quite similar to P4 but the parafossette is much smaller or missing in heavily worn M1/2 (GPIT/MA/10731, 17163) while the hypoflexus is elongated. In two cases of M1/2, meso- and metaflexus/fossette are interconnected at mid length (GPIT/MA/13820 and SNSB-BSPG 2020 XCIV-1391; Figs. 3R, U, 4H, I); in one separate case they are fused at the terminal end of the metaflexus (GPIT/MA/16134; Fig. 3V). In the least worn M1/2 (GPIT/MA/13820 and SNSB-BSPG 2020 XCIV 5366), the para- and metafossette are of irregular outline (Figs. 3Q, R, 4G, H). Three slightly worn M1/2 show an additional tiny enamel column/stylid at the base of the mesostria (GPIT/MA/13820, SNSB-BSPG 2020 XCIV-5377 and 5368; Figs. 3R, Z, 4H, M). All M1/2 have three roots: one dominant lingual root and two small buccal roots (Fig. 4K₂, N₂).

M3: The M3 is the shortest tooth of the toothrow (Fig. 4Q₂, P₂). The occlusal outline of the M3 is square but slightly elongated distally. The hypostria ends well above the crown base and is the longest stria like in the other upper molars. Only in two specimens, representing unworn, unrooted and thus not fully developed M3, the hypostria ends very slightly above the crown base (SNSB-BSPG XCIV-1320 and 3388; Fig. 4O₂, P₂). Buccal striae are short and terminate within the first third of the height of the tooth crown. The mesostria is the longest buccal stria, usually followed by the parastria.

The metastrria is very short and only present in four lesser worn M3 where it is located at the distobuccal corner in three specimens (GPIT/MA/10990, 12562 and SNSB-BSPG 2020 XCIV-0446; Figs. 3AH, AI, AL, 4R) and slightly shifted to the posterior side in SNSB-BSPG 2020 XCIV-0415 (Figs. 3AG, 4Q).

The two unworn M3 show a para- and a mesoflexus/-stria but no metastrria (and thus a primary metafossette) (SNSB-BSPG 2020 XCIV-1320; Figs. 3AF, 4P₁, P₂) or a very short

← Fig. 4. Upper (A–T) and lower (U–AM) cheek teeth of the beaver *Steneofiber depereti* Mayet, 1908, from the early Later Miocene locality Hammerschmiede (Bavaria, Germany), local stratigraphic levels HAM 5 and HAM 4. Deciduous premolars: (A, B, U–V); premolars (C–F, W–AA); molars (G–N, O–T, AB–AI, AJ–AN). Occlusal (A, B₁, C, D₁–F₁, G–J, K₁, L, M, N₁–P₁, Q–U, V₁–X₁, Y, Z₁, AA₁, AB, AC₁–AF₁, AI–AH, AJ₁, AK, AL, AM₁, AN), lingual (B₂, D₂–F₂, K₂, N₂–P₂, W₂, X₂, AC₂, AD₂, AE₂, AF₂, AJ₂, AM₂), and buccal (B₃, D₃, K₃, N₃, O₃, P₃, V₂–X₂, Z₂, AA₂, AC₃, AD₂, AJ₂, AM₃) views. Left DP4: (A) GPIT/MA/10744, HAM 5. Right DP4: (B) GPIT/MA/17763, HAM 4. Left P4: (C) SNSB-BSPG 2020 XCIV-3891, HAM 4; (D) GPIT/MA/10989, HAM 4; (E) GPIT/MA/10746, HAM 5. Right P4: (E) GPIT/MA/16935, HAM 4. Left M1/2: (G) SNSB-BSPG 2020 XCIV-5366, HAM 4; (H) GPIT/MA/13820, HAM 5. Right M1/2: (I) SNSB-BSPG 2020 XCIV-1391, HAM 4; (J) SNSB-BSPG 2020 XCIV-5372, HAM 4; (K) GPIT/MA/16845, HAM 4; (L) SNSB-BSPG 2020 XCIV-5370, HAM 4; (M) SNSB-BSPG 2020 XCIV-5368, HAM 4; (N) SNSB-BSPG 2020 XCIV-1726, HAM 4. Right M3: (O) SNSB-BSPG 2020 XCIV-3388, HAM 4. Left M3: (P) SNSB-BSPG 2020 XCIV-1320, HAM 4; (Q) SNSB-BSPG 2020 XCIV-0415, HAM 4; (R) GPIT/MA/12562, HAM 4; (S) GPIT/MA/16530, HAM 4; (T) SNSB-BSPG 2020 XCIV-1729, HAM 4. Right dp4: (U) GPIT/MA/13826, HAM 5; (V) GPIT/MA/10785, HAM 5. Right p4: (W) GPIT/MA/10745, HAM 4; (X) SNSB-BSPG 2020 XCIV-5362, HAM 4. Left p4 (Y) SNSB-BSPG 2020 XCIV-0487, HAM 4; (Z) SNSB-BSPG 2020 XCV-0303, HAM 5; (AA) GPIT/MA/09896, HAM 5. Right m1/2: (AB) GPIT/MA/16915, HAM 4; (AD) GPIT/MA/10987, HAM 4; (AE) GPIT/MA/16672, HAM 4; (AF) GPIT/MA/09906, HAM 5; (AI) GPIT/MA/12260, HAM 5. Left m1/2: (AC) SNSB-BSPG 2020 XCIV-5364, HAM 4; (AG) GPIT/MA/12342, HAM 5; (AH) GPIT/MA/13824, HAM 5. Right m3: (AJ) SNSB-BSPG 2020 XCIV-1722, HAM 4; (AK) GPIT/MA/13823, HAM 5; (AN) GPIT/MA/09907, HAM 5. Left m3: (AL) GPIT/MA/17388, HAM 4; (AM) SNSB-BSPG 2020 XCIV-1719, HAM 4.

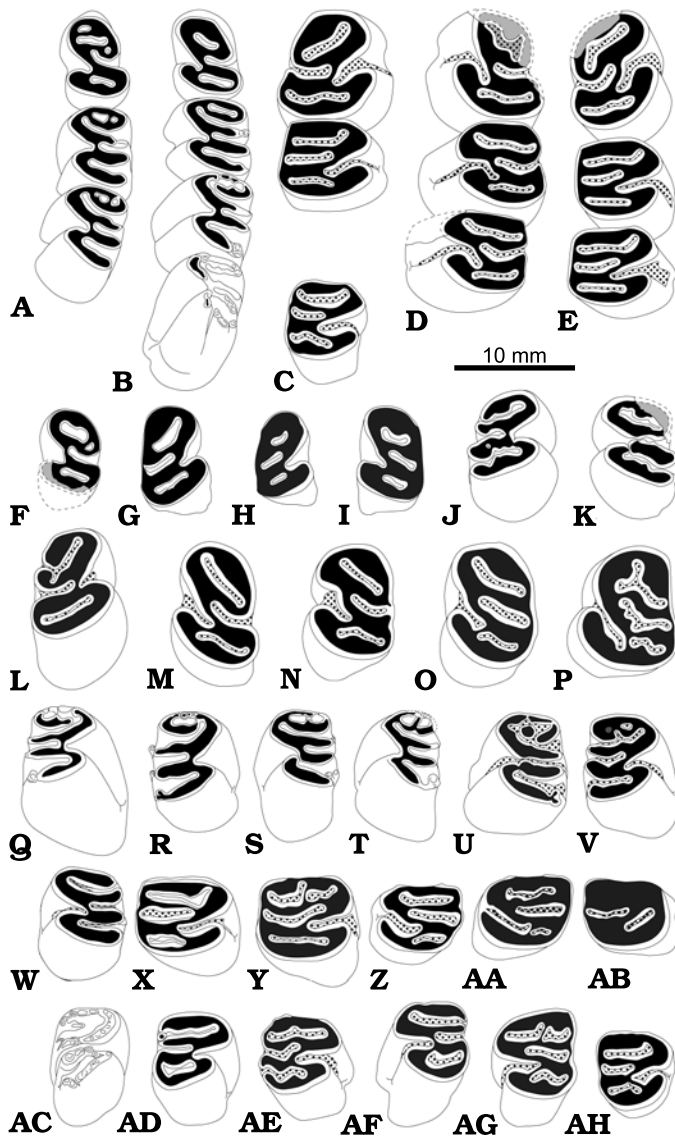


Fig. 5. Occlusal pattern of lower cheek teeth of the beaver *Stenofiber depereti* Mayet, 1908, from the early Late Miocene locality Hammerschmiede (Bavaria, Germany), local stratigraphic levels HAM 5 and HAM 4. Mandibular tooth rows (A–E), deciduous premolars (F–I), premolars (J–P), molars (Q–AF). Left dp4–m2: (A) GPIT/MA/17569, HAM 4; (B) GPIT/MA/16950, HAM 4. Right p4–m1 and m3, lacking m2: (C) GPIT/MA/09909, HAM 5. Left p4–m2: (D) GPIT/MA/17068, HAM 4. Right p4–m2: (E) GPIT/MA/16839, HAM 4. Left dp4: (F) GPIT/MA/10782, HAM 5; (I) SNSB-BSPG 2020 XCIV-5365, HAM 4. Right dp4: (G) GPIT/MA/13826, HAM 5; (H) GPIT/MA/10785, HAM 5. Right p4: (J) GPIT/MA/10745, HAM 5; (L) SNSB-BSPG 2020 XCIV-5362, HAM 4. Left p4: (K) GPIT/MA/10727, HAM 5; (M) GPIT/MA/13980, HAM 5; (N) GPIT/MA/09896, HAM 5; (O) SNSB-BSPG 2020 XCV-0303, HAM 5; (P) SNSB-BSPG 2020 XCIV-0487, HAM 4. Right m1/2: (Q) GPIT/MA/16915, HAM 4; (R) GPIT/MA/16672, HAM 4; (V) GPIT/MA/10987, HAM 4; (X) GPIT/MA/09903, HAM 5; (Y) SNSB-BSPG 2020 XCIV-5360, HAM 4; (AB) GPIT/MA/12260, HAM 5. Left m1/2: (S) GPIT/MA/09906, HAM 5; (T) GPIT/MA/10728, HAM 5; (U) SNSB-BSPG 2020 XCIV-5364, HAM 4; (W) GPIT/MA/09902, HAM 5; (Z) GPIT/MA/12342, HAM 5; (AA) GPIT/MA/13824, HAM 5. Right m3: (AC) SNSB-BSPG 2020 XCIV-1722, HAM 4; (AD) GPIT/MA/13823, HAM 5; (AE) GPIT/MA/10751, HAM 5; (AH) GPIT/MA/09907, HAM 5. Left m3: (AF) SNSB-BSPG 2020 XCIV-1719, HAM 4; (AG) GPIT/MA/17388, HAM 4. Enamel in white, dentine in black, cement as dotted area, completions in grey.

para-, a dominant meso- and a nearly as dominant metaflexus/stria (SNSB-BSPG 2020 XCIV-3388; Figs. 3AE, 4O₁, O₃). The former M3 shows a well-expressed paraflexus forming a “U”, crossing the tooth buccolingually and then turning back mesially to the buccal margin. The latter M3 exhibits additional enamel columns/stylids within the mesostria, the metastria and at the lingual hypostria (Fig. 4O).

In more advanced wear stages, the paraflexus/fossette is randomly separated into a large mesial and a small distal fossette (GPIT/MA/10748, 10990, 12562 and SNSB-BSPG 2020 XCIV-0415; Figs. 3AG–AI, AK, 4Q, R). The slightly worn GPIT/MA/12562 shows an additional third paraflexus/stria that is small but open buccally (Figs. 3AH, 4R). The most heavily worn M3 show in two cases only one hypo-, para-, meso-, and metafossette (GPIT/MA/16530 and SNSB-BSPG 2020 XCIV-1728; Figs. 3AM, AN, 4S) and in one case only hypo-, meso-, and a tiny metafossette (SNSB-BSPG 2020 XCIV-1729; Figs. 3AO, 4T).

All M3 have three roots, like the M1/2, with one dominant lingual root and two small buccal roots. Only the two unworn M3 (SNSB-BSPG 2020 XCIV-1320 and 3388) are still rootless and open at the base (Fig. 4O₃, P₂).

Lower dentition: The material consists of 12 i2 (seven isolated tips, two fragments in situ, three complete teeth in situ), six dp4 (two still in their mandible), 18 p4 (four preserved in their mandible), 44 m1/2 and 14 m3, of which 18 molars are still in situ in ten jaw fragments (nine m1, seven m2 and two m3).

i2: Seven of the 12 lower incisor specimens include a preserved tip. In contrast to the upper incisor, the wear facet of the lower i2s is constantly angled and smooth. The wear facet is longer than in the upper I2 and extends from the labial enamel tip to the lingual edge. In cross section the lower incisors show a lingually elongated triangle. The lingual tip of the triangle is rounded and situated mesially. The mesial surface is nearly flat and parallel with the symphysis of the mandibles. The enamel face is convex in juvenile specimens (GPIT/MA/16436, 16985, and 17569), but it is “semiflat-tened” in older individuals, with a flattened mesial and a convex distal half of the enamel face.

dp4: All six dp4 are worn and para- and metafossetids are visible (Fig. 5A, B, F–H). Three of the dp4 are strongly worn and a closed mesoflexid is visible (GPIT/MA/13826, 10785, SNSB-BSPG 2020 XCIV-5365; Figs. 4U, V₁, 5G–I,). In the medium worn specimens, the mesoflexid is open and associated with a short mesostriid (Fig. 5A, B, F). All dp4 show a well-expressed hypoflexid with an associated hypostriid that terminates shortly above the crown base but extends as a groove until the tooth base (Fig. 4V₂). The mesostriid is clearly longer than the meta- and parastriid (if present), but the hypostriid is always the longest. Synclines of the dp4 are never filled with cement. In all dp4 with preserved roots, two dominant main roots diverge mesially and distally, and a tiny third root protrudes buccally, mesially to the hypostriid (GPIT/MA/10785, 16950, and 17569; Fig. 4V₂). GPIT/MA/17569 shows two additional small and circular

fossettids: one mesiobuccal (preparafossettid) and another distolingual (premesofossettid) (Fig. 5A).

p4: In premolars that are only slightly or medium worn, the typical eight-shaped occlusal outline is visible (Figs. 4W₁, X₁, 5J–L). With increasing wear, the anterior part of the worn surface of the *p4* extends in length mesially, whereas its width remains unchanged. With the last wear phase, an antero-lingual edge is forming that extends the mesiolingual part of the *p4* up to the level of its distal part (Figs. 4Y, AA₁, 5C, D, N–P). The hypostriid always ends very close (approximately 3 mm) to the base of the crown. Slightly below the closure of the hypostriid, a well-expressed groove extends to the base of the tooth (Fig. 4W₂, X₂, Z₂, AA₂). The closure of the hypostriid can easily be overlooked in teeth of higher wear stages due to the increased accumulation of cementum in the striids; therefore, the continuing groove can be misinterpreted as an open hypostriid that reaches the tooth base.

Only in slightly worn *p4* (GPIT/MA/10727, 10745), para- and meta-striids of equal length are exposed and are closing within the first quarter of the tooth length (Figs. 4W₁, W₃, 5J, K). In all specimens with more advanced wear stages the para- and metaflexid/striid are closed and their para- and metafossettid are visible. Generally, lower premolars show a well-developed mesostriid/flexid extending at least halfway down to the tooth base (Fig. 4W₃, X₃). Only in the most heavily worn *p4* (GPIT/MA/09896, SNSB-BSPG 2020 XCV-0303, 0487) the mesostriid/flexid is just closed and the mesofossettid is present (Figs. 4Y, Z₁, AA₁, 5N–P). In slightly worn *p4* the hypoflexid is straight and diagonally oriented in medio-distal direction. The hypoflexid crosses approximately one third of tooth width and ends between the meso- and metaflexid. Only in the least worn premolars (GPIT/MA/10727, 10745 and SNSB-BSPG 2020 XCIV-5362), the hypoflexid ends in line with the ends of the meso- and metaflexid (Figs. 4W₁, X₁, 5J–L). In GPIT/MA/10727 the meso- and metaflexid are fused with the hypoflexid (Fig. 5K). In moderate to heavy wear stages, the hypoflexid of lower premolars is hook-shaped and oriented more distally, never crossing the midline of tooth width. In these advanced wear stages, the mesoflexid/fossettid are more elongated, run mesially side by side with the terminating hypoflexid by forming a mesiobuccally oriented hook (GPIT/MA/09896, 13980, 16839 and SNSB-BSPG 2020 XCIV-0487; Figs. 4Y, AA₁, 5E, M, N, P), or stay straight (SNSB-BSPG 2020 XCV-0303; Figs. 4Z₁, 5O). The mesoflexid is the shortest of the lingual flexids/fossettids and it slightly crosses the midline of the tooth width. The para- and metaflexids/fossettids run two thirds along the tooth width before they terminate. The shape of the paraflexid/fossettid on the occlusal surface is variable, showing a straight course or a convex (GPIT/MA/16839; Fig. 5E) to concave (GPIT/MA/09909; Fig. 5C) hook-shaped orientation. The metaflexids/fossettids are slightly undulating. In SNSB-BSPG 2020 XCIV-0487 all lingual fossettids are heavily undulating (Figs. 4Y, 5P).

m1/2/3: The typical outline of the lower molars is rectangular. The hypostriid/flexid is the longest striid/flexid and

ends shortly above the crown base and closes to a hypofossettid without any lingual groove in contrast to the *p4*. The mesostriid is always longer than the para- and meta-striid, both of which having the same length. Para- and meta-striid are only present in the first millimetres of wear and they close within the first fourth of the tooth crown length. In contrast the mesostriid continues downwards until it closes before reaching half of the tooth crown height in *m1/2* (Fig. 4AC₂, AD₃, AE₂, AF₂), but surpasses the half length of the crown height in *m3* (Fig. 4AJ₃, AM₂). The latter is bucco-lingually slightly narrower and approximately 20% shorter in crown height than a typical *m1/2* (compare Fig. 4AC₂, AC₃, AJ₂, AJ₃, AM₂, AM₃). In unworn and slightly worn molars, some special features in lingual flexids/fossettids are obvious: unworn molars show a U-shaped paraflexid that is oriented transversally on the occlusal surface, nearly reaching the buccal margin until it is reversing mesially all way back near the lingual tooth margin (Figs. 4AB, AC₁, AJ₁, 5B, Q, U, AC). In slightly worn *m1/2* this “U” is divided and yields a typical straight transversal paraflexid and one elongated preparafossettid (Figs. 4AE₁, 5B, R). With continuing wear this preparafossettid splits in two preparafossettids, a lingual and a buccal preparafossettid (GPIT/MA/09906, 10728, 10987, and 17569 [m1]; Figs. 4AF₁, AD₁, 5A, S, T, V). In a single case a third preparafossettid appears (GPIT/MA/17569 [m2]; Figs. 5A, 6C₂). Another singular specimen shows a Y-shaped paraflexid where the two endings encompass the buccal preparafossettid. Furthermore, the same *m1/2* shows a second, lingual preparafossettid that is barely visible and nearly worn out (GPIT/MA/10987; Figs. 4AD, 5V). All preparafossettids are removed due to tooth wear before any lingual flexid closes. The medium worn GPIT/MA/17388 (*m3*) and the heavily worn SNSB-BSPG 2020 XCIV-5360 (*m1/2*) exhibit an interrupted parafossettid that is split into a lingual and a buccal parafossettid of equal dimensions (Figs. 4AL, 5Y, AG). In the most heavily worn molar only a hypo- and mesofossette is present (GPIT/MA/12260) (Figs. 4AI, 5AB). Three molars show tiny additional enamel columns or stylids at the lower ends of some lingual striids (GPIT/MA/16672, *m1/2*: parastriid and mesostriid; Figs. 4AE₁, AE₂, 5R; GPIT/MA/09906, *m1/2*: parastriid and mesostriid, Figs. 4AF₁, AF₂, 5S; GPIT/MA/13823, *m3*: only one stylid at the paraflexid, Figs. 4AK, 5AD). In general, paraflexid/fossettid, mesoflexid/fossettid and metaflexid/fossettid are straight or slightly undulating and transversely oriented on the occlusal surface.

Mandibles: The description of the mandible is mainly based on the four better preserved specimens: a nearly complete right mandible comprising of the angular process, part of the coronoid process, *i2* and *m1* (GPIT/MA/13813, Fig. 6A); a well-preserved right mandible with articular process, *p4*, *m1*, and *m3* (GPIT/MA/09909, Fig. 6B); a mandible fragment with *i2* (fragment) and *p4*–*m2* (GPIT/MA/17068, Fig. 6D); and a juvenile left mandible with *i2* and *dp4*–*m2* (GPIT/MA/17569, Fig. 6C). In addition to that, the mandibular material consists of two isolated articular processes (GPIT/MA/16586, 17215) and eight smaller mandibular

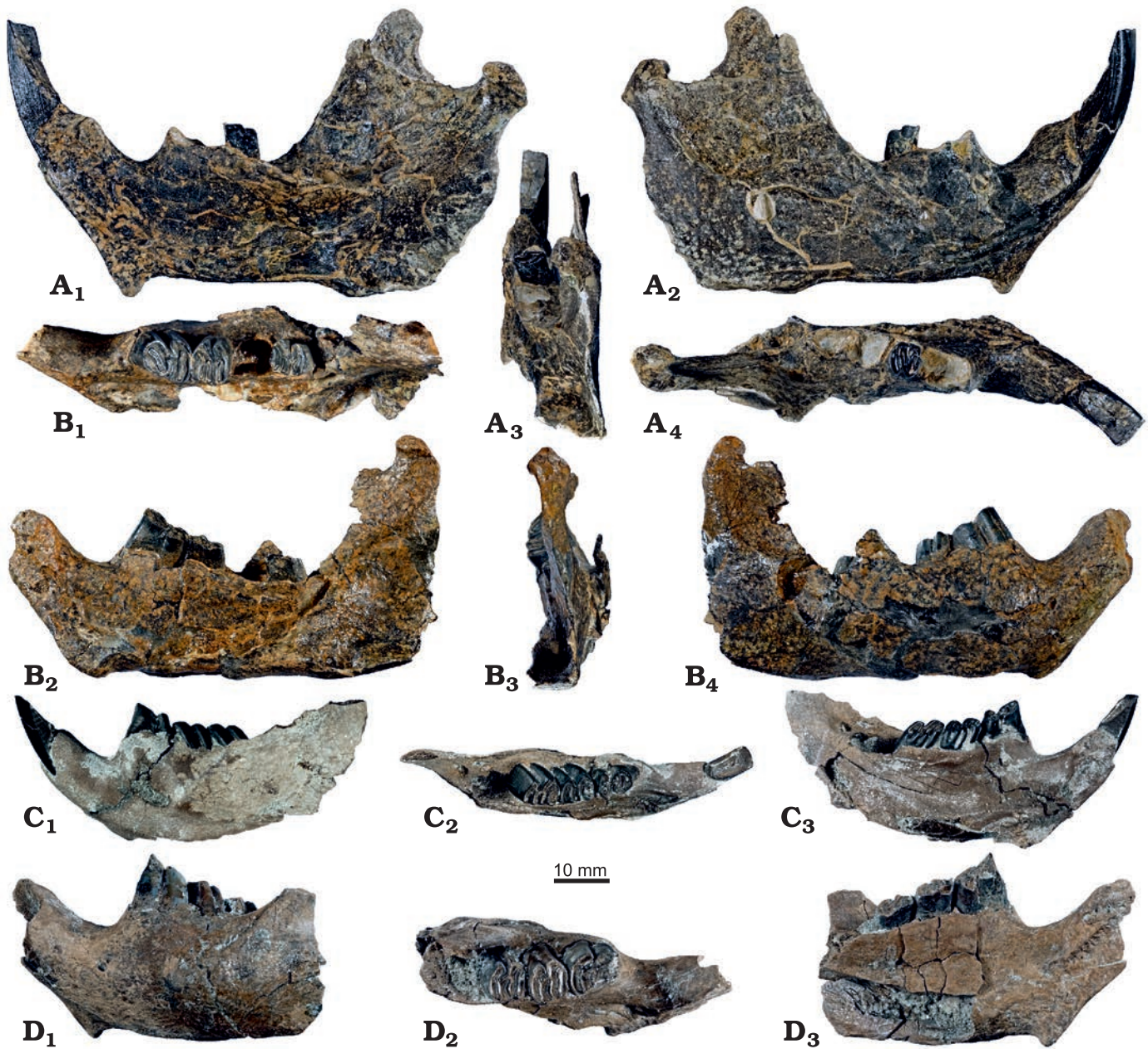


Fig. 6. Mandibles of the beaver *Steneofiber depereti* Mayet, 1908, from the early Late Miocene locality Hammerschmiede (Bavaria, Germany), local stratigraphic levels HAM 5 and HAM 4. **A.** GPIT/MA/13813, HAM 5, right mandible with angular process, part of the coronoid process, i2 and m1 in lingual (A₁), buccal (A₂), distal (A₃) and occlusal (A₄) views. **B.** GPIT/MA/09909, HAM 5, right mandible with angular process, p4, m1 and m3 in occlusal (B₁), lingual (B₂), distal (B₃) and buccal (B₄) views. **C.** GPIT/MA/17569, HAM 4, left mandible with i2, dp4, m1 and m2 (juvenile) in buccal (C₁), occlusal (C₂) and lingual (C₃) views. **D.** GPIT/MA/17068, HAM 4, left mandible with i2 (fragment), p4 (fragment), m1 and m2 in buccal (D₁), occlusal (D₂) and lingual (D₃) views.

fragments (GPIT/MA/10742, 16767, 16839, 16950, 17280, 18106, SNSB-BSPG 2020 XCIV-1494 and 2134).

In lateral view, the chin process is pointed postero-ventrally; it is situated anterior to the p4 in the older individuals (GPIT/MA/09909, 13813, and 17068; Fig. 6A₂, B₄, D₁) and at the same height as the dp4 in the juvenile specimen (GPIT/MA/17569; Fig. 6C₁). The mental foramen is situated anterior to the p4 (GPIT/MA/09909, 17068) and at the same height as the anterior margin of dp4 (GPIT/MA/17569). The m3 and parts of the m2 are hidden by the anterior margin of

the coronoid process (GPIT/MA/09909, 17068, 17569) and a deep masseteric fossa is situated dorsal to the posterior end of the incisor (GPIT/MA/09909, 13813).

In lingual view, the angular shelf (crista pterygoidea) starts posterior to the m3; it bends horizontally and is expanded at the ventral margin (GPIT/MA/09909, 13813), thus a clear and distinct fossa for the pterygoid muscle is visible (Fig. 6A₁, B₂). GPIT/MA/13813 has an elongated mandibular foramen that is situated posteriorly to the m3 at a crest starting at the lingual alveolar rim and continuing to the

condylar process (Fig. 6A₁, A₄). In the juvenile specimen (GPIT/MA/17569) this foramen is situated labially to this crest, directly posterior to the m3 alveolus (Fig. 6C₂, C₃). The symphysis is pointed to the chin process and expands dorsally. The occlusal margin of the toothrow is concave and slightly inclined posteriorly.

In posterior view, the coronoid and the angular processes are arranged in a vertical line (Fig. 6A₃). The articular process is shifted lingually to this line (GPIT/MA/09909, 13813; Fig. 6A₃, B₃).

Results and discussion

The taxonomic differentiation of fossil castorids is mainly limited to a few dental and cranial characters (Huguency 1999). In the present case the lower premolar (p4) exhibits the only character that allows to assign the material of the larger castorid from Hammerschmiede to *Steneofiber depereti*, and not *Chalicomys jaegeri*. In a further analysis, a metric comparison with other Miocene beavers focusing on lower premolars (p4) and mandibular tooth row length is conducted. Furthermore, the dp4/p4 tooth is permanently in use during the entire lifetime of the beaver and thus offers the possibility to analyse the complete dental “attritional” record for *Steneofiber depereti* from Hammerschmiede from birth to death in a mortality analysis.

Comments on the genus *Steneofiber*.—The dental morphology of *Steneofiber depereti* is very similar to *Chalicomys jaegeri*; therefore, the distinction between the two genera remains difficult. Generally, *Chalicomys jaegeri* is considered to be the successor of *Steneofiber depereti* (Ginsburg 1971; Stefen 1997; Mörs and Stefen 2010). So far, the following features are usually used to distinguish *Steneofiber* spp. from *Chalicomys* spp.: increasing hypsodonty in *Chalicomys* spp.; development of a clear tetralophodont pattern with well-expressed striids on the lingual side in *Chalicomys* spp.; and cement filling of the striids even in early wear stages in *Chalicomys* spp. (Huguency 1999; Casanovas-Vilar et al. 2008; Stefen 2009; Mörs and Stefen 2010). As already suggested by Mörs and Stefen (2010), the only clear difference is a hypostriid that always reaches the base of the tooth in *Chalicomys* spp. at least in its fourth lower premolar. Here we use this character as a potential synapomorphy of the clade including the genera *Chalicomys* and *Castor*. Therefore, all lower p4 with a hypostriid that does not reach the base of the tooth crown can be attributed to the genus *Steneofiber*.

Comments on the species of *Steneofiber*.—*Steneofiber* comprises two clearly distinguished species, the stratigraphically older mesodont *S. eseri* (MN 1–MN 2) and the younger hypsodont *S. depereti* (MN 3–MN 10). Both species are also characterized based on their dental metric data (Huguency 1999). However, a third species, *S. subpyrenaicus* was discussed by Mörs and Stefen (2010) and they pointed out that

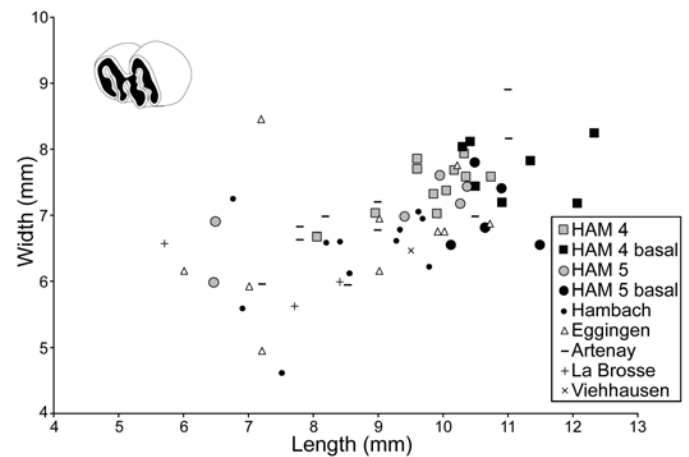


Fig. 7. Length/width dimensions of lower premolars of the beaver *Steneofiber depereti* Mayet, 1908, from the early Late Miocene locality Hammerschmiede (Bavaria, Germany), local stratigraphic levels HAM 5 and HAM 4, compared to other *S. depereti* material from Miocene localities in France and Germany. Data for Hambach from Mörs and Stefen (2010), for Eggingen-Mittelhart from Sach and Heizmann (2001) and Mörs and Stefen (2010), for Artenay from Mörs and Stefen (2010), for La Brosse from Ginsburg et al. (2000), and for Viehhausen from Seemann (1938). Measurements for HAM 5 and HAM 4 material is additionally compared by occlusal (grey) and basal (black) tooth measurements. Measurements for Hambach and Eggingen-Mittelhart contain both occlusal and basal tooth measurements. Data for Artenay, La Brosse and Viehhausen only include occlusal measurements.

the material of *S. subpyrenaicus* might be undiagnostic or conspecific with *S. depereti*. We agree with Mörs and Stefen (2010) about their proposal that a subspecies differentiation should not be used for the European *Steneofiber* species, especially *S. depereti*. Since the morphology and metrics of the larger Hammerschmiede beaver correspond to the usual variability of *S. depereti* (Fig. 7), we assign the material described here to this species.

Tooth differences between *Chalicomys jaegeri* and *Steneofiber depereti* and the impact of increased cement filling.—*Chalicomys jaegeri* from the type locality Eppelsheim is characterized by hypsodont teeth with a hypostriid extending to the crown base, three well-expressed lingual striids and conspicuous cement in the synclines of the teeth already at early wear stages (Huguency 1999; Stefen 2009; Mörs and Stefen 2010). According to previous studies, *Steneofiber depereti* exhibits subhypsodont to hypsodont teeth, closed hypostria/-iids, and only a labial mesostriid; it further lacks substantial cement in the synclines (Mayet 1908; Ginsburg 1971; Stefen 1997; Huguency 1999; Sach and Heizmann 2001; Mörs and Stefen 2010). In the present sample from Hammerschmiede, the cheek teeth of a large castorid are subhypsodont to hypsodont. Lower cheek teeth of the Hammerschmiede beaver comprise three lingual striids with a dominant mesostriid and small additional para- and meta-striids, but these are not as dominant and long as in *Chalicomys jaegeri* from Eppelsheim (Huguency 1999; Stefen 2009) or Soblay (see Huguency 1999: fig. 28.6E1). Furthermore, cheek teeth of the large beaver from

Table 2. Material list with dimensions (in mm) of upper and lower teeth of the beaver *Steneofiber depereti* Mayet, 1908, from the early Late Miocene locality Hammerschmiede (Bavaria, Germany) and the local stratigraphic levels HAM 5 and HAM 4. L, left; R, right. Cement codes the occurrence of cement filling in cheek teeth flexids with (0) no cement, (1) first, faint traces of cement, and (2) complete filling with cement; wear stages are defined as (1), unworn: no wear can be observed, deciduous dentition in use, (2) slightly worn: first occlusal contact, (3) worn: para/metaflexus/-id is closing or just closed, (4) medium worn: mesoflexus/-id is closing or just closed, (5) deeply worn: hypoflexus/-id is near to closing, (6) heavily worn: hypoflexus/-id is closed; length occlusal, mesio-distal length at occlusal surface of cheek teeth and length across anterior enamel band for incisors; length at base, mesio-distal length at basal tooth position (where possible); width occlusal, bucco-lingual width at occlusal surface of cheek teeth and incisors; width at base, bucco-lingual width at basal tooth position (where possible). Estimated values of measurements are marked by an asterisk (*).

Tooth position		Repository number	Layer	Cement [0–2]	Wear stage [1–6]	Occlusal		Base	
						length	width	length	width
I2	R	GPIT/MA/17456	HAM 4				6.87		
		GPIT/MA/17807	HAM 4			6.49	6.24		
		SNSB-BSPG 2020 XCIV-661	HAM 4			7.06	7.42		
		GPIT/MA/10753	HAM 5			5.77	5.85		
	L	GPIT/MA/10749	HAM 5			6.84	6.4		
DP4	R	GPIT/MA/17763	HAM 4	0	3	6.61	5.45	5.08	7.82
		SNSB-BSPG 2020 XCIV-0879	HAM 4	0	3	6.24	4.19	5.58	7.42
		SNSB-BSPG 2020 XCIV-1731	HAM 4	0	4		7.1		
	L	GPIT/MA/12416	HAM 4	0	3	6.59	4.48	6.8	9.82
		GPIT/MA/12489	HAM 4	0	4		5.88		8.45
		GPIT/MA/10744	HAM 5	0	3	6.1	5.51	5	7.61
		GPIT/MA/10781	HAM 5	0	4	5.76	6	5.6	7.52
P4	R	SNSB-BSPG 2020 XCIV-1510	HAM 4	1	2			7.99	8.21
		GPIT/MA/17367	HAM 4	1	3			8.26	9.45
		GPIT/MA/17422	HAM 4	2	4	9.19	8.11	7.95	9.28
		GPIT/MA/17772	HAM 4	2	4	8.92	8.81	8.02	9.84
		GPIT/MA/16935	HAM 4	2	4	8.96	9.58	8.01	9.15
		GPIT/MA/17081	HAM 4	2	4	8.5	8.33	7.59	8.83
		GPIT/MA/17163-2	HAM 4	2	4	7.74	8.94		
	L	GPIT/MA/10989	HAM 4	1	3	7.95	7.39	8.2	8.94
		GPIT/MA/17205	HAM 4	2	4	8.43	9.05	8.35	8.95
		GPIT/MA/17163-1	HAM 4	2	4	7.62	8.9		
		SNSB-BSPG 2020 XCIV-1725	HAM 4	1	5	9.56*	8.74*	7.62	8.38
		GPIT/MA/16979	HAM 4	2	5	8.42	9.32		
		SNSB-BSPG 2020 XCIV-3891	HAM 4	2	1	7.61	7.74	8.05	8.66
M1	R	GPIT/MA/17163-1	HAM 4	2	5	5.5	7.75		
	L	GPIT/MA/17367	HAM 4	1	4			5.47	7.7
M1–M2	R	GPIT/MA/16845	HAM 4	1	3	6.52	5.85	5.47	7.27
		SNSB-BSPG 2020 XCIV-1391	HAM 4	2	3	6.44	5.76	5.3	6.89
		GPIT/MA/17358	HAM 4	2	4	6.12	7.53	6.02	7.43
		SNSB-BSPG 2020 XCIV-1727	HAM 4	2	4	5.93	5.96	5.61	6.76
		SNSB-BSPG 2020 XCIV-1726	HAM 4	1	5	5.94	7.9	5.58	7.8
		SNSB-BSPG 2020 XCIV-5368	HAM 4	1	3	6.04	5.4	5.13	6.77
		SNSB-BSPG 2020 XCIV-5370	HAM 4	2	3	6.56	6.3	5.77	7.79
		SNSB-BSPG 2020 XCIV-5372	HAM 4	1	3	6.24	5.2	4.98	6.53
		SNSB-BSPG 2020 XCIV-5369	HAM 4	1	4	6.18	6.58	5.71	6.94
		SNSB-BSPG 2020 XCIV-5367	HAM 4	1	1	6.2	4.59	6.18	6.96
		SNSB-BSPG 2020 XCIV-5377	HAM 4	2	3	6.22	6.72	5.23	7.69
		SNSB-BSPG 2020 XCIV-5376	HAM 4	2	4	6.51	6.46	6.25	6.92
		SNSB-BSPG 2020 XCIV-5378	HAM 4	2	4	6.45	6.99	6.41	7.52
		SNSB-BSPG 2020 XCIV-5374	HAM 4	2	5	6.13	7.69	5.91	6.84
		SNSB-BSPG 2020 XCIV-4059	HAM 4	2	4	5.73	7.37	5.45	7.1
		GPIT/MA/12604	HAM 5	1	4	6.18	6.76	5.58	7.47
		GPIT/MA/13825	HAM 5	0	4	5.93	6.37	5.76	6.41

M1–M2	L	SNSB-BSPG 2020 XCIV-1724	HAM 4	1	3	6.18	6.18	6.02	6.47
		GPIT/MA/16134	HAM 4	1	3	6.19	5.82	5.94	6.93
		GPIT/MA/16755	HAM 4	1	4	7.4	5.77	5.75	7.97
		GPIT/MA/12490	HAM 4	2	4	5.54	6.47	5.22	6.6
		SNSB-BSPG 2020 XCIV-5366	HAM 4	1	1	6.1	4.3	5.7	6.63
		SNSB-BSPG 2020 XCIV-5371	HAM 4	1	2	5.93	5.02		
		GPIT/MA/13820	HAM 5	0	2	5.96	4.06	5.06	6.83
		GPIT/MA/10731	HAM 5	2	5	5.57	7.14	5.18	6.38
M2	R	GPIT/MA/17367	HAM 4	1	4			6.04	7.02
M3	R	SNSB-BSPG 2020 XCIV-1730	HAM 4	0	1	5.52	4.73	5.16	5.09
		GPIT/MA/10990	HAM 4	2	3	5.85	6.05	6.29	6.3
		SNSB-BSPG 2020 XCIV-0446	HAM 4	2	4	6.18	6.53	6.32	6.52
		SNSB-BSPG 2020 XCIV-3388	HAM 4	1	1	5.65	4.62	6.03	5.64
		SNSB-BSPG 2020 XCIV-5373	HAM 4	2	4	6.33	6.46	6.41	6.76
	L	SNSB-BSPG 2020 XCIV-1320	HAM 4	0	1	5.72	3.97	5.76	5.79
		SNSB-BSPG 2020 XCIV-0415	HAM 4	2	2	5.42	5.31	5.55	5.91
		GPIT/MA/12562	HAM 4	2	3	5.61	5.52	5.88	6.01
		GPIT/MA/16530	HAM 4	2	5	6.1	7	5.52	6.31
		SNSB-BSPG 2020 XCIV-1728	HAM 4	2	6			6.02	6.55
		SNSB-BSPG 2020 XCIV-1729	HAM 4	2	6			5.62	6.98
		GPIT/MA/10748	HAM 5	1	3	5.62	5.75	5.46	5.46
		GPIT/MA/12152	HAM 5	2	4	5.92	6.76	5.82	6.41
i2	R	GPIT/MA/16512	HAM 4			7.92	6.99		
		GPIT/MA/16928	HAM 4			7.3	6.95		
		GPIT/MA/16436	HAM 4			5.3	4.6		
		GPIT/MA/10742	HAM 5			7.19	7.47		
		GPIT/MA/10729	HAM 5			6.62	6.42		
		GPIT/MA/13813	HAM 5			7.88	7.16		
	L	SNSB-BSPG 2020 XCIV-1100	HAM 4			7.26	6.44		
		GPIT/MA/17569	HAM 4			5.38	4.54		
		GPIT/MA/16985	HAM 4			6.84	6.91		
		GPIT/MA/10743	HAM 5			4.14	4.15	4.94	4.47
dp4	R	GPIT/MA/10785	HAM 5	0	5	7.03	4.76		
		GPIT/MA/13826	HAM 5	0	4	8.26	5.51		
	L	GPIT/MA/16950	HAM 4	0	3	6.64	5.13	7.5	5.66
		GPIT/MA/17569	HAM 4	0	3	6.73	4.99	7.75	5.07
		SNSB-BSPG 2020 XCIV-5365	HAM 4	0	4	7.63	5.42		
		GPIT/MA/10782	HAM 5	0	3	6.56*	4.52*		
p4	R	GPIT/MA/18113	HAM 4	2	3	10.05	7.38		
		SNSB-BSPG 2020 XCIV-2276	HAM 4	2	3			10.9*	7.2*
		GPIT/MA/16839	HAM 4	2	3	9.85*	7.32		
		SNSB-BSPG 2020 XCIV-5362	HAM 4	2	3	8.95	7.02	11.35	7.82
		GPIT/MA/10745	HAM 5	0	2	6.47	5.98	10.9	7.4
		GPIT/MA/09909	HAM 5	2	3	9.95	7.6	10.5	7.79
	L	SNSB-BSPG 2020 XCIV-0179	HAM 4	2	3	9.9*	7.02*		
		SNSB-BSPG 2020 XCIV-1246	HAM 4	1	3	8.06*	6.67*	10.3*	8.04*
		GPIT/MA/17068	HAM 4	2	3	9.6*	7.7*		
		SNSB-BSPG 2020 XCIV-1494	HAM 4	2	3	9.6	7.86	10.42	8.11
		GPIT/MA/17352	HAM 4	2	4	10.35	7.58	12.07	7.18
		GPIT/MA/17296	HAM 4	2	4	10.74	7.58	10.5	7.44
		SNSB-BSPG 2020 XCIV-0487	HAM 4	1	5	10.33	7.94		
		SNSB-BSPG 2020 XCIV-3726	HAM 4	2	3	10.17	7.68	12.34	8.23
		GPIT/MA/10727	HAM 5	1	2	6.5*	6.9*		
GPIT/MA/13980	HAM 5	2	3	10.27	7.17	11.5	6.55		
GPIT/MA/09896	HAM 5	2	4	9.42	6.97	10.13	6.55		
SNSB-BSPG 2020 XCV-303	HAM 5	2	4	10.38	7.43	10.65	6.81		

m1	R	GPIT/MA/17280	HAM 4	1	4	6.67	7.17	6.8	8.04
		GPIT/MA/16839	HAM 4	2	4	6.7	7.1		
		GPIT/MA/09909	HAM 5	2	4	6.84	7.83	6.64	7.66
		GPIT/MA/13813	HAM 5	2	5	6.33	6.63		
	L	GPIT/MA/16950	HAM 4	0	2	6.18	5.57		
		GPIT/MA/17569	HAM 4	0	2	6.44	5.1		
		GPIT/MA/18106	HAM 4	2	4	6.38	6.52	6.14	6.88
		GPIT/MA/17068	HAM 4	2	4	6.9	7.12		
		SNSB-BSPG 2020 XCIV-1494	HAM 4	2	4	6.95	7.9		
m1-m2	R	GPIT/MA/16915	HAM 4	1	2	6.47	5.77	6.31	8.37
		GPIT/MA/16672	HAM 4	1	2	7.63	5.34	6.64	6.9
		GPIT/MA/10987	HAM 4	1	2	7.26	5.83	6.03	7.38
		SNSB-BSPG 2020 XCIV-1185	HAM 4	1	2	6.18	4.86	6.32	7.04
		SNSB-BSPG 2020 XCIV-1468	HAM 4	1	2	6.63	5.44	6.13	7.15
		SNSB-BSPG 2020 XCIV-1723	HAM 4	1	3	7.41	7.33	6.64	7.93
		SNSB-BSPG 2020 XCIV-3903	HAM 4	2	4	6.49	7.51	6.07	7.33
		SNSB-BSPG 2020 XCIV-5360	HAM 4	2	5	6.99	7.9	6.6	8.09
		SNSB-BSPG 2020 XCIV-5357	HAM 4	2	4	8.02	7.71	6.88	8.29
		SNSB-BSPG 2020 XCIV-5358	HAM 4	1	4	7.07	6.81	6.14	6.99
		GPIT/MA/09903	HAM 5	1	4	6.59	7.8	6.66	7.46
		GPIT/MA/13821	HAM 5	1	4	6.34	7.25	5.89	6.75
		GPIT/MA/12032	HAM 5	2	5	6.7	7.34		
		GPIT/MA/12260	HAM 5	2	6			5.94	7.25
	L	GPIT/MA/16908	HAM 4	1	3	7.32	6.26	6.03	7.34
		SNSB-BSPG 2020 XCIV-3572	HAM 4	1	2	6.36	5.6	5.8	6.82
		SNSB-BSPG 2020 XCIV-3745	HAM 4	2	3	6.59	7.04	7.67	5.93
		SNSB-BSPG 2020 XCIV-5364	HAM 4	1	1	7.1	5.49	6.61	7.84
		SNSB-BSPG 2020 XCIV-5363	HAM 4	2	4	6.73	7.79	6.46	7.86
		SNSB-BSPG 2020 XCIV-5359	HAM 4	2	3	7.18*	7.5*	7.17*	7.11*
		GPIT/MA/09906	HAM 5	1	2	6.3	5.26	5.94	6.86
		GPIT/MA/10728	HAM 5	0	2	6.38	4.55	6.03	7.13
		GPIT/MA/09902	HAM 5	1	3	6.02	5.91	5.99	6.88
		GPIT/MA/09897	HAM 5	1	3	6.46	6.95	6.97	6.64
		GPIT/MA/13822	HAM 5	1	4	6.22	6.94	6.09	7.17
		GPIT/MA/12342	HAM 5	1	5	5.74	7.08		
		GPIT/MA/10784	HAM 5	1	5	6.37	6.85	5.89	6.72
		GPIT/MA/13824	HAM 5	2	6			6.21	7.43
		m2	R	SNSB-BSPG 2020 XCIV-2134	HAM 4	1	3	6.66	6.94
GPIT/MA/17280	HAM 4			1	4	7.42	6.8		
GPIT/MA/16839	HAM 4			2	4	6.65	7.35		
L	GPIT/MA/16950		HAM 4	0	2	6.38	5.22		
	GPIT/MA/17569		HAM 4	0	2	6.47	5.23		
	GPIT/MA/17068		HAM 4	2	4	6.8	7.25		
	SNSB-BSPG 2020 XCIV-1494		HAM 4	2	4	6.9	7.8		
m3	R	GPIT/MA/17666	HAM 4	1	4	6.86	6.01	6.27	6.4
		SNSB-BSPG 2020 XCIV-1722	HAM 4	1	1			6.2	6.54
		SNSB-BSPG 2020 XCIV-1720	HAM 4	1	4	6.91	6.46	6.51	6.01
		SNSB-BSPG 2020 XCIV-1721	HAM 4	2	4	6.6	6.63	6.56	6.49
		GPIT/MA/13823	HAM 5	0	3	6.22	6.39	6.5	6.55
		GPIT/MA/10751	HAM 5	2	3	6.68	6.7	6.57	6.24
		GPIT/MA/09909	HAM 5	2	4	6.64	6.5	7.23	5.92
	L	GPIT/MA/09907	HAM 5	2	5	6.75	6.38		
		GPIT/MA/16950	HAM 4	0	1	5.87	5.17	7.37	7.05
		SNSB-BSPG 2020 XCIV-0416	HAM 4	2	3	5.78	5.88	5.78	5.63
		SNSB-BSPG 2020 XCIV-1114	HAM 4	2	3	6.75	6.31	6.32	6.34
		GPIT/MA/17388	HAM 4	2	4	7.77	6.9	6.76	6.02
		SNSB-BSPG 2020 XCIV-1719	HAM 4	2	4	6.7	6.16	6.17	6.45
		SNSB-BSPG 2020 XCIV-5361	HAM 4	2	4	7.53	6.45	6.33	6.48

Hammerschmiede exhibit filling of cement in dental synclines that increases considerably with higher individual age. Table 2 and Figs. 2 and 3 show that deciduous (juvenile beavers) teeth never exhibit cement filling (Figs. 3A–E, 5A, B, F–I) and teeth assigned to WS 1 and WS 2 (juvenile and young adult beavers) comprise no or only slight cement agglomeration (Figs. 3Q, R, AE, AF, 5A, B, J, K, Q–T, AC–AD). At WS 3 and WS 4 (mature and senile beavers) this character state changes to first traces of cement (Figs. 3S–U, 5W, X) and completely cement-filled dental synclines (Figs. 3F–P, V–AD, AG–AO, 5C–E, L–P, U–V, Y–AB, AE–AH). This continuous increase of cement filling in dental synclines with higher wear stages and thus individual age indicates that the deposition of cement in Hammerschmiede beavers (and possibly any other European Miocene beaver) is a secondary effect during dental development. Compared to other European Miocene beaver species, the larger Hammerschmiede castorid represents an intermediate stage between the first forms of *Steneofiber* (*S. eseri*, *S. castorinus* and earlier forms of *S. depereti*; no cement in synclines), later forms of *Steneofiber depereti* (e.g., from Hambach, MN 5/6; with slight cement filling of dental synclines for individuals of higher ages) and *Chalicomys jaegeri* (cement-filled synclines already at juvenile individuals). A similar intermediate position becomes apparent when comparing the tooth crown height of cheek teeth (hypso-donty). The increase of cement accumulation possibly correlates with the increase of hypso-donty; therefore, it appears questionable to use this character as a diagnostic character at the species or even genus level in European castorids. Consequently, only one clear character remains to differentiate between *Chalicomys jaegeri* and *Steneofiber depereti*: the hypostriid, that closes before and does not reach the crown base in *Steneofiber depereti*, specifically in lower premolars.

Metric comparison of the lower premolar.—In addition to their identical morphology, the dimensions of the lower premolars from the two different Hammerschmiede layers are overlapping; the beavers from the HAM 5 and HAM 4 layers are thus considered as conspecific (Fig. 7). For further analyses, HAM 5 and HAM 4 material is merged. The age difference between these two layers is estimated to approximately 180 ka (Kirscher et al. 2016). The stratigraphically slightly younger beavers from HAM 4 exhibit the largest teeth in width and length (Fig. 7). This could indicate a slight tendency of body size enlargement through time or it might be explained with slightly changed environmental conditions as indicated by the wider and deeper river deposits of HAM 4 in contrast to the small rivulet of HAM 5 (Böhme et al. 2019; Mayr et al. 2020a).

The material from Hammerschmiede fits quite well into the size variability of other medium-sized Miocene beaver populations of Europe (Figs. 6, 7). The largest dimensions of the lower p4 from Hammerschmiede tend to be greater compared to other Miocene *Steneofiber* spp., but also *Chalicomys* spp. finds from Germany and France (Fig. 8).

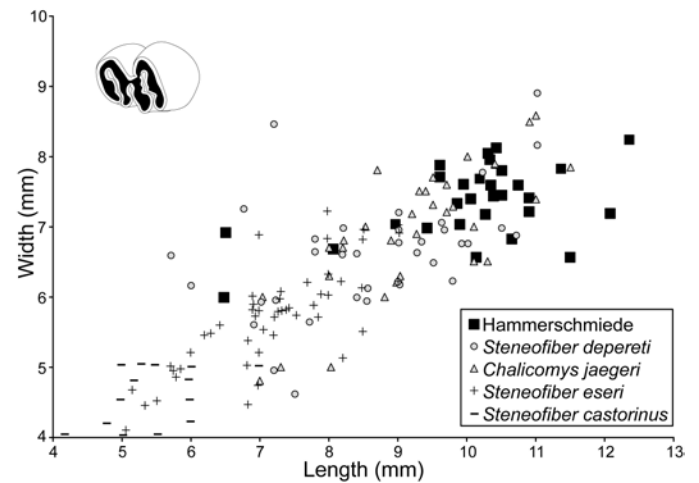


Fig. 8. Length/width dimensions of lower premolars of the beaver *Steneofiber depereti* Mayet, 1908, from the early Late Miocene locality Hammerschmiede (Bavaria, Germany), local stratigraphic levels HAM 5 and HAM 4, compared to *S. depereti* and several other castorid species from other European Miocene localities. Data for non Hammerschmiede *S. depereti* from Mörs and Stefen (2010) and citations therein, for *Chalicomys jaegeri* from Stefen (2009) and citations therein, for *Steneofiber eseri* from Stefen (1997), and for *Steneofiber castorinus* from Filhol (1879). Data points for all taxa resemble both occlusal and basal tooth measurements.

The smallest values for the lower p4 mesio-distal length from Hammerschmiede consist of occlusal measurements of slightly worn teeth. This observation is based on the typical morphology of the lower premolar, where in a buccal view the mesio-distal length increases heavily within the first wear stage. Therefore, occlusal measurements of unworn and very slightly worn p4 do not represent the typical tooth dimensions of the larger Hammerschmiede castorid.

Mandibular tooth row size.—In addition to the metrical analysis of lower premolars from different fossil Miocene localities, some authors compared the lengths of mandibular tooth rows at the occlusal surface and the alveolar length (Stefen 2009; Mörs and Stefen 2010; Stefen 2011). Following this approach, the available mandibular material of *Steneofiber depereti* from Hammerschmiede is added to the dataset and compared in the same way (Fig. 9). The length of the mandibular tooth rows of *S. depereti* from the combined HAM 4 and HAM 5 shows a similarly high intraspecific variability as other comparable comprehensive records of *Steneofiber* from Hambach (MN 5/6), Pontlevoy (MN 5), Ulm-Westtangente (MN 2a), and St. Geränd le Puy (MN 2a) (Fig. 9). In direct comparison, the small Early Miocene (MN 2) *Steneofiber eseri* and *Steneofiber castorinus* exhibit a clearly shorter mandibular tooth row. The lengths of *S. depereti* tooth rows from Hammerschmiede overlap with those of *S. depereti* (formerly *S. depereti caliodorensis*) from Chilleurs-aux-Bois (MN 3) and *S. depereti* from Hambach (MN 5/6). Considering the alveolar length, measurements of *S. depereti* (formerly *S. depereti janvieri*) from Denezé (base MN 3) do not overlap with those from Hammerschmiede. Furthermore, the tooth

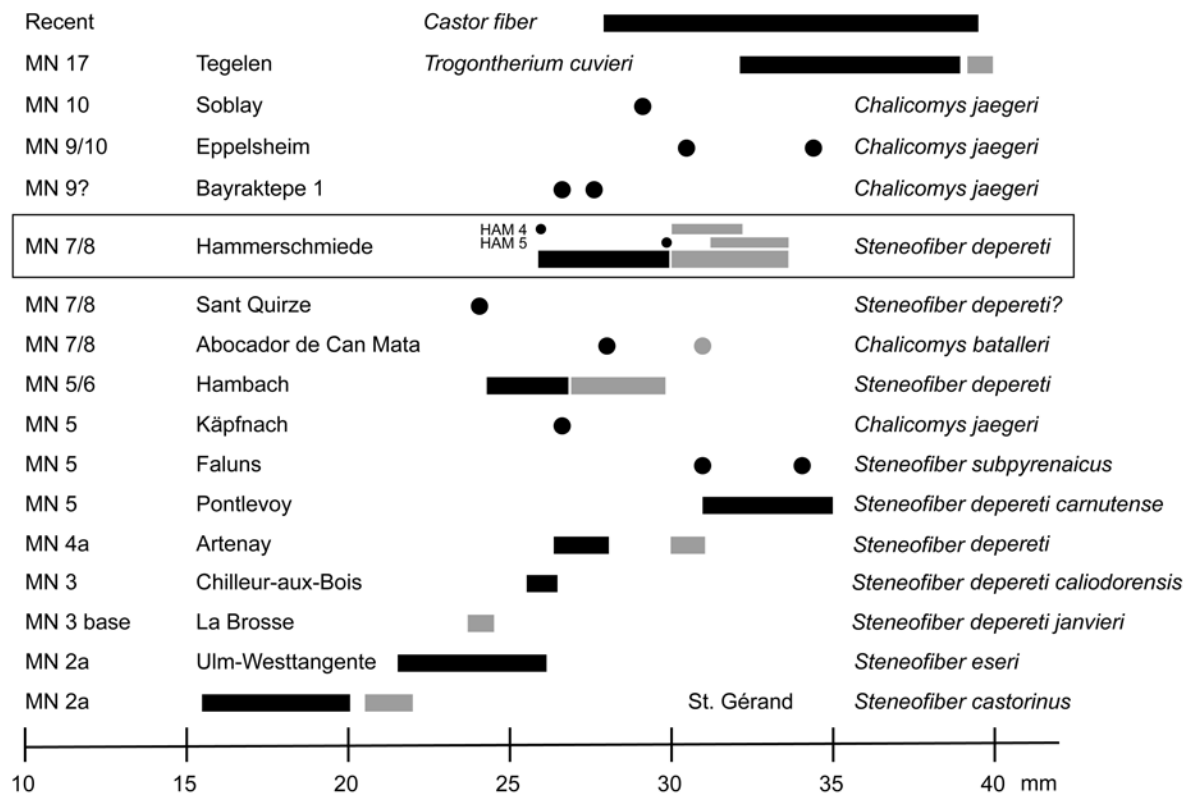


Fig. 9. Mandibular tooth row lengths of the beaver *Steneofiber depereti* Mayet, 1908, from the early Late Miocene locality Hammerschmiede (Bavaria, Germany), local stratigraphic levels HAM 5 and HAM 4, in comparison to representative European Miocene castorid species. Occlusal surface lengths are given as single measurements (black dots) or ranges (black bars). Alveolar lengths are given in grey dots or bars respectively. Measurements adapted from Stefen (2009), Mörs and Stefen (2010), Stefen (2011), and citations therein. Biostratigraphic positions of the localities according to the Mammal Neogene (MN) zones (sensu Mein 1975).

row lengths of the Early Miocene material from Käpfnach (MN 5) assigned to *Chalicomys jaegeri*, the Late Miocene *Chalicomys jaegeri* from Bayraktepe 1 (MN 9?), Soblay (MN 10) and Eppelsheim (MN 9/10), and also *Chalicomys batalleri* from Abocador de Can Mata (MN 7/8) are within the size range of Hammerschmiede mandibular tooth rows.

Wear stages of lower premolars and their step-length relation.—The highly different states of preservation of the dental material make it difficult to gather age groups based on tooth abrasion by measuring the tooth height directly. In order to include most available tooth specimens, the age groups are characterized by defined changes in the occlusal patterns of the cheek teeth depending on their dental wear stages. To avoid data duplication by multiple counting of individuals, the analysis is restricted to the lower dp4/p4 tooth position. Furthermore, this tooth position provides the only mortality record from birth (deciduous dentition) to death (permanent dentition). Morphological characters that define the wear stages of the p4 are not equally distributed along the entire tooth height. Therefore, the absolute age information differs according to the actual step-length between the wear stages (Fig. 10). In the least worn and isolated specimens of lower p4 (GPIT/MA/10727 and 10745) the absolute distribution of wear stages can be estimated by “percentage of dental lifespan” with the wear stages according to a max-

imum tooth height plus the lifetime of a juvenile individual with the dp4 still in use.

WS 1 represents the time range when a deciduous premolar (dp4) is used by a juvenile beaver (p4 is unerupted and unused at this stage). To avoid potential individual duplication by counting shed out deciduous teeth, which therefore do not represent the time of death of the beaver individual, dp4 with resorbed roots were excluded from counting. The attritional lifetime of the dp4 (WS 1) (interval between time of tooth eruption and time when dp4 is shed out) is of unknown relation to the wear stages of the p4 (WS 2–6). The entire p4 tooth height represents 100%. The relation of direct measurements of the wear stage step lengths of the example p4s leads to following approximate step length proportions (Fig. 10): WS 2 is a short (17%) step-length compared to the longest WS 3 (33%) and WS 4 (28%). WS 5 (11%) and WS 6 (11%) exhibit the shortest step-lengths of the p4 with approximately one third of WS 3 (Fig. 10). In consequence, this means that with the beginning of WS 4, 50% of the absolute dental lifespan of the lower p4 is worn and with the end of WS 4, 77% of the available enamel tooth height is abraded. Finally, a tentative assignment of wear stages and age groups results in: WS 1, juvenile; WS 2, young/prime adult; WS 3, mature/elder; WS 4 and higher wear stages, old/senile.

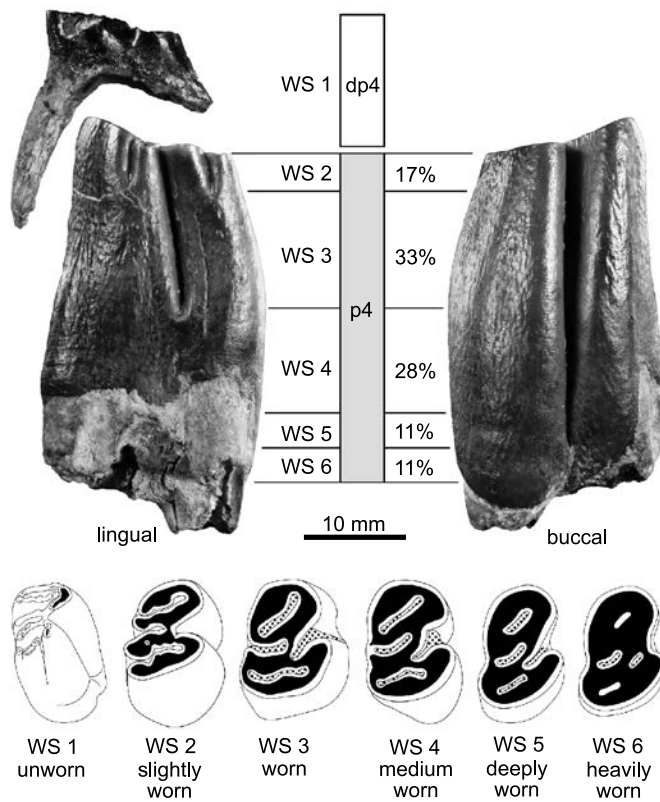


Fig. 10. Wear stages (WS) and step-length between wear stages for the lower premolar dp4/p4 of the beaver *Steneofiber depereti* Mayet, 1908, from the early Late Miocene locality Hammerschmiede (Bavaria, Germany). The step-length of wear stages is given as an approximate percentage of the entire p4 tooth crown height (100%). Lower right dp4 (GPIT/MA/10785) in buccal (mirrored) view and lower left p4 (SNSB-BSPG 2020 XCIV-0487) for step-length of “age groups” definition in lingual and buccal views. WS 1, unworn: no wear can be observed, deciduous dentition in use; WS 2, slightly worn: first occlusal contact; WS 3, worn: para/metaflexus/id is closing or just closed; WS 4, medium worn: mesoflexus/id is closing or just closed; WS 5, deeply worn: hypoflexus/id is near to closing; WS 6, heavily worn: hypoflexus/id is closed. Occlusal pattern of lower right p4: WS 1, 3, 5 and 6: line drawings not based on specific specimens, WS 2: GPIT/MA/10745, WS 4: GPIT/MA/09896 (mirrored). WS 1–6 not to scale.

Mortality analysis.—In a following analysis, all unshed lower dp4 and p4 specimens from HAM 5 and HAM 4 strata representing the medium sized castorid *Steneofiber depereti* were counted and categorized by wear stage and an age-frequency distribution (Mortality profile) following Lyman (1994) was performed (Fig. 11).

In addition to the wear stage definitions as provided in the Material and Methods paragraph, the material representing WS 1 includes dp4s that are still in situ in the mandible, as well as isolated (used) dp4s, if they do not show signs of tooth resorption. Furthermore, unworn p4s would also relate to this age group and could duplicate dp4 data due to simultaneous occurrence, but no p4 in this wear stage is available from Hammerschmiede.

The mortality profiles according to the wear stages of the lower dp4/p4 specimens show different distributions in HAM 5 and HAM 4 (Fig. 11). In the HAM 4 profile, WS

1 (20%) and WS 3 (60%) dominate, while WS 4 (13.33%) and WS 5 (6.67%) are underrepresented and WS 2 and WS 6 are missing (Fig. 11). A different pattern occurs in the HAM 5 material, with high distributions in WS 1 (33%) and a consistent value for WS 2, WS 3 and WS 4 (22% each), with WS 4 being the highest available wear stage (Fig. 11).

The mortality profile of the HAM 4 layer complies with the typical U-shaped frequency distribution, referred to as “attritional” or “normal” mortality (Lyman 1994). This means that juvenile, mature and old individuals dominate the fossil material and young adults (WS 2) are lacking. This arrangement represents a natural ecological mortality (Lyman 1994). It can thus be assumed, that the HAM 4 river represents the natural ecosystem the beaver inhabited. A possible explanation for the low number of WS 1 and the complete absence of WS 2 material in HAM 4 could indicate a great ecological similarity of the larger Hammerschmiede castorid with the extant species of the *Castor*. Today’s beavers mostly prefer deeper waters, which correspond roughly to rivers of 1st or 2nd stream orders (according to the classic stream order following Hack 1957) (Beier and Barret 1987; Dieter and McCabe 1989; Hartman 1996; Hartman and Törnlov 2006), where HAM 4 is assumed to fit 2nd stream order. Since Hugueneu and Escuillié (1995) already have documented K-strategy and two-year parental investment in the very early *Steneofiber eseri* from Montaigu-le-Blin (France, MN 2) and since a similar behaviour is known from the extant beaver (Hinze 1950), this behaviour can possibly also be assumed for *S. depereti* from Hammerschmiede. Compared to *Castor fiber*, WS 1 would then represent the first year of live where predation pres-

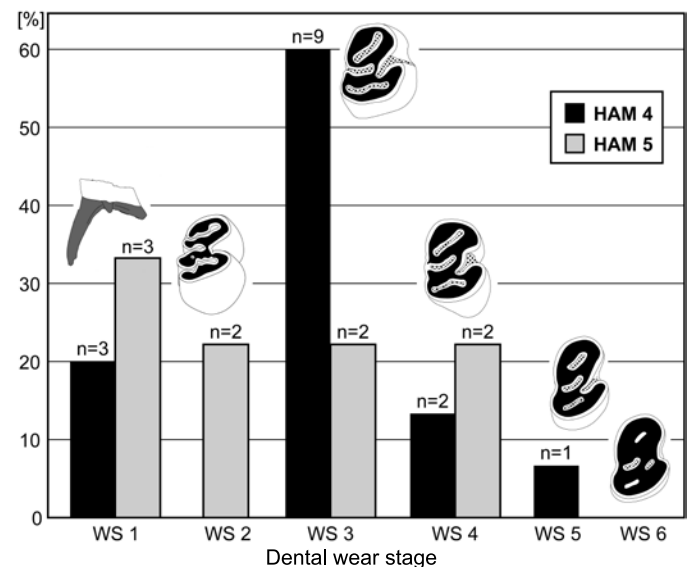


Fig. 11. Mortality profiles (age-frequency distribution) of the beaver *Steneofiber depereti* Mayet, 1908, from the early Late Miocene locality Hammerschmiede (Bavaria, Germany) based on lower dp4 and p4 tooth positions from the local stratigraphic levels HAM 5 and HAM 4. Each bar corresponds to an age class, defined by occlusal dental wear stages (WS 1–6). Vertical axis represents the percentage of individuals.

sure is moderate because of a small radius of movement close to the beaver lodge. WS 2 would include second year beavers, which migrate and are looking for their own territory, often on smaller tributaries (3rd stream order) because preferred territories are already occupied, as in extant beavers (Semyonoff 1951; Curry-Lindhal 1967; Żurowski and Kasperczyk 1986; Pupinnikas 1999; Gorshkov et al. 2002; Hartman and Törnlov 2006). The greatest predation pressure in the *S. depereti* population of HAM 4 seems to be on prime age beavers (WS 3) with a continuous staircase slope towards old (WS 4) and senile (WS 5) individuals (Fig. 11), which indicates continuous colonisation by larger family groups in the habitat. In contrast to HAM 4, the HAM 5 age-frequency distribution cannot be assigned to a generalised mortality pattern (U-shaped or L-shaped according to Lyman 1994). In the mortality profile of HAM 5, teeth for WS 2 ($n = 2$) are present and of equal value with WS 3 and WS 4 (22% each). Except for the slightly higher value for WS 1, all available beaver ages in HAM 5 (WS 1–4) seem to show a similar predation pressure. A possible explanation for this observation could be that the HAM 5 rivulet was a sporadically colonised habitat of only small founder populations of *S. depereti*, where the locality would not match the preferred habitat requirements. This would be consistent with the observation that HAM 5 corresponds to a shallow river or rivulet of 3rd stream order, which would neither be the preferred habitat of extant beavers (Beier and Barret 1987; Dieter and McCabe 1989; Hartman 1996; Hartman and Törnlov 2006), and thus would provide a niche for young adult beavers (especially WS 2) looking for a new territory.

Conclusions

The dental material of a medium sized castorid from the Hammerschmiede locality adds valuable morphological and metric data to the hitherto fragmentary record of European beavers of the early Late Miocene age. Furthermore, the material is characterised by a morphological intermediate stage between *Chalicomys jaegeri* and *Steneofiber depereti*. The still debated transitional evolution of *Steneofiber depereti*–*Chalicomys jaegeri*–*Castor fiber* implies that a differentiation between those taxa can be difficult (Mörs and Stefen 2010). The nominal types of this lineage, the early forms of *S. depereti* from the Early Miocene (MN 4) and the late forms of *C. jaegeri* from the Late Miocene (MN 9/10) are easily distinguishable. In contrast, the late forms of *S. depereti* and *C. jaegeri* share many dental characters (subhypodont to hypodont cheek teeth, three lingual striids, closure of roots at moderate or higher age, and synclines filled with cement at least at higher age) and can hardly be separated. In contrast, the Early Miocene European *Steneofiber eseri* and *Steneofiber castorinus*, characterized by a smaller size and mesodont cheek dentition, no cement in synclines, the absence of the

three lingual striids, and the closure of roots at juvenile age, can be easily distinguished from both *S. depereti* and *C. jaegeri*. With the medium size Hammerschmiede castorid sample, the taxonomic distinction between the two latter species is reduced to one character of the lower premolar: a hypostrid that does not reach the crown base in *S. depereti*. Whether it is appropriate to differentiate two species at the genus level with only one character is questionable and beyond the scope of this study.

By categorising the dental wear stages of lower premolars of *S. depereti* from Hammerschmiede in an age-frequency distribution (Mortality analysis), it can be proposed, that the Hammerschmiede beaver shows similarities in demography and ecology, including similar habitat requirements, with extant beavers. The 2nd order stream HAM 4 can be interpreted as a typical beaver habitat with continuous occupation by larger family groups (temporal and spatial), while the 3rd order stream HAM 5 is interpreted as not optimally matching the habitat requirements of *S. depereti*, resulting in a discontinuous occupation by smaller family groups, and thus primarily offering a niche for young adult beavers looking for a new territory.

Finally, the beavers from the locality Hammerschmiede in Southern Germany are part of a highly diverse river, rivulet and floodplain ecosystem of the early late Miocene that is an ideal environment for castorids. Thus, it is not surprising, that a second, but smaller beaver species, *Euroxenomys minutus*, is also inhabiting this environment. Due to similarities in the ecological behaviour of castorids, most fossil beaver sites contain only one species, and only a few localities comprise two or more species (Rekovets et al. 2020). If more than one beaver taxon is found at a fossil site, usually one is much more abundant. This is not the case for the Hammerschmiede beavers. Here, both the large *S. depereti* and the small *E. minutus* are frequently found.

Acknowledgements

The authors wish to thank Ingmar Werneburg (GPIT) for providing access to the specimens under his care (GPIT and SNSB-BSPG stored at GPIT). Further, we wish to thank Wolfgang Lechner (Nawilab, Trostberg, Germany) for providing recent reference material. We thank Henrik Stöhr (GPIT) for the preparation of the specimens and Agnes Fatz (Senckenberg Center HEP, Tübingen, Germany) for assistance and access to the photo laboratory. We further acknowledge all participants of the numerous excavations in the Hammerschmiede fossil site, who helped to detect and collect the studied material. The excavations and associated research were supported by the Bavarian State Ministry of Research and the Arts and by the Bavarian Natural History Collections (SNSB). We would also like to thank Ilona Gold, Christian Dietzel, Panagiotis Kampouridis, Felix Augustin, and Andreas Matzke (all GPIT) for fruitful discussions and improvement of the manuscript. Finally, we thank the editor Olivier Lambert (Royal Belgian Institute of Natural Sciences, Belgium), Clara Stefen (Senckenberg Naturhistorische Sammlungen Dresden, Germany), and an anonymous reviewer for helpful comments and suggestions on the manuscript.

References

- Aldana Carrasco, E. 1992. Los Castoridae (Rodentia, Mammalia) del Neógeno de Cataluña (España). *Treballs del Museu de Geologia de Barcelona* 2: 99–141.
- Beier, P. and Barrett, R.H. 1987. Beaver habitat use and impact in Truckee River Basin, California. *Journal of Wildlife Management* 51: 794–799.
- Böhme, M., Spassov, N., DeSilva, J.M., and Begun, D.R. 2020. Reply to: Reevaluating bipedalism in *Danuvius*. *Nature* 586: E4–E5.
- Böhme, M., Spassov, N., Fuss, J., Tröscher, A., Deane, A.S., Prieto, J., Kirscher, U., Lechner, T., and Begun, D.R. 2019. A new Miocene ape and locomotion in the ancestor of great apes and humans. *Nature* 575: 489–493.
- Bowdich, T.E. 1821. *An Analysis of the Natural Classifications of Mammalia for the Use of Students and Travellers*. 115 pp. J. Smith, Paris.
- Casanovas-Vilar, I. and Alba, D.M. 2011. The never-ending problem of Miocene beaver taxonomy. *Acta Palaeontologica Polonica* 56: 217–220.
- Casanovas-Vilar, I., Alba, D.M., Almécija, S., Robles, J.M., Galindo, J., and Moyà-Solà, S. 2008. Taxonomy and paleobiology of the genus *Chalicomys* Kaup, 1832 (Rodentia, Castoridae), with the description of a new species from Abocador De Can Mata (Vallès-Penedès Basin, Catalonia, Spain). *Journal of Vertebrate Paleontology* 28: 851–862.
- Curry-Lindahl, K. 1967. The beaver, *Castor fiber* Linnaeus, 1758 in Sweden—extinction and reappearance. *Acta Theriologica* 12 (1): 1–15.
- Dieter, C.D. and McCabe, T.R. 1989. Factors influencing beaver-lodge site selection on a prairie river. *The American Midland Naturalist* 122 (2): 408–411.
- Fahlbusch, V. and Mayr, H. 1975. Microtoide Cricetiden (Mammalia, Rodentia) aus der Oberen Süßwasser-Molasse Bayerns. *Palaeontologische Zeitschrift* 49: 78–93.
- Filhol, M.H. 1879. Etude des mammifères fossiles de Saint-Gérand-le-Puy (Allier). *Annales des Sciences géologiques* 10: 1–252.
- Fischer von Waldheim, G. 1809. Sur l'Elasmotherium et le Trogontherium, deux animaux fossiles et inconnus de la Russie. *Études palaeontologiques sur les environs de Moscou* 2: 250–268.
- Franzen, J.L. and Storch, G. 1975. Die unterpliozäne (turoliche) Wirbeltierfauna von Dorn-Dürkheim, Rheinhessen (SW-Deutschland); 1. Entdeckung, Geologie, Mammalia: Carnivora, Proboscidea, Rodentia. Grabungsergebnisse 1972–1973. *Senckenbergiana lethaea* 56: 233–303.
- Freye, H.-A. 1959. Deskriptive Anatomie des Craniums vom Elbe-Biber (*Castor fiber albicus* MATSCHIE 1907). *Wissenschaftliche Zeitschrift der Martin-Luther-Universität Halle-Wittenberg. Mathematisch-naturwissenschaftliche* 8: 913–962.
- Fuss, J., Prieto, J., and Böhme, M. 2015. Revision of the boselaphin bovid *Miotragocerus monacensis* Stromer, 1928 (Mammalia, Bovidae) at the Middle to Late Miocene transition in Central Europe. *Neues Jahrbuch für Geologie und Paläontologie Abhandlungen* 276: 229–265.
- Geoffroy-Saint-Hilaire, E.-F. 1833. Considérations sur des ossements fossils la plupart inconnus, trouvés et observés dans les bassins de l'Auvergne. *Revue encyclopédique (Paris)* 59: 76–95.
- Ginsburg, L. 1971. Sur l'évolution des *Steneofiber* (Mammalia, Rodentia) en France. *Comptes rendus de l'Académie des sciences, Paris, Série D: Sciences naturelles* 272: 2159–2161.
- Ginsburg, L., Cheneval, J., Janvier, P., Pouit, D., and Sen, S. 2000. Les Vertébrés des sables continentaux d'âge orléanien inférieur (MN 3) de Mauvières à Marcilly-sur-Maulne (Indre-et-Loire), La Brosse à Meigné-le-Vicomte (Maine-et-Loire) et Chitenay (Loir-et-Cher). *Geodiversitas* 22: 597–631.
- Gorshkov, Y.U., Gorshkov, D.Y., Easter-Pilcher, A.L., and Pilcher, B.K. 2002. First results of beaver (*Castor fiber*) reintroduction in Volga-Kama national nature Zapovednik (Russia). *Folia Zoologica* 51: 64–74.
- Hack, J.T. 1957. Studies of longitudinal stream profiles in Virginia and Maryland. Shorter contributions to general geology. *U.S. Geological Survey Professional Paper* 294-B: 45–97.
- Hartman, G. 1996. Habitat selection by European beaver (*Castor fiber*) colonizing a boreal landscape. *Journal of Zoology (London)* 240: 317–325.
- Hartman, G. and Törnlov, S. 2006. Influence of watercourse depth and width on dam-building behaviour by Eurasian beaver (*Castor fiber*). *Journal of Zoology (London)* 268: 127–131.
- Hartung, J. and Böhme, M. 2022. Unexpected cranial sexual dimorphism in the tragulid *Dorcatherium nauii* based on cranial material from the middle to late Miocene localities of Eppelsheim and Hammerschmiede (Germany). *PLOS ONE*. [published online, <https://doi.org/10.1371/journal.pone.0267951>]
- Hartung, J., Lechner, T., and Böhme, M. 2020. New cranial material of *Miotragocerus monacensis* (Mammalia: Bovidae) from the late Miocene hominid locality Hammerschmiede (Germany). *Neues Jahrbuch für Geologie und Paläontologie Abhandlungen* 298: 269–284.
- Heinrich, W.-D. and Maul, L.C. 2020. Mortality profiles of *Castor* and *Trogontherium* (Mammalia: Rodentia, Castoridae), with notes on the site formation of the Mid-Pleistocene hominin locality Bilzingsleben II (Thuringia, Central Germany). *Fossil Imprint* 76: 40–58.
- Hemprich, G. 1820. *Grundriss der Naturgeschichte für höhere Lehranstalten*. 29 pp. August Rücker, Berlin.
- Hinze, G. 1950. *Der Biber*. 216 pp. Körperbau und Lebensweise-Verbreitung und Geschichte Akademie-Verlag, Berlin.
- Huguency, M. 1999. Family Castoridae. In: G.E. Rössner and K. Heissig (eds.), *The Miocene Land Mammals of Europe*, 281–300. Verlag Friedrich Pfeil, Munich.
- Huguency, M. and Duranthon, F. 2012. Les Castoridae (Rodentia) de Sansan. In: S. Peigné (ed.), *Mammifères de Sansan. Mémoires du Muséum National d'Histoire Naturelle*, 95–118. Publications Scientifiques du Muséum, Paris.
- Huguency, M. and Escuillié, F. 1995. K-strategy and adaptive specialization in *Steneofiber* from Montaigu-le-Blin (dept. Allier, France; Lower Miocene, MN 2a, ±23 Ma): first evidence of fossil life-history strategies in castorid rodents. *Palaeogeography, Palaeoclimatology, Palaeoecology* 113: 217–225.
- Jäger, G.F. 1835. *Ueber die fossilen Säugethiere, welche in Württemberg aufgefunden worden sind*. 70 pp. C. Erhard, Stuttgart.
- Kargopoulos, N., Kampouridis, P., Lechner, T., and Böhme, M. 2021a. A review of *Semigenetta* (Viverridae, Carnivora) from the Miocene of Eurasia based on material from the hominid locality of Hammerschmiede (Germany). *Geobios* 69: 25–36.
- Kargopoulos, N., Kampouridis, P., Lechner, T., and Böhme, M. 2021b. Hyaenidae (Carnivora) from the Late Miocene hominid locality of Hammerschmiede (Bavaria, Germany). *Historical Biology* [published online, <https://doi.org/10.1080/08912963.2021.2010193>]
- Kargopoulos, N., Valenciano, A., Abella, J., Kampouridis, P., Lechner, T., Böhme, M. 2022. The exceptionally high diversity of small carnivorans from the Late Miocene hominid locality of Hammerschmiede (Bavaria, Germany). *PLOS ONE* 17 (7): e0268968.
- Kargopoulos, N., Valenciano, A., Kampouridis, P., Lechner, T., and Böhme, M. 2021c. New early late Miocene species of *Vishnuonyx* (Carnivora, Lutrinae) from the hominid locality of Hammerschmiede, Bavaria, Germany. *Journal of Vertebrate Paleontology* 41. [published online, <https://doi.org/10.1080/02724634.2021.1948858>]
- Kaup, J.J. 1832. Beschreibung dreier Gattungen urweltlicher Nager des zoologischen Museums zu Darmstadt, welche von den jetzt lebenden Genera verschieden sind. *Isis* 9: 992–996.
- Kaup J.J. 1833. Mitteilungen an Professor Bronn [letter to Bronn]. *Neues Jahrbuch für Mineralogie, Geognosie, Geologie und Petrefaktenkunde* 1833: 419–420.
- Kirscher, U., Prieto, J., Bachtadse, V., Abdul Aziz, H., Doppler, G., Hagmaier, M., and Böhme, M. 2016. A biochronologic tie-point for the base of the Tortonian stage in Europe terrestrial settings: Magnetostratigraphy of the topmost Upper Freshwater Molasse sediments of the North Alpine Foreland Basin in Bavaria (Germany). *Newsletters on Stratigraphy* 49: 445–467.
- Lambrecht, K. 1916. Die Gattung *Plotus* im ungarischen Neogen. *Mitteilungen aus dem Jahrbuche der königlichen ungarischen Geologischen Reichsanstalt* 24: 1–24
- Lechner, T.S. and Böhme, M. 2020. *Castor*-like postcranial adaptation in an

- uppermost Miocene beaver from the Staniantsi Basin (NW Bulgaria). *Fossil Imprint* 76: 128–164.
- Linnaeus, C. 1758. *Systema naturae Per Regna Tria Naturae, Secundum Classes, Ordines, Genera, Species cum Characteribus, Differentiis, Synonymis, Locis*. 824 pp. Laurentius Salvius, Holmiae (Stockholm).
- Lyman, R.L. 1994. *Vertebrate Taphonomy. Cambridge Manuals in Archaeology*. 524 pp. Cambridge University Press, Cambridge.
- Mayet, L. 1908. Étude des mammifères miocènes des sables de l'Orléanais et des faluns de la Touraine. *Annales de l'Université de Lyon. Nouvelle Série, I. Sciences, Médecine* 24: 1–336.
- Mayr, G., Lechner, T., and Böhme, M. 2020a. A skull of a very large crane from the late Miocene of Southern Germany, with notes on the phylogenetic interrelationships of extant Gruinae. *Journal of Ornithology* 161: 923–933.
- Mayr, G., Lechner, T., and Böhme, M. 2020b. The large-sized darter *Anhinga pannonica* (Aves, Anhingidae) from the late Miocene hominid Hammerschmiede locality in Southern Germany. *PLOS ONE* 15 (5): 0232179.
- Mayr, G., Lechner, T., and Böhme, M. 2022. Nearly complete leg of an unusual, shelduck-sized anseriform bird from the earliest late Miocene hominid locality Hammerschmiede (Germany). *Historical Biology*. [published online, <https://doi.org/10.1080/08912963.2022.2045285>].
- Mayr, H. and Fahlbusch, V. 1975. Eine unterpliozäne Kleinsäugerfauna aus der Oberen Süßwasser-Molasse Bayerns. *Mitteilungen der Bayerischen Staatssammlung für Paläontologie und Historische Geologie* 15: 91–111.
- Mein, P. 1975. Résultats du groupe de travail des vertébrés: Biozonation du Néogène méditerranéen à partir des mammifères. In: J. Senes (ed.), *Report on Activity of the RCMNS Working Groups (1971–1975)*, 78–81. Bratislava.
- Mörs, T. and Stefen, C. 2010. The castorid *Steneofiber* from NW Germany and its implications for the taxonomy of Miocene beavers. *Acta Palaeontologica Polonica* 55: 189–198.
- Pomel, A. 1847. Note sur des animaux fossiles découverts dans le département de l'Allier. *Bulletin de la Société géologique de France* 4: 378–385.
- Prieto, J. 2012. The genus *Eomyops* Engesser, 1979 (Rodentia, Eomyidae) from the youngest deposits of the German part of the North Alpine Foreland Basin. *Swiss Journal of Palaeontology* 131: 95–106.
- Prieto, J. and van Dam, J.A. 2012. Primitive Anourosoricini and Allosoricinae from the Miocene of Germany. *Geobios* 45: 581–589.
- Prieto, J. and Rummel, M. 2009. Evolution of the genus *Collimys* Daxner-Hock, 1972 (Rodentia, Cricetidae) a key to Middle to Late Miocene biostratigraphy in Central Europe. *Neues Jahrbuch für Geologie und Paläontologie Abhandlungen* 252: 237–247.
- Prieto, J., van den Hoek Ostende, L.W., Böhme, M., and Braze, M. 2011. Reappearance of *Galerix* (Erinaceomorpha, Mammalia) at the Middle to Late Miocene transition in South Germany: biostratigraphic and palaeoecologic implications. *Contributions to Zoology* 80: 179–189.
- Pupinnikas, S. 1999. The state of the beaver (*Castor fiber*) populations and characteristics of beaver sites in Lithuania. *Acta Zoologica Lithuanica* 9: 20–26.
- Rekovets, L., Kopij, G., and Nowakowski, D. 2009. Taxonomic diversity and spatio-temporal distribution of late Cenozoic beavers (Castoridae, Rodentia) of Ukraine. *Acta Zoologica Cracoviensia. Series A: Vertebrata* 52: 95–105.
- Rekovets, L., Stefen, C., and Demeshkant, V. 2020. Beavers (Castoridae, Rodentia) from the late Miocene (MN 9) locality Grytsiv in Ukraine. *Fossil Imprint* 76: 165–173.
- Roger, O. 1898. Wirbeltierreste aus dem Dinotheriensande der bayerisch-schwäbischen Hochebene. *Bericht des Naturwissenschaftlichen Vereins für Schwaben und Neuburg* 33: 1–46.
- Sach, V.J. and Heizmann, E.P.J. 2001. Stratigraphie und Säugetierfauna der Brackwassermolasse in der Umgebung von Ulm (Südwestdeutschland). *Stuttgarter Beiträge zur Naturkunde Serie B (Geologie und Paläontologie)* 310: 1–95.
- Samson, P. and Radulesco, C. 1973. Remarques sur l'évolution des Castoridés (Rodentia, Mammalia). In: Traian Orghidan (ed.), *Livre du cinquantenaire de L'Institut de Spéléologie "Emile Racovitza"*, 437–449. Academiae Republicii Socialiste România, Bucarest.
- Schlosser, M. 1884. Die Nager des europäischen Tertiärs nebst Betrachtungen über die Organisation und die geschichtliche Entwicklung der Nager überhaupt. *Palaeontographica* 31: 19–162.
- Schlosser, M. 1902. Beiträge zur Kenntniss der Säugethierreste aus den süddeutschen Bohnerzen. *Geologische und Palaeontologische Abhandlungen Jena* 5 (3): 117–258.
- Seemann, I. 1938. Die Insektenfresser, Fledermäuse und Nager aus der obermiocänen Braunkohle von Viehhausen bei Regensburg. *Palaeontographica A* 89: 1–56.
- Semyonoff, B.T. 1951. The river beaver in Archangel Province. In: *Translation of Russian Game Reports, Vol. 1*, 5–45. Canadian Wildlife Services, Ottawa.
- Stefen, C. 1997. *Steneofiber eseri* (Castoridae, Mammalia) von der Westtangente bei Ulm im Vergleich zu anderen Biberpopulationen. *Stuttgarter Beiträge zur Naturkunde, Serie B* 255: 1–78.
- Stefen, C. 2001. Barstovian (Miocene) beavers from Stewart Valley, Nevada, and a discussion of the genus *Monosaulax* based on tooth morphology. *PaleoBios* 21: 1–14.
- Stefen, C. 2009. The European Tertiary beaver *Chalicomys jaegeri* (Rodentia: Castoridae) revisited. *Kaupia-Darmstädter Beiträge zur Naturgeschichte* 16: 161–174.
- Stefen, C. 2011. A brief overview of the evolution of European tertiary beavers. *Baltic Forestry* 17 (1): 148–153.
- Stefen, C. 2018. The castorids (Mammalia, Castoridae) from the (early) middle Miocene of Gračanica (Bosnia-Herzegovina). *Palaeobiodiversity and Palaeoenvironments* 100: 301–305.
- Stefen, C. and Mörs, T. 2008. The beaver *Anchitheriomys* from the Miocene of central Europe. *Journal of Paleontology* 82: 1009–1020.
- Stirton, R.A. 1935. A review of the Tertiary beavers. *University of California Publications in Geological Sciences* 23: 391–458.
- Stromer von Reichenbach, E. 1928. Wirbeltiere im obermiocänen Flnz Münchens. *Abhandlungen der Bayerischen Akademie der Wissenschaften, mathematisch-naturwissenschaftliche* 32: 1–74.
- Von Meyer, H. 1838. Mittheilungen an Professor Bronn gerichtet, Frankfurt a. M., den 26. Juli 1838. In: K.C. Leonhard and H.G. Bronn (eds.), *Neues Jahrbuch für Mineralogie, Geognosie, Geologie und Petrefaktenkunde*, 1838: 413–418.
- Von Meyer, H. 1846. Mittheilungen an Prof. Bronn. *Neues Jahrbuch für Mineralogie, Geologie und Paläontologie, Stuttgart* 1846: 462–476.
- Von Meyer, H. 1846. Mittheilungen an Professor Bronn gerichtet, Frankfurt a. M., 4. Mai 1846. In: K.C. Leonhard and H.G. Bronn (eds.), *Neues Jahrbuch für Mineralogie, Geognosie, Geologie und Petrefaktenkunde* 1846: 462–476.
- Williams, S.A., Prang, T.C., Meyer, M.R., Russo, G.A., and Shapiro, L.J. 2020. Reevaluating bipedalism in *Danuvius*. *Nature* 586: E1–E3.
- Żurowski, W. and Kasperczyk, B. 1986. Characteristics of a European beaver population in the Suwalki Lakeland. *Acta Theriologica* 31: 311–325.

Chapter 8



Taxonomy and Ecology of the beaver *Euroxenomys minutus* (Mammalia, Castoridae)

Published in

Lechner, T., Böhme, M., 2023. The largest record of the minute beaver *Euroxenomys minutus* (Mammalia, Castoridae) from the early Late Miocene hominid locality Hammerschmiede (Bavaria, Southern Germany) and palaeoecological considerations. *Historical Biology*, 1–16. <https://doi.org/10.1080/08912963.2023.2215236>

This chapter is a reprint of the published version and differs from the general chapter numbering of this dissertation.

The largest record of the minute beaver *Euroxenomys minutus* (Mammalia, Castoridae) from the early Late Miocene hominid locality Hammerschmiede (Bavaria, Southern Germany) and palaeoecological considerations

Thomas Lechner  and Madelaine Böhme 

Senckenberg Centre for Human Evolution and Palaeoenvironment (HEP), Eberhard Karls University of Tübingen, Institute for Geoscience, Tübingen, Germany

ABSTRACT

In this study, we describe the dental remains of a very minute beaver from the early Late Miocene locality Hammerschmiede (MN 7/8) located at the Northern Alpine Foreland Basin (Southern Germany, Bavaria). The finds represent the so far most comprehensive (>1.000 dental specimens) collection of the trogontheriine castorid *Euroxenomys minutus*. Metrically and morphologically, the large data set demonstrates an extensive intraspecific variability of this beaver from Hammerschmiede that covers most finds of other European localities and confirms previous species assignments. The subspecies *Euroxenomys minutus rhenanus* from Dorn-Dürkheim (Germany), clearly isolates from this range of variation and can thus be validated. The performed age-frequency distributions for *Euroxenomys minutus* from the local stratigraphic levels HAM 5 (rivulet) and HAM 4 (river) correspond roughly and also resemble *Euroxenomys* from the swamp deposit Rudabánya (Hungary). Since previous mortality studies on the also occurring larger beaver *Steneofiber depereti* from Hammerschmiede demonstrated dominance of behavioural or internal factors, this cross-ecosystem similarity in mortality for the small beaver species is likely explained by external factors, such as predation. Supported by a taphonomic bone analysis, a multitude of predators are finally considered to prey on *Euroxenomys minutus* and indicate a predatory bone assemblage.

ARTICLE HISTORY

Received 12 April 2023
Accepted 14 May 2023

KEYWORDS

Mammalia; Castoridae;
Euroxenomys minutus;
ecology; mortality analysis;
Hammerschmiede locality

Introduction



For almost half a century now, the Hammerschmiede fossil site has been providing new scientific discoveries (Fahlbusch and Mayr 1975; Mayr and Fahlbusch 1975). At least seven fossil-bearing strata are known to date, with most of the finds coming from the local stratigraphic levels HAM 5 and HAM 4, dated to 11.62 and 11.44 Ma, respectively, by Kirscher et al. (2016). Since new excavation efforts by the University of Tübingen began in the early 2000s, the constantly growing amount of material available has increased to more than 30,000 specimens, which comprise at least 146 different vertebrate taxa. The still ongoing excavations continue to yield new discoveries year after year, which contribute to our knowledge on these unique early Late Miocene ecosystems in Central Europe. The most famous discovery of the Hammerschmiede is for sure the arboreal biped hominid *Danuvius guggenmosi* Böhme et al. (2019), which attracted international interest (Böhme et al. 2019, 2020; Williams et al. 2020). Many different vertebrates from Hammerschmiede have already been subject of scientific research, including carnivores (Kargopoulos et al. 2021a, 2021b, 2021c, 2022), artiodactyles (Fuss et al. 2015; Hartung et al. 2020, 2022), small mammals (Mayr and Fahlbusch 1975; Prieto 2009, 2012; Prieto et al. 2011; Prieto and van Dam 2012) and birds (Mayr et al. 2020a, 2020b, 2022). A preliminary taxa list of the Hammerschmiede fauna was published by Kirscher et al. (2016) and updated by Böhme et al. (2019).


Beavers have also been included in scientific studies on the Hammerschmiede fauna. Mayr and Fahlbusch (1975) have already

mentioned the occurrence of two beaver species, a small form '*Steneofiber minutus*' = *Euroxenomys minutus* (von Meyer 1838) and a large beaver species '*Steneofiber jaegeri*' = *Chalicomys jaegeri* Kaup (1832) were mentioned by a small number of teeth and fragments. The large form, referred to a single incisor fragment, was further listed by Huguene (1999), Kirscher et al. (2016) and Böhme et al. (2019) as *Chalicomys jaegeri* Kaup (1832). Recently, Lechner and Böhme (2022) assigned the now significantly more extensive material collection of this large beaver to the species of *Steneofiber depereti* Mayet (1908). The small beaver form from Hammerschmiede was already correctly recognised by several authors as one of the various synonymous combinations like *Trogotherium* (*Euroxenomys*) *minutum* in Huguene (1999) and *Euroxenomys minutus* in Kirscher et al. (2016), Böhme et al. (2019) and Lechner and Böhme (2022). Here, we follow the latter in their assignment to the combination *Euroxenomys minutus* (von Meyer 1838).

Euroxenomys represents with much over 1.000 dental and at least as many postcranial specimens a very abundant rodent in Hammerschmiede, being next to *Anomalomys gaudryi* (Anomalomyidae) the second most common small mammal species after *Microcricetus molassicus* (Cricetidae).

The current beaver biodiversity is limited to one genus including two species, whereas the family of Castoridae was much more diverse during the Miocene time period. The European Neogene beaver record is very rich and contains up to seven genera, *Anchitheriomys* Roger (1898), *Chalicomys* Kaup (1832), *Dipoides*

CONTACT Thomas Lechner  thomas.lechner@senckenberg.de  Senckenberg Centre for Human Evolution and Palaeoenvironment (HEP), Eberhard Karls University of Tübingen, Institute for Geoscience, Sigwartstraße 10, 72074 Tübingen, Germany

 Supplemental data for this article can be accessed online at <https://doi.org/10.1080/08912963.2023.2215236>.

© 2023 The Author(s). Published by Informa UK Limited, trading as Taylor & Francis Group.

This is an Open Access article distributed under the terms of the Creative Commons Attribution-NonCommercial-NoDerivatives License (<http://creativecommons.org/licenses/by-nc-nd/4.0/>), which permits non-commercial re-use, distribution, and reproduction in any medium, provided the original work is properly cited, and is not altered, transformed, or built upon in any way. The terms on which this article has been published allow the posting of the Accepted Manuscript in a repository by the author(s) or with their consent.

Jäger (1835), *Eucastor?* (*Schreuderia*) Aldana Carrasco (1992), *Euroxenomys* Samson and Rădulescu (1973), *Steneofiber* Geoffroy-Saint-Hilaire (1833) and *Trogontherium* Fischer von Waldheim (1809) (Hugueney 1999; Stefen 2009). There are localities with only one beaver species recorded and others, containing a higher beaver diversity (Hugueney 1999; Rekovets et al. 2020). It is quite rare that several large beavers occur simultaneously in one site, whereas the combination of one large beaver like *Steneofiber* or *Chalicomys* and the minute beaver *Euroxenomys minutus* is quite typical (Hugueney 1999).

The biology and ecology of fossil representatives of the *Steneofiber-Chalicomys-Castor* lineage can probably be considered quite similar to those of present-day castorids. Physiognomy with excellent swimming and burrowing ability and behavioural strategies or ecological parameters seem to differ only marginally from today's beavers (Schreuder 1929; Hugueney and Escuillié 1995, 1996; Lechner and Böhme 2020, 2022). The knowledge about the ecology of the small beaver *Euroxenomys minutus* is much more limited and therefore it is not fully understood how coexistence with large beaver species is possible. It seems clear that the small beaver deviates from the typical beaver construction plan simply because of its small body size (size of a muskrat), but also other physiognomic differences (no wide and flattened tail; different long-bone proportions) and thus is likely to represent a different ecology, possibly comparable to the extant muskrat – *Ondatra zibethicus* (Stefen and Rummel 2003; Daxner-Höck 2004). We know from present-day beavers that they can easily exist sympatrically in the same habitats with the muskrat, which is also semi-aquatic (Mott et al. 2013). For a deeper palaeoecological analysis, in addition to dental investigations, profound functional-morphological analyses of the entire skeleton must of course be carried out. Even though especially the long bones of the extremities are often fragmented and broken, more than 1000 pieces are available for such investigations. The postcranial fundus will be the subject of future investigations and is not part of the present study.

The aim of our study is to describe the large amount of dental material of the minute beaver *Euroxenomys minutus* from Hammerschmiede and compare with other finds of European localities. Since the Hammerschmiede material probably represents the most extensive collection of material of this fossil beaver species, a unique insight into its intraspecific variability can be gained here. Furthermore, the material is analysed taphonomically to find potential traces of predation. Finally, mortality analyses based on dental wear stages are created that can provide further evidence for the ecological classification of this small beaver and makes it possible to compare it with other beaver species from similar and different fossil habitats.

Geological setting

The Hammerschmiede fossil site is an actively operated clay mine near the small village of Pforzen (Bavaria, Southern Germany). The 26-metre-thick profile of the clay pit exhibits fluvio-alluvial flood plain deposits (clay, silt, fine-sand, lignite) of the Northern Alpine Foreland Basin. The two main fossiliferous levels HAM 5 and HAM 4 represent early Late Miocene (base of Tortonian, MN 7/8) channel fillings with very fossil enriched channel lag deposits and have been dated to 11.62 and 11.44 Myr, respectively (Kirscher et al. 2016). The older HAM 5 is assumed to represent a rivulet of approximately 5 m width, whereas HAM 4 corresponds to a larger river of about 50 m width and 4–5 m depth (Mayr et al. 2020a; Lechner and Böhme 2022).

Material and methods

The studied specimens were collected from the local fossil layers HAM 5 and HAM 4 of the Hammerschmiede site over the period from 2011 to 2021 (later collected specimens are not included). Since 2016, all excavated sediments of the find layers are screened for small finds (>1 mm) by means of screen washing and rotational sieving system. However, a large part of the sediments from the grain size range 1–5 mm has not yet been sorted out, so that a statistical distribution of tooth sizes of small teeth (last molars) to large teeth (premolars) is probably statistically biased. In total, 1115 teeth (981 specimens) were examined, of which 465 (452 specimens: 10 tooth row specimens, 442 isolated teeth) are from the HAM 5 layer and 650 (529 specimens: 75 tooth row specimens, 454 isolated teeth) from the HAM 4 layer.

The entire material is deposited in the palaeontological collection of the University of Tübingen, Germany (GPIT), and is labelled either with GPIT (for excavation years 2011 to 2019 inclusive) or SNSB-BSPG (Bavarian State Collection of Palaeontology and Geology in Munich, Germany; for excavation years 2020 to 2022). SNSB-BSPG 2020 XCIV encodes the inventory from the layer HAM 4 and SNSB-BSPG 2020 XCV from the layer HAM 5.

The morphological nomenclature of dental material follows Stirton (1935) and Hugueney (1999) (Figure 1). The nomenclature of skull and mandibular features follows Freye (1959) and Stefen and Rummel (2003).

Measurements were taken with a digital calliper (rounded to the first decimal point). The maximum mesio-distal length (L) and bucco-lingual width (W) of cheek teeth were measured at the occlusal surface (occlusal measurements) and at the basal tooth crown position (basal measurements) where possible. In the upper and lower incisors, the length (L) corresponds to the antero-posterior and the width (W) to the mesio-distal extent.

Crown height measurements of lower premolars (p4) follow Kordos (2020) and have been taken at the position of the buccal hypostriid: (1) from the occlusal surface of the tooth to the base of the hypoflexid and (2) from the base of the hypoflexid to the base of the tooth crown. Both measurements were added to determine a tooth crown height.

The evaluation of dental wear stages (WS) used for tooth descriptions are modified according to Stefen (1997, 2001, 2018), Stefen and Mörs (2008), Heinrich and Maul (2020) and Lechner and Böhme (2022): (1) unworn: no wear can be observed, deciduous dentition in use; (2) slightly worn: first clear occlusal contact; (3) worn: para-/metaflexus/-id is closing or closed and mesoflexus/-id in most cases open; (4) medium worn: mesoflexus/-id is closing or just closed; (5) deeply worn: hypoflexus/-id is near to closing; (6) heavily worn: hypoflexus/-id is closed. Due to the very short lingual striids in the available material from Hammerschmiede, the wear stages from unworn to worn teeth represent approximately the first quarter of tooth crown height and therefore these wear stages defined on morphological criteria cannot be used for evenly graded age estimation and thus for a mortality analysis.

The dental wear stages for the preparation of mortality analyses were taken at the lower premolar tooth position and combine morphological and metric data. The first two wear stages are morphologically determined age stages defined by unused (WS 1, deciduous tooth in use) and first and slightly used lower p4 (WS 2, milk tooth replaced). During these two wear stages, the tooth crown of the lower p4 is not fully grown and the crown height cannot be measured. For the remaining p4 material (> WS 2), the wear stages are calculated based on the crown height. The difference between the largest and the smallest measured tooth crown height is divided into four evenly distributed size ranges and the teeth are

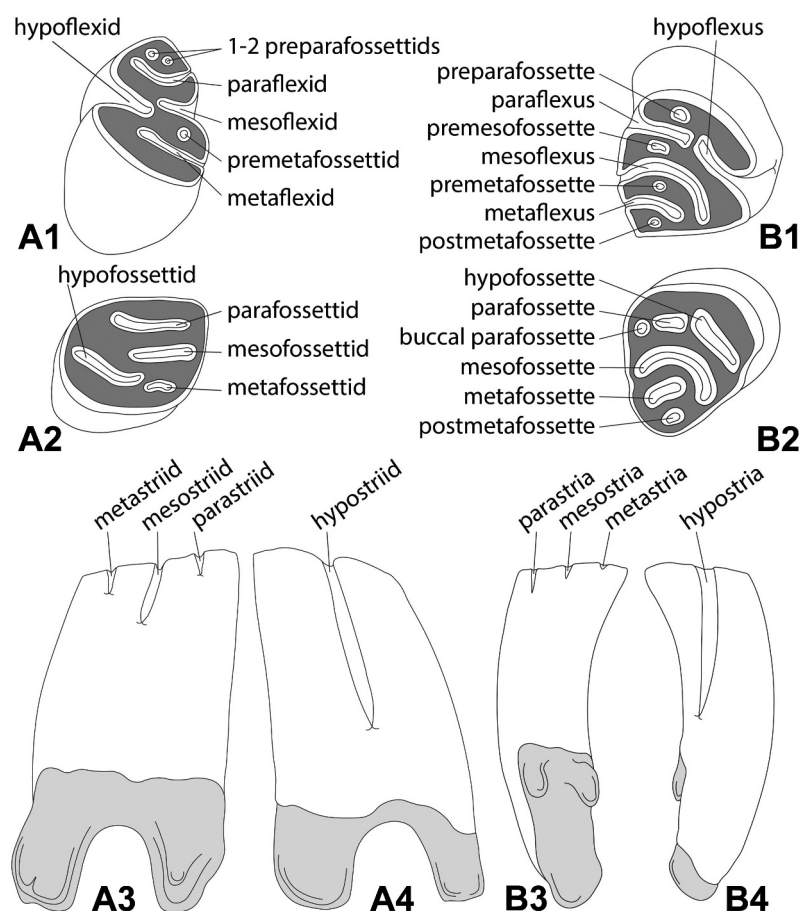


Figure 1. Morphological nomenclature and the general tooth scheme of left lower (A) and right upper (B) cheek teeth (premolars and molars) used for the descriptions and comparisons of the minute beaver *Euroxenyomys minutus* (von Meyer 1838), from the early Late Miocene locality Hammerschmiede (Bavaria, Germany). (A1) and (B1), occlusal views of early wear stages; (A2) and (B2), occlusal views of later wear stages; (A3) and (B4), lingual views; (A4) and (B3), buccal views. Enamel in white, dentine in dark grey, roots in light grey. Line drawings are not based on actual specimens and are not to scale. Nomenclature follows Stirton (1935) and Huguency (1999).

assigned to these size categories as WS 3 to WS 6 according to their measured value. Due to the high metric variability within the existing tooth material, it did not seem reasonable to define more than 4 wear stages based on measurements.

Systematic palaeontology

Family Castoridae Hemprich (1820)

Genus *Euroxenyomys* Samson and Rădulesco (1973)

Comment

The generic assignment of *Euroxenyomys* is still under discussion. In some studies, *Euroxenyomys* is classified at the subgenus level (e.g. Huguency 1999; Stefen and Rummel 2003; Giersch et al. 2010; Kordos 2020) or as a valid genus (e.g. Samson and Rădulesco 1973; Korth 2001; Huguency and Duranthon 2012; Prieto et al. 2014; Rekovets et al. 2020; Mörs et al. 2022).

Here, we follow Huguency and Duranthon (2012) and place *Euroxenyomys* at generic level.

Type species

Chalicomys minutus von Meyer (1838)

Type locality

Elgg (Switzerland), Middle Miocene.

Euroxenyomys minutus (von Meyer 1838)

Subspecies of *Euroxenyomys*: *E. minutus minutus* (von Meyer 1838), *E. minutus rhenanus* (Franzen and Storch 1975)

Euroxenyomys minutus minutus (von Meyer 1838)

(Figures 2–5; Measurements see Figures 6–7, Table 1 and Table 2 supplement)

Material

Hammerschmiede locality, Germany, early Late Miocene, base of Tortonian, MN 7/8. For measurements see Table 1 and Table 2 supplement. The material comprises a total of 1115 teeth (981 specimens: 896 isolated teeth; 32 jaws with in situ dentition) from layer HAM 5 and HAM 4 together. The HAM 5 material includes 465 teeth (452 specimens: 442 isolated teeth; 4 jaws with in situ dentition) and the HAM 4 material includes 650 teeth (529 specimens: 454 isolated teeth; 28 jaws with in situ dentition). HAM 5: 24 i2, 34 dp4, 68 p4, 84 m1/2, 21 m3, 18 I2, 17 DP4, 67 P4, 91 M1/2, 37 M3; HAM 4: 89 i2, 9 dp4, 143 p4, 130 m1/2, 19 m3, 45 I2, 6 DP4, 115 P4, 72 M1/2, 22 M3. The MNI (minimum number of individuals) based on the maximum number of a tooth position on one side is 35 for HAM 5 (based on right lower p4 and left upper P4) and 82 for Ham 4 (right lower p4).

Diagnosis

See Prieto et al. (2014) and emended diagnosis therein. Furthermore, see diagnosis in Samson and Rădulesco (1973) for

Table 1. Dimensions of upper and lower teeth of the minute beaver *Euroxenomys minutus* (von Meyer 1838), from the early Late Miocene locality Hammerschmiede (Bavaria, Germany), with combined treatment of the material from the local stratigraphic levels HAM 5 and HAM 4. L, mesio-distal length at occlusal surface and at basal crown position (where possible) for cheek teeth and length across anterior enamel band for incisors; W, bucco-lingual width at occlusal surface and at basal crown position (where possible) for cheek teeth; m, measurement; n, number of measurements (sum of occlusal and basal values); All measurements in mm.

Tooth	m	n	min	max	mean	standard deviation	variance
i	L	101	2.36	4.29	3.35	0.36	0.13
	W	101	2.27	3.67	2.99	0.31	0.10
I	L	70	2.65	3.89	3.43	0.23	0.06
	W	70	2.12	3.40	2.95	0.24	0.06
dp4	L	37	3.07	3.89	3.54	0.19	0.03
	W	38	2.29	2.96	2.68	0.18	0.03
p4	L	352	2.95	6.25	4.89	0.58	0.34
	W	363	2.52	4.15	3.47	0.33	0.11
m1/2	L	324	2.37	3.63	2.98	0.32	0.10
	W	328	2.63	4.36	3.43	0.27	0.07
m3	L	63	2.58	3.75	3.11	0.29	0.08
	W	64	2.64	3.75	3.31	0.24	0.06
DP4	L	20	2.85	3.30	3.09	0.11	0.01
	W	20	2.42	3.25	2.87	0.26	0.07
P4	L	308	2.97	4.73	3.93	0.28	0.08
	W	312	2.74	4.92	4.08	0.39	0.16
M1/2	L	284	2.10	3.25	2.69	0.30	0.09
	W	280	2.29	3.97	3.20	0.25	0.06
M3	L	106	2.79	4.67	3.60	0.35	0.13
	W	107	2.61	3.99	3.17	0.21	0.04

the then assumed monospecific genus *Euroxenomys* and see Hugueney (1999), Daxner-Höck and Bernor (2009) and Kordos (2020) for detailed dental descriptions of *Euroxenomys minutus*.

Description (Figures 2–5)

Maxilla and palatine (Figure 2)

There are several cranial specimens of *Euroxenomys minutus* available from Hammerschmiede, mostly comprising fragments of the toothrow or maxilla and palatine. The description of maxilla and palatine follows the rather complete specimens (SNSB-BSPG 2020 XCIV-9124, 9522, 9523). In ventral view, the tooth rows diverge from anterior to distal (Fig. 2A3, B2, C1). The palatine shows

a small anterior palatine foramen and a slightly larger lateral distal palatine foramen is fragmentary preserved in SNSB-BSPG 2020 XCIV-9522 (Fig. 2C1). The distal end of the palatine is medially trapezoidal carved without an aboral nasal spine as it typically occurs with *Castor*. The anterior palatine suture separates the maxillaries almost in a straight line on between M1 and M2. Maxillary grooves start at the anterior palatal foramen and extend slightly anterior to P4 enclosing a medially aligned palatine sulcus. A laterally very widely projecting zygomatic process is fragmentarily indicated (Fig. 2A2).

I2

Upper incisors are robust, rounded triangular and show a smooth and convex anterior enamel surface, a convex to nearly straight

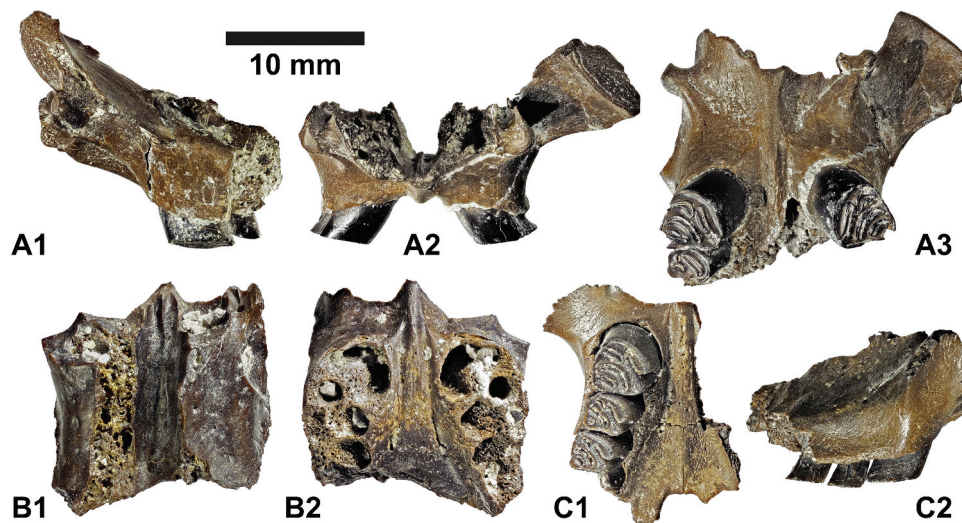


Figure 2. Cranial fragments of the minute beaver *Euroxenomys minutus* (von Meyer 1838), from the early Late Miocene locality Hammerschmiede (Bavaria, Germany), local stratigraphic level HAM 4. (A) SNSB-BSPG 2020 XCIV-9124, maxillae and fragmentary palatine with left P4 and right P4-M1 in left buccal (A1), mesial (A2) and occlusal (A3) views. (B) SNSB-BSPG 2020 XCIV-9523, maxillae and fragmentary palatine without dentition but with preserved alveoli of left P4-M3 and right P4-M2 in dorsal (B1) and occlusal (B2) views. (C) SNSB-BSPG 2020 XCIV-9522, right maxilla and fragmentary palatine with right P4-M2 in occlusal (C1) and right buccal (C2) views. Scale bar equals 10 mm.

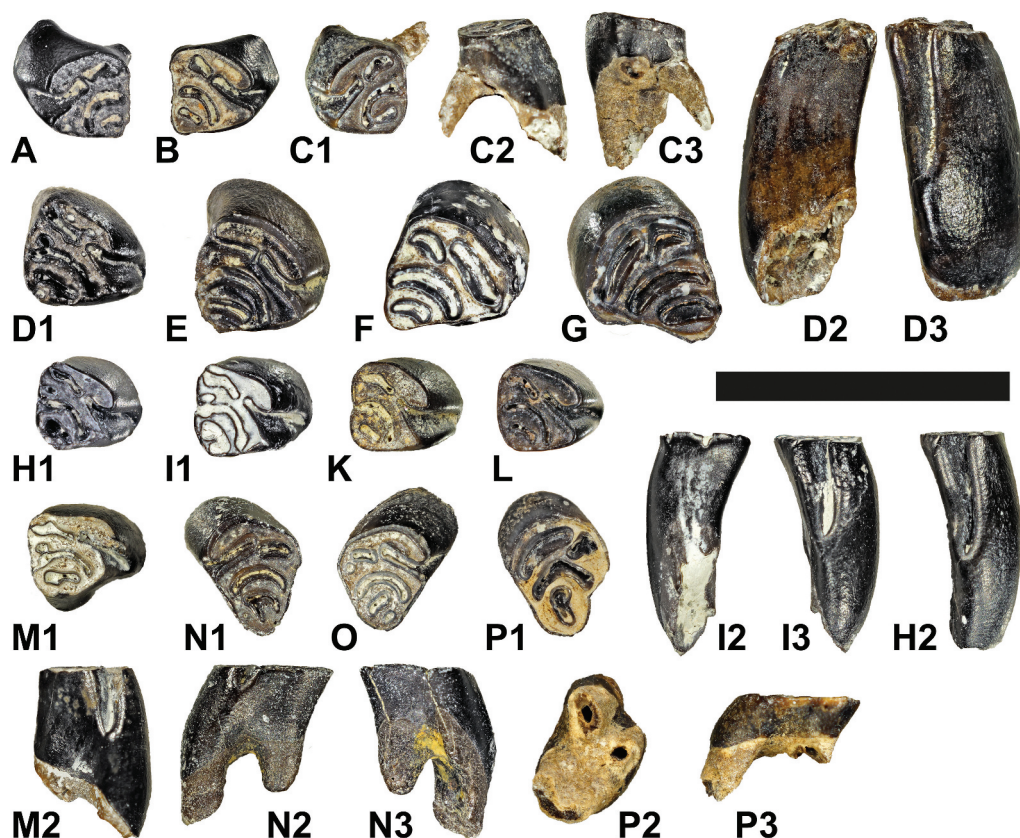


Figure 3. Upper cheek teeth of the minute beaver *Euroxenomys minutus* (von Meyer 1838), from the early Late Miocene locality Hammerschmiede (Bavaria, Germany), local stratigraphic levels HAM 5 and HAM 4. Deciduous premolars: (A-C); premolars (D-G); molars (H-P). Occlusal (A, B, C1, D1, E, F, G, H1, I1, K, L, M1, N1, O, P1), lingual (D3, H2, I3, M2, N2, P3), buccal (D2, I2, N3) and apical (P2) views. Scale bar equals 10 mm. Left DP4: (A) GPIT/MA/12001; (C) GPIT/MA/12058. Right DP4: (B) GPIT/MA/19158. Left P4: (G) GPIT/MA/18783. Right P4: (D) GPIT/MA/19060; (E) GPIT/MA/18780; (F) GPIT/MA/18835. Right M1/2: (H) GPIT/MA/18866; (I) GPIT/MA/18872; (K) SNSB-BSPG 2020 XCIV-6959; (L) GPIT/MA/19131. Left M3: (N) GPIT/MA/19088; (P) GPIT/MA/19127. Right M3: (M) SNSB-BSPG 2020 XCIV-6949; (O) SNSB-BSPG 2020 XCIV-2170.

mesial and a convex rounded distal tooth surface. The mesial and distal tooth surfaces may show slight longitudinal striations of irregular arrangement (GPIT/MA/19176, 19177). In contrast to the lower incisors, the wear area in upper I2 is short and the anterior enamel edge is straight. There are two wear facets, one runs evenly diagonally over the distal wear area, whereas the other dips steeply into the dentin along the anterior enamel band and results in a mesial depression in which the tip of the lower i2 can insert (GPIT/MA/19177), as in the modern muskrat *Ondatra zibethicus*.

DP4 (Figure 3A-C)

The upper deciduous premolar is very short crowned (brachydont) and exhibits in unused specimens a rather rectangular, with increasing wear rather triangular occlusal outline. The buccal and posterior tooth margins are straight and the anterolingual tooth wall is convex rounded. The buccal side of the DP4 is clearly lower crowned than the lingual one. The hypoflexus is open in all available specimens and the hypostria almost reaches the tooth crown base. Only in unworn or slightly worn DP4, the buccal para-, meso- and metaflexus/-stria is open. Most specimens show moderate wear stages with all of the buccal flexus/striae close to the fossettes. The long and straight paraflexus (GPIT/MA/12002, unworn) is oriented posterolingually and meets straight in line with the obliquely oriented hypoflexus. The mesoflexus is long and bent, runs across the entire tooth width and ends at the posterolingual corner. In barely worn specimens, the mesoflexus can be connected to the

metaflexus/-fossette. In more worn DP4, the long mesofossette spans the small round metafossette, that is placed at the posterobuccal edge (GPIT/MA/19158). The upper deciduous premolar is three-rooted with one large transverse lingual and two equally small and circular buccal roots at the anterolingual and posterolingual corners (GPIT/MA/12001, GPIT/MA/12058).

P4 (Figure 3D-G)

The upper P4 is very high-crowned and represents the largest tooth of the upper tooth row. In most of the specimens (unworn to higher worn P4) the occlusal outline is triangular with convex anterolingual and buccal sides. In very heavily worn specimens, also the buccal side can be straight or slightly concave (GPIT/MA/18783). The straight posterior tooth wall together with the buccal side forms a posterobuccal apex. The entire tooth crown is bent diagonally towards posterobuccal resulting in a very high anterolingual and a shorter posterobuccal crown. The lingual hypoflexus/-fossette, and the buccal para-, meso- and metaflexus/-fossette are general occlusal elements of the P4. The paraflexus/-fossette is straight, oriented posterolingually and meets in straight line the equally sized hypoflexus/-fossette, which is directed oblique anterobuccally. In heavily worn upper premolars the hypofossette is short, protrudes slightly between para- and mesofossette (GPIT/MA/18783, 18835) and can be angled posteriorly (GPIT/MA/18783).

The mesoflexus/-fossette is the longest occlusal element, can be less, more or heavily convex and ends at the posterior margin of the P4. Similar to the DP4 the short metaflexus/-fossette is straight or

very slightly curved and enclosed by the mesoflexus/-fossette at the posterobuccal corner. A wide range of variations within the occlusal elements of the extensive material can be found: a divided parafofsette (GPIT/MA/19066), an additional preparafofsette (GPIT/MA/19059, SNSB-BSPG 2020 XCIV-7000) or a small premetafofsette at the posterior margin between the meso- and the metafofsette (GPIT/MA/16866). In SNSB-BSPG 2020 XCIV-7001, the meta- and mesofossette are fused resulting in a U-shape and in the special case of SNSB-BSPG 2020 XCIV-7025 an additional elongated fossette is placed and oriented perpendicular between the ends of the hypo- and parafofsette, in anterodistal orientation.

The hypostria is the longest of all striae and in unworn or slightly worn P4 (GPIT/MA/19060), it runs down half of the tooth crown, closing at high wear stages. The parastria is the longest buccal stria closing within the first quarter of the tooth-crown at moderate dental wear stages. The mesostris, in general the second shortest stria, closes within the first millimetre of tooth wear (assessed on unworn teeth). A very short metastris/-flexus is only present in unworn or very slightly worn P4 (GPIT/MA/12436, 16191, 17302, 19055, 19056, SNSB-BSPG 2020 XCIV-3449, 7004, 7017, 7023). In most of the material the metastris is the shortest stria but in two worn P4, the mesostris is already closed while para- and metastris are still open (GPIT/MA/19052, SNSB-BSPG 2020 XCIV-7008). In a single case is the mesostris the longest and only buccal stria, while para- and metastris are already closed (GPIT/MA/19066). Upper premolars show two heteromorphic roots, one massive that follows the anterolingual outline of the tooth in a crescent shape and one short, small circular and columnar shaped posterobuccal root.

M1/2 (Figure 3H-L)

In general, the upper first and second molars occlusally show high morphological similarities with upper premolars. Deviating from this, upper M1/2 are smaller and more square in occlusal outline. With wear, the mesio-distal length gets shorter, while the width remains approximately the same (rectangular outline). The buccal and posterior tooth walls are straight and oriented perpendicular to each other, while the anterior and lingual ones are more rounded. The tooth crowns of the M1/2 are bent diagonally so that the posterobuccal corner slightly overhangs. Very young dental ages (unworn or slightly worn) of M1/2 show all typical occlusal elements of the P4. The lingual hypoflexus/-fossette is long, straight and oriented oblique in anterobuccal direction, crossing half of the tooth width. The parafofsette is short, straight or slightly bent posteriorly and ends slightly directing posteriorly to the end of the hypoflexus/-fossette. Like with the P4, the mesoflexus/-fossette is the longest occlusal element. It is slightly, more or heavily curved posteriorly and ends at the posterior margin of the M1/2. Similar to DP4 and P4 the short metafofsette is straight or very slightly curved and enclosed by the mesoflexus/-fossette at the posterobuccal corner. The lingual hypostris runs down half of the tooth crown, being the longest stria. Meso- and parastris correspond to each other in length but are very short. There are slightly worn M1/2 that show a buccally open para- and mesoflexus (GPIT/MA/18866, 18872, 19121) and in two worn specimens only the mesoflexus/-stria is open at the buccal tooth wall (GPIT/MA/12057, 19136). The metastris is the shortest of all striae – if existing at all. There are two specimens representing slightly worn M1/2, that show all four flexus/striae in an open phase (hypo-, para-, meso- and metafofsette/-stria; GPIT/MA/19009, 19010). In highly worn upper first and second molars, the hypoflexus/-stria is closed (GPIT/MA/12028, 12030, 18863, 18896, 18909, 19007, 19120, SNSB-BSPG 2020 XCIV-6962). M1/2 of very high wear stages show only occlusal fossettes and in two cases the metafofsette is worn down and missing (GPIT/MA/18863, 19120). Upper M1/2 are three-rooted with one large and massive root that

follows in a crescent shape the anterolingual margin of the tooth wall and two short, small and round roots located at the anterobuccal and posterobuccal corners.

M3 (Figure 3M-P)

Upper third molars are triangular in occlusal outline and highly elongated in anterodistal direction. The convex anterior face marks the greatest tooth width and the straight buccal and posterolingual faces merge in a distally pointed and round corner. The tooth crown of the M3 is slightly bent and overhanging at the posterobuccal tip. Furthermore, the anterolingual margin is higher crowned than the posterobuccal one. In early dental wear stages, the M3 is rather rectangular and shows a weak distal elongation, which strengthens and lengthens with higher wear stages. With wear, mesio-distal length gets longer, while the width remains approximately the same. As a basic pattern, a lingual hypoflexus/-fossette and the buccal para-, meso- and metafofsette can be observed. The straight anterobuccally oriented hypoflexus/-fossette terminates at median tooth width anteriorly to the parafofsette. Mesoflexus/-fossette in the upper third molars, as in all other upper cheek teeth, is more or less curved or angled posteriorly and encloses the metafofsette anteriorly. Para- and metafofsette are equally small, shorter than the mesoflexus/-fossette and display marked variability in size, orientation and shape. Occurring occlusal variations are: a split in two parafofsettes (or additional, a small and circular buccal parafofsette; GPIT/MA/18752); an additional premetafofsette (GPIT/MA/19124); an additional small and circular fossette lingually (GPIT/MA/18753, 19124) or posteriorly to the metafofsette (postmetafofsette: GPIT/MA/19125, 19126); a straight buccolingually oriented (SNSB-BSPG 2020 XCIV-6949), an antero-posteriorly oriented (GPIT/MA/19127), a posteriorly inverted U-shaped (GPIT/MA/19124) or a Y-shaped metafofsette (GPIT/MA/19125). The hypostris is the longest striid closing at very high wear stages (GPIT/MA/18760, 19127, SNSB-BSPG 2020 XCIV-4606, 6956). GPIT/MA/18997 is the only M3 showing three open buccal striae (slightly worn) but all very short. In other cases, the parastris is closed while meso- and metastris are open (worn; GPIT/MA/18995, SNSB-BSPG 2020 XCIV-6954); the para- and mesostris are open, while the metastris is closed (slightly worn or worn; GPIT/MA/18999, 19,124, SNSB-BSPG 2020 XCIV-6953), or only the mesostris is open buccally (slightly worn or worn; GPIT/MA/18752, 18753, SNSB-BSPG 2020 XCIV-6955). The third upper molar shows two or three roots. A marked crescent-shaped root runs along the anterior tooth margin and a slightly smaller and round root is placed under the posterior tooth tip. A third, very small root may occur adjacent to the anterolingual margin of the former main root (GPIT/MA/19088) or is somewhat more pronounced and shifted further into the lingual centre of the tooth (GPIT/MA/19127).

Mandible (Figures 4, 9)

There are several mandibular specimens of *Euroxenomys minutus* available from Hammerschmiede mostly comprising fragments of the tooththrow or anterior portion. GPIT/MA/12168 represents the most complete specimen with the ramus and angular process preserved but crushed and slightly displaced. Furthermore, the description of mandibles follows the rather complete specimens (GPIT/MA/16523, 17127, SNSB-BSPG 2020 XCIV-0310, 4551, 5287, 5289). The tooth row lengths show values between 13.38 and 14.59 mm (SNSB-BSPG 2020 XCIV-5287, 13.38 mm; GPIT/MA/17444, 13.4 mm; GPIT/MA/17700, 13.61 mm; GPIT/MA/16523, 14.1 mm; SNSB-BSPG 2020 XCIV-4551, 14.58 mm; SNSB-BSPG 2020 XCIV-0310, 14.59 mm). The alveolar length of the mandibular tooththrow is between 14.36 and 15.62 mm (SNSB-BSPG 2020 XCIV-5287, 14.36; SNSB-BSPG 2020 XCIV-4551,

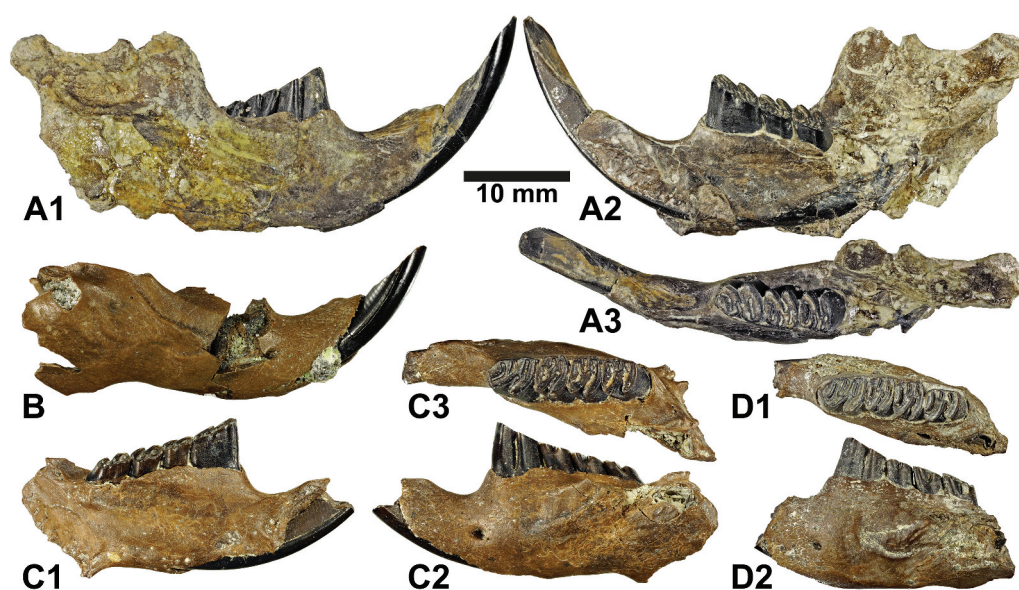


Figure 4. Mandibles of the minute beaver *Euroxenomys minutus* (von Meyer 1838), from the early Late Miocene locality Hammerschmiede (Bavaria, Germany), local stratigraphic levels HAM 5 and HAM 4. Scale bar equals 10 mm. (A) GPIT/MA/12168, right mandible with angular process, part of the coronoid process, i2, p4-m2 in buccal (A1), lingual (A2) and occlusal (A3) views. (B) GPIT/MA/17127, right mandible with i2 in buccal view. (C) GPIT/MA/16523, left mandible with broken i2 and complete cheek tooththrow p4-m3 in lingual (C1), buccal (C2) and occlusal (C3) views. (D) SNSB-BSPG 2020 XCIV-5287, left mandible fragment with complete cheek tooththrow p4-m3 in occlusal (D1) and buccal (D2) views.

14.42 mm; GPIT/MA/16523, 14.77 mm; SNSB-BSPG 2020 XCIV-0310, 14.99 mm; GPIT/MA/17444, 15.09 mm; GPIT/MA/17127, 15.12; GPIT/MA/16521, 15.22 mm; GPIT/MA/17419, 15.25 mm; GPIT/MA/17700, 15.62 mm).

Broken margins of the ventral side of the posterior portion of the mandibles indicate a large pterygoid fossa with a wide shelf. On the buccal side, the masseteric fossa is marked and placed at the level of the occlusal surface of the tooththrow in superposition to the posterior end of the incisor, between the coronoid process and the angular process. There is a distinct groove at the anterior ascending ramus that runs anteroventrally until it terminates at a shallow and tiny punctual depression, arranged in line with the buccal hypostridium of the lower premolar and placed slightly occlusal to the foramen mentale. This depression is the origin of another groove that is running posteriorly at a more ventral position and terminates at about the level of the posterior m3.

In buccal view, the small chin process is in line with the foramen mentale, shortly anterior to the premolar. The diastema is posteriorly asymmetrical and reaches approximately the length of the occlusal p4-m2 (10 mm). The posterior end of the lingual symphysis is placed below the anterior margin of the m1.

i2

Lower incisors are robust, show a smooth and convex anterior enamel surface, a convex distal and a straight mesial tooth surface that roughly describe a triangular cross-section. The wear area is elongated (longer than in the upper I2) and separated into a slightly mesially and a slightly distally angled wear facet, terminating in a central tooth tip, as in the modern muskrat *Ondatra zibethicus*.

dp4 (Figure 5A-E)

The lower deciduous premolar corresponds morphologically to a brachydont miniature of the permanent lower premolar. Basic elements include a buccal hypoflexid with a hypostridium that does not reach the crown base, a parafossettid (closed in all specimens), a metaflexid/fossettid with a metastridium as the second longest lingual striid and a mesoflexid/fossettid with the longest of the lingual

striids, the mesostriid. Two of the hardly worn specimens show an open metaflexid that is closed in all other dp4 to a metafossettid. Mesoflexid is only closed in some dp4 of higher wear stages forming a mesofossettid (GPIT/MA/18993, 19096, 19097, 19098). In exceptional cases, the following variations may occur in deviation from the basic construction plan: presence of one or two small and circular preparafossettids (one preparafossettid: GPIT/MA/19093, 19169, 19172, 19173; two preparafossettids: GPIT/MA/18988, 19092, 19166); parafossettid is U-shaped (GPIT/MA/19095); In a single case, the paraflexid is connected to the mesoflexid, elongating the mesoflexid in antero-buccal direction (GPIT/MA/11999). In the HAM 5 material 2 out of 34 dp4 have preserved roots, while in the HAM 4 material all 9 available lower deciduous premolars are only preserved as rootless tooth crowns. The dp4 is two-rooted with one anteriorly and one posteriorly diverging root (GPIT/MA/18988, 18993).

p4 (Figure 5F-M)

The lower premolar clearly represents the largest tooth of the lower tooth row and is slightly inclined anteriorly. The occlusal outline is elongated and figure eight shaped and generally four flexids/fossettids are exposed, one buccal hypoflexid and three lingual flexids (para-, meso- and metaflexid). With progressive wear, the occlusal tooth dimensions increase in longitudinal and transverse direction with a stronger increase of the mesio-distal length. Lingual flexids are straight or slightly curved and oriented mesiobuccally, opposing the hypoflexid. All striids end before reaching the crown base. The hypoflexid presents the longest striid and is open in all available p4 and age categories, except for a single, very heavily worn p4 in which a hypofossettid is formed (GPIT/MA/18725) and one tooth exposes a closing hypoflexid (GPIT/MA/18711). In a few cases of very young age classes (unworn or slightly worn teeth), a very short and mesially open paraflexid can be present (GPIT/MA/12480, 17240, 17307, 18671, 18682, 18694, 18695, 18700, 18702, 18704, 18707, 18723, 18727, 18729, 18732, SNSB-BSPG 2020 XCIV-6870, 6876, 6899), but in most cases, it is close to a parafossettid. A similar observation can be made for the metaflexid, that can be lingually

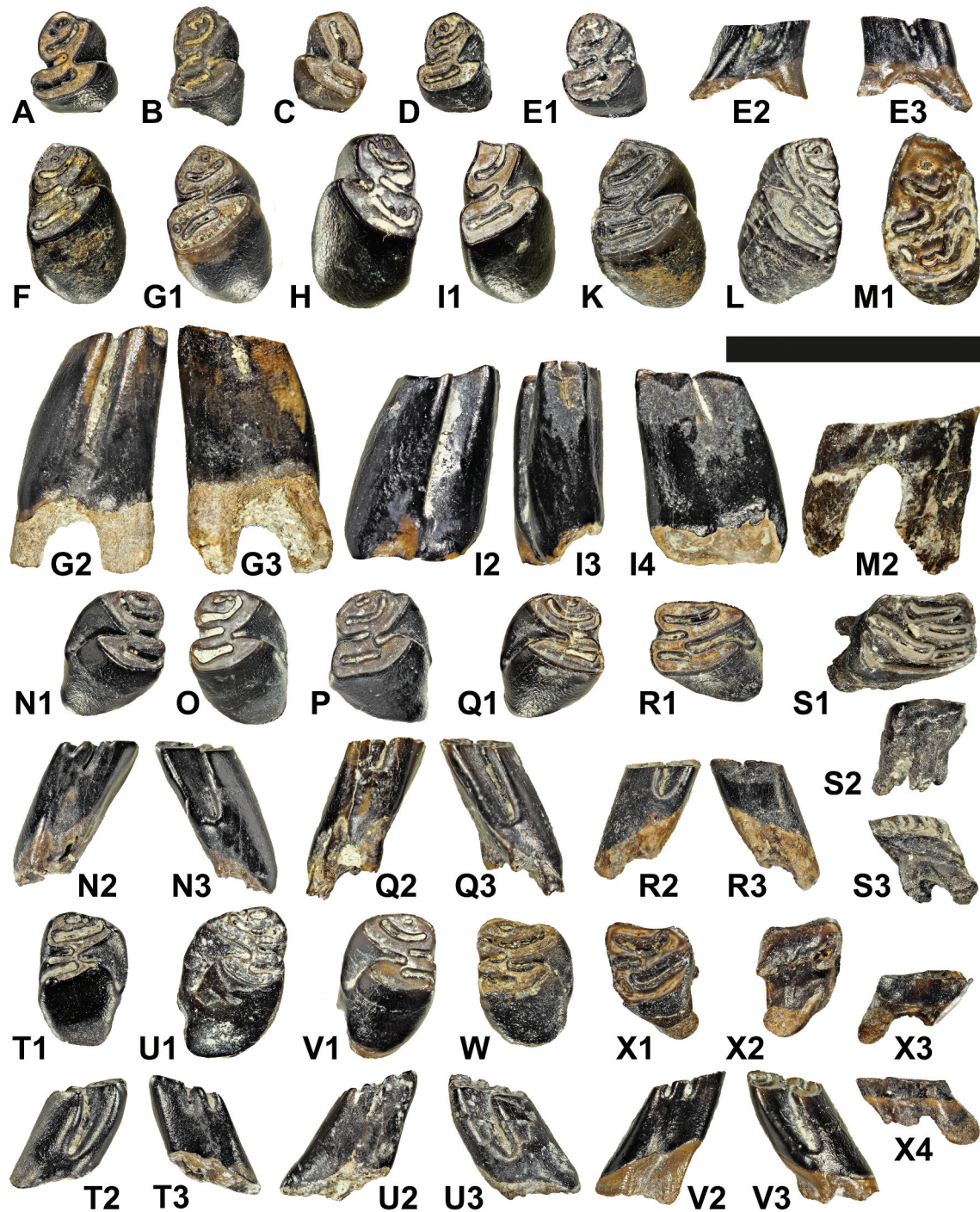


Figure 5. Lower cheek teeth of the minute beaver *Euroxenomys minutus* (von Meyer 1838), from the early Late Miocene locality Hammerschmiede (Bavaria, Germany), local stratigraphic levels HAM 5 and HAM 4. Deciduous premolars: (A-E); premolars (F-M); molars (N-X). Occlusal (A, B, C, D, E1, F G1, H, I1, K, L, M1, N1, O, P, Q1, R1, S1, T1, U1, V1, W, X1), lingual (E3, G3, I4, N2, Q2, R3, S2, T3, U2, V2, X4), buccal (E2, G2, I2, M2, N3, Q3, R2, S3, T2, U3, V3, X3), mesial (I3) and apical (X2) views. Scale bar equals 10 mm. Left dp4: (C) GPIT/MA/11999. Right dp4: (A) GPIT/MA/19166; (B) GPIT/MA/19095; (D) GPIT/MA/19093; (E) GPIT/MA/18988. Left p4: (H) GPIT/MA/18699; (L) SNSB-BSPG 2020 XCIV-6894. Right p4: (F) GPIT/MA/18678; (G) SNSB-BSPG 2020 XCIV-6889; (I) GPIT/MA/18732; (K) GPIT/MA/18676; (M) GPIT/MA/18725. Left m1/2: (N) GPIT/MA/19150; (Q) GPIT/MA/18964; (S) GPIT/MA/19021. Right m1/2: (O) GPIT/MA/19023; (P) GPIT/MA/19019; (R) SNSB-BSPG 2020 XCIV-7037. Left m3: (U) GPIT/MA/18982; (V) SNSB-BSPG 2020 XCIV-6983. Right m3: (T) SNSB-BSPG 2020 XCIV-6985; (W) GPIT/MA/19086; (X) GPIT/MA/19122.

open (and slightly longer than the parastriid), in unworn and slightly worn p4. The mesoflexid exhibits the longest lingual striid and remains open until higher age classes (only medium, deeply and highly worn p4 show a mesofossettid). In unworn and slightly worn p4, it can be connected to the hypoflexid. Further features can be one to two preparafossettids (one: GPIT/MA/12480, 17240,

17419, 17444, 18664, 18670, 18674, 18685, 18693, 18699, 18716, SNSB-BSPG 2020 XCIV-6889; two: GPIT/MA/10756, 17700, 18668, 18678, 18730, SNSB-BSPG 2020 XCIV-6874, 6893) and/or premetafossettids (one: GPIT/MA/18664, 18668, 18683, 18722, SNSB-BSPG 2020 XCIV-6889; two: SNSB-BSPG 2020 XCIV-6887, divided parafossettids (SNSB-BSPG 2020 XCIV-6875) and/or

metafossetids (GPIT/MA/18693) or bifurcated parafofossetids (GPIT/MA/17444, SNSB-BSPG 2020 XCIV-6894, 6903). The lower premolar has two equally sized roots with a crescent shaped cross-section.

m1-2 (Figure 5N-S)

The m1/2 is shorter crowned than the p4 and inclined anteriorly within the lower tooth row. The occlusal outline of lower m1/2 is nearly square with a straight and transverse anterior and a slightly convex posterior tooth wall. With wear, mesio-distal length becomes shorter, while the width remains approximately the same (rectangular outline). The principal morphology is similar to that of the p4 but teeth are shorter. In general, an oblique posteriorly oriented hypoflexid and a slightly anteriorly oriented mesoflexid are present. Both flexids end at the median line of the tooth with the hypoflexid located between the mesoflexid and metaflexid/-fossettid. Only in a few unworn and slightly worn m1/2 an open paraflexid is present (GPIT/MA/19035, 19150, SNSB-BSPG 2020 XCIV-0725-2), while an open metaflexid is more frequently observed (GPIT/MA/10995, 17710-2, 17949-1, 17949-2, 18964, 19030, 19032, 19035, 19037, 19104, 19140, 19150, SNSB-BSPG 2020 XCIV-0725-2, 6915-2, 6978, 6981, 7035, 7041, 7044-2). The mesoflexid closes at medium wear stages and in a few cases of very heavily and deeply worn m1/2 the hypoflexid is close to a hypofossettid (GPIT/MA/10757, 12479-1, 18934, 18949, 18968, 19021, 19149, SNSB-BSPG 2020 XCIV-4235). The paraflexid/-fossettid is curved and oriented anteriorly and is placed in the centre of the anterior m1/2. In many cases of up to moderately worn m1/2, a tiny preparafossettid exists (GPIT/MA/10995, 12432, 12480-1, 12480-2, 16433-1, 17240-2, 17444-1, 17444-2, 17710-1, 17710-2, 17766-2, 17949-1, 17949-2, 17952, 19019, 19029, 19030, 19032, 19037, 19039, 19040, 19041, 19044, 19102, 19103, 19104, 19141, 19143, 19144, 19145, SNSB-BSPG 2020 XCIV-0725-1, 0725-2, 6915-1, 6915-2, 6975, 6977, 6978, 6980, 6981, 7035, 7038, 7044-1, 7044-2), that sometimes can be connected with the paraflexid/-fossettid to form a lingually open U-bend (GPIT/MA/19035, 19146, 19148, 19150). In a single case, two preparafossettid exist and are connected to form a horizontal figure eight (GPIT/MA/19023). The metaflexid/-fossettid is rather straight and aligned in parallel to the posterior tooth margin. The hypostriid is the longest striid that ends short above the base of the tooth crown. The mesostriid is the second longest striid reaching approximately half of the tooth crown, while para- and metastriid are only present in some cases and often only observed in early wear stages. The tree-rooted m1/2 show two equally short and small anterior roots and one large transverse posterior one.

m3 (Figure 5T-X)

The m3 is the shortest-crowned tooth of the lower tooth row, strongly inclined anteriorly, comprising a similar principal morphology as the m1/2 but instead of a square occlusal outline, the molar is slightly elongated and tapers buccally from the posterior half of the tooth. No significant dimensional changes can be observed with progressive wear. Lower m3 comprises a straight obliquely oriented buccal hypoflexid, and the tree lingual para-, meso- and metaflexids/-fossettid. A paraflexid can only be observed in few slightly worn specimens (GPIT/MA/12269, 18982, 18983, 19110), whereas in the other teeth a parafofossettid is expressed that is slightly concave and spans transversely the entire anterior portion of the tooth. One to two small preparafossettid can be placed within this anterior-opened arch (one: GPIT/MA/17444-3, 17700-3, 19086, 19109, 19110, SNSB-BSPG 2020 XCIV-6983, 6984; two: SNSB-BSPG 2020 XCIV-6985). In less worn teeth, this preparafossettid can be connected to the anterior tooth wall and the parafofossettid can be open anteriorly (GPIT/MA/18974, SNSB-BSPG 2020 XCIV-6985). The mesoflexid/-fossettid is slightly shorter than the metaflexid/-fossettid, which both are straight and reach near to the half

of the tooth width and terminate near to the anterior and posterior end of the hypoflexid. The hypostriid is the longest striid reaching nearly the end of the tooth crown but still closes in a heavily worn specimen (GPIT/MA/19122). The mesostriid is the second longest striid and reaches the first third of the tooth crown, closely followed by the shorter metastriid. A parastriid is rarely formed and when present it is extremely short and closes during the very first wear. The m3 is three rooted, with two very tiny anterior roots and one large one, that runs transverse along the convex posterior tooth wall.

Results and discussion

Morphologic comparison

The dental material from the HAM 5 and HAM 4 levels of the Hammerschmiede fossil site show the typical characters for *Euroxenomys minutus* following Hugueney (1999) and Daxner-Höck and Bernor (2009) with additions after Prieto et al. (2014), Kordos (2020) and Mörs et al. (2022).

(1) Small size; (2) upper premolar (P4) subtriangular in occlusal outline and clearly larger than upper molars; (3) lower premolar (p4) that is elongated, significantly larger than lower molars and forming an anteriormost edge; (4) rooted and high crowned cheek teeth with mostly parallel-oriented flexus/fossettes and flexids/fossettid without cement in synclines and hypostriae/-ids that do not reach the crown base; (5) characteristic enlarged upper third molar (M3)

The extensive dental material collection of *Euroxenomys minutus* from the Hammerschmiede fossil site is morphologically highly variable but fits well with other Eurasian Miocene localities, such as Tagay (MN 5) in Siberia (Mörs et al. 2022), Sansan (MN 6) in France (Hugueney and Duranthon 2012), Gratkorn (MN 7/8) in Germany (Prieto et al. 2014), Mataschen (MN 7/8) in Austria (Daxner-Höck 2004), Anwil (MN 7/8) in Switzerland (Engesser 1972), Felsötárkány (MN 7/8) in Hungary (Hír 2004), Atzelsdorf (MN 9) in Austria (Daxner-Höck and Bernor 2009), Höwenegg (MN 9) in Germany (Giersch et al. 2010) and Rudabánya (MN 9) in Hungary (Kordos 2020). An additional mesial preparafossettid/fossette (occurring in Hammerschmiede material at all lower cheek tooth positions and the first time documented for the upper P4) usually visible at earlier wear stages is already described in material from Tagay (p4 and m3), Rudabánya (m2 and m3), Anwil (dp4, m3), Sansan and Atzelsdorf (p4 and m1/2) (Engesser 1972; Daxner-Höck and Bernor 2009; Hugueney and Duranthon 2012; Kordos 2020; Mörs et al. 2022). Moreover, duplicate preparafossettid, or additional premetafossettid/fossette, premesofossette or postmetafossette can be varying supplementary characters (Figure 1). Further possible variations within the enormous cheek teeth collection are differences in length, course and orientation as well as possible bipartitions, bifurcations or connections of occlusal flexids/flexus or fossettid/fossettes.

Metric comparison (Figures 6–7)

In order to investigate the subjective influence of the measurer on values obtained, additionally to the Hammerschmiede material, own measurements were taken for *Euroxenomys minutus rhenum* from the Dorn-Dürkheim site, where values deviate slightly from those from the literature and differences mainly concern the width values. This methodological uncertainty may explain to some extent differences in especially the width values from teeth of the compared fossil sites taken from literature, which means that slight ranges of metric variation should not be weighted too much and

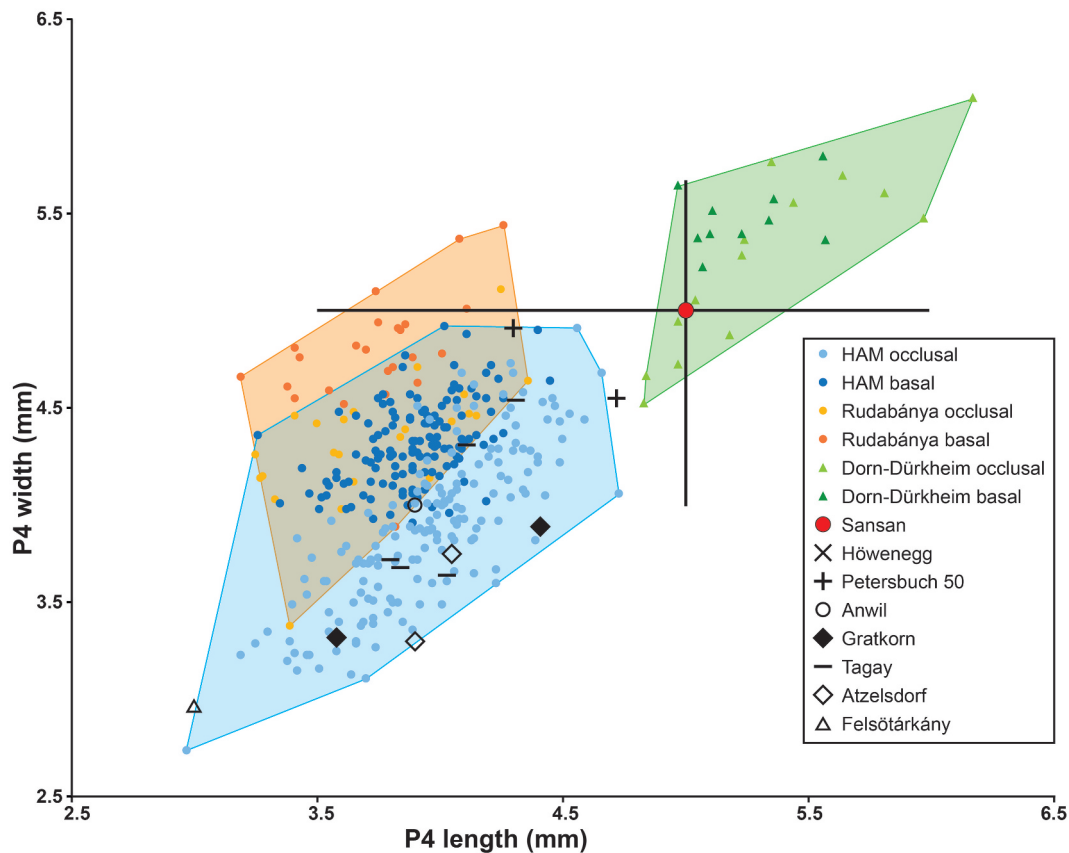


Figure 6. Length/width dimensions of upper premolars of the minute beaver *Euroxenomys minutus* (von Meyer 1838), from the early Late Miocene locality Hammerschmiede (Bavaria, Germany), local stratigraphic levels HAM 5 and HAM 4, compared to *Euroxenomys* material from other Eurasian Miocene localities. Measurements for Hammerschmiede (HAM), Rudabánya and Dorn-Dürkheim additionally distinguish occlusal and basal tooth measurements while the other sites only include occlusal values. Data for Rudabánya from L. Kordos personal communication, for Dorn-Dürkheim own measurements, for Sansan from Huguency and Duranthon (2012), for Höwenegg from Giersch et al. (2010), for Petersbuch 50 from Stefen and Rummel (2003), for Anwil from Engesser (1972), for Gratkorn from Prieto et al. (2014), for Tagay from Mörs et al. (2022), for Atzelsdorf from Daxner-Höck and Bernor (2009) and for Felsötárkány from Hír (2004)

could be based on methodological differences in measurement techniques.

Measurements for lower and upper teeth from the local stratigraphic levels HAM 5 and HAM 4 from the Hammerschmiede deposits exactly overlap and can unambiguously be used as one dataset (HAM). The smallest values of upper premolars correspond to occlusal measurements of less worn teeth. In contrast to lower premolars, basal measurements of upper premolars and thus also teeth of higher wear stage and age show similar length values, but a slightly higher width and occlusal measurements show a higher scatter than basal ones (Figure 6). A similar pattern can be observed in the collection of *Euroxenomys minutus* teeth from Rudabánya in Hungary (Figure 6). The smallest values of lower premolars correspond to occlusal measurements of less worn teeth, the larger values enclose measurements taken at the base of the crown, which in turn match occlusal values of some very worn teeth. With progressive tooth wear (age), lower premolars become slightly wider but significantly longer (Figure 7).

Metrically, the upper premolars from Hammerschmiede fit well with *Euroxenomys minutus* from Tagay (MN 5), Gratkorn (MN 7/8), Anwil (MN 7/8) and Atzelsdorf (MN 9) (Figure 6). The single P4 from Petersbuch 50 (MN 8) corresponds with the highest, and from Felsötárkány (MN 7/8) with the lowest values of Hammerschmiede specimens. The large collection from Rudabánya (MN 9) fits well with the highest width values and overlaps best the basal measurements of upper Hammerschmiede premolars. The Rudabánya

material also shows even greater width values at the basal P4 (Figure 6). Upper premolars from Sansan (MN 6) partly match the highest values and Dorn-Dürkheim specimens (*Euroxenomys minutus rhenanus*) are substantially larger than those from Hammerschmiede (Figure 6).

The lower p4 from Hammerschmiede match with material from Elgg (MN 5), Anwil (MN 7/8), Felsötárkány (MN 7/8), Petersbuch 50 (MN 8), Atzelsdorf (MN 9) and Höwenegg (MN 9) (Figure 7). Lower p4 from Gratkorn (MN 7/8) are within the maximum width limit of the Hammerschmiede material and the Tagay (MN 5) specimen is slightly wider, but within the length range of Hammerschmiede p4 (Figure 7). Rudabánya (MN 9) p4 fit very well, but the shortest length values show a higher width maximum at the occlusal tooth portion, while basal tooth measurements agree with the values for lower premolars from Hammerschmiede (Figure 7). Rudabánya and Hammerschmiede both show a very high variability in p4 length with a close match in the range of values (Figure 7). Lower p4 from Sansan (MN 6) show consistency in their lower range of values, however most measurements are wider than the maximum width of Hammerschmiede specimens (possibly different measuring sections are used) (Figure 7). Dorn-Dürkheim p4 (own measurements) are larger and wider and follow a different regression line than the Hammerschmiede measurements (Figure 7).

To distinguish finally between the two subspecies (or possibly species) *Euroxenomys minutum minutum* and *E. minutum*

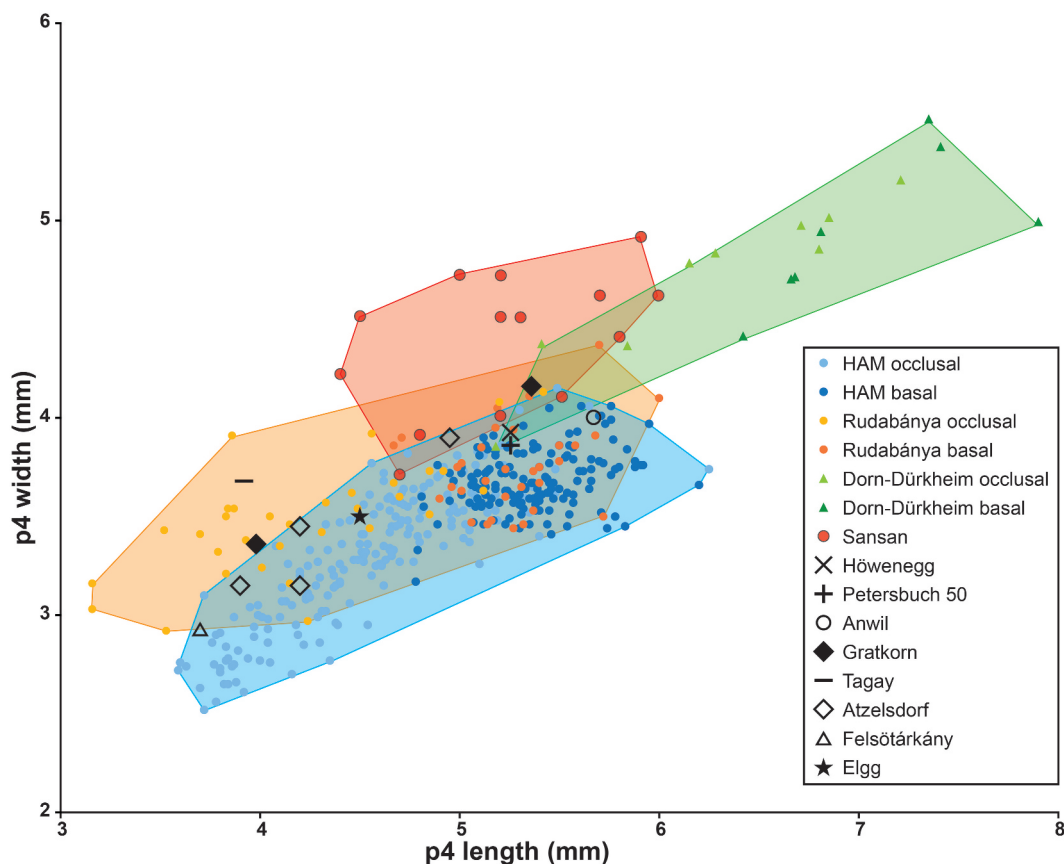


Figure 7. Length/width dimensions of lower premolars of the minute beaver *Euroxenomys minutus* (von Meyer 1838), from the early Late Miocene locality Hammerschmiede (Bavaria, Germany), local stratigraphic levels HAM 5 and HAM 4, compared to *Euroxenomys* material from other Eurasian Miocene localities. Measurements for Hammerschmiede (HAM), Rudabánya and Dorn-Dürkheim additionally distinguish occlusal and basal tooth measurements while the other sites only include occlusal values. Data for Rudabánya from L. Kordos personal communication, for Dorn-Dürkheim own measurements, for Sansan and Elgg from Hugueneu and Duranthon (2012), for Höwenegg from Giersch et al. (2010), for Petersbuch 50 from Stefen and Rummel (2003), for Anwil from Engesser (1972), for Gratkorn from Prieto et al. (2014), for Tagay from Mörs et al. (2022), for Atzelsdorf from Daxner-Höck and Bernor (2009) and for Felsötárkány from Hír (2004)

rhenanum, the differences already mentioned by Franzen and Storch (1975) can be maintained and confirmed. Even the extremely large data set from Hammerschmiede does not manage to match the range of large values for upper and lower premolars from Dorn-Dürkheim. Finally, the diagnosis for *E. minutum rhenanum* made by Franzen and Storch (1975) remains valid and the best criteria to distinguish from *E. minutum minutum* are (1) the larger premolars in absolute terms and in comparison to M1/2 and m1/2, (2) the M3, which are significantly longer in absolute terms and compared to M1/2 and (3) M1 and m1, which are wider compared to M2 and m2 in *E. minutum rhenanum*. This also results in a longer jaw tooth row length in *E. minutum rhenanum*.

Taphonomy and signs of predation (Figure 8)

The presented tooth and jaw material of *Euroxenomys minutus* from Hammerschmiede shows a significantly high quantity of isolated teeth compared to in situ tooth rows and jaw fragments (HAM 5: 442/10; HAM 4: 454/75). In both studied strata, this ratio of disarticulation is high with 83% isolated dental specimens at HAM 4 and very high with 98% at HAM 5. A considerable proportion of dental specimens shows moderate and heavy corrosive lesions (Figure 8). In most cases, it is mainly the enamel that is affected, and in jaw specimens with in situ dentition, the bone itself is hardly or not at all dissolved, while the crowns of the teeth have been considerably corroded. Corrosive lesions mainly affect the visible part of the enamel.

Areas of enamel that are still hidden in the jawbone remain largely undamaged as it is best visible on incisors (Figs. 8B1, C2). It is obvious that corrosive effects on molars are greatest at the more basal enamel areas, just above the alveolar rim of the jawbone, while enamel close to the occlusal surface exhibits only weak corrosive lesions (Figs. 8A3, A4, C3).

Some incisors show strongly corroded, striated enamel patterns, which were carved out and highlighted by the corrosion and presumably represent the rhythm of diurnal incremental tooth growth lines (Figs. 8C2, E1, E2). Possibly cyclic changes in tooth properties provide weak points or inhibitions for acids to work.

In addition to dental corrosions, it is striking that long bones in particular are in many cases only preserved in broken form. According to several studies, the degree and position of the corrosive lesions could correspond to digestive corrosions observed on prey bones in recent predators that have an acidic digestive system, such as mammalian carnivores (Andrews and Evans 1983; Lopez et al. 2017, Figure 3; Marin-Monfort et al. 2019) or predatory birds, e.g., owls (Andrews 1990; Fernández-Jalvo and Andrews 2016, Fig. A767; Fernández et al. 2019). According to Andrews (1990), there is no other alteration process that can replicate the corrosive effects of digestion, which makes such traces, especially on teeth, a clear indicator of predatory bone assemblages. In contrast to digestive corrosion, bone fractures alone are not good indicators of a predator assemblage, as it cannot be ruled out that further modifications may have been caused by processes like weathering, trampling or sediment compression (Andrews 1990), including

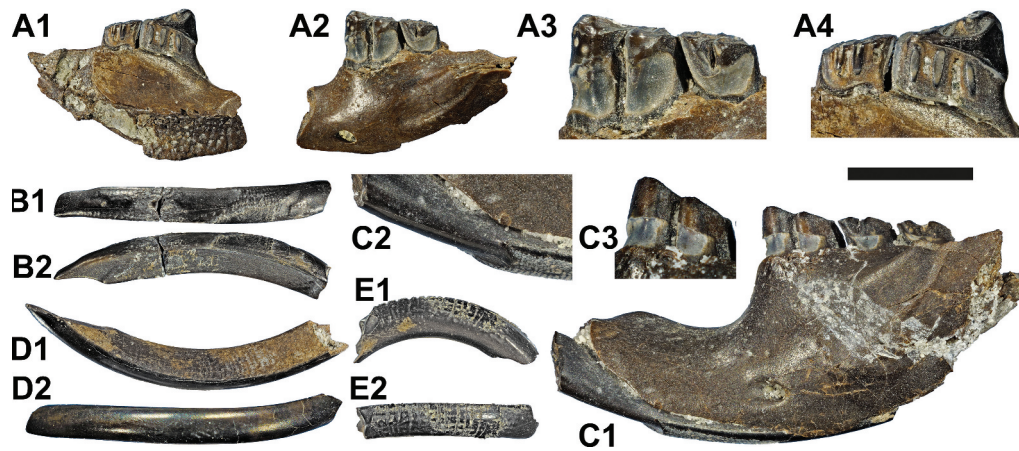


Figure 8. Signs of digestive corrosion on dental material of the minute beaver *Euroxenomys minutus* (von Meyer 1838), from the early Late Miocene locality Hammerschmiede (Bavaria, Germany), local stratigraphic levels HAM 5 and HAM 4. (a) SNSB-BSPG 2020 XCIV-6917, left mandible with corrosion on p4 and m1 enamel in lingual (A1, A4), buccal (A2-A3) views and double magnifications of the corroded enamel regions (A3, A4). (B) GPIT/MA/19190, left lower incisor i2 with corrosion on enamel regions in labial/anterior (B1) and mesial (B2) views. Enamel of the tooth tip region is already completely missing while the proximal half preserves some portions of enamel. (C) GPIT/MA/17703, left mandible with broken i2 and cheek teeth p4-m2 with corrosion of the tooth enamel at the i2 and at the base of the molars in buccal (C1-C3) and double magnified (C2-C3) views. (D) GPIT/MA/19188, left lower incisor i2 without corrosion effects for comparison purposes with the corroded incisors in buccal (D1) and labial/anterior (D2) views. (E) SNSB-BSPG 2020 XCIV-0607, upper right incisor i2 in buccal (E1) and labial/anterior (E2) views, with signs of dental enamel corrosion that possibly amplify the incremental rhythm of growth lines. Scale bar equals 10 mm except for magnifications A3, A4, C2 and C3 where it corresponds to 5 mm.

excavation artefacts. Generally, each predator species produces a different type of alteration on the tooth and bone material, which means that some predators can be assigned to their traces (Andrews 1990). With approximately the body size of a muskrat, large birds of prey as well as medium- and large-sized mammalian carnivores are certainly possible predators of *Euroxenomys minutus* at the Hammerschmiede fossil site. However, we lack corresponding studies on the respective individual corrosive effects of digestion of the numerous possible fossil predator species.

Mortality analysis (Figure 9)

To map the entire lifespan of beaver individuals in a mortality analysis, the tooth position of the lower dp4 and p4 is used (Heinrich and Maul 2020; Kordos 2020; Lechner and Böhme 2022). The general problem with using deciduous teeth (here dp4) in the mortality analysis is the possible duplication of individuals, by interpreting teeth as deceased juvenile individuals and later duplicating the same individual by an adult p4 with the actual wear stage it died. For this reason, when using deciduous teeth, meticulous care must be taken to ensure that only teeth that show no signs of resorbed roots are used. In addition, when using deciduous teeth, the permanent p4 must not be supplemented at the same time if it shows no signs of wear, as both are in the juvenile jaw at the same time.

In the present case of the Hammerschmiede, the data from dp4 and unused p4 were compared with each other, and it turns out that only two out of 34 dp4 at the HAM 5 and none of the nine from HAM 4 show preserved roots. All 'unrooted' dp4 have lost their roots, possibly through root resorption (shedding) or have been mechanically eroded during transportation processes in the alluvial system, what cannot be definitively determined. In contrast, there are four unused p4 from HAM 5 and seven from HAM 4, which should finally generate a larger and thus better data security for this age group, also since the larger lower premolars have a better chance of being found in the field and during wet sieving than the very small dp4. Although the shed deciduous premolars cannot be used for the mortality study, as they represent a 'life process', they

indicate autochthony of *Euroxenomys minutus* at both HAM 5 and HAM 4 habitats.

All available lower premolars of appropriate preservation from HAM 5 and HAM 4 strata representing the small beavers *Euroxenomys minutus* were counted and categorised by wear-stage definitions provided in the material and methods paragraph. With the final counts on the six wear stages, an age-frequency distribution – Mortality profile – following Lyman (1994) was performed (Figure 9).

The age-frequency distributions for *Euroxenomys minutus* are based on 70 lower premolars from the local stratigraphic level HAM 5 and 131 p4 from the HAM 4 layer. In general, the shape of the two resulting mortality profiles is quite similar but a slight shift by one wear stage, to an older age at death in the HAM 5 material can be observed (Figure 9). In the HAM 5 profile, WS 1 (5.7%, n = 4) and WS 2 (5.7%, n = 4) show very low values, followed by the most dominant WS 3 (31.4%, n = 22) and WS 4 (37.1%, n = 26) counts. WS 5 (18.6%, n = 13) still exposes a quite high value, while WS 6 (1.4%, n = 1) is the most underrepresented age class. The age-frequency distribution of lower premolars from HAM 4 reveals a similarly low WS 1 (5.3%, n = 7) as in HAM 5. In contrast to the latter, WS 2 already exhibits a considerably higher score (17.6%, n = 23) in the HAM 4 material, followed by the highest mortality proportion during WS 3 (40.1%, n = 53) and a slightly lower value in WS 4 (26%, n = 34). In contrast to HAM 5, WS 5 (9.9%, n = 13) from HAM 4 is already low, while both share a very low value for WS 6 (0.8%, n = 1).

The mortality profiles of both HAM 5 and HAM 4 layers neither correspond with the typical U-shaped (attritional death model) age-frequency distribution nor with the characteristic L-shaped (catastrophic death model) mortality pattern after Voorhies (1969) and Lyman (1994). In the case of both Hammerschmiede mortality profiles, the shape is more likely to be described as a 'pyramid'-shaped pattern. A typical peak in the form of a high mortality in juveniles is not observed in both HAM 5 and HAM 4 age-frequency distributions. Instead, the highest mortality is among individuals in the 'prime' age group (WS 3 and WS 4). The peak of the mortality 'pyramid' of HAM 5 is located at WS 4 and in HAM 4 at WS 3, and thus shifted by one wear stage. Apart from that, the two profiles are extremely similar.

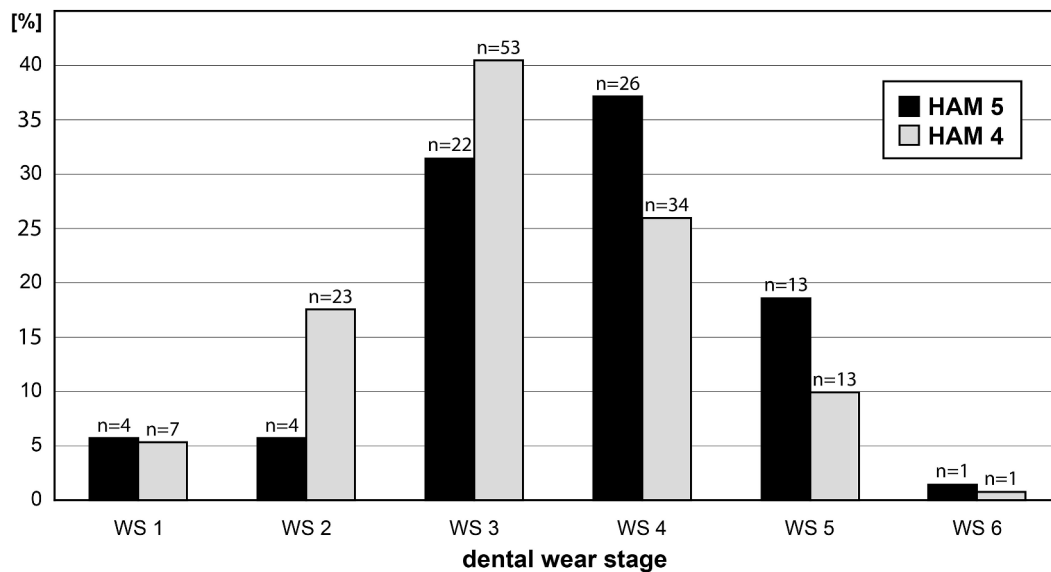


Figure 9. Mortality profiles (age-frequency distribution) of the minute beaver *Euroxenomys minutus* (von Meyer 1838), from the early Late Miocene locality Hammerschmiede (Bavaria, Germany), based on lower premolars from the local stratigraphic levels HAM 5 and HAM 4. Each bar corresponds to an age class, defined by either morphologic criteria (WS 1-WS 2) or mathematical spread of the tooth crown height (WS 3-WS 6) as defined in the materials and methods section. Vertical axis represents the percentage of individuals within the corresponding local stratigraphic level.

In a second mortality analysis, a ternary diagram following the basic methods introduced by Stiner (1990) and modified after Discamps and Costamagno (2015) was created (Figure 10). Here only three age groups are used (juvenile, prime adult and old adult). These three groups are obtained by always combining the counts of two wear stages (juvenile = WS 1+ WS 2, prime adult = WS 3+ WS 4 and old adult = WS 5+ WS 6). In addition to the classic L-shaped (JPO dominated zone) and U-shaped (JOP dominated zone) mortality profiles, the ternary diagram can be used to compare more options. To display the four dominance zones (Juveniles-Old-Prime = JOP; Juveniles-Prime-Old = JPO; Old = O; and Prime = P) introduced by Discamps and Costamagno (2015) a reference point must be defined, which is maintained due to the species-specific lifetime distribution. Since we do not know the relative distribution of the three age groups compared to the average lifetime expectancy in *Euroxenomys minutus*, this point was derived as follows. While for the large beaver species from Hammerschmiede *Steneofiber depereti*, the lifetime distribution is assumed to be similar to today's beavers, this is not necessarily applicable to *Euroxenomys minutus*, especially due to the tiny body size. Given the extremely high functional morphological and presumably ecological similarity of *Euroxenomys minutus* to today's muskrat (*Ondatra zibethicus*), its life cycle could be a possible assumption for comparison. Muskrats have a significantly shorter life span of about 3 years (Godin 1977; Willner et al. 1980; Nowak 1991). The muskrat reaches sexual maturity and thus the end of the juvenile period with about 7 months (Heidecke and Seide 1989; Birnbaum 2013). Until the end of the second year of life, the muskrat is considered a prime adult and from the second year of life onwards an old adult. This roughly corresponds to a distribution of 20% juvenile (7 months), 47% prime adult (17 months) and 33% old adult (12 months). Since the reference point used for *Castor fibre* from extant studies and Pleistocene sites of a corresponding analysis from Campbell (2009) and Heinrich and Maul (2020) marks a similar point (24% young, 43% prime, 33% old) in the ternary diagram as the calibration just derived for the muskrat, the decision between both calibration points is not necessary and we continue to work with the muskrat data.

As already indicated in the mortality profile, the mortalities of the compared *Euroxenomys* sites do not correspond to any of those classically differentiated zones, but in a separate area called 'P' (prime dominated zone). Hereby, it can be further specified that HAM 5 is located in a subzone $P > O > J$ and HAM 4 and Rudabanya are located in the subzone $P > J > O$. However, these subtle differences are probably of marginal importance and are not the focus of our further discussion. It must be emphasised that the points are not located in the standard fields, but in the prime dominated zone, which should not be the case in a classical normal mortality (Discamps and Costamagno 2015). Thus, a special influence is required for a mortality to shift from juvenile dominance, which would be expected due to typically high infant mortality, to prime adult dominance. Such prime adult dominance has hardly been described in beavers so far, but is rather found in archaeological contexts. Heinrich and Maul (2020) describe an almost identical mortality in *Castor fibre* from the Pleistocene sites Bilzingsleben II, Weimar-Ehringsdorf and Weimar-Taubach. The authors explain this taphonomic filter as an accumulation of similarly aged beavers that were selectively hunted by hominins. Since we exclude hominin/hominid hunting on beavers for Hammerschmiede, a dominating influence by other predators is the most likely explanation.

We already published the age-frequency distribution of another, much larger beaver species from Hammerschmiede locality – *Steneofiber depereti* (Lechner and Böhme 2022). For this large beaver, a massive difference in the mortality distribution between the two layers (HAM 5 and HAM 4) was found, which we attribute mainly to ecological reasons of *Steneofiber depereti* and the observation that HAM 5 represents a rivulet and HAM 4 a larger river with different environmental parameters. *S. depereti*, a beaver slightly smaller in size than today's beavers, most probably preferred the larger river (represented by HAM 4 sediments) as the core habitat, while the HAM 5 rivulet was a temporary habitat for young adult beavers in search of their own territory (Lechner and Böhme 2022). Although such observations and differences in mortality can be made for the large beaver species from Hammerschmiede, the age-frequency distribution of the tiny

Euroxenomys minutus shows a totally different pattern. A possible explanation for these major differences could be a different ecologic lifestyle of these beaver species and also the huge difference in size. *Euroxenomys minutus* possibly is subject to strong predation influence due to its small size, in contrast to the much larger and therefore more defensible *Steneofiber depereti*. The body size of *Euroxenomys minutus* should be about the same as the extant muskrat, with an average weight of approximately 1100 g (750–1575 g) provided for the muskrat by Fuller (1951). For rodents of this weight class, a very large number of avian and mammalian predators are available in the Hammerschmiede ecosystems, e.g., several aquatic/semiaquatic as well as terrestrial carnivores and birds of prey. A predatory selection in *Euroxenomys minutus* according to life age seems possible if especially the young animals are not accessible for the predators for certain reasons. However, the low number of very young *Euroxenomys* beavers in the mortality is possibly based on habitat or behavioural reasons. Perhaps young *Euroxenomys* stayed hidden in burrows inaccessible to predators or they moved mainly in more by vegetation protected areas near the dwelling, while adults that cover much greater distances in search of food and resources, were easy targets of predators in the water and on land.

As already described before, there is no data on the lifetime of the fossil *Euroxenomys minutus* and consequently we can only assume which time-steps the age-frequency distribution covers. While in the large *Steneofiber depereti*, the lifetime probably corresponds to that of today's large beaver species and other large rodents (up to 15–24 years living in the wild; Brown 1979; Grzimek 1990; Bobick and Peffer 1993), the lifetime expectancy of

Euroxenomys minutus is assumed to correspond with that of smaller rodents like the muskrat (*Ondatra zibethicus*) with an estimated 3 years of life (Godin 1977; Willner et al. 1980; Nowak 1991). With such a short-life expectancy, mortality analyses would react much more sensitive and could depict processes that take place over a period of a few months only. The probability of dying during a short juvenile phase (*Ondatra*) is of course much lower than if this phase lasts longer (*Castor*). This certainly has an influence on the relative frequency of juvenile teeth to adult teeth.

For an intraspecific comparison of *Euroxenomys minutus*, the age-frequency distribution from the slightly younger fossil site of Rudabánya in Hungary is compared (Kordos 2020). Here, very young and very old beavers are also quite rare in the mortality analysis, while the main count is represented by medium-aged beavers (Kordos 2020). The age frequency distribution in the mortality analyses for *Euroxenomys minutus* from Rudabánya is therefore very similar to that observed at HAM 5 and HAM 4 (Figure 10). This finding is particularly interesting also by the fact that Rudabánya represents a fossil swamp environment (Kordos 2020). Thus, in addition to the channel of HAM 5 interpreted as a small rivulet and the HAM 4 channel representing larger river deposits, a third environment interpreted as a swamp (Rudabánya) now also shows a very comparable mortality distribution (Böhme et al. 2019; Kordos 2020). In contrast to the larger Miocene beaver species *Steneofiber depereti* (which is not found at Rudabánya site) our results show that on one hand *Euroxenomys minutus* is an ubiquitous dweller of various aquatic habitats (swamp, rivulet and river), much as the muskrats today, on the other hand, the small beaver in all of these habitats seems to be under an influence that produces a very similar age distribution and mortality. As a possibly very dominant external factor, especially because of the small body size of *Euroxenomys minutus* as a prey, a selective predation on prime age *Euroxenomys* by the afore mentioned large amount of different available predators (diurnal and nocturnal avian and terrestrial and aquatic/semiaquatic mammalian carnivores) is probably one of the most causal reasons for these similarities in the age-frequency distributions of those habitats. Another explanation could be a special behaviour of the young beavers, which makes them more difficult to reach for predators.

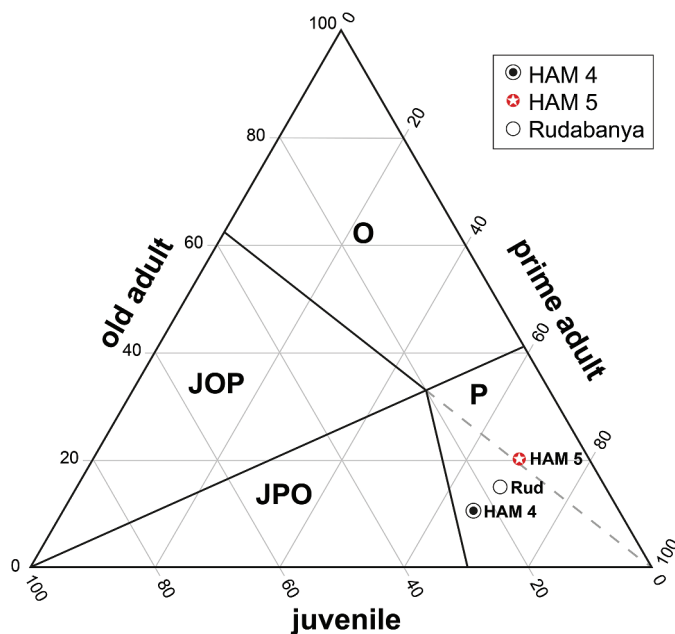


Figure 10. Ternary diagram of the relative age-frequency distributions (mortality) differentiated into the three age groups juvenile, prime adult and old adult individuals (in %) of the small beaver species *Euroxenomys minutus* (von Meyer 1838) from the early Late Miocene localities Hammerschmiede (Bavaria, Germany), including the local stratigraphic levels HAM 5 and HAM 4 and from Rudabánya (Hungary); Data from Kordos 2020 based on lower premolars. Calibration of the zoning point corresponds to the relative lifetime distribution of the extant muskrat, *Ondatra zibethicus* (see text). Abbreviations of zones follow Discamps and Costamagno (2015): JOP, juveniles-old adults-prime adults dominated zone; JPO, juveniles-prime adults-old adults dominated zone; P, prime adults dominated zone. All three fossil samples are located in the prime dominated zone.

Conclusion

Beavers are extremely abundant finds at the early Late Miocene Hammerschmiede locality. The two local stratigraphic levels worked on here represent a small rivulet (HAM 5) and a river (HAM 4) and in both there occurs a common large beaver (*Steneofiber depereti*) as well as an even more frequent small beaver form. We assign the small form to the trogontheriine beaver *Euroxenomys minutus* (von Meyer 1838). The extensive set of dental remains from Hammerschmiede represent the largest Miocene record for this beaver species at all. This facilitates a very realistic insight into the metric and morphological intraspecific variability of this small beaver, which is marked by an enormous range of variation in these points. *Euroxenomys minutus* from Hammerschmiede includes the hitherto rather heterogeneous individual data from the many other Eurasian discovery sites and proves their affiliation to one species. Furthermore, a clear delimitation to teeth from the locality Dorn-Dürkheim (Germany) can be confirmed and the status of this morphotype at least at subspecies level (*Euroxenomys minutus rhenanus*) is approved as correct.

In contrast to the large beaver species *Steneofiber depereti* from Hammerschmiede, where the local stratigraphic levels HAM 5

(rivulet) and HAM 4 (river) demonstrate significantly different mortality patterns, the age-frequency distributions of *Euroxenyomys minutus* reveal a higher degree of similarity for both of these fossil habitats. In addition to that, the age-frequency distribution of *Euroxenyomys minutus* from Rudabánya in Hungary, that is assumed to be a fossil swamp, is consistent with this image, despite the fact that no large beaver species is found here. In all three habitats a very low number of individuals is represented by very young beavers, a high mortality indicates the midlife and only few very old animals were found. This high similarity in the mortality profiles of the river, rivulet and swamp habitats indicates, that on one hand, the ecology of the small *Euroxenyomys minutus* could be different from that of the large beaver, and on the other hand, that the small beaver is probably more vulnerable to external factors like predators, due to its size. The latter hypothesis is supported by traces of corrosive lesions on several dental specimens, which could be attributed to corrosive effects of digestion by mammalian carnivores or predatory birds. Furthermore, the extremely high proportion of fragmented cranial (more than 90% of dental material are single teeth) and postcranial material and especially the long bones could indicate that finds of *Euroxenyomys minutus* at the Hammerschmiede represent a predatory bone assemblage.

Acknowledgments

The authors would like to thank I. Werneburg (GPIT) for providing access to the objects stored in the Tübingen collection (GPIT and SNSB-BSPG stored at GPIT) and T. Lehmann for access to the specimens from Dorn-Dürkheim under his care (Senckenberg, Frankfurt, Germany). Moreover, we are very grateful to L. Kordos (Eötvös Loránd University, Budapest) for providing his records and measurements on the beaver material from Rudabánya. Further, we thank W. Lechner (Nawilab, Trostberg, Germany) for providing the most recent reference material. We thank A.-C. Grupp (GPIT and SNSB-BSPG), D. Wedekind (Senckenberg Centre HEP, Tübingen, Germany) and J. Franke (SNSB-BSPG) and H. Stöhr (GPIT) for the preparation of the specimens. We further acknowledge all participants of the numerous excavations in the Hammerschmiede fossil site, who helped to detect and collect the studied material, with special thanks to the members of the organisation team of the excavation years 2020–2022: F. Augustin, A. Ayvazyan, C. Dietzel, H. El Atfy, J. Hartung, P. Kampouridis, N. Kargopoulos, U. Kirscher, C. Kyriakouli, M. Lex, T. Massonne, A. Matzke and M. Neuhof. The excavations and associated research were supported by the Bavarian State Ministry of Research and the Arts and by the Bavarian Natural History Collections (SNSB). We would also like to thank I. Gold, C. Dietzel, P. Kampouridis, F. Augustin, and A. Matzke (all GPIT) for fruitful discussions and improvement of the manuscript. Finally, we thank the editor G. Dyke, and the reviewers T. Mörs and an anonymous reviewer for helpful comments and suggestions on the manuscript.

Disclosure statement

No potential conflict of interest was reported by the author(s).

Funding

Research was partially supported by the Bavarian State Ministry of Research and the Arts, and by the Bavarian Natural History Collections (SNSB).

ORCID

Thomas Lechner  <http://orcid.org/0009-0003-3087-7487>

Madelaine Böhme  <http://orcid.org/0000-0003-2100-6164>

References

- Aldana Carrasco E. 1992. Los Castoridae (Rodentia, Mammalia) del Neógeno de Cataluña (España). Treballs del Museu de Geologia de Barcelona. 2:99–141. Spanish
- Andrews P. 1990. Owls, Caves and Fossils. Chicago: University of Chicago Press; pp. 231.

- Andrews P, Evans EM. 1983. Small mammal bone accumulations produced by mammalian carnivores. *Paleobiology*. 9(3):289–307. doi:10.1017/S0094837300007703.
- Birnbaum C 2013. NOBANIS – invasive alien species fact sheet – *Ondatra zibethicus*. – from: online database of the European Network on invasive alien species – NOBANIS www.nobanis.org, Date of access 2023 March 30.
- Bobick JE, Peffer M 1993. Science and technology desk reference. Gale research Inc. Washington (D.C).
- Böhme M, Spassov N, DeSilva JM, Begun DR. 2020. Reply to: Reevaluating bipedalism in *Danuvius*. *Nature*. 586(7827):E4–E5. doi:10.1038/s41586-020-2737-3.
- Böhme M, Spassov N, Fuss J, Tröscher A, Deane AS, Prieto J, Kirscher U, Lechner T, Begun DR. 2019. A new Miocene ape and locomotion in the ancestor of great apes and humans. *Nature*. 575(7783):489–493. doi:10.1038/s41586-019-1731-0.
- Brown MK. 1979. Two old beavers from the Adirondacks. *New York Fish and Game J*. 26:92.
- Campbell RD 2009. Demography and life history of the Eurasian beaver *Castor fiber*. Ph.D. thesis. – MS, Department of Zoology, University of Oxford, Oxford, 282 pp. (thesis available online)
- Daxner-Höck G. 2004. Biber und ein Zwerghamster aus Mataschen (Unter-Pannonium, Steirisches Becken). *Joannea, Geologie und Paläontologie*. 5:19–33. German
- Daxner-Höck G, Bernor RL. 2009. The early Vallesian vertebrates of Atzelsdorf (Late Miocene, Austria) 8. *Anchitherium*, Suidae and Castoridae (Mammalia). *Annalen des Naturhistorischen Museums in Wien*. 111 (A):557–584.
- Discamps E, Costamagno S. 2015. Improving mortality profile analysis in zooarchaeology: a revised zoning for ternary diagrams. *Journal of Archaeological Science*. 58:62–76. doi:10.1016/j.jas.2015.03.021.
- Engesser B. 1972. Die obermiozäne Säugetierfauna von Anwil (Baselland). Tätigkeitsbericht Naturforschende Gesellschaft Baselland. 28:1–363. German
- Fahlbusch V, Mayr H. 1975. Microtoide Cricetiden (Mammalia, Rodentia) aus der Oberen Süßwasser-Molasse Bayerns. *Paläontologische Zeitschrift*. 49(1/2):78–93. doi:10.1007/BF02988068. German
- Fernández FJ, Hadler P, Cherem JJ, Saldanha JP, Stutz NS, Dias AS, Pardiñas UFJ. 2019. Holocene small mammals hunted by owls and humans in southern Brazil: taphonomic evidence and biological significance. *Boreas*. 48(4):953–965. doi:10.1111/bor.12399.
- Fernández-Jalvo Y, Andrews P. 2016. Atlas of taphonomic identifications. Dordrecht: Springer; pp. 359.
- Fischer von Waldheim G. 1809. Sur l'*Elasmotherium* et le *Trogontherium*, deux animaux fossiles et inconnus de la Russie. *Études palaeontologiques sur les environs de Moscou* 2: 250–268. French
- Franzen JL, Storch G. 1975. Die unterpliozäne (turolische) Wirbeltierfauna von Dorn-Dürkheim, Rheinhessen (SW-Deutschland); 1. Entdeckung, Geologie, Mammalia: Carnivora, Proboscidea, Rodentia. *Grabungsergebnisse 1972–1973. Senckenbergiana lethaea*. 56. 233–303. German
- Freye H-A. 1959. Deskriptive Anatomie des Craniums vom Elbe-Biber (*Castor fiber albicus* MATSCHIE 1907). *Wissenschaftliche Zeitschrift der Martin-Luther-Universität Halle-Wittenberg. Math-naturwissenschaftliche Reihe*. VIII. 913–962. German
- Fuller WA. 1951. Measurements and weights of Northern Muskrats. *Journal of Mammalogy*. 32(3):360–362. doi:10.1093/jmammal/32.3.360.
- Fuss J, Prieto J, Böhme M. 2015. Revision of the boselaphin bovid *Miotragocerus monacensis* Stromer, 1928 (Mammalia, Bovidae) at the Middle to Late Miocene transition in Central Europe. *Neues Jahrbuch für Geologie und Paläontologie Abhandlungen*. 276(3):229–265. doi:10.1127/njgpa/2015/0481.
- Geoffroy-Saint-Hilaire É. 1833. Palaeontographie. Considérations sur des ossements fossiles la plupart inconnus trouvés et observés dans les bassins de l'Auvergne. *Revue Encyclopédique*. 59(LIX):76–95. French
- Giersch S, Munk W, Ziegler R. 2010. The first record of a beaver – *Trogontherium (Euroxenyomys) minutum* – in the Höwenegg fauna (Miocene, southern Germany). *Palaeodiversity*. 3:235–239.
- Godin AJ. 1977. Wild mammals of New England. Baltimore: Johns Hopkins University Press; p. 304.
- Grzimek B. ed. 1990. Grzimek's animal life encyclopedia. Mammals I - IV. ed. Series. Grzimek, B. Vol. I-IV. New York: McGraw-Hill Publishing Company.
- Hartung J, Böhme M. 2022. Unexpected cranial sexual dimorphism in the tragulid *Dorcotherium naui* based on material from the middle to late Miocene localities of Eppelsheim and Hammerschmiede (Germany). *PLOS ONE*. 17(5):e0267951. [published online] 10.1371/journal.pone.0267951
- Hartung J, Lechner T, Böhme M. 2020. New cranial material of *Miotragocerus monacensis* (Mammalia: Bovidae) from the late Miocene hominid locality Hammerschmiede (Germany). *Neues Jahrbuch für Geologie und Paläontologie Abhandlungen*. 298(3):269–284. doi:10.1127/njgpa/2020/0948.
- Heidecke D, Seide P. 1989. *Bisamratte Ondatra zibethicus* (L.). *Buch der Hege Band 1 Haarwild*. Stubbe H ed., Berlin: VEB Deutscher Landwirtschaftsverlag Berlin. German. p. 640–666.

- Heinrich W-D, Maul LC. 2020. Mortality profiles of *Castor* and *Trogontherium* (Mammalia: Rodentia, Castoridae), with notes on the site formation of the Mid-Pleistocene hominid locality Bilzingsleben II (Thuringia, Central Germany). Fossil Imprint. 76(1):40–58. doi:10.37520/fi.2020.004.
- Hemprich W 1820. Grundriss der Naturgeschichte für höhere Lehranstalten. 29 pp. August Rücker, Berlin. German.
- Hír J. 2004. The Middle Miocene (late Astaracian, MN7-8) rodent Fauna of Felsőtárkány 3/2 (Hungary). Acta Palaeontol Rom. 4:125–136.
- Huguency M. 1999. Family Castoridae. In: Rössner GE, Heissig K, editors. The Miocene Land Mammals of Europe. Munich: Verlag Friedrich Pfeil; p. 281–300.
- Huguency M, Duranthon F. 2012. Les Castoridae (Rodentia) de Sansan. In: Peigné S, editor. Mammifères de Sansan, Mémoires du Muséum National d'Histoire Naturelle. French: Publications Scientifiques du Muséum, Paris; p. 95–118.
- Huguency M, Escuillié F. 1995. K-strategy and adaptative specialization in *Steneofiber* from Montaigu-le-Blin (dept. Allier, France; Lower Miocene, MN 2a, ± 23 Ma): first evidence of fossil life-history strategies in castorid rodents. Palaeogeography Palaeoclimatol Palaeoecol. 113(2–4):217–225. doi:10.1016/0031-0182(95)00050-V.
- Huguency M, Escuillié F. 1996. Fossil evidence for the origin of behavioral strategies in early Miocene Castoridae, and their role in the evolution of the family. Paleobiology. 22(4):507–513. doi:10.1017/S0094837300016493.
- Jäger GF 1835. Über die fossilen Säugethiere, welche in Württemberg aufgefunden worden sind. 70 pp. C. Erhard, Stuttgart. German.
- Kargopoulos N, Kampouridis P, Lechner T, Böhme M. 2021a. A review of *Semigenetta* (Viverridae, Carnivora) from the Miocene of Eurasia based on material from the hominid locality of Hammerschmiede (Germany). Geobios. 69:25–36. doi:10.1016/j.geobios.2021.07.001.
- Kargopoulos N, Kampouridis P, Lechner T, Böhme M. 2021b. Hyaenidae (Carnivora) from the Late Miocene hominid locality of Hammerschmiede (Bavaria, Germany). Historical Biology. doi:10.1080/08912963.2021.2010193.
- Kargopoulos N, Valenciano A, Abella J, Kampouridis P, Lechner T, Böhme M. 2022. The exceptionally high diversity of small carnivorans from the Late Miocene hominid locality of Hammerschmiede (Bavaria, Germany). PLOS ONE. 17(7):e0268968. doi:10.1371/journal.pone.0268968.
- Kargopoulos N, Valenciano A, Kampouridis P, Lechner T, Böhme M. 2021c. New early late Miocene species of *Vishnuonyx* (Carnivora, Lutrinae) from the hominid locality of Hammerschmiede, Bavaria, Germany. Journal of Vertebrate Paleontology. 41(3):[published online] 10.1080/02724634.2021.1948858
- Kaup JJ. 1832. Beschreibung Dreyer Gattungen urweltlicher Nager des zoologischen Museums zu Darmstadt, welche von den jetzt lebenden Genera verschieden sind. Isis. IX. 992–996. German
- Kirscher U, Prieto J, Bachtadse V, Abdul Aziz H, Doppler G, Hagmaier M, Böhme M. 2016. A biochronologic tie-point for the base of the Tortonian stage in Europe terrestrial settings: magnetostratigraphy of the topmost upper freshwater molasse sediments of the North Alpine Foreland Basin in Bavaria (Germany). Newsl on Stratigr. 49(3):445–467. doi:10.1127/nos/2016/0288.
- Kordos L. 2020. *Trogontherium minutum* (Rodentia, Castoridae) from the late Miocene of Rudabánya, Hungary. Tertiary & Quaternary Strata. 2020(1):1–7.
- Korth WW. 2001. Occurrence of the European genus of beaver *Euroxonomys* (Rodentia: Castoridae) in North America. Paludicola. 3:73–79.
- Lechner T, Böhme M. 2020. *Castor*-like postcranial adaptation in an uppermost Miocene beaver from the Staniantzi Basin (NW Bulgaria). Fossil Imprint. 76(1):128–164. doi:10.37520/fi.2020.009.
- Lechner T, Böhme M. 2022. The beaver *Steneofiber depereti* from the lower Upper Miocene hominid locality Hammerschmiede and remarks on its ecology. Acta Palaeontologica Polonica. 67(4):807–826. doi:10.4202/app.00997.2022.
- López JM, Rosi MI, Tabeni S, Bender B, Chiavazza H. 2017. Taphonomic analysis of small mammal bone remains preyed upon by wildcats (Carnivora: Felidae) from the central Monte Desert (Mendoza, Argentina). Boreas. 46(2):282–293. doi:10.1111/bor.12211.
- Lyman RL 1994. Vertebrate taphonomy. Cambridge manuals in archaeology. Cambridge University Press, Cambridge, New York, Melbourne. 524 pp.
- Marin-Monfort MD, García-Morato S, Olucha R, Yravedra J, Piñeiro A, Barja J, Andrews P, Fernández-Jalvo Y. 2019. Wildcat scats: taphonomy of the predator and its micromammal prey. Quaternary Science Reviews. 225:1–16. doi:10.1016/j.quascirev.2019.106024.
- Mayet L. 1908. Étude des Mammifères Miocènes des Sables de l'Orléanais et des Faluns de la Touraine. Annales de L'Université de Lyon - Nouvelle Série, I. Sciences, Médecine. 24. 1–336. French
- Mayr H, Fahlbusch V. 1975. Eine unterpliozäne Kleinsäugerfauna aus der Oberen Süßwasser-Molasse Bayerns. Mitt der Bayerischen Staatssammlung für Paläontol und Historische Geol. 15. 91–111. German
- Mayr G, Lechner T, Böhme M. 2020a. A skull of a very large crane from the late Miocene of Southern Germany, with notes on the phylogenetic interrelationships of extant Gruinae. J Ornith. 161(4):923–933. doi:10.1007/s10336-020-01799-0.
- Mayr G, Lechner T, Böhme M. 2020b. The large-sized darter *Anhinga pannonica* (Aves, Anhingidae) from the late Miocene hominid Hammerschmiede locality in Southern Germany. PLOS ONE. 15(5):0232179. doi:10.1371/journal.pone.0232179.
- Mayr G, Lechner T, Böhme M. 2022. Nearly complete leg of an unusual, shelduck-sizedanseriform bird from the earliest late Miocene hominid locality Hammerschmiede (Germany). Historical Biology. doi:10.1080/08912963.2022.2045285.
- Meyer H von. 1838. Mittheilungen, an Professor Bronn gerichtet. In Leonhard KC, Bronn HG, editors. Neues Jahrbuch für Mineralogie, Geognosie, Geologie und Petrefaktenkunde.(1838):413–418. German
- Mörs T, Häggglund S, Erbjaveva MA, Alexeeva N, Shchetnikov AA, Daxner-Höck G. 2022. The northernmost Eurasian Miocene beavers: *Euroxonomys* (Castoridae, Mammalia) from Olkhon Island, Lake Baikal (Eastern Siberia). Palaeobiodivers and Palaeoenviron. 102(4):873–883. doi:10.1007/s12549-022-00555-x.
- Mott CL, Bloomquist CK, Nielsen CK. 2013. Within-lodge interactions between two ecosystem engineers, beavers (*Castor canadensis*) and muskrats (*Ondatra zibethicus*). Behav. 150(11):1325–1344. doi:10.1163/1568539X-00003097.
- Nowak RM. 1991. Walker's Mammals of the World. Vol. I, 5th ed. Baltimore: Johns Hopkins University Press.
- Prieto J. 2009. Evolution of the genus *Collimys* Daxner-Hock, 1972 (Rodentia, Cricetidae) a key to Middle to Late Miocene biostratigraphy in Central Europe. Neues Jahrbuch für Geologie und Paläontologie - Abhandlungen. 252(2):237–247. doi:10.1127/0077-7749/2009/0252-0237.
- Prieto J. 2012. The genus *Eomyops* Engesser, 1979 (Rodentia, Eomyidae) from the youngest deposits of the German part of the North Alpine Foreland Basin. Swiss Journal of Palaeontology. 131(1):95–106. doi:10.1007/s13358-011-0033-4.
- Prieto J, Casanovas-Vilar I, Gross M. 2014. *Euroxonomys minutus minutus* (Rodentia, Castoridae) from Gratkorn (Austria, Styria). In: Böhme M, Gross M, Prieto J, editors. The Sarmatian vertebrate locality Gratkorn, Styrian Basin. Palaeobiodiversity and Palaeoenvironments. Vol. 94(1). 163–170
- Prieto J, van Dam JA. 2012. Primitive Anourosoricini and Allosoricinae from the Miocene of Germany. Geobios. 45(6):581–589. doi:10.1016/j.geobios.2012.03.001.
- Prieto J, van den Hoek Ostende LW, Böhme M. 2011. Reappearance of *Galerix* (Erinaceomorpha, Mammalia) at the Middle to Late Miocene transition in South Germany: biostratigraphic and palaeoecologic implications. Contributions to Zoology. 80(3):179–189. doi:10.1163/18759866-08003002.
- Rekovets L, Stefan C, Demeshkant V. 2020. Beavers (Castoridae, Rodentia) from the late Miocene (MN 9) locality Grytsiv in Ukraine. Fossil Imprint. 76(1):165–173. doi:10.37520/fi.2020.010.
- Roger O. 1898. Wirbeltierreste aus dem Dinotheriensande der bayerisch-schwäbischen Hochebene. Bericht des Naturwissenschaftlichen Vereins für Schwaben und Neuburg. 33: 1–46. German
- Samson P, Rădulescu C. 1973. Rémarques sur l'évolution des Castoridés (Rodentia, Mammalia). In: Orghidan T, editor. Livre du cinquantenaire de L'Institut de Spéléologie "Emile Racovitza". French: Academie Republicii Socialiste România, Bucarest. Romanian; p. 437–449.
- Schreuder A. 1929. *Conodontes* (*Trogontherium*) and *Castor* from the Teglian clay compared with the Castoridae from other localities. Archives du Musée Teyler. 3:99–320.
- Stefen C 1997. *Steneofiber eseri* (Castoridae, Mammalia) von der Westtangente bei Ulm im Vergleich zu anderen Biberpopulationen. Stuttgarter Beiträge zur Naturkunde - Serie B (Geologie und Paläontologie) 255:1–73. German.
- Stefen C. 2001. Barstovian (Miocene) beavers from Stewart Valley, Nevada, and a discussion of the genus *Monosaulax* based on tooth morphology. Paleobios. 21(1):1–14.
- Stefen C. 2009. The European Tertiary beaver *Chalicomys jaegeri* (Rodentia: Castoridae) revisited. Kaupia - Darmstädter Beiträge zur Naturgeschichte. 16:161–174.
- Stefen C. 2018. The castorids (Mammalia, Castoridae) from the (early) middle Miocene of Gračanica (Bosnia-Herzegovina). Palaeobiodivers and Palaeoenviron. 100(2):301–305. doi:10.1007/s12549-018-0365-9.
- Stefen C, Mörs T. 2008. The beaver *Anchitheriomys* from the Miocene of Central Europe. J Paleontol. 82(5):1009–1020. doi:10.1666/06-049.1.
- Stefen C, Rummel M. 2003. *Trogontherium* (*Euroxonomys*) *minutum* (Castoridae: Mammalia) from Petersbuch 50, Miocene, South Germany. Neues Jahrb für Geol und Paläontol, Monatsh. 2003(1):11–34. doi:10.1127/njgpm/2003/2003/11.
- Stiner MC. 1990. The use of mortality patterns in archaeological studies of hominid predatory adaptations. Journal of Anthropological Archaeology. 9(4):305–351. doi:10.1016/0278-4165(90)90010-B.
- Stirton RA. 1935. A review of the tertiary beavers. Univ Calif Publ Geol Sci. 23:391–458.
- Voorhies MR. 1969. Taphonomy and population dynamics of an early Pliocene vertebrate fauna, Knox county, Nebraska. Rocky Mountain Geol. 8:1–69.
- Williams SA, Prang TC, Meyer MR, Russo GA, Shapiro LJ. 2020. Reevaluating bipedalism in *Danuvius*. Nature. 586(7827):E1–E3. doi:10.1038/s41586-020-2736-4.
- Willner GR, Feldhamer GA, Zucker EE, Chapman JA. 1980. *Ondatra zibethicus*. Mamm Species. 141(141):1–8. doi:10.2307/3504016.

Conclusion and future perspectives

The early Late Miocene Hammerschmiede locality had already been known for more than half a century to science. Before the work on this dissertation was started several studies on the flora and fauna of the Hammerschmiede were already carried out, but rather focused to a taxonomic level. More recent changes in the accessibility of the outcrops and above all, the use of more advanced and renewed methods opened up a new scope of information for this fossil site. The introduction of special documentation and excavation techniques multiplied the quality and quantity of finds and supplemented metadata. New approaches in spatial data analyses for the Hammerschmiede fossil site provided insights into sedimentary processes as well as biostratigraphic findings.

The focus of this dissertation was the study of the local stratigraphic levels HAM 5 and HAM 4. Previous investigations had assumed that these fossil-bearing layers comprise fluvial channel deposits, which could fundamentally be confirmed. Both levels clearly contain fine-grained fluvial deposits including typical structures of cross-bedding, trough cross-bedding, fining upward sequences, sorting with the deposition of placers of heavy minerals (garnet) and an enrichment of coarse grained material in channel lag deposits. The latter provide the majority of osteological finds but also include erosive clasts of the channel base. Gravel is almost completely absent and the coarsest elements are represented by biogenic components (bones, shells, plant remains). Both HAM 5 and HAM 4 could be clearly traced by an eroded channel structures in the outcrop of the Hammerschmiede clay pit. This enabled the excavations to be focussed precisely on the channel fillings which were documented over a considerable extent in various areas of the clay pit. In this way, many smaller patches provided sedimentological and taphonomic insights that could be combined to a large-scale view.

It was shown that both deposits HAM 5 and HAM 4 are small- to medium scale multiphase sedimentological sequences, which shared some similarities but also had significant differences. In both channels, allochthonous, as well as autochthonous elements were identified.

The channel structure of HAM 4 meanders slight S-curved from south-west to north-east. This was confirmed by observations of the outcropping channel structures in the clay pit area, supplemented by multiple small-scale flow direction analyses based on elongated objects orientations (bones and plant remains) as well as directional analyses of the longitudinal axes of mass accumulations of freshwater pearl mussels. The taphonomic observations on possible individual skeletal strewnfields served as further evidence for this. It was further assumed that

the actual drain direction of the HAM 4 river was oriented from south to north, as this is also consistent with the general geological and tectonic idea of a northward flow from the Alpine uplift direction. The observed northerly inclination of the HAM 4 channel cannot be used as evidence for this, as it corresponds to the general inclination of the entire Hammerschmiede sediments. The absence of alpine gravels must be clarified in the future, but may indicate a river origin in the folded molasse in fine-grained sediments such as the Upper Marine Molasse.

The exact flow behaviour of the HAM 5 rivulet could not be clearly reconstructed due to the small extent of available documented excavation area. Nevertheless, a slightly meandering course was suggested due to field investigations. The HAM 5 flow direction was supposed mainly based on sedimentological evidences. The numerous reconstructed skeletal strewnfields of presumed single vertebrate individuals clearly indicated that a flow direction from south to north can be regarded as definite.

The local stratigraphic level HAM 5 most likely represented a smaller channel, more in the size of a rivulet and rather stable in place. The HAM 5 showed a main erosive channel depression, which was successively filled by two generations of fining upward-sequences including basal channel lag deposits and on top vegetation markers (roots) indicated slight temporal separations. These two channel fillings mostly enriched osteological specimens in channel lag deposits. Taxonomic, osteological and preservative heterogeneity of the found material showed a strong intermixing and accumulation of objects from the closer but also more distant regions over a certain period of time, as many specimens are placed incoherently next to each other. Evidence that carcasses from the immediate vicinity were also washed into the HAM 5 channel was provided by the reconstruction of a bony strewnfield representing a male individual of the great ape *Danuvius guggenmosi*. This discovery, as well as other skeletal strewnfields, proved that those were introduced into the area at a fairly late stage, short before the final burial and thus possibly represent autochthonous elements of the rivulet surrounding ecosystem. A third and final phase of sediments at the HAM 5 level additionally overlies a lateral overbank area of the main channel, which is characterised by low contents of aquatic vertebrates and a different qualitative and quantitative fossil composition compared to the first two phases. It was shown that this lateral overbank deposit was subject to significantly less reworking and thus exhibits various detectable relations between finds. A variety of mammalian strewnfields consisting of a juvenile deinothere, an antelope, two tragulids as well as a beaver and a large feliform carnivore revealed a unique enrichment of carcasses for the Hammerschmiede. The

precise nature of this accumulation must be clarified in future studies but nevertheless proved the presence and possible autochthony of the various vertebrates for this habitat.

The eroded channel structure of HAM 4 covers a significantly greater extent as the HAM 5, comparable in size to a river. Furthermore, HAM 4 showed small-scale and large-scale differences in sedimentation. No clear general sedimentation phases could be identified over the entire deposit, with the exception of a basal channel lag deposit. The channel fill is characterised by heterogeneous, small-scale accumulation phases with obliquely dipping, fossil-rich layers that converge with the basal channel deposit and cannot be clearly separated in some cases. Due to detected flow direction changes of the channel, these structures demonstrate the lateral migration of channel meanders in cut bank direction, and channel lag sedimentation at the channel base and at the obliquely dipping point bar of the inner bank. This proved that the observed eroded channel width does not correspond to the actual channel width of the river, at least during the final sedimentation of the channel fill. The spatial documentation of finds furthermore revealed that, due to the inclining channel lags, specimens collected from different elevations can contribute the same event of sedimentation and those gathered from similar elevation can be of different phases. According to sedimentological or outcrop observations supplemented by the orientation of elongated objects within the channel deposits, a clearly meandering, sinuous course from the south-west to the north-east throughout the clay pit outcrop could be established. As in HAM 5, skeletal strewnfields were detected at different excavation areas within the HAM 4 level (a suid, a tragulid, an antelope and avian remains). Furthermore, articulated finds of turtle shells and a bird leg (*Allgoviachen tortonica*) were made. Several anatomically arranged skeletal elements indicated that at least connected parts of carcasses were introduced to the fluvial system (connected e.g. by ligaments). This suggested at least partial carcass dehydration during the decomposition out of reach of scavengers and an introduction, transported and deposition of these elements by the river. This furthermore demonstrated the small-scale nature of the HAM 4 river system with at least non-permanent water fill over the entire channel area during the final channel filling. The bone content within the channel lags was, similar to HAM 5, very heterogeneous and mixed. Elements of assumed strewnfields of individuals were exceptions and most likely represent carcasses that were inserted late before the final burial.

Hammerschmiede strewnfields provided an atypical pattern of bone distribution in fluvial channels. Previous assumptions assume that the distribution of the bones depends primarily on their density and surface properties as well as on the flow velocity. The Hammerschmiede

deposits contained accumulates of bones which are actually quite easy to transport (e.g. ribs) together with the heaviest and densest elements (e.g. teeth, skull), while most of the vertebrae and many other bones were missing. It has been hypothesized that this effect is produced by an influence of the soft-bottomed nature of the river channels, that adhesively sucked flat bones in particular onto the bottom. More voluminous objects were possibly leveraged by the current and transported away. The requirement for this, however, is that the carcass (carcass fragment) was introduced to the river and deposited in one piece, where it was first completely decomposed and disarticulated at rest so that all the bones are could fell loose to the ground. This suggested, that the HAM 4 river was subject to strong fluctuations in currents and water supply.

In addition to possible abiogenic abrasion (rolling) and fragmentation, the majority of the specimens found at HAM 4 and HAM 5 also exhibited a large number of biogenic traces. These proved that the bone materials in particular were decomposed and further utilized by larger carnivores, smaller vertebrates or arthropods as well as plants and possibly algae and bacteria. Root traces prove that some bones were embedded in rooted soils over several time until they were secondarily relocated. Possible arthropod (dermestids, termites, ants) traces as well as small mammal gnawing indicate skeletal remains have also decomposed under terrestrial conditions. An immense number of bone splinters proved that a major proportion of mammal carcasses was consumed and fragmented by larger carnivores and those remains were introduced and enriched within the river deposits. Similarly, suspected traces of digestive corrosion indicate that small mammals, such as the small beaver (*Euroxenomys minutus*) in particular, were preyed upon, and the finds largely represent digestive remains of e.g. birds of prey or carnivorous mammals.

Next to digestive corrosion, a second form of bone surface etching was detected on most of the fossil bones, which may be referred to as biofilm corrosion (or corrosion by aquatic vegetation). This traces possibly proved, that bones were superimposed to or at least half embedded at the channel ground and exposed to the water column for a certain period of time. This hardground was possibly colonised by algae or bacteria, which superficially corroded and roughened the bones for phosphatic fertilizers.

In addition to sedimentological and biostratinomic observations, another focus was on the ecological assessment of selected animal species. In a first approach, beavers were selected as

a potentially autochthonous element of the fluvial ecosystem which is also characterised by a particularly high frequency of finds. With a presumed semi-aquatic lifestyle, beavers should provide an insight into ecological parameters of the fossil HAM 5 and HAM 4 habitats. A taxonomic review assigned the specimens to the large beaver *Steneofiber depereti* (Minimal number of individuals, MNI: 9 for HAM 5; 15 for HAM 4) and the small *Euroxenomys minutus* (MNI: 35 for HAM 5; 82 for HAM 4). Mortality analyses were carried out on the basis of the most common tooth positions (lower premolar, p4) through defined dental (age) wear stages. It was found that the mortality distributions of *Steneofiber depereti* differed significantly between the local stratigraphic levels of HAM 5 and HAM 4. In contrast, the small beaver showed an almost identical mortality distribution not only between the Hammerschmiede strata but also compared to the Rudabánya (Hungary) fossil site, representing swamp deposits. Using actualistic considerations, it could be shown that the mortality on the large beaver correspond fairly closely to those of modern beavers. The optimal habitat of *Steneofiber depereti* refers to larger rivers (such as HAM 4) and the HAM 5 rivulet represents a rather inappropriate habitat. The age frequency distribution indicated a “natural“, “attritional“ mortality controlled by intraspecific, ecologic parameters. This observation further showed that the ecology of the fossil *Steneofiber* possibly was very similar to that of modern beavers, possibly lived in family groups with multi-year parental investment, and prime adult migrations to poorer habitats, in search of own territories. The small beaver (*Euroxenomys minutus*), on the other hand, is ubiquitous (similar to the modern muskrat) and inhabits large rivers, as well as smaller rivulets or swamp regions. The resulted age frequency distribution could not be assigned to either the typical L-shaped or U-shaped mortality but shows a dominance of prime adults. Due to its body size, mortality is controlled by external predation pressures rather than intraspecific parameters.

In addition to biostratigraphic, ecologic and partly necrologic parameters, also postgenetic and thus diagenetic influences on fossil preservation were analysed. HAM 5 and HAM 4 showed clear differences in preservability of different types of material. Diagenetic compaction was identified as one of the strongest impacts on deposited bones. Discrepancies between HAM 4 and HAM 5 are primarily due to the different sediment composition. The clay-rich HAM 5 strata showed a high diagenetic compressibility (pore space reduction through water expulsion) and bones are more often compressed. In contrast, finds in the rather fine sandy HAM 4 deposits were more easily preserved in three dimensions as the surrounding sediment is less compactible. The compression pressure was probably mainly caused by the sedimentary overburden, which could be assumed to be very high, and only to a lesser extent by the glacial load during

Pleistocene ice ages. In certain cases, modern compression and dislocation or shearing of bones by load and movement of mining vehicles as well as mining activities could not be ruled out. Finally, excavations are of course also responsible for damage to some finds or modification by chemical substances (e.g. adhesives).

Supplementary to mechanical preservation influences, geochemical observations were also made at the Hammerschmiede deposits. High pyrite and uranium contents in HAM 4 and HAM 5 fossils indicated strong redox reactions in the subsurface of the channel sediments. This raised the question of whether this could be reconciled with the well-ventilated channel waters indicated by various faunal elements. It turns out that the sediments themselves are responsible for this, regardless of the water running over them. Presumably due to the high proportion of fine clastic sediments (clay and silt) and organic contents, the pore water chemistry was influenced since sediment formation affecting redox reactions during water infiltration. It remains unexplained why the high iron-sulfate incorporation in wood becomes unstable after exhumation and causes the wood to disintegrate and impossible to store in the collection, while the iron-sulfide content in the bones remains stable. Future investigations could clarify whether this difference is possibly due to mineralogical variations and whether pyrite in bones and marcasite in wood was formed as iron sulphide and therefore explain why this is the case.

Finally, this dissertation was able to show that comprehensive conclusions on fossil site genesis, taphonomy and in detail also biostratigraphy were mostly possible to properly and extensively documented excavations. However, such techniques have not yet been widely adopted in palaeontology. Only a few sites such as Untermassfeld (Pleistocene; Germany, Thuringia) show a similar comprehensive approach (e.g. Kahlke 2006). Particularly in sites with several fossil-bearing layers in superposition, small-scale investigations are extremely useful for documenting changes within the site. Fossil localities such as Sandelzhausen (Miocene; Bavaria, Germany) have been excavated in precisely this way, but the stratified distinctions are only processed further in a few exceptions (Böhme 2010). The Hammerschmiede sites show to a unique extent the documentation of the entire river channel deposits revealing many autochthonous and allochthonous elements. The question of why these channel fillings are so rich in fossils and other fluvial deposits in the Molasse are seem to be not, remains exciting and unresolved. It is possible that other river deposits equally rich in fossils and that this interpretation is a bias of observation. It also took some time for the Hammerschmiede investigations to get on the right track. Systematic excavation only began because of large vertebrate fossils were found by chance. The excavations themselves finally revealed the actual abundance of fossils within the

identified levels. The success of this fossil site resulted from initial stratigraphic excavations, which were eventually changed to a planum technique. However, many sites represent small-scale singular outcrops in which it is not so easy to excavate and document on a large scale.

The data and discoveries already generated from the Hammerschmiede excavations will multiply in the future. Based on the dental material of the Hammerschmiede beavers an initial ecological evaluation was carried out using mortality analyses. This method can now be applied to many other faunal elements of the fossil Hammerschmiede ecosystems. The possible confirmation that terrestrial mammals could represent autochthonous elements of the habitats opens up the opportunity of carrying out further investigations here too. Future analyses could reveal migration movements of animals, show seasonality by changing water availability, or provide ecological insights into animal species and groups.

For the moment, it remains unclear for what duration of time sediments were accumulated and deposited but the multiphase nature suggested a minimum of several events. A better three-dimensional understanding of the deposits will certainly make it possible to assemble further skeletal strewnfields into singular individuals, which will continue to provide us with morphological information on vertebrate species. There are only a few places in the world where such a comprehensive insight into fossil ecosystems can be gained at different points in time in one place. Excavations will certainly continue in the Hammerschmiede and the existing areas could yield a large number of new finds over the next decades which could massively enrich our understanding of fossil ecosystems.

References

- Augustin, F.J., Matzke, A.T., Csiki-Sava, Z., Pfretzschner, H.-U., 2019. Bioerosion on vertebrate remains from the Upper Cretaceous of the Hațeg Basin, Romania and its taphonomic implications. *Palaeogeography, Palaeoclimatology, Palaeoecology* 534. <https://doi.org/10.1016/j.palaeo.2019.109318>.
- Augustin, F.J., Matzke, A.T., Maisch, M.W., Pfretzschner, H.-U., 2021. Dinosaur taphonomy of the Jurassic Shishugou Formation (Northern Junggar Basin, NW China) – insights from bioerosional trace fossils on bone. *Ichnos* 1–10. <https://doi.org/10.1080/10420940.2021.1890590>
- Backwell, L.R., Parkinson, A.H., Roberts, E.M., d’Errico, F., Huchet, J.-B., 2012. Criteria for identifying bone modification by termites in the fossil record. *Palaeogeography, Palaeoclimatology, Palaeoecology* 337–338, 72–87. <https://doi.org/10.1016/j.palaeo.2012.03.032>.
- Behrensmeyer, A.K., 1975. The Taphonomy and Paleoecology of Plio-Pleistocene Vertebrate Assemblages east of Lake Rudolf, Kenya. *Bull. Mus. Comp. Zool* 146, 473–578.
- Behrensmeyer, A.K., 1988. Vertebrate preservation in fluvial channels. *Palaeogeography, Palaeoclimatology, Palaeoecology* 63(1-3), 183–199. [https://doi.org/10.1016/0031-0182\(88\)90096-x](https://doi.org/10.1016/0031-0182(88)90096-x)
- Behrensmeyer, A.K., 1990. Transport / hydrodynamics of Bones. In: Briggs, D.E.G., Crowther, P.R. (Eds.), *Palaeobiology: A Synthesis*. 232–235.
- Behrensmeyer, A.K., Kidwell, S.M. 1985. Taphonomy’s Contributions to Paleobiology. *Paleobiology* 11(1), 105–119.
- Behrensmeyer, A.K., Kidwell, S.M., Gastaldo, R.A., 2000. Taphonomy and paleobiology. *Paleobiology* 26, 103–147. <https://doi.org/10.1017/S0094837300026907>
- Böhme, M., 2002. Freshwater fishes from the Pannonian of the Vienna Basin with special reference to the locality Sandberg near Götzendorf, Lower Austria. *Courier Forschungsinstitut Senckenberg* 237, 151–173.
- Böhme, M., 2010. Ectothermic vertebrates (Actinopterygii, Allocaudata, Urodela, Anura, Crocodylia, Squamata) from the Miocene of Sandelzhausen (Germany, Bavaria) and their implications for environment reconstruction and palaeoclimate. *Paläontologische Zeitschrift* 84, 3–41. <https://doi.org/10.1007/s12542-010-0050-4>
- Böhme, M., Braun, R., Breier, F., 2019. *Wie wir Menschen wurden: Eine kriminalistische Spurensuche nach den Ursprüngen der Menschheit – Spektakuläre Funde im Alpenraum*. Heyne Verlag. 336 pp.
- Böhme, M., Ilg, A., Ossig, A., Küchenhoff, H., 2006. New method to estimate paleoprecipitation using fossil amphibians and reptiles and the middle and late Miocene precipitation gradients in Europe. *Geology* 34 (6), 425–428. <https://doi.org/10.1130/G22460.1>
- Böhme, M., Ilg, A., Winklhofer, M., 2008. Late Miocene “washhouse” climate in Europe. *Earth and Planetary Science Letters* 275, 393–401. <https://doi.org/10.1016/j.epsl.2008.09.011>
- Böhme, M., Spassov, N., DeSilva, J.M., Begun, D.R., 2020. Reply to: Reevaluating bipedalism in *Danuvius*. *Nature* 586, E4–E5. <https://doi.org/10.1038/s41586-020-2737-3>

- Böhme, M., Spassov, N., Fuss, J., Tröscher, A., Deane, A.S., Prieto, J., Kirscher, U., Lechner, T., Begun, D.R., 2019. A new Miocene ape and locomotion in the ancestor of great apes and humans. *Nature* 575, 489–493. <https://doi.org/10.1038/s41586-019-1731-0>
- Böhme, M., Vasilyan, D., Winklhofer, M., 2012. Habitat tracking, range dynamics and palaeoclimatic significance of Eurasian giant salamanders (Cryptobranchidae) – indications for elevated Central Asian humidity during Cenozoic global warm periods. *Palaeogeography, Palaeoclimatology, Palaeoecology* 342–343, 64–72. <https://doi.org/10.1016/j.palaeo.2012.04.032>
- Böhme, M., Winklhofer, M., Ilg, A., 2011. Miocene precipitation in Europe: Temporal trends and spatial gradients. *Palaeogeography, Palaeoclimatology, Palaeoecology* 304, 212–218. <https://doi.org/10.1016/j.palaeo.2010.09.028>
- Bolliger, T., 1999. Family Anomalomyidae. In: Rössner, G.E., Heissig, K. (Eds.), *The Miocene Land Mammals of Europe*. Verlag Dr. Friedrich Pfeil, Munich. 411–420.
- Daams, R., 1999. Family Gliridae. In: Rössner, G.E., Heissig, K. (Eds.), *The Miocene Land Mammals of Europe*. Verlag Dr. Friedrich Pfeil, Munich. 301–318.
- Discamps, E., Costamagno, S., 2015. Improving mortality profile analysis in zooarchaeology: a revised zoning for ternary diagrams. *Journal of Archaeological Science* 58, 62–76. <https://doi.org/10.1016/j.jas.2015.03.021>
- de Bruijn, H., Daams, R., Daxner-Höck, G., Fahlbusch, V., Ginsburg, L., Mein, P., Morales, J., Heinzmann, E., Mayhew, D.F., van der Meulen, A.J., Schmidt-Kittler, N., Telles Antunes, M., 1992. Report of the RCMNS working group on fossil mammals, Reisenburg 1990. *Newsletters on Stratigraphy* 26(2/3), 65–118.
- Dentzien-Dias, P., Hunt, A.P., Lucas, S.G., Francischini, H., Gulotta, M., 2021. Coprolites from shallow marine deposits of the Nanjemoy Formation, Lower Eocene of Virginia, USA. *Lethaia* 54, 26–39. <https://doi.org/10.1111/let.12380>
- Doppler, G., 1989. Zur Stratigraphie der nördlichen Vorlandmolasse in Bayerisch-Schwaben. *Geologica Bavarica* 94, 83–133. Munich.
- Doppler, G., Heissig, K., Reichenbacher, B., 2005. Die Gliederung des Tertiärs im süddeutschen Molassebecken. *Newsletters on Stratigraphy* 41(1-3), 359–375. <https://doi.org/10.1127/0078-0421/2005/0041-0359>
- Efremov, I.A., 1940. Taphonomy: a new branch of paleontology. *Pan-American Geologist* 74, 81–93.
- Etter, W., 1994. *Palökologie: eine methodische Einführung*. Birkhäuser Verlag, Basel, Boston, Berlin. 294 pp.
- Fahlbusch, V., Mayr, H., 1975. Microtoide Cricetiden (Mammalia, Rodentia) aus der Oberen Süßwasser-Molasse Bayerns. *Paläontologische Zeitschrift* 49, 78–93.
- Fejfar, O., 1999. Microtoid Cricetids. In: Rössner, G.E., Heissig, K. (Eds.), *The Miocene Land Mammals of Europe*. Verlag Dr. Friedrich Pfeil, Munich. 365–373.
- Fernández-Jalvo, Y., Andrews, P., 2016. *Atlas of Taphonomic Identifications: 1001+ Images of Fossil and Recent Mammal Bone Modification, Vertebrate Paleobiology and Paleoanthropology*. Springer Netherlands, Dordrecht. <https://doi.org/10.1007/978-94-017-7432-1>

- Frison, G.C., Todd, L.C., 1986. The Colby mammoth site: taphonomy and archaeology of a Clovis kill in northern Wyoming. Albuquerque, University of New Mexico Press.
- Fürsich, F.T., Mayr, H., 1981. Non-marine Rhizocorallium (trace fossil) from the Upper Freshwater Molasse (Upper Miocene) of southern Germany. *Neues Jahrbuch für Geologie und Paläontologie – Monatshefte* Jg. 1981, 321–333. <https://doi.org/10.1127/njgpm/1981/1981/321>
- Fuss, J., Prieto, J., Böhme, M., 2015. Revision of the boselaphin bovid *Miotragocerus monacensis* Stromer, 1928 (Mammalia, Bovidae) at the Middle to Late Miocene transition in Central Europe. *Neues Jahrbuch für Geologie und Paläontologie - Abhandlungen* 276, 229–265. <https://doi.org/10.1127/njgpa/2015/0481>
- Gregor, H.-J., 1982. Die jungtertiären Floren Süddeutschlands: Paläokarpologie, Phytostratigraphie, Paläoökologie, Paläoklimatologie. I. Enke, Stuttgart. 278 pp.
- Gross, M., Prieto, J., Grímsson, F., Bojar, H.-P., 2023. Hyena and ‘false’ sabre-toothed cat coprolites from the late Middle Miocene of south-eastern Austria. *Historical Biology* 1–20. <https://doi.org/10.1080/08912963.2023.2237979>
- Gümbel, C.W. von, 1861. Geognostische Beschreibung des bayerischen Alpengebirges und seines Vorlandes. Gotha. 950 pp.
- Hanson, C.B., 1980. 9. Fluvial taphonomic processes: models and experiments, in: Behrensmeyer, A.K., Hill, A.P. (Eds.), *Fossils in the Making: Vertebrate Taphonomy and Paleoecology*. University of Chicago Press, Chicago, pp. 156–181.
- Hartung, J., Böhme, M., 2022. Unexpected cranial sexual dimorphism in the tragulid *Dorcatherium nauii* based on material from the middle to late Miocene localities of Eppelsheim and Hammerschmiede (Germany). *PLOS ONE* 33.
- Hartung, J., Lechner, T., Böhme, M., 2020. New cranial material of *Miotragocerus monacensis* (Mammalia: Bovidae) from the late Miocene hominid locality Hammerschmiede (Germany). *Neues Jahrbuch für Geologie und Paläontologie - Abhandlungen* 298, 269–284. <https://doi.org/10.1127/njgpa/2020/0948>
- Hugueney, M., 1999. Family Castoridae. In: Rössner, G.E., Heissig, K. (Eds.), *The Miocene Land Mammals of Europe*. Verlag Dr. Friedrich Pfeil, Munich. 281–300.
- Hulbert, R.C., Jr., 1982. Population dynamics of the three-toed horse *Neohipparion* from the Late Miocene of Florida. *Paleobiology* 8, 159–167.
- Iyagbaye, L., Iyagbaye, R., Omoigberale, M., 2017. Mayflies (Order Ephemeroptera) Distribution as Indicators of the Water Quality Status of a Stretch of Ovia River (Iguoriakhi), Edo State, Southern Nigeria. *International Journal Of Innovative Research & Development* 6. <https://doi.org/10.24940/ijird/2017/v6/i9/SEP17041>
- Jung, W., Mayr, H., 1980. Neuere Befunde zur Biostratigraphie der Oberen Süßwassermolasse Süddeutschlands und ihre palökologische Deutung. *Mitteilungen der Bayerischen Staatssammlung für Paläontologie und historische Geologie*. 20, 159–173.
- Kahlke, R.-D., Gaudzinski, S., 2005. The blessing of a great flood: differentiation of mortality patterns in the large mammal record of the Lower Pleistocene fluvial site of Untermassfeld (Germany) and its relevance for the interpretation of faunal assemblages from archaeological sites. *Journal of Archaeological Science* 32, 1202–1222. <https://doi.org/10.1016/j.jas.2005.03.004>

- Kahlke, R.-D., 2006. Untermassfeld: a late early Pleistocene (Epivillafranchian) fossil site near Meiningen (Thuringia, Germany) and its position in the development of the European mammal fauna, BAR international series. Archaeopress, Oxford.
- Kargopoulos, N., Kampouridis, P., Lechner, T., Böhme, M., 2021a. A review of *Semigenetta* (Viverridae, Carnivora) from the Miocene of Eurasia based on material from the hominid locality of Hammerschmiede (Germany). *Geobios* 69, 25–36. <https://doi.org/10.1016/j.geobios.2021.07.001>
- Kargopoulos, N., Kampouridis, P., Lechner, T., Böhme, M., 2021b. Hyaenidae (Carnivora) from the Late Miocene hominid locality of Hammerschmiede (Bavaria, Germany). *Historical Biology* 1–10. <https://doi.org/10.1080/08912963.2021.2010193>
- Kargopoulos, N., Valenciano, A., Abella, J., Kampouridis, P., Lechner, T., Böhme, M., 2022. The exceptionally high diversity of small carnivorans from the Late Miocene hominid locality of Hammerschmiede (Bavaria, Germany). *PLOS ONE* 64.
- Kargopoulos, N., Valenciano, A., Kampouridis, P., Lechner, T., Böhme, M., 2021c. New early late Miocene species of *Vishnuonyx* (Carnivora, Lutrinae) from the hominid locality of Hammerschmiede, Bavaria, Germany. *Journal of Vertebrate Paleontology* 41, e1948858. <https://doi.org/10.1080/02724634.2021.1948858>
- Kirscher, U., Prieto, J., Bachtadse, V., Abdul Aziz, H., Doppler, G., Hagmaier, M., Böhme, M., 2016. A biochronologic tie-point for the base of the Tortonian stage in Europe terrestrial settings: Magnetostratigraphy of the topmost Upper Freshwater Molasse sediments of the North Alpine Foreland Basin in Bavaria (Germany). *Newsletters on Stratigraphy* 49, 445–467. <https://doi.org/10.1127/nos/2016/0288>
- Kitching, J.W., 1980. On some fossil arthropoda from the Limeworks. Makapansgat, Potgietersrus. *Palaeontologia Africana* 23, 63–68.
- Kivell, T.L., 2019. Fossil ape hints at how walking on two feet evolved. *Nature* 575, 445–446. <https://doi.org/10.1038/d41586-019-03347-0>
- Klein, R.G., 1982. Patterns of ungulate mortality and ungulate mortality profiles from Langebaanweg (Early Pliocene) and Elandsfontein (Middle Pleistocene), South-Western Cape Province, South Africa. *Annals of the South African Museum* 90, 49–94.
- Klein, S., 1937. Der Oberste Feinflinz im Alpenvorland und südlichen Tertiärhügelland. Studie I zur Geologie und Morphologie südbayerischer Jungtertiär- und Diluviallandschaften. *Zeitschrift der Deutschen Geologischen Gesellschaft* 89, 384–409.
- Klein, S., 1938. Die Ausformung der Münchner Ebene durch fluvioglaziale Erosion jungtertiärer Schichten. Studie II zur Geologie und Morphologie südbayerischer Jungtertiär- und Diluviallandschaften. *Zentralblatt für Mineralogie, Geologie und Paläontologie in Verbindung mit dem Neuen Jahrbuch für Mineralogie, Geologie und Paläontologie, Abteilung B: Geologie und Paläontologie* 1938, 279–299.
- Klein, S., 1939. Die miocän-pliocänen Grenzschichten nördlich von München. Südbayerische Jungtertiär- und Quartärstudien IV (Schluß). *Zentralblatt für Mineralogie, Geologie und Paläontologie in Verbindung mit dem Neuen Jahrbuch für Mineralogie, Geologie und Paläontologie, Abteilung B: Geologie und Paläontologie* 1939, 278–292.
- Klembara, J., Böhme, M., Rummel, M., 2010. Revision of the anguine lizard *Pseudopus laurillardii* (Squamata, Anguinae) from the Miocene of Europe, with comments on paleoecology. *Journal of Paleontology* 84(2), 159–196.

- Konidaris, G.E., Lechner, T., Kampouridis, P., Böhme, M., 2023. *Deinotherium levius* and *Tetralophodon longirostris* (Proboscidea, Mammalia) from the Late Miocene hominid locality Hammerschmiede (Bavaria, Germany), and their biostratigraphic significance for the terrestrial faunas of the European Miocene. *Journal of Mammalian Evolution*. 1–39. <https://doi.org/10.1007/s10914-023-09683-3>.
- Kordiuk, B., 1938. Zur Entwicklung des subalpinen Molassetroges. Berlin. 47 pp.
- Kreutzer, L.A., 1988. Megafaunal butchering at Lubbock Lake, Texas: a taphonomic reanalysis. *Quaternary Research* 30, 221–231.
- Kurtén, B. (1953). On the variation and population dynamics of fossil and recent mammal populations. Doctoral dissertation, Societas pro fauna et flora Fennica.
- Laatsch, W., 1931. Die Biostratonomie der Ganoidfische des Kupferschiefers. *Palaeobiologica* 4.
- Lechner, T., Böhme, M., 2022. The beaver *Steneofiber depereti* from the lower upper Miocene hominid locality Hammerschmiede and remarks on its ecology. *Acta Palaeontologica Polonica* 67(4), 807-826. <https://doi.org/10.4202/app.00997.2022>
- Lechner, T., Böhme, M., 2023. The largest record of the minute beaver *Euroxenomys minutus* (Mammalia, Castoridae) from the early Late Miocene hominid locality Hammerschmiede (Bavaria, Southern Germany) and palaeoecological considerations. *Historical Biology* 1–16. <https://doi.org/10.1080/08912963.2023.2215236>.
- Lemcke, K., 1988. Das bayerische Alpenvorland vor der Eiszeit. *Geologie von Bayern* 1. Schweizerbart, Stuttgart. 175 pp.
- Lovich, E., Gotte, W., Ernst, H., Harshbarger, C., Laemmerzahl, F., Whitfield, J., 1996. Prevalence and Histopathology of shell disease in turtles from lake Blackshear, Georgia. *Journal of Wildlife Disease* 32(2), 259–265.
- Lyman, R.L., 1994. *Vertebrate taphonomy*, Cambridge manuals in archaeology. Cambridge University Press, Cambridge [England]; New York. 524 pp.
- Mayr, G., Lechner, T., Böhme, M., 2020a. A skull of a very large crane from the late Miocene of Southern Germany, with notes on the phylogenetic interrelationships of extant Gruinae. *Journal of Ornithology* 161, 923–933. <https://doi.org/10.1007/s10336-020-01799-0>
- Mayr, G., Lechner, T., Böhme, M., 2020b. The large-sized darter *Anhinga pannonica* (Aves, Anhingidae) from the late Miocene hominid Hammerschmiede locality in Southern Germany. *PlosOne* 15, 19. <https://doi.org/10.1371/journal.pone.0232179>
- Mayr, G., Lechner, T., Böhme, M., 2022. Nearly complete leg of an unusual, shelduck-sized anseriform bird from the earliest late Miocene hominid locality Hammerschmiede (Germany). *Historical Biology* 1–10. <https://doi.org/10.1080/08912963.2022.2045285>
- Mayr, H., Fahlbusch, V., 1975. Eine unterpliozäne Kleinsäugerfauna aus der Oberen Süßwasser-Molasse Bayerns. *Mitteilungen der Bayerischen Staatssammlung für Paläontologie und historische Geologie* 15, 91–111.
- Mein, P., 1989. Updating of MN zones. In: E. Lindsay, V. Fahlbusch & P. Mein, editors. *European Neogene Mammal Chronology*. NATO ASI Series 180, 73–90.
- Meyer, B.L., 1956. Mikrofloristische Untersuchungen an jungtertiären Braunkohlen im östlichen Bayern. *Geologica Bavarica* 25, 100–128.

- Müller, A.H., 1951. Grundlagen der Biostratonomie. Deutsche Akademie der Wissenschaften zu Berlin, Abhandlungen 1950, No. 3.
- Müller, A.H., 1963. Lehrbuch der Paläozoologie, Band 1: Allgemeine Grundlagen. G. Fischer Verlag, Jena. 387 pp.
- Parkinson, A.H., Backwell, L.R., Roberts, E.M., D’Errico, F., Huchet, J.-B., Val, A., 2010. Effects of termites on mammal and bird bone. In: Mostovski, M.B., Ovechkina, M.N. (Eds.), Proceedings of the 16th Conference of the Palaeontological Society of Southern Africa. Pietermaritzburg, South Africa, pp. 79.
- Pesquero, M.D., Ascaso, C., Alcalá, L., Fernández-Jalvo, Y., 2010. A new taphonomic bioerosion in a Miocene lakeshore environment. *Palaeogeography, Palaeoclimatology, Palaeoecology* 295, 192–198. <https://doi.org/10.1016/j.palaeo.2010.05.037>
- Prieto, J., 2007. Kleinsäuger-Biostratigraphie und Paläoökologie des höheren Mittelmiozäns (MN8) Bayerns: Spaltenfüllungen der Fränkischen Alb und Lokalitäten der Oberen Süßwassermolasse im Vergleich. PhD thesis, Fakultät für Geowissenschaften der Ludwig-Maximilians-Universität München, Munich, Germany.
- Prieto, J., 2012. The Genus *Eomyops* Engesser, 1979 (Rodentia, Eomyidae) from the youngest deposits of the German part of the North Alpine Foreland Basin. *Swiss Journal of Palaeontology* 131, 95–106. <https://doi.org/10.1007/s13358-011-0033-4>
- Prieto, J., Rummel, M., 2009a. The genus *Collimys* Daxner-Höck, 1972 (Rodentia, Cricetidae) in the Middle Miocene fissure fillings of the Frankian Alb (Germany). *Zitteliana* 48/49, 75–88.
- Prieto, J., Rummel, M., 2009b. Evolution of the genus *Collimys* Daxner-Hock, 1972 (Rodentia, Cricetidae) a key to Middle to Late Miocene biostratigraphy in Central Europe. *Neues Jahrbuch für Geologie und Paläontologie - Abhandlungen* 252, 237–247. <https://doi.org/10.1127/0077-7749/2009/0252-0237>
- Prieto, J., van Dam, J.A., 2012. Primitive Anourosoricini and Allosoricinae from the Miocene of Germany. *Geobios* 45, 581–589. <https://doi.org/10.1016/j.geobios.2012.03.001>
- Prieto, J., van den Hoek Ostende, L.W., Böhme, M., Braze, M., 2011. Reappearance of *Galerix* (Erinaceomorpha, Mammalia) at the Middle to Late Miocene transition in South Germany: biostratigraphic and palaeoecologic implications. *CTOZ* 80, 179–189. <https://doi.org/10.1163/18759866-08003002>
- Schleich, H.H., 1984. Neue Reptilienfunde aus dem Tertiär Deutschlands. 1. Schildkröten aus dem Jungtertiär Süddeutschlands. *Naturwissenschaftliche Zeitschrift für Niederbayern* 30, 63–93.
- Schneider, S., Prieto, J., 2011. First record of an autochthonous community of fluviatile freshwater molluscs from the Middle/Late Miocene Upper Freshwater Molasse (southern Germany). *Archiv für Molluskenkunde International Journal of Malacology* 140, 1–18. <https://doi.org/10.1127/arch.moll/1869-0963/140/001-018>
- Scholz, H., 2016. Bau und Werden der Allgäuer Landschaft – Alpen und schwäbisches Alpenvorland - zwischen Ammer und Bodensee, Eine süddeutsche Erd- und Landschaftsgeschichte. 3rd edition. 354 pp. Schweizerbart, Stuttgart.
- Schwerd, K., Doppler, H., Unger, H.-J., 1996. Gesteinsfolge des Molassebeckens und der inneralpinen Tertiärbecken. In: Freudenberger, W., Schwerd, K., (eds) Erläuterungen

- zur Geologischen Karte von Bayern 1:500.000. Bayerisches Geologisches Landesamt, Munich. 141-149.
- Seitner, L., 1987. Miozäne Mikrofloren aus Sedimenten der Süßbrackwassermolasse und der Oberen Süßwassermolasse Süddeutschlands. PhD thesis, Fakultät für Geowissenschaften der Ludwig-Maximilians-Universität München, Munich, Germany.
- Steininger, F.F., Bernor, R.L., Fahlbusch, V., 1989. European Neogene marine/continental chronologic correlations. In: Lindsay, E.H., Fahlbusch, V., Mein, P. [eds.]: European Neogene mammal chronology. 15–46. New York (Plenum).
- Stiner, M.C., 1994. Honor among Thieves: A Zooarchaeological Study of Neandertal Ecology. Princeton University Press, Princeton.
- Uchman, A., Mikuláš, R., Stachacz, M., 2017. Mayfly Burrows in Firmground of Recent Rivers from the Czech Republic and Poland, with Some Comments on Ephemeropteran Burrows in General. *Ichnos* 24, 191–203. <https://doi.org/10.1080/10420940.2016.1257488>
- van Dam, J.A., 2010. Anourosoricini (Soricidae, Mammalia): new taxa and systematic position in the light of molecular phylogenetics. *Journal of Vertebrate Paleontology* 30, 1221–1228.
- Voorhies, M.R., 1969. Taphonomy and Population Dynamics of an Early Pliocene Vertebrate Fauna, Knox County, Nebraska. University of Wyoming, Laramie, WY. https://doi.org/10.2113/gsrocky.8.special_paper_1.1
- Wang, J., Yan, Y., Bai, J., Su, X., 2020. Influences of riverbed siltation on redox zonation during bank filtration: a case study of Liao River, Northeast China. *Hydrology Research* 51, 1478–1489. <https://doi.org/10.2166/nh.2020.107>
- Watson, J.A.L., Abbey, H.M., 1986. The effects of termites (Isoptera) on bone: some archaeological implications. *Sociobiology* 11, 245–254.
- Weigelt, J., 1919. Geologie und Nordseefauna: *Steinbruch* 14, 228–231, 244–246.
- Weigelt, J., 1928. *Rezente Wirbeltierleichen und ihre paläobiologische Bedeutung*. 3rd edition, 1999, Bad Vilbel (Dieter W. Berger). 288 pp.
- Wiedenmann, L., 2011. *Historischer Kohlenbergbau und Bergbauversuche auf Kohlen im Allgäu – Irsee. Eine Archiv-Dokumentation eines (fast) vergessenen Erwerbszweigs*. Bauer-Verlag GmbH, Thalhofen. 373 pp.
- Williams, S.A., Prang, T.C., Meyer, M.R., Russo, G.A., Shapiro, L.J., 2020. Reevaluating bipedalism in *Danuvius*. *Nature* 586, E1–E3. <https://doi.org/10.1038/s41586-020-2736-4>
- Ziegler, R., 1999. Order Insectivora. In: Rössner, G.E., Heissig, K. (Eds.), *The Miocene Land Mammals of Europe*. Verlag Dr. Friedrich Pfeil, Munich. 53–74.